Dysfonctions mitochondriales et paragangliomes métastatiques : voies d'oncogenèse médiées par les différents gènes SDHx

Judith Goncalves

Université de Paris

École doctorale n°561 « Hématologie, Oncogenèse, Biothérapies »

Laboratoire : INSERM UMR 970 – PARIS CENTRE DE RECHERCHE CARDIOVASCULAIRE (PARCC)

DYSFONCTIONS MITOCHONDRIALES ET PARAGANGLIOMES METASTATIQUES : VOIES D'ONCOGENESE MEDIEES PAR LES DIFFERENTS GENES *SDHx*

Par Judith Goncalves

Thèse de doctorat de Biologie, spécialité Oncogenèse

Dirigée par Dr Judith Favier

Présentée et soutenue publiquement le 5 février 2021

Devant un jury composé de :

Dr Judith Favier, DR2 INSERM, Université de Paris	Directrice de thèse
Pr Olivier Chabre, PU-PH, Université Grenoble-Alpes	Rapporteur
Dr Laurent Le Cam, DR2 INSERM, Université de Montpellier	Rapporteur
Dr Pierre Rustin, DRE INSERM, Université de Paris	Examinateur
Dr Géraldine Gentric, CRCN INSERM, Université de Paris	Examinatrice
Dr Sophie Vasseur, DR2 INSERM, Université de Aix-Marseille	Examinatrice

Remerciements

En premier lieu je tiens à remercier très sincèrement les membres du jury :

Le Pr Olivier Chabre et le Dr Laurent Le Cam pour avoir accepté avec enthousiasme, la lourde charge d'être rapporteurs de cette thèse.
Le Dr Pierre Rustin qui, après avoir accepté de suivre mes travaux au cours de ces quatre dernières années en tant que membre de mon comité de suivi, me fait aujourd'hui l'honneur d'examiner l'aboutissement de ce travail. Merci d'avoir pris le temps de me transmettre une partie de votre savoir avec la passion et la gentillesse qui vous caractérisent.
Le Dr Géraldine Gentric, pour avoir accepté avec enthousiasme de faire partie de ce jury, ainsi que pour m'avoir partagé ses précieuses connaissances à plusieurs reprises avec patience et bienveillance.
Le Dr Sophie Vasseur pour avoir accepté de participer à ce jury et de juger ce travail.

Merci au Dr Judith Favier et au Pr Anne-Paule Gimenez-Roqueplo de m'avoir chaleureusement accueilli au sein de leur équipe. Merci pour votre soutien au cours de ces (presque) cinq dernières années et pour m'avoir confié un si beau projet. C'est un honneur pour moi d'avoir pu réaliser ma thèse au sein d'une équipe dirigée par deux femmes aussi brillantes que vous.

Je tiens à remercier tout particulièrement Judith pour sa confiance, sa patience, sa disponibilité et sa bienveillance tout au long de cette thèse. J'ai beaucoup appris à tes côtés, professionnellement et personnellement, aussi bien par ton enseignement que par ton exemple. Merci pour toutes les opportunités que tu m'as données, pour ton écoute, pour tes conseils avisés, pour ton humanité et pour ton humour qui ont grandement contribués au bon déroulement et au plaisir que j'ai pris à faire cette thèse. Je serais toujours reconnaissante et fière d'avoir été ton étudiante de thèse. Merci pour tout.

Un grand merci à l'ensemble des membres, passés et présents, de l'équipe 13 (Nelly, Charlotte, Laurence, Aurélie, Luis, Alexandre, Sophie, Tom, Estelle, Justine, Karen, Patricia, Mélanie, Marie, Déborah, Yasmin, Manon, Aurélien et Élisa) pour leur aide précieuse, leurs conseils et leur soutien au quotidien. Travailler à vos côtés a été un réel plaisir.

Je tiens à remercier sincèrement Aurélie pour son soutien inouï, à tous niveaux. Merci pour ta grande patience, ton indétrônable pédagogie et ta gentillesse dès mon arrivée au laboratoire alors que j'étais encore une petite étudiante de M2 et ce tout au long de ma thèse. Merci pour ta générosité et tout ce que tu as pris le temps de me transmettre avec passion et bonne humeur. J'ai d'abord eu la grande chance de t'avoir pour encadrante et d'apprendre à tes côtés, et désormais de te compter parmi mes proches amis. Pensée particulière pour Mathieu, mon partenaire de danse préféré et Patrick, qui ont bien animés les fêtes de Noël du PARCC.

Je remercie vivement Charlotte pour sa disponibilité, sa bonne humeur et son enthousiasme perpétuel. J'ai également beaucoup apprécié travailler à tes côtés. Merci pour tout ce que tu m'as appris et pour ton soutien aussi bien au niveau professionnel que personnel tout au long de ces années.

Merci à Nelly pour ses suggestions toujours très pertinentes, ses bons conseils et sa bienveillance. Merci de toujours te soucier du bien-être de chacun.

Un grand merci à Estelle et Isa, mes deux mamans du labo (très jeunes mamans bien-sûr). Merci pour votre soutien si précieux, votre aide à toute heure (vous m'avez sauvés la mise plus d'une fois et je ne l'oublierai pas), votre écoute attentive, les fous-rires, les larmes et nos petits restos qui vont bien me manquer. Merci pour vos grands cœurs et d'avoir été présentes dans les bons comme dans les moins bons moments.

Je tiens également à remercier chaleureusement l'ensemble de la plateforme administrative, notamment Cyrille, Bruno, Annette, Camille. Merci Stéphanie pour ta bonne humeur quotidienne et ta disponibilité à chaque fois que j'en ai eu besoin. Un merci tout particulier à Catherine Tritscher pour sa bienveillance, son savoir-faire et pour son aide précieuse.
Merci également à l'ensemble du personnel du PARCC avec qui j'ai pu interagir et en particulier aux membres des équipes du 1er étage avec qui j'ai partagé de très beaux moments. Une pensée particulière à nos copains de l'équipe Aldo : travailler à vos côtés a véritablement été un plaisir.

Je remercie affectueusement le Dr Fatima Mechta-Grigoriou et le Dr Pierre Rustin, pour avoir accepté avec enthousiasme de m'accueillir dans leurs laboratoires à plusieurs occasions, et m'avoir ainsi permis de me former à de nouvelles techniques et expériences passionnantes. Merci à Paule Bénit pour son aide et sa patience.

A mes collègues et amis du BDE, actuels et passés, un merci tout particulier. Alexandre, Hélène, Rami, Georgios, Sophie, Tom, Elisa, Alaa, Kelly, Bakhta, Aurélien, Didi et Bettina se fut un réel plaisir de partager ce bureau et cette belle aventure avec vous tous. Merci à chacun d'entre vous pour les bons moments, les conseils, les discussions scientifiques et beaucoup moins scientifiques aussi, les fous-rires, les verres, les cafés, les anniversaires et les repas de noël. Ce bureau est vraiment spécial et j'y ai fait des rencontres fabuleuses. Merci pour la bonne humeur permanente dans laquelle nous avons pu travailler et pour votre soutien.
Alex, un grand merci pour ton soutien indéfectible à toute heure et à toute épreuve. Merci pour ta patience, ton humour, ta gentillesse et tous tes compliments qui ont vraiment égayés mon quotidien au cours de ces cinq dernières années. J'ai été très chanceuse de t'avoir pour co-thésard. Merci d'avoir si bien pris soin de moi au labo, merci pour toutes tes attentions, tous les post-its, pour les madeleines, les concerts, ton écoute perpétuelle et tes précieux conseils. Je serais toujours très reconnaissante pour tout.
Rami, tu es vite devenu l'un de mes plus proches amis au labo et ce dès mon arrivée. Merci pour ta gentillesse, ton aide, ton réconfort quand j'en avais besoin, nos échanges musicaux et tous les moments passés ensemble.
Hélène, ma grande amie de thèse. On en a traversé des choses ensembles et tous ces moments et les souvenirs qui y sont associés resteront toujours avec moi. Merci pour tout. Tu as été un rayon de soleil au labo et en dehors. Je suis très fière de toi et de tout le chemin que tu as parcouru. J'ai eu beaucoup de chance de vivre ces années à tes côtés.
A Sophie, un immense merci ! Merci pour ta douceur, ta gentillesse, ton humour. Merci pour tous les cafs, tous les repas, les verres, les potins, nos discussions, nos coups de folies (souvent musicaux), notre passion commune (aka Alexis) et pour ton précieux soutien. Merci pour m'avoir écouté râler et vider mon sac quand j'en avais besoin. Merci pour tes conseils, ton réconfort et toutes tes belles attentions à mon égard. J'ai eu beaucoup de chance que tu nous rejoignes au labo et de vivre mes deux dernières années de thèse en ta compagnie. Tu vas accomplir de grandes choses je n'en doute pas une seconde et j'ai hâte d'assister à tout ça !
Merci à mon Dj préféré, notre Gilbert international, Dr Dro, et j'en passe… Tom, je suis très heureuse que tu aies intégré l'équipe et la famille BDE. Merci pour tous les fous-rires, ta bonne humeur quotidienne, ton soutien, tes conseils toujours pertinents et très bienveillants. J'ai adoré partager tous ces moments avec toi et je suis certaine que tu vas faire un excellent doctorant.

Élisa, un très grand merci. Tu as été une très belle rencontre au cours de cette thèse. Nous avons beaucoup de chance de t'avoir eu avec nous au quotidien pendant quelques mois au labo. Merci pour ta présence toujours solaire, ta joie de vivre communicative, ta gentillesse, tes belles attentions, les fous rires, les messages, les horoscopes, les réconforts, la retraite, les crises maniaques… qui m'ont beaucoup apporté et ont été d'un grand soutien. Fifi et toi avez réellement ensoleillé mes journées ces deux dernières années et je suis très chanceuse et reconnaissante pour cette belle amitié.

Un merci spécial à mes amis pour leur soutien indéfectible tout au long de ces années. Amal, tu as toujours été à mes côtés, présente et disponible même quand moi je ne l'étais pas trop, sans jugement ni critiques, au premier rang pour me soutenir à toute heure du jour et de la nuit. Je ne te remercierai jamais assez pour tout. Tu es et sera toujours une inspiration pour moi. A Juliette et Marion, nous avons commencé et terminons cette grande aventure ensemble et j'en suis très fière. Merci pour tous les beaux moments (et voyages exceptionnels) en votre compagnie. J'ai hâte de vivre ces prochaines étapes à vos côtés. Aux rirififi (Leticia, Vincent, Flo, Max, Marlène, Rigaud, Marie, Cotton, Caro, Val e Gaelzinho) merci pour votre grand soutien au cours de ces dernières années et plus particulièrement ces derniers mois. Merci pour toutes les soirées, les week-ends, les vacances qui ont été de véritables bouffées d'oxygène dans ce tourbillon. Tous vos mots d'encouragements, l'intérêt porté sur ce que je faisais et où j'en étais et même vos « alors t'as trouvé quelque chose ? » m'ont porté, merci à tous. Clem, Gab et Paolo merci pour votre soutien et votre amitié précieuse. Merci à Eric Penaud et à Geoffroy LePrado pour le grand intérêt qu'ils portent à la recherche et plus particulièrement à mon sujet de thèse. Nos discussions ont toujours été très enrichissantes, stimulantes et encourageantes.

Enfin, je remercie du fond du cœur mes parents pour leur incroyable soutien. Papa, maman, merci d'avoir cru en moi depuis toujours et de m'avoir continuellement répété que je pourrais accomplir tout ce que je voulais si je m'en donnais les moyens. Merci de m'avoir inculqué vos valeurs et de m'avoir montré l'exemple. Merci d'avoir tout fait pour que nous puissions avoir un bel avenir et pour vos sacrifices. Je suis très fière d'être votre fille et c'est en grande partie grâce à vous que je suis devenue la personne que je suis aujourd'hui. Cette thèse vous est également dédiée (tu vois maman j'ai pas fini à la NASA mais finalement c'est pas si mal non plus). Tout simplement merci. Merci infiniment à mon frère Yann, pour son soutien sans faille depuis toujours. Merci d'avoir toujours dit que j'étais la meilleure et de continuer à me considérer (à tort) comme un génie même après toutes ces années. Merci à l'ensemble de ma famille et en particulier à ma marraine, ma mamie Élisa et mon petit Jojo pour avoir toujours réussis à dissiper mes nuages, pour vos belles leçons de vie, vos encouragements incessants et pour votre amour inconditionnel.

Guillaume, ces derniers mots seront pour toi. Je ne sais par où commencer tellement je te suis reconnaissante. Tu as sans aucun doute été la personne qui m'a le plus soutenue ces dernières années, sans aucune condition, plainte, ou critique. Merci d'avoir toujours tout écouté et ce même quand je te répétais pour la 10ème fois la même chose (désolé) et d'avoir pris le temps de me donner tes précieux conseils. Merci d'avoir été d'une patience inégalable et d'avoir réussi à me supporter. Merci pour ta compréhension à toute épreuve. Merci pour ta passion pour SDHC (t'as toujours pas compris mais ça viendra). Merci pour tes encouragements hors du communs. Merci d'avoir toujours su me réconforter et me porter. Merci de croire en moi plus que quiconque et cela même quand je n'y crois plus moi-même. Tu es une source d'inspiration inépuisable de par ta vision de la vie, ton intelligence et ta gentillesse. Merci pour toutes tes attentions quotidiennes qui ensoleillent ma vie. Tu es mon pilier. Tout simplement merci d'être toi et de partager ce bout de chemin avec moi.

À Augusto Azevedo Ferreira,

RESUME

Les paragangliomes et les phéochromocytomes (PPGL) sont des tumeurs neuroendocrines rares qui se développent aux dépens du système nerveux sympathique et parasympathique. Bien qu'elles soient le plus souvent bénignes, des formes métastatiques sont observées dans environ 15% des cas. La malignité du PPGL est en effet définie par l'apparition d'une métastase à distance d'un site paraganglionnaire. Il n'existe à ce jour aucun traitement curatif des formes métastatiques. Une mutation sur le gène *SDHB* constitue le principal facteur de risque de malignité et de mauvais pronostic des PPGL. Les gènes *SDHx (SDHA, B, C* et *D)* codent pour les 4 sous-unités de la succinate déshydrogénase (SDH), une enzyme mitochondriale impliquée à la fois dans le cycle de Krebs et dans la chaîne respiratoire. Les mutations *SDHx* conduisent toutes à une accumulation de succinate, résultant en un phénotype hyperméthylateur. Toutefois, une plus importante méthylation de l'ADN a été observée dans les tumeurs *SDHB* versus les autres mutations *SDHx*, ce qui pourrait participer à l'acquisition du phénotype métastatique de ces tumeurs. Les raisons de ces différences et la question de la malignité associée aux mutations *SDHB* restent cependant totalement inexpliquées.

L'objectif principal de mon projet de thèse était d'élucider les mécanismes expliquant le phénotype métastatique des tumeurs liées à *SDHB*, en comparant des modèles de cellules chromaffines murines (imCC) porteuses d'une inactivation des gènes *Sdhb* ou *Sdhd*. L'analyse de la distribution de la 5-méthylcytosine et de la 5-hydroxyméthylcytosine à l'échelle du génome dans les tumeurs mutées sur *SDHB* et dans les imCC *Sdhb-/-*, a montré que la perte d'activité des enzymes TET est responsable du phénotype hyperméthylateur marqué de ces tumeurs. Cette étude a également mis en évidence l'impact de l'hyperméthylation, en synergie avec l'activation de HIF2α pour favoriser l'acquisition de traits métastatiques. Par la suite, des approches Omics (métabolome, transcriptome, méthylome, matrisome) ont permis la caractérisation complète des différents modèles d'imCCs (WT, *Sdhb-/-* et *Sdhd-/-*) disponibles au laboratoire et de la matrice extracellulaire (MEC) secrétée *in vitro* par ces cellules. Ces travaux ont validé la pertinence de ces modèles cellulaires, qui récapitulent l'ensemble du phénotype des tumeurs humaines porteuses de mutations sur les gènes *SDHB* et *SDHD*. Ainsi, des études comparatives ont mis en évidence les principaux mécanismes d'oncogenèse associés spécifiquement à un déficit de SDHB, à savoir une plus forte inhibition des PHD et des TET, un déséquilibre de l'homéostasie du cuivre et du fer considérablement exacerbé, ainsi qu'un niveau de stress oxydant élevé. Ces modèles ont également révélé un remodelage de la MEC secrétée par les imCC *Sdhb-/-,* ainsi que son impact sur le phénotype métastatique de ces cellules. Enfin, ces études ont mis en lumière l'intérêt prometteur de l'ascorbate à forte dose, pour traiter les formes agressives de PPGL SDHB-dépendants.

Mes travaux de thèse ont donc permis d'apporter des éléments clés à la compréhension des mécanismes d'oncogenèse liés à SDHB, faisant progresser une question cruciale dans le domaine depuis plus de 20 ans. Mes résultats devraient ouvrir la voie à des essais précliniques et ainsi permettre des avancées majeures dans la prise en charge thérapeutique des patients atteints de PPGL métastatiques.

Mots clés : Paragangliomes, succinate-déshydrogénase, dioxygénases 2-OG dépendantes, métastases, oncogenèse, stress oxydant, fer, cuivre, HIF2α, matrice-extracellulaire

ABSTRACT

Paragangliomas and pheochromocytomas (PPGL) are rare neuroendocrine tumors developing at the expense of the sympathetic and parasympathetic nervous system. Although usually benign, metastatic forms are detected in about 15% of cases. Indeed, PPGL malignancy is defined by the appearance of a distant metastasis from a paraganglionic site. To date, there is no curative treatment for metastatic forms. A mutation in the *SDHB* gene is the main risk factor for malignancy and poor prognosis for PPGLs. The *SDHx* genes (SDHA, B, C and D) encode the 4 subunits of succinate dehydrogenase (SDH), a mitochondrial enzyme involved both in the Krebs cycle and in the respiratory chain. *SDHx* mutations all lead to the accumulation of succinate, resulting in a hypermethylator phenotype. However, greater DNA methylation was observed in *SDHB* tumors versus other *SDHx* mutations, which may participate in the acquisition of the metastatic phenotype of these tumors. However, these differences and the malignancy specifically associated with *SDHB* mutations, remain totally unexplained.

The main objective of my doctoral project was to elucidate the mechanisms explaining the metastatic phenotype of SDHB-related tumors, by comparing models of murine chromaffin cells (imCC) carrying inactivation of the *Sdhb* or *Sdhd* genes. Analysis of the distribution of 5-methylcytosine and 5-hydroxymethylcytosine at the genome level in mutated tumors on *SDHB* and in imCC *Sdhb-/-,* showed that TET enzymes loss of activity is responsible for the marked hypermethylator phenotype of these tumors. This study also demonstrated the impact of hypermethylation, in synergy with the activation of HIF2α to promote the acquisition of metastatic traits. Subsequently, Omics approaches (metabolome, transcriptome, methylome, matrisome) allowed the complete characterization of the different imCCs models (WT, *Sdhb-/-* and *Sdhd-/-*) available in the laboratory and of the extracellular matrix (ECM) secreted *in vitro* by these cells. This work validated the relevance of these cellular models, which emulate the phenotype of human tumors carrying mutations in either the *SDHB* or the *SDHD* genes. Thus, comparative studies have highlighted the main mechanisms of oncogenesis associated specifically with a deficit of SDHB, namely a stronger inhibition of PHD and TET, an imbalance of iron and copper homeostasis considerably exacerbated, as well as elevated oxidative stress levels. These models also revealed the remodeling of the ECM secreted by the *Sdhb-/-* imCC, as well as its influence on the metastatic phenotype of these cells. Finally, these studies highlighted the promising interest of high-dose ascorbate to treat aggressive forms of SDHB-dependent PPGL.

Therefore, the work carried out during my thesis has provided key elements for understanding the mechanisms of oncogenesis linked to SDHB, advancing a crucial question in the field for more than 20 years. My results should pave the way for preclinical trials and thus allow major advances in the therapeutic management of patients with metastatic PPGL.

Keywords: Paragangliomas, succinate dehydrogenase, 2-OG dependent dioxygenases, metastases, oncogenesis, oxidative stress, iron, copper, HIF2α, extracellular matrix

LISTE DES PRINCIPALES ABREVIATIONS

2-HG : 2-hydroxyglutarate
5-mC : 5-méthylcytosine
5-hmC : 5-hydroxyméthylcytosine
α-KG : α-kétoglutarate
CMT : carcinome médullaire de la thyroïde
COMT : catéchol-O-méthyl transférase
CVD : cyclophosphamide, vincristine, dacarbazine
DAC : décitabine
EMT : transition épithélio-mésenchymateuse
ETC : chaîne respiratoire mitochondriale
^{18}F-DOPA : ^{18}F- dihydroxyphénylalanine
^{18}F-FDG : ^{18}F-Fluorodeoxyglucose
Fe-S : fer-souffre
FH : Fumarate hydratase
FT : facteur de transcription
GIST : tumeur gastrointestinale stromale
GLUT : transporteurs de glucose
^{1}H-SRM : spectroscopie protonique
HIF : facteur induit par l'hypoxie
HNPGL : paragangliome de la tête et du cou
HPTH : hyperparathyroïdie
HRLCC : Hereditary Leiomyomatosis and Renal Cell Cancer
HTA : hypertension artérielle
^{123}I-MIBG : ^{123}I-métaiodobenzylguanidine
IDH : isocitrate déshydrogénase
IHC : immunohistochimie
ImCC : cellules chromaffines murines immortalisées
IRM : imagerie à résonance magnétique
KDM : lysine déméthylase
KO : knock-out
L-DOPA : L-dihydroxyphényléthylamine
LOH : perte d'hétérozygotie
LOX : lysyl-oxydase
3-MT : 3-méthoxytyramine
MAO : monoamine oxydase
MB : membrane basale
MEC : matrice extracellulaire
miR : micro ARN
MnSOD : superoxide dismutase mitochondriale
MN : métanéphrines
NMN : normétanéphrines

NMT : transition neuroendocrino-mésenchymateuse
NEM2 : néoplasies endocriniennes multiples de type 2
NF1 : neurofibromatose de type 1
NGS : séquençage de nouvelle génération à haut débit
NRF2 : nuclear factor erythroid 2-related factor 2
OMS : organisation mondiale de la santé
P4H : prolyl-4-hydroxylase des collagènes
PA : pression artérielle
PCC : phéochromocytome
PGL : paragangliome
PHD : prolyl-hydroxylases
PPGL : phécohromocytome et paragangliome
PNMT : Phényléthanolamine N-méthyl transférase
RCC : carcinome rénal
RE : réticulum endoplasmique
ROS : espèces réactives de l'oxygène
SDH : succinate déshydrogénase
SOD : superoxide dismutase
TAPPGL : paragangliome thoraco-abdomino-pelvien
TCGA : The Cancer Genome Atlas
TDM : tomodensitométrie
TEP : tomographie par émission de positons
TET : Ten eleven translocase (déméthylases de l'ADN)
TKI : inhibiteur de récepteurs à tyrosine kinase
VEGF : vascular endothelial growth factor
VHL : maladie de von Hippel-Lindau
WT : wild-type (sauvage)

INTRODUCTION

LES PARAGANGLIOMES ET PHEOCHROMOCYTOMES

1) Définition et épidémiologie

Les paragangliomes (PGL) sont des tumeurs neuroendocrines rares et richement vascularisées, se développant aux dépens des ganglions sympathiques et parasympathiques du système nerveux autonome. Un phéochromocytome (PCC) est un PGL qui se développe spécifiquement à partir des cellules chromaffines de la glande médullo-surrénale. Ces tumeurs, classées parmi les maladies orphelines (OMIM 171300 et OMIM 606864), ont une incidence estimée entre 5 cas par million d'habitants par an et une prévalence estimée à moins de 0,05 % de la population générale (1). Les PGL et PCC (PPGL) affectent autant les hommes que les femmes (2). Néanmoins, la prévalence des PPGL augmente chez les patients présentant une hypertension artérielle (HTA), où elle est estimée à environ 0,4% des patients, ainsi que chez les patients ayant une masse surrénalienne de découverte fortuite (nommée incidentalome), où elle atteint les 4%. Il est important de noter que les nombreuses formes asymptomatiques et le manque de spécificité des symptômes conduisent souvent à un sous-diagnostique de ces tumeurs. Certaines études ont ainsi montré qu'après autopsie, un PCC était trouvé dans 0,05% des cas, indiquant une incidence beaucoup plus élevée que celle actuellement estimée (3).

2) Physiologie

a) Origine embryologique

Les cellules chromaffines sont des cellules neuroendocrines, hautement spécialisées dans la synthèse et la libération de diverses hormones, dérivées de la crête neurale (4). La crête neurale est une structure transitoire qui se forme au cours de la vie embryonnaire à la fin de la gastrulation, suite à l'association du tube neural avec l'ectoderme dorsal. Ces crêtes neurales engendrent des cellules pluripotentes capables de migrer et de coloniser tout l'embryon, grâce à un processus appelé Transition Epithélio-Mésenchymateuse (EMT), donnant ainsi naissance à de nombreux types cellulaires et tissus (Figure 1). Elles sont notamment à l'origine des os, cartilages et muscles de la face, des mélanocytes et de la quasi-totalité du système nerveux périphérique (système sympathique, parasympathique et sensoriel) (5). Plus particulièrement, elles sont à l'origine de nombreuses cellules du système endocrinien, appelées alors « cellules neuroendocrines », telles que les cellules C de la thyroïde et les cellules chromaffines de la médullo-surrénale et des paraganglions (6).

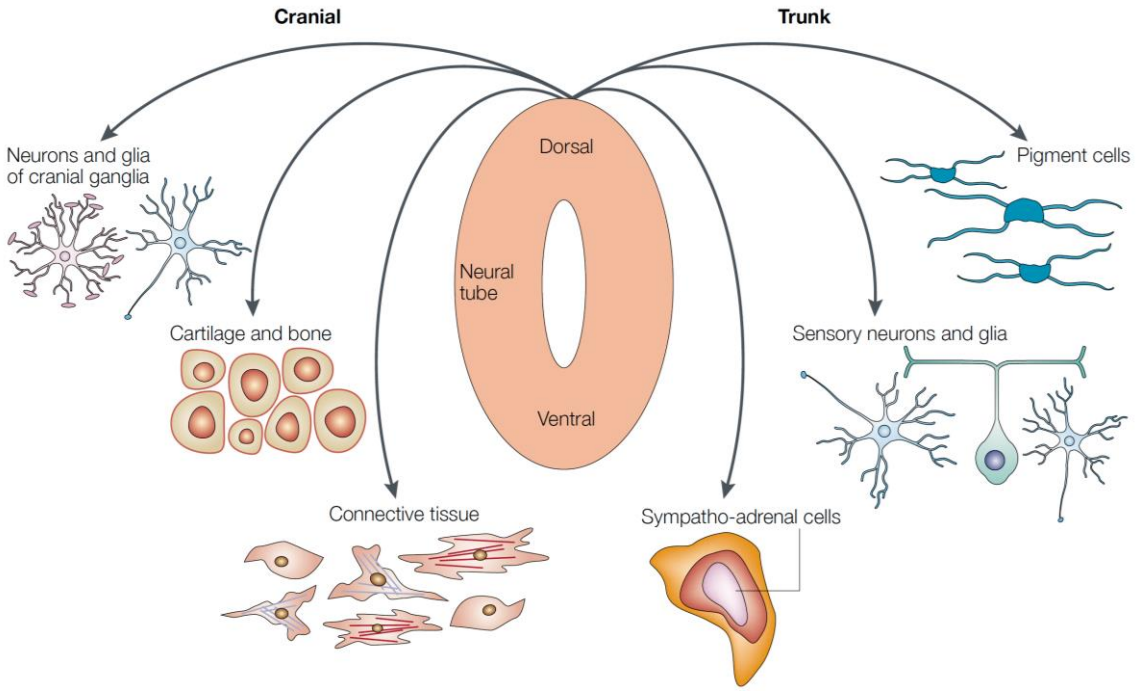

Figure 1 : Principaux types cellulaires dérivés des cellules de la crête neurale. *D'après (7)*

Toutefois, des études plus récentes suggèrent que les cellules chromaffines de la médullo-surrénale et des systèmes nerveux sympathiques et parasympathiques, subiraient des étapes de développement différentes selon leur localisation anatomique et ne proviendraient peut-être pas d'un seul lignage cellulaire dérivé de la crête neurale (4). Ainsi, le développement du système nerveux sympathique se ferait en une seule étape, à partir de précurseurs directs de la crête neurale (8), contrairement au développement du système nerveux parasympathique qui aurait lieu en deux étapes. Des précurseurs multipotents des cellules de Schwann auraient la capacité de migrer de la crête neurale, pour former des niches cellulaires le long des axones, avant de migrer à nouveau le long de ces axones afin de donner naissance au système nerveux parasympathique (9). Le développement de la médullo-surrénale se ferait par l'association des deux mécanismes antérieurement décrits (8).

b) Localisation

Les PPGL sont retrouvés au niveau de la partie basse du crâne, du cou, des ganglions sympathiques thoraco-abdominaux-pelviens et de la médullosurrénale (10) (Figure 2). Ainsi, on distingue classiquement :

- Les PGL issus des ganglions du système nerveux parasympathique, qui se développent généralement dans la région cervicale, c'est-à-dire au niveau des glomus tympanique

et jugulaire au niveau de la tête, et des glomus carotidien et vagal dans le cou. Ces PGL ne secrètent généralement pas d'hormones, ils sont dits non-fonctionnels.

- Les PGL se développant à partir de la chaine ganglionnaire du système nerveux sympathique, qui se retrouvent généralement dans les régions thoraciques, abdominales et pelviennes. Ces PGL se développent principalement le long des chaines ganglionnaires para-aortiques, des chaines pré-vertébrales et para-vertébrales thoraciques et abdominales, au sein de l'organe de Zuckerkandl, au niveau de la fourche aortique et de la région pelvienne (ovaires, testicules, prostate, urètre et plus particulièrement de la vessie). Plus rarement, des PGL ont été décrits au niveau du système digestif (ampoule de Vater, estomac, foie et pancréas) (10,11). Les PCC sont les PGL sympathiques les plus fréquents, ils se développent à partir des cellules chromaffines de la médullo-surrénale.

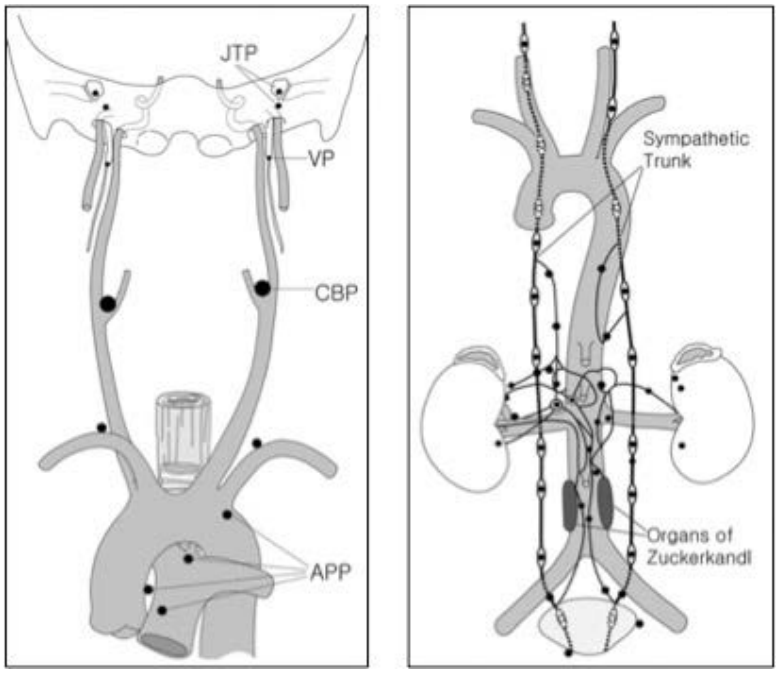

Figure 2 : Illustration du système paraganglionnaire montrant les principales localisations anatomiques des paraganglions de la région cervicale (gauche) et thoraco-abdomino-pelvienne (droite). *D'après (12). JTP : paraganglion jugulotympanique, VP : paraganglion vagal, CBP : paraganglion carotidien, APP : paraganglions aortiques*

c) Sécrétion

A l'instar d'autres tumeurs neuroendocrines, certains PGL, notamment ceux dérivant du système nerveux sympathique, ont la capacité de produire et de sécréter des

catécholamines (adrénaline, noradrénaline, dopamine). On parle alors de tumeurs fonctionnelles. Les catécholamines sont des neuro-hormones bio-synthétisées à partir de la L-tyrosine (Figure 3) provenant de l'alimentation ou du métabolisme hépatique de la phénylalanine. La métabolisation de la tyrosine en dihydroxyphényléthylamine (L-DOPA) par la tyrosine hydroxylase (TH) dans le cytoplasme des cellules chromaffines de la médullo-surrénale, amorce la synthèse des catécholamines et correspond à l'étape limitante de la réaction. Les catécholamines exercent un rétrocontrôle négatif de leur propre synthèse par inhibition compétitive (13). La L-DOPA est ensuite transformée en dopamine par la dopa décarboxylase. La biosynthèse se poursuit alors par la transformation de la dopamine en noradrénaline, en dehors des neurones dopaminergiques, par la dopamine β hydroxylase. Enfin, l'adrénaline est synthétisée à partir de la noradrénaline par la phényléthanolamine N-méthyltransférase (PNMT) dans le cytoplasme des cellules de la médullo-surrénale et des neurones adrénergiques du système nerveux central (14).

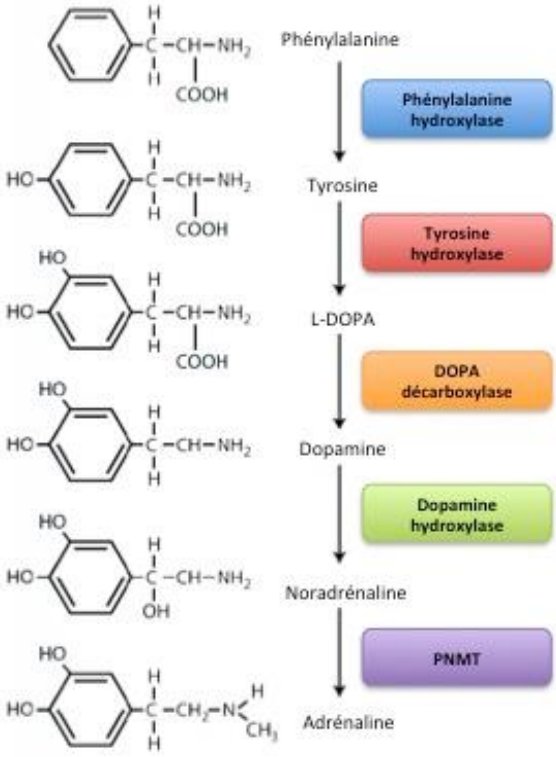

Figure 3 : Biosynthèse des catécholamines à partir de la phénylalanine.

Par la suite, les catécholamines sont stockées dans des granules (pool de réserve, correspondant à 80% des catécholamines synthétisées), ou libres dans le cytoplasme (pool libre, représentant 20% des catécholamines totales). Pour maintenir cet équilibre, les catécholamines sont transférées d'un pool à l'autre par des transporteurs vésiculaires (VMAT-

1 dans les cellules neuroendocrines et VMAT-2 dans les terminaisons nerveuses) (15,16). La sécrétion des catécholamines est ensuite déclenchée par la stimulation des récepteurs nicotiniques à l'acétylcholine au niveau de la médullo-surrénale ou par l'activation des canaux sodiques voltages-dépendants dans les neurones sympathiques périphériques (17). Après sécrétion, une partie des catécholamines libérées est recaptée pour reconstituer le pool de réserve (18). Les catécholamines ayant échappé à la recapture sont transportées dans la circulation avant d'être inactivées, par dégradation chimique, au niveau des neurones, de la médullo-surrénale ou des organes périphériques (en particulier le foie et le rein). La monoamine oxydase (MAO) et la catéchol-O-méthyl transférase (COMT), sont les deux enzymes principalement responsables de cette dégradation (18). Après cette étape, les catécholamines sont enfin sulfo-conjuguées et excrétées dans les urines (19).

3) Présentation clinique et diagnostic

a) Signes cliniques

Comme évoqué précédemment, les symptômes des patients porteurs de PPGL sont souvent aspécifiques, voire inexistants. Les PPGL se déclarent habituellement soit par une hypersécrétion de catécholamines, dans le cas des PGL fonctionnels, soit par un syndrome de compression. Le délai moyen entre l'apparition des symptômes et le diagnostic a été estimé à 3 ans (20). Une HTA secondaire à la sécrétion de catécholamines est retrouvée dans 85% des cas, constituant ainsi un des symptômes les plus répandus. Elle peut être soit permanente (50 % des cas), soit paroxystique (35 % des cas) et due à l'augmentation des résistances vasculaires périphériques, de la fréquence cardiaque et de l'activation du système rénine-angiotensine-aldostérone, responsable d'un hyperaldostéronisme secondaire. Une hypotension peut également être retrouvée notamment chez les patients porteurs de paragangliomes produisant préférentiellement de la dopamine (10). Les patients porteurs de PGL fonctionnels souffrent également de malaises, correspondants à des décharges catécholaminergiques et se présentant par des céphalées (60 à 90 % des cas), des sueurs (55 à 75%) et des palpitations (50 à 70%). L'ensemble de ces symptômes, pouvant survenir simultanément ou de façon isolée, porte le nom de « triade de Plouin-Ménard ». Les signes de cette triade, associés à une pâleur caractéristique après un malaise, ont une spécificité de 90% pour le diagnostic de PGL fonctionnel (21). D'autres symptômes peuvent se manifester, tels que des nausées, un amaigrissement, une hyperglycémie, des troubles psychologiques (anxiété, attaques de

panique), ainsi qu'un syndrome polyuro-polydipsique chez l'enfant. En outre, 10 à 15 % des PGL fonctionnels sont diagnostiqués au cours d'une complication cardiovasculaire aigue, comme par exemple une cardiopathie adrénergique ou un accident vasculaire cérébral (22). Du fait de leur production épisodique ou continue de catécholamines, les PPGL sont souvent associées à une morbidité et mortalité cardiovasculaires.

L'absence de sécrétions catécholaminergiques rend le diagnostic des PGL non fonctionnels plus difficiles. Ces tumeurs sont découvertes soit de façon fortuite sur un bilan d'imagerie, on parle alors d'incidentalome (20), soit par palpation ou sur des signes de compression nerveuse pouvant conduire à des acouphènes, à une hypoacousie, à une paralysie faciale ou encore à des troubles de la déglutition (23). Ce syndrome tumoral est majoritairement retrouvé dans la région cervicale.

b) Indications du dépistage

La recherche d'un PPGL est indiquée :

- chez les patients présentant des symptômes pouvant être associés à des sécrétions catécholaminergiques,
- chez les patients présentant une HTA résistante au traitement, qui se définie par une pression artérielle (PA) systolique supérieure ou égale à 140 mmHg et/ou une PA diastolique supérieure ou égale à 90 mmHg sous 3 antihypertenseur dont au moins un diurétique,
- chez les patients présentant une labilité tensionnelle importante objectivée,
- chez les patients présentant un incidentalome surrénalien,
- chez les patients de moins de 50 ans, hypertendus, diabétiques, ayant un indice de masse corporelle inférieur à 25,
- chez les patients atteints d'une maladie génétique prédisposant aux PPGL ou suite à la découverte d'un gène de prédisposition aux PPGL chez des sujets asymptomatiques dans le cadre du dépistage familial (24).

c) Diagnostic biologique

L'objectif principal du diagnostic biologique des PPGL est d'identifier d'éventuels PGL fonctionnels. Ce diagnostic repose sur l'augmentation des concentrations de métanéphrine (MN) et de normétanéphrine (NMN), traduisant une hypersécrétion de catécholamines. En

effet, l'adrénaline est dégradée en métanéphrine, la noradrénaline en normétanéphrine. Du fait de leur excellente sensibilité et spécificité, le dosage de ces métabolites constitue une étape cruciale dans la mise en évidence des PGL fonctionnels (24). Le dosage des MN et NMN plasmatiques et urinaires ayant été démontré, à de nombreuses reprises, comme étant supérieur aux dosages de catécholamines, auparavant utilisés (25). Les MN et NMN sont sulfoconjuguées avant d'être éliminées par voie urinaire. Par conséquent, les dosages des NMN et MN plasmatiques représentent les NMN et MN libres alors que les NMN et MN urinaires représentent les NMN et MN conjuguées (26). Actuellement, ces dosages sont effectués par des techniques de chromatographie en phase liquide à haute performance (HPLC) ou de spectrométrie de masse, permettant la séparation des MN et NMN en métanéphrines fractionnées, et assurant une excellente reproductibilité (27). La sensibilité et la spécificité de ces dosages sont également remarquables, de nombreuses études ayant montré une sensibilité dépassant les 95% et une spécificité supérieure à 85 %. Les dosages des MN et NMN urinaires nécessitent un recueil urinaire complet sur une durée de 24h (28), néanmoins ces métabolites restant stables pendant 8 jours (29), il n'est pas nécessaire de reproduire ces dosages sur plusieurs jours.

En ce qui concerne les dosages des formes libres plasmatiques de MN et NMN, ils sont plus simples pour le patient que les dosages urinaires mais également plus susceptibles d'augmenter le nombre de faux positifs obtenus quand ils sont réalisés en position assise. C'est pourquoi il est recommandé de réaliser ce dosage sur un prélèvement sanguin effectué chez un patient ayant passé au moins 30 minutes au repos en position allongée (25,30). Le diagnostic est considéré comme étant hautement probable lorsque les dosages de MN et NMN montrent une élévation supérieure à trois fois la normale et suspecté lorsque la concentration se situe entre deux et trois fois la normale. De plus, le profil sécrétoire des tumeurs mis en évidence lors de ces dosages (à savoir prédominance des MN ou des NMN) peut également orienter vers une origine génétique (31). Ainsi, les PPGL porteurs de mutations sur les gènes *SDHx*, *VHL* et *FH,* sécrètent majoritairement des NMN, contrairement aux PPGL avec mutations sur les gènes *RET*, *NF1*, *TMEM127* et *MAX*, qui ont plutôt un profil sécrétoire de type adrénergique. Le dosage des MN et NMN est considéré comme étant le gold standard pour diagnostiquer une hyperproduction de catécholamines. Néanmoins, l'équipe de G. Eisenhofer a démontré qu'il était intéressant d'associer ces examens biologiques au dosage d'un dérivé méthoxylé de la dopamine, la 3-méthoxytyramine (3-MT).

Ce dosage étant d'autant plus justifié que certains PGL, notamment cervicaux, produisent uniquement de la dopamine. Ils avaient également suggéré que la 3-MT aurait une valeur diagnostique et pronostique dans les formes malignes de PGL (32), ce qui n'a cependant pas été validé dans les études suivantes (33,34).

Par ailleurs, certains médicaments, tels que des bêtabloquants, des antidépresseurs tricycliques ou des inhibiteurs de la monoamine oxydase, peuvent biaiser les résultats de dosages de MN et NMN, induisant ainsi des faux positifs, soit par l'augmentation de la synthèse des catécholamines, soit en interférant avec les méthodes de dosage (24). Le dosage de la chromogranine A (CgA), un marqueur général de nombreuses tumeurs neuroendocrines présentant des concentrations sériques proportionnelles au volume tumoral, peut également être réalisé. Néanmoins, la CgA étant moins sensible et moins spécifique que les dosages de MN et NMN, elle est rarement utilisée pour le diagnostic des PPGL (35). Les dosages de CgA peuvent toutefois être utilisés pour le suivi post-opératoire ou pour la surveillance des patients ayant une forme métastatique ou un PGL non fonctionnel, chez qui une élévation de la CgA avait déjà été observée au moment du diagnostic.

d) Imagerie

Suite à une présentation clinique évocatrice permettant de suspecter une tumeur, de par un syndrome tumoral ou des dosages de MN et NMN mettant en évidence un excès de catécholamines, il est primordial de localiser le(s) PGL responsable(s), notamment dans l'optique de procéder à l'exérèse chirurgicale, qui reste à l'heure actuelle le seul traitement curatif. L'imagerie s'avère alors être un outil indispensable.

i. Imagerie conventionnelle

L'imagerie conventionnelle (tomodensitométrie (TDM) et imagerie à résonnance magnétique (IRM)) apporte des informations anatomiques sur la structure et la localisation précise de la tumeur et permet d'obtenir des clichés de très haute résolution. Une TDM est indiquée en première intention pour la recherche de PPGL localisés dans la région thoraco-abdomino-pelvienne, selon les recommandations internationales publiées en 2014. L'examen de référence pour le dépistage des PGL de la région cervicale est l'angio-IRM. De plus, l'IRM étant un examen non-irradiant, il est grandement privilégié chez les enfants et les femmes enceintes (36). Ainsi, ces examens présentent une excellente sensibilité, 98% pour la TDM et 100 % pour

l'IRM, mais une spécificité moindre, 70 % et 67 % respectivement (37). Par conséquent, il est souvent nécessaire de compléter ces examens par une imagerie fonctionnelle métabolique.

ii. Imagerie fonctionnelle

L'imagerie fonctionnelle présente l'avantage d'informer sur le statut physiopathologique des tumeurs et d'être hautement spécifique. De plus, elle est préférable à la biopsie, contre-indiquée au vu des risques majeurs qui sont associés à la manipulation tumorale, notamment des risques d'hémorragie et de crise hypertensive (38). Elle est cependant de sensibilité variable en fonction de la localisation tumorale, des techniques utilisées et du statut génétique des patients (cf. 4. Génétique des PPGL). L'imagerie fonctionnelle s'appuie sur l'utilisation d'agents radiomarqués très spécifiques qui permettent de mettre en évidence les cellules chromaffines tumorales (39).

Les principales imageries fonctionnelles utilisées pour la détection des PPGL sont :

- La Scintigraphie à la ^{123}I-métaiodobenzylguanidine (^{123}I-MIBG), qui correspond à une scintigraphie du corps entier, réalisée grâce à un marquage à l'iode 123 de la MIBG, un dérivé proche de la noradrénaline, qui utilise le même transporteur membranaire NET (NorEpinephrine Transporter). La ^{123}I-MIBG s'accumule de façon sélective dans les tumeurs produisant des catécholamines et permet ainsi de révéler des atteintes multifocales et des localisations secondaires sécrétantes. Cette scintigraphie est notamment à privilégier dans un contexte métastatique menant à un traitement par ^{131}I-MIBG (24) ;
- La Scintigraphie des récepteurs de la somatostatine par ^{111}In-pentetréotide (Octréoscan®), qui utilise le pentetréotide, un analogue de la somatostatine présentant une affinité pour les sous-types 2 et 5, qui sont les récepteurs exprimés par par la plupart des tumeurs endocrines et préférentiellement les PPGL sus-diaphragmatiques (40) ;
- La TEP au ^{18}F-Fluorodeoxyglucose (^{18}F-FDG), est un examen réalisé grâce à l'utilisation du ^{18}F-FDG, un analogue du glucose marqué au fluor 18 qui constitue le traceur le plus utilisé en oncologie. Le principe de cet examen est la mise en évidence de l'augmentation de la consommation du glucose par les tissus, induite dans un contexte tumoral. La fixation est d'autant plus intense dans un contexte métastatique associé à une prolifération tumorale intense. Remarquablement, cet examen présente une forte sensibilité pour les PGL SDHB-dépendants (80 à 100 %) mais une faible spécificité (41–43) ;

- La TEP à la dihydroxyphénylalanine marquées au fluor 18 (^{18}F-FDOPA), repose sur l'utilisation de la forme marquée au fluor-18 de la L-DOPA, qui est captée avec une très forte affinité par les PGL (44) et en particulier pour les PGL cervicaux SDHD-dépendants (45,46). Toutefois, ce traceur présente chez les patients porteurs d'une mutation *SDHB*, une sensibilité significativement inférieure (évaluée à 20 %) à celle du ^{18}F-FDG (47,48) ;
- La TEP aux analogues de la somatostatine marqués au Gallium 68 (^{68}Ga-DOTATATE), qui repose sur l'utilisation de trois peptides (DOTATOC, DOTATATE et DOTANOC) en tant que traceurs. Cet examen cible les récepteurs de la somatostatine, comme l'Octréoscan® mais avec une bien meilleure résolution grâce à la technologie TEP et offre des résultats prometteurs notamment pour le diagnostic des PGL de la tête et du cou, des PPGL métastatiques et des PPGL associés à des mutations *SDHx* (49–51) (Figure 4).

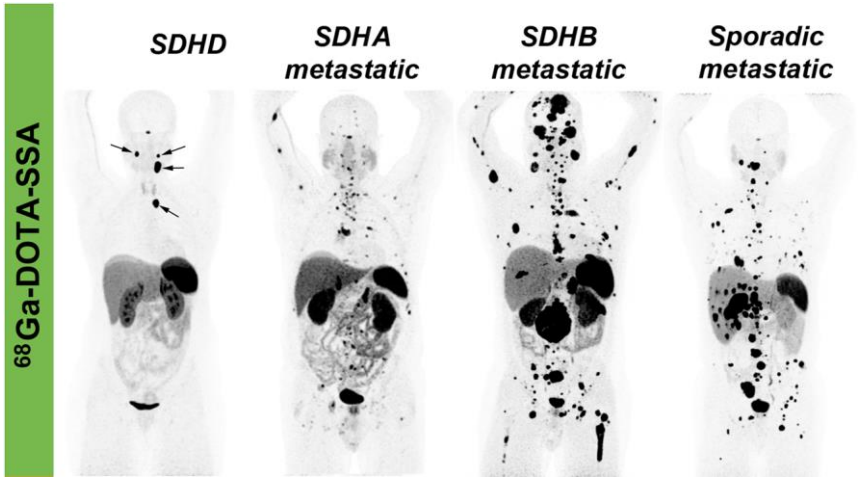

Figure 4 : Efficacité de la TEP au 68Ga-DOTATATE pour la détection des PPGL métastatique SDHB-dépendant. *D'après (52)*

e) Diagnostic histologique

Le diagnostic histologique des PCC consistait anciennement en une coloration au bichromate de potassium aboutissant en une coloration brune caractéristique des cellules contenant des catécholamines, à l'origine de leur nom de cellules « chromaffines ». Ces techniques de coloration ont été abandonnées au profit de techniques plus récentes d'immunohistochimie (IHC). Désormais le diagnostic histologique des PPGL repose essentiellement sur la mise en évidence d'une positivité pour les marqueurs généraux des tumeurs neuroendocrines, à savoir la CgA et la synaptophysine, associée à un réseau caractéristique de cellules sus-tentaculaires visibles grâce au marquage de la protéine S100. Un immunomarquage positif des enzymes impliquées dans la synthèse des catécholamines,

telles que la tyrosine hydroxylase, constitue un diagnostic histologique plus spécifique des PPGL (53,54). De plus, la plupart des PPGL présentent une architecture caractéristique en coloration à l'hématoxyline et à l'éosine (HES). Les cellules chromaffines tumorales, dans lesquelles se trouvent de nombreuses vésicules de sécrétion, sont alors organisées en niches appelées historiquement « Zellballen » (Figure 5). Ces niches sont séparées par des capillaires et entourées par les cellules sus-tentaculaires, qui assurent le soutien de ces structures particulières (55,56).

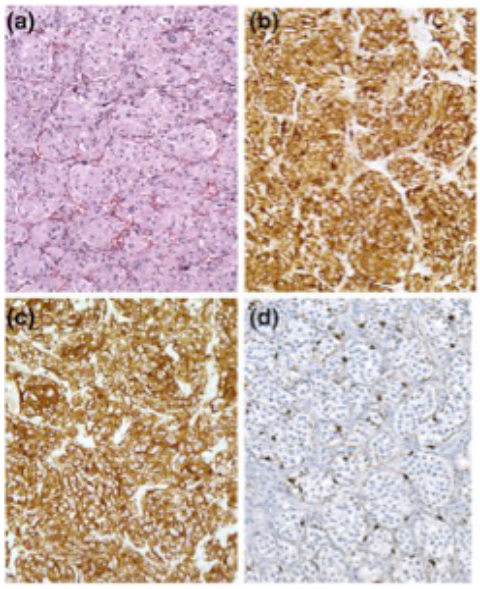

Figure 5 : Histologie d'un PGL. Ilots de Zellballen vus par HES d'un PGL (a), IHC anti-chromogranineA (b), synaptophysine (c) et S-100 (d). *D'après (57)*

4) Génétique des Phéochromocytomes et Paragangliomes

L'une des principales particularités des PPGL est leur fort déterminisme génétique. On considère désormais que les PGL sont les tumeurs humaines les plus fréquemment héréditaires. En effet, les progrès des techniques d'exploration génétique effectués ces vingt dernières années ont permis l'identification d'une vingtaine de gènes de prédisposition au PPGL (Figure 6). Ainsi, une mutation constitutionnelle sur l'un de ces gènes de prédisposition est retrouvée dans environ 40% des cas, avec une transmission autosomique dominante (58–63). Ces récentes données permettent d'infirmer le dogme qui existait au début des années 2000 postulant que seuls 10% des PPGL avaient une origine génétique (64). De plus, une méta-analyse récemment menée a permis de mettre en évidence une mutation constitutionnelle dans un de ces gènes de prédisposition chez environ 12% des patients avec un PGL de

présentation apparemment sporadique (65). Parmi la vingtaine de gènes de prédisposition au PGL, seuls *RET*, *HIF2A*, *GOT2* et *DNMT3A* sont considérés comme étant des oncogènes. Les autres gènes de prédisposition sont des gènes suppresseurs de tumeurs, ce qui implique que le mécanisme de tumorigenèse requiert l'association d'une mutation constitutionnelle et d'un second événement génétique somatique, telle qu'une perte d'hétérozygotie, une seconde mutation ou une hyperméthylation sur l'autre allèle, selon le modèle des « two hits » de Knudson (66).

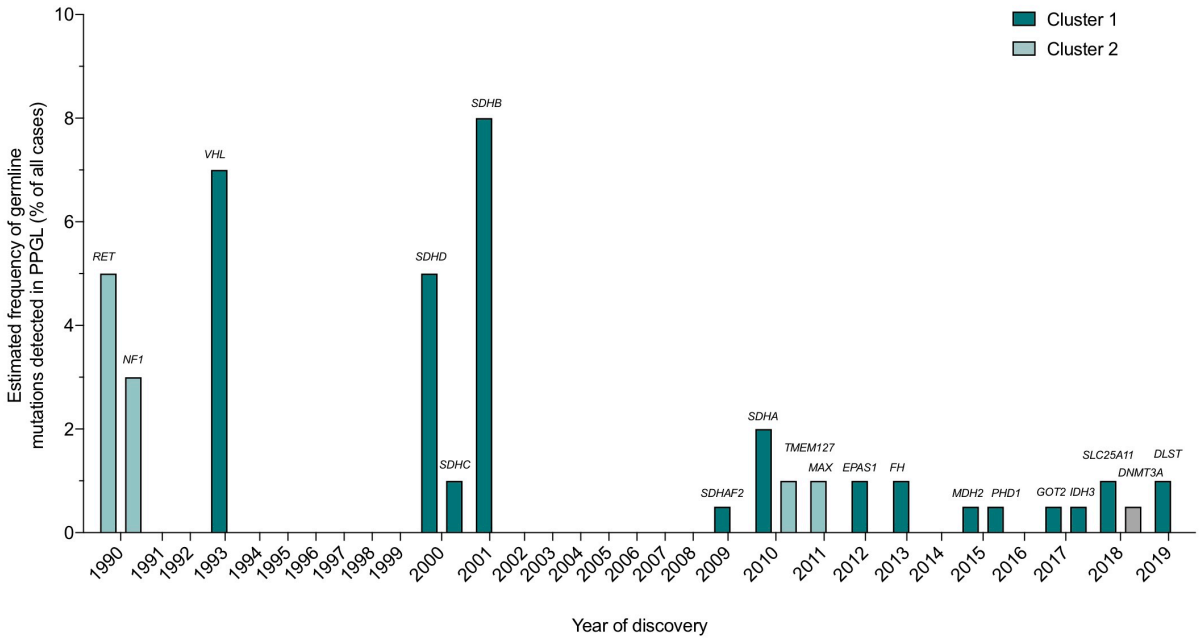

Figure 6 : Fréquence estimée des mutations constitutionnelles détectées sur les principaux gènes de prédisposition au PPGL en fonction de la chronologie de la découverte et du cluster d'expression d'appartenance de chaque gène.

Ces découvertes sont primordiales dans la prise en charge actuelle des PPGL. Elles ont été essentielles pour la meilleure compréhension des mécanismes moléculaires impliqués dans leur tumorigenèse, permettant l'association du statut génétique des tumeurs à une signature moléculaire et à un phénotype tumoral particulier (Tableau 1). Ainsi, la connaissance du statut génétique constitue désormais l'un des éléments clés de la prise en charge médicale des patients, impactant leur diagnostic, leurs suivi et leur pronostic.

a) Formes syndromiques

i. La neurofibromatose de type 1 (gène NF1)

La neurofibromatose de type 1 (NF1) ou maladie de Von Recklinghausen (OMIM 162200) est une pathologie génétique fréquente, à forte pénétrance, dont la prévalence est estimée à

1/3000 (67,68) et l'incidence à 1 nouveau cas pour 2500 naissances (69). Les mutations du gène *NF1* sont responsables de cette affection autosomique dominante. Il s'agit d'un gène suppresseur de tumeur codant une protéine inhibant la protéine RAS, la neurofibromine. Le diagnostic de la maladie chez l'adulte est relativement simple et essentiellement clinique. Il repose sur les sept critères cardinaux du consens du NIH, établis en 1988 (70). La pathologie est diagnostiquée si au moins deux de ces critères sont réunis chez un même individu. Il est ainsi posé dans 95% des cas sur ces seuls critères cliniques dès l'âge de 11 ans (71). La NF1 prédispose au développement de PGL dans 0,1 à 5,7 % des cas, vers l'âge de 40 ans (72,73). Il s'agit la plupart du temps de PCC, sécrétant de l'adrénaline, parfois bilatéraux (20 à 40 % des cas) et rarement métastatiques (10 % des cas)(72,74,75). Ces PCC sont découverts fortuitement dans 30% des cas (74,76) et moins de 20% des patients présentent des symptômes catécholaminergiques (73). De façon intéressante, plusieurs études récentes ont permis l'identification de mutations constitutionnelles du gène *NF1* chez plusieurs patients porteurs de PCC, qui ne présentaient pas de phénotype clinique clair de NF1 mais seulement des signes cliniques modérés de la maladie. Ces résultats ont été possibles grâce au séquençage systématique du gène *NF1* par Next Generation Sequencing dans l'ADN constitutionnel de patients avec un PCC d'apparence sporadique, suggérant l'importance de l'analyse du gène *NF1* en routine chez tous les patients avec un PCC (77,78). Par conséquent, le diagnostic de NF1 chez un patient avec un PCC doit reposer sur l'association entre un examen clinique soigneux et l'analyse attentive des antécédents familiaux du patient.

ii. La maladie de von Hippel-Lindau (gène VHL)

La maladie de von Hippel-Lindau (VHL) est une maladie de transmission autosomique dominante, avec une pénétrance quasi-complète à 65 ans et dont l'incidence est estimée à 1/36 000 naissances (79). Les mutations constitutionnelles du gène suppresseur de tumeur *VHL* prédisposent à cette pathologie (80). Il code une E3 ubiquitine ligase et joue un rôle majeur dans l'ubiquitination et la dégradation par le protéasome de la sous-unité alpha des facteurs de transcription de réponse à l'hypoxie (HIF-1α et 2α) (81) (Figure 7). Ce syndrome est caractérisé par le développement de différents types de tumeurs. L'atteinte rénale constitue l'une des manifestations cliniques principales, un carcinome rénal à cellules claires étant retrouvé chez 70% des patients à 60 ans (79).

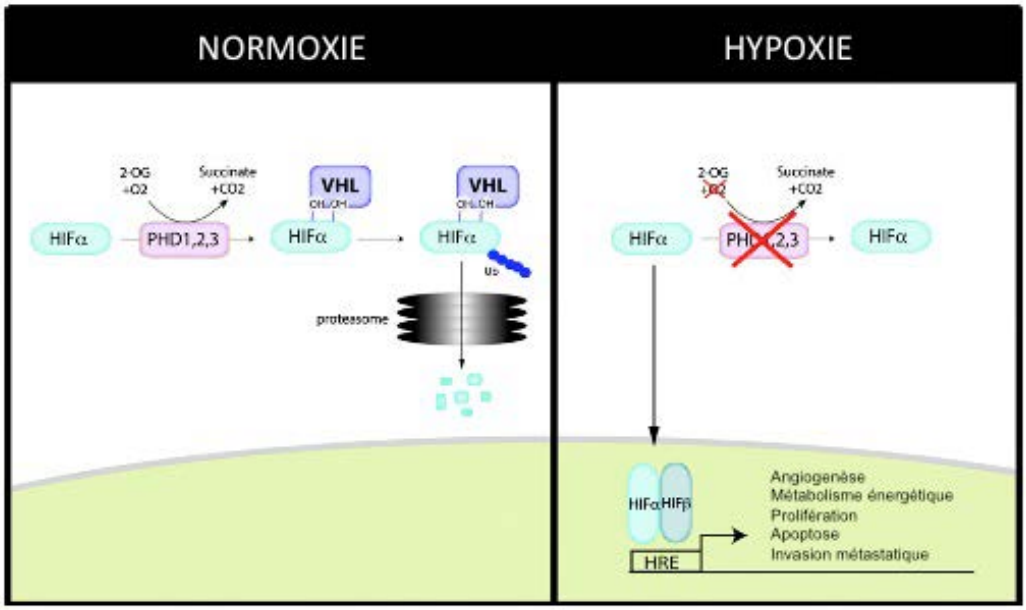

Figure 7 : Schéma représentant la voie de régulation de l'hypoxie et la participation de la protéine pVHL. *D'après (82)*

Des tumeurs neuroendocrines pancréatiques et/ou des kystes sont également retrouvées dans 12 % et 80 % des cas, respectivement. Des hémangioblastomes rétiniens et/ou du système nerveux central (atteignant le cervelet, le tronc cérébral et/ou la moelle épinière) sont diagnostiqués dans 80 % et 75 % respectivement. Des tumeurs du sac endolymphatique peuvent également survenir chez 10 à 15 % des patients (83) ou encore des cystadénomes épididymaires ou ligamentaires larges. Enfin, des PPGL sont retrouvés chez 24 % des patients porteurs d'une mutation constitutionnelle de *VHL.* Il s'agit le plus souvent de PCC, mais des PGL extra-surrénaliens peuvent être observés. Historiquement, deux grands sous-types du syndrome VHL ont été définis chez les patients atteints, fondés sur le risque de développer ou non un PPGL (84). Ainsi, on distingue :

- La maladie de VHL de type 1, dans laquelle les patients ont un faible risque de développer un PPGL
- La maladie de VHL de type 2 est quant à elle subdivisé en 3 sous-groupes et est associée à un risque important de développer un PGL :
    - VHL de type 2A, associé à un risque élevé de développer un carcinome rénal ;
    - VHL de type 2B, associé à un faible risque de développer un carcinome rénal ;
    - VHL de type 2C, où les patients développent exclusivement des PPGL.

De façon intéressante, les mutations responsables du VHL de type 1 sont généralement des mutations tronquantes, alors que celles conduisant au VHL de type 2 sont le plus souvent des mutations faux-sens. De plus, l'étude d'une grande famille atteinte de la maladie de VHL a récemment permis de décrire une mutation dans l'intron 1, d'un exon cryptique *VHL*. Ces mutations conduisent à la sous-expression de la protéine VHL et semblent être des événements rares chez les patients atteints de PPGL (85,86). La maladie de VHL se révèle en général chez de jeunes patients. Ainsi, un PPGL est souvent retrouvé avant l'âge de 20 ans chez ces patients. Ces PPGL sont souvent bilatéraux, synchrones ou métachrones (40 à 60% des cas). Des antécédents familiaux de la maladie de VHL ou des lésions syndromiques associées aux PPGL sont retrouvés dans environ 66 % des cas (72).

iii. Les néoplasies endocriniennes multiples de type 2 (gène RET)

La néoplasie endocrinienne multiple de type 2 (NEM2) est un syndrome de transmission autosomique dominante à pénétrance complète, affectant 1/30 000 individus (87). Les mutations gain de fonction du proto-oncogène *RET* ont été identifiées depuis le début des années 90 comme étant responsables de la NEM2 (88). Elles conduisent à une auto-activation du récepteur RET et sont associées à trois présentations cliniques différentes avec très bonnes corrélations génotype/phénotype :

- la NEM2A ou syndrome de Sipple, forme la plus fréquente (70% à 80 % des cas), se caractérise par la survenue d'un carcinome médullaire de la thyroïde (CMT), associé à un PCC et à une hyperparathyroïdie (HPTH). Un lichen amyloïde est aussi retrouvé chez certains patients.
- la NEM2B ou syndrome de Gorlin, plus rare (5 % des cas), se caractérise par l'émergence d'un CMT, associé à un PCC, à des neuromes muqueux, ainsi qu'à une gangliomatose gastrique ou intestinale, et une dysmorphie marfanoïde.
- le carcinome médullaire thyroïdien familial ou syndrome de Farndon (10 à 12 % des NEM2) se caractérise par le développement isolé d'un CMT (89). Le pronostic global de la maladie est fondé sur l'agressivité du CMT. Ainsi, l'American Thyroid Association a classé les CMT en fonction de leur degré d'agressivité selon trois niveaux : modéré, élevé, plus élevé (90). Les mutations responsables de la NEM2B, forme la plus sévère et précoce, sont la plupart du temps retrouvées sur l'exon 6 (p.Met918Thr), contrairement aux mutations responsables de la NEM2A qui sont le plus souvent localisées dans les exons 10 et 11 (91,92). Ce syndrome présente la particularité de prédisposer quasi-uniquement aux PCC et non aux PGL. Un seul

cas de PGL cervical associé à un CMT a été décrit chez un patient atteint d'une NEM2 (93). De plus, un PCC est retrouvé chez environ 50 % des patients atteints de MEN2A ou MEN2B. Ces PCC se développent généralement vers l'âge de 30 ans (89) et ils sont classiquement bénins et bilatéraux (20,94).

iv. Les syndromes PGL-polyglobulie (cas des mutations EPAS1 et EGLN1)

A l'instar de *VHL*, les gènes *EPAS1* (également appelé *HIF2A*) et *EGLN1* (*PHD2*) codent pour deux protéines impliquées dans la réponse hypoxique. *EPAS1* est un gène codant pour la sous-unité alpha du facteur de réponse à l'hypoxie HIF2. *EGLN1* code pour la prolyl-hydroxylase 2 (PHD2), l'une des dioxygénases dépendante du 2-oxoglutarate, ayant pour rôle l'hydroxylation de HIF2α, ce qui permet sa reconnaissance par VHL et sa dégradation par le protéasome (Figure 7). Au début des années 2000 des mutations constitutionnelles de *EPAS1* et *EGLN1* ont été identifiées dans des polyglobulies congénitales de transmission autosomique dominante (95,96). C'est en 2008, qu'une mutation constitutionnelle sur le gène *EGLN1* a été décrite pour la première fois comme pouvant être responsable du développement de PPGL (97). La mutation a été identifiée chez un patient atteint d'une polyglobulie et d'un PGL abdominal, qui présentait une mutation constitutionnelle perte de fonction de *EGLN1* associée à une perte d'hétérozygotie (LOH) au niveau du PGL. L'implication des mutations du gène *EGLN1* dans la tumorigenèse des PPGL a été validée quelques années plus tard avec l'identification d'une mutation *EGLN1* chez un nouveau patient porteur de PGL multiples (97,98). Les premières mutations somatiques sur le gène *EPAS1* associées au développement de PPGL ont été identifiées en 2012 par l'équipe de K. Pacak. Ces mutations somatiques « gain de fonction » ont été identifiées chez des patients atteints de polyglobulie congénitale, PPGL et somatostatinome (99). Par la suite, ces données ont été largement validées par plusieurs études. Notre équipe a notamment identifiée des mutations de *EPAS1*, présentes à l'état de mosaïque somatique, ce qui suggère un évènement mutationnel *de novo* post-zygotique. Des mutations à l'état de mosaïque constitutionnelle ont également été décrites, suggérant une possible transmission à la descendance (100).

Les mutations *EPAS1* semblent prédisposer aux PPGL sécrétant préférentiellement de la noradrénaline et de l'EPO, ils sont multiples dans 50 % des cas et surviennent plutôt chez des sujets jeunes (99–103). L'ensemble des mutations *EPAS1* identifiées jusqu'à présent sont localisées dans les exons 9 et 12. Ces deux exons codent pour les deux prolines qui sont

normalement reconnues et hydroxylées par les PHDs, nécessaires à la dégradation de HIF2α. Par conséquent, la mutation de ces prolines inhibe l'hydroxylation et donc la dégradation de HIF2α, conduisant ainsi à une stabilisation anormale de la protéine et à une activation inappropriée de la voie de réponse à l'hypoxie. Des mutations somatiques *EPAS1* seraient également responsables du développement des PPGL associés à une cardiopathie cyanogène, suggérant que l'hypoxie chronique peut favoriser leur apparition (104,105).

b) Les PPGL héréditaires

i. Les gènes SDHx (SDHA, SDHB, SDHC, SDHD, SDHAF2)

C'est au tout début des années 2000 que l'implication des gènes *SDHx* dans la tumorigenèse des PPGL a été découverte, révolutionnant ainsi les connaissances sur la génétique de ces tumeurs (106,107). Les gènes *SDHA, SDHB, SDHC* et *SDHD* codent pour les 4 sous-unités de la succinate déshydrogénase (SDH). La SDH est une enzyme mitochondriale localisée dans la membrane mitochondriale interne, au carrefour de deux voies métaboliques : le cycle de Krebs, dans lequel elle oxyde le succinate en fumarate et la chaine respiratoire mitochondriale, où elle constitue le complexe II et participe au transfert d'électrons par la réduction de l'ubiquinone (coenzyme Q). Les sous-unités SDHC et SDHD constituent les protéines d'ancrage de ce complexe mitochondrial, alors que les sous-unités SDHA et SDHB correspondent au centre catalytique de l'enzyme (Figure 8). Le gène *SDHAF2* code pour une protéine permettant la flavination de la sous-unité SDHA, essentielle à l'assemblage de la SDH.

Les gènes *SDHx* sont des gènes suppresseurs de tumeurs et une mutation constitutionnelle sur l'un d'eux est retrouvée dans 50 % des cas de PPGL héréditaires (108,109). Ces tumeurs peuvent prendre des formes diverses (souvent multiples), avec différentes localisations (PGL cervical, PGL thoraco-abdomino-pelvien (TAP) ou PCC), et parfois métastatiques (110). Elles ont une survenue plus précoce, puisque l'âge moyen d'apparition est de 36 ans, contrairement aux formes sporadiques qui se développent vers l'âge de 50 ans (111). Une mutation constitutionnelle dans l'un des gènes *SDHx,* combinée à une perte d'hétérozygotie (LOH) au niveau somatique conduit à une perte le plus souvent complète de l'activité de la SDH, ce qui a pour conséquence une accumulation cytosolique de succinate, considéré comme l'oncométabolite principal de la tumorigenèse des PPGL (112,113).

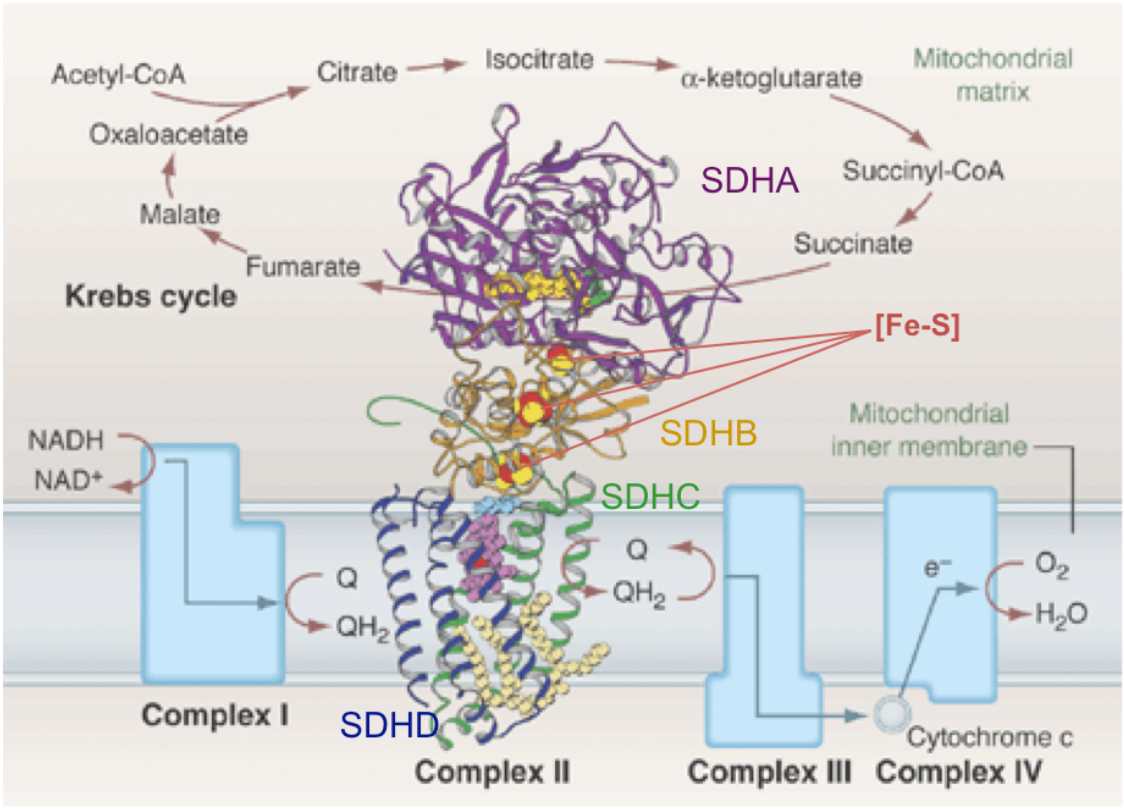

Figure 8 : Structure cristallographique de la succinate déshydrogénase au sein de la chaine respiratoire mitochondriale et du cycle de Krebs. *D'après (114)*

Des études de liaison génétique menées dans de grandes familles atteintes de PPGL ont tout d'abord permis d'identifier en 2000 le gène *SDHD* comme gène de prédisposition au PPGL (106). Ce gène est localisé sur le chromosome 11q23, comporte 4 exons et code pour une petite protéine de 160 acides aminés. La transmission de la maladie liée à *SDHD* est soumise à empreinte génomique maternelle. Une femme transmettant une mutation *SDHD* ne transmettra donc pas la maladie à sa descendance. Néanmoins quelques études ont rapporté des cas de violation de cette empreinte génomique maternelle (115,116). Récemment, une étude prospective menée par mon équipe d'accueil a estimée à environ 5 %, le risque auquel sont confrontés les patients ayant hérités d'une mutation *SDHD* de leur mère, de développer un PPGL au cours de leur vie (117). Transmises par le père, les mutations sur le gène *SDHD* prédisposent presque exclusivement aux formes cervicales de PGL (plus de 97 % des cas), souvent multiples. De surcroit, ces mutations ont une pénétrance quasi complète (86 % à 50 ans) et des antécédents familiaux sont retrouvés dans 60 à 80 % des cas (111,118).

La découverte des mutations sur le gène *SDHC* a rapidement suivi en 2000. *SDHC* est un gène localisé en 1q21, comportant 6 exons et codant, tout comme *SDHD,* pour une petite protéine de 150 acides aminés (119,120). Le gène *SDHC* est le gène *SDHx* le plus rarement muté chez les patients atteints de PPGL. Toutefois les mutations *SDHC* ont une pénétrance importante et prédisposent le plus souvent au développement de PGL cervicaux (111,121).

Les mutations sur le gène *SDHB* ont ensuite été identifiées en 2001 (107). Le gène *SDHB,* localisé en 1p36, est composé de 8 exons et code pour une protéine de 180 acides aminés. Les mutations constitutionnelles sur le gène *SDHB* sont transmises de façon autosomique dominante et prédisposent majoritairement au développement de PGL dans la région thoraco-abdomino-pelvienne (60 % des cas). Des PGL cervicaux associés aux mutations *SDHB* sont retrouvés dans environ 40 % des cas (36,122). A l'instar des patients porteurs de mutations *SDHD,* l'âge moyen de présentation de la maladie est de 30 ans (111,123) et la pénétrance de la mutation *SDHB* est estimée à 50 % à 50 ans et peut augmenter jusqu'à 70 % à l'âge de 60 ans (124,125).

L'identification d'une mutation *SDHB* est considérée comme le principal facteur de risque de malignité des PPGL (20,72,72,126,126–129). En effet, 50 à 70 % des patients porteurs de mutations *SDHB* développent des PPGL métastatiques contre seulement 5 % des patients porteurs d'une mutation *SDHD* ou *SDHC* (72,94,111,118). Parmi les patients atteints de formes métastatiques de la maladie, 36 % sont porteurs d'une mutation constitutionnelle sur le gène *SDHB*. De plus, les premières études menées au début des années 2000 rapportaient que parmi les patients atteints de PGL métastatiques, ceux qui étaient porteurs de mutations *SDHB* avaient un pronostic plus sombre (130,131). Ainsi, la survie globale des patients avec un PGL métastatique associé à une mutation *SDHB* était estimée à 42 mois après la détection de la première métastase versus 244 mois chez les patients ayant un PGL métastatique sans mutation *SDHB* (Figure 9) (132). Ces observations ont récemment été contestées dans une grande étude internationale réalisée sur 169 patients atteints de PPGL métastatiques, dans laquelle la mutation *SDHB* n'est plus associée au mauvais pronostic (133). L'interprétation de ces résultats est cependant sujet à caution. Il est en effet fort probable qu'un meilleur suivi des patients porteurs de mutations *SDHB* mis en place cours de la dernière décennie explique cette amélioration de leur pronostic (133,134).

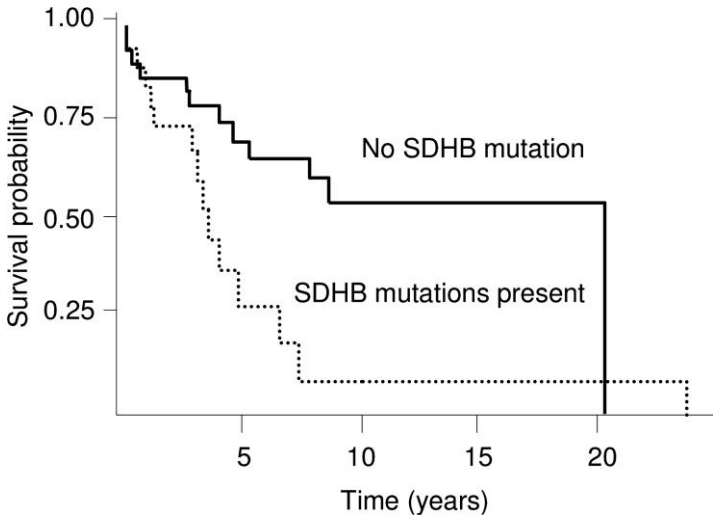

Figure 9 : Survie globale des patients atteints de PPGL métastatiques après le diagnostic de la première métastase selon le statut SDHB. *D'après (132)*

Ce n'est que bien plus tard que les mutations sur les gènes *SDHAF2* et *SDHA* ont été identifiées. Ainsi, les premières mutations sur le gène *SDHAF2* ont été décrites en 2009, suite à l'identification d'une même mutation faux-sens retrouvée chez plusieurs patients issus de deux familles différentes, présentant tous des PGL cervicaux uniques ou multiples (135–137). Le gène *SDHAF2* est un gène de 4 exons, localisé en 11q13, qui code pour une protéine assurant la stabilisation du complexe II mitochondrial, grâce à son action de flavination de la sous-unité SDHA (135). Les mutations sur le gène *SDHAF2* sont les plus rarement décrites chez les patients atteints de PPGL.

L'implication du gène *SDHA* (15 exons, localisé en 5p15) a finalement été démontrée en 2010, suite à l'identification par mon équipe d'accueil de la première mutation de ce gène chez une patiente atteinte d'un PGL abdominal fonctionnel (138). Les mutations *SDHA* ne sont quasiment jamais associée à une histoire familiale de la maladie. Leur incidence, tout d'abord considérée comme très faible, a récemment augmenté de façon importante suite au test génétique systématique qui est désormais réalisé par NGS. Aujourd'hui, on considère que les mutations *SDHA* représentent 10 à 15 % de l'ensemble des mutations identifiées dans les PPGL. Les formes cervicales sont majoritaires, bien que des formes thoraciques ou abdominales soient parfois décrites (139).

Les mutations des gènes *SDHx* sont également impliquées dans le développement d'autres types tumoraux, dont les cancers du rein (RCC) et les tumeurs stromales gastro-

intestinales (GIST). Ainsi, ces mutations seraient responsables de 0,05 à 0,2% des cancers du rein (140) et le risque de développer un cancer du rein est estimé entre 2 et 3 % chez les patients avec une mutation *SDHx* (125,141). Ces cancers du rein *SDHx*-dépendants sont reconnus comme un nouveau sous-type de RCC par l'OMS depuis 2016 et sont le plus souvent décrits chez des patients jeunes, porteurs de mutations *SDHB.*

L'implication des gènes *SDHx* dans le développement des GIST a d'abord été établie chez des patients présentant une association de PGL multiples et de GIST multifocaux, aujourd'hui connue sous le nom dyade (ou syndrome) de Carney-Stratakis » (142–144). Depuis, des mutations *SDHx* ont également été retrouvées chez des patients avec GIST isolés, sans mutation dans les gènes *PDGFRA* et *KIT* (145). En effet, des mutations somatiques activatrices sur les gènes *KIT* ou *PDGFRA* sont retrouvées dans la grande majorité des GIST (85 % des GIST de l'adulte et 15 % des GIST pédiatriques) (146). Parmi les GIST sans mutation *KIT* ou *PDGFRA*, une mutation sur un gène *SDHx* est retrouvée dans plus de 80 % des cas (147). Dans ces GIST *SDHx*-dépendants, des mutations somatiques de *SDHA* sont le plus souvent retrouvées (147–149). Les mutations *SDHx* prédisposent surtout à l'apparition précoce de GIST multiples et malignes (147). Des GIST secondaires à des épimutations du gène *SDHC*, consistant en une inhibition de sa transcription due à une hyperméthylation de son promoteur, ont également été décrites (150).

Finalement, les mutations *SDHx* ont été associées à des adénomes hypophysaires, sans que le lien de causalité soit véritablement démontré (151). En effet, un seul véritable cas clinique d'adénome hypophysaire secondaire à une mutation du gène *SDHD*, conduisant à une perte d'expression de la protéine dans la tumeur a été décrit (152). L'implication des mutations *SDHx* dans la tumorigenèse des adénomes hypophysaires reste encore controversée, notamment en raison de l'absence d'études fonctionnelles et de données d'IHC qui sont la plupart du temps absentes ou contradictoires dans les différents cas publiés (152).

ii. Le gène FH

Le gène *FH* est un gène codant pour une enzyme du cycle de Krebs (Figure 10), la fumarate hydratase ou fumarase, qui est une lyase catalysant l'hydratation du fumarate en L-malate. Des mutations du gène *FH* ont d'abord été décrites en 1986 par Zinn *et al*., associées à des encéphalopathies précoces sévères (153,154). Depuis, l'implication des mutations

constitutionnelles du gène *FH* a également été démontrée dans les syndromes de léiomyomes cutanés et utérins multiples (MCUL, multiple cutaneous and uterin leiomyomata) ou syndrome de Reed. Chez certains patients ce syndrome peut être associé à des atteintes rénales (kystes ou carcinome rénal papillaire de type 2), on parle alors de syndrome HLRCC (hereditary leiomyomatosis and renal cell cancer) (155,156).

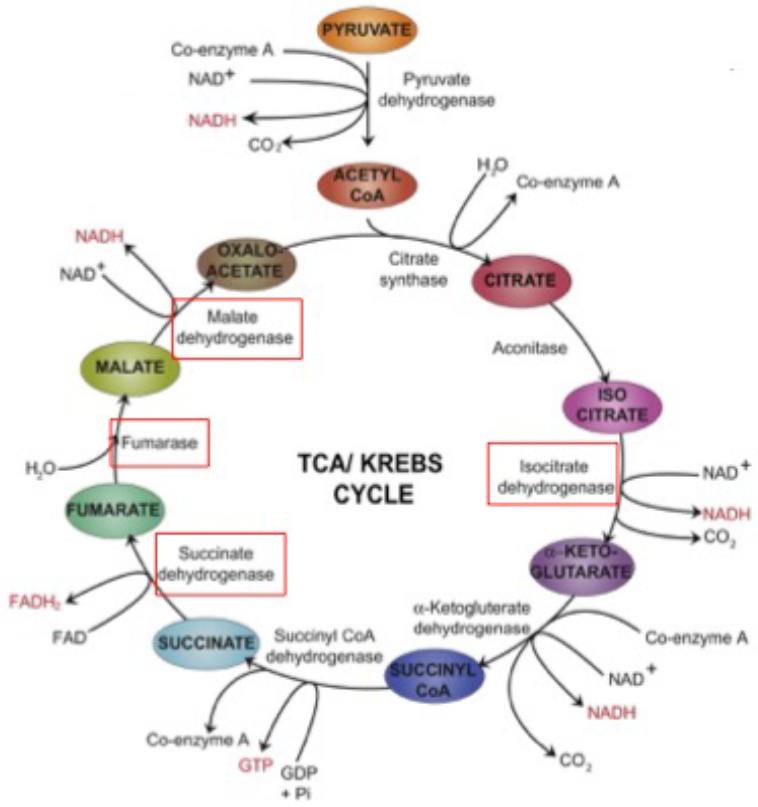

Figure 10 : Principales enzymes du cycle de Krebs impliquées dans la prédisposition aux PPGL.

Des léiomyomes cutanés sont retrouvés chez 70% des patients atteints, des léiomyomes utérins chez 80 % des femmes atteintes à partir de l'âge de 30 ans et plus rarement des léiomyosarcomes. Des carcinomes rénaux papillaires de type 2 sont retrouvés dans 15 à 19 % des cas (157,158), mais sont associés à un mauvais pronostic du fait de leur caractère majoritairement métastatique (159).

Depuis 2013, il est connu que les mutations *FH* peuvent également prédisposer au développement de PPGL. En effet, mon équipe d'accueil a montré que ces mutations sont retrouvées dans environ 1 % des cas de PPGL. La première mutation *FH* associée à un PGL a été mise en évidence grâce au séquençage de l'exome d'une patiente, qui portait une tumeur

se classant, au niveau moléculaire, avec les tumeurs *SDHx*. Chez cette patiente, une mutation constitutionnelle hétérozygote sur le gène *FH* associée à une mutation somatique avaient été identifiée (160). D'autres études de cohortes ont ensuite validé ces observations et révélé le caractère agressif de ces PGL *FH*-dépendants, qui sont dans 40% des cas de nature métastatiques ou multiples (161,162).

c) PCC familiaux

i. Le gène TMEM127

Le gène *TMEM127* est un gène de susceptibilité au PCC, ayant été identifié en 2010, grâce à des approches dites de génomique intégrative (analyse de liaison, études transcriptomiques et analyse du nombre de copies), au sein d'une famille dans laquelle plusieurs sujets présentaient des PCC (163). A l'instar des mutations *RET* et *NF1,* les mutations sur le gène *TMEM127* prédisposeraient exclusivement au développement de PCC. Néanmoins les mutations *TMEM127* seraient responsables de 1 à 2 % des cas de PCC seulement, avec une présentation de la maladie après 35 ans (164,165). Ces PCC sécrètent généralement de l'adrénaline et peuvent être bilatéraux (15 à 66 % des cas). Une histoire familiale est retrouvée dans 15 à 30 % des cas et la pénétrance est estimée à 32% avant 65 ans (165,166). Plus récemment, il a été montré que des mutations *TMEM127* pouvaient également prédisposer aux ccRCC (167).

ii. Le gène MAX

La technique de séquençage nouvelle génération de l'ensemble des exons ou « whole-exome sequencing » a permis d'identifier *MAX* comme gène de prédisposition au PPGL (168). Ainsi, les mutations sur le gène *MAX* sont responsables d'environ 1 % des PGL ; il s'agit la plupart du temps de PCC ou de PGL abdominaux, sécrétant des catécholamines (adrénaline, noradrénaline), volontiers bilatéraux (50% des cas) et parfois métastatiques. L'âge moyen d'apparition de la maladie est de 34 ans et des antécédents familiaux sont retrouvés chez 40 % des patients atteints (169). Le gène *MAX* code pour une protéine avec une structure de type « leucine zipper », appartenant au réseau des facteurs de transcription MYC/MAX/MXD1. Les interactions au sein de cet axe sont directement impliquées dans la régulation de la prolifération, la différenciation cellulaire et l'apoptose. Ainsi, les hétérodimères formés par

l'association de MAX avec l'oncogène MYC favorisent les processus précédents, alors que ceux formés par l'interaction MAX-MXD1 ont à l'opposé une action répressive de ces fonctions (170). MAX est également capable de réguler la transformation cellulaire dépendante de MYC en formant des homodimères qui inhibent les cibles du complexe MAX-MYC.

d) Gènes de prédisposition plus rares

Au cours de ces cinq dernières années, de nombreux gènes de susceptibilité aux PPGL ont été découverts grâce à l'évolution importante des techniques de séquençage de l'ADN. Toutefois, l'implication de ces gènes a été démontrée dans un nombre très limité de cas et des études plus larges sont nécessaires pour valider leur rôle dans la prédisposition au PPGL.

i. Gènes impliqués dans le métabolisme mitochondrial (MDH2, GOT2, SLC25A11, DLST)

Parmi ces nouveaux gènes identifiés, la plupart sont impliqués dans le métabolisme mitochondrial. Ainsi, *MDH2* et *DLST* sont deux gènes suppresseurs de tumeurs qui codent pour deux protéines du cycle de Krebs : la malate déshydrogénase de type 2, une enzyme mitochondriale catalysant l'étape en aval de la production de fumarate par la FH dans le cycle de Krebs (Figure 10), et la dihydrolipoamide S-succinyltransférase qui constitue la sous-unité E2 de l'α-cétoglutarate déshydrogénase, respectivement (61,63). Les gènes *GOT2* et *SLC25A11* sont quant à eux impliqués dans la navette malate-aspartate (Figure 11), un autre processus mitochondrial essentiel. Ils codent respectivement pour la transaminase glutamique-oxaloacétique mitochondriale (GOT2) et le transporteur mitochondrial malate/α-kétoglutarate ou oxoglutarate carrier (OGC) (60)(62)(61). L'ensemble de ces mutations, rarement décrites, semblent être associées à des formes métastatiques ou multiples de PPGL.

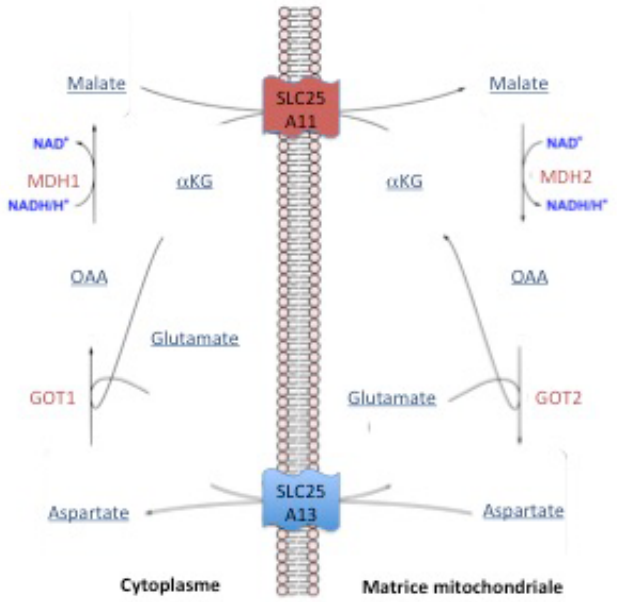

Figure 11 : Représentation schématique de la navette malate-aspartate. *Le transporteur SLC25A11 est impliqué dans la prédiposition aux PPGL métastatiques.*

ii. Gènes impliqués dans la voie de signalisation MAPK (MET, MERTK)

MET et *MERTK* sont deux gènes qui codent pour des récepteurs à tyrosine kinase et qui prédisposent aux PPGL. Les mutations du gène *MET* sont plus souvent retrouvées au niveau somatique bien qu'une mutation constitutionnelle ait récemment été découverte au sein d'une famille où plusieurs sujets étaient porteurs de PCC. Les mutations *MET* sont également associées au carcinome papillaire à cellules rénales de type 1 et les mutations sur le gène *MERTK* au CMT (59)(171).

iii. Gènes impliqués dans la méthylation de l'ADN (H3F3A, DNMT3A, KIF1B)

Les gènes *H3F3A, DNMT3A* et *KIF1Bβ* codant l'histone H3.3, une méthyltransférase de l'ADN et une protéine appartenant à la superfamille des kinésines respectivement, semblent également prédisposer aux PPGL (Tableau 1). La mutation décrite de *H3F3A* correspond à une mutation récurrente à l'état de mosaïque somatique sur un hot spot de mutation et semble être systématiquement associées aux tumeurs osseuses à cellules géantes (59)(172). Les mutations du gène *DNMT3A* identifiées sont des mutations constitutionnelles gain de fonction (173) et *KIF1B* est quant à lui considéré comme un gène suppresseur de tumeur (174–176).

Gène	Année de découverte	Fonction protéique	Cluster d'expression	Présentation clinique	Risque métastatique
RET	1990	Récepteur de la tyrosine kinase	C2	Syndrome NEM2 (PCC, CMT)	faible
NF1	1990	Neurofibromine 1, régulateur négatif de la voie de signalisation RAS	C2	Syndrome NF1 (PCC multiples, neurofibromes, nodules de Lisch, taches de rousseur axillaires et inguinales, lésions osseuses, gliomes optiques, sarcomes, GIST, ccRCC)	faible
VHL	1993	Protéine Von Hippel-Lindau, E3 ubiquitine ligase	C1B	VHL syndrome (PCC, TAPPGL, ccRCC, hémangioblastomes du systèm nerveux central ou de la rétine, kystes rén et pancréatiques, tumeurs neuroendocrin pancréatiques, tumeurs du sac endolymphatique et cystadénomes épididymaires)	faible
SDHD	2000	Sous-unité d'ancrage D de la SDH	C1A	HNPGL multiples, GIST, ccRCC, AH	faible
SDHC	2000	Sous-unité d'ancrage C de la SDH	C1A	HNPGL, GIST, RCC	faible
SDHB	2001	Sous-unité catalytique B de la SDH	C1A	TAPPGL, GIST, RCC, AH	élevé
SDHAF2	2009	Facteur d'assemblage de la SDH	C1A	HNPGL	faible
SDHA	2010	Sous-unité catalytique A de la SDH	C1A	HNPGL, GIST, RCC, AH	faible
TMEM127	2010	Régulateur négatif de la voie mTOR	C2	PCC multiples, ccRCC	faible
MAX	2011	Facteur de transcription de type Leucine zipper	C2	PCC multiples, oncocytome rénal	faible
EPAS1	2012	Sous-unité alpha du facteur de transcription 2 induit par l'hypoxie	C1B	PCC, TAPPGL, polyglobulie, somatostatinome	faible
FH	2013	Fumarate déshydrogénase	C1A	TAPPGL, leïomyomes rénal	élevé
MDH2	2015	Malate déshydrogénase mitochondriale	C1A	PCC multiples, TAPPGL	élevé
PHD1	2015	Hydroxylase dépendante du 2-oxoglutarate	C1B	PGL multiples, polyglobulie précoce	faible
GOT2	2017	Transaminase glutamique-oxaloacétique	C1A	TAPPGL multiples,	élevé ?
IDH3	2017	Isocitrate déshydrogénase 3 spécifique au NAD	C1A ?	HNPGL, LMA	?
SLC25A11	2018	Transporteur mitochondrial 2-oxoglutarate/malate	C1A	TAPPGL	élevé
DNMT3A	2018	Méthyltransférase de l'ADN		HNPGL, LMA	faible
DLST	2019	Sous-unité E2 de la 2-oxoglutarate déshydrogénase mitochondriale (OGDH)	C1A	TAPPGL multiples	faible

Tableau 1 : Principaux gènes de prédisposition aux PPGL et présentation clinique associée. *TAPPGL : thoracic, abdominal or pelvic paraganglioma ; HNPGL : head and neck ; ccRCC : clear cell renal cell carcinoma ; GIST: gastrointestinal stromal tumor ; AML : acute myeloid leukemia ; PA: pituitary adenoma.*

e) Génétique somatique

Comme mentionné précédemment, de grandes études, dont une menée par mon équipe d'accueil, ont étudié spécifiquement les atteintes somatiques retrouvées chez les patients porteurs de PPGL (171,177). Ces études ont permis d'acquérir de nombreuses connaissances, et de démontrer l'implication de certains gènes qui avaient alors un rôle prépondérant connu dans d'autres types de cancers, mais qui n'étaient pas associés au développement des PPGL. Ainsi, des mutations somatiques ont été décrites dans deux grands types de gènes (Figure 12) :

- dans les différents gènes de prédisposition aux PPGL connus (*VHL, RET, EPAS1, SDHB, NF1, MET, …*). Dans ce cas, la mutation somatique est considérée comme étant le « driver » de la tumorigenèse du PPGL (59,77,171,178,179).

- dans des gènes intervenants dans les processus d'oncogenèse (tels que *HRAS, TP53, CDKN2A, FGFR1, ATRX, …)* (171,179–183).

Ces études ont pu identifier ces mutations somatiques dans 30 à 40 % des PPGL, consolidant donc l'intérêt porté à l'identification de la cause génétique des PPGL, puisqu'elles permettent l'élévation à 70 % de la part de PPGL génétiquement déterminés, qui était alors de 40 % pour les PPGL avec mutations constitutionnelles. Les PPGL sont ainsi les tumeurs avec le plus fort déterminisme génétique (77,171,178).

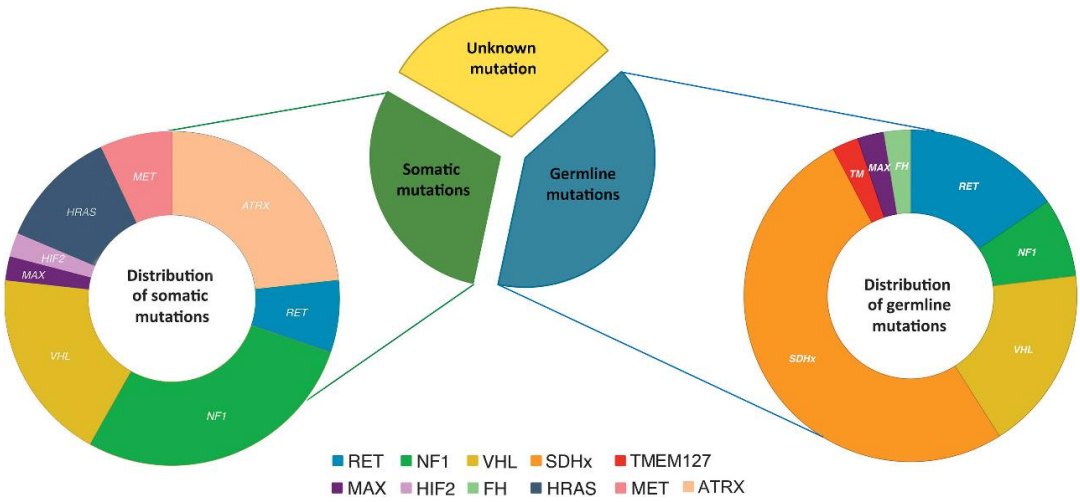

Figure 12 : Estimation de la répartition des mutations constitutionnelles et somatiques des gènes de prédisposition aux PPGL. *D'après (184)*

Les mutations somatiques ne présentent aucun risque de transmission d'ordre familial, n'en sont pas moins cruciales pour orienter la prise en charge du patient. En effet, ces

différentes mutations définissent les voies de tumorigenèse activées et le phénotype tumoral. Par exemple, une mutation somatique sur les gènes *RET* ou *NF1* entraine préférentiellement le développement d'un PGL sécrétant de l'adrénaline, contrairement à un PGL associé à une mutation somatique *VHL* qui sécrétera plutôt de la noradrénaline (77,176,178). En outre, plusieurs études soulignent l'importance de l'identification des mutations somatiques sur le gène *ATRX* qui sont retrouvées dans 12 % des PPGL, parfois associées à une mutation constitutionnelle sur un gène *SDHx* et qui pourrait constituer un marqueur pronostic de l'agressivité de la tumeur (185) (cf. 5. Malignité des PPGL)

f) Test génétique

En raison de ce fort déterminisme génétique, il est primordial de connaître le statut génétique des patients atteints de PPGL. C'est pourquoi, il est à présent recommandé de proposer systématiquement un test génétique à tous les patients atteints (24,186). Les tests génétiques étaient auparavant effectués de manière séquentielle par séquençage Sanger et principalement orientés en fonction du phénotype du patient et dans certains cas selon les résultats d'IHC sur le tissu tumoral inclus en paraffine (169,187,188). Aujourd'hui, grâce à la généralisation des nouvelles techniques de séquençages haut débit (NGS), l'utilisation de panels spécifiques permet le séquençage simultané de tous les gènes de prédisposition au PPGL (189). Des recommandations internationales pour encadrer la pratique de ces tests par NGS ont ainsi été récemment publiées (190). L'identification de la mutation permet ensuite de proposer au patient un suivi adapté selon son génotype (24,186), prenant en compte la présentation clinique et le potentiel métastatique associés. Des recommandations internationales ont été proposées, sur la base d'avis d''experts (1,186).

Mon laboratoire a récemment mis en évidence les bénéfices cliniques de cette connaissance précoce du statut génétique chez les patients porteurs d'une mutation *SDHx* ou *VHL* (134). L'amélioration du suivi de ces patients dont on sait qu'ils sont à risque, suffit en effet à elle seule à améliorer leur pronostic, en permettant une détection plus précoce des lésions et des éventuelles récidives et/ou métastases.

Dans le cas où une mutation constitutionnelle est identifiée, un test pré-symptomatique peut également être réalisé chez les sujets apparentés. Un consensus international, mené par mon équipe d'accueil, est en cours de publication pour les recommandations du suivi de ces sujets asymptomatiques (Amar et al, Submitted).

g) Validation des variants génétiques identifiés

Les tests génétiques peuvent conduire à l'obtention de résultats difficiles d'interprétation. Ainsi, plusieurs biomarqueurs ont été développés afin d'estimer la pathogénicité des variants de signification inconnue (VSI) identifiés. Ces approches présentent un enjeu majeur, car elles conduisent à une identification rapide d'un éventuel déficit en SDHB ou FH, particulièrement associés avec une évolution métastatique de la maladie, permettant ainsi une prise en charge personnalisée et précoce des patients.

La méthode la plus couramment employée pour détecter l'expression de la SDH reste l'IHC anti-SDHB réalisée sur les tumeurs FFPE (formalin-fixed paraffin-embedded). Les différentes interprétations de l'ensemble des IHC impliquées dans le diagnostic des PPGL SDH-dépendants sont récapitulées dans le Tableau 2.

IHC	Interprétation	Se/Spé	Utilisation	Références
SDHB	Marquage granulaire mitochondrial, négatif dans les cellules tumorales avec une mutation *SDHx* (*SDHA, SDHB, SDHC, SDHD et SDHAF2*). Un marquage cytosolique faible et diffus doit être considérée comme négatif	94%/84%	clinique	(188,191,192).
SDHA	Marquage négatif dans les tumeurs mutées *SDHA* mais positif dans toutes les autres tumeurs	75%/93%	clinique	(187,192)
SDHD	Utilisé en cas d'interprétation difficile de l'IHC SDHB (marquage faible et diffus); négatif dans les PGL non *SDHx* et m positif (signal cytoplasmique avec accumulation irrégulière) dans les PGL mutés *SDHx*	96%/97%	recherche	(193)
Méthylation de l'ADN (5hmc)	Coloration 5hmC plus faible (voire absente) dans les noyaux des cellules tumorales mutées *SDHx* par rapport aux cellules endothéliales ou sustentaculaires	Non déterminé	recherche	(160,194)
Méthylation des histones (H3K4me3, H3K9me3, H3K27me3)	Marquage de H3K9me3 positif dans les tumeurs SDH-dépendantes (pas de changement pour les marquages de H3K4me3 et H3K27me3)	Non déterminé	recherche	(160)

Tableau 2 : Interprétation des immunohistochimies des PPGL SDH-déficients. *IHC: immunohistochimie; Se: sensibilité; Spé : spécificité*

Par ailleurs, des IHC anti-FH et anti-OGC négatives ont également été décrites dans des tumeurs mutées *FH* et *SLC25A11 respectivement* (62). En revanche, les PPGL avec une mutation *GOT2* présentent une IHC positive, reflétant l'expression plus élevée de GOT2 observée dans ces tumeurs (60). Enfin, une forte corrélation entre un marquage CA9 membranaire et la présence d'une mutation VHL (germinale ou somatique) a été récemment décrite par mon équipe d'accueil (195).

Des approches métabolomiques ont également été développées et constituent une autre stratégie pertinente (bien que moins facile d'accès) pour aider à l'interprétation des variants génétiques dans les cas de mutations liées aux déficits mitochondriaux (196). Ces approches reposent sur la quantification de certains métabolites, et en particulier du succinate, (mais aussi du fumarate et du 2-hydroxyglutarate) dans les tumeurs. Elles sont réalisées par chromatographie liquide couplée à la spectrométrie de masse (LCMS), permettant l'identification de PPGL avec une mutation germinale (ou somatique) sur les gènes *SDHx, FH* ou plus rarement *IDHx* (197). Une étude comparative récente a montré que la LCMS présentait une spécificité plus élevée que l'IHC anti-SDHB, avec une sensibilité similaire pour détecter les mutations *SDH*x. Elle a montré la forte complémentarité des deux techniques suggérant l'utilisation des deux stratégies pour une bonne prise en charge des patients (198).

Enfin, une séquence de spectrométrie par résonnance magnétique (1H-MRS) permettant la détection de l'accumulation du succinate *in vivo* a été développée ces dernières années par mon équipe d'accueil. Cette technique, non invasive, s'est avérée particulièrement efficace pour détecter l'accumulation de succinate dans les tumeurs des patients (199,200). Suite à des études de preuves de concept, une étude de validation a récemment été réalisée sur 50 patients atteints de PPGL, démontrant les performances diagnostiques élevées de cette approche chez les porteurs de mutations *SDHx* (201).

5) Malignité des PPGL

La classification de l'OMS de 2004, révisée en 2017, définie la malignité du PPGL par l'émergence de cellules tumorales à distance d'un site paraganglionnaire. Les recommandations actuelles incitent donc à abandonner l'appellation de PPGL « malin » au profit de PPGL « métastatique ». Environ 15% des PPGL (10% des PCC et 40% des PGL) sont

susceptibles de présenter une évolution métastatique. Les foyers métastatiques préférentiels des PPGL sont les ganglions lymphatiques, les os, le foie, et les poumons (20). Toutefois, les tumeurs à potentiel métastatique ne présentent pas de manifestations cliniques propres et la similitude de leurs symptômes avec ceux des tumeurs bénignes rend leur diagnostic difficile. Le délai d'apparition des métastases est très variable et s'étend sur une période allant de 3 mois à 30 ans (20,132). Le pronostic de ces formes métastatiques est mauvais, la survie globale à 5 ans étant estimée inférieure à 50 % (202,203). L'absence de marqueurs spécifiques pour le diagnostic et le suivi de ces formes métastatique constitue donc un enjeu majeur. D'autant que les critères cliniques utilisés jusqu'à présent sont les mêmes que ceux utilisés pour l'identification d'un PPGL et reposent principalement sur la détection d'une l'hypersécrétion hormonale (204).

a) Diagnostic des formes métastatiques

i. Critères cliniques

Des analyses multivariées effectuées dans plusieurs études de cohortes ont permis la mise en évidence de 3 facteurs de risque de malignité considérés comme étant les plus robustes : une taille tumorale supérieure à 5 cm au diagnostic ; une localisation extra-surrénalienne de la tumeur primaire (40 à 70 % des patients présentant une tumeur primaire localisée dans la région thoraco-abdomino-pelvienne sont associés à un développement métastatique (128,205,206) ; et l'identification d'une mutation constitutionnelle sur le gène *SDHB* (20). L'âge du patient lors du diagnostic a également été considéré mais n'étant pas retrouvé de manière systématique dans toutes les études, il n'apparait pas comme un facteur diagnostic assez robuste (20,126,128,132).

ii. Biomarqueurs des formes métastatiques

Il n'existe pas de critères histologiques fiables permettant de prédire le potentiel métastatique des PPGL sur l'analyse de la tumeur primaire (207,208). Ces dernières années, l'expansion des études de génomique a permis l'identification de biomarqueurs, permettant de prédire ce risque métastatique. Une signature constituée de six microARN (miRs), à savoir miR-21-3p, miR-183-5p, miR-182-5p, miR-96-5p, miR-551b-3p et miR-202-5p, a ainsi été associée à un risque plus élevé de développer des métastases chez les patients atteints de

PPGL. Les biopsies liquides de ces patients ont également montré des niveaux d'expression plus élevés de 5 de ces miRs. Notamment, miR-21-3p est associé à l'activation de la voie mTOR et présente une bonne corrélation avec une signature prédictive de la réponse à l'inhibiteur de mTOR, dans les PPGL et d'autres cancers (209). En outre, les longs ARN non codants (lncRNA) ont été récemment associés à une dérégulation transcriptionnelle des PPGL. Quatre lncRNA semblent corrélés avec les différents clusters d'expression des PPGL. Un lncRNA (GenBank : BC063866) en particulier, est considéré comme un facteur de risque indépendant de malignité et de mauvais pronostic clinique chez les patients mutés sur l'un des gènes *SDHx*. Ces lncRNA et miRs se présentent ainsi comme des biomarqueurs innovants pour la détection de tumeurs potentiellement métastatiques chez ces patients (210,211).

Des altérations somatiques des gènes impliqués dans la préservation des télomères et l'immortalisation cellulaire, comme *ATRX* ou *TERT* sembleraient aussi favoriser le développement métastatique de la maladie (179,183,212). En effet, *Job et al.* ont récemment montré que 18,5% des PPGL subissent un mécanisme d'immortalisation (212). Cette étude a révélé que l'activation de la télomérase se produisait principalement dans les paragangliomes métastatiques mutés sur le gène *SDHB*, tandis que les mutations *ATRX* étaient principalement retrouvées dans les tumeurs métastatiques mutées sur les gènes *SDHB* ou *FH*. L'activation de la télomérase et les mutations *ATRX* sont des facteurs indépendants de mauvais pronostic et doivent être évalués afin d'identifier les PPGL métastatiques, en particulier dans les tumeurs à haut risque de progression.

6) Prise en charge thérapeutique

Une fois le(s) PPGL précisément identifié(s), la prise en charge thérapeutique peut prendre plusieurs formes, en fonction du caractère fonctionnel ou non de la tumeur, de sa localisation, de son potentiel métastatique et de son déterminisme génétique.

La chirurgie demeure actuellement le seul traitement curatif pour traiter les PPGL, à condition qu'elle soit réalisée précocement. Toutefois, l'acte chirurgical reste un acte complexe pouvant présenter des difficultés principalement liées au risque de décharges catécholaminergiques, au cours du geste chirurgical et de la mobilisation de la tumeur. Des risques hémorragiques existent également du fait du caractère hypervasculaire de ces tumeurs (213,214). Afin d'éviter ces complications, une préparation médicale du patient en préopératoire, de sept à

quatorze jours avant la chirurgie, est recommandée. Cette préparation consiste essentiellement en une réhydratation associée à un traitement à base d'alpha-bloquants, préconisé pour leurs effets anti-hypertensifs. Afin de contrecarrer une éventuelle tachycardie secondaire à ce traitement, des bêtabloquants peuvent également être prescrits. Il a été démontré que cette prémédication des patients a permis d'abaisser le taux de mortalité péri-opératoire à moins de 3% (213). Pour les PCC, quand la taille tumorale le permet, la surrénalectomie est réalisée sous cœlioscopie, technique moins invasive et qui présente donc moins de risques de complications post-opératoires. Concernant les PGL, l'intervention consiste généralement en une tumorectomie. Toutefois, une laparotomie est préconisée lorsque les lésions sont de grande taille (supérieures à 6 cm), pour les PPGL invasifs et pour les PGL cervicaux (24). Une surrénalectomie bilatérale peut également être réalisée mais afin de palier à l'insuffisance surrénalienne qui en résulte, elle astreint le patient à un traitement à vie en hormones corticoïdes (hydrocortisone et fludrocortisone dans 90% des cas). Ainsi, la tumorectomie, chirurgie épargnant la région corticale de la surrénale, peut constituer une alternative à ce traitement pour les PCC familiaux de petite taille, mais augmente le risque de récidive sur la partie de la surrénale restante (215,216).

En ce qui concerne les PGL cervicaux, la chirurgie peut être contestée. En effet, un risque supplémentaire d'hémorragie et/ou de paralysies locales définitives existe, en raison de la présence de nombreux vaisseaux et nerfs à proximité de ces tumeurs. La chirurgie dépend alors de la localisation, de la taille et de l'envahissement vasculaire de la tumeur (217). Ainsi, la chirurgie est envisageable dans le cas d'un PGL du glomus carotidien de petite taille.

Enfin, dans les cas de formes malignes de PGL, la chirurgie peut également constituer un traitement palliatif. On parle alors de chirurgie réductrice ayant pour but de restreindre les conséquences fonctionnelles causées par les fortes sécrétions catécholaminergiques (218).

Bien qu'elle ne soit pas indiquée pour les PGL fonctionnels, la radiothérapie peut être privilégiée pour la prise en charge des PGL cervicaux plus volumineux, envahissant la carotide ou adjacentes à la base du crâne, afin de limiter la morbidité associée à l'intervention chirurgicale (219). Le traitement radiochirurgical peut également être une option pour les PGL de petite taille (220). Ces radiothérapies ont montré une stabilisation de la taille tumorale à 10 ans, dans environ 96% des cas (221). En outre, la proton-thérapie a récemment montré des résultats prometteurs (222).

a) Prise en charge des formes métastatiques

La prise en charge des formes métastatiques consiste en premier lieu au traitement des symptômes, dont notamment la régulation de l'HTA et des autres conséquences, souvent sévères, d'un excès de catécholamines dans la circulation (constipation, malaises, palpitations...) pouvant conduire au décès du patient. Malheureusement, il n'existe encore actuellement que peu d'options thérapeutiques pour traiter les formes métastatiques de la maladie. Ces différentes options reposent principalement sur la radiothérapie métabolique par ^{131}I-MIBG et la chimiothérapie CVD (cyclophosphamide, vincristine, dacarbazine) dont l'efficacité limitée a été démontrée (223). Toutefois, les différentes études menées ces dernières années pour approfondir la génomique et élucider les mécanismes de pathogenèse impliqués dans le développement des PPGL métastatiques, ont permis l'émergence de cibles thérapeutiques potentielles. Ces études semblent ainsi ouvrir la voie à l'utilisation, dans un futur proche, de thérapies ciblées et de la médecine de précision pour le traitement des formes métastatiques de PPGL (58). Néanmoins, la résection chirurgicale, quand elle est possible, reste encore actuellement le traitement de référence. Ainsi, d'après le centre national de référence COMETE-CANCER :

- La radiothérapie métabolique à l'^{131}I-MIBG permet une amélioration globale des symptômes dans environ 80 % des cas et est associée à une rémission partielle chez 30 à 50 % des patients, bien qu'une rémission complète ne soit observée que chez 5 à 13 % des patients (10,224).
- La combinaison CVD constitue la chimiothérapie de référence dans le traitement des PPGL. Elle est estimée efficace dans 55 % des cas et permettrait une rémission partielle chez 44 % des patients et une rémission totale dans 11 % des cas. Néanmoins, ce traitement est associé à de nombreux effets indésirables et a une réponse éphémère, sans réelle amélioration en termes de survie globale .
- Le temozolomide est une alternative orale à la chimiothérapie intra-veineuse qui présente l'avantage d'être moins toxique mais aussi efficace que la CVD. Une réponse partielle serait observée chez près de 33 % des patients. Le temozolomide est particulièrement efficace lorsque l'enzyme dé réparation MGMT (O(6)-methylguanine-DNA-methyltransferase) est sous-exprimée. Du fait d'une sous-expression particulière de cette enzyme dans les tumeurs SDHB (due à l'hyperméthylation de son promoteur (cf 7. Tumorigenèse)), ces patients sont apparemment de meilleurs répondeurs à ce traitement, avec une survie sans progression plus importante que les patients sans mutation *SDHB* (19,7 mois contre 2,9 mois) (228).

b) Thérapies ciblées anti-angiogéniques

L'angiogenèse joue un rôle crucial dans le développement tumoral des PPGL, notamment ceux ayant un profil pseudo-hypoxique (129,229–232). L'utilisation de thérapies anti-angiogéniques, ayant notamment pour cible la voie du VEGF, est donc apparue donc comme une stratégie particulièrement pertinente pour le traitement des formes métastatiques et en particulier celles associées à une mutation *SDHB*. Le sunitinib est un inhibiteur oral de récepteurs à tyrosine kinase (TKI), tels que les récepteurs au VEGF, au PDGF, ainsi que les récepteurs RET et c-kit. Plusieurs études rétrospectives évaluant la réponse à ce traitement ont montré des résultats prometteurs, avec notamment une réponse partielle ou une stabilisation chez plusieurs patients qui étaient devenus résistants aux thérapies classiques comme la radiothérapie métabolique à l'^{131}I-MIBG ou la chimiothérapie. De façon remarquable, la majorité des patients présentant une réponse au sunitinib dans ces études étaient porteurs d'une mutation sur les gènes *SDHB* ou *VHL* .

Des études prospectives visant à évaluer l'efficacité de ce médicament dans le traitement des PPGL ont été menées ces dernières années. Une première étude clinique internationale de phase II (SNIPP) a récemment évalué à 13,4 mois la survie sans progression de la maladie suite au traitement par sunitinib de 23 patients réfractaires. Néanmoins, le taux de réponse objective était très faible et seuls 3 patients, avec des mutations *SDHA, SDHB* et *RET,* ont présenté une réponse partielle (238). Les résultats du premier essai clinique randomisé international menée en double aveugle évaluant l'efficacité du sunitinib versus placebo (FIRSTMAPPP, NCT01371201) devraient être révélés très prochainement. Cet essai clinique de phase II est réalisé chez 78 patients atteints de PPGL métastatiques progressifs. D'autres TKI sont actuellement en cours d'évaluation (axitinib, pazopanib, lenvatinib, cabozantinib), mais malgré des résultats préliminaires encourageants, la plupart semblent être associées à de lourds effets indésirables, notamment à de l'hypertension sévère (239). En outre, les patients développent fréquemment une résistance aux thérapies anti-angiogéniques, comme cela a déjà été démontré dans d'autres types de cancers dont le RCC (240). Il est donc essentiel de développer d'autres stratégies thérapeutiques alternatives, qui pourraient être administrées seules ou en combinaison avec les anti-angiogéniques. Les progrès dans la compréhension des mécanismes de tumorigenèse sont essentiels à de tels développements.

7) Tumorigenèse des PPGL du cluster 1A

Ces quinze dernières années, plusieurs grandes études génomiques ont été menées sur des collections tumorales internationales et indépendantes, apportant une meilleure connaissance des mécanismes de tumorigenèse impliqués dans le développement des PPGL (178,229,241–243). Ainsi, les données transcriptomiques ont permis de classer les PPGL en trois différents sous-groupes, appelés clusters, reflétant les différents mécanismes de tumorigenèse impliqués (171,179) (Figure 13).

Le premier cluster ou cluster C1 est caractérisé par une signature moléculaire évoquant une activation constitutive des voies de réponse à l'hypoxie, appelée « pseudo-hypoxie ». Le deuxième cluster (cluster C2) est particulièrement caractérisé par l'activation des voies de signalisation kinases-dépendantes (voies MAP kinase et mTOR). Enfin, un troisième cluster a récemment été mis en évidence grâce aux données transcriptomiques issues des études du consortium TCGA. Ce cluster est caractérisé par une activation de la voie Wnt-β-catenine. L'implication de cette voie a été reconnue dans le développement de nombreux types tumoraux et un gène de fusion comportant le gène *MAML3* (mastermind-like transcriptional coactivator 3) semble responsable de son induction dans les PPGL appartenant à ce troisième cluster (179).

Le cluster C1 pseudo-hypoxique regroupe les PPGL secondaires aux mutations des gènes *SDHx*, *FH, MDH2*, *SLC25A11*, *GOT2*, *DLST* et *VHL*, alors que le cluster C2 regroupe toutes les tumeurs avec mutations *RET*, *NF1*, *TMEM127*, *MAX, MET, MERTK* et *HRAS*. Par ailleurs, deux sous-groupes sont reconnus au sein du cluster C1. Le C1A contient les PPGL secondaires aux mutations *SDHx* et *FH* (160), auxquels ce sont joints plus récemment de nouveaux gènes de prédisposition aux PPGL impliqués dans le métabolisme mitochondrial (*MDH2*, *SLC25A11*, *GOT2*, *DLST)* (60–63,244). Ce sous-groupe est associé à l'induction de nombreux gènes impliqués dans la prolifération et la survie cellulaire, le métabolisme énergétique, l'angiogenèse ainsi que dans les processus d'invasion et la formation de métastases (113,161,229). Le deuxième sous-groupe correspond (C1B) comporte, quant à lui, les PPGL avec mutations *VHL* et se différencie notamment par une induction des gènes codant pour les enzymes de la glycolyse.

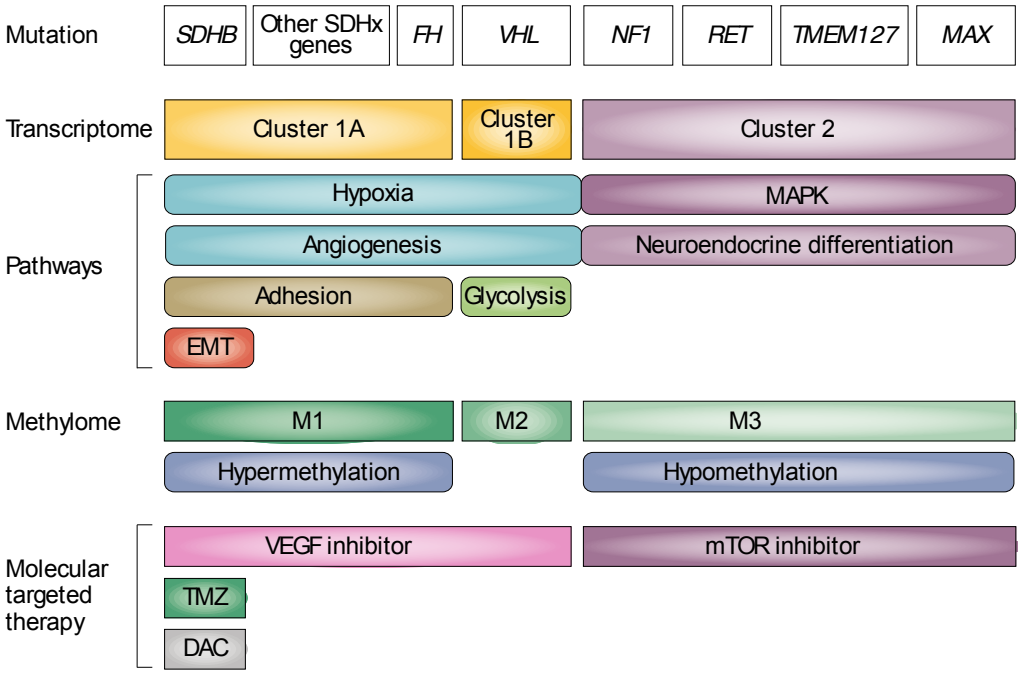

Figure 13 : Voies de tumorigenèse en fonction du cluster d'expression et de méthylation des gènes de prédisposition aux PPGL. *D'après (196)*

a) Le stress oxydant

Le stress oxydant est l'une des premières voies dont l'implication a été suspectée pour expliquer la tumorigenèse des PPGL du C1A. Il se définit par un déséquilibre entre la production et l'élimination des espèces réactives de l'oxygène (ROS), qui sont des espèces chimiques dérivées de l'O_2, plus réactives que lui-même et résultant d'un état d'oxydation différent de ce dernier. Cette dénomination comprend ainsi des radicaux libres de l'oxygène (i.e. associés à des électrons libres ou non appariés), tels que l'anion superoxyde ($O_2^{\bullet -}$) et le radical hydroxyle ($HO^{\bullet}$), mais également certains dérivés non radicalaires, comme le peroxyde d'hydrogène (H_2O_2) (245–247). Dans les cellules animales, les ROS sont générés au cours de réactions métaboliques et la mitochondrie est considérée comme étant leur principale source cellulaire (248,249). Une caractéristique commune aux différents types de ROS est leur capacité à causer des dommages oxydatifs aux protéines, à l'ADN et aux lipides (249,251,252)(321). Ainsi, les ROS sont capables d'induire des réponses biologiques très différentes en fonction de leurs niveaux cellulaires. Des ROS présents en petite ou moyenne quantité agissent comme des molécules de signalisation, alors qu'une accumulation excessive de ROS endommage les composants cellulaires (253,254). Une régulation stricte de

l'homéostasie redox, assurant l'équilibre entre les voies d'induction et de détoxification des ROS est donc essentielle pour assurer le maintien des fonctions cellulaires et de la survie (248).

i. Production des espèces réactives de l'oxygène (ROS)

La production de ROS a lieu en continu dans la cellule, par le biais d'une cascade de réactions (enzymatiques ou non), initiées par la génération d'anions superoxyde ($O_2^{\bullet -}$). Le flux d'($O_2^{\bullet -}$) est directement corrélé à la concentration de donneurs d'électrons potentiels et à la concentration locale d'O_2 (251). La chaîne respiratoire mitochondriale (ou chaine de transport des électrons, ETC) est la source majoritaire, non enzymatique, de ROS et les complexes I et III de l'ETC sont considérés comme étant les principaux sites de production (255,256) (Figure 14). Le complexe I génère principalement les anions superoxydes dans la matrice mitochondriale, tandis que ceux produits par le complexe III se retrouvent à la fois dans la matrice et dans l'espace intermembranaire. Un transport d'électrons défectueux n'aboutissant pas à une production normale d'ATP, ainsi que des ratios élevés de NADH/NAD+ constituent deux cas de figure conduisant généralement à une production massive d'$O_2^{\bullet -}$ par l'ETC (247,251). Indépendamment du site de production des ROS dans la mitochondrie, les premières étapes de la production des ROS mitochondriaux consistent systématiquement en la génération d'$O_2^{\bullet -}$ qui subit une dismutation rapide en H_2O_2 (257,258). Cette conversion peut s'effectuer de façon spontanée en fonction des conditions cellulaires (comme suite à une diminution de pH) ou par l'action d'une enzyme de la famille des superoxyde dismutase (SOD). Il existe trois formes de SOD : la SOD1 correspondant à la forme cytoplasmique, la SOD2 (ou MnSOD) localisée dans la matrice mitochondriale et la SOD3 située dans la matrice extracellulaire. Ces enzymes, notamment la SOD2, jouent un rôle majeur dans la régulation des ROS mitochondriales et dans l'homéostasie redox. La majorité des atteintes cellulaires secondaires à $O_2^{\bullet -}$ et à H_2O_2 résultent de leur transformation en espèces encore plus réactives et donc plus toxiques. C'est le cas du radical hydroxyle OH^-, qui est un des produits de la réaction de Fenton à partir de H_2O_2. Néanmoins, H_2O_2 reste considérée comme étant la forme la plus réactive de ROS. En effet, sa longue durée de vie et sa capacité élevée à traverser les membranes cellulaires semblent lui conférer un rôle majeur dans les signalisations inter- et intra-cellulaires (247,253). Il est désormais globalement admis que les ROS ont la capacité de fonctionner comme des molécules de signalisation, favorisant la prolifération et la

différenciation cellulaires, et permettant l'activation des voies de défense contre les agents pathogènes (259).

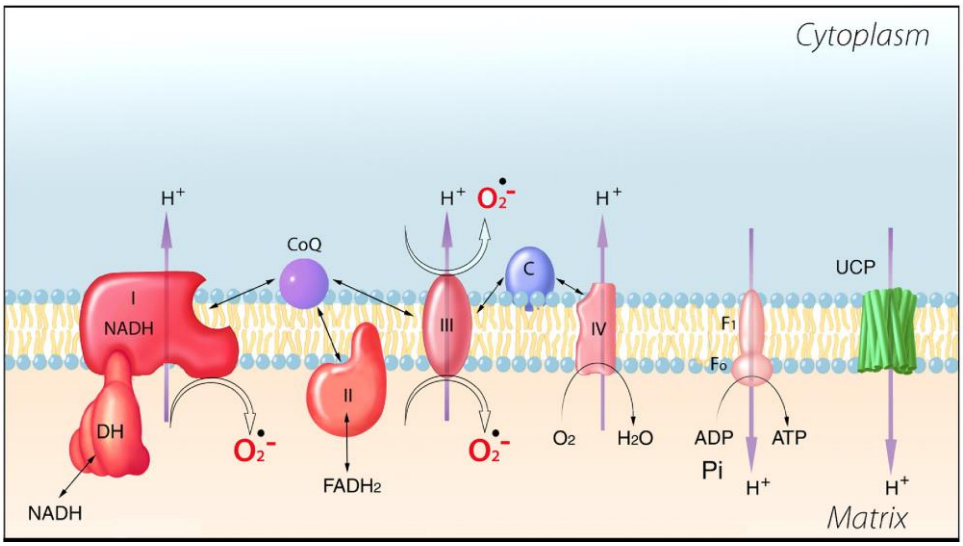

Figure 14 : Représentation schématique de la production de ROS par les complexes I et III de la chaîne respiratoire mitochondriale. *Adapté de (252)*

ii. Mécanismes de détoxification des ROS

Dans un contexte physiologique les ROS sont piégés par différents composants cellulaires, dits « antioxydants », qui activent les voies de réponse aux stress. L'expression des gènes antioxydants est donc sous le contrôle d'une régulation fine (Figure 15) et dépend largement de certains composants régulateurs. NRF2 (nuclear factor erythroid 2-related factor 2) est un facteur de transcription constituant le principal régulateur des réponses antioxydantes intracellulaires (260,261). Au repos c'est-à-dire quand l'organisme ne doit pas activer ses mécanismes de réponses au stress, NRF2 est sous le contrôle du complexe ligase E3 (KEAP1-CUL3) qui entretient sa dégradation constitutive. Dans un contexte de stress oxydant, KEAP1 se retrouve oxydé et dans l'incapacité de se lier à NRF2, résultant en la stabilisation et la translocation vers le noyau de ce dernier (262). NRF2 peut ensuite activer l'expression de nombreux gènes codant pour des enzymes ayant des fonctions antioxydantes (l'hème oxygénase, HMOX1 ; les glutathion S-transférases, GST ; la NAD(P)H quinone oxydoréductase 1, NQO1 et les UDP-glucuronosyl-transférases, UGT. De plus, NRF2 est l'unique facteur régulateur des enzymes responsables de la production du glutathion (GSH) (262).

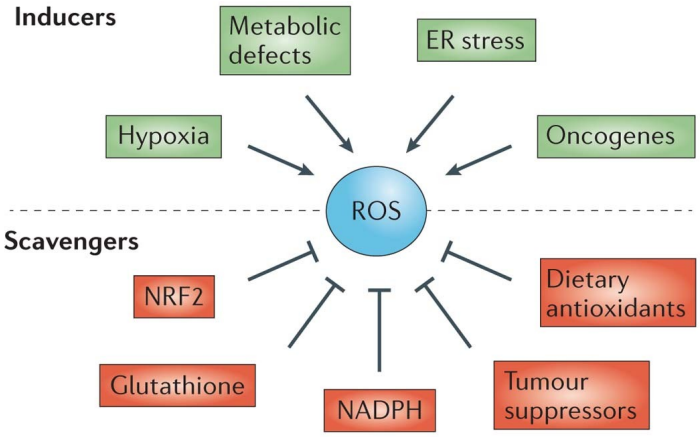

Figure 15 : Représentation schématique des principaux régulateurs de ROS. *D'après (248)*

Le glutathion (GSH) est la molécule non-enzymatique avec des propriétés antioxydantes, présente en plus grande quantité dans la cellule. Elle est essentielle à la survie cellulaire et au maintien de l'équilibre redox, notamment par son action dans l'élimination de H_2O_2 (263,264). Plusieurs études ont rapporté des modifications du métabolisme du GSH dans différents types tumoraux. L'agent réducteur NADPH est également un régulateur cellulaire essentiel. En plus de son rôle important pour la régénération du GSH, il agit dans la régulation de la thiorédoxine (TXN), un autre facteur participant activement à l'élimination de H_2O_2 (265). Malgré leurs rôles majeurs dans l'arrêt du cycle cellulaire et l'apoptose, l'implication dans la prévention du stress oxydant intracellulaire de certains suppresseurs de tumeurs, comme le facteur de transcription FOXO et la protéine p53, a également été rapporté. Ils pourraient ainsi stimuler l'expression de certains gènes antioxydants (254). Des sources externes d'antioxydants telles que les antioxydants alimentaires (vitamine C, vitamine E, sélénium, β-carotène) sont des composés non enzymatiques qui semblent jouer un rôle majeur dans l'activation des mécanismes de réponse cellulaire au stress oxydant (266). Parmi ces régulateurs non endogènes, la vitamine C semble particulièrement importante et essentielle aux fonctions cellulaires sous sa forme redox (ascorbate), de par son activité réductrice et son rôle de cofacteur enzymatique, notamment pour les dioxygénases 2-OG dépendantes (267).

iii. Principaux inducteurs des ROS

De façon paradoxale, la vitamine C peut également exercer des effets pro-oxydants, notamment en présence de certains métaux réactifs, comme le fer qui est un ion métallique essentiel à de nombreuses protéines (268). La capacité unique du Fer à passer efficacement

d'un état d'oxydation réduit (on parle alors de fer ferreux Fe^{2+}) à un état oxydé (fer ferrique Fe^{3+}), le rend indispensable à de nombreux organismes. En conditions physiologiques, le fer labile doit être majoritairement séquestré par la transferrine (Tf) dans le plasma et stocké dans la ferritine à l'intérieur de la cellule. Il se retrouve également incorporé comme cofacteur dans de nombreuses protéines (269). C'est notamment le cas de l'hème et des protéines portant des clusters Fer-Souffre dont la protéine SDHB. Néanmoins, des petits pools de fer labile Fe^{2+} subsistent à l'intérieur des cellules, dans le cytosol et la matrice mitochondriale (269). Ce fer labile est capable de réagir avec H_2O_2 pour générer, par la réaction de Fenton, le radical hydroxyle (• OH) hautement réactif (270) (Figure 16). L'ascorbate est également un cofacteur de cette réaction en donnant des électrons au Fe^{3+}, conduisant à la régénération de la forme réactive Fe^{2+} et ainsi à une production continue de ROS. Par ailleurs, une multitude d'études a révélé l'action pro-oxydante de l'ascorbate *in vitro* résultant en une surproduction de H_2O_2, ayant pour conséquence directe la mort de cellules cancéreuses (271–273). Ce rôle pro-oxydant de l'ascorbate serait secondaire à sa capacité à s'auto-oxyder lorsqu'il est présent en quantité supra-physiologiques (274,275). De plus, le Fe^{2+} labile serait également capable de catalyser cette réaction d'auto-oxydation (276,277).

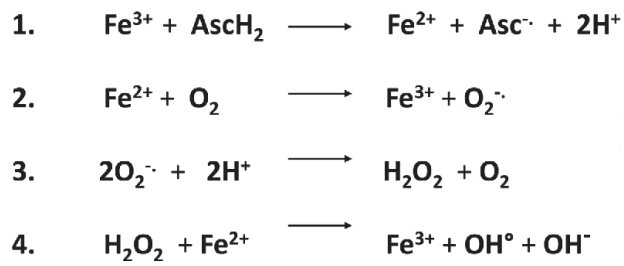

Figure 16 : Différentes étapes de la réaction de Fenton Haber-Weiss médiée par l'ascorbate.
D'après (278)

Plusieurs voies de signalisation impliquées dans le développement tumoral favorisent l'accumulation intracellulaire de ROS (Figure 15), telles que l'hypoxie (279,280), les altérations métaboliques et notamment une respiration mitochondriale soutenue (281), l'activation de certains oncogènes et l'inhibition de la catalase ou de la SOD mitochondriale (SOD2) (282,283). Plus récemment, l'inactivation de la SOD extracellulaire (SOD3) a été associée à l'accumulation de ROS dans le microenvironnement tumoral (284). Plusieurs études ont démontré l'implication des ROS dans le remodelage de la matrice extracellulaire (MEC), notamment par la conversion des fibroblastes en myofibroblastes (247,285). Une production continue de ROS peut donc aboutir à un stress oxydant chronique et par conséquent à la

stimulation de processus d'oncogenèse (initiation de la croissance tumorale et formation de métastases). Des niveaux élevés de ROS sont généralement considérés comme délétères pour les cellules et ont été détectés dans plusieurs types de cancers, tels que les cancers du sein, de l'ovaire, du foie ou du côlon. Toutefois le statut redox des cellules cancéreuses diffère de celui des cellules normales. Ces dernières ont la capacité de s'adapter à des niveaux élevés de ROS (Figure 17) (286,287) demeurant compatibles avec un bon fonctionnement cellulaire. Ce phénomène ne s'oppose pas au développement tumoral car des niveaux modérés de ROS peuvent induire des mutations de l'ADN et stimuler l'activation des voies de signalisations pro-oncogéniques (288,289). À des niveaux élevés, les ROS favorisent la mort cellulaire et de graves dommages cellulaires.

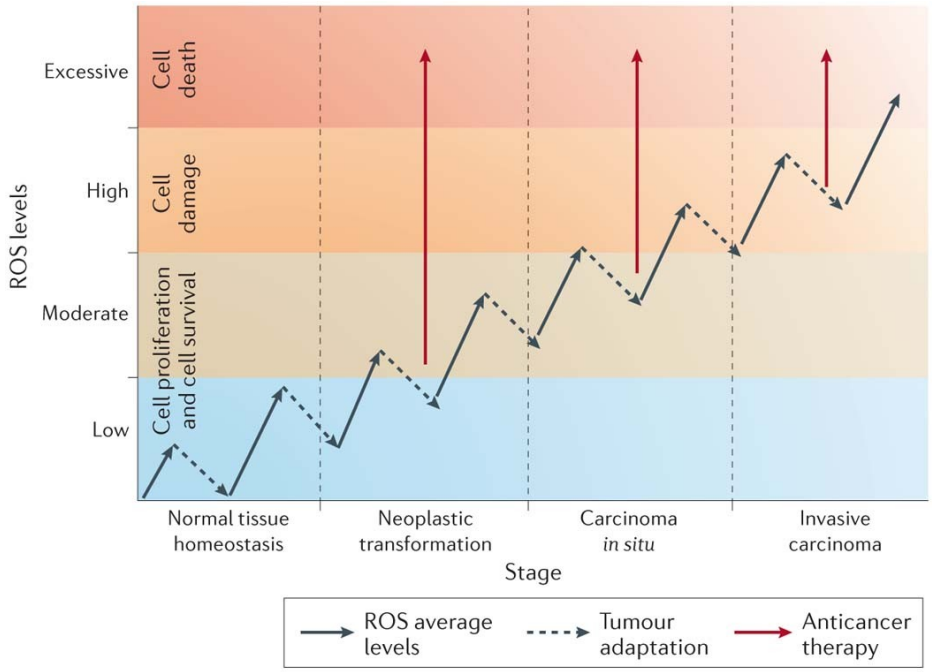

Figure 17 : Interactions entre les niveaux de ROS et les différentes étapes de la tumorigenèse.
D'après (248)

L'association entre la SDH et les ROS est évoquée depuis le début des années 2000, bien que controversée, le lien entre la production de ROS et la tumorigenèse SDH-dépendante faisant toujours débat. Certaines études suggèrent qu'un défaut en SDH est associé à une production accrue de ROS (290) et d'autres au contraire s'opposent à cette hypothèse (291–293). Ainsi, *Selak et al*. ont d'abord rapporté en 2006, une absence de stress oxydant dans des cellules avec un knock-down (KD) du gène *Sdhd* (291). Deux ans plus tard, *Guzy et al.* ont publié une étude suggérant, au contraire, une production plus importante de ROS suite à un défaut

de la sous-unité SDHB, en précisant toutefois que cette observation n'était pas valable suite à la perte seule de la sous-unité SDHA. Dans cette étude, il a été proposé un mécanisme expliquant la tumorigenèse des PPGL SDH-dépendants, qui reposerait sur l'action des ROS comme messagers capables d'activer les voies de réponse à l'hypoxie (290). Conformément à ces résultats, une autre étude a rapporté qu'un défaut de la sous-unité SDHB conduisait à une production élevée de ROS, associée à la stabilisation nucléaire de HIF1α et à l'expression accrue du facteur anti-apoptotique Bcl-2 (294). Enfin, une étude réalisée à partir d'un modèle de levure a rapporté que l'augmentation des niveaux de ROS observés, suite à un défaut de la sous-unité SDHB, serait à l'origine d'un taux élevé de mutagenèse de l'ADN, contribuant ainsi à la tumorigenèse (295). Ces discordances s'expliquent probablement par l'hétérogénéité des modèles étudiés, ainsi que les différentes méthodes utilisées pour inhiber l'activité de la SDH. En effet, ces modèles présentent la plupart du temps à une inactivation partielle de la SDH, associée à différentes mutations des gènes *Sdhx* (*Sdhd, Sdhb ou Sdha*), ce qui pourrait expliquer les différents degrés de production de ROS. L'impact des ROS dans la tumorigenèse SDH-dépendante était donc, jusqu'à récemment, encore très discutée et nécessitait une étude approfondie. L'article 2 présenté dans ce manuscrit aborde cette question et a permis d'apporter quelques éléments de réponse à cette controverse.

b) Les dioxygénases dépendantes du 2-OG

En raison de ces contradictions, l'élucidation des mécanismes impliqués dans la tumorigenèse des PPGL SDHx-dépendants s'est surtout axée autour de l'étude des conséquences directes de l'accumulation de succinate. Il a ainsi été établi que la tumorigenèse des PPGL SDHx-dépendants repose principalement sur l'inhibition des dioxygénases dépendantes du 2-OG (296). La première preuve d'un rôle tumorigénique des oncométabolites (succinate, fumarate) dans les PPGL du cluster C1A est apparue avec l'identification du mécanisme de pseudo-hypoxie dans ces tumeurs.

i. Les PHDs des HIFs et la pseudo-hypoxie

C'est au début des années 2000 que le mécanisme moléculaire responsable de la réponse cellulaire à l'hypoxie a été découvert par les équipes de William Kaelin et de Peter Ratcliff (297,298), découverte qui leur value le Prix Nobel de Médecine en 2019, conjointement avec

Greg Semenza pour l'identification du facteur HIF1α au début des années 90' (Figure 7). La voie de la réponse hypoxique est médiée par la stabilisation des facteurs de transcription HIF1α et HIF2α (Hypoxia Inducible Factors). En conditions physiologiques et normoxiques, les protéines HIFα sont d'abord hydroxylées sur deux prolines par des enzymes appartenant à la famille des dioxygénases dépendantes du Fe(II) et du 2-oxoglutarate (2-OG), les prolyl-hydroxylases (PHD). L'activité de ces enzymes particulières repose sur la disponibilité, en concentrations suffisantes selon leurs différents K_m (Tableau 3), de leurs principaux co-facteurs, qui sont en plus du 2-OG : le fer (299), l'oxygène (300) et l'ascorbate (301).

Cosubstrate	C-P4H-I	C-P4H-II	C-P4H-III	HIF-P4H-1	HIF-P4H-2	HIF-P4H-3
	K_m, μM					
Fe^{2+}	2	2	0.5	0.03	0.03	0.1
2-Oxoglutarate	20	22	20	2	1	12
O_2	40	N.D.[b]	N.D.	230	250[c]	230
O_2					100[d]	
O_2					65–85[e]	
Ascorbate	300	340	370	170	180	140

Tableau 3 : Valeurs des différents Km des prolyl-hydroxylases des HIFs (PHD) et du collagène (P4H) en fonction de leurs principaux co-facteurs *(O_2, 2-OG, Fe^{2+} et Ascorbate). D'après (302)*

Cette réaction d'hydroxylation est primordiale puisqu'elle permet la fixation d'une ubiquitine ligase E3, la protéine VHL, sur les protéines HIFα, qui subissent alors une polyubiquitination, avant d'être dégradées par le protéasome. Ce processus se déroule très rapidement étant donné la courte demi-vie des HIFα dans le cytosol, estimée à 5 minutes (303). En situation de faible pression partielle en oxygène (ou hypoxie) les PHD, qui utilisent l'O_2 comme substrat, ne peuvent plus assurer la réaction d'hydroxylation. Les sous-unités HIFα sont donc stabilisées et capables de transloquer au noyau, où elles s'associent à la sous-unité constitutivement stable, HIF1β (ou ARNT). L'hétérodimère nouvellement formé est alors capable d'induire l'expression de gènes cibles impliqués dans l'adaptation cellulaire et tissulaire à l'hypoxie. Dans les tumeurs du cluster C1, cette voie de réponse à l'hypoxie est activée, même en conditions normoxiques. La stabilisation anormale des protéines HIFα est expliquée par l'absence d'ubiquitination dans les PPGL secondaires à des mutations perte de fonction du gène *VHL*, tandis qu'elle s'explique par l'accumulation des oncométabolites (succinate, fumarate ou 2-hydroxyglutarate) secondaire à une mutation sur les gènes *SDHx*, *FH* ou *DLST* respectivement (61,304) (Figure 18). Ces métabolites agissent comme des inhibiteurs

compétitifs des dioxygénases dépendantes du Fe(II) et du 2-OG (dont les PHDs), entrainant ainsi la stabilisation anormale des HIFα (305,306).

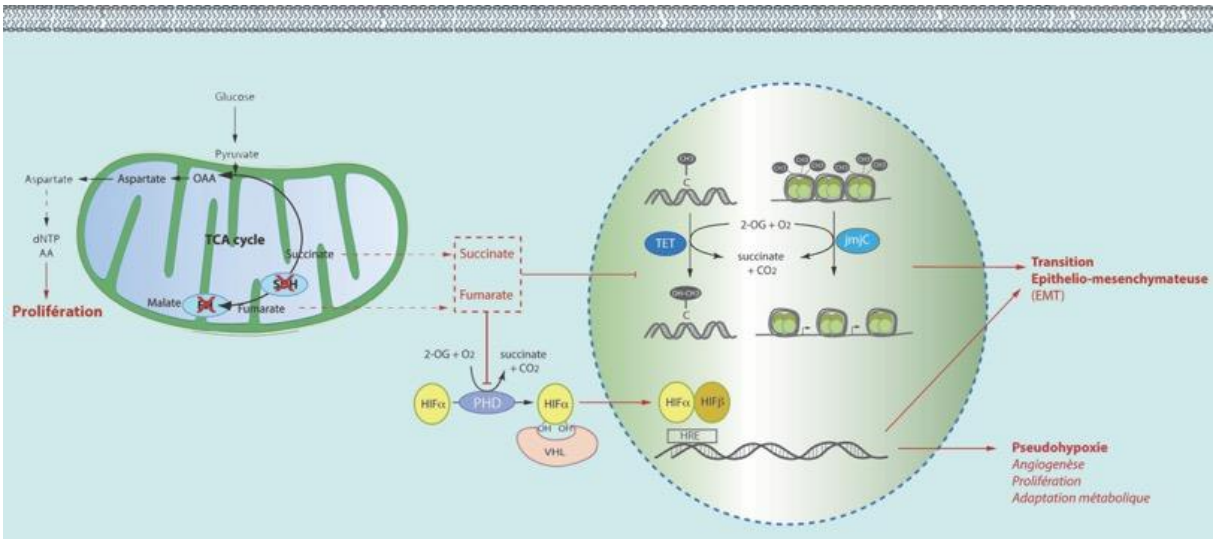

Figure 18 : Voies de tumorigenèse médiées par l'accumulation des oncométabolites succinate et fumarate, résultant des mutations des gènes SDHx et FH. *D'après (112)*

Les facteurs de transcription HIF ont la capacité d'induire l'expression d'une multitude de gènes cibles et par ce biais d'activer les processus d'angiogenèse (307), de prolifération et de survie cellulaires ainsi que le métabolisme glucidique ou l'EMT (308) (Tableau 4). La pseudo-hypoxie est donc susceptible d'agir sur la tumorigenèse des PPGL à différents niveaux (Figure 19).

L'angiogenèse

Comme proposé par Judah Folkman au début des années 70', il est aujourd'hui bien établi qu'au-delà d'un volume tumoral de 1 à 3 mm^3, la vascularisation est essentielle à la croissance d'une tumeur. Les HIF ont la capacité de réguler l'expression de plusieurs gènes pro-angiogéniques, favorisant le développement de vaisseaux sanguins à partir du système vasculaire préexistant (82). Parmi ces cibles, le Vascular Endothelial Growth Factor (VEGF) et ses récepteurs, ainsi que le couple Angiopoïétine-2 (Ang-2) / Tie2 semblent jouer un rôle crucial dans l'initiation du processus de néovascularisation. Ainsi, dans un contexte de pseudo-hypoxie, la sécrétion de VEGF par les cellules tumorales permet l'activation de la signalisation VEGFR-2, favorisant alors la survie, prolifération et migration des cellules endothéliales (309). Une surexpression du VEGF et une densité vasculaire plus importante sont notamment

observées au sein des tumeurs secondaires à des mutations *SDHx* ou *VHL* en comparaison à des tumeurs appartenant au cluster C2 mutées sur *RET* ou *NF1* (229).

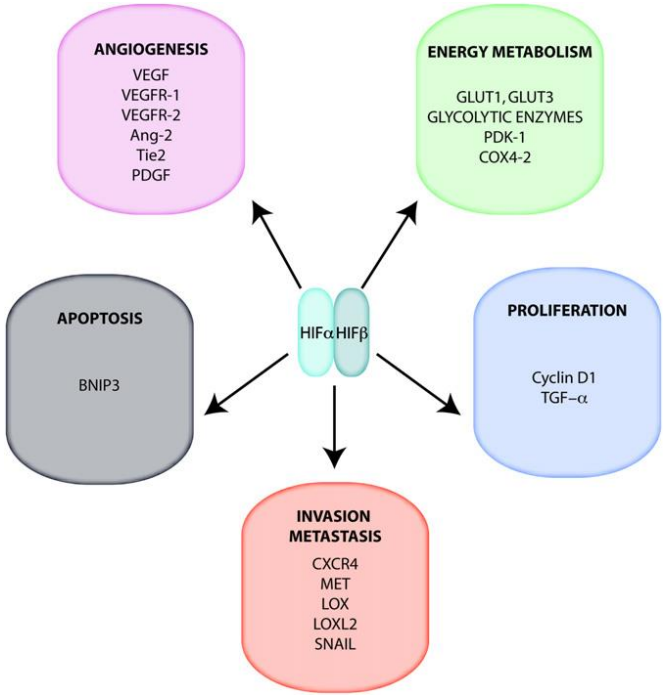

Figure 19 : Gènes cibles et voies de signalisation favorisées par la stabilisation du complexe HIFα/HIFβ. *D'après (82)*

Le métabolisme énergétique

Le « switch métabolique » de la respiration aérobie vers une respiration anaérobie est un processus central de l'adaptation à l'hypoxie. De nombreux gènes impliqués dans le métabolisme glucidique constituent ainsi des cibles des HIFα : HIF1α induit l'expression des transporteurs du glucose GLUT1 et GLUT3 et de nombreuses enzymes de la glycolyse, telles que l'hexokinase 2 et la lactate déshydrogénase A (310), tandis que HIF2α induit l'expression de GLUT1 (311). Ce phénotype fait écho à celui décrit par Otto Warburg, Prix Nobel de Médecine en 1931, qui avait émis l'hypothèse avant-gardiste d'un lien majeur entre le dysfonctionnement mitochondrial et le cancer. Après avoir observé que les cellules cancéreuses utilisent préférentiellement la glycolyse anaérobie même en présence d'oxygène, Warburg suggère ainsi que des défauts au niveau de la phosphorylation oxydative seraient à l'origine du cancer (312). Cet « effet Warburg » est aujourd'hui observé suite à des altérations génétiques conduisant à l'activation de la pseudo-hypoxie. De plus, l'augmentation de la captation en glucose qui en découle est un principe tellement fiable qu'il a donné lieu à

une technique d'imagerie permettant la détection de métastases qui est couramment utilisé en clinique : la tomographie par émission de positons au ^{18}F-fluorodésoxyglucose (FDG-PET). Le mécanisme moléculaire à l'origine de cet effet Warburg est resté une énigme pendant des décennies et ce n'est que dans les années 2000 que l'implication des HIF dans ce processus a été démontré (313). La reprogrammation métabolique est à présent considérée comme l'une des huit caractéristiques majeures des cancers, comme définies par Weinberg et Hanahan dans leur article de référence « The Hallmarks of Cancer » (314).

Gène (protéine)	Fonction protéique	Gène cible de HIF1α	Gène cible de HIF2α	Type cellulaire
***SLC25A11* (GLUT1)**	Transporteur mitochondrial du glucose	+	+	ccRCC
***PLIN2* (ADRP)**	Métabolisme lipidique	+	+	ccRCC
***CA12* (CAXII)**	Homéostasie acido-basique (pH)	+	+	ccRCC
***FLG* (filaggrine)**	Cytosquelette	+	+	ccRCC
***IL6* (IL-6)**	Cytokine participant à la fonction immunitaire	+	+	ccRCC
ADM (adrenomedulline)	Angiogenèse	+	+	ccRCC
VEGFA (VEGFA)	Angiogenèse	+	+	ccRCC
VEGFA (VEGFA)	Angiogenèse	+	-	Cellules souches embryonnaires
***BNIP3* (BNIP3)**	Autophagie et apoptose	+	-	ccRCC
***HK1* (hexokinase1)**	Glycolyse	+	-	
***HK2* (hexokinase2)**	Glycolyse	+	-	ccRCC
***PFK* (phosphofructokinase)**	Glycolyse	+	-	ccRCC
***ALDOA* (ALDA)**	Glycolyse	+	-	ccRCC
***PGK1* (PGK1)**	Glycolyse	+	-	ccRCC
***LDHA* (LDHA)**	Glycolyse	+	-	ccRCC
***NOS2* (iNOS)**	Production de NO	-	+	Macrophages
***ABL2* (ARG)**	Inhibiteur de la production de NO	-	+	Macrophages
***EPO* (érythropoïétine)**	Erythropoïèse	-	+	Cellules du rein et hépatocytes
***POUSF1* (OCT4)**	Différenciation des cellules souches	-	+	Cellules souches embryonnaires
***SCGB3A1* (secretoglobine 3A1)**	Cytokine inhibant la croissance ?	-	+	Carcinome pulmonaire non-à-petites cellules
***TGFA* (TGFa)**	Facteur de croissance	-	+	ccRCC
***CCND1* (cycline D1)**	Acteur du cycle cellulaire	-	+	ccRCC
***DLL4* (DLL4)**	Signalisation Notch	-	+	Cellules souches embryonnaires
***ANGPT2* (angiopoietine 2)**	Remodelage des vaisseaux sanguins	-	+	Cellules souches embryonnaires

Tableau 4 : Principaux gènes cibles régulés par HIF1α et HIF2α. *Adapté de (323).* *ccRCC : carcinome rénal à cellules claires.*

Les HIF sont impliqués dans la stimulation de la glycolyse (Tableau 4) et mais aussi dans l'inhibition de la phosphorylation oxydative mitochondriale, notamment par l'intermédiaire

de HIF1α qui stimule l'expression de la pyruvate déshydrogénase kinase 1 (PDKZ1), enzyme inhibitrice de la pyruvate déshydrogénase (PDH) et qui limite l'entrée du pyruvate dans le cycle de Krebs (315–317). En conditions d'hypoxie, HIF2α jouerait quant à lui un rôle direct sur l'ETC en stimulant l'expression de la sous-unité COX4-2 du complexe IV ou cytochrome c oxydase (COX). Cette activation se fait au détriment de la sous-unité COX4-1, et entraine une inhibition de l'activité globale de la COX (317,318). De plus, de nombreux modèles de souris invalidés pour le gène *Hif2α* ont démontré que l'inactivation de HIF2 a pour conséquence une diminution de l'activité de plusieurs complexes de l'ETC, tels que COX et SDH, ainsi qu'une altération plus globale de l'activité du cycle de Krebs (319). L'ensemble de ces données obtenues *in vitro* et *in vivo* suggéraient une implication majeure des HIF dans le mécanisme conduisant à l'effet Warburg observé dans les tissus tumoraux. Cette implication a ensuite été confirmée dans plusieurs types tumoraux associés à la pseudo-hypoxie, dont le ccRCC, qui présente une mutation somatique du gène *VHL* dans environ 80% des cas, ayant pour conséquence la surexpression de nombreuses enzymes glycolytiques et la sous-expression d'enzymes mitochondriales, qui seraient donc le résultat de la stabilisation des HIF (320–322).

L'implication des HIF dans les mécanismes de pathogenèse associés aux PPGL a également été démontrée par plusieurs études. Ainsi, mon équipe d'accueil a démontré que l'expression protéique et l'activité enzymatique de l'ensemble des complexes de la chaîne respiratoire mitochondriale étaient diminuées chez les patients porteurs de mutations *SDHx* et *VHL* en comparaison aux patients avec des mutations *RET* et *NF1,* au sein d'une cohorte de 68 PPGL héréditaires analysées par micro-array (229). Néanmoins, bien que l'augmentation des transporteurs du glucose (GLUT1 et GLUT3) soit retrouvée à la fois dans les PPGL mutés *VHL* et *SDHx,* traduisant une stimulation de la glycolyse anaérobie lié à la stabilisation des HIF, seules les tumeurs *VHL* présentent une surexpression des enzymes glycolytiques. Ces analyses avaient à l'époque déjà permis de classer les PPGL en trois groupes (*SDHx, VHL* et *RET/NF1*) soulignant la pertinence de l'étude des voies du métabolisme énergétique dans les PPGL. L'ensemble de ces résultats suggéraient donc un rôle central de HIF1α et HIF2α dans la régulation du métabolisme énergétique au sein des PPGL *VHL* et de HIF2α uniquement dans les tumeurs *SDHx*-dépendantes.

L'apoptose PHD3-dépendante

Les HIFα jouent également un rôle dans la régulation du processus de mort cellulaire programmée ou apoptose. Toutefois ces rôles peuvent être opposés en fonction du type tumoral ou du sous-type de HIFα impliqué (Tableau 4). Ainsi, HIF1α exerce un effet pro-apoptotique via la stimulation de l'expression de BNIP3 et la stabilisation de p53 (324), alors que HIF2α manifesterait un effet anti-apoptotique dans les ccRCC, par l'inhibition de BNIP3 (325). La sous-expression de *BNIP3* a été observée dans les PPGL avec mutations *SDHB* et *HIF2A* (230) suggérant à nouveau une implication plus importante de HIF2α, en comparaison à HIF1α, dans la pathogenèse des PPGL *SDHx*-dépendants.

En 2005, *Lee et al.* ont mis en lumière l'implication d'une voie d'apoptose développementale médiée par l'une des trois prolyl-hydroxylase des HIF, PHD3 (également appelée EglN3), dans la tumorigenèse des PPGL avec mutation sur les gènes *RET, NF1, VHL* et *SDHx* (326). Cette voie correspondrait à un mécanisme d'apoptose embryonnaire provoqué par PHD3, permettant la différenciation d'un nombre convenable de cellules neuronales sympathiques, à partir desquelles les phéochromocytomes sont dérivés. Elle serait régulée par la présence de facteurs neurotrophiques et notamment du NGF (Nerve Growth Factor). Ainsi, la privation en NGF de certaines de ces cellules neuronales aboutirait à leur mort cellulaire par apoptose PHD3-dépendante. Ce mécanisme d'apoptose serait indépendant des facteurs HIF1α et HIF2α, ce qui suggère l'existence d'autres cibles de PHD3 (327). De manière remarquable, cette voie semble être affectée à différents niveaux en fonction des gènes de susceptibilité aux PPGL mutés. Ainsi, dans les PPGL mutés *VHL,* l'inhibition de l'apoptose s'effectuerait par l'inactivation indirecte du facteur de transcription c-Jun, secondaire à l'accumulation de JunB tandis que chez les patients porteurs de mutations *SDHx* constitutionnelles, l'accumulation de succinate inhiberait directement PHD3, altérant l'apoptose embryonnaire et potentialisant la transformation néoplasique.

Ces études suggèrent donc qu'une SDH fonctionnelle est nécessaire pour l'induction de l'apoptose, néanmoins il semblerait que la mort cellulaire puisse également être induite lorsque la fonction de la SDH est inhibée, comme l'ont rapporté *Kluckova et al.* en 2015, suite à une mutation dans le site de liaison à l'ubiquinone. Dans cette étude, l'apoptose s'est avérée être dépendante de la génération de ROS. L'induction de la mort cellulaire par inhibition du

site de liaison à l'ubiquinone a alors été suggérée comme une stratégie anti-tumorale intéressante (328). L'apoptose pourrait donc être stimulée par plusieurs mécanismes en fonction des mutations identifiées et du type de cellules dans lesquelles l'accumulation de succinate et de ROS pourraient jouer un rôle déterminant dans le destin cellulaire.

Finalement, un mécanisme supplémentaire a récemment été identifié associant SDH et apoptose. La SDH agirait comme un capteur direct d'apoptose en détectant les variations de pH (329,330). Des études récentes ont proposé que l'acidification du milieu intracellulaire et l'afflux de Ca^{2+} dans les mitochondries secondaires à l'apoptose, conduiraient à la dissociation du dimère catalytique de la SDH (SDHA/SDHB) du reste du complexe. Ce phénomène entrainerait une génération plus importante de ROS, induisant un stress oxydant trop important pour la cellule et aboutissant à la mort cellulaire (329,331).

ii. Dioxygénases impliquées dans les modifications épigénétiques et génétiques

L'épigénétique se définit comme la présence de modifications chimiques qui affectent l'expression génique, sans modifier la séquence d'ADN (332). En 2013, mon équipe d'accueil a procédé à l'analyse du méthylome des PPGL à partir d'une collection de 145 tumeurs issues de la cohorte française COMETE. Cette étude a validé l'importance des mutations « driver » sur le phénotype moléculaire des PPGL, en montrant que la classification des échantillons basée sur la méthylation de l'ADN permettait, à nouveau de les classer en fonction de leur génotype: cluster M1 (tumeurs *SDHx* et *FH*), cluster M2 (tumeurs *VHL*) et cluster M3 (tumeurs *RET, NF1, TMEM127, MAX* et tumeurs sporadiques) (113). Les tumeurs appartenant au cluster M1 présentent une hyperméthylation globale de l'ADN, retrouvée dans, et à l'extérieur des îlots CpG. Simultanément, une équipe américaine a rapporté un phénotype similaire dans une collection de GIST SDH-dépendants (333). Ces articles ont eu un retentissement très important, révélant pour la première fois que les modifications épigénétiques constituent sans doute l'un des mécanismes clés de la tumorigenèse des PPGL induite par les oncométabolites (160,171,196)

L'accumulation des oncométabolites est ainsi apparue comme responsable de l'inhibition d'autres dioxygénases 2-OG dépendantes, telles que des déméthylases de l'ADN (TET ou « Ten eleven translocase ») et des histones (histone lysine déméthylases KDM contenant un

domaine JmjC) (334) (Figure 20), ayant pour conséquence une hyperméthylation globale de l'ADN (113) et des modifications structurelles de la chromatine (212).

Les dioxygénases TET hydroxylent les cytosines méthylées de l'ADN (5-méthylcytosine, 5mC) en 5-hydroxy-méthylcytosine (5hmC)(335,336). Par conséquent, l'inhibition des enzymes TET par les oncométabolites résulte en une forte méthylation de l'ADN et une faible hydroxyméthylation de l'ADN. Cette dérégulation de l'épigénome conduit à la sous-expression de nombreux gènes, notamment des gènes suppresseurs de tumeurs, des gènes impliqués dans la propagation métastatique, et des gènes responsables de la différenciation neuroendocrine (337). Ce modèle d'hyperméthylation globale de l'ADN et des histones explique ainsi plusieurs des caractéristiques des PPGL liés à la SDH. L'hyperméthylation des îlots CpG dans le promoteur des gènes suppresseurs de tumeur joue certainement un rôle important dans la tumorigenèse et constitue souvent le « deuxième évènement » du modèle de Knudson (338,339).

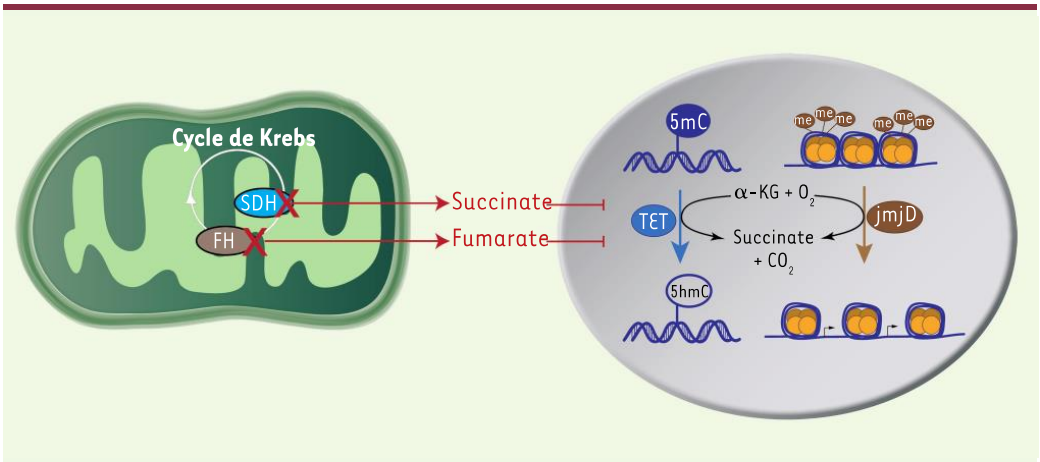

Figure 20 : Mécanismes d'hyperméthylation de l'ADN et des histones favorisés par les mutations SDHx et FH. *Me : méthyl ; 5mC : 5 méthylcytosine ; 5hmC : 5 hydroxyméthylcytosine. D'après (340)*

Plus récemment, il a été montré que l'accumulation de ces oncométabolites était à l'origine de l'inhibition des lysine déméthylases KDM4A et KDM4B, ayant pour conséquence la dérégulation des voies de recombinaison homologue et de réparation de l'ADN dans les tumeurs mutées *SDHx* et *FH* (341,342). Le mécanisme par lequel les oncométabolites perturbent les processus de réparation de l'ADN (ou HDR « homology-dependent repair ») implique une hyperméthylation aberrante de la lysine 9 de l'histone 3 (H3K9) au niveau des

locus entourant les cassures de l'ADN, ce qui a pour conséquence directe de masquer le signal de triméthylation normalement détecté sur H3K9 et essentiel à la bonne réalisation des processus d'HDR. L'absence d'identification du signal empêche le recrutement des facteurs de réparation qui interviennent dans ces processus et aboutit à une absence de recombinaison homologue et à une instabilité génomique conséquente. Ces résultats sont très prometteurs et pourraient permettre l'émergence de stratégies thérapeutiques efficaces, ce mécanisme confèrant une sensibilité accrue aux inhibiteurs de PARP (343), une enzyme hautement conservée qui répare les cassures d'ADN simple brin et stabilise la réplication de l'ADN. L'efficacité de ces iinhibiteurs est actuellement évaluée dans des essais cliniques.

iii. Autres dioxygénases dépendantes du 2-OG, dont les P4H

Plusieurs enzymes impliquées dans les modifications post-traductionnelles des collagènes, telles que les collagènes prolyl 4- hydroxylases (P4HA1, P4HA2, P4HA3), les collagènes prolyl 3-hydroxylases et les 3 isoformes de la collagène lysyl-hydroxylase (PLOD1, PLOD2, PLOD3), sont également des dioxygénases dépendantes du 2-OG (Figure 21). Les P4H sont les principales enzymes responsables de l'hydroxylation des résidus proline du collagène, résultant en des résidus 4-hydroxyproline.

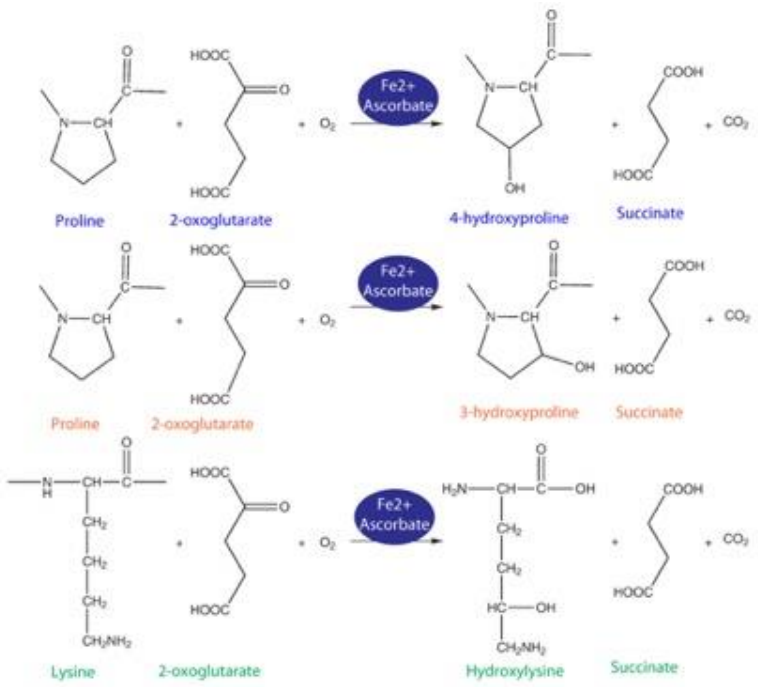

Figure 21 : Réactions catalysées par les différents types de collagènes hydroxylases *(P4H, P3H et PLOD de haut en bas). D'après (344)*

Elles jouent un rôle majeur dans la formation et la stabilisation de la triple hélice de collagène (345–348), leur action étant essentielle pour aboutir à la maturation correcte des fibrilles de collagènes dans le réticulum endoplasmique (RE) et à leur sécrétion dans le milieu extracellulaire (349–351) (Figure 22). Par ailleurs, des études ont montré que l'inhibition de l'hydroxylation entrainait un stress au niveau du RE (352). Les résidus 4-hydroxyproline, sont les principaux résidus hydroxylés retrouvés dans l'ensemble des collagènes. La P4H du collagène pourrait donc constituer une cible thérapeutique particulièrement intéressante pour le traitement de certaines pathologies, associées à une accumulation excessive de collagènes (353) ou à une dérégulation de la matrice extracellulaire (MEC). En effet, les collagènes sont les principaux composants de la MEC (90%) (354). Les collagènes de type I et de type IV, qui sont respectivement les principaux constituants de la matrice interstitielle et de la membrane basale (MB), sont les formes les plus répandues (355,356).

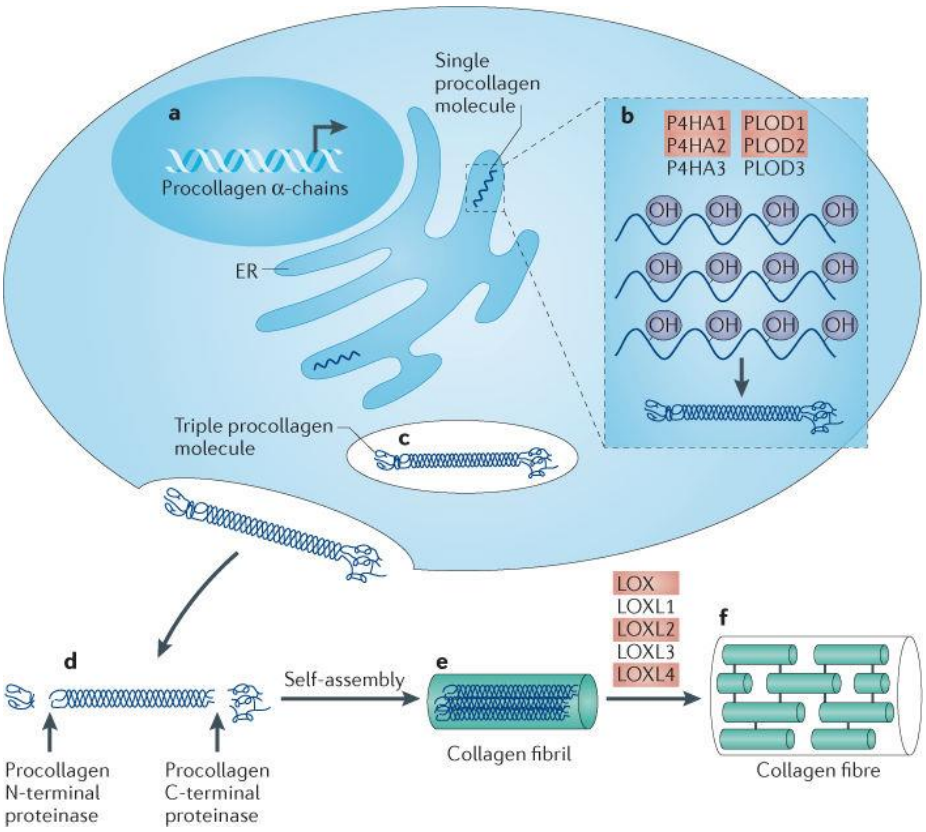

Figure 22 : Voie de synthèse des collagènes fibrillaires. *D'après (349)*

Ainsi, la question de l'impact du succinate sur ces P4H s'est rapidement posée au sein de mon équipe d'accueil. C'est pourquoi, au cours de ma thèse je me suis intéressée à ces enzymes et

à l'implication de la MEC dans l'acquisition du phénotype métastatique associé aux PPGL *SDHB*-dépendant, ce travail en cours de finalisation, faisant l'objet du 3ème article présenté dans ce manuscrit. La MEC qui est un ensemble de protéines extracellulaires, sécrétées par les cellules et soutenant les tissus, est apparu comme un élément d'étude intéressant pour la compréhension des mécanismes de tumorigenèse des PPGL SDH-dépendants. Ces dernières années un nombre croissant d'études ont révélé des implications majeures de la MEC dans de nombreux processus cellulaires (357) (358), notamment dans des contextes pathologiques. Ainsi, dans un contexte tumoral la MEC participe à la prolifération, l'invasion, la progression métastatique et peut également influer sur la réponse thérapeutique (359). La capacité des cellules tumorales invasives à remodeler la MEC est aujourd'hui bien connue et cette dernière montre une implication dans un nombre croissant de cancers.

c) L'hypoxie et la MEC : deux alliés dans la progression métastatique ?

Bien que considérés pendant longtemps comme des contributeurs indépendants de la progression métastatique, l'émergence de nouvelles données suggère une implication collaborative majeure de l'hypoxie et de la MEC dans la formation de métastases. L'hypoxie agirait directement sur la composition et l'organisation de la MEC, notamment en stimulant le recrutement de composants des cellules stromales du microenvironnement tumoral (360,361). Plusieurs signaux microenvironnementaux pourraient influencer de manière synergique l'issue métastatique. La matrice ainsi remodelée dans les régions hypoxiques intratumorales pourrait constituer un atout pour les métastases cancéreuses (362–365). Certaines cibles de l'hypoxie étroitement liées à la MEC sont d'ailleurs considérées comme des marqueurs de mauvais pronostic dans de nombreux cancers (cancer colorectal, RCC, cancer du sein, cancer de la prostate, cancer de l'estomac, cancer du pancréas). Ainsi, l'hypoxie induit la surexpression des enzymes appartenant à la famille des LOX, ayant pour conséquence l'augmentation du nombre de liaisons covalentes des fibres de collagènes qui se déposent autour de la tumeur. Ces modifications entrainent une modification topographique de la MEC, résultant en un microenvironnement tumoral particulièrement rigide et donc propice à l'invasion tumorale (366). Les composants de la MEC peuvent alors jouer un rôle chimio-attractif, en stimulant le recrutement de cellules immunitaires. L'infiltration des macrophages est notamment facilitée par la topographie des fibres de collagène I (367). L'hypoxie est également responsable de l'induction de facteurs de croissance dans la tumeur

primaire, favorisant l'accumulation de macrophages. Les macrophages répondent alors rapidement au microenvironnement hypoxique en modifiant leurs patrons d'expression génique (368–370). Dans un contexte hypoxique, les macrophages produisent et sécrètent des molécules bioactives, tels que des facteurs de croissance et des facteurs pro-angiogéniques (TGFα, TGFβ1, VEGF, FGF, PDGF, TNFα, IL-1 et IL-8), qui peuvent à leur tour stimuler le recrutement d'autres macrophages et de cellules mésenchymateuses supplémentaires, tels que les fibroblastes et les cellules endothéliales (371). Ainsi, les macrophages favorisent l'angiogenèse et le processus d'intravasation des cellules cancéreuses dans les vaisseaux sanguins voisins (372). Enfin, les macrophages sécrètent également des MMPs, contribuant au renouvellement de la MEC (371). L'inflammation peut donc conférer un avantage pour la tumeur en facilitant l'angiogenèse, l'invasion et la formation de métastases (314). L'ensemble de ces données soutiennent donc un rôle majeur de la signalisation hypoxique dans le remodelage de la MEC (Figure 23).

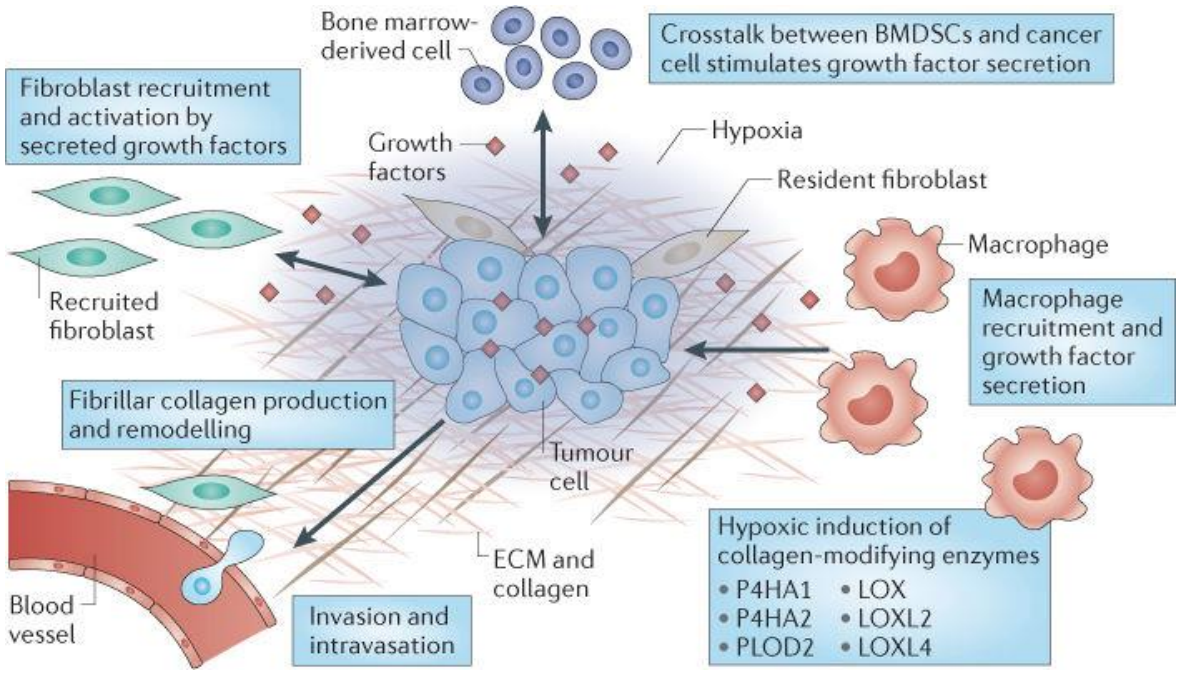

Figure 23 : L'hypoxie favorise le recrutement de cellules du microenvironnement induisant la synthèse de collagènes fibrillaires. *D'après (349)*

8) Oncogenèse liée à la perte de la sous-unité SDHB

La progression métastatique repose sur la capacité des cellules tumorales à migrer hors du foyer primaire en traversant la barrière formée par la MEC pour accéder à la circulation sanguine, afin de coloniser un foyer secondaire à distance et d'établir ainsi des métastases (373). Pour devenir cancéreuse, une cellule doit donc acquérir de nombreuses propriétés oncogéniques, telles que des capacités de prolifération, de migration, d'adhésion et d'invasion (Figure 24). Comme évoqué précédemment, les tumeurs *SDHB*-dépendantes sont particulièrement associées à des formes métastatiques de PPGL (72,126) et l'origine de cette agressivité constitue une question majeure dans le domaine.

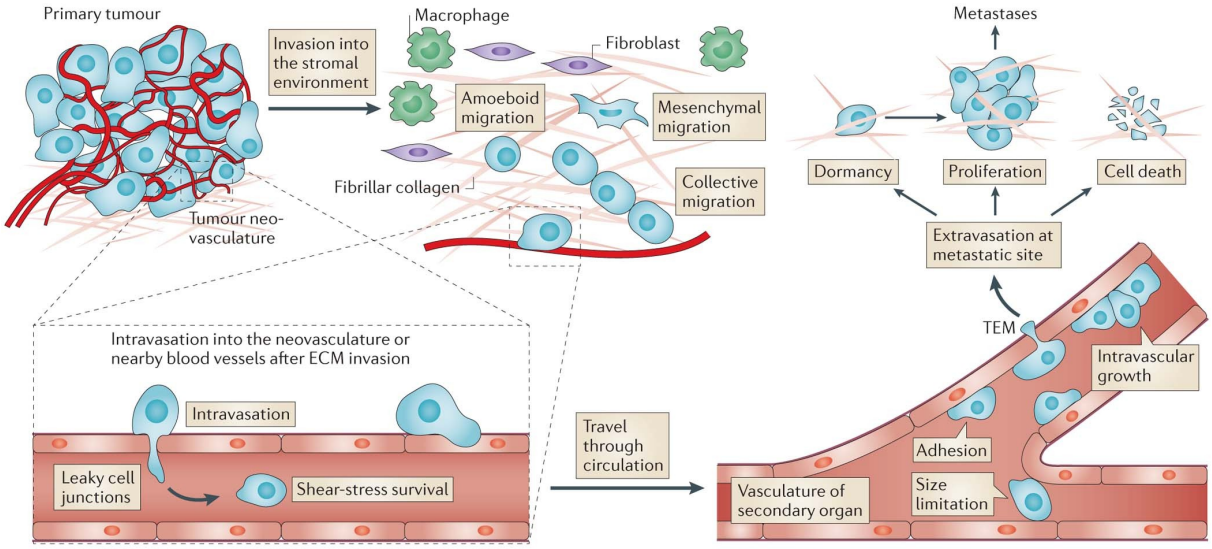

Figure 24 : Les différentes étapes nécessaires à la dissémination métastatique. *Adapté de (374)*

Au cours des dix dernières années, plusieurs études ont tenté d'élucider les mécanismes d'oncogenèse liés à la perte de la sous-unité SDHB. En raison de son rôle central dans la tumorigenèse SDH-dépendante, le succinate a longtemps été considérée comme le principal élément déclencheur de la tumorigenèse des PPGL. Il a d'abord été suggéré que des niveaux de succinate plus élevés résultant d'une inactivation plus complète de la SDH en fonction des différentes mutations *SDHx,* pourraient expliquer les différentes présentations cliniques observées (375,376).

L'Analyse ciblée du transcriptome a ensuite permis pour la première fois, de différencier les tumeurs avec une mutation *SDHB* des autres tumeurs *SDHx* (Figure 25). Mon équipe d'accueil

a mis en évidence l'activation d'un processus rappelant l'EMT et donc nommée transition neuroendocrino-mésenchymateuse (NMT), au sein des PPGL métastatiques *SDHB*-dépendants qui n'était pas retrouvé dans les autres types de mutations *SDHx* (377).

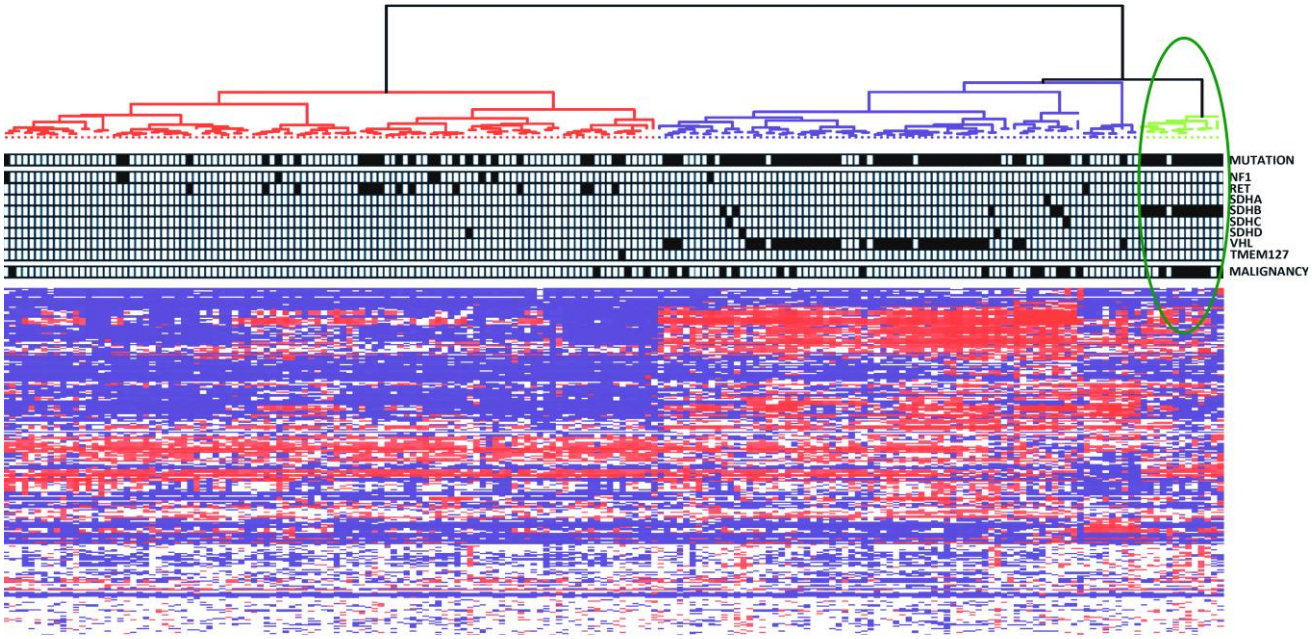

Figure 25 : Analyse de clustering hiérarchique non supervisée de 188 échantillons selon l'expression de 94 gènes impliqués dans la voie de l'EMT. *Les profils d'expression sont présentés sous forme de carte thermique indiquant une expression élevée (rouge) et faible (bleue) selon une échelle transformée en log2. La partition la plus élevée permet de distinguer tous les PPGL métastatiques SDHB de tous les autres patients. D'après (377)*

Cette étude a également permis de montrer que la surexpression de certains marqueurs de l'EMT, tels que *LOXL2* et *TWIST1,* ainsi que la translocation nucléaire de SNAI1 étaient spécifiquement associés aux PPGL métastatiques *SDHB*-dépendants. L'EMT est un processus physiologique essentiel au développement embryonnaire, permettant la différenciation et la migration de cellules épithéliales en cellules mésenchymateuses. Ainsi, ce terme est également associé à la capacité à changer de phénotype et à migrer qu'ont certaines cellules à l'âge adulte, pouvant avoir lieu dans un contexte physiologique (cicatrisation, régénération tissulaire...) ou pathologique (développement tumoral, fibrose...) (378). Dans un contexte pathologique de développement tumoral, l'EMT se caractérise par l'expression de protéines impliquées dans l'adhésion cellulaire, au détriment des jonctions cellulaires, et permet donc l'interaction des cellules avec la matrice extracellulaire. Ces interactions pouvant être impliqués dans la croissance tumorale et l'induction des processus métastatiques.

Suite à l'identification de cette signature transcriptomique particulière, l'étude du méthylome a permis une avancée supplémentaire dans l'identification de spécificités génomiques liées à la perte de la sous-unité SDHB. En effet, cette classification a montré que ce phénotype hyperméthylateur était particulièrement accentué dans les tumeurs *SDHB*-dépendantes par rapport aux autres sous-types de tumeurs déficientes en SDH (Figure 26).

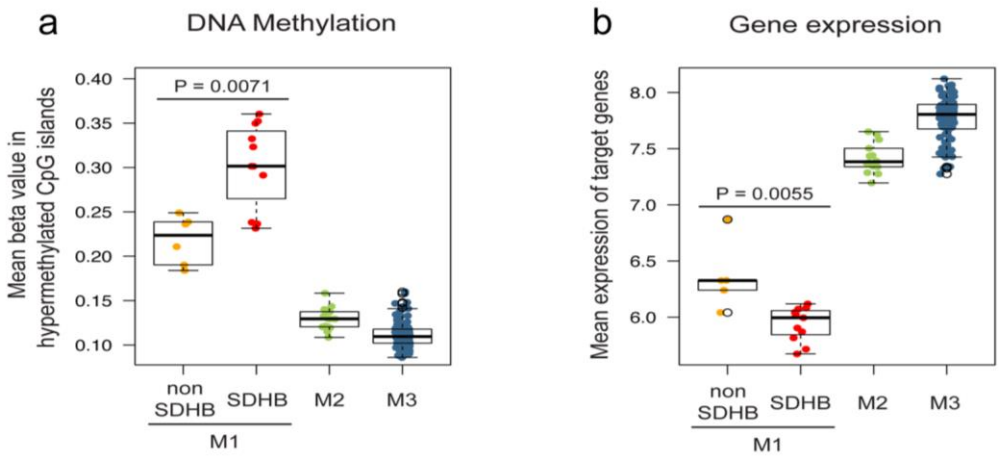

Figure 26 : Phénotype hyperméthylateur particulièrement sévère des tumeurs mutées SDHB. *(a) Méthylation moyenne de toutes les sondes d'îlots CpG significativement hyperméthylées dans les tumeurs M1, selon le sous-groupe des tumeurs. Les tumeurs M1 sont séparées en tumeurs SDHB mutées et SDHB de type sauvage. (b) Expression moyenne des gènes significativement hyperméthylés et sous-exprimés dans les tumeurs M1, selon le sous-groupe des tumeurs. D'après (160)*

Ces résultats suggèrent le rôle de la reprogrammation épigénétique dans l'acquisition des capacités métastatiques des tumeurs mutées sur *SDHB*. Cette étude a également permis de mettre en lumière une corrélation entre le phénotype « super-hyperméthylateur » des PPGL *SDHB*-dépendants et l'activation de l'EMT observée dans ces tumeurs. Ainsi l'hyperméthylation de plusieurs gènes codant pour des marqueurs de l'EMT, tel que *KRT19*, a été démontrée et suggère une contribution de la méthylation dans l'activation du processus d'EMT observé dans les PPGL métastatiques liés à SDHB (377).

Mon équipe d'accueil a ensuite généré le premier modèle de cellules chromaffines murines immortalisées (ou imCC pour « immortalized mouse chromaffin cells »), invalidé pour le gène *Sdhb* par la méthode Cre/Lox et présentant une inactivation complète de la SDH. Ces cellules récapitulaient les caractéristiques retrouvées au sein des tumeurs SDHB-dépendantes (hyperméthylation globale de l'ADN plus élevée en comparaison aux cellules contrôles imCCs

Wild-Type (WT), propriétés adhésives et migratoires accrues). L'obtention de ce modèle a permis d'approfondir les études précédentes et de démontrer que les capacités migratoires accrues des imCC *Sdhb* KO étaient réprimées par un traitement à la décitabine (DAC). Ces résultats ont permis d'établir un premier lien fonctionnel entre le déficit en SDH, la méthylation et la NMT. Cette découverte suggère que l'intérêt de thérapies ciblant les voies épigénétiques pour le traitement des PPGL métastatiques liés à SDHB (113).

L'ensemble de ces observations constitue des progrès majeurs dans la compréhension des conséquences oncogéniques de la perte de fonction de SDHB. Néanmoins, la cause exacte du phénotype métastatique et particulièrement agressif associé aux mutations *SDHB* demeurait essentiellement inexpliqué au début de mon travail de thèse. Déceler l'origine de ce phénotype constitue donc une question cruciale, non résolue depuis près de 20 ans. Elle pourrait avoir un impact considérable sur la compréhension de la biologie mitochondriale, ainsi que sur la prise en charge des patients.

OBJECTIFS ET PRESENTATION DU TRAVAIL DE THESE

OBJECTIFS ET PRESENTATION DU TRAVAIL DE THESE

Bien qu'ils soient bénins la plupart du temps, les paragangliomes et phéochromocytomes (PPGL) subissent une transformation métastatique dans environ 15% des cas. Néanmoins, il n'existe toujours pas de critère anatomopathologique fiable de prédiction de malignité lors de l'examen histologique de la tumeur primaire et la seule approche thérapeutique efficace à ce jour reste l'ablation chirurgicale de la tumeur, qui peut causer de nombreuses complications, comme évoqué précédemment. Ainsi, les PPGL posent de difficiles problèmes de diagnostic, de pronostic, de traitement et de surveillance à long terme. Toutefois, mon équipe d'accueil a montré que la présence d'une mutation sur le gène *SDHB* constituait un facteur de risque de progression métastatique et de mauvais pronostic.

Mon équipe d'accueil est un membre actif du réseau COMETE, qui collecte depuis 1993 les histoires cliniques, l'ADN et les tumeurs (congelées et inclues en paraffine) de patients atteints de PPGL pris en charge dans l'Unité d'HTA de l'HEGP (Pr Plouin) et dans le service d'Endocrinologie de l'Hôpital Cochin (Pr Bertagna, puis Pr Bertherat). Grâce à cette collection unique de tumeurs surrénaliennes et de PGL, elle a pu intégrer le programme **Carte d'Identité des Tumeurs (CIT)** mené par la Ligue Nationale contre le Cancer, qui avait pour but de réaliser la cartographie génomique précise et intégrée des cancers. Une collection de 202 PGL/PCC a ainsi été étudiée en utilisant différentes plateformes du CIT, qui ont permis de générer : des données de **transcriptome** (*Affymetrix GeneChip® HG U133 Plus 2.0HG*), la cartographie fine des **pertes et des gains chromosomiques** (*BAC array CGH* et *SNP-array Illumina*), le **méthylome** (*Illumina Infinium HumanMethylation27 et 450 BeadChips*) et le **miRNome** (*HiSeq sequencing, Illumina*). Ces données ont été analysées en collaboration étroite avec les bioinformaticiens de l'Équipe CIT.

Ces travaux antérieurs de mon équipe ont ainsi montré que les tumeurs *SDHB* métastatiques présentaient un phénotype moléculaire rappelant la transition épithélio-mésenchymateuse (EMT), associé à l'augmentation des capacités migratoires, invasives et adhésives des cellules. Un taux de méthylation de l'ADN significativement accru a été observé dans les tumeurs avec mutation *SDHB* versus celles avec d'autres mutations *SDHx*, ce qui pourrait également participer aux modifications phénotypiques associées aux mutations *SDHB*. Néanmoins, les causes exactes de la malignité SDHB-dépendante demeuraient globalement inexpliquées au

début de mon travail de thèse (2016). Déceler l'origine de ce phénotype métastatique constitue donc une question cruciale, non résolue, depuis près de 20 ans.

Dans ce contexte, l'objectif de mon projet de thèse était d'étudier et de comparer des modèles de cellules chromaffines murines (imCC) porteuses d'inactivation des gènes *Sdhb* et *Sdhd*, générés au laboratoire par les techniques Cre-Lox et CrispR-Cas9 respectivement. J'ai donc tenté de répondre à cette difficile question au cours de mon travail de thèse, qui s'est articulé autour de trois axes principaux.

Dans une première partie, j'ai participé à l'étude des mécanismes expliquant l'hyperméthylation plus importante observée dans l'ADN des PPGL SDHB-dépendants, ainsi que l'impact de celle-ci dans la tumorigenèse associée aux mutations *SDHB.* Nous avons procédé à l'analyse de la distribution de la 5-méthylcytosine et de la 5-hydroxyméthylcytosine à l'échelle du génome dans les tumeurs mutés *SDHB* et dans les cellules imCC *Sdhb-/-*. Nous avons également étudié la corrélation de l'hyperméthylation avec les niveaux d'expression génique dans ces deux modèles. Nous avons ainsi montré dans les imCC *Sdhb-/-,* qu'un déficit en Sdhb favorise un phénotype hyperméthylateur marqué, médié par la perte d'activité des enzymes TET, agissant en synergie avec l'activation de HIF2 pour favoriser l'acquisition de traits métastatiques. Cette étude fait l'objet du premier article présenté dans mon manuscrit de thèse, publié en mars 2020 dans la revue *Cell Reports,* que je signe en deuxième auteure.

Par la suite, grâce à la disponibilité au laboratoire d'une nouvelle lignée de cellules chromaffines murines invalidée pour le gène *Sdhd*, j'ai pu procéder à des études de caractérisation et de comparaison des différents modèles d'imCCs (WT, *Sdhb-/-* et *Sdhd-/-)*, notamment par l'utilisation d'approches Omics (métabolome, transcriptome, méthylome), dans le but de mettre en évidence les différents mécanismes spécifiques aux mutations *Sdhb*, qui expliqueraient ainsi le phénotype métastatique particulièrement associé à ces mutations. Ces travaux m'ont permis de valider la pertinence de ce nouveau modèle cellulaire, qui récapitule l'ensemble du phénotype des tumeurs humaines porteuses de mutations du gène *SDHD.* Grâce à ces études comparatives j'ai ensuite pu mettre en évidence plusieurs mécanismes impliqués uniquement, ou de façon plus marquée, dans les imCC *Sdhb-/-,* expliquant ainsi l'agressivité particulière associée à ces mutations : une inhibition plus forte des PHD et des TET et un déséquilibre dans l'homéostasie du cuivre et du fer

considérablement exacerbé, associé à une augmentation du stress oxydant. Cette étude nous a également permis de mettre en lumière l'intérêt prometteur de l'ascorbate à forte dose, pour traiter les formes agressives de PPGL SDHB-dépendants. Ces résultats ont donné lieu à un article actuellement en révision dans la revue *Cancer Research* dont je suis la première auteure.

Enfin, la deuxième partie de ma thèse a consisté en la caractérisation de la matrice extracellulaire (MEC) sécrétée *in vitro* par les différentes lignées d'imCCs (WT, *Sdhb-/-* et *Sdhd-/-),* par des études du matrisome de chacun de ces modèles cellulaires. Nous avons ainsi pu corréler les données obtenues avec les données transcriptomiques des imCCs. Ces travaux nous ont permis de mettre en évidence l'implication de la MEC dans l'acquisition du phénotype métastatique des imCC *Sdhb-/-*, grâce à la réalisation de tests fonctionnels montrant que la MEC sécrétée par ces cellules est capable d'induire l'adhésion et la migration cellulaire contrairement à la MEC produite par les imCCs WT et *Sdhd-/-*. Au cours de cette étude, j'ai également pu mettre en évidence que la MEC des cellules *Sdhd* KO était même à l'inverse, particulièrement appauvrie, soulignant ainsi la spécificité du remodelage de la MEC observé dans les imCC *Sdhb-/-* et l'implication de celle-ci dans l'acquisition du phénotype métastatique. *Ces résultats font l'objet d'un troisième article actuellement en préparation, que je signe en co-premier auteure.*

CHAPITRE 1

Impact de l'hyperméthylation sur le phénotype métastatique des PPGL SDHB-dépendants

CONTEXTE

Mon équipe d'accueil a décrit que les tumeurs avec une mutation sur le gène *SDHB* étaient associées à un phénotype hyperméthylateur particulièrement marqué, ainsi qu'à des caractéristiques transcriptomiques, morphologiques et phénotypiques de transition neuroendocrino-mésenchymateuse (NMT) telles que la surexpression de SNAIL ou TWIST, et l'augmentation des capacités migratoires, invasives et adhésives des cellules. Ces caractéristiques n'étant pas retrouvées dans des PPGL mutés sur d'autres gènes *SDHx* (*SDHA, SDHC et SDHD*).

Cette étude princeps d'analyse du méthylome avait été réalisée grâce à l'utilisation de puces à méthylation dans la cohorte de PPGL du réseau Français COMETE et par séquençage au bisulfite à représentation réduite (RRBS) dans un modèle unique de cellules chromaffines murines spontanément immortalisées (imCC) avec knockout (KO) complet du gène *Sdhb*, généré par Cre-Lox. Les expériences réalisées *in vitro* suggéraient que le mécanisme associé à l'hyperméthylation pouvait être une inhibition par le succinate des TET déméthylases, responsables de l'hydroxylation des cytosines méthylées (5mC) en cytosines hydroxyméthylées (5hmC). Cette hypothèse, bien que probable, n'avait pas été véritablement démontrée car les techniques de séquençage au bisulfite ne permettent pas de dissocier les bases 5mC des 5hmC. De même, la participation de ce phénotype hyperméthylé à l'acquisition des caractéristiques mésenchymateuses des cellules n'avait pas été démontrée. L'objectif de ce projet était donc de s'attaquer à ces deux questions fondamentales.

TRAVAUX PERSONNELS

Pour approfondir l'étude de la méthylation et de l'hydroxyméthylation de l'ADN dans les tumeurs et le modèle cellulaire *Sdhb-/-,* différentes techniques ont été utilisées : le séquençage par immunoprécipitation d'ADN méthylé (meDIP-seq) ou hydroxyméthylé (hmeDIP-seq) ainsi que la technique de RRBS oxydatif (oxRRBS). Ces approches ont été mises en place par Aurélie Morin, post-doctorante au laboratoire. Des études fonctionnelles ont ensuite été réalisées après avoir généré de nouvelles lignées d'imCC, porteuses d'un knock-down des enzymes TET 1 et 2 dans les cellules sauvages (WT), ou des facteurs HIF2a et HIF1a dans les cellules *Sdhb-/-.* Dans ces cellules, nous avons étudié la méthylation de l'ADN (par

ELISA et RRBS), mais aussi l'impact de l'hypoxie chronique, et les modifications phénotypiques associées à la NMT.

J'ai personnellement contribué à cette étude en participant au traitement sur le long terme (jusqu'à 7 passages) des différentes lignées d'imCC avec du GSK343, un inhibiteur spécifique de PRC2, ainsi qu'à la préparation des échantillons traités pour les analyses subséquentes. J'ai également aidé à l'optimisation des conditions et à la mise en hypoxie des cellules, ainsi qu'à la préparation des échantillons pour les expériences de RRBS réalisées ensuite par les plateformes Integragen. Enfin, j'ai participé aux études fonctionnelles sur ces lignées en effectuant des tests de prolifération, d'adhésion et de migration.

Ce travail a fait l'objet du premier article de ma thèse, publié au mois de mars 2020 dans la revue *Cell Reports.*

ARTICLE 1

TET-mediated hypermethylation primes SDH-deficient cells for HIF2α-driven mesenchymal transition

Aurélie Morin, Judith Goncalves, Sophie Moog, Luis-Jaime Castro-Vega, Sylvie Job, Alexandre Buffet, Marie-Joséphine Fontenille, Justine Woszczyk, Anne-Paule Gimenez-Roqueplo, Eric Letouzé, Judith Favier

Cell Rep. 2020 Mar 31;30(13):4551-4566.e7.

Article

Cell Reports

TET-Mediated Hypermethylation Primes SDH-Deficient Cells for HIF2α-Driven Mesenchymal Transition

Graphical Abstract

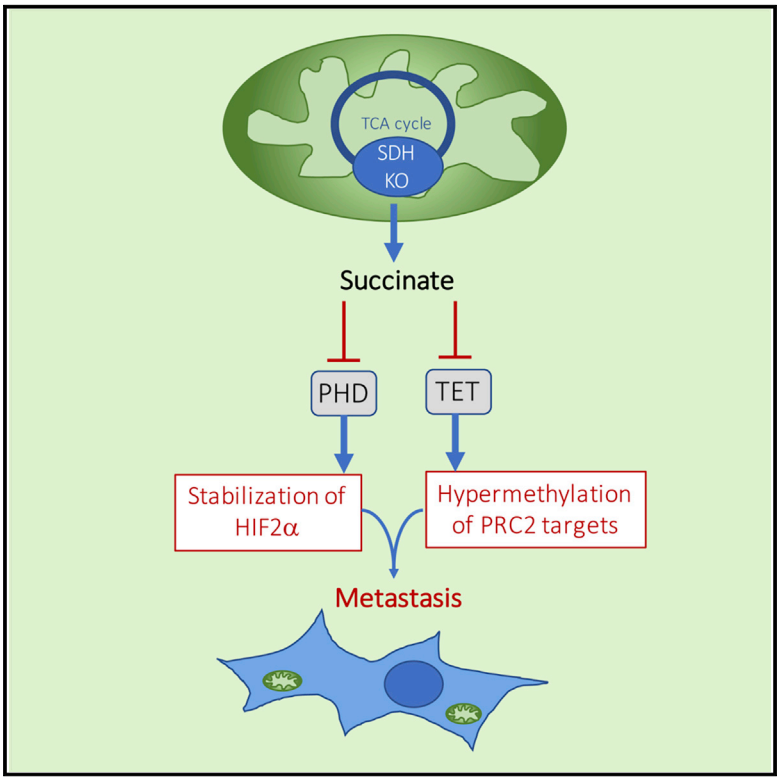

Authors

Aurélie Morin, Judith Goncalves, Sophie Moog, ..., Anne-Paule Gimenez-Roqueplo, Eric Letouzé, Judith Favier

Correspondence

judith.favier@inserm.fr

In Brief

Morin et al. investigate the hypermethylator phenotype of SDHB-deficient human paragangliomas and *Sdhb*$^{-/-}$ mouse cells and its link with metastatic hallmark acquisition. They reveal synergy between TET-mediated hypermethylation and pseudohypoxia that drives transition of *SDHB*-mutated tumors toward metastasis, providing a rationale for targeting HIF2α and DNA methylation in SDH-associated malignancies.

Highlights

- SDHB-mutated tumors and cells show low hydroxymethylation
- Hypermethylation in SDHB-mutated tumors preferentially affects PRC2 target genes
- TET knockdown recapitulates the hypermethylated phenotype of SDHB-deficient cells
- Combining TET inhibition and HIF2 activation mimics the SDHB metastatic phenotype

Morin et al., 2020, Cell Reports *30*, 4551–4566
March 31, 2020
https://doi.org/10.1016/j.celrep.2020.03.022

CellPress

Cell Reports
Article

TET-Mediated Hypermethylation Primes SDH-Deficient Cells for HIF2α-Driven Mesenchymal Transition

Aurélie Morin,[1] Judith Goncalves,[1] Sophie Moog,[1] Luis-Jaime Castro-Vega,[1] Sylvie Job,[2] Alexandre Buffet,[1,3] Marie-Joséphine Fontenille,[1] Justine Woszczyk,[1] Anne-Paule Gimenez-Roqueplo,[1,3] Eric Letouzé,[4,5] and Judith Favier[1,5,6,*]

[1]Université de Paris, PARCC, INSERM, Equipe Labellisée par la Ligue contre le Cancer, 75015 Paris, France
[2]Programme Cartes d'Identité des Tumeurs, Ligue Nationale Contre Le Cancer, 75013 Paris, France
[3]Department of Genetics, Assistance Publique-Hôpitaux de Paris, Hôpital Européen Georges Pompidou, 75015 Paris, France
[4]Functional Genomics of Solid Tumors Laboratory, Centre de Recherche des Cordeliers, Université de Paris, INSERM, 75006 Paris, France
[5]Senior author
[6]Lead Contact
*Correspondence: judith.favier@inserm.fr
https://doi.org/10.1016/j.celrep.2020.03.022

SUMMARY

Loss-of-function mutations in the SDHB subunit of succinate dehydrogenase predispose patients to aggressive tumors characterized by pseudohypoxic and hypermethylator phenotypes. The mechanisms leading to DNA hypermethylation and its contribution to SDH-deficient cancers remain undemonstrated. We examine the genome-wide distribution of 5-methylcytosine and 5-hydroxymethylcytosine and their correlation with RNA expression in SDHB-deficient tumors and murine *Sdhb*$^{-/-}$ cells. We report that DNA hypermethylation results from TET inhibition. Although it preferentially affects PRC2 targets and known developmental genes, PRC2 activity does not contribute to the DNA hypermethylator phenotype. We also prove, *in vitro* and *in vivo*, that TET silencing, although recapitulating the methylation profile of *Sdhb*$^{-/-}$ cells, is not sufficient to drive their EMT-like phenotype, which requires additional HIF2α activation. Altogether, our findings reveal synergistic roles of TET repression and pseudohypoxia in the acquisition of metastatic traits, providing a rationale for targeting HIF2α and DNA methylation in SDH-associated malignancies.

INTRODUCTION

Succinate dehydrogenase (SDH) is the mitochondrial enzyme that catalyzes oxidation of succinate into fumarate in the tricarboxylic acid (TCA) cycle. It consists of 4 subunits encoded by the *SDHA*, *SDHB*, *SDHC*, and *SDHD* (*SDHx*) genes. Germline mutations in one of these genes predispose to pheochromocytoma and paraganglioma (PPGL), rare neuroendocrine tumors that arise in the adrenal medulla and the parasympathetic or sympathetic nervous systems, respectively. Notably, mutations in the *SDHB* gene are associated with increased risk of metastatic disease (Gimenez-Roqueplo et al., 2003) and poor prognosis (Amar et al., 2007).

Mutations affecting other TCA cycle enzymes, such as fumarate hydratase (germline mutations on *FH*) and isocitrate dehydrogenase (somatic mutations on *IDH1* or *IDH2*) are found, although infrequently, in PPGL (Castro-Vega et al., 2014; Clark et al., 2014) and often lead to other forms of cancer (Morin et al., 2014).

Mechanistically, mutations affecting SDH, fumarate hydratase (FH), or isocitrate dehydrogenase (IDH) enzymes induce accumulation of oncometabolites (succinate, fumarate, and (R)-2-hydroxyglutarate, respectively), which inhibits 2-oxoglutarate (2-OG)-dependent dioxygenases such as hypoxia-inducible factors (HIF) prolyl-hydroxylases (PHDs); ten-eleven translocation (TET) dioxygenases that hydroxylate DNA-methylated cytosines (5-methylcytosine [5mC]) into 5-hydroxymethylcytosine (5hmC), and JmjC domain-containing histone lysine demethylases (KDM). Nevertheless, the affinity of each oncometabolite for these various dioxygenases varies greatly (Rose et al., 2011), and the specific contributions of these impaired enzymatic activities in the tumor phenotype remain undetermined.

PHD inhibition results in pseudohypoxia; i.e., abnormal stabilization of HIF1α and/or HIF2α transcription factors and subsequent expression of hypoxia-inducible genes, even in normoxia. It was the first discovered oncometabolite-induced pathway. Because tumor hypoxia is a known inducer of epithelial-to-mesenchymal transition (EMT), cancer stem cell phenotypes, and metastases (Marie-Egyptienne et al., 2013), pseudohypoxia has long been considered a driver mechanism in the invasive and metastatic behavior of oncometabolite-driven tumors.

KDM and TET enzymes are involved in epigenetic regulation, which is altered in most cancers. For example, global DNA hypomethylation and specific promoter CpG island hypermethylation are hallmarks of cancer. In particular, polycomb repressive complex 2 (PRC2) targets are highly prone to cancer-specific hypermethylation (Ohm et al., 2007;

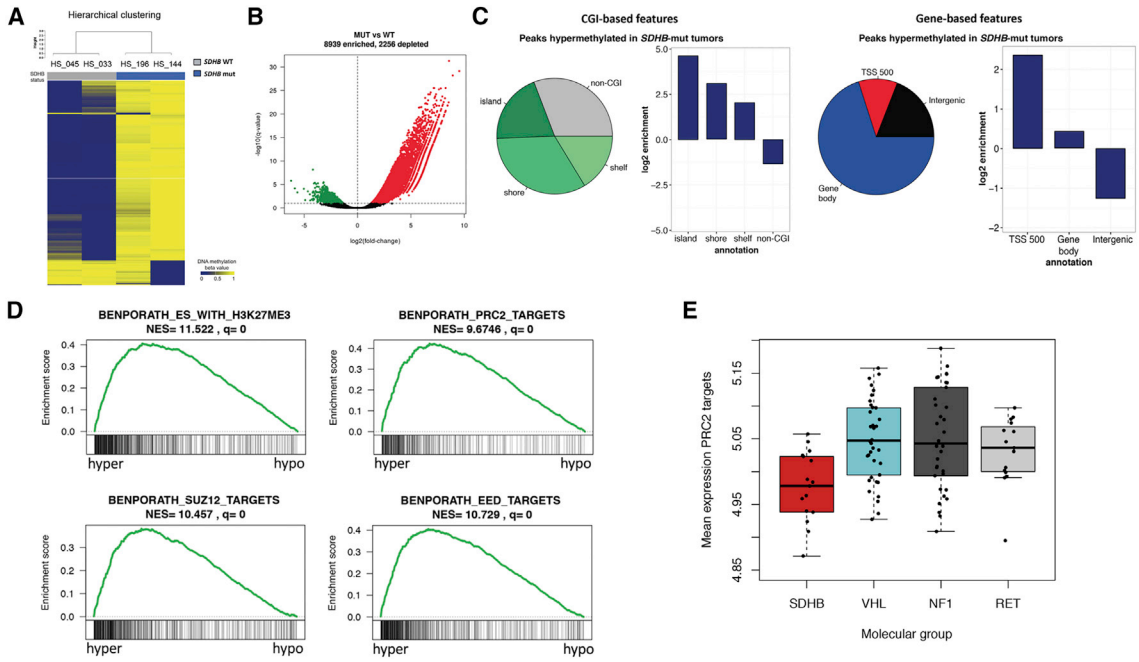

Figure 1. MeDIP-Seq Analysis of DNA Methylation in *SDHB*-mut Tumors Identifies Enrichment in PRC2 Targets

(A) Hierarchical clustering of the tumors based on methylation of the 1,000 most variant peaks.

(B) Volcano plot indicating the number of differentially methylated peaks between *SDHB*-mut and *SDHB*-wild-type (WT) PPGL.

(C) Preferential location of hypermethylated peaks in *SDHB*-mut versus *SDHB*-WT tumors and segregation in CGI-based or gene-based features.

(D) Hypermethylated peaks in *SDHB*-mut versus *SDHB*-WT tumors (identified by meDIP-seq) are strongly enriched in genes marked by H3K27me3 or targeted by SUZ12, EED, or PRC2 in ESCs (gene sets described by Ben-Porath et al. 2008). The gene set called "PRC2_targets" is composed of genes that possess the H3K27me3 mark at their promoters and are bound by SUZ12 and EED Polycomb proteins in ESCs. A description of genomic features used to analyze meDIP-seq is provided in Figure S1.

(E) Microarray-based analysis of expression of PRC2 targets in a cohort of 113 genetically determined PPGL tumors described in Letouzé et al. (2013). Middle bar, median; box, interquartile range; bars extend to 1.5 times the interquartile range.

See also Figure S1.

Schlesinger et al., 2007). PRC2 is a transcriptionally repressing complex catalyzing tri-methylation of lysine 27 of histone H3 (H3K27me3). In embryonic stem cells (ESCs), it is involved in repression of poised developmental genes (Lee et al., 2006). The PRC2 complex can also recruit the DNA methyltransferases DNMT1 and DNMT3a to its target genes (Viré et al., 2006) and has been implicated in DNA hypermethylation in cancers not driven by oncometabolites (Ohm et al., 2007; Schlesinger et al., 2007). Several studies have suggested a link between TET and PRC2 (Haffner et al., 2013; Putiri et al., 2014; Verma et al., 2018), but it remains unexplored whether PRC2 participates in DNA methylation in oncometabolites-driven tumors.

The role of TET enzymes in shaping the DNA methylome of such tumors has been partially investigated. Several groups, including ours, studied the methylome of oncometabolite-driven tumors and reported enhanced DNA methylation in (Killian et al., 2013; Letouzé et al., 2013; Lu et al., 2013) and outside CpG islands (Killian et al., 2013; Letouzé et al., 2013). However, these studies were performed using methylome arrays or reduced-representation bisulfite sequencing (enrichment in CG-rich regions), and no genome-wide, unbiased method has been used so far. Besides, the classical bisulfite conversion used in these studies is not able to distinguish 5mC from 5hmC. Global 5hmC levels in these tumors were measured using immunolabeling (Figueroa et al., 2010; Killian et al., 2013; Letouzé et al., 2013; Xiao et al., 2012), fluorescence-activated cell sorting (FACS) (Figueroa et al., 2010; Turcan et al., 2012), or dot blot (Xiao et al., 2012). These experiments showed a reduction in global levels of 5hmC that parallels the increased 5mC levels. Rampal et al. (2014) reported, in the first study published so far regarding oncometabolite-driven tumors, the genome-wide 5mC and 5hmC patterns in *TET2, WT1*, and *IDH*-mutated acute myeloid leukemia but did not assess the correlation between 5mC and 5hmC in these tumors.

In the present study, we analyze DNA methylation and hydroxymethylation along the genome in SDHB-deficient tumors. We used a tractable cellular model that recapitulates most of the phenotypic characteristics of *SDHB*-mutated tumors to determine how the pattern of hypermethylation and related transcriptional changes are established. We also provide evidence that pseudohypoxia cooperates with hypermethylation in inducing an EMT-like phenotype, suggesting synergistic requirements for tumor initiation and progression of aggressive *SDHB*-mutated tumors.

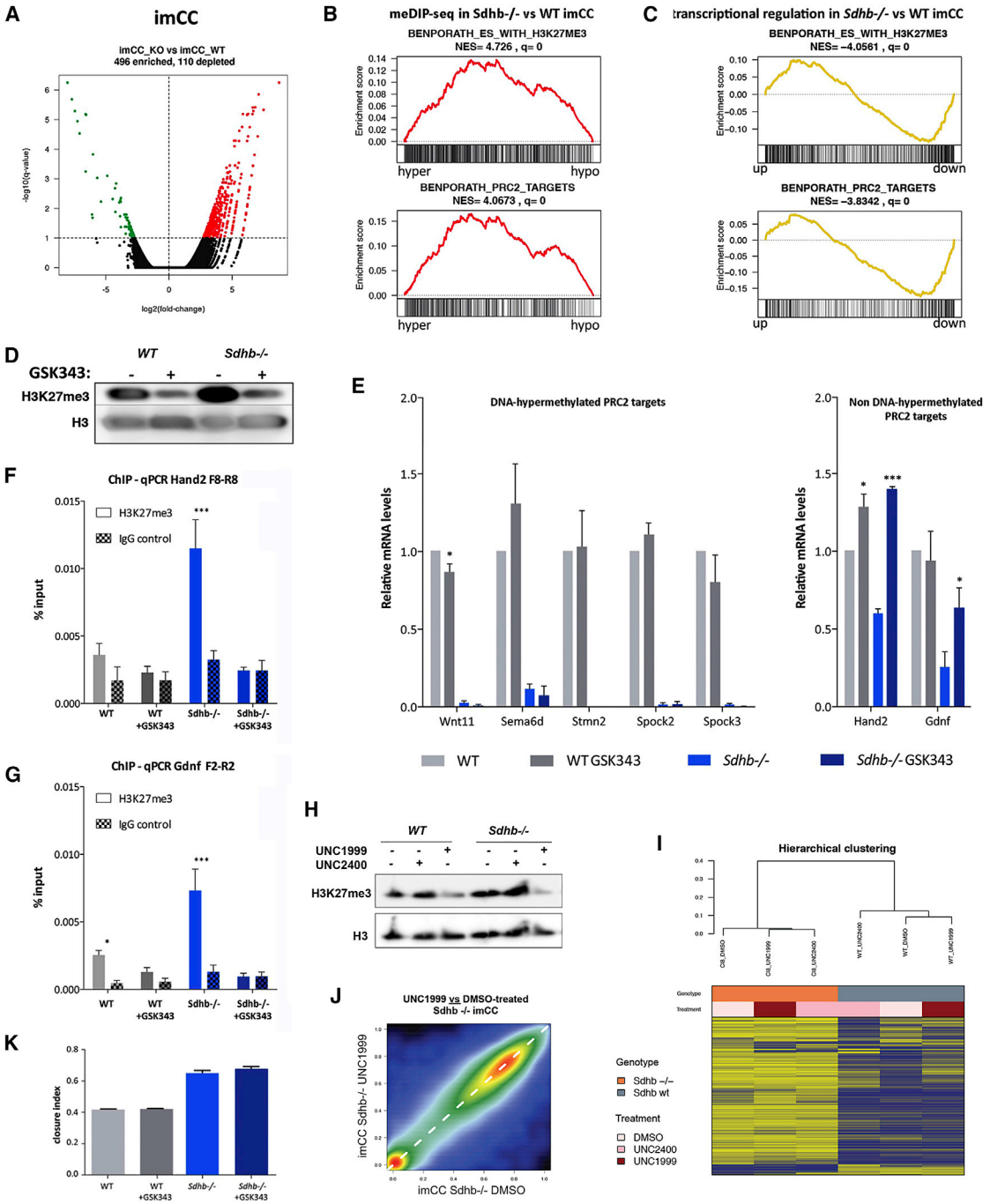

Figure 2. PRC2 Targets Are Enriched among Hypermethylated and Downregulated Genes in *Sdhb*$^{-/-}$ versus Wild-type (WT) imCCs, but PRC2 Inhibition Does Not Alter the DNA Methylation or Cell Phenotype of *Sdhb*$^{-/-}$ imCCs

(A) Volcano plot indicating the number of differentially methylated peaks between *Sdhb*$^{-/-}$ and *Sdhb*-WT imCCs.

(B) Hypermethylated peaks in *Sdhb*$^{-/-}$ compared with *Sdhb* WT imCCs (identified by meDIP-seq) are strongly enriched in genes marked by H3K27me3 or targeted by PRC2 in ESCs.

(C) Downregulated genes in *Sdhb*$^{-/-}$ compared with *Sdhb*-WT imCCs (identified in RNA sequencing [RNA-seq] data) are enriched in genes marked by H3K27me3 or targeted by PRC2 in ESCs.

(D) Inhibition of trimethylation of H3K27 by the PRC2 inhibitor GSK343 (3 μM).

(E) qRT-PCR dosage of known PRC2 targets (DNA hypermethylated or not in *Sdhb*$^{-/-}$ imCCs) in cells treated with GSK343 for 5–7 passages.

(legend continued on next page)

RESULTS

Genome-wide DNA Methylation and the PRC2 Pathway in SDHB-Deficient Tumors and Cells

Using methylation arrays and reduced-representation bisulfite sequencing (RRBS), we have previously described a hypermethylator phenotype in tumors carrying an *SDHx* mutation and in spontaneously immortalized mouse chromaffin cells (imCCs) with complete *Sdhb* knockout (Letouzé et al., 2013). To further investigate DNA methylation patterns using an un-biased and genome-wide method, we used methylated DNA Immunoprecipitation sequencing (meDIP-seq) in human PPGL carrying or not carrying *SDHB* mutations. As expected, we found strong DNA hypermethylation (80% of differentially methylated peaks) in *SDHB*-mutated (*SDHB*-mut) compared with *SDHB* wild-type (WT) tumors (Figures 1A and 1B). Hypermethylated peaks were more frequent at CpG islands (CGIs) and promoters (defined as 500 bp before and after the transcription start sites [TSSs] and hereafter referred to as TSS 500), but they were also detectable in the rest of the genome (Figures 1C and S1A).

Gene set analysis of hypermethylated genes in *SDHB*-mut tumors revealed strong enrichment in genes deregulated in cancer and in genes encoding proteins involved in pluripotency or development. The most significantly enriched sets of genes were polycomb targets and genes marked by H3K27me3 in ESCs and neural precursor cells (Figure 1D; Table S1). A heatmap of DNA methylation, established from the methylome array data from the French COMETE (COrtico et MEdullo-surrénale, les Tumeurs Endocrines) cohort (4 non-tumoral samples and 145 PPGL samples) (Letouzé et al., 2013) and restricted to the gene set BENPORATH_ES_WITH_H3K27ME3, showed strong hypermethylation in tumors carrying an *SDHx* gene mutation (Figure S1B). To address whether this hypermethylation was accompanied by reduced RNA expression, we used the transcriptomics data on the COMETE cohort of PPGL encompassing 17 *SDHB*-, 40 *VHL*-, 37 *NF1*-, and 19 *RET*-mutated PPGL samples. *SDHB*-mut tumors showed the lowest mean expression of PRC2 targets among all PPGL subgroups (Figure 1E).

We also compared expression of the PRC2 core components EZH2, SUZ12, and EED among the expression clusters described in Burnichon et al. (2011). EZH2 and SUZ12 were overexpressed in cluster C1A, which is composed of tumors with mutations on genes encoding TCA cycle enzymes (Figure S1C), whereas the PRC1 components RING1 and BMI1 were not (Figure S1D). EZH2 and SUZ12 were also overexpressed in metastatic compared with benign tumors (Figure S1E).

To investigate whether PRC2 participates in the DNA hypermethylator phenotype, we used the *Sdhb*$^{-/-}$ imCC model, which recapitulates the strong DNA hypermethylation observed by meDIP-seq in SDH tumors (Figure 2A) and the enrichment in PRC2 among hypermethylated (Figure 2B) or transcriptionally repressed genes (Figure 2C). We treated imCCs with a specific PRC2 inhibitor, GSK343, a potent and highly selective EZH2 inhibitor (Verma et al., 2012), for up to 7 passages. GSK343 treatment resulted in sustained inhibition of H3K27me3 (Figure 2D) but did not modify global 5mC levels (Figure S2A) or 5hmC levels (Figure S2B). Nevertheless, most polycomb targets downregulated in *Sdhb*$^{-/-}$ cells were also hypermethylated at their TSS 500. We thus selected seven PRC2 targets that were downregulated in *Sdhb*$^{-/-}$ cells. These genes are involved in neural differentiation (Hand2 [Stanzel et al., 2016], Gdnf [Roussa and Krieglstein, 2004], Stmn2 [Liu et al., 2002], and Wnt11 [Elizalde et al., 2011]) and cell migration and subsequent development of the central nervous system (Sema6d [Toyofuku et al., 2004], Spock2 [Schnepp et al., 2005], and Spock3 [Yamamoto et al., 2014]). Five of them were also hypermethylated at their TSS 500 and two were not. Treatment with GSK343 did not reactivate the expression of DNA-hypermethylated genes, whereas it promoted re-expression of the two genes that were not DNA methylated (Figure 2E). We showed, by chromatin immunoprecipitation, that the H3K27me3 mark was detected in these 2 genes only in *Sdhb*$^{-/-}$ cells, which returned to baseline following GSK343 treatment (Figures 2F and 2G). In contrast, genes that were DNA hypermethylated in *Sdhb*$^{-/-}$ cells did not bear an increased H3K27me3 mark in *Sdhb*$^{-/-}$ compared with WT cells (Figure S2C), showing that their repression was solely mediated by DNA rather than histone methylation.

To confirm these results with a different PRC2 inhibitor and using a global methylation technique, we used the UNC1999 inhibitor, highly selective for EZH2 and EZH1, and its close analog UNC2400 (>1,000-fold less potent than UNC1999) as a negative control (Figure 2H) and analyzed their effect on methylation profiles using RRBS. Unsupervised hierarchical clustering based on the 1,000 most variant features showed that the methylation profiles of UNC1999-treated cells remained very close to that of UNC2400-treated or untreated cells, regardless of the genotype (Figure 2I). In particular, *Sdhb*$^{-/-}$ imCCs remained hypermethylated when treated with the EZH1/2 inhibitor UNC1999 (Figure 2J).

We have shown previously that *Sdhb*$^{-/-}$ cells display a mesenchymal-like phenotype with increased adhesion and migration properties (Loriot et al., 2015). Notably, PRC2 inhibition did not reduce the migration or adhesion capacities of *Sdhb*$^{-/-}$ cells (Figures 2K and S2D). Altogether, these results suggest that, although PRC2 represses a subset of its targets through deposition of H3K27me3 marks in SDH-deficient cells,

(F and G) Chromatin immunoprecipitation using an antibody against H3K27me3 or negative control rabbit immunoglobulin G (IgG) was performed on the indicated cell lines. The Hand2 (F) and Gdnf (G) genes were quantified by qPCR using primer pairs, as indicated in Figure S7B. Shown is the mean of 3 experiments (+SEM). Student's test was performed to compare the H3K27me3 chromatin immunoprecipitation (ChIP) signal with the background IgG signal.
(H) Inhibition of H3K27me3 by the PRC2 inhibitor UNC1999 compared with vehicle or the negative control UNC2400.
(I) Unsupervised hierarchical clustering based on the 1,000 most variant features in RRBS data from cells treated with UNC1999, UNC2400, or vehicle.
(J) Smooth scatterplot comparing methylation levels identified by RRBS in *Sdhb*$^{-/-}$ cells treated with UNC1999 or vehicle.
(K) Collective migration was followed using a wound scratch assay after treatment with GSK343. Migration is represented as the closure percentage of the wound. The data in (E) and (K) are the mean of 3 independent experiments (+SEM). Student's tests were performed to compare GSK343-treated with untreated cells (*$p < 0.05$, ***$p < 0.001$). Quantification of global 5mC and 5hmC levels in cells treated with GSK343, ChIP-qPCR experiments with additional primer pairs, and adhesion experiments are provided in Figure S2.

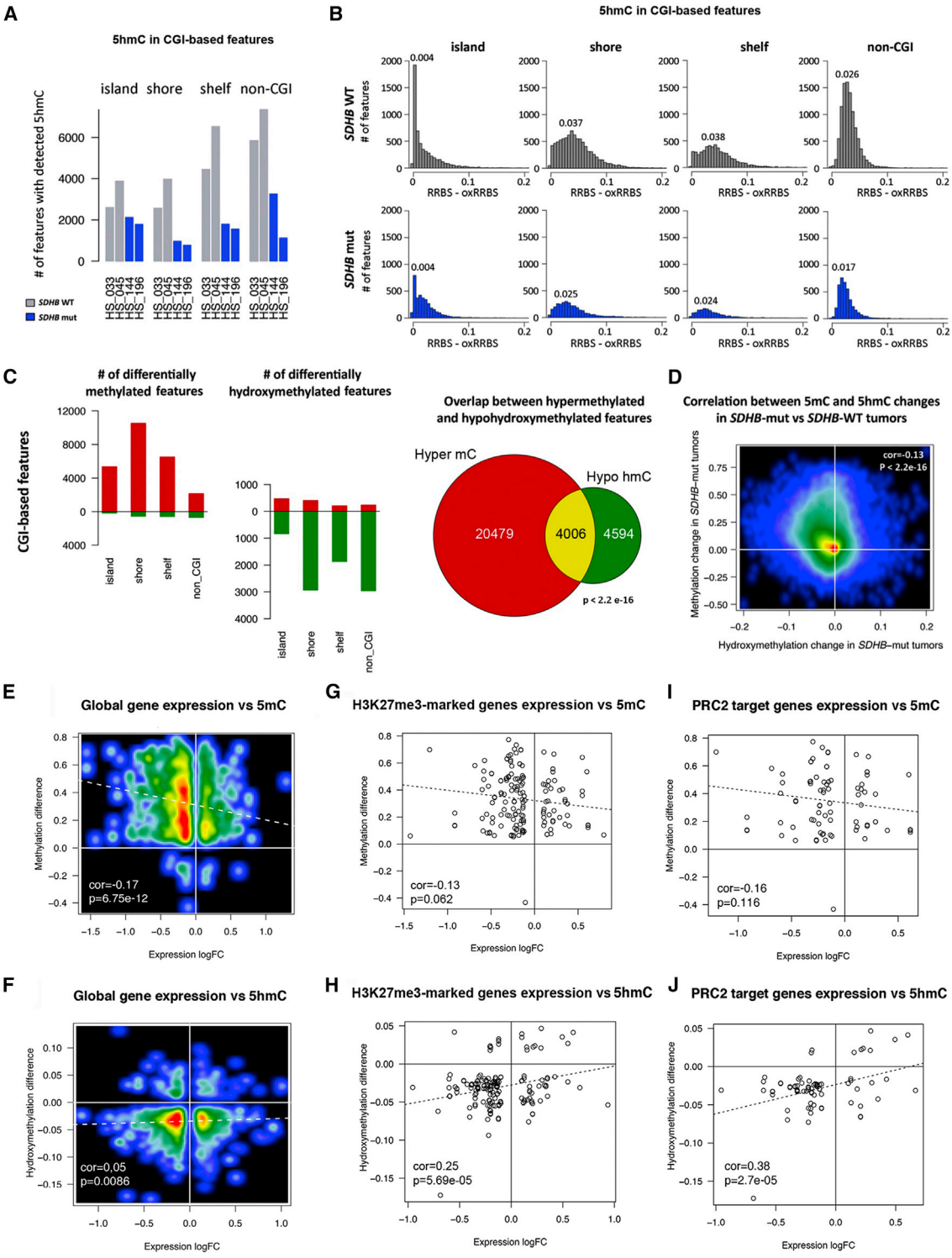

Figure 3. Detection of Methylation or Hydroxymethylation in *SDHB*-mut Compared with *SDHB* Wild-type (WT) Tumors and Correlation between Methylation or Hydroxymethylation Difference and Gene Expression Changes

(A) Number of regions in which 5hmC was detected by (ox)RRBS.

(B) Distribution of 5hmC rates (RRBS-oxRRBS) in regions where it was detected in *SDHB* WT (top) or *SDHB*-mut (bottom) tumors.

(C) Number and overlap of differentially methylated and hydroxymethylated regions in S*DHB*-mut compared with *SDHB*-WT tumors.

(legend continued on next page)

it is not responsible, per se, for the DNA hypermethylation or for the aggressive phenotype of *Sdhb*$^{-/-}$ cells.

Analysis of DNA Hydroxymethylation in SDHB-Deficient Tumors and Cells

Previous studies suggested that DNA hypermethylation could result from succinate-driven inhibition of TET demethylases. To directly test this hypothesis, we precisely quantified 5mC and 5hmC modifications along the genome after enrichment for CpG-rich regions using oxidative RRBS (oxRRBS) (Booth et al., 2012) in human tumors and imCCs. DNA methylation data were highly correlated with meDIP-seq data (Figure S3A) and confirmed the enrichment of PRC2 targets among genes hypermethylated at their TSS 500 in *SDHB*-mut tumors (Benjamini-Hochberg (BH) adjusted p values: BENPORATH_ES_WITH_H3K27ME3 = 1.41E−38; BENPORATH_SUZ12_TARGETS = 1.35E−35; BENPORATH_EED_TARGETS = 5.06E−21; BENPORATH_PRC2_TARGETS = 1.25E−24).

5hmC mapping in tumors from the same genotype was highly correlated, indicating the robustness of the method (Figure S3C). Hydroxymethylation was more abundant in gene bodies than in promoter regions (Figures S3D, S4A, S4B, S5A, and S5B).

Hydroxymethylation was reduced in *SDHB*-mut compared with *SDHB*-WT tumors and cells, sustaining the hypothesis that the hypermethylator phenotype is caused by inhibition of oxidative demethylation. In human tumors, the number of features with detectable 5hmC was reduced by 40% in CGIs, 73% in CGI shores, 69% in CGI shelves, and 67% outside of CGIs (Figure 3A). In terms of gene features, the number of features with detectable 5hmC was reduced by 32% in promoter regions and 54% in gene bodies (Figure S4A). Furthermore, in these features, where 5hmC was detected, the level of hydroxymethylation (RRBS-oxRRBS) was decreased in *SDHB*-mut tumors regardless the feature considered (Figures 3B and S4B). For instance, the peak of the 5hmC rate in gene bodies was 2.9% in *SDHB* WT tumors but only 1.6% in *SDHB*-mut tumors (Figure S4B). Similar results were observed in the cellular model (Figures S5A and S5B).

There was a significant ($p < 2.2e{-}16$, Fisher's exact test) overlap between 5mC gain and 5hmC loss, with above 4,000 features being both hypermethylated and hypohydroxymethylated (Figures 3C and S4C). We also observed a significant anti-correlation between delta-5mC and delta-5hmC in *SDHB*-mut *versus SDHB* WT tumors, both in CGI-based (Figure 3D) and gene-based features (Figure S4D). Similarly, we found a significant correlation between increased 5mC and decreased 5hmC following *Sdhb* knockout (KO) in cells (Figures S5C and S5D).

As expected, enhanced 5mC levels and reduced 5hmC levels both correlated with a reduction in gene expression (Figures 3E and 3F). Restricting this analysis to PRC2 targets or genes marked by H3K27me3 shows that, as observed in other tumor types (Ohm et al., 2007; Schlesinger et al., 2007), most PRC2 targets were repressed by DNA methylation and not only by histone H3K27 methylation (Figures 3G and 3H). Interestingly, these repressed PRC2 targets also mostly showed low 5hmC levels (Figures 3I and 3J).

Combined Tet1/Tet2 Knockdown Mimics the Methylator Phenotype of Sdhb-Deficient Cells

To evaluate the contribution of TET enzyme inhibition to the hypermethylator phenotype, we knocked down their coding genes in WT imCCs. Because *Tet3* was barely expressed in imCCs (Figure S6A), we generated a double knockdown (KD) by infecting WT imCCs with lentiviruses expressing short hairpin RNAs (shRNAs) targeting *Tet1* and *Tet2*, which led to 50% to 60% inhibition of expression of both enzymes in two different clones (Figure 4A). Global quantification of 5mC and 5hmC by ELISA showed reduced 5hmC and increased 5mC levels in *Tet1*+*Tet2*^{KD} cells, comparable with those observed in *Sdhb*-deficient cells (Figure 4B). RRBS analysis of DNA methylation in shSCR (short hairpin scramble RNA) and *Tet1*+*Tet2*^{KD} imCCs (clone 74) revealed that the hypermethylator phenotypes induced by *Sdhb* KO or *Tet1*+*Tet2*^{KD} were highly similar (Figures 4C and S6B), with a significant overlap of hypermethylated loci at the level of individual CpG sites (Figure 4D) and gene features (Figure S6C; $p < 2.2e{-}16$, Fisher's exact test). Molecular Signatures Database (MSigDB) enrichment analysis showed strong enrichment in PRC2 targets among the genes hypermethylated at their TSS 500 in *Tet1*+*Tet2*^{KD} cells (Figure S7A), as in *Sdhb*$^{-/-}$ cells. Accordingly, PRC2 targets that are both downregulated and DNA hypermethylated in *Sdhb*$^{-/-}$ cells were also repressed in *Tet1*+*Tet2*^{KD} cells. In contrast, the few targets downregulated but not DNA hypermethylated were only repressed and marked by H3K27me3 in *Sdhb*$^{-/-}$ cells but not in *Tet1*+*Tet2*^{KD} cells (Figures 4E and S7B). Altogether, these data reinforce the demonstration that, in *Sdhb*$^{-/-}$ cells, DNA methylation of most PRC2 targets is the result of TET enzyme inhibition rather than increased PRC2 activity and recruitment of DNA methyltransferase. They are in accordance with other studies in ESCs showing that TET1 and PRC2 have redundant targets (Williams et al., 2011a).

We then investigated the phenotype of *Tet1*+*Tet2*^{KD} imCCs and compared it with *Sdhb*-deficient cells. The proliferation rate of *Tet1*+*Tet2*^{KD} imCCs was lower than that of WT and shSCR cells but slightly higher than that of *Sdhb*$^{-/-}$ cells (Figure 4F). Moreover, *Tet1*+*Tet2*^{KD} imCCs exhibited increased

(D) Correlation between delta-5mC and delta-5hmC in *SDHB*-mut versus *SDHB*-WT tumors. Characteristics of genome-scale mapping of 5mC and 5hmC are provided in Figure S3. 5hmC detection in gene-based features in *SDHB*-mut compared to *SDHB* WT tumors is provided in Figure S4. 5hmC detection in *Sdhb*$^{-/-}$ compared with *Sdhb*-WT imCCs is provided in Figure S5.

(E) Gene expression change versus methylation difference at TSS 500.

(F) Gene expression change versus hydroxymethylation difference at gene bodies.

(G and H) Analysis restricted to gene set "BENPORATH_ES_WITH_H3K27ME3." Shown is gene expression change versus methylation (G) or hydroxymethylation (H) difference at TSS 500.

(I and J) Analysis restricted to gene set "BENPORATH_PRC2_TARGETS." Shown is gene expression change methylation (I) or hydroxymethylation (J) at TSS 500.

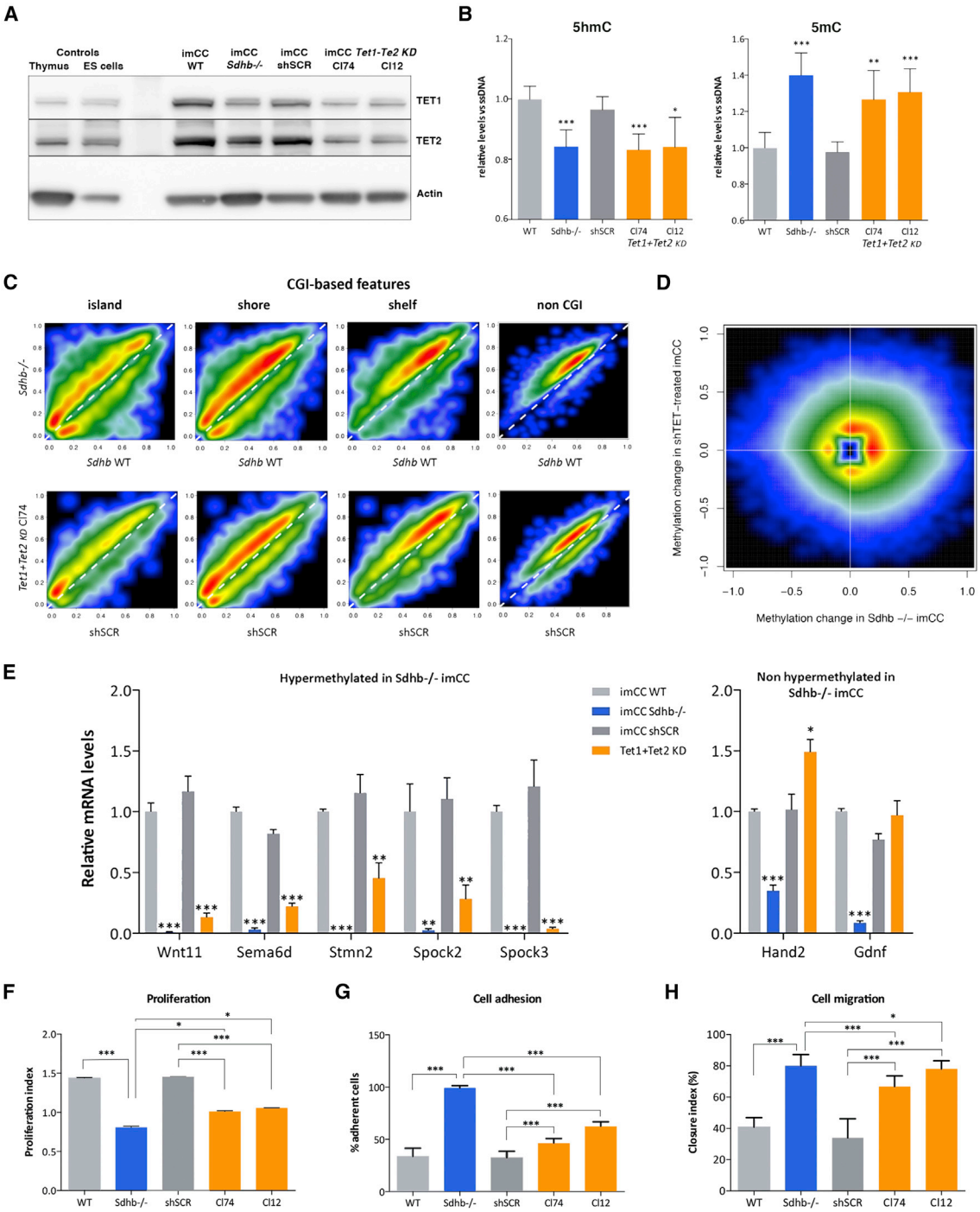

Figure 4. Double Knockdown (KD) of *Tet1* and *Tet2* in Wild-type (WT) imCCs Recapitulates the DNA Hypermethylation Observed in *Sdhb*$^{-/-}$ Cells

(A) Western blot analysis of TET1 and TET2 in total protein extracts from imCCs of the indicated genotypes.

(B) ELISA dosage of global 5hmC (left) and 5mC (right) levels in imCCs infected by scramble shRNA (shSCR) or *Tet1+Tet2* shRNA.

(C) Smooth scatterplot of significantly differentially methylated features (identified by RRBS) in *Sdhb*$^{-/-}$ versus *Sdhb*-WT imCCs (top) or *Tet1+Tet2*^{KD} versus *shSCR* imCCs (bottom) in each kind of CGI-based feature.

(D) Comparison of methylation changes induced by *Tet1+Tet2*^{KD} and *Sdhb*$^{-/-}$ imCCs, considering all differentially methylated CpG sites (delta > 0.1) in at least one condition.

(E) qRT-PCR dosage of known PRC2 targets (hypermethylated or not in *Sdhb*$^{-/-}$ imCCs) in cells of the indicated genotypes.

(F) Proliferation index of the indicated cell lines.

(legend continued on next page)

adhesion and migration compared with WT and shSCR cells but did not reach the levels of adhesion and migration of *Sdhb*$^{-/-}$ cells (Figures 4G and 4H).

DNA Hypermethylation and Hypoxia Act in Synergy to Fully Recapitulate the Sdhb-Deficient Phenotype

Because *Sdhb*$^{-/-}$ cells also exhibit a pseudohypoxic phenotype, we investigated whether hypoxia drives mesenchymal transition in these cells. Pseudohypoxia was characterized by massive overexpression of HIF2α but not HIF1α (Figure 5A). In all cell types, HIF2α stabilization and nuclear translocation can be induced at levels similar to that of *Sdhb*$^{-/-}$ cells by O_2 deprivation for 72 h (Figure 5B). Indeed, cultivating all *Sdhb* WT cells at 2% O_2 induced transient activation of the HIF1α pathway from 4–24 h of hypoxia (as shown by expression of its preferential targets Glut1, Pgk1, and Ldha), whereas the HIF2α pathway (as revealed by Epas1, Mmp9, and Tgfa mRNAs) was induced only after 72 h of hypoxia (Figures 5C and 5D). This is in agreement with transcriptomics analysis in our large cohort of PPGL, which comprised 23 *SDHx*-mutated tumors. We used a list of 11 genes that have been described as HIF1α-specific targets (Figure 5E) and of 9 HIF2α-specific (Figure 5F) targets (Keith et al., 2011) and compared their mean expression in the group of *SDH*-mutated PPGL with *VHL*-, *NF1*-, and *RET*-mutated ones. This analysis showed that SDH- and Von Hippel-Lindau (VHL)-related tumors display a HIF2α signature compared with *RET* or *NF1*-mutated tumors. In contrast, HIF1α targets are highly expressed in VHL-mutated PPGL but not SDH tumors.

In line with previous reports (Thienpont et al., 2016), RRBS and ELISA analyses showed that this modest hypoxia was not sufficient to repress TET activity (Figures 5G and 5H). Indeed, only 1,374 features were differentially methylated between normoxia and hypoxia, whereas over 12,000 were differentially methylated following *Sdhb* KO. These changes were balanced between hyper- and hypomethylation (Figure 5G).

Cultivating cells for 72 h at 2% O_2 mimics the pseudohypoxic features of Sdhb$^{-/-}$ cells. Interestingly, these hypoxic conditions had no or a moderate effect on WT or shSCR cells but enhanced adhesion and migration of *Tet1*+*Tet2*^{KD} imCCs (Figures 6B and 6C). Notably, under these conditions, *Tet1*+*Tet2*^{KD} imCCs reached the migration capacity of *Sdhb* KO cells.

Sdhb$^{-/-}$ cells display a mesenchymal morphology, highlighted by intense staining of actin filaments in all of the cytoplasm, whereas in *Tet1*+*Tet2*^{KD} imCCs, like in WT cells, staining was mainly cortical in normoxia. Strikingly, cultivating *Tet1*+*Tet2*^{KD} imCCs in hypoxia modified their morphology toward an *Sdhb* deficiency-like mesenchymal phenotype (Figure 6D). Accordingly, hypoxic *Tet1*+*Tet2*^{KD} imCCs displayed molecular hallmarks of neuro-endocrine-to-mesenchymal transition, such as Snai1 and Twist1 overexpression and Cdh2 (N-Cadherin is the main cadherin expressed in neuroendocrine cells) downregulation (Figure 6E).

To investigate whether hypoxia could also induce metastatic traits in *Tet1*+*Tet2*^{KD} imCCs *in vivo*, we grew these cells for 72 h in normoxia or hypoxia before injection into the tail vein of immunocompromised mice. This metastatic model has a lung tropism. We therefore sacrificed the mice 41 days after grafting and harvested the lungs, in which the number of metastatic cells was quantified by qPCR on genomic DNA. We showed that the metastatic burden was twice as high in mice injected with hypoxic cells than in those with normoxic cells, confirming *in vivo* the contribution of hypoxia to the metastatic phenotype (Figure 6F).

These data suggest that HIF2α inhibition could counteract metastatic traits of *SDHB*-mut PPGL. To further investigate the effect of HIF2α inhibition on *Sdhb*$^{-/-}$ cells, we silenced HIF2α using specific shRNA lentiviral vectors. To avoid a potential HIF1α response counteracting HIF2α loss, we also infected cells with a lentiviral vector expressing a HIF1α-targeting shRNA together with the shHIF2α (Figures 7A and 7B), and we selected 3 clones bearing only HIF2α or HIF2α+HIF1α silencing. HIF2α inhibition reversed the overexpression of *Mmp9*, *Tgfa*, and *Snai1* observed in *Sdhb* KO cells (Figure 7C). It also had a strong effect on the phenotype of *Sdhb*-deficient cells, leading to changes in cell morphology (Figure 7D) as well as decreased proliferation and migration. In contrast, HIF2α loss had little effect on cell adhesion, in agreement with the small effect of hypoxia on adhesion of Tet-depleted cells (Figures 7E–7G). HIF1α repression had no additional effect on all of these features.

Altogether, our data demonstrate that hypermethylation and repression of PRC2 targets and developmental genes increase phenotypic plasticity, allowing acquisition of mesenchymal traits induced by HIF2α to recapitulate the SDHB deficiency phenotype.

DISCUSSION

In this study, we investigated the mechanisms by which hypermethylation occurs in SDH-deficient tumors and cells. Because of the low levels of 5hmC in tumors and cultured somatic cells, there have been very few studies that analyzed the content and distribution of 5hmC in non-embryonic cells and cancer. Hence, the link between SDH tumor hypermethylation and TET inhibition has been postulated but actually never truly demonstrated. Our data show that SDH-driven hypermethylation does result from TET inhibition and subsequent loss of 5hmC.

It may seem contradictory that the hypermethylator phenotype of SDH-deficient tumors mainly affects CGIs, whereas hypo-hydroxymethylation is mostly observed in gene bodies. However, it is important to note that hypo-hydroxymethylation in CGIs is very difficult to detect because of the very low level of 5hmC in these features (about 0.4% in our data). Because of this very low level at baseline, we are

(G) Adhesion of the indicated cell lines 3 h after plating.
(H) Closure index of the wound scratch assay after 15-h migration of the indicated cell lines.
The data in (B), (E), (F), (G) and (H) are the mean of 3 experiments (+SEM). Student's test was performed to compare *Sdhb*$^{-/-}$ cells with WT cells and *Tet1*+*Tet2*^{KD} cells with shSCR cells and *Sdhb*$^{-/-}$ cells (*p < 0.05, **p < 0.01, ***p < 0.001). TET3 protein levels and RRBS analyses for each kind of gene-based features are provided in Figure S6.

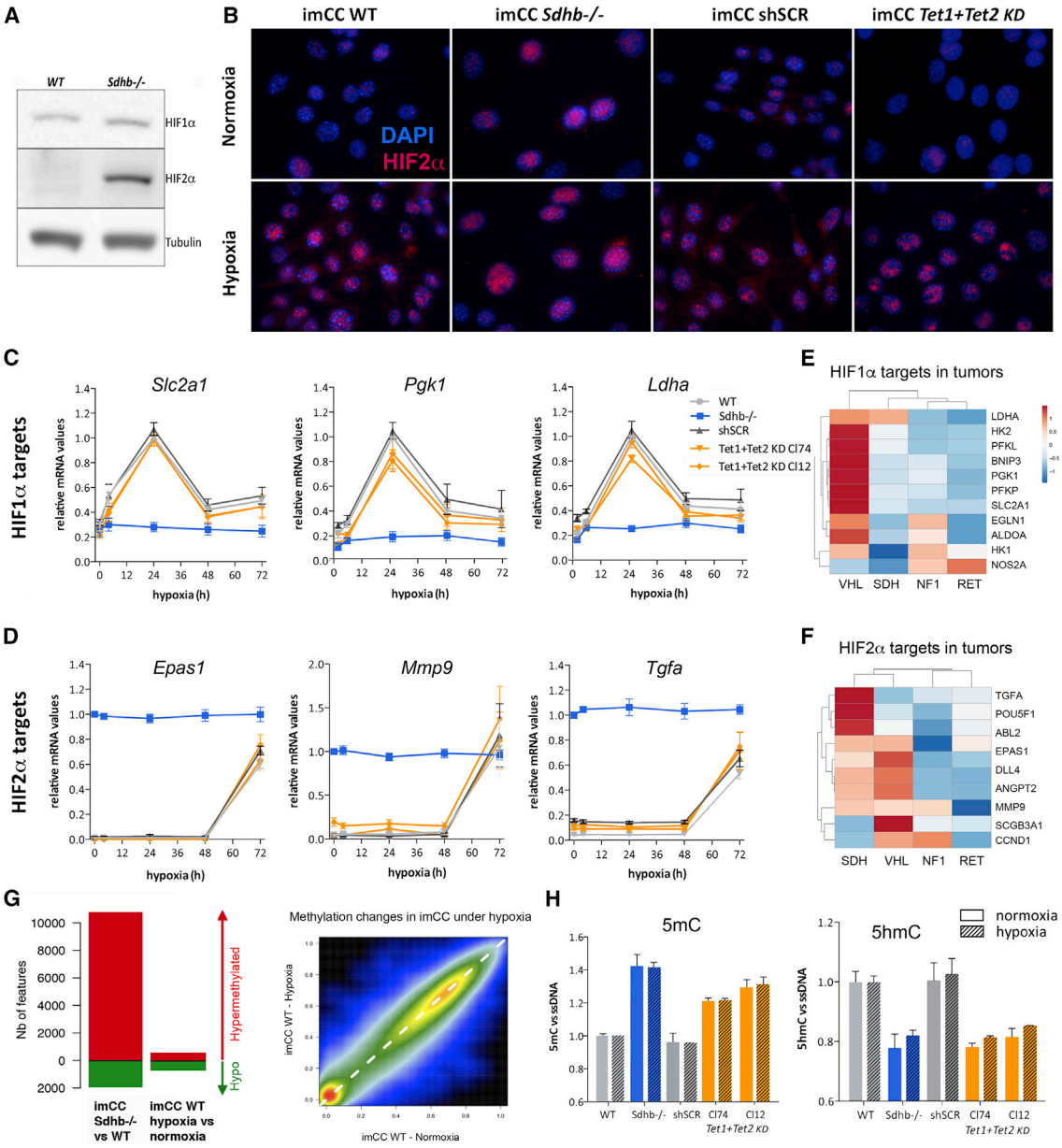

Figure 5. Pseudohypoxia in *Sdhb*$^{-/-}$ imCCs Leads to Stabilization of HIF2α and Can Be Mimicked by Long-Term Moderate Hypoxia

(A) Western blot of HIF1α and HIF2α in total cellular extracts of WT or *Sdhb*$^{-/-}$ imCCs cultured in normoxia (21% O_2).

(B) HIF2α immunofluorescence staining in cells cultivated in normoxia or hypoxia (2% O_2) for 72 h.

(C and D) Kinetics of induction of various (C) HIF1α or (D) HIF2α targets by qRT-PCR measurements in the indicated cell lines cultured at 2% O_2 in a hypoxic chamber.

(E and F) Heatmap based on mean expression of (E) HIF1α or (F) HIF2α target genes in human PPGL with *SDH* (n = 23), *VHL* (n = 40), *NF1* (n = 37), or *RET* (n = 19) driver mutations.

(G) Left: number of differentially methylated features in *Sdhb*$^{-/-}$ (versus WT) or hypoxic (versus normoxic) imCCs. Right: smooth scatterplot of methylation levels identified by RRBS in hypoxic compared with normoxic WT imCCs.

(H) Global 5hmC and 5mC levels, measured by ELISA in cells incubated for 72 h at 21% or 2% O_2. Student's test was performed to compare normoxic and hypoxic conditions for 5hmC and 5mC quantification. No significant difference was observed.

The data in (C), (D) and (H) are the mean of 3 experiments (+ SEM).

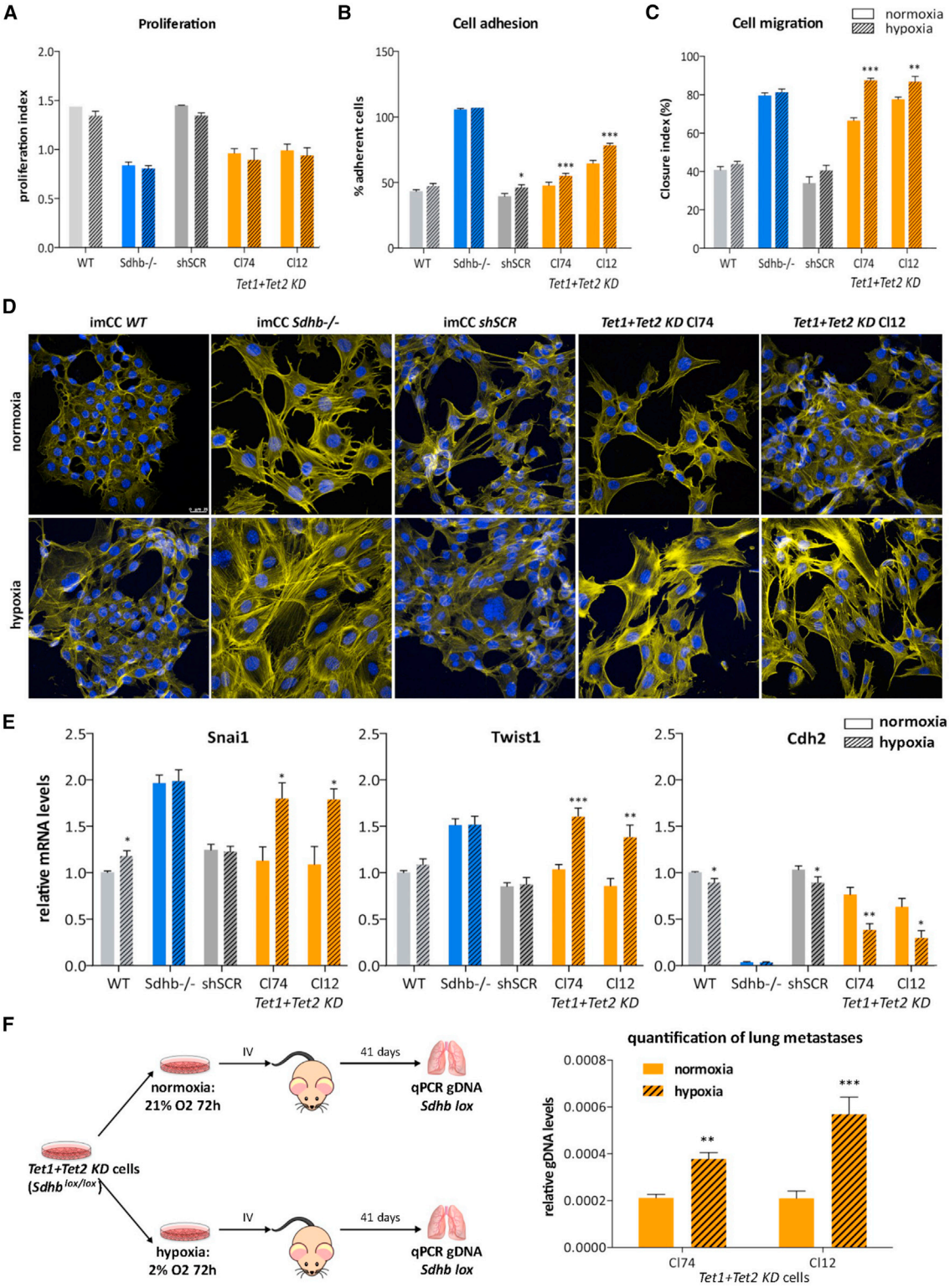

Figure 6. Hypoxia Synergizes with TET Inhibition to Drive Neuro-endocrine-to-Mesenchymal Transition and Subsequent Metastatic Traits

(A) The indicated cell lines were cultivated for 72 h at 21% (normoxia) or 2% O_2 (hypoxia) before running a 7 day proliferation test in normoxia or hypoxia.

(B) After 72 h of incubation at 21% or 2% O_2, the indicated cell lines were plated in normoxia or hypoxia, and the percentage of adherent cells was quantified 3 h later.

(legend continued on next page)

underpowered to detect a decrease of 5hmC within a single CGI. However, we detect 5hmC in a lower number of CGIs in SDH-mut compared with SDH WT tumors (Figure 3B). Thus, 5hmC decreases in CGIs following SDH deficiency, even though this phenomenon is hard to quantify at the level of a single island. The correlation between the intensity of 5mC and 5hmC changes (Figure 3D) is also a strong argument for the pairing of these two changes.

We reveal that a significant fraction of genes hypermethylated consecutive to *SDHB* mutation are known PRC2 targets and genes marked by H3K27me3 histone modification in ESCs. Polycomb groups are mainly involved in transient repression of developmental genes in ESCs through deposition of the H3K27me3 mark at bivalent promoters. Strikingly, several studies have shown that polycomb targets are more prone (up to 12-fold) to cancer-specific hypermethylation (Ohm et al., 2007; Schlesinger et al., 2007) in cancers not driven by oncometabolites, supporting a stem cell origin of cancer in which reversible gene repression would be replaced by permanent silencing. This switch would not cause *de novo* repression but might significantly reduce epigenetic plasticity, locking the cell into a perpetual state of self-renewal and predisposing it to subsequent malignant transformation. The fact that polycomb targets are not highly methylated in non-SDH PPGL suggests a different oncogenic origin in these mostly benign tumors. Thus, our results are in accordance with studies showing that underexpression of polycomb-regulated genes is restricted to poorly differentiated tumors and associated with poor clinical outcome (Ben-Porath et al., 2008).

Because two PRC2 core components, EZH2 and SUZ12, are overexpressed in SDH-deficient tumors, we investigated whether hypermethylation of these gene sets was caused by PRC2 activity. Although a subset of PRC2 targets are indeed repressed by PRC2-mediated trimethylation of H3K27, PRC2 pharmacological inhibition does not counteract DNA hypermethylation in *Sdhb*$^{-/-}$ cells, and *Tet1*+*Tet2*^{KD} imCCs also show DNA hypermethylation, preferentially at PRC2 targets. This points to a prominent role of oncometabolite-mediated inhibition of TET enzymes rather than the DNA methyltransferases DNMT1 and DNMT3a recruited by PRC2.

Several studies have shown redundancy between PRC2 and TET targets in ESCs (Pastor et al., 2011; Verma et al., 2018; Williams et al., 2011a; Wu et al., 2011). Neri et al. (2013) showed a physical interaction between TET1 and the PRC2 complex specifically in ESCs, whereas Williams et al. (2011a) failed to find this interaction in HEK293 cells. It thus remains unclear whether TET enzymes still convert 5mC to 5hmC at PRC2 targets in differentiated cells and in cancer cells. Redundancy between TET and PRC2 targets in cancer cells has been demonstrated by some studies (Putiri et al., 2014; Thomson et al., 2016) but denied by others (Fernandez et al., 2018; Uribe-Lewis et al., 2015). Our study differs in that we did not compare normal with cancer tissues, but we compared tumor samples carrying or not carrying *SDHB* mutations and isogenic cells carrying or not carrying *Sdhb* deletion or *Tet1*+*Tet2* KD. Under these conditions, we were able to demonstrate that, in PPGL tumors and in mouse cells originating from the adrenal medulla, TET enzymes counteract DNA methylation preferentially at genes marked by H3K27me3 and targeted by PRC2 in ESCs. Thus, TET inhibition leads to repression of PRC2 target genes notably involved in neural differentiation (*Stmn2* [Liu et al., 2002] and *Wnt11* [Elizalde et al., 2011]) and cell migration and subsequent development of the central nervous system (*Sema6d* [Toyofuku et al., 2004], *Spock2* [Schnepp et al., 2005], and *Spock3* [Yamamoto et al., 2014]).

Mechanistic insights into the PRC2-TET relationship could be gained from the literature on *WT1* mutations in acute myeloid leukemia (AML), which are mutually exclusive with *IDH1/2, TET2* (Wang et al., 2015), and *EZH2* (Bolouri et al., 2018) mutations. Interestingly, WT1 can recruit EZH2 (Xu et al., 2011), TET2 (Wang et al., 2015), (Rampal et al., 2014) and TET3 (Rampal et al., 2014) to specific targets and may therefore be the clue to explain the redundancy between PRC2 and TET targets. Accordingly, Sinha et al. (2015) showed that *WT1* mutations lead to hypermethylation of PRC2 targets in AML. However, WT1 is hardly expressed in PPGL cells and imCCs (data not shown), so another, still unknown transcription factor and/or non-coding RNA is probably involved in recruiting TET enzymes at PRC2 target promoters in PPGL.

In the second part of this study, we analyzed the functional consequences of DNA hypermethylation because of TET silencing and HIF2α stabilization. We show that the mesenchymal-like phenotype and metastatic behavior of *Sdhb*-deficient cells result from synergistic effects of TET inhibition and pseudohypoxia. Her et al. (2015) showed that TET inhibition by succinate is oxygen dependent in SDH loss models of PPGL. They suggested that the increased incidence and worst prognosis of SDH-related PPGL in patients living at high altitude or with chronic hypoxia because of respiratory or circulatory pathologies is due to TET inhibition by hypoxia. In contrast, we showed previously, in a large cohort of PPGL from patients living at normal altitude, that DNA hypermethylation was evidenced in all SDH-mutated PPGL (Letouzé et al., 2013). Similarly, *Sdhb* KO in imCCs results in TET-mediated DNA hypermethylation even under normoxic conditions. The hypoxic conditions we used in this study were neither

(C) Closure index of the wound scratch assay after 15-h migration of the indicated cell lines pre-cultured for 72 h at 21% or 2% O_2.
(D) Actin staining was performed using fluorescent phalloidin toxin in the indicated cell lines cultivated for 72 h at 21% or 2% O_2.
(E) qRT-PCR measurement of known drivers of neuro-endocrine-to-mesenchymal transition (Loriot et al., 2015) in the indicated cell lines incubated for 72 h at 21% or 2% O_2. All data are the mean of 3 experiments.
(F) Evaluation of *in vivo* metastatic behavior of *Tet1*+*Tet2* KD imCCs (Cl74 and Cl12) precultured for 72 h at 21% or 2% O_2. After preculture in normoxia or hypoxia, 10^6 cells were injected in PBS in the tail vein of NMRI nude mice. 41 days later, the mice were sacrificed, and the lungs were snap frozen in liquid nitrogen. genomic DNA (gDNA) extraction was performed on entire lungs, and metastatic charge was quantified by qPCR using primers specific for the loxP site present in imCCs. The data in (A), (B), (C) and (E) are the mean of 3 experiments (+ SEM). Student's test was performed to compare normoxic and hypoxic conditions (*$p < 0.05$, **$p < 0.01$, ***$p < 0.001$).

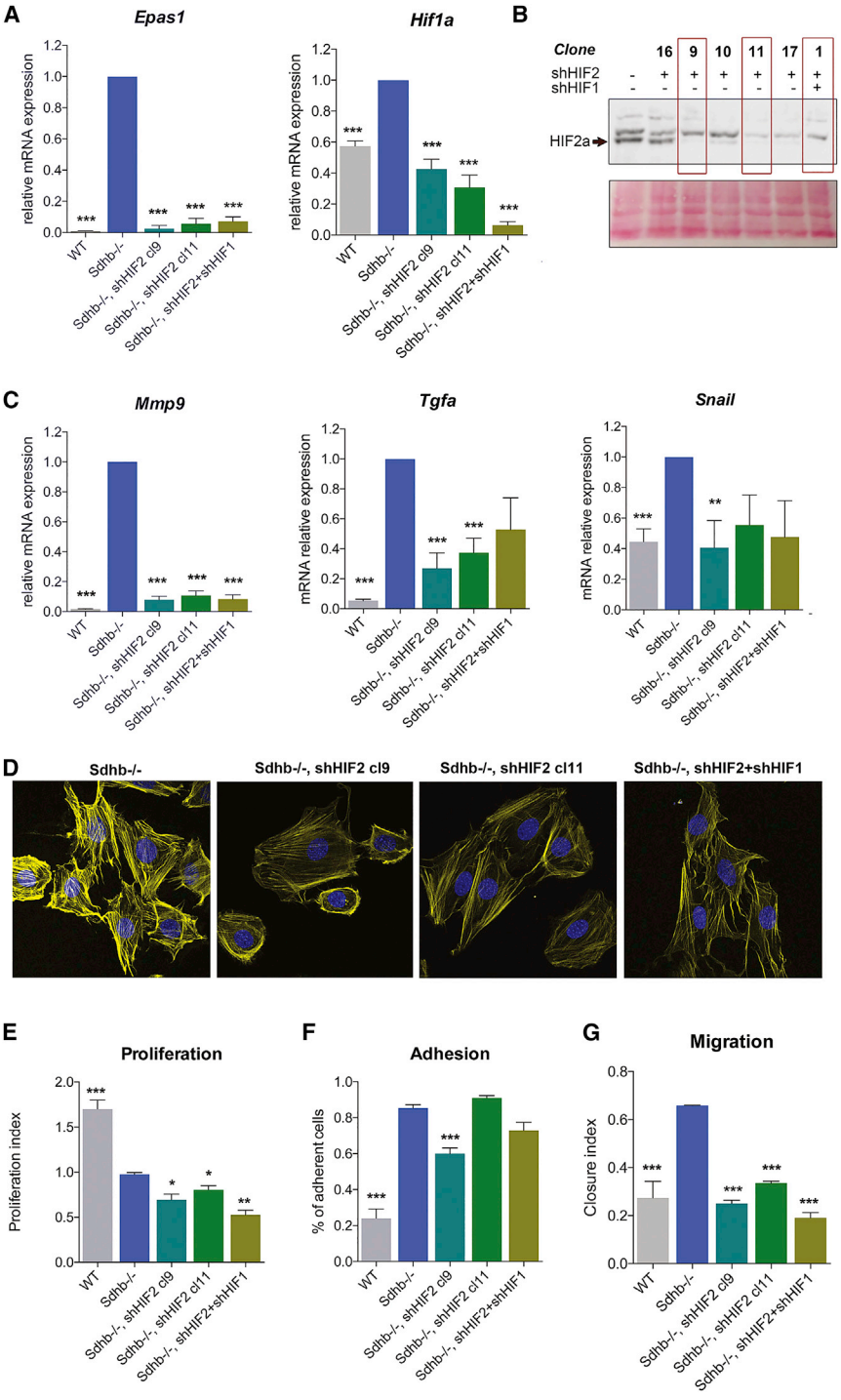

Figure 7. HIF2α Silencing Counteracts Pseudohypoxia in *Sdhb*$^{-/-}$ Cells and Reverses Their Mesenchymal Phenotype

(A) qRT-PCR measurement of *Epas1* and *Hif1α* expression in the indicated cell lines and clones.

(B) Protein expression of Hif2α in pure clones of *Sdhb*$^{-/-}$ imCCs stably expression shRNAs targeting Hif2α (clones 16, 9, 10, 11, and 17) or HIF2α and HIF1α (clone 1). Clones 9, 11, and 1 had nearly complete extinction of Hif2α expression and were selected for further experiments.

(C) qRT-PCR measurement of *Mmp9* and *Tgfa* (markers of pseudohypoxia) and *Snai1* (EMT marker) expression in the indicated cell lines and clones.

(D) Actin staining was performed using fluorescent phalloidin toxin in the indicated cell lines and clones.

(E) Proliferation index of the indicated cell lines and clones.

(F) Adhesion of the indicated cell lines 1 h after plating.

(G) Closure index of the wound scratch assay after 10-h migration of the indicated cell lines.

The data in (A), (C), (E), (F), and (G) are the mean of 3 experiments (+ SEM). Student's test was performed to compare all cell lines with *Sdhb*$^{-/-}$ cells (*p < 0.05, **p < 0.01, ***p < 0.001).

necessary nor sufficient to inhibit TET activity in our cells. Therefore, the effect of hypoxia we observed on cell behavior is not mediated by increased DNA methylation but, rather, by HIF2α-mediated gene transcription. Thienpont et al. (2016) showed that acute hypoxia is necessary to repress TET activity because the Michaelis Constant (Km) for TET1 and TET2 were, respectively, 0.31% and 0.53% O_2. Thus, altitude may synergize with oncometabolites and intra-tumoral acute hypoxia in repression of TET enzymes, but it is probably not the leading mechanism.

HIF1α and HIF2α proteins have been found to be overexpressed in the nuclei of some SDH-deficient tumors, but a few studies suggest that HIF2α plays a more important role than HIF1α in tumorigenesis (Favier et al., 2009; Holmquist-Mengelbier et al., 2006; Nilsson et al., 2005; Qin et al., 2014). Here we demonstrate that pseudohypoxia in *Sdhb*$^{-/-}$ and in SDH-mutated PPGL is driven by HIF2α stabilization rather than HIF1α and that the kinetics of stabilization of both proteins may explain this observation. Indeed, HIF1α is stabilized in short-term acute hypoxia, whereas HIF2α is stabilized in moderate but prolonged hypoxia (Holmquist-Mengelbier et al., 2006; Uchida et al., 2004). We confirmed previous observations that HIF1α levels decline after several hours of hypoxia (Koh et al., 2011; Uchida et al., 2004), whereas HIF2α levels increase later in long-term hypoxia (Holmquist-Mengelbier et al., 2006; Uchida et al., 2004). Several mechanisms may play a role in HIF1α decline in long-term hypoxia: HIF-mediated expression of antisense transcripts from the *HIF1A* locus (Uchida et al., 2004); HAF-, HSP70-, or Carboxyl terminus of HSC70-interacting protein (CHIP)-mediated HIF1α-specific degradation (Koh

et al., 2008, 2011; Luo et al., 2010). Thus, pseudohypoxia mimics long-term hypoxia with massive HIF2α stabilization but no HIF1α stabilization.

High HIF2α levels have been implicated in the undifferentiated and aggressive phenotype of some pseudohypoxic cancers (Myszczyszyn et al., 2015; Pietras et al., 2010). Here we show that, in chromaffin cells, hypoxia is not sufficient to induce EMT but synergizes with epigenetic modifications resulting from SDHB loss to drive neuro-endocrine-to-mesenchymal transition and subsequent invasive behavior. This may explain why pseudohypoxic *VHL*-mutated PPGL (which are not highly hypermethylated) are rarely metastatic, whereas *SDHB*-mut PPGL are more prone to metastasis.

Similarly, all oncometabolites do not identically repress the various 2-OG-dependant dioxygenases, which could be a clue regarding the different phenotypes of oncometabolite-mediated tumors. Indeed, histone demethylases such as JMJD2A are inhibited by all oncometabolites (Chowdhury et al., 2011; Xiao et al., 2012), with higher affinity for 2-hydroxyglutarate (2-HG) than for succinate and fumarate, whereas the affinity of TET enzymes for 2-HG is lower than for succinate and fumarate (Laukka et al., 2016). Finally, PHDs are inhibited by succinate and fumarate (Isaacs et al., 2005; Selak et al., 2005), but the effect of the R-enantiomer of 2-hydroxylglutarate (R-2-HG) is still debated (Chowdhury et al., 2011; Williams et al., 2011b; Zhao et al., 2009) and may even activate these enzymes (Koivunen et al., 2012; Losman et al., 2013). In consequence, *IDH*-mutated gliomas, which have a good prognosis, would be hypermethylated but not pseudohypoxic. Conversely, SDH and FH tumors, which are both pseudohypoxic and DNA hypermethylated, are associated with increased risk of regional and distant spread in PPGL as well as hereditary leiomyomatosis and renal cell cancer (caused by germline *FH* mutations). Thus, the comparison of the distinct metastatic susceptibility of VHL, IDH, and FH tumors (Henegan and Gomez, 2016) is in accordance with our data showing that TET inhibition and pseudohypoxia are needed to synergistically drive malignancy.

We show that, surprisingly, cell adhesion was very high in *Sdhb*$^{-/-}$ cells compared with WT or *Tet1*+*Tet2*^{KD} cells but was not highly affected by HIF2α inhibition or hypoxia. This suggests that the remarkably high adhesion properties of *Sdhb*$^{-/-}$ cells may be in great part driven by pathways other than DNA methylation and pseudohypoxia; for example, metabolic reprogramming (Lussey-Lepoutre et al., 2015; Sousa et al., 2019).

Although these findings do not explain why only half of all *SDHB*-mut tumors become metastatic, we and others have shown recently that *TERT* activation and *ATRX* mutations are frequently associated with metastatic progression of these tumors (Fishbein et al., 2015; Svahn et al., 2018; Dwight et al., 2018; Job et al., 2019). Nonetheless, it should be noted that imCCs have achieved spontaneous immortalization right before *Sdhb* inactivation (Letouzé et al., 2013). Thus, we propose a tripartite model where TET-mediated hypermethylation, pseudohypoxia, and immortalization propel the transition of *SDHB*-mut tumors toward metastasis.

STAR★METHODS

Detailed methods are provided in the online version of this paper and include the following:

- KEY RESOURCES TABLE
- LEAD CONTACT AND MATERIALS AVAILABILITY
- EXPERIMENTAL MODEL AND SUBJECT DETAILS
  - Patients and tumor samples
  - Mammalian cell line
  - Data generated
  - Mouse model
- METHOD DETAILS
  - MeDIP-seq analysis
  - RNA-seq analysis
  - oxRRBS and RRBS Analyses
  - 5hmC detection using (ox)RRBS data
  - Differential (hydroxy)methylation analysis
  - Gene set enrichment analysis
  - Inhibition of PRC2 activity
  - Proliferation assay
  - Adhesion assay
  - Wound scratch assay
  - shRNA stable transduction
  - Reversed Transcription and Quantitative Real-Time PCR
  - ChIP-qPCR
  - 5mC and 5hmC ELISA
  - Western Blot analysis
  - Fluorescent staining
  - *In vivo* metastasis assay
- QUANTIFICATION AND STATISTICAL ANALYSIS
- DATA AND CODE AVAILABILITY

SUPPLEMENTAL INFORMATION

Supplemental Information can be found online at https://doi.org/10.1016/j.celrep.2020.03.022.

ACKNOWLEDGMENTS

We thank Charles Marcaillou, Sylvain Guibert, and Céline Vallot for technical contributions and advice and Catherine Tritscher for precious administrative help. This work has received funding from the European Union (FP7/2007-2013 no. 259735), The Plan Cancer, Epigénétique et Cancer (EPIG201303 METABEPIC), The Paradifference Foundation, and the Cancer Research for Personalized Medicine (CARPEM) project (Site de Recherche Intégré sur le Cancer [SIRIC]). We thank all members of the Genetics Department, Biological Resources Center and Tumor Bank Platform, Hôpital Européen Georges Pompidou (BB-0033-00063). This work is part of the "Cartes d'Identité des Tumeurs (CIT) program" funded and developed by the Ligue Nationale contre le Cancer. S.M. is the recipient of a fellowship from La Fondation pour la Recherche Médicale. J.G. is the recipient of a fellowship from La Ligue Nationale contre le Cancer.

AUTHOR CONTRIBUTIONS

A.M. contributed to acquisition, analysis, and interpretation of data; management of the project; and preparation and writing of the manuscript. J.G., S.M., A.B., M.-J.F., and J.W. contributed to acquisition of data. L.-J.C.-V. contributed to the acquisition and analysis of data. S.J. contributed to analysis of transcriptomics data. A.-P.G.-R. contributed to management of the project. E.L.

contributed to conception of the study, analysis of sequencing data, and preparation and revision of the manuscript. J.F. contributed to conception of the study, management of the project, analysis and interpretation of data, and preparation and revision of the manuscript.

DECLARATION OF INTERESTS

The authors declare no competing interests.

Received: February 6, 2019
Revised: January 24, 2020
Accepted: March 6, 2020
Published: March 31, 2020

REFERENCES

Akalin, A., Kormaksson, M., Li, S., Garrett-Bakelman, F.E., Figueroa, M.E., Melnick, A., and Mason, C.E. (2012). methylKit: a comprehensive R package for the analysis of genome-wide DNA methylation profiles. Genome Biol. *13*, R87.

Amar, L., Baudin, E., Burnichon, N., Peyrard, S., Silvera, S., Bertherat, J., Bertagna, X., Schlumberger, M., Jeunemaitre, X., Gimenez-Roqueplo, A.P., and Plouin, P.F. (2007). Succinate dehydrogenase B gene mutations predict survival in patients with malignant pheochromocytomas or paragangliomas. J. Clin. Endocrinol. Metab. *92*, 3822–3828.

Anders, S., and Huber, W. (2010). Differential expression analysis for sequence count data. Genome Biol. *11*, R106.

Anders, S., Pyl, P.T., and Huber, W. (2015). HTSeq–a Python framework to work with high-throughput sequencing data. Bioinformatics *31*, 166–169.

Ben-Porath, I., Thomson, M.W., Carey, V.J., Ge, R., Bell, G.W., Regev, A., and Weinberg, R.A. (2008). An embryonic stem cell-like gene expression signature in poorly differentiated aggressive human tumors. Nat. Genet. *40*, 499–507.

Bolouri, H., Farrar, J.E., Triche, T., Jr., Ries, R.E., Lim, E.L., Alonzo, T.A., Ma, Y., Moore, R., Mungall, A.J., Marra, M.A., et al. (2018). The molecular landscape of pediatric acute myeloid leukemia reveals recurrent structural alterations and age-specific mutational interactions. Nat. Med. *24*, 103–112.

Booth, M.J., Branco, M.R., Ficz, G., Oxley, D., Krueger, F., Reik, W., and Balasubramanian, S. (2012). Quantitative sequencing of 5-methylcytosine and 5-hydroxymethylcytosine at single-base resolution. Science *336*, 934–937.

Burnichon, N., Vescovo, L., Amar, L., Libé, R., de Reynies, A., Venisse, A., Jouanno, E., Laurendeau, I., Parfait, B., Bertherat, J., et al. (2011). Integrative genomic analysis reveals somatic mutations in pheochromocytoma and paraganglioma. Hum. Mol. Genet. *20*, 3974–3985.

Castro-Vega, L.J., Buffet, A., De Cubas, A.A., Cascón, A., Menara, M., Khalifa, E., Amar, L., Azriel, S., Bourdeau, I., Chabre, O., et al. (2014). Germline mutations in FH confer predisposition to malignant pheochromocytomas and paragangliomas. Hum. Mol. Genet. *23*, 2440–2446.

Chowdhury, R., Yeoh, K.K., Tian, Y.M., Hillringhaus, L., Bagg, E.A., Rose, N.R., Leung, I.K., Li, X.S., Woon, E.C., Yang, M., et al. (2011). The oncometabolite 2-hydroxyglutarate inhibits histone lysine demethylases. EMBO Rep. *12*, 463–469.

Clark, G.R., Sciacovelli, M., Gaude, E., Walsh, D.M., Kirby, G., Simpson, M.A., Trembath, R.C., Berg, J.N., Woodward, E.R., Kinning, E., et al. (2014). Germline FH mutations presenting with pheochromocytoma. J. Clin. Endocrinol. Metab. *99*, E2046–E2050.

Dwight, T., Flynn, A., Amarasinghe, K., Benn, D.E., Lupat, R., Li, J., Cameron, D.L., Hogg, A., Balachander, S., Candiloro, I.L.M., et al. (2018). *TERT* structural rearrangements in metastatic pheochromocytomas. Endocr. Relat. Cancer *25*, 1–9.

Elizalde, C., Campa, V.M., Caro, M., Schlangen, K., Aransay, A.M., Vivanco, Md., and Kypta, R.M. (2011). Distinct roles for Wnt-4 and Wnt-11 during retinoic acid-induced neuronal differentiation. Stem Cells *29*, 141–153.

Favier, J., Brière, J.J., Burnichon, N., Rivière, J., Vescovo, L., Benit, P., Giscos-Douriez, I., De Reyniès, A., Bertherat, J., Badoual, C., et al. (2009). The Warburg effect is genetically determined in inherited pheochromocytomas. PLoS ONE *4*, e7094.

Fernandez, A.F., Bayón, G.F., Sierra, M.I., Urdinguio, R.G., Toraño, E.G., García, M.G., Carella, A., López, V., Santamarina, P., Pérez, R.F., et al. (2018). Loss of 5hmC identifies a new type of aberrant DNA hypermethylation in glioma. Hum. Mol. Genet. *27*, 3046–3059.

Figueroa, M.E., Abdel-Wahab, O., Lu, C., Ward, P.S., Patel, J., Shih, A., Li, Y., Bhagwat, N., Vasanthakumar, A., Fernandez, H.F., et al. (2010). Leukemic IDH1 and IDH2 mutations result in a hypermethylation phenotype, disrupt TET2 function, and impair hematopoietic differentiation. Cancer Cell *18*, 553–567.

Fishbein, L., Khare, S., Wubbenhorst, B., DeSloover, D., D'Andrea, K., Merrill, S., Cho, N.W., Greenberg, R.A., Else, T., Montone, K., et al. (2015). Whole-exome sequencing identifies somatic ATRX mutations in pheochromocytomas and paragangliomas. Nat. Commun. *6*, 6140.

Gimenez-Roqueplo, A.P., Favier, J., Rustin, P., Rieubland, C., Crespin, M., Nau, V., Khau Van Kien, P., Corvol, P., Plouin, P.F., and Jeunemaitre, X.; COMETE Network (2003). Mutations in the SDHB gene are associated with extra-adrenal and/or malignant phaeochromocytomas. Cancer Res. *63*, 5615–5621.

Guo, W., Fiziev, P., Yan, W., Cokus, S., Sun, X., Zhang, M.Q., Chen, P.Y., and Pellegrini, M. (2013). BS-Seeker2: a versatile aligning pipeline for bisulfite sequencing data. BMC Genomics *14*, 774.

Haffner, M.C., Pellakuru, L.G., Ghosh, S., Lotan, T.L., Nelson, W.G., De Marzo, A.M., and Yegnasubramanian, S. (2013). Tight correlation of 5-hydroxymethylcytosine and Polycomb marks in health and disease. Cell Cycle *12*, 1835–1841.

Heger, A., Webber, C., Goodson, M., Ponting, C.P., and Lunter, G. (2013). GAT: a simulation framework for testing the association of genomic intervals. Bioinformatics *29*, 2046–2048.

Henegan, J.C., Jr., and Gomez, C.R. (2016). Heritable Cancer Syndromes Related to the Hypoxia Pathway. Front. Oncol. *6*, 68.

Her, Y.F., Nelson-Holte, M., and Maher, L.J., 3rd. (2015). Oxygen concentration controls epigenetic effects in models of familial paraganglioma. PLoS ONE *10*, e0127471.

Holmquist-Mengelbier, L., Fredlund, E., Löfstedt, T., Noguera, R., Navarro, S., Nilsson, H., Pietras, A., Vallon-Christersson, J., Borg, A., Gradin, K., et al. (2006). Recruitment of HIF-1alpha and HIF-2alpha to common target genes is differentially regulated in neuroblastoma: HIF-2alpha promotes an aggressive phenotype. Cancer Cell *10*, 413–423.

Isaacs, J.S., Jung, Y.J., Mole, D.R., Lee, S., Torres-Cabala, C., Chung, Y.L., Merino, M., Trepel, J., Zbar, B., Toro, J., et al. (2005). HIF overexpression correlates with biallelic loss of fumarate hydratase in renal cancer: novel role of fumarate in regulation of HIF stability. Cancer Cell *8*, 143–153.

Job, S., Draskovic, I., Burnichon, N., Buffet, A., Cros, J., Lépine, C., Venisse, A., Robidel, E., Verkarre, V., Meatchi, T., et al. (2019). Telomerase activation and ATRX mutations are independent risk factors for metastatic pheochromocytoma and paraganglioma. Clin. Cancer Res. *25*, 760–770.

Keith, B., Johnson, R.S., and Simon, M.C. (2011). HIF1α and HIF2α: sibling rivalry in hypoxic tumour growth and progression. Nat. Rev. Cancer *12*, 9–22.

Killian, J.K., Kim, S.Y., Miettinen, M., Smith, C., Merino, M., Tsokos, M., Quezado, M., Smith, W.I., Jr., Jahromi, M.S., Xekouki, P., et al. (2013). Succinate dehydrogenase mutation underlies global epigenomic divergence in gastrointestinal stromal tumor. Cancer Discov. *3*, 648–657.

Kim, D., Pertea, G., Trapnell, C., Pimentel, H., Kelley, R., and Salzberg, S.L. (2013). TopHat2: accurate alignment of transcriptomes in the presence of insertions, deletions and gene fusions. Genome Biol. *14*, R36.

Koh, M.Y., Darnay, B.G., and Powis, G. (2008). Hypoxia-associated factor, a novel E3-ubiquitin ligase, binds and ubiquitinates hypoxia-inducible factor 1alpha, leading to its oxygen-independent degradation. Mol. Cell. Biol. *28*, 7081–7095.

Koh, M.Y., Lemos, R., Jr., Liu, X., and Powis, G. (2011). The hypoxia-associated factor switches cells from HIF-1α- to HIF-2α-dependent signaling

promoting stem cell characteristics, aggressive tumor growth and invasion. Cancer Res. *71*, 4015–4027.

Koivunen, P., Lee, S., Duncan, C.G., Lopez, G., Lu, G., Ramkissoon, S., Losman, J.A., Joensuu, P., Bergmann, U., Gross, S., et al. (2012). Transformation by the (R)-enantiomer of 2-hydroxyglutarate linked to EGLN activation. Nature *483*, 484–488.

Konze, K.D., Ma, A., Li, F., Barsyte-Lovejoy, D., Parton, T., Macnevin, C.J., Liu, F., Gao, C., Huang, X.P., Kuznetsova, E., et al. (2013). An orally bioavailable chemical probe of the Lysine Methyltransferases EZH2 and EZH1. ACS Chem. Biol. *8*, 1324–1334.

Langmead, B., and Salzberg, S.L. (2012). Fast gapped-read alignment with Bowtie 2. Nat. Methods *9*, 357–359.

Laukka, T., Mariani, C.J., Ihantola, T., Cao, J.Z., Hokkanen, J., Kaelin, W.G., Jr., Godley, L.A., and Koivunen, P. (2016). Fumarate and Succinate Regulate Expression of Hypoxia-inducible Genes via TET Enzymes. J. Biol. Chem. *291*, 4256–4265.

Lee, T.I., Jenner, R.G., Boyer, L.A., Guenther, M.G., Levine, S.S., Kumar, R.M., Chevalier, B., Johnstone, S.E., Cole, M.F., Isono, K., et al. (2006). Control of developmental regulators by Polycomb in human embryonic stem cells. Cell *125*, 301–313.

Letouzé, E., Martinelli, C., Loriot, C., Burnichon, N., Abermil, N., Ottolenghi, C., Janin, M., Menara, M., Nguyen, A.T., Benit, P., et al. (2013). SDH mutations establish a hypermethylator phenotype in paraganglioma. Cancer Cell *23*, 739–752.

Li, H., Handsaker, B., Wysoker, A., Fennell, T., Ruan, J., Homer, N., Marth, G., Abecasis, G., and Durbin, R.; 1000 Genome Project Data Processing Subgroup (2009). The Sequence Alignment/Map format and SAMtools. Bioinformatics *25*, 2078–2079.

Liu, Z., Chatterjee, T.K., and Fisher, R.A. (2002). RGS6 interacts with SCG10 and promotes neuronal differentiation. Role of the G gamma subunit-like (GGL) domain of RGS6. J. Biol. Chem. *277*, 37832–37839.

Loriot, C., Domingues, M., Berger, A., Menara, M., Ruel, M., Morin, A., Castro-Vega, L.J., Letouzé, É., Martinelli, C., Bemelmans, A.P., et al. (2015). Deciphering the molecular basis of invasiveness in Sdhb-deficient cells. Oncotarget *6*, 32955–32965.

Losman, J.A., Looper, R.E., Koivunen, P., Lee, S., Schneider, R.K., McMahon, C., Cowley, G.S., Root, D.E., Ebert, B.L., and Kaelin, W.G., Jr. (2013). (R)-2-hydroxyglutarate is sufficient to promote leukemogenesis and its effects are reversible. Science *339*, 1621–1625.

Lu, C., Venneti, S., Akalin, A., Fang, F., Ward, P.S., Dematteo, R.G., Intlekofer, A.M., Chen, C., Ye, J., Hameed, M., et al. (2013). Induction of sarcomas by mutant IDH2. Genes Dev. *27*, 1986–1998.

Luo, W., Zhong, J., Chang, R., Hu, H., Pandey, A., and Semenza, G.L. (2010). Hsp70 and CHIP selectively mediate ubiquitination and degradation of hypoxia-inducible factor (HIF)-1alpha but Not HIF-2alpha. J. Biol. Chem. *285*, 3651–3663.

Lussey-Lepoutre, C., Hollinshead, K.E., Ludwig, C., Menara, M., Morin, A., Castro-Vega, L.J., Parker, S.J., Janin, M., Martinelli, C., Ottolenghi, C., et al. (2015). Loss of succinate dehydrogenase activity results in dependency on pyruvate carboxylation for cellular anabolism. Nat. Commun. *6*, 8784.

Marie-Egyptienne, D.T., Lohse, I., and Hill, R.P. (2013). Cancer stem cells, the epithelial to mesenchymal transition (EMT) and radioresistance: potential role of hypoxia. Cancer Lett. *341*, 63–72.

Mohammad, F., Weissmann, S., Leblanc, B., Pandey, D.P., Højfeldt, J.W., Comet, I., Zheng, C., Johansen, J.V., Rapin, N., Porse, B.T., et al. (2017). EZH2 is a potential therapeutic target for H3K27M-mutant pediatric gliomas. Nat. Med. *23*, 483–492.

Morin, A., Letouzé, E., Gimenez-Roqueplo, A.P., and Favier, J. (2014). Oncometabolites-driven tumorigenesis: From genetics to targeted therapy. Int. J. Cancer *135*, 2237–2248.

Myszczyszyn, A., Czarnecka, A.M., Matak, D., Szymanski, L., Lian, F., Kornakiewicz, A., Bartnik, E., Kukwa, W., Kieda, C., and Szczylik, C. (2015). The Role of Hypoxia and Cancer Stem Cells in Renal Cell Carcinoma Pathogenesis. Stem Cell Rev. Rep. *11*, 919–943.

Neph, S., Kuehn, M.S., Reynolds, A.P., Haugen, E., Thurman, R.E., Johnson, A.K., Rynes, E., Maurano, M.T., Vierstra, J., Thomas, S., et al. (2012). BEDOPS: high-performance genomic feature operations. Bioinformatics *28*, 1919–1920.

Neri, F., Incarnato, D., Krepelova, A., Rapelli, S., Pagnani, A., Zecchina, R., Parlato, C., and Oliviero, S. (2013). Genome-wide analysis identifies a functional association of Tet1 and Polycomb repressive complex 2 in mouse embryonic stem cells. Genome Biol. *14*, R91.

Nilsson, H., Jögi, A., Beckman, S., Harris, A.L., Poellinger, L., and Påhlman, S. (2005). HIF-2alpha expression in human fetal paraganglia and neuroblastoma: relation to sympathetic differentiation, glucose deficiency, and hypoxia. Exp. Cell Res. *303*, 447–456.

Ohm, J.E., McGarvey, K.M., Yu, X., Cheng, L., Schuebel, K.E., Cope, L., Mohammad, H.P., Chen, W., Daniel, V.C., Yu, W., et al. (2007). A stem cell-like chromatin pattern may predispose tumor suppressor genes to DNA hypermethylation and heritable silencing. Nat. Genet. *39*, 237–242.

Pastor, W.A., Pape, U.J., Huang, Y., Henderson, H.R., Lister, R., Ko, M., McLoughlin, E.M., Brudno, Y., Mahapatra, S., Kapranov, P., et al. (2011). Genome-wide mapping of 5-hydroxymethylcytosine in embryonic stem cells. Nature *473*, 394–397.

Pietras, A., Johnsson, A.S., and Påhlman, S. (2010). The HIF-2α-driven pseudo-hypoxic phenotype in tumor aggressiveness, differentiation, and vascularization. Curr. Top. Microbiol. Immunol. *345*, 1–20.

Putiri, E.L., Tiedemann, R.L., Thompson, J.J., Liu, C., Ho, T., Choi, J.H., and Robertson, K.D. (2014). Distinct and overlapping control of 5-methylcytosine and 5-hydroxymethylcytosine by the TET proteins in human cancer cells. Genome Biol. *15*, R81.

Qin, N., de Cubas, A.A., Garcia-Martin, R., Richter, S., Peitzsch, M., Menschikowski, M., Lenders, J.W., Timmers, H.J., Mannelli, M., Opocher, G., et al. (2014). Opposing effects of HIF1α and HIF2α on chromaffin cell phenotypic features and tumor cell proliferation: Insights from MYC-associated factor X. Int. J. Cancer *135*, 2054–2064.

Quinlan, A.R., and Hall, I.M. (2010). BEDTools: a flexible suite of utilities for comparing genomic features. Bioinformatics *26*, 841–842.

Rampal, R., Alkalin, A., Madzo, J., Vasanthakumar, A., Pronier, E., Patel, J., Li, Y., Ahn, J., Abdel-Wahab, O., Shih, A., et al. (2014). DNA hydroxymethylation profiling reveals that WT1 mutations result in loss of TET2 function in acute myeloid leukemia. Cell Rep. *9*, 1841–1855.

Rose, N.R., McDonough, M.A., King, O.N., Kawamura, A., and Schofield, C.J. (2011). Inhibition of 2-oxoglutarate dependent oxygenases. Chem. Soc. Rev. *40*, 4364–4397.

Roussa, E., and Krieglstein, K. (2004). GDNF promotes neuronal differentiation and dopaminergic development of mouse mesencephalic neurospheres. Neurosci. Lett. *361*, 52–55.

Schlesinger, Y., Straussman, R., Keshet, I., Farkash, S., Hecht, M., Zimmerman, J., Eden, E., Yakhini, Z., Ben-Shushan, E., Reubinoff, B.E., et al. (2007). Polycomb-mediated methylation on Lys27 of histone H3 pre-marks genes for de novo methylation in cancer. Nat. Genet. *39*, 232–236.

Schnepp, A., Komp Lindgren, P., Hülsmann, H., Kröger, S., Paulsson, M., and Hartmann, U. (2005). Mouse testican-2. Expression, glycosylation, and effects on neurite outgrowth. J. Biol. Chem. *280*, 11274–11280.

Selak, M.A., Armour, S.M., MacKenzie, E.D., Boulahbel, H., Watson, D.G., Mansfield, K.D., Pan, Y., Simon, M.C., Thompson, C.B., and Gottlieb, E. (2005). Succinate links TCA cycle dysfunction to oncogenesis by inhibiting HIF-alpha prolyl hydroxylase. Cancer Cell *7*, 77–85.

Sinha, S., Thomas, D., Yu, L., Gentles, A.J., Jung, N., Corces-Zimmerman, M.R., Chan, S.M., Reinisch, A., Feinberg, A.P., Dill, D.L., and Majeti, R. (2015). Mutant WT1 is associated with DNA hypermethylation of PRC2 targets in AML and responds to EZH2 inhibition. Blood *125*, 316–326.

Sousa, B., Pereira, J., and Paredes, J. (2019). The Crosstalk Between Cell Adhesion and Cancer Metabolism. Int. J. Mol. Sci. *20*, 1933.

Stanzel, S., Stubbusch, J., Pataskar, A., Howard, M.J., Deller, T., Ernsberger, U., Tiwari, V.K., Rohrer, H., and Tsarovina, K. (2016). Distinct roles of hand2 in developing and adult autonomic neurons. Dev. Neurobiol. *76*, 1111–1124.

Stark, R., and Brown, G. (2011). DiffBind: Differential binding analysis of ChIP-Seq peak data. In Bioconductor (Cambridge, UK: University of Cambridge).

Svahn, F., Juhlin, C.C., Paulsson, J.O., Fotouhi, O., Zedenius, J., Larsson, C., and Stenman, A. (2018). Telomerase reverse transcriptase promoter hypermethylation is associated with metastatic disease in abdominal paraganglioma. Clin. Endocrinol. (Oxf.) *88*, 343–345.

Thienpont, B., Steinbacher, J., Zhao, H., D'Anna, F., Kuchnio, A., Ploumakis, A., Ghesquière, B., Van Dyck, L., Boeckx, B., Schoonjans, L., et al. (2016). Tumour hypoxia causes DNA hypermethylation by reducing TET activity. Nature *537*, 63–68.

Thomson, J.P., Ottaviano, R., Unterberger, E.B., Lempiäinen, H., Muller, A., Terranova, R., Illingworth, R.S., Webb, S., Kerr, A.R., Lyall, M.J., et al. (2016). Loss of Tet1-Associated 5-Hydroxymethylcytosine Is Concomitant with Aberrant Promoter Hypermethylation in Liver Cancer. Cancer Res. *76*, 3097–3108.

Toyofuku, T., Zhang, H., Kumanogoh, A., Takegahara, N., Suto, F., Kamei, J., Aoki, K., Yabuki, M., Hori, M., Fujisawa, H., and Kikutani, H. (2004). Dual roles of Sema6D in cardiac morphogenesis through region-specific association of its receptor, Plexin-A1, with off-track and vascular endothelial growth factor receptor type 2. Genes Dev. *18*, 435–447.

Turcan, S., Rohle, D., Goenka, A., Walsh, L.A., Fang, F., Yilmaz, E., Campos, C., Fabius, A.W., Lu, C., Ward, P.S., et al. (2012). IDH1 mutation is sufficient to establish the glioma hypermethylator phenotype. Nature *483*, 479–483.

Uchida, T., Rossignol, F., Matthay, M.A., Mounier, R., Couette, S., Clottes, E., and Clerici, C. (2004). Prolonged hypoxia differentially regulates hypoxia-inducible factor (HIF)-1alpha and HIF-2alpha expression in lung epithelial cells: implication of natural antisense HIF-1alpha. J. Biol. Chem. *279*, 14871–14878.

Uribe-Lewis, S., Stark, R., Carroll, T., Dunning, M.J., Bachman, M., Ito, Y., Stojic, L., Halim, S., Vowler, S.L., Lynch, A.G., et al. (2015). 5-hydroxymethylcytosine marks promoters in colon that resist DNA hypermethylation in cancer. Genome Biol. *16*, 69.

Verma, S.K., Tian, X., LaFrance, L.V., Duquenne, C., Suarez, D.P., Newlander, K.A., Romeril, S.P., Burgess, J.L., Grant, S.W., Brackley, J.A., et al. (2012). Identification of Potent, Selective, Cell-Active Inhibitors of the Histone Lysine Methyltransferase EZH2. ACS Med. Chem. Lett. *3*, 1091–1096.

Verma, N., Pan, H., Doré, L.C., Shukla, A., Li, Q.V., Pelham-Webb, B., Teijeiro, V., González, F., Krivtsov, A., Chang, C.J., et al. (2018). TET proteins safeguard bivalent promoters from de novo methylation in human embryonic stem cells. Nat. Genet. *50*, 83–95.

Viré, E., Brenner, C., Deplus, R., Blanchon, L., Fraga, M., Didelot, C., Morey, L., Van Eynde, A., Bernard, D., Vanderwinden, J.M., et al. (2006). The Polycomb group protein EZH2 directly controls DNA methylation. Nature *439*, 871–874.

Wang, Y., Xiao, M., Chen, X., Chen, L., Xu, Y., Lv, L., Wang, P., Yang, H., Ma, S., Lin, H., et al. (2015). WT1 recruits TET2 to regulate its target gene expression and suppress leukemia cell proliferation. Mol. Cell *57*, 662–673.

Wassef, M., Luscan, A., Aflaki, S., Zielinski, D., Jansen, P.W.T.C., Baymaz, H.I., Battistella, A., Kersouani, C., Servant, N., Wallace, M.R., et al. (2019). EZH1/2 function mostly within canonical PRC2 and exhibit proliferation-dependent redundancy that shapes mutational signatures in cancer. Proc. Natl. Acad. Sci. USA *116*, 6075–6080.

Williams, K., Christensen, J., Pedersen, M.T., Johansen, J.V., Cloos, P.A., Rappsilber, J., and Helin, K. (2011a). TET1 and hydroxymethylcytosine in transcription and DNA methylation fidelity. Nature *473*, 343–348.

Williams, S.C., Karajannis, M.A., Chiriboga, L., Golfinos, J.G., von Deimling, A., and Zagzag, D. (2011b). R132H-mutation of isocitrate dehydrogenase-1 is not sufficient for HIF-1α upregulation in adult glioma. Acta Neuropathol. *121*, 279–281.

Wu, H., D'Alessio, A.C., Ito, S., Wang, Z., Cui, K., Zhao, K., Sun, Y.E., and Zhang, Y. (2011). Genome-wide analysis of 5-hydroxymethylcytosine distribution reveals its dual function in transcriptional regulation in mouse embryonic stem cells. Genes Dev. *25*, 679–684.

Xiao, M., Yang, H., Xu, W., Ma, S., Lin, H., Zhu, H., Liu, L., Liu, Y., Yang, C., Xu, Y., et al. (2012). Inhibition of α-KG-dependent histone and DNA demethylases by fumarate and succinate that are accumulated in mutations of FH and SDH tumor suppressors. Genes Dev. *26*, 1326–1338.

Xu, B., Zeng, D.Q., Wu, Y., Zheng, R., Gu, L., Lin, X., Hua, X., and Jin, G.H. (2011). Tumor suppressor menin represses paired box gene 2 expression via Wilms tumor suppressor protein-polycomb group complex. J. Biol. Chem. *286*, 13937–13944.

Yamamoto, A., Uchiyama, K., Nara, T., Nishimura, N., Hayasaka, M., Hanaoka, K., and Yamamoto, T. (2014). Structural abnormalities of corpus callosum and cortical axonal tracts accompanied by decreased anxiety-like behavior and lowered sociability in spock3- mutant mice. Dev. Neurosci. *36*, 381–395.

Zhang, Y., Liu, T., Meyer, C.A., Eeckhoute, J., Johnson, D.S., Bernstein, B.E., Nusbaum, C., Myers, R.M., Brown, M., Li, W., and Liu, X.S. (2008). Model-based analysis of ChIP-Seq (MACS). Genome Biol. *9*, R137.

Zhao, S., Lin, Y., Xu, W., Jiang, W., Zha, Z., Wang, P., Yu, W., Li, Z., Gong, L., Peng, Y., et al. (2009). Glioma-derived mutations in IDH1 dominantly inhibit IDH1 catalytic activity and induce HIF-1alpha. Science *324*, 261–265.

STAR★METHODS

KEY RESOURCES TABLE

REAGENT or RESOURCE	SOURCE	IDENTIFIER
Antibodies		
anti-H3K27me3	Diagenode	Cat# C15410069, RRID: AB_2814977
anti-5mC	Calbiochem	Cat# NA81-50UG, RRID: AB_213180
anti-5hmC	Active Motif	Cat# 39769, RRID: AB_10013602
anti-ssDNA	Millipore	Cat# MAB3299, RRID: AB_94795
biotinylated secondary antibody	VECTOR	Cat# BA-1000, RRID: AB_2313606
HRP-conjugated mouse secondary antibodies	Biovision	Cat# 6402-05, RRID: AB_657968
HRP-conjugated rabbit secondary antibodies	Biorad	Cat# 170-6515, RRID: AB_11125142
anti-actin	Sigma-Aldrich	Cat# A5316, RRID: AB_476743
anti-TET1	Millipore	Cat# 09-872, RRID: AB_10806199
anti-TET2	Proteintech	Cat# 21207-1-AP, RRID: AB_10734584
anti-TET3	Active motif	Cat#61744 clone 23B9; RRID: AB_2793753
anti-HIF2α	Abcam	Cat# ab8365, RRID: AB_306519
anti-HIF2α	Abcam	Cat# ab109616, RRID: AB_11156727
Anti-H3K27me3	Active Motif	Cat# 39156, RRID: AB_2636821
anti-H3-Cterminal	Active Motif	Cat# 39451, RRID: AB_2793242
Anti-Hif2α antibody	R&D Systems	Cat# AF2997, RRID: AB_2098218
Donkey anti-rabbit secondary antibody, Alexa Fluor 594	Invitrogen	Cat# A-21207, RRID: AB_141637
Bacterial and Virus Strains		
pLKO.1 empty vector	Sigma-Aldrich	
Tet1 shRNA pLKO.1-puro vector	Sigma-Aldrich	TRCN0000341849
Tet2 shRNA pLKO.1-puro vector	Sigma-Aldrich	TRCN0000250894
HIF1α pLKO.1-puro vector	Sigma-Aldrich	TRCN0000232220
HIF2α pLKO.1-puro vector	Sigma-Aldrich	TRCN000082304
shSCR pLKO.1-puro vector	Sigma-Aldrich	SHC016
Biological Samples		
HUMAN: Frozen paraganglioma samples	COMETE Collection	N/A
Chemicals, Peptides, and Recombinant Proteins		
DMEM (Dulbecco Modified Eagle Medium)	GIBCO	31966-021
Fetal bovine serum	GIBCO	10270
Penicillin/Streptomycin	GIBCO	15140-122
UNC1999	Sigma-Aldrich	SML0778
UNC2400	SGC	https://www.thesgc.org/chemical-probes
GSK343	Sigma-Aldrich	SML0766
DMSO	Sigma-Aldrich	D4540
trypsin-EDTA 0.05%	GIBCO	25300-054
puromycin	Invivogen	CAS 58-58-2
polybrene	Sigma-Aldrich	TR-1003-G
proteinase K	Sigma-Aldrich	1245680500
PBS	GIBCO	10010-015
QiaAmp DNA mini kit,	QIAGEN	51306
DNA coating buffer	Thermofisher	17250
Kathon	Supelco	5-00127

(*Continued on next page*)

Continued

REAGENT or RESOURCE	SOURCE	IDENTIFIER
Tween 20	Sigma-Aldrich	P1379
Streptavidin HRP	BD Bioscience	554066
RIPA buffer	Abcam	Ab156034
NuPAGE® Novex 4–16% Bis-Tris gradient gel	Invitrogen	NP0335BOX
PVDF membrane	Millipore	IPVH00010
nitrocellulose membrane	Amersham	10600001
H2SO4	VWR	20700.298
trichloroacetic acid	Sigma-Aldrich	T6399
acetone	VWR	E646-1L
formaldehyde	VWR	11699404
triton buffer	Sigma-Aldrich	T8787
Phalloidin-TRITC toxin	Sigma-Aldrich	#P1951
vectashield with Dapi	VECTOR	H-1200
Critical Commercial Assays		
AllPrep extraction kit	QIAGEN	80204
NEXTflex PCR-Free DNA Sequencing kit	Diagenode	ref. C02010021
MagMeDIP kit	Diagenode	C02010021
Genomic DNA Clean & Concentrator kit	Zymo Research	ref. D4010
RNeasy plus mini-kit	QIAGEN	74134
iScript enzyme	BioRad	1708891
TrueMethyl 24 kit	Cambridge Epigenetix	N/A
SuperScript SybrGreen	BioRad	#1725151
iDeal ChIP-qPCR kit	Diagenode	#C01010180
GenElute Mammalian genomic DNA kit	Sigma-Aldrich	#G1N350
Genomic DNA Clean & Concentrator kit	Zymo Research	ref. D4010
Deposited Data		
MeDIP-seq, RRBS and oxRRBS data	European Genome Phenome Archive	EGA: EGAS00001004252
Experimental Models: Cell Lines		
MOUSE: imCC WT	Letouzé et al., 2013	N/A
MOUSE: imCC Sdhb−/−	Letouzé et al., 2013	N/A
Experimental Models: Organisms/Strains		
NMRI nude mice	Janvier Lab	N/A
Oligonucleotides		
Oligonucleotides	This study	Table S3
Software and Algorithms		
bowtie2	Langmead and Salzberg, 2012	http://bowtie-bio.sourceforge.net/bowtie2/index.shtml
Picard Tools	Broadinstitute	http://picard.sourceforge.net
SAMtools	Li et al., 2009	http://samtools.sourceforge.net
MACS	Zhang et al., 2008	https://github.com/taoliu/MACS
bedtools	Quinlan and Hall, 2010	https://bedtools.readthedocs.io/en/latest/
GAT	Heger et al., 2013	https://gat.readthedocs.io/en/latest/
Bioconductor DiffBind package	Stark and Brown, 2011	https://bioconductor.org/packages/release/bioc/html/DiffBind.html
Bedmap tool from the BEDOPS suite	Neph et al., 2012	https://bedops.readthedocs.io/en/latest/
Bioconductor DESeq package	Anders and Huber, 2010	https://bioconductor.org/packages/release/bioc/html/DESeq.html

(*Continued on next page*)

Continued

REAGENT or RESOURCE	SOURCE	IDENTIFIER
FastQC	Babraham Bioinformatics	http://www.bioinformatics.babraham.ac.uk/projects/fastqc/
tophat2	Kim et al., 2013	https://ccb.jhu.edu/software/tophat/index.shtml
HTSeq	Anders et al., 2015	https://htseq.readthedocs.io/en/release_0.11.1/
R statistical software	The R Foundation	https://cran.r-project.org
BS-Seeker2	Guo et al., 2013	https://github.com/BSSeeker/BSseeker2
methylKit package	Akalin et al., 2012	https://bioconductor.org/packages/release/bioc/html/methylKit.html
R code from the GSEA website		https://www.gsea-msigdb.org/gsea/index.jsp
PRISM 8	Graphpad	https://www.graphpad.com/scientific-software/prism/
NIS-advanced imaging software	Nikon	https://www.microscope.healthcare.nikon.com/products/software/nis-elements
Other		
MSigDB database version 5.1	UCSD, Broad Institute	https://www.gsea-msigdb.org/gsea/msigdb/index.jsp

LEAD CONTACT AND MATERIALS AVAILABILITY

Further information and requests should be directed to and will be fulfilled by the Lead Contact, Judith Favier (judith.favier@inserm.fr). This study did not generated new unique reagents.

EXPERIMENTAL MODEL AND SUBJECT DETAILS

Patients and tumor samples

We used tumor samples from 4 patients (see gender and age of the patients in the table Data generated) recruited in the COMETE network and previously characterized by HM27 methylome Chip and transcriptomic arrays in Letouze et al., 2013. This seminal paper identified 3 clusters: M1 (mainly SDH tumors), M2 (contains most VHL tumors), and M3 (included NF1, RET, and sporadic tumors). To be homogeneous, 2 *NF1*-mutated pheochromocytomas were selected in cluster M3, and compared to 2 *SDHB*-mutated pheochromocytomas from cluster M1.

Mammalian cell line

imCC were cultured in DMEM (Dulbecco Modified Eagle Medium, GIBCO) with 10% FBS (Fetal bovine serum, GIBCO) and 1% antibiotics (penicillin/streptomycin, GIBCO). Cells were grown at 37°C, in 5% CO2.

Data generated

Genotype	Sample	Gender	Age at surgery	meDIP-seq	oxRRBS	RRBS	Transcriptomic
SDHB-WT (*NF1*-mut)	Human tumor HS_033	Female	66	yes	yes	yes	arrays
SDHB-WT (*NF1*-mut)	Human tumor HS_045	Female	52	yes	yes	yes	arrays
SDHB-mut	Human tumor HS_144	Male	28	yes	yes	yes	arrays
SDHB-mut	Human tumor HS_196	Female	31	yes	yes	yes	arrays
$Sdhb^{lox/lox}$ (WT)	imCC	Female		yes	yes	yes	RNA-seq
$Sdhb^{-/-}$	imCC	Female		yes	yes	yes	RNA-seq
$Tet1{+}Tet2^{KD}$	imCC Cl74	Female		no	no	yes	no

Mouse model

Athymic nude NMRI female mice (6-weeks old, Janvier Labs, France) were maintained in specific pathogen-free conditions in a temperature-controlled environment with 12 h light, 12 h dark cycles and received food and water *ad libitum* at the animal facility of the PARCC Paris, France. Animal experiments were performed by certified personal following the French law on animal experimentation n°2013-118 and were approved by the French Ethical Committee (#16922-2017122215408962v4).

METHOD DETAILS

MeDIP-seq analysis

gDNA extracted with AllPrep extraction kit (QIAGEN) was fragmented by sonication and used to prepare non-amplified DNA libraries with the NEXTflex PCR-Free DNA Sequencing kit. 1ug of the equimolar pool of all sample libraries (with internal IP "spike-in" controls added) was kept as input, and 3ug was used for meDIP-seq with MagMeDIP kit (Diagenode ref. C02010021). Immunoprecipitation was conducted following manufacturer instructions. Briefly, after heat-denaturation, DNA was incubated overnight with magnetic beads coated with anti-5mC antibody. Beads were washed and then eluted by proteinase K digestion of the antibody. Eluted DNA was further purified with Genomic DNA Clean & Concentrator kit (Zymo Research ref. D4010). IP efficiency and specificity was verified by qPCR targeting the internal controls. Sequencing was performed on an Illumina HiSeq2000 as paired-end 75 bp reads.

Fastq files were aligned to the reference human genome hg19 and mouse genome mm10 with bowtie2 (Langmead and Salzberg, 2012). We filtered and kept only reads mapping to one location. Duplicated reads were removed from the datasets using Picard Tools (http://picard.sourceforge.net) and total number of reads were down-sized to the minimum available read count for each type of samples (MeDIP 48.10^6 reads and INPUT 74.10^6 reads for human samples, and MeDIP 62.10^6 reads and INPUT 73.10^6 reads for mouse samples) using SAMtools (Li et al., 2009). Peaks were identified using MACS (Zhang et al., 2008) (-s 50 -p 10^{-5} -m 10,30) and associated to closest TSS using bedtools (Quinlan and Hall, 2010). We used GAT (Heger et al., 2013) to perform genomic association analysis of our peaks with gene annotations and CpG island, shore, and shelf annotation. We used the Bioconductor *DiffBind* package (Stark and Brown, 2011) to define a common set of peaks between all samples (peaks common to at least two samples are considered). We used the bedmap tool from the BEDOPS suite (Neph et al., 2012) to collect read counts for all MeDIP and INPUT samples within the common set of peaks. We created a normalized binding matrix with, for each peak and MeDIP sample, a read count normalized with peak size. The log2 normalized binding matrix from the 1,000 most variant peaks (based on standard deviation of the normalized read counts) was used to classify the samples according to their binding patterns using hierarchical clustering (with Euclidian distance and Ward method). We used the Bioconductor *DESeq* package (Anders and Huber, 2010) to test for differential read counts between samples, without correcting for size factors as libraries had been previously down-sized.

RNA-seq analysis

Quality of reads was assessed for each sample using FastQC (http://www.bioinformatics.babraham.ac.uk/projects/fastqc/). Fastq files were aligned to the reference Human genome hg19/GRCh37 or to the reference Mouse genome mm10 with tophat2 (-p 16 -r 150 -g 2–library-type fr-firststrand) (Kim et al., 2013). We removed reads mapping to multiple locations. We used HTSeq (Anders et al., 2015) to obtain the number of reads associated to each gene in the Gencode vM9 (Mouse) database, restricting to protein-coding genes, antisense and lncRNAs. We used the Bioconductor DESeq package (Anders and Huber, 2010) to import raw HTSeq counts for each sample into R statistical software and extract the count matrix. After normalizing for library size, we normalized the count matrix by the coding length of genes to compute FPKM scores (number of fragments per kilobase of exon model and millions of mapped reads). We used the Bioconductor *DESeq* package to obtain size factors and dispersion estimates, and perform differential expression analysis.

oxRRBS and RRBS Analyses

RRBS was performed by Integragen SA (Evry, France), as previously described (Letouze et al.). This analysis does not distinguish 5mC from 5hmC, and considering the low levels of 5hmC compared to 5mC, it represents a good estimation of 5mC levels.

oxRRBS analysis is required for 5hmC quantification. An additional oxidative step converts 5hmC to 5fC which is sensitive to bisulfite treatment, unlike 5mC and 5hmC. Each sample is thus run for both RRBS and oxRRBS procedures in parallel. 5hmC levels are calculated by subtracting RRBS – oxRRBS signals.

oxRRBS was performed by Integragen SA (Evry, France), as described in Letouzé et al. (2013) for the MspI Reduced Representation part, and following the TrueMethyl 24 kit manufacturer protocol user guide version 3.1 (https://www.nugen.com/support/user-manuals) for the OxBS part. In brief, 4 μg of genomic DNA plus CeGX Sequencing Control (3% W/W) were digested with MspI (NEB) then SPRI 2.2X purified. After end-repair, A-tailing, and ligation to methylated Illumina adapters, the library fragments of 40–220 bp were gel isolated, and oxidative bisulfite- and only bisulfite-converted DNA templates were generated using the TrueMethyl 24 kit (Cambridge Epigenetix) for each sample according to the manufacturer's instructions. Last, oxRRBS- and RRBS-converted DNA were PCR amplified with 16 cycles, SPRI 1.8X purified and sequenced on an Illumina HiSeq2000 or HiSeq4000 as paired-end 75 bp reads.

We generated approximately 30 millions uniquely aligned reads for each sample, which covered ≈8 million CpG (Figure S1C; Table S2). We used BS-Seeker2 (Guo et al., 2013) to map RRBS data to the human genome hg19/GRCh37 or Mouse genome mm10 and retrieve the number of methylated and unmethylated cytosines at each covered CpG site. Methylation rates were then integrated across CpG island (CGI)-based and gene-based features. CGI-based features were defined as follows: CpG islands (from UCSC database hg19/GRCh37 or Mouse mm10), shores (2 kb on each side of the island) and shelves (2 kb on each side of the shores). DNA methylation outside CpG islands was analyzed by grouping CpG sites not located in CGI-based features every 100kb window. Gene-based features were defined based on Ensembl *Homo sapiens* GRCh37.p13 or *Mus musculus* GRCm38.78

assembly. We calculated for each gene the methylation rate across the promoter region (TSS ± 500bp) and the gene body (Figure S1A).

5hmC detection using (ox)RRBS data

To detect the presence of 5hmC, we compared the proportions of converted C bases between the RRBS and oxRRBS experiments in each CGI- and gene-based feature using Fisher's exact tests, corrected for multiple testing using Benjamini Hochberg procedure. We verified that >90% of features with a significant difference ($q < 0.05$) had an excess of converted bases in the oxRRBS experiment, as expected, indicating that we detected true 5hmC signal and not random noise. Finally, we considered that 5hmC was detected in a feature when the q value of the Fisher's exact test was < 0.05, with ≥ 100 CpGs analyzed, and we estimated the 5hmC rate as the delta between the proportions of converted C bases in the RRBS and oxRRBS experiments. For other features the 5hmC rate was considered to be zero.

Differential (hydroxy)methylation analysis

We compared methylation rates across all CGI-based and gene-based features (covered by at least 50 reads). q values were computed by comparing the number of (hydroxy) methylated and un(hydroxy)methylated reads in each condition using a logistic regression and the SLIM method for pvalue adjustment, as implemented in the methylKit package (Akalin et al., 2012). We also calculated the methylation rate difference (delta) between each pair of test and reference sample. We considered as differentially methylated every region with a q-value < 0.05 and a methylation delta >0.05 or <−0.05 in at least 80% of test-reference pairs.

Gene set enrichment analysis

We used the GSEA method (Subramanian et al., 2005) to identify gene sets overrepresented among up/down- regulated and hyper/hypomethylated genes. The GSEA method calculates an enrichment score that reflects the degree to which genes belonging to a given gene set are overrepresented at the top or bottom of a gene list, ranked for example by their expression fold-change between two conditions. The statistical significance (nominal p value) of the enrichment score is derived using a permutation test procedure, and p values across gene sets are adjusted for multiple testing. We used the R code downloaded from the GSEA website (https://www.gsea-msigdb.org/gsea/index.jsp) to calculate enrichment scores, significance p values and q-values, which we adapted to be able to provide any ranked gene list as input. For RNA-seq analyses, genes were ranked according to their expression fold-change between the two conditions (e.g., *Sdhb*−/− versus wild-type cells). For MeDIP-seq analyses, genes were ranked according to the fold-change of methylation signal within their TSS region (TSS ± 500 bp) between the two conditions. For RR(ox)BS analyses, genes were ranked according to the methylation rate difference (delta) within their TSS region (TSS ± 500 bp) between the two conditions. We downloaded gene sets from the MSigDB database (version 5.1) and restricted our analysis to the hallmark (H), curated (C2) and oncogenic (C6) gene sets.

Inhibition of PRC2 activity

When stated they WT or *Sdhb*−/− imCC were treated with GSK343 or vehicle (DMSO) for 5 to 7 passages (17 to 24 days), or treated with UNC1999, UNC2400 or vehicule (DMSO) for 15 days, or cultured for indicated times at 2% O2 in a nitrogen-supplemented hypoxic incubator. For GSK343 treatments, the classical of dose of 3 μM was chosen (Mohammad et al., 2017) as it allows a potent EZH2 inhibition (IC_{50} = 4nM) and has been described as the growth IC_{50} value (2.9 μM) in the most sensitive cell lines studied (prostate cancer cell line LNCaP) (Verma et al., 2012). For UNC1999 and UN2400 (Konze et al., 2013) we chose a dose of 1 μM as used in Wassef et al. (2019).

Proliferation assay

Proliferation curves were established on a 7 days period. When stated, cells were preincubated for 72h in normoxia or hypoxia before cell counting. Proliferation index were calculated as the differential coefficient of the linear regression from cell proliferation curves.

Adhesion assay

After complete detachment from their plate using trypsin-EDTA 0.05% (GIBCO), cells were plated in 12-wells dishes. Cell adhesion was analyzed by taking picture 1 to 3 h post-seeding. Percentage of adhesive cells at 1 to 1.5 h allowed accurate comparison of WT to *Sdhb*−/− cells. 3 h were more appropriate to distinguish Tet1+Tet2^{KD} cells from shSCR cells, but at that time point, 100% *Sdhb*−/− cells were adherent, in normoxia as in hypoxia.

Wound scratch assay

Wound scratch assays were performed as described elsewhere (Loriot et al., 2015) and analyzed using ImageJ software or using Nikon videomicroscope and NIS-advanced imaging software. The experiments were performed in triplicates.

shRNA stable transduction

Lentiviral constructs were purchased at Sigma-Aldrich. pLKO.1 is the parental viral vector without shRNA. WT imCC (30000) were infected in a serum-free medium containing 8 μg/mL polybrene by either 10 MOI of Tet1 (TRCN0000341849) and 10 MOI of Tet2

(TRCN0000250894) shRNA vectors, or 20 MOI of scramble shRNA vector targeting no known mammalian genes (shSCR SHC016). 48 h post-infection, transduced cells were selected by puromycin treatment (4 μg/mL) for 13 days and sub-cloned. Clones were screened for Tet1 and Tet2 knockdown by qRT-PCR and protein inhibition in selected clones was confirmed by Western Blot.

Sdhb−/− imCC (50,000) were seeded in 48-well plates. 24 h later, cells were washed twice with PBS and transduced with 10 MOI of lentiviral vectors (pLKO.1-puro, Sigma-Aldrich) encoding shRNAs for HIF1α (TRCN0000232220) or HIF2α (TRCN000082304) in the presence of polybrene [8 μg/ml] and serum-free medium. Double transductions (HIF1α +HIF2α) were performed at a MOI of 20. 24 h later, fresh complete medium was added and selection was started with puromycin [4 μg/ml] for wild-type or [2 μg/ml] for *Sdhb*−/−. After 1 week of selection, cells were trypsinized and amplified. Then, to obtain clones, a limiting dilution assay was performed for each condition in 96-well plates. Clones were screened for HIF2 or HIF1+HIF2 knockdown by qRT-PCR and HIF2α protein inhibition in selected clones was confirmed by Western Blot.

Reversed Transcription and Quantitative Real-Time PCR

Total RNAs were extracted from cell pellets using RNeasy plus mini-kit (QIAGEN) as described by the manufacturer. Reverse transcription was performed using random primers and iScript enzyme (BioRad), during 30 mn at 42°C. qRT-PCR was run with SuperScript SybrGreen (BioRad) and normalization was performed with Ubc, B2m and 18S amplifications, and comparisons were calculated using the ΔΔCt method. Primers' sequences were as follows:

Ubc: F 5′-AGCCCAGTGTTACCACCAAG-3′; R 5′-ACCCAAGAACAAGCACAAG-3′;
18 S: F 5′-CGCGGTTCTATTTTGTTGGT-3′; R 5′-AACCATAAACGATGCCGAC-3′;
B2m: F 5′-ATTCACCCCCACTGAGACTG-3′; R 5′-TGCTATTTCTTTCTGCGTGC-3′
Hand2: F 5′-CCAGCTACATCGCCTACCTC-3′; R 5′-TGGTTTTCTTGTCGTTGCTG-3′
Gdnf: F 5′-CTGTCTGCCTGGTGTTGCT-3′; R 5′-CTGCCGCTTGTTTATCTGGT-3′
Wnt11: F 5′-TCCGATGCTCCTATGAAGGT-3′; R 5′-CTGACAGGTAGCGGGTCTTG-3′
Sema6d: F 5′-GCTTCCCAGAAGACGATGAG-3′; R 5′-CTGTTTGGGGGATTTCATTT-3′
Stmn2: F 5′-CTACGACGACATGGAGGTGA-3′; R 5′-CCTCTTCTCTGCCAACTGCT-3′
Spock2: F 5′-CCATCGGTTGGATGTTCTCT-3′; R 5′-GACACCTGGCTTCTTCTTGG-3′
Spock3: F 5′-AGGATTCACTTGGCTGGATG-3′; R 5′-TTTATCCCCTGTCGCTTCTG-3′
Snai1: F 5′-TGGAAAGGCCTTCTCTAGGC-3′; R 5′-AAAAGCACGGTTGCAGTGG-3′
Twist1: F 5′-GACTCCAAGATGGCAAGCTG-3′; R 5′-TTCTCTGGAAACAATGACATCTAGGT-3′
Cdh2: F 5′-GAAGATGTTTACAGCGCAGTCTT-3′; R 5′-CTCGCTGCTTTCATACTGAACTT-3′
Epas1: F 5′-AGGGCCACAGCAAAGAGAG-3′; R 5′-CATCACGGGATTTCTCCTTC-3′
Glut1: F 5′-AAACATGGAACCACCGCTAC-3′; R 5′-GGAGAAGCCCATAAGCACAG-3′
Hif1a: F 5′-TCAGCATACAGTGGCACTCA-3′; R 5′-AAGGGAGCCATCATGTTCCA-3′

ChIP-qPCR

Chromatin immunoprecipitation was performed on $1*10^6$ cells using the iDeal ChIP-qPCR kit (Diagenode #C01010180) following manufacturer instructions with 1 μL of anti-H3K27me3 antibody (Diagenode #C15410069) or 1 μL of rabbit IgG from the kit as a negative control. qPCR was performed using the following primer pairs: Hand2 F8/Hand2 R8; Hand2 F3/Hand2 R3; Binding site for PRC1 on Gdnf (https://www.chipprimers.com): Gdnf F1/Gdnf R1; Binding site for PRC2 on Gdnf (https://www.chipprimers.com):Gdnf F2/Gdnf R2; Wnt11 F/Wnt11 R; Sema6d-Iso1 F/Sema6d-Iso1 R; Sema6d-Iso2 F/Sema6d-Iso2 R; Stmn2 F/Stmn2 R; Spock2 F/Spock2 R; Spock3 F/Spock3 R. Primers sequences are detailed in Table S3.

Results of immunoprecipitation were represented as percentage of input. Experiments were repeated 3 times.

5mC and 5hmC ELISA

Colorimetric detection of global levels of 5mC and 5hmC was performed by ELISA. Briefly, 1 μg of purified (QiaAmp DNA mini kit, QIAGEN) DNA was added to 1mL of DNA coating buffer (Thermofisher). After denaturation, 200 μL of DNA (ELISA 5hmC and ssDNA) or 100 μL of DNA + 100 μL of coating buffer (ELISA 5mC) were dropped in duplicates in a 96-well plate and incubated for 2 h at 37°C. After blocking for 30 min with PBS 0.5% BSA 0.05% Kathon, anti-5mC (Calbiochem NA81 1/5000), anti-5hmC (Active Motif #39769 1/200) or anti-ssDNA (Millipore MAB3299 1/200), and secondary antibodies were added to the wells and incubated overnight at 4°C. Antibodies were diluted in blocking buffer supplemented with 0.1% Tween 20. Finally, Avidin HRP (BD Bioscience) 1/2500 was incubated for 30 mn and reaction was developed using TMB and stopped with 1N H2SO4. The absorbance was read at 450 nm. 5mC and 5hmC levels were normalized by absorbance of ssDNA ELISA. Experiments were repeated 3 times.

Western Blot analysis

Total proteins were extracted in RIPA buffer, resolved on NuPAGE® Novex 4%–16% Bis-Tris gradient gel (Invitrogen), transferred on PVDF membrane (for TET western blotting) or nitrocellulose membrane (for HIF western blotting). After blocking in PBS-milk solution (5%), membranes were incubated with specific primary antibodies, followed by incubation with corresponding HRP-conjugated secondary antibodies. The antibodies used were: anti-actin (Sigma-Aldrich A5316 1/50000), anti-TET1 (Millipore #09-972 1/500),

anti-TET2 (Proteintech #21207-1-AP 1/400), anti-TET3 (Active motif #61744 clone 23B9 1/400), anti-HIF2α (Abcam #ab8365 1/1000; Figure 6) or, anti-HIF2α (Abcam ab109616, 1/500; Figure 7).

For H3K27me3 and H3-Cterminal western blots, proteins were extracted by acidic lysis with 0,2M H2SO4, and precipitated with trichloroacetic acid. Pellets were washed with acetone and resuspended in diluted loading buffer and sonicated. Western blot conditions were identical. Proteins were transferred on nitrocellulose membrane. Anti-H3K27me3 (Active Motif #39156) was diluted 1/1000 and anti-H3-Cterminal (Active Motif #39164) was diluted 1/2000.

Fluorescent staining

Actin staining was performed on cultured cells fixed for 5 mn with ice cold 4% formaldehyde and permeabilized with 0.5% triton buffer for 10 mn. Phalloidin-TRITC toxin (Sigma #P1951) diluted 1/1000 was incubated for 1h and washed before mounting the coverslip in vectashield with Dapi. Fluorescence was observed on a confocal microscope and 13 z stacks of 0.5 μm were merged.

Hif2α immunofluorescence was performed on cultured cells fixed for 5 mn with ice cold 4% formaldehyde. After blocking for 30 mn with PBS 1% BSA 0.1% triton, coverslips were incubated of 2h with Hif2α antibody (R&D Systems #AF2997) diluted 1/100 in blocking buffer. Primary antibody was washed and coverslips were blocked in PBS 1% BSA and incubated for 2h with secondary antibody before mounting in vectashield with Dapi.

In vivo metastasis assay

Tet1+Tet2 KD imCC were cultured for 72h at 21% O_2 (normoxia) or 2% O_2 (hypoxia), and subsequently trypsinized, centrifuged, and resuspended in PBS before injection. 10^6 cells were injected in the tail vein of immunocompromised NMRI nude mice. Two different clones of *Tet1+Tet2 KD* imCC were injected in 10 mice per clone, 5 mice for normoxic cells and 5 for hypoxic cells. 41 days after inoculation, mice were sacrificed and lungs were snap-frozen in liquid nitrogen. Genomic DNA extraction was performed on entire lungs using GenElute Mammalian genomic DNA kit (Sigma #G1N350). Metastatic burden was quantified by qPCR using primer pairs specific for the loxP site present in imCC (Letouzé et al., 2013) (but absent from mice lungs):

Forward primer in Sdhb intron 1 and Reverse primer in Sdhb intron1 and loxP site (Table S3).

We previously verified in gDNA extracted from normal mouse tissue that this primer pair does not allow any DNA amplification (data not shown). 18S primer pair was used for normalization.

QUANTIFICATION AND STATISTICAL ANALYSIS

Data are represented as mean (of at least 3 independent experiments) ± SEM (standard error of the mean). Student tests were performed using PRISM software. For additional information, see Table S4.

DATA AND CODE AVAILABILITY

All raw sequence data have been deposited to the European Genome Phenome Archive. The accession number for the MeDIP-seq, RRBS, and oxRRBS data reported in this paper is EGA: EGAS00001004252.

Cell Reports, Volume *30*

Supplemental Information

TET-Mediated Hypermethylation Primes SDH-Deficient Cells for HIF2α-Driven Mesenchymal Transition

Aurélie Morin, Judith Goncalves, Sophie Moog, Luis-Jaime Castro-Vega, Sylvie Job, Alexandre Buffet, Marie-Joséphine Fontenille, Justine Woszczyk, Anne-Paule Gimenez-Roqueplo, Eric Letouzé, and Judith Favier

TET-mediated hypermethylation primes SDH-deficient cells for HIF2α-driven mesenchymal transition

Aurélie Morin, Judith Goncalves, Sophie Moog, Luis-Jaime Castro-Vega, Sylvie Job, Alexandre Buffet, Marie-Joséphine Fontenille, Justine Woszcyk, Anne-Paule Gimenez-Roqueplo, Eric Letouzé and Judith Favier

Supplementary data

- **Figure S1**
- **Figure S2**
- **Figure S3**
- **Figure S4**
- **Figure S5**
- **Figure S6**
- **Figure S7**
- **Supplemental Table S2**
- **Supplemental Table S3 – Oligonucleotides**
- **Supplemental Table S4 – Statistical section**

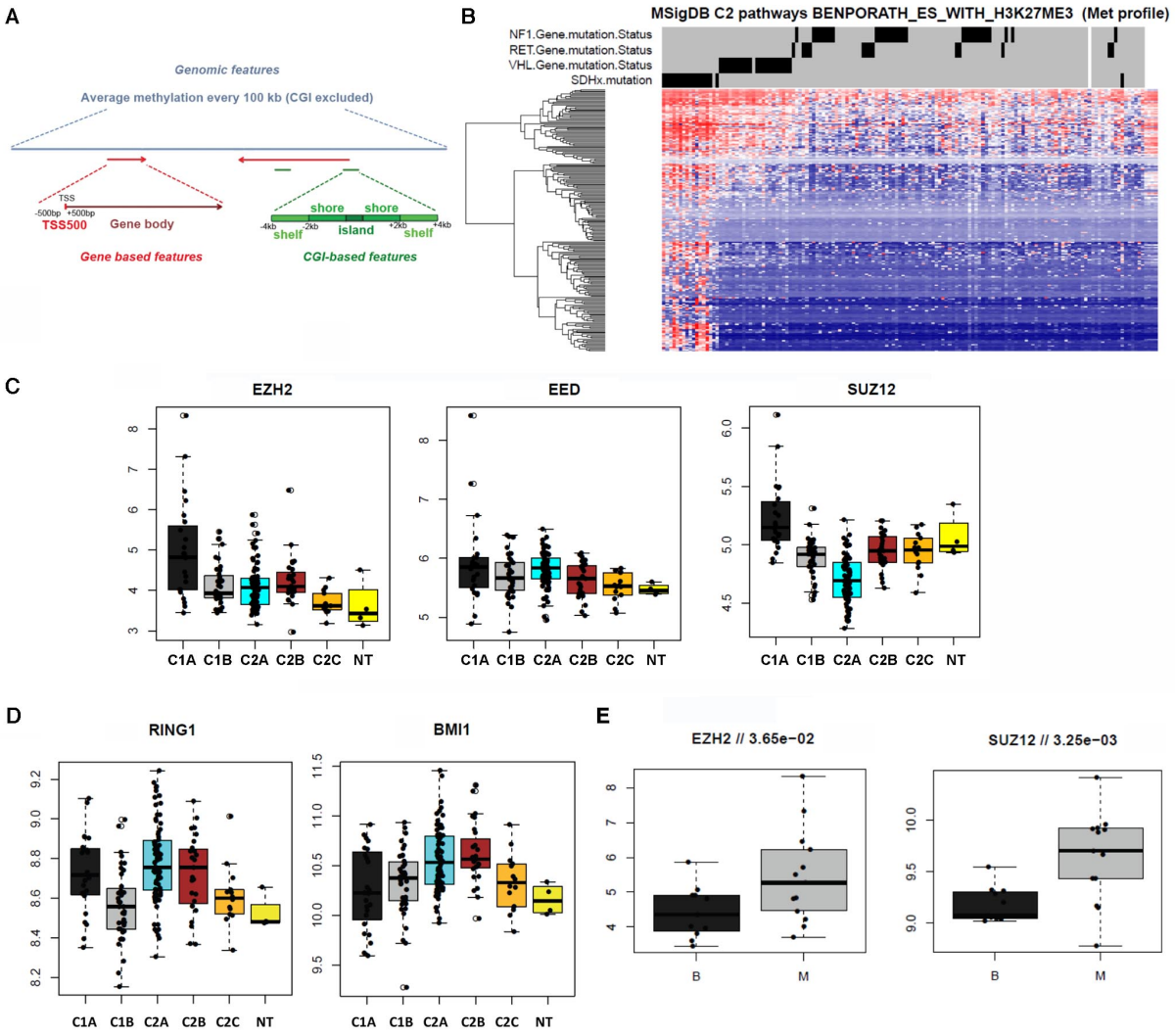

Figure S1. Related to Figure 1. Polycomb pathway in SDH-deficient tumors. A, Description of genomic features used to analyze meDIP-seq and (ox)RRBS data. **B,** Heatmap of DNA methylation obtained from the methylome array data fromLetouzé et al., 2013, restricted to the gene set "BENPORATH_ES_WITH_H3K27ME3". **C,** Microarray-based expression analysis of PRC2 components EZH2, EED and SUZ12 in a cohort of 4 non-tumoral samples and 145 PPGL tumors. Expression clusters have been described in Burnichon et al., 2011. EZH2 and SUZ12 are overexpressed in C1A cluster encompassing tumors with SDH deficiency. **D,** Expression of PRC1 components RING1 and BMI1 in the same cohort. No overexpression of RING1 or BMI1 is observed in C1A cluster. **E,** Microarray-based expression analysis of PRC2 components EZH2 and SUZ12 in the same cohort, comprising 130 benign (B) and 15 metastatic (M) tumors.

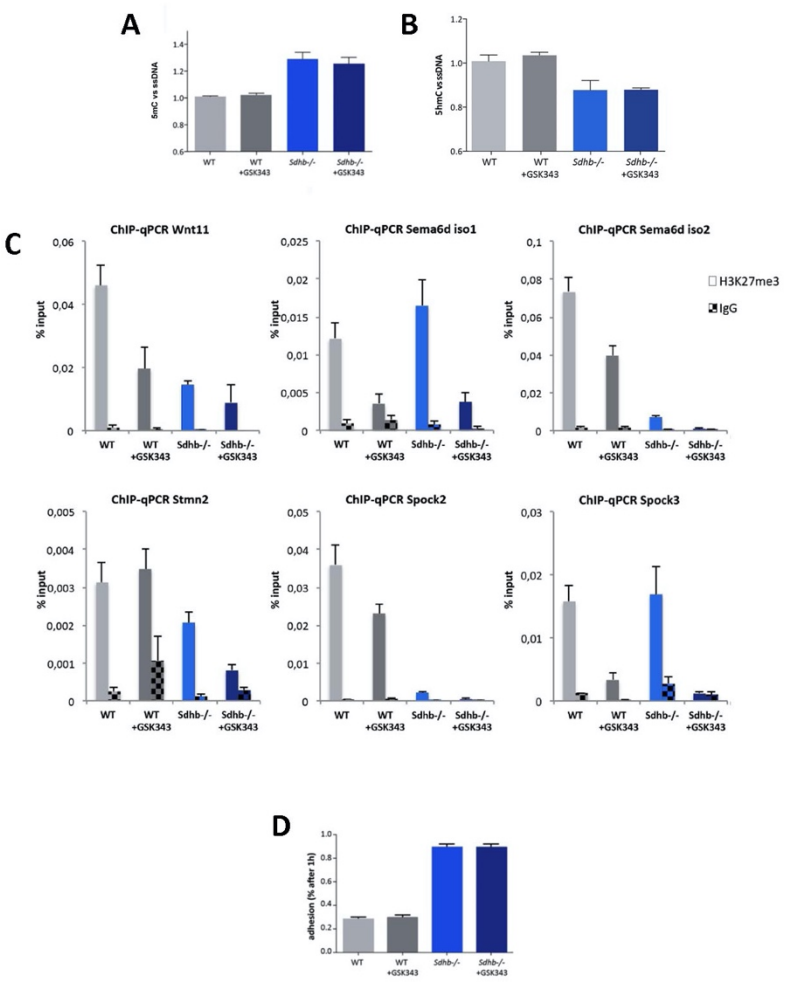

Figure S2. Related to Figure 2. Effects of PRC2 inhibition in imCC. A, B, Quantification of global 5mC and 5hmC levels by ELISA in cells treated with 3µM GSK343 or vehicle for 5 to 7 passages (mean of 3 experiments + SEM). Student test was performed to compare GSK343-treated to untreated cells. No significant difference was observed. **C,** Chromatin immunoprecipitation using an antibody against H3K27me3 or negative control rabbit IgG was performed on indicated cell lines. *Wnt11, Sema6d, Stmn2, Spock2* and *Spock3* genes were quantified by qPCR. Mean of 3 experiments (+ SEM). **D,** Quantification of cell adhesion 1 hour after seeding. Cells were pretreated with the 3µM GSK343 or vehicle for 5 to 7 passages (mean of 3 experiments + SEM). Student test was performed to compare GSK343-treated to untreated cells. No significant difference was observed.

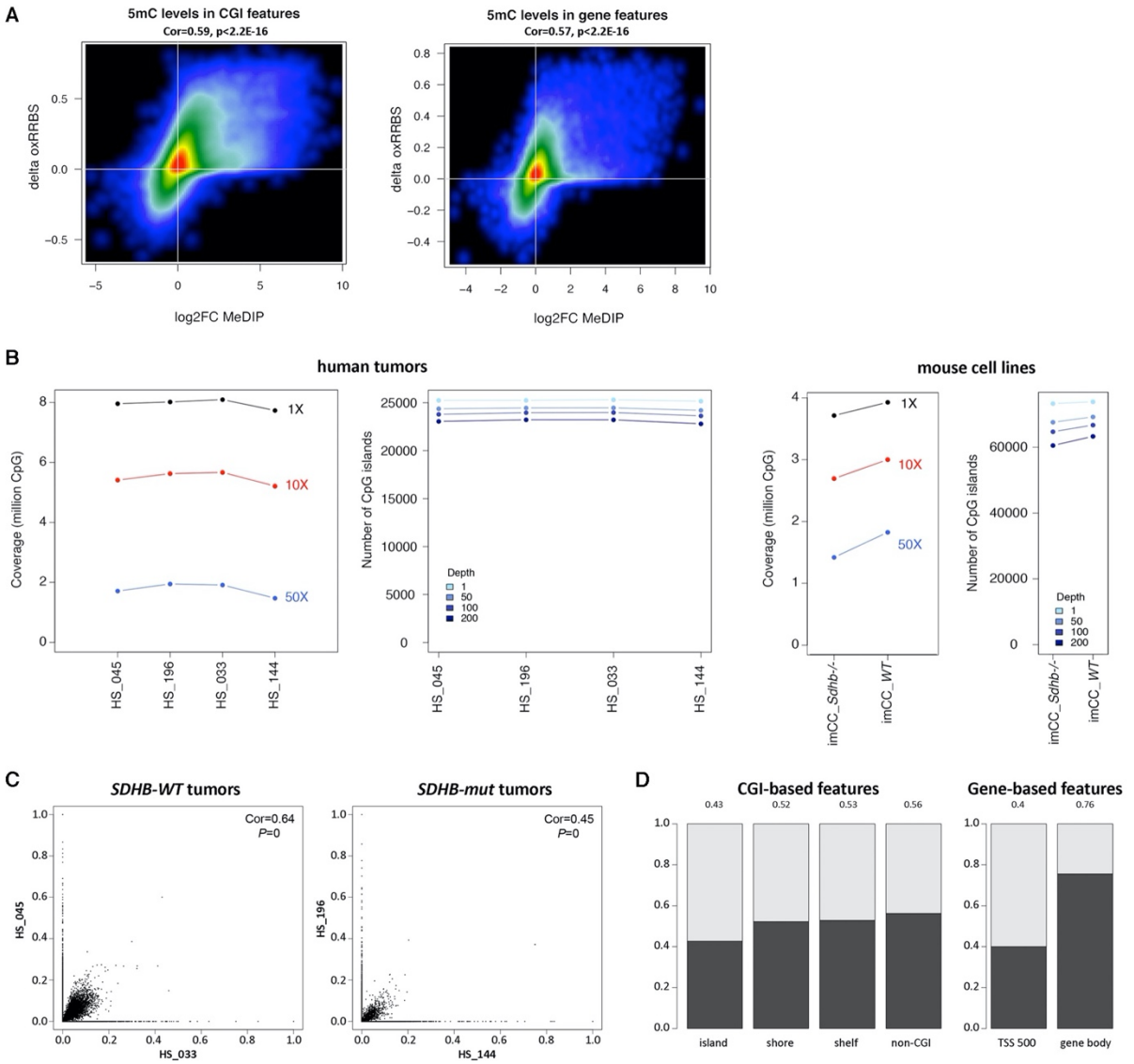

Figure S3. Related to Figure 3. Characteristics of genome-scale mapping of 5mC and 5hmC. A, Correlation of 5mC change between *SDHB*-mut and *SDHB*-WT tumors quantified by oxRRBS versus meDIP-seq. **B,** Coverage and sequencing depth of oxRRBS experiments in each tumor and cell line. **C,** 5hmC levels quantified by oxRRBS in each genomic feature. Correlation between tumors of same genotype. **D,** Proportion of features with detectable 5hmC (coverage >1000, positive value for RRBS-oxRRBS signal, and a significant q-value in at least one sample)

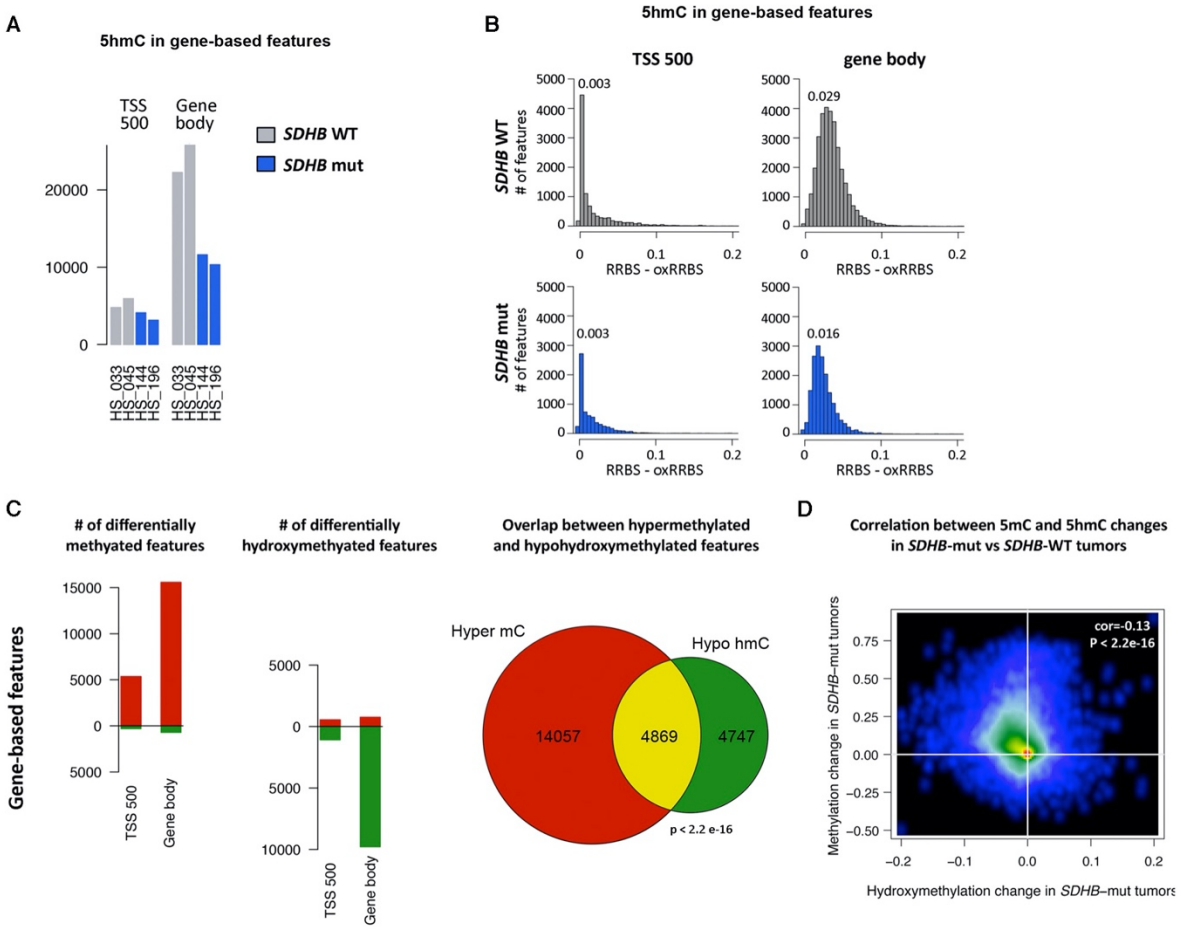

Figure S4. Related to Figure 3. 5-hmC detection in gene-based features in *SDHB*-mutated compared to *SDHB*-wild-type tumors. A, Number of regions in which 5hmC was detected. **B,** Distribution of 5hmC rates in regions where it was detected in *SDHB*-wild-type (top) or *SDHB*-mutated (bottom) tumors. **C,** Number and overlap of differentially methylated and hydroxymethylated regions in S*DHB*-mutated compared to *SDHB*-WT tumors. **D,** Correlation between delta-5mC and delta-5hmC in S*DHB*-mutated *vs SDHB*-WT tumors.

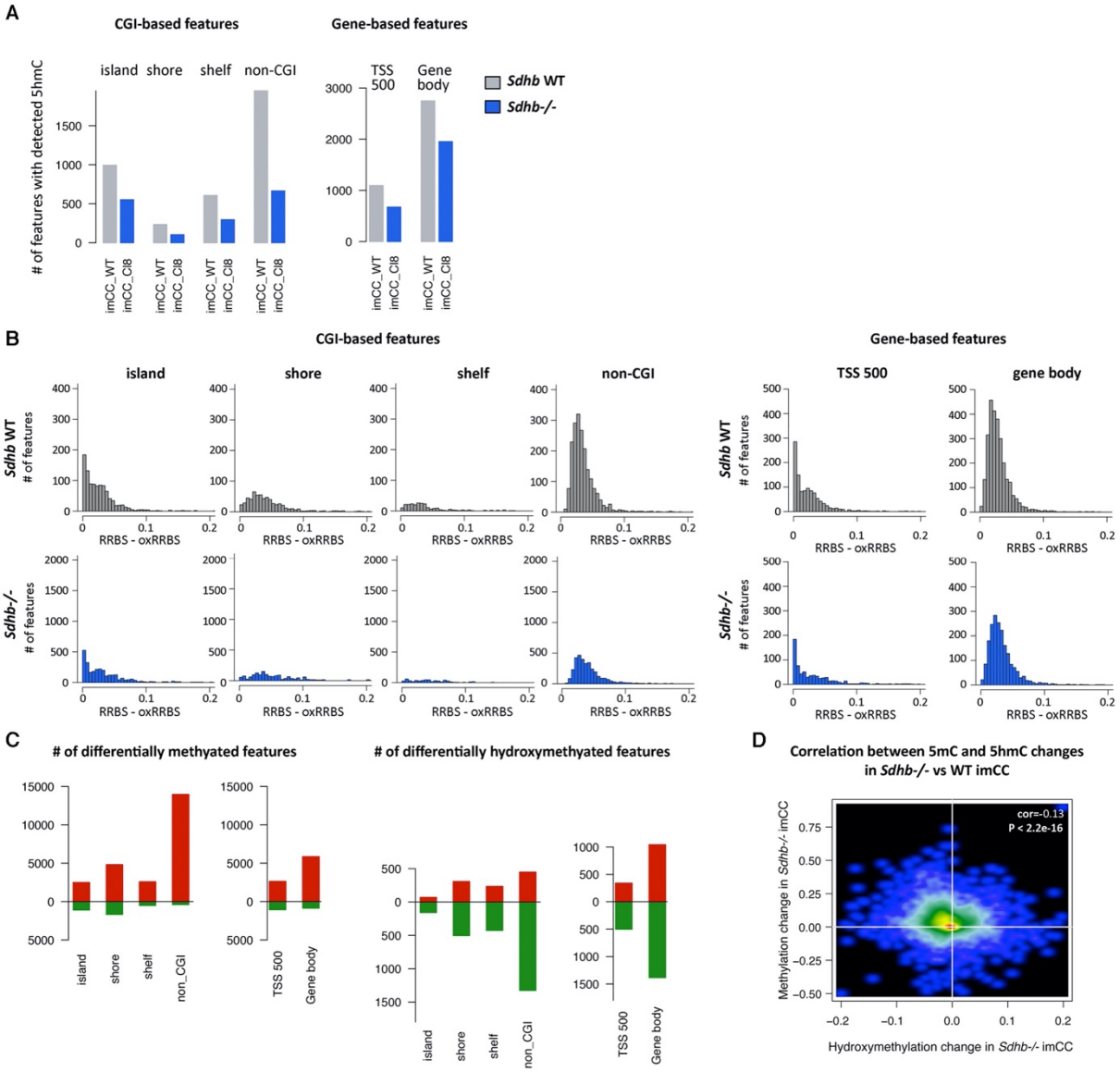

Figure S5. Related to Figure 3. 5-hmC detection in *Sdhb*-/- compared to *Sdhb*-wild-type imCC. A, Number of regions in which 5hmC was detected. **B,** Distribution of 5hmC rates in regions where it was detected in *Sdhb* WT (top) or *Sdhb*-/- (bottom) cells. **C,** Number of differentially methylated and hydroxymethylated regions in *Sdhb*-/- compared to *Sdhb*-WT cells. **D,** Correlation between delta-5mC and delta-5hmC in *Sdhb*-/- vs *Sdhb*-WT cells.

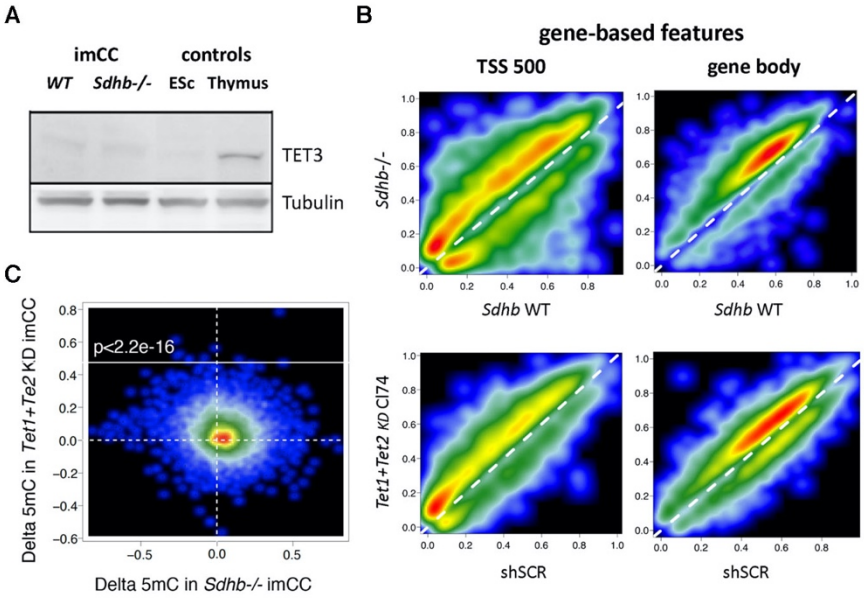

Figure S6. Related to Figure 5. Effects of *Tet1* and *Tet2* knock-down in imCC. A, Western blot analysis of TET3 in total protein extracts from imCC, mouse embryonic stem cells and mouse thymus. **B,** Smoothscatter plot from significantly differently methylated features in *Sdhb-/- vs Sdhb*-WT imCC (top) or *Tet1+Tet2*^{KD} *vs shSCR* imCC (bottom) **C,** Correlation of hypermerthylated gene-based features in *Tet1+Tet2*^{KD} *vs Sdhb-/-* imCC.

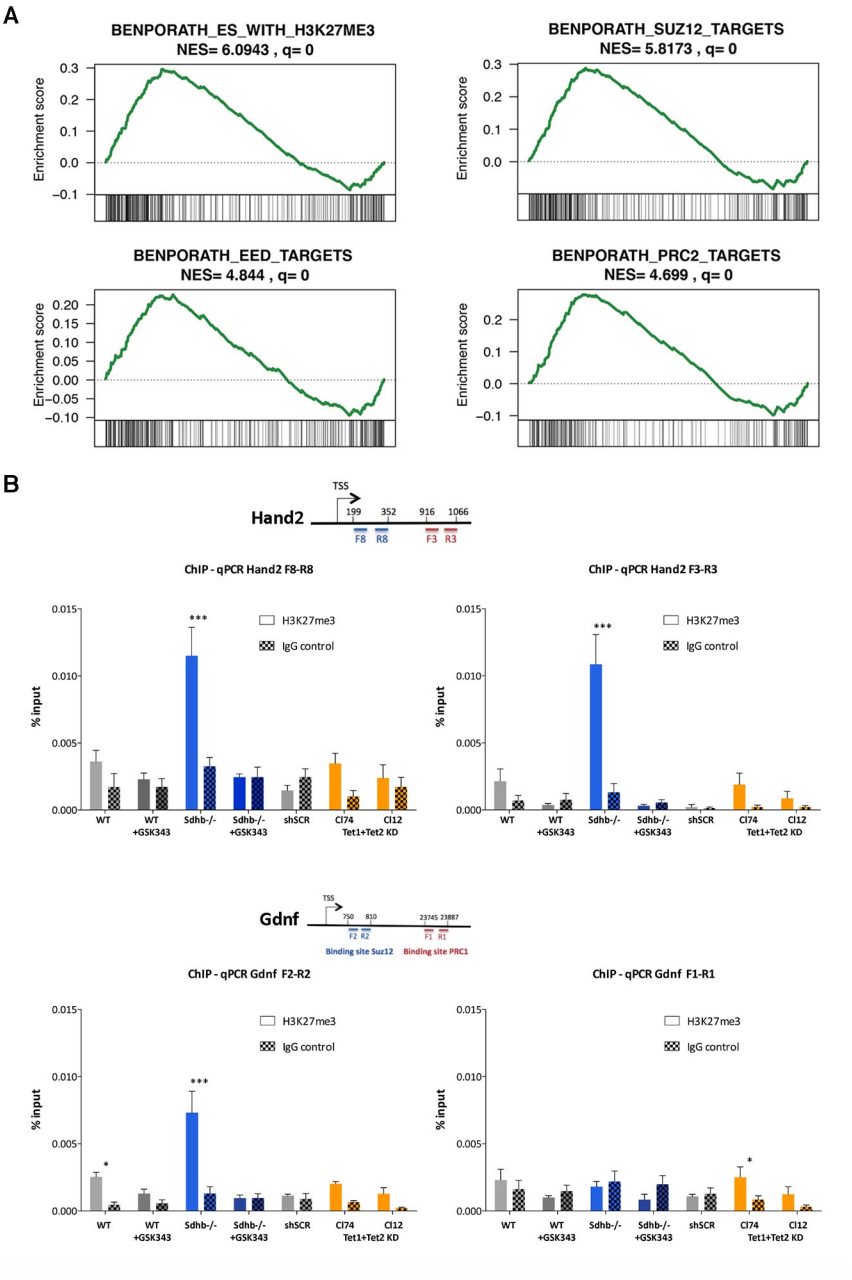

Figure S7. Related to Figure 5. PRC2 and TET have redundant targets in chromaffin cells. A, Hypermethylated genes in *Tet1+Tet2*^{KD} imCC compared to *shSCR* imCC are enriched in genes marked by H3K27me3 or targeted by SUZ12, EED or PRC2 in ES cells. **B,** Chromatin immunoprecipitation using an antibody against H3K27me3 or negative control rabbit IgG was performed on indicated cell lines. Hand2 and Gdnf genes were quantified by qPCR using 2 different primer pairs as indicated. Mean of 3 experiments (+ SEM). Student test was performed to compare H3K27me3 ChIP signal to background IgG signal.

Supplementary Table 2. Related to Figure 1: Number of features with detected 5hmC in human tumors

CGI-based features

	island.HS_033	island.HS_045	island.HS_144	island.HS_196	shore.HS_033	shore.HS_045	shore.HS_144	shore.HS_196	shelf.HS_033	shelf.HS_045	shelf.HS_144	shelf.HS_196
Number of features with sufficient coverage	23010	23010	23010	23010	32717	32717	32717	32717	21410	21410	21410	21410
Number of features with significant difference in oxRRBS	3003	4320	2789	2331	4689	6782	2141	1862	2670	4091	1165	915
Number of features with significant positive difference in oxRRBS	2599	3871	2125	1788	4448	6523	1795	1560	2562	3970	963	772
Proportion of good coverage features with significant positive difference	0.1129509	0.1682312	0.0923512	0.0777053	0.1359538	0.1993765	0.0548644	0.0476816	0.1196637	0.1854274	0.0449790	0.0360579

Gene-based features

	TSS500.HS_033	TSS500.HS_045	TSS500.HS_144	TSS500.HS_196	body.HS_033	body.HS_045	body.HS_144	body.HS_196
Number of features with sufficient coverage	46455	46455	46455	46455	58799	58799	58799	58799
Number of features with significant difference in oxRRBS	5880	7022	5629	4467	22645	26152	12425	10979
Number of features with significant positive difference in oxRRBS	4767	5939	4105	3145	22260	25767	11606	10329
Proportion of good coverage features with significant positive difference	0.1026154	0.1278442	0.0883651	0.0676999	0.3785779	0.4382217	0.1973843	0.1756663

Supplemental Table S3. Related to STAR Methods - Oligonucleotides

Ubc F	5′-AGCCCAGTGTTACCACCAAG-3′
Ubc R	5′-ACCCAAGAACAAGCACAAG-3′
18S F	5′-CGCGGTTCTATTTTGTTGGT-3′
18S R	5′-AACCATAAACGATGCCGAC-3′
B2m F	5’-ATTCACCCCCACTGAGACTG-3’
B2m R	5’-TGCTATTTCTTTCTGCGTGC-3’
Hand2 F	5’-CCAGCTACATCGCCTACCTC-3’
Hand2 R	5’-TGGTTTTCTTGTCGTTGCTG-3’
Gdnf F	5’-CTGTCTGCCTGGTGTTGCT-3’
Gdnf R	5’-CTGCCGCTTGTTTATCTGGT-3’
Wnt11 F	5’-TCCGATGCTCCTATGAAGGT-3’
Wnt11 R	5’-CTGACAGGTAGCGGGTCTTG-3’
Sema6d F	5’-GCTTCCCAGAAGACGATGAG-3’
Sema6d R	5’-CTGTTTGGGGGATTTCATTT-3’
Stmn2 F	5’-CTACGACGACATGGAGGTGA-3’
Stmn2 R	5’-CCTCTTCTCTGCCAACTGCT-3’
Spock2 F	5’-CCATCGGTTGGATGTTCTCT-3’
Spock2 R	5’-GACACCTGGCTTCTTCTTGG-3’
Spock3 F	5’-AGGATTCACTTGGCTGGATG-3’
Spock3 R	5’-TTTATCCCCTGTCGCTTCTG-3’
Snai1 F	5’-TGGAAAGGCCTTCTCTAGGC-3’
Snai1 R	5’-AAAAGCACGGTTGCAGTGG-3’
Twist1 F	5’-GACTCCAAGATGGCAAGCTG-3’
Twist1 R	5’-TTCTCTGGAAACAATGACATCTAGGT-3
Cdh2 F	5’-GAAGATGTTTACAGCGCAGTCTT-3’
Cdh2 R	5’-CTCGCTGCTTTCATACTGAACTT-3’
Epas1 F	5’-AGGGCCACAGCAAAGAGAG-3’
Epas1 R	5’-CATCACGGGATTTCTCCTTC-3’
Glut1 F	5’-AAACATGGAACCACCGCTAC-3’
Glut1 R	5’-GGAGAAGCCCATAAGCACAG-3’
Hif1a F	5’-TCAGCATACAGTGGCACTCA-3’
Hif1a R	5’-AAGGGAGCCATCATGTTCCA-3’
Hand2 F8	5’-GAAAATGGATGCGCTGAGAC-3’
Hand2 R8	5’-GTTCTTGGGCGCTTATTGTT-3’
Hand2 F3	5’-AAGGCGAGATGAGTCTGGTG-3’
Hand2 R3	5’-TAAGCCAGCCGTGGAAGTAG-3’
Gdnf F1	5’-TGGGCTATGAAACCAAGGAG-3’
Gdnf R1	5’-CAACATGCCTGGCCTACTTT-3’
Gdnf F2	5’-CTCTGGCCTTTTGCTTCAAC-3’
Gdnf R2	5’-CTAATCTCGACCCCGCATAA-3’
Wnt11 F	5’-GAGAGCCGAGCACAACTGAC-3’
Wnt11 R	5’-GCGAGGATAGCTTCTTCCAG-3’
Sema6d-Iso1 F	5’-TCCACAGAAGCGCCATAGAC-3’
Sema6d-Iso1 R	5’-GGGAGCTGAGAGCGTAACAC-3’
Sema6d-Iso2 F	5’-CTGTGGATGGTGCCTTGTT-3’
Sema6d-Iso2 R	5’-GACACCCTAGTAGCCGCTCA-3’
Stmn2 F	5’-GACCCTTCTCCTTTGCCTTC-3’
Stmn2 F R	5’-GATGTGCACGCACGGAGT-3’
Spock2 F	5’-ATTTCATGGAGGACGAGCAA-3’
Spock2 R	5’-TACTGCGAGATGGACGACAG-3’
Spock3 F	5’-TGGCTCACGACAATCTCTCA-3’
Spock3 R	5’-CGTCTCGGAATTTGTTCCAC-3’
Sdhb intron 1 Forward	5’-CTCATCGGGCTCCAGTTAAA-3’
Sdhb intron1 and loxP site reverse	5’-GCCGGCCATTTCTGACAC-3’

Supplemental Table S4. Related to Methods – Statistical section

figure	statistical test	n	analysis details	statistical details	Stastistical software
Fig 1 A - C. Fig 2 A		2 tumors / genotype	in Method section "MeDIP-seq analysis"	in figure legend	R statistical software
Fig1 D. Fig 2 B - C	enrichment score and nominal p-value	2 tumors / genotype	in Method section "Gene set enrichment analysis"	in Method section "Gene set enrichment analysis"	R code downloaded from the GSEA website
Fig 1 E	median with interquartile range	cohort of 113 genetically-determined PPGL tumors described in Letouze et al., 2013.	in Method section "RNA-seq analysis"	in figure legend	R statistical software and Bioconductor DESeq package
Fig 2 E	mean with SEM	3 independant experiments. In each experiment, 3 wells of each cell line. qPCR in triplicates.	in Method section "Reversed Transcription and Quantitative Real-Time PCR"	student test between treated and untreated cells: * $p<0.05$, ** $p<0.001$, *** $p<0.0001$	Graphpad Prism
Fig 2 F - G	mean with SEM	3 independant experiments. qPCR in triplicates.	in Method section "ChIP-qPCR"	student test: * $p<0.05$, ** $p<0.001$, *** $p<0.0001$	Graphpad Prism
Fig 2 I - J	logistic regression and the SLIM method for pvalue adjustment	1 RRBS experiment per treatment and cell type	in Method section "oxRRBS and RRBS Analyses"	in Method section "Differential (hydroxy)methylation analysis"	methylKit package (Akalin et al., 2012)
Fig 2 K	mean with SEM	3 independant experiments	in Method section "Wound scratch assay"	student test between treated and untreated cells: * $p<0.05$, ** $p<0.001$, *** $p<0.0001$	Graphpad Prism
Fig 3 & 5 C		Fig. 3: 4 tumor samples (2 SDHB-mutated and 2 SDHB-wt). Fig. 5C: 4 cell line samples (1 Sdhb wt, 1 Sdhb -/-, 1 sh_Scr, 1 sh_TET).	in Method section "oxRRBS and RRBS Analyses"	in Method sections "5hmC detection using (ox)RRBS data" and "Differential (hydroxy)methylation analysis"	Fisher's exact tests, corrected for multiple testing using Benjamini Hochberg procedure
Fig 3 D. Fig 4. Fig 5D	correlation	Fig. 3D and Fig. 4: 4 tumor samples (2 SDHB-mutated and 2 SDHB-wt). Fig. 5D: 4 cell line samples (1 Sdhb wt, 1 Sdhb -/-, 1 sh_Scr, 1 sh_TET).	in Method section "oxRRBS and RRBS Analyses" and "RNA-seq analysis"	Pearson correlation.	R statistical software
Fig 5 B	mean with SEM	3 independant experiments. ELISA in triplicates	in Method section "5mC and 5hmC ELISA"	student test between Sdhb-/- and WT and between shTet and shSCR cells: * $p<0.05$, ** $p<0.001$, *** $p<0.0001$	Graphpad Prism
Fig 5 E. Fig 6 C - D	mean with SEM	3 independant experiments. In each experiment, 3 wells of each cell line. qPCR in triplicates.	in Method section "Reversed Transcription and Quantitative Real-Time PCR"	student test between Sdhb-/- and WT and between shTet and shSCR cells: * $p<0.05$, ** $p<0.001$, *** $p<0.0001$	Graphpad Prism

Fig 5 F	mean with SEM	3 independant experiments	in Method section "Proliferation assay"	student test between Sdhb-/- and WT and between shTet and shSCR cells: * p<0.05, ** p<0.001, *** p<0.0001	Graphpad Prism
Fig 5 G	mean with SEM	3 independant experiments	in Method section "Adhesion assay"	student test between Sdhb-/- and WT and between shTet and shSCR cells: * p<0.05, ** p<0.001, *** p<0.0001	Graphpad Prism
Fig 5 H	mean with SEM	3 independant experiments	in Method section "Wound scratch assay"	student test between Sdhb-/- and WT and between shTet and shSCR cells: * p<0.05, ** p<0.001, *** p<0.0001	Graphpad Prism
Fig 6 E - F		119 tumors (SDH (n=23), VHL (n=40), NF1 (n=37) or RET (n=19))	in figure legend	hierarchical clustering was performed using the ClustVis software with default settings. https://biit.cs.ut.ee/clustvis/	
Fig 6 H	mean with SEM	3 independant experiments. ELISA in triplicates	in Method section "5mC and 5hmC ELISA"	student test between normoxic and hypoxic cells: no significative difference	Graphpad Prism
Fig 7 A	mean with SEM	3 independant experiments	in Method section "Proliferation assay"	student test between normoxic and hypoxic cells: * p<0.05, ** p<0.001, *** p<0.0001	Graphpad Prism
Fig 7 B	mean with SEM	3 independant experiments	in Method section "Adhesion assay"	student test between normoxic and hypoxic cells: * p<0.05, ** p<0.001, *** p<0.0001	Graphpad Prism
Fig 7 C	mean with SEM	3 independant experiments	in Method section "Wound scratch assay"	student test between normoxic and hypoxic cells: * p<0.05, ** p<0.001, *** p<0.0001	Graphpad Prism
Fig 7 E	mean with SEM	3 independant experiments. In each experiment, 3 wells of each cell line. qPCR in triplicates.	in Method section "Reversed Transcription and Quantitative Real-Time PCR"	student test between normoxic and hypoxic cells: * p<0.05, ** p<0.001, *** p<0.0001	Graphpad Prism
Fif 7 F	mean with SEM	Two different clones of *Tet1+Tet2 KD* imCC injected in 10 mice per clone, 5 mice for normoxic cells and 5 for hypoxic cells	in Method section "In vivo metastasis assay"	student test between normoxic and hypoxic cells: * p<0.05, ** p<0.001, *** p<0.0001	Graphpad Prism
Fig 8 A & C	mean with SEM	3 independant experiments. In each experiment, 3 wells of each cell line. qPCR in triplicates.	in Method section "Reversed Transcription and Quantitative Real-Time PCR"	student test relative to Sdhb-/- cells: * p<0.05, ** p<0.001, *** p<0.0001	Graphpad Prism
Fig 8 E	mean with SEM	3 independant experiments	in Method section "Proliferation assay"	student test relative to Sdhb-/- cells: * p<0.05, ** p<0.001, *** p<0.0001	Graphpad Prism
Fig 8 F	mean with SEM	3 independant experiments	in Method section "Adhesion assay"	student test relative to Sdhb-/- cells: * p<0.05, ** p<0.001, *** p<0.0001	Graphpad Prism
Fig 8 G	mean with SEM	3 independant experiments	in Method section "Wound scratch assay"	student test relative to Sdhb-/- cells: * p<0.05, ** p<0.001, *** p<0.0001	Graphpad Prism

DISCUSSION

Cette étude s'est donc articulée autour de deux questions :

- Élucider les mécanismes responsables de l'hyperméthylation dans les cellules et tumeurs avec un déficit en SDH, et en particulier suite à une mutation sur le gène *SDHB.*
- Analyser les conséquences fonctionnelles de l'hyperméthylation de l'ADN dans des cellules déficientes en Sdhb.

Dans un premier temps, ces travaux ont mis en évidence les mécanismes moléculaires à l'origine de l'hyperméthylation marquée, secondaire à un déficit en SDHB. Ainsi, nous avons démontré pour la première fois, le lien entre l'hyperméthylation des tumeurs avec mutations *SDHx* et l'inhibition des TET, qui avait déjà été postulé mais jamais précisément démontré. L'analyse de l'ensemble des gènes hyperméthylés dans les tumeurs mutées sur *SDHB* a révélé un enrichissement important en gènes dérégulés dans le cancer et en gènes codant pour des protéines impliquées dans la pluripotence ou le développement. Ces séquences d'ADN hyperméthylées étaient particulièrement enrichies en gènes cibles du complexe répresseur de polycomb 2 (PRC2). Toutefois, nous avons montré que l'activité de PRC2 ne contribue pas à l'acquisition du phénotype hyperméthylateur induit suite à un défaut de SDH, ce qui suggère un tropisme particulier des TET pour les régions d'ADN des gènes cibles de PRC2.

Dans une deuxième partie, nous avons étudié la corrélation entre l'inhibition des TET, le phénotype pseudohypoxique et le phénotype mésenchymateux des cellules *Sdhb* KO. Nos résultats montrent que le phénotype mésenchymateux et le comportement métastatique des cellules mutées sur le gène *Sdhb* résultent des effets synergiques de l'inhibition du TET et de la stabilisation de HIF2α. Cette étude nous a également permis de valider une hypothèse émise depuis une dizaine d'années, suggérant que dans les PPGL HIF2α joue un rôle plus important que HIF1α. Nous démontrons ici que c'est la stabilisation de HIF2α, et non de HIF1α, qui est principalement induite dans les imCC *Sdhb-/-* et dans les PPGL SDH-dépendants, ce qui peut s'expliquer par la cinétique de stabilisation différente de ces deux protéines.

Enfin, nous révélons *in vitro* que bien qu'elle soit insuffisante pour induire la NMT secondaire à la perte de SDHB, l'hypoxie permet la NMT en agissant en synergie avec l'hyperméthylation,

aboutissant à terme en un comportement invasif. Ainsi, ces observations pourraient expliquer pourquoi les PPGL mutés sur le gène *VHL*, présentant un phénotype pseudohypoxique mais une faible hyperméthylation, sont rarement métastatiques, contrairement aux PPGL avec mutations *SDHB* ou *FH*. Toutefois, ces résultats ne suffisent pas à expliquer pourquoi les patients porteurs de mutations sur les autres gènes *SDHx (SDHA, SDHC et SDHD)* développent rarement des PPGL métastatiques. En effet, les études du génome, du transcriptome et du méthylome réalisées précédemment, montrent que l'ensemble des mutations *SDHx* résultent en un phénotype pseudohypoxique et hyperméthylateur.

Par conséquent, bien que ces résultats représentent des avancées majeures dans la connaissance de certains des mécanismes moléculaires impliqués dans la tumorigenèse liée aux mutations *SDHB* et dans l'acquisition de traits caractéristiques d'un état mésenchymateux, ils ne permettent pas totalement d'expliquer la malignité SDHB-dépendante. En outre, nos travaux ont également révélé que les propriétés d'adhésion remarquablement élevées des imCC *Sdhb-/-* n'étaient pas totalement expliquées par l'action synergique de l'hypoxie et de l'hyperméthylation. Des études complémentaires, permettant la comparaison de plusieurs modèles mutés sur des gènes *SDHx* différents apparaissent donc nécessaires. De telles études pourraient permettre une compréhension plus poussée des mécanismes spécifiquement impliqués dans les PPGL mutés *SDHB,* et ainsi la mise en évidence des causes de la malignité SDHB-dépendante.

CHAPITRE 2

Mécanismes intracellulaires responsables de la transformation métastatique des PPGL mutés *SDHB*

CONTEXTE

Comme déjà évoqué, les données de transcriptome et de méthylome générées par mon équipe d'accueil dans le cadre du projet CIT-COMETE avait mis en évidence une signature d'expression mésenchymateuse spécifique des tumeurs métastatiques mutées sur SDHB ainsi qu'une élévation des niveaux globaux de méthylation de l'ADN en comparaison des autres tumeurs SDHx. Ces observations ont été les premières à avoir mis en évidence des différences entre les tumeurs SDHB à fort potentiel métastatique et les autres tumeurs SDHx, le plus souvent bénignes, suggérant que la méthylation pourrait constituer l'une des clés pour comprendre cette hétérogénéité phénotypique.

Des études fonctionnelles étaient bien évidemment essentielles pour décortiquer ces mécanismes. Une lignée cellulaire de cellules murines immortalisées spontanément (imCC) et porteuses d'un KO de gène *Sdhb* a donc été générée et extensivement caractérisée par mon équipe d'accueil. Comme les tumeurs SDH, ces cellules présentent un phénotype pseudo-hypoxique et une hyperméthylation de l'ADN associés à un phénotype mésenchymateux, une augmentation des capacités de migration, d'adhésion, et d'invasion. Les travaux réalisés jusqu'à présent ont donc suggéré un rôle central du succinate, qui s'accumule de façon massive dans ces cellules et qui est considéré comme l'oncométabolite prinicipal de la tumorigenèse SDH-dépendante via la modulation de l'activité des dioxygénases dépendantes du 2-OG.

Par ailleurs, les imCC *Sdhb-/-* présentent une reprogrammation métabolique qui leur permet de survivre au déficit en SDH (Lussey-Lepoutre et al., Nat Commun 2015). Ainsi, la survie et la prolifération des imCC *Sdhb-/-* reposent sur la synthèse d'aspartate, devenue la source majeure de carbone pour l'anabolisme de ces cellules. Cette synthèse métabolique étant principalement maintenue par carboxylation réductrice.

Malgré les avancées importantes que constituent ces résultats, ils n'expliquent pas*, per se,* le phénotype agressif spécifiquement associé aux mutations *SDHB*. Il était crucial de disposer d'un modèle exactement comparable aux imCC *Sdhb-/-,* qui représenterait un modèle de PPGL SDH-dépendant bénin. Les mutations *SDHC* sont très rares, et les mutations *SDHA* ayant été décrites plus récemment, le recul sur d'éventuelles corrélations génotype/phénotype y est moins clairs. Il a donc été décidé de générer, à partir des imCC WT, un KO du gène *Sdhd*, qui

est aussi fréquemment muté que *SDHB* chez l'homme, et dont les mutations sont associées à un risque de développement d'une forme métastatique 10 fois moindre.

TRAVAUX PERSONNELS

A mon arrivée au laboratoire, j'ai donc eu la chance d'avoir immédiatement accès à ce nouveau modèle d'étude, la lignée imCC *Sdhd-/-* qui venait d'être générée par une post-doctorante de mon équipe d'accueil par CRISPR-Cas9. Mon objectif était alors de pouvoir comparer ce nouveau modèle à la lignée imCC *Sdhb-/-*, afin d'identifier les différents mécanismes impliqués en fonction du gène *Sdhx* muté et ainsi comprendre la malignité SDHB-dépendante.

Du fait de l'ampleur des études à réaliser, de nombreuses collaborations ont été mises en place afin d'effectuer la caractérisation la plus complète possible de ces modèles cellulaires.
Dans un premier temps, je me suis donc attachée à la caractérisation primaire des cellules (séquençage, validation de l'expression des gènes *Sdhx* et de l'expression de certains marqueurs de la NMT ou de la pseudohypoxie par RT-qPCR, immunofluorescence ou western blot). La caractérisation métabolique a été effectuée en collaboration avec Daniel Tennant à l'Université de Birmingham. J'ai réalisé les expériences de flux métaboliques avec du Glucose et de la Glutamine radiomarqués au ^{13}C et la préparation de l'ensemble des métabolites qui ont ensuite été analysés sur la plateforme de spéctrométrie de masse à Birmingham. Les expériences de génomique (transcriptome par RNAseq, méthylome par RRBS) ont été réalisées sur les plateformes Integragen et analysées en collaboration avec Eric Letouzé (Inserm U1162).
Les premiers résultats obtenus au cours de ce projet, ainsi que certaines propriétés fondamentales de la sous-unité SDHB, m'ont alors amené à étudier le métabolisme du fer et du cuivre dans ces cellules. Les mesures de Fer et de cuivre ont été effectuées par Sebastian Muller (Équipe R. Rodriguez, Institut Curie) pour la partie cellulaire, et par l'équipe de Cynthia Andoniadou (King's College London) pour l'approche par LA-ICP-MS. Afin d'étudier le stress oxydant dans ces cellules, nous avons collaboré avec Géraldine Gentric et Fatima Mechta-Grigoriou (Institut Curie) avec qui j'ai pu réaliser les premières séries d'expériences (marquages et analyses en cytométrie en flux). J'ai ensuite établi et poursuivi ces expériences

au sein de mon laboratoire d'accueil. Enfin, j'ai réalisé l'ensemble des traitements et des analyses subséquentes, pour évaluer l'impact de la NAC, de l'ascorbate ou du fer sur ces différents modèles cellulaires.

L'ensemble de cette étude avait pour objectif d'améliorer la connaissance et la compréhension des mécanismes à l'origine du phénotype métastatique SDHB-dépendant. Ces travaux ont fait l'objet de l'article 2 présenté dans ce manuscrit, pour lequel je suis premier auteur et qui est actuellement en révision favorable dans la revue *Cancer Research.*

ARTICLE 2

Loss of SDHB, but not SDHD, promotes dysregulated iron and copper homeostasis, oxidative stress and vulnerability to ascorbate.

Judith Goncalves, Aurélie Morin, Géraldine Gentric, Sebastian Müller, Cynthia L. Andoniadou, Sophie Moog, Katarína Kľučková, Alexander P. Morrell, Theodora J. Stewart, Charlotte Lussey-Lepoutre, Paule Bénit, Alpesh Thakker, Raphaël Rodriguez, Fatima Mechta-Grigoriou, Anne-Paule Gimenez-Roqueplo, Eric Letouzé, Daniel A. Tennant and Judith Favier

(Septembre 2020 : article en révision dans la revue Cancer Research)

Loss of SDHB, but not SDHD, promotes dysregulated iron and copper homeostasis, oxidative stress and vulnerability to ascorbate.

Judith Goncalves[1,2], Aurélie Morin[1,2], Géraldine Gentric[3], Sebastian Müller[4], Cynthia L. Andoniadou[5], Sophie Moog[1,2], Katarína Kľučková[6], Alexander P. Morrell[7], Theodora J. Stewart[8], Charlotte Lussey-Lepoutre[1,9], Paule Bénit[10], Alpesh Thakker[6], Raphaël Rodriguez[4], Fatima Mechta-Grigoriou[3], Anne-Paule Gimenez-Roqueplo[1,2,11], Eric Letouzé[12], Daniel A. Tennant[6] and Judith Favier[1,2*]

1 PARCC, INSERM UMR970, Equipe Labellisée par la Ligue contre le Cancer, Paris, France.
2 Université de Paris, Paris, France
3 Institut Curie, Stress and Cancer Laboratory, Equipe Labellisée par la Ligue Nationale contre le Cancer, PSL Research University; Inserm, U830, 26, rue d'Ulm, Paris 75005, France
4 Chemical Biology of Cancer Team, Labellisée par la Ligue Contre le Cancer. PSL Research University, CNRS UMR3666 -INSERM U1143, Institut Curie, Paris, France
5 Centre for Craniofacial & Regenerative Biology, Faculty of Dentistry, Oral and Craniofacial Sciences, King's College London
6 Institute of Metabolism and Systems Research, University of Birmingham, Edgbaston, Birmingham, B15 2TT. UK
7 Centre for Oral, Clinical & Translational Sciences, Faculty of Dentistry, Oral and Craniofacial Sciences, King's College London
8 London Metallomics Facility, King's College London and Imperial College London, London, UK
9 Assistance Publique-Hôpitaux de Paris, Pitie-Salpêtrière Hospital, Department of Nuclear Medicine, Sorbonne Université, F-75013, Paris, France
10 Université de Paris, INSERM, UMR 1141, Hôpital Robert Debré, Paris, France
11 Assistance Publique-Hôpitaux de Paris, Hôpital Européen Georges Pompidou, Department of Genetics, 75015 Paris, France
12 Centre de Recherche des Cordeliers, Sorbonne Université, Inserm, USPC, Université Paris Descartes, Université Paris Diderot, Université Paris 13, Functional Genomics of Solid Tumors Laboratory, 75006 Paris, France

Running title: Targeting therapy of *SDHB*-dependent metastatic paraganglioma with ascorbate

Keywords: metastatic paraganglioma, *SDHB*, iron homeostasis, oxidative stress, ascorbate

Additional information:

Financial support:

This work has received funding from The Plan Cancer, Epigénétique et Cancer (EPIG201303 METABEPIC), The Paradifference Foundation, Ligue Contre le Cancer (Equipe Labellisée) and the Cancer Research for Personalized Medicine - CARPEM project (Site de Recherche Intégré sur le Cancer - SIRIC). The London Metallomics Facility is funded by the Wellcome trust (grant No 202902/Z/16/Z). Sophie Moog is the recipient of a fellowship from la Fondation pour la Recherche

Médicale. Judith Goncalves is the recipient of a fellowship from la Ligue Nationale contre le Cancer. The R.R. research group is funded by the European Research Council (ERC) under the European Union's Horizon 2020 research and innovation programme (grant agreement No [647973]), the Fondation Charles Defforey-Institut de France and Ligue Contre le Cancer (Equipe Labellisée).

***Correspondence to:**
Dr Judith Favier
Genetics and Metabolism of Rare Cancers team
INSERM, UMR970
Paris-Cardiovascular Research Center
56 rue Leblanc, 75015 Paris, France
Phone: +33 1 53 98 80 45
e-mail: judith.favier@inserm.fr

Conflict of interest disclosure statement: the authors declare no potential conflicts of interest

Word count: 5361

Number of figures: 5

Abstract

All four subunits of succinate dehydrogenase are tumor suppressor genes predisposing to paraganglioma but *SDHB* mutations only are associated with increased risk of metastasis. Here, we generated an *Sdhd* knockout chromaffin cell line and compared it to *Sdhb*-deficient cells. Both cell types exhibited similar SDH loss-of-function, metabolic adaptation and succinate accumulation. In contrast, *Sdhb*-/- cells only showed hallmarks of mesenchymal transition associated with increased DNA hypermethylation and a massive pseudo-hypoxic phenotype. Loss of SDHB specifically leads to increased oxidative stress associated with dysregulated iron and copper homeostasis, in the absence of NRF2 activation. High dose of ascorbate exacerbated the increase in mitochondrial reactive oxygen species, leading to cell death. Our data establish a mechanism linking oxidative stress to iron and copper homeostasis that specifically occurs in *Sdhb-/-* cells and may promote metastasis by inhibiting TET enzymes and HIF-prolyhydroxylases. They highlight high-dose ascorbate as a promising therapeutic strategy for SDHB-related cancers.

Introduction

Succinate dehydrogenase (SDH) is a key enzyme localized in the inner mitochondrial membrane where it participates both in the tricarboxylic acid (TCA) cycle and the electron transport chain (ETC), as complex II. In the TCA cycle, SDH catalyzes the oxidation of succinate into fumarate while in the ETC, it allows the transfer of electrons from succinate to the ubiquinone pool. SDH is constituted of two anchoring subunits (SDHC, SDHD) and two catalytic subunits (SDHA, SDHB) encoded by the four *SDHx* nuclear genes *(SDHA, SDHB, SDHC* and *SDHD)*. SDHA is a flavoprotein to which the substrate succinate binds in order to be oxidized to fumarate, while the resulting electrons are channeled to ubiquinone, through the three Fe-S clusters of SDHB. Since the initial discovery of *SDHD* mutations in 2000(1), all four *SDHx* genes have been demonstrated to act as tumor-suppressor genes(2),(3), (4). Their mutations predispose to pheochromocytoma and paraganglioma (PPGL), rare neuroendocrine tumors arising from chromaffin cells of the adrenal medulla and from the sympathetic and parasympathetic nervous systems, respectively; as well as gastro-intestinal stromal tumors (GIST) and rare forms of renal cell carcinomas. It is now estimated that mutations in *SDHx* genes stand for almost 50% of inherited cases of PPGL. Interestingly, *SDHB* mutations have been shown to be the highest risk factor of malignancy in patients with PPGL: approximately 50% of PPGL patients carrying *SDHB* mutations will ultimately develop a metastatic form of the disease and a germline mutation in *SDHB* is found in up to 36% of all metastatic PPGL cases(5). In contrast, metastatic forms of the disease are found in only 5% of patients with an *SDHD* gene mutation. Moreover, *SDHB* mutated cancers are more aggressive than non-mutated metastatic ones. The overall survival of patients with metastatic *SDHB*-related PPGL was initially estimated at 42 months after diagnosis of the first metastasis versus 244 months for patients with a metastatic PPGL but without an *SDHB* gene mutation(6). Interestingly, recent studies have revealed that increased follow-up of patients with genetically determined PPGL has significantly improved their survival, demonstrating the beneficial impact of genetic testing in these patients(7,8).

In all cases, germline *SDHx* mutations are associated with loss of heterozygosity, which causes the complete loss of SDH function in the tumor(9) and a subsequent accumulation of its substrate, succinate(10). Succinate (as other TCA cycle intermediates such as fumarate and 2-hydroxyglutarate) is considered as an oncometabolite, driving aberrant activation of transcription factors and global epigenetic reprogramming. Indeed, high steady-state levels of these metabolites are known to inhibit 2-oxoglutarate (2-OG) dependent dioxygenases, such as the hypoxia-inducible transcription factor (HIF) prolyl-hydroxylases (PHDs) and Ten-eleven translocation (TET) DNA demethylases(11). These enzymes belong to the large family of iron (Fe) and 2-OG-dependent dioxygenases, which activity is based on the use of iron(12), oxygen(13) and ascorbate(14) as main co-factors. Inhibition of PHDs promotes the abnormal stabilization, and thus activity of HIF1 and HIF2, while TET inhibition leads to a lack of DNA demethylation, resulting in pseudo-hypoxic and hypermethylator phenotypes, respectively. These observations were initially revealed in genomic studies performed on large PPGL tumor collections, resulting in a better understanding of the mechanisms of SDH-related tumorigenesis. In these studies, all *SDHx* and *FH* mutated tumors clustered together, showing a transcriptome signature characterized by activation of the hypoxic response pathway(2,15),(16) and a DNA hypermethylator phenotype(17). Despite this apparent homogeneity, some differences have emerged suggesting that *SDHB*-mutated tumors may display a particularly marked hypermethylator phenotype associated with hallmarks of neuroendocrine-to-mesenchymal transition (NMT), which were not observed in other types of *SDHx*-mutated cases (i.e *SDHA, SDHC* and *SDHD* mutated)(18). In order to decipher these mechanisms at the cellular level, we have generated an immortalized mouse chromaffin cell (imCC) line knocked-out for the *Sdhb* gene(17). In these cells, we showed that *Sdhb*-deficiency does promote a marked hypermethylator phenotype mediated by TET1 and/or TET2 blockade, which acts in synergy with HIF2 activation to promote NMT and metastatic dissemination(19), (20). *Sdhb-/-* cells also undergo significant metabolic reprogramming becoming critically dependent on aspartate synthesis as a major source of carbon for anabolic purposes, which supports their viability and proliferation, maintained mainly through reductive carboxylation(21).

Despite these important advances in the understanding of the oncogenic consequences of SDHB loss of function, the exact cause of the metastatic phenotype of *SDHB*-related tumors remain mostly unexplained. *SDHA* and *SDHC* mutations are rare in PPGL patients, probably because of low penetrance of the disease in mutation carriers. In contrast, *SDHB* and *SDHD* are the most frequently described mutations in PPGL, with an incidence of 8-10 and 5-7% among all PPGL cases, respectively(22). Genotype-phenotype correlation studies performed in patients with *SDHB* or *SDHD* mutations have undoubtedly demonstrated their different clinical behavior in terms of invasiveness. To address this crucial question in the field, we have generated *Sdhd* knocked-out cell lines in the imCC model. In this new and unique model, we have investigated the different pathways previously identified in SDH-related tumors in order to identify the specificities that may explain their different clinical behavior.

Results

Loss of SDHB or SDHD leads to similar metabolic dysfunction and respiratory profiles

To investigate the mechanisms underlying the metastatic characteristics of *SDHB* mutated-PPGL but not of *SDHD*-deficient tumors, we knocked-out the *Sdhd* gene using the CRISPR/Cas9 procedure in wild-type (WT) imCC(17). We obtained two independent *Sdhd*-/- clones (ClA and ClB) each containing a different homozygous point mutation on exon 3 of *Sdhd*, c.119delC and c.120_121delCA, respectively, both leading to premature stop codons (Fig. 1A). These mutations were predicted to lead to the translation of truncated proteins of 79 and 68 amino acids, respectively, instead of the 159 amino acids of the entire WT SDHD protein. To attest for the absence of off-target effects in *Sdhd-/-* cells, we generated a third cell line, in which SDHD loss was rescued by stably transfecting an *Sdhd*-expressing vector in the *Sdhd*-/- ClA (clone *Sdhd-R*). *Sdhd*-mutated cells showed a decrease in *Sdhd* RNA levels (Supplementary Fig. 1A) when compared with WT and *Sdhd-R* cells, which may be suggestive of nonsense-mediated decay in the mutant clones, and particularly in cloneA.

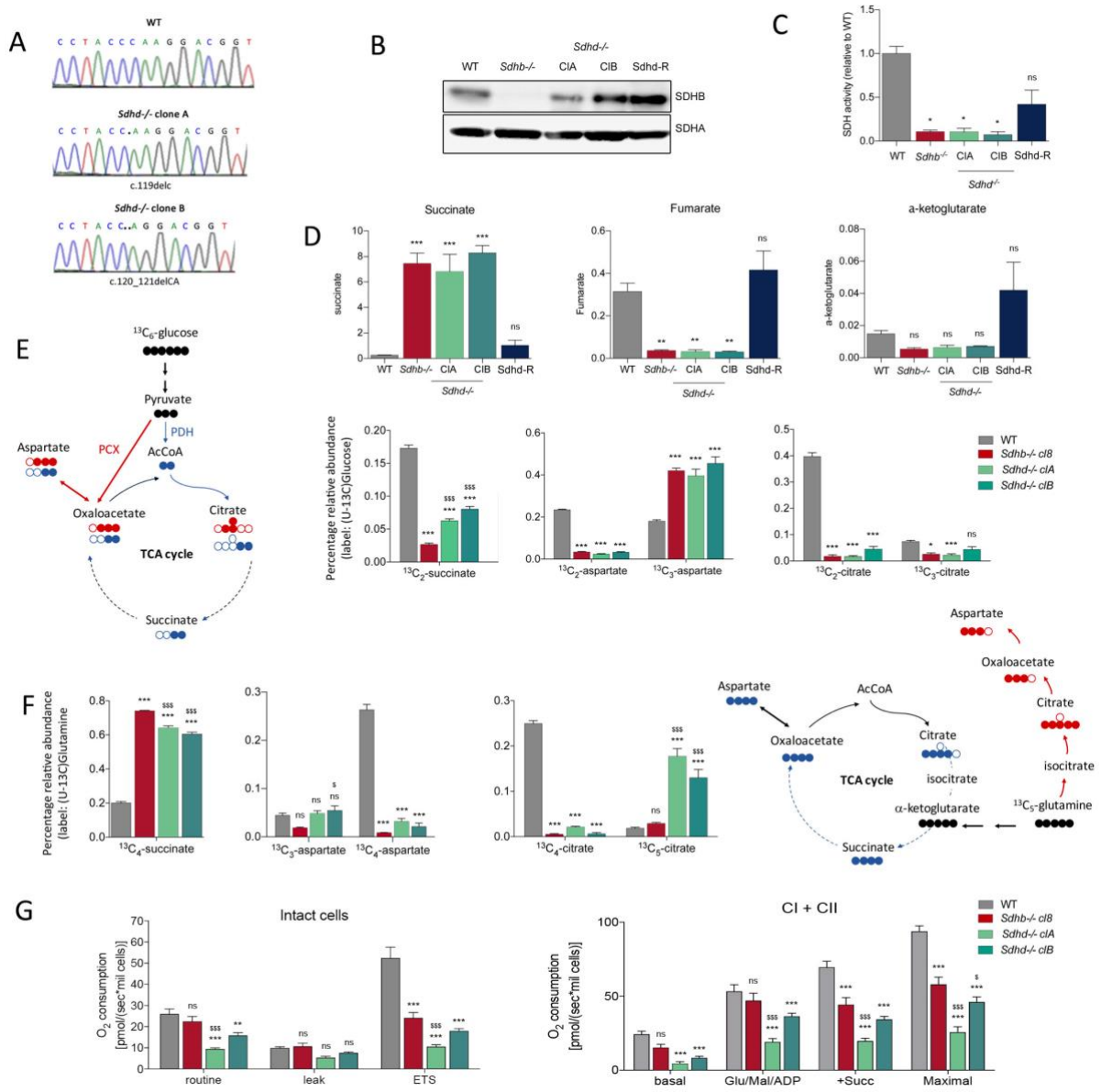

Fig. 1 Generation of *Sdhd*-deficient immortalized mouse chromaffin cells reveals similar metabolic and respiratory profiles with *Sdhb-/-* cells

A, Electrophoregrams of Sanger sequencing of the exon 3 of *Sdhd* gene showing both homozygous point mutations c.119delC and c.120_121delCA of ClA and ClB respectively compared to a control DNA (WT). **B,** Western-blot showing SDHB protein expression in *Sdhb-/-* cells, in two *Sdhd-/-* clones (ClA and ClB) and *Sdhd* rescued cells (*Sdhd*-R) in comparison to WT control. **C,** Spectrophotometrical measurement of SDH activity following the oxidation of added reduced cytochrome c. **D,** Steady-state assessment of TCA cycle organic acids using GS-MS (n=3) revealing a massive increase in succinate in all SDH-deficient cells, associated with a decrease in fumarate and α-ketoglutarate versus WT and *Sdhd*-R2. **E,** Diagram describing the incorporation of carbons from glucose through PDH (blue) or PCX (red) enzymes activity. Abbreviations in metabolic diagram: PDH, pyruvate dehydrogenase; PCX, pyruvate carboxylase; AcCoA, acetyl coenzyme A. Both *Sdhb-/-* and *Sdhd-/-* cell models were incubated for 24 h with $^{13}C_6$-glucose, and cell extracts subjected to NMR spectroscopy analysis of resulting incorporation of ^{13}C into succinate, aspartate and citrate (n=3, error bars are SEM). Isotopomers ^{13}C atoms are shown as filled circles, whereas ^{12}C atoms are empty circles. **F,** Incorporation of $^{13}C_5$-glutamine into succinate, aspartate and citrate in *Sdhb-/-* and *Sdhd-/-* cells versus WT cells and the associated diagrammatic representation of their oxidative (blue) and

reductive (red) metabolism. **G,** Oxygen consumption (respiration) of intact and permeabilized (CI + CII) cells. ETS refers to electron transfer system capacity and basal respiration to oxygen consumption in non-permeabilised cells. Results shown are from at least three independent experiments, presented as mean ± SEM. In (C) and (D) One-way ANOVA was used to assess statistical significance. In (E), (F) and (G) 2-way ANOVA was performed; ns, not significant, *P≤0.05, **P≤0.01, ***P≤0.001 relative to WT and $P≤0.05, $$$P≤0.001 relative to *Sdhb-/-* imCC.

SDHD protein expression could not be estimated due to the lack of efficient antibody in mouse. It is worth noting that *Sdhd* mRNA levels were also reduced in *Sdhb*-deficient cells. In contrast, *Sdhb* mRNA levels were absent in *Sdhb-/-* cells, but not significantly reduced in *Sdhd-/-* imCC (Supplementary Fig. 1B). It has previously been reported that disassembly of the SDH complex in case of *SDHx* mutations leads to the degradation of the SDHB subunit in all *SDHx* mutant cells(23). However, our data show that *Sdhd-/-* clones retain a small but significant level of SDHB protein (Fig. 1B). Similarly, evaluation of SDHB protein by immunohistochemistry in SDH-related PPGL frequently leads to a weak diffuse signal in SDHD deficient tumors, while it is totally negative in SDHB-mutated ones, suggesting that some SDHB remains present in this type of mutants(24). Nevertheless, they exhibited a complete loss of SDH enzymatic activity, similar to that observed in *Sdhb*-deficient cells (Fig. 1C), and in accordance with observations in mutated human PPGL(25,26). Interestingly, it has previously been suggested that succinate accumulation might be less important in SDHD-deficient tumors, which may account for their different metastatic potential(27). Analysis of intracellular succinate levels revealed a substantial accumulation of succinate in *Sdhd-/-* cells that reached that observed in the $Sdhb^{-/-}$ imCC model (Fig. 1D). Similarly, levels of the related metabolites, fumarate and 2-oxoglutarate, were strongly reduced in all SDH-deficient cells regardless of the subunit inactivated. *Sdhd-R* cells showed a profile similar to that of WT imCC (Fig. 1D).

Next, we assessed the metabolic and respiratory phenotypes of both types of SDH-deficient cells. ^{13}C-glucose tracing experiments revealed that in accordance with previous work(21), cells deficient in SDH-activity undergo a metabolic rewiring in the absence of a fully functional TCA cycle. Like *Sdhb-/-* cells, the synthesis of aspartate by *Sdhd-/-* imCC cannot rely on oxidative TCA cycle metabolism (Fig.

1E, m+2 isotopomer) and instead increase the aspartate produced through pyruvate carboxylation (PC) (Fig. 1E, m+3 isotopomer) for anabolic purposes. Equally, their synthesis of citrate from glucose, a central metabolite for cellular anabolism, was greatly reduced (Fig. 1E). The metabolism of another key nutrient, glutamine was therefore examined. Although both cell lines retain some oxidative metabolism of glutamine to produce succinate (Fig. 1F), *Sdhd-/-* imCC appear to significantly increase their synthesis of aspartate and citrate using reductive carboxylation (Fig. 1F), which is not observed to the same degree in *Sdhb-/-* imCC. However, this increase doesn't appear to be sufficient to compensate for their metabolic dysfunction. We then measured oxygen consumption of intact and permeabilized imCC. In both cases, *Sdhb-/-* imCC exhibited no significant change in basal respiration, while *Sdhd-/-* cells showed a decrease (Fig.1G), suggesting that a more significant defect in respiration exists in the *Sdhd-/-* cells compared to *Sdhb-/-.* Maximal respiratory capacity (FCCP-mediated uncoupled respiration) was significantly reduced in both SDH-deficient imCC models, in compliance to that previously reported in *Sdhb-/-* cells(28). Altogether, these results suggest that massive succinate accumulation and rewired metabolism do not constitute relevant triggers for SDHB-related malignancy, although the extent of mitochondrial respiratory deficit may vary between the two models.

Sdhb knockout in mouse chromaffin cells promotes neuroendocrine-to-mesenchymal transition (NMT), unlike Sdhd knockout

We previously reported that *Sdhb-/-* imCC exhibit a mesenchymal-like phenotype with increased adhesion, migration and invasion capacities(19). Morphological observation following phalloidin staining revealed that *Sdhd-/-* cells did not display the dense and wider actin mesh observed in *Sdhb-/-* imCC (Fig. 2A), suggesting that only *Sdhb-/-* cells undergo mesenchymal transformation. Accordingly, markers of NMT activation such as *Snai1*, *Mmp9, Fn1* (Fig. 2B) were overexpressed in *Sdhb-/-* imCC but not in *Sdhd-/-* cells and *NCadh* was downregulated (Supplementary Fig. 2A). *Sdhd-/-* cells showed moderate increase in adhesion (Fig. 2C), and no

increase in migration, evaluated both in collective (Fig. 2D) and individual migration assays (Supplementary Fig. 2C). Similarly, *Sdhd-/-* imCC exhibited a much slower cell growth than *Sdhb-/-* cells (Supplementary Fig. 2D). Hence, despite similar SDH loss-of-function and succinate levels, *Sdhd*-deficient cells do not display the invasive phenotype of *Sdhb* KO cells, as observed in human paraganglioma(18).

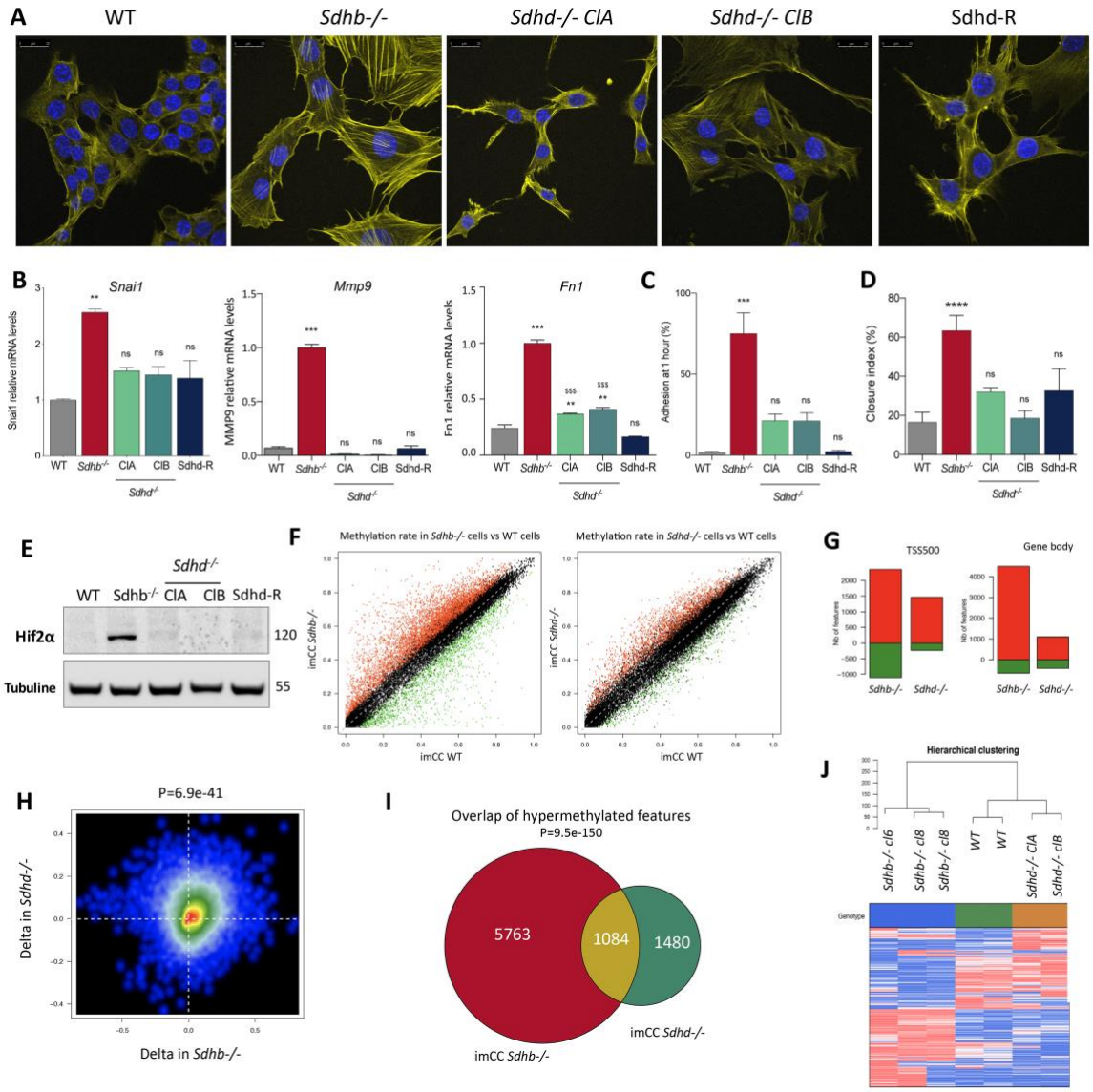

Fig. 2 *Sdhb,* but not *Sdhd* knockout in mouse chromaffin cells initiates a mesenchymal metastaticphenotype due to stronger 2OG-dependent dioxygenases inhibition. A, Actin staining was performed using fluorescent phalloidin toxin in the indicated cell lines. **B,** qRT-PCR analysis of known epithelial-to-mesenchymal markers (*Snai1*, *Mmp9, Fn1)*. **C,** Quantification of cell adhesion one hour after plating. **D,** Collective migration was evaluated using a wound scratch assay. Cell migration was assessed after ten hours. Migration is represented as the closure percentage of the wound. **E,** Western blot of HIF2α in total cellular extracts of WT, *Sdhb-/-, Sdhd-/-* and *Sdhd*-rescued imCCs. **F,** Scatterplot representative of methylation rates identified by RRBS in *Sdhb-/-* cells versus WT cells and *Sdhd-/-* cells versus WT cells, respectively. **G,** number of differentially methylated

features in S*dhb-/-* and *Sdhd-/-* imCC (versus WT) in TSS500 and gene body regions. **H,** Comparison of methylation changes generated by *Sdhd* and *Sdhb* knockout in imCC. **I,** Number and overlap of differentially methylated features in *Sdhb-/-* imCC compared with *Sdhd-/-* imCCs. **J,** Heatmap representation of transcriptome-based classification of imCCs according to their genotype resulting in hierarchical clustering showing that surprisingly the expression profile of *Sdhd-/-* imCC remains closer to that of wild-type imCC and not *Sdhb-/-* imCC. In **A, B, C, D** and **E** data shown are from at least three independent experiments, presented as mean ± SEM. One-way ANOVA was used to assess statistical significance; ns, not significant, **P≤0.01, ***P≤0.001 relative to WT and $$$P≤0.001 relative to *Sdhb-/-* imCC.

Sdhb-deficient cells show greater inhibition of 2OG-dependent dioxygenases

We have previously established that *SDHB*-mutated PPGL and *Sdhb-/-* imCC display pseudohypoxic and hypermethylator phenotypes, caused by inhibition of PHD and TET enzymes and involved in the mesenchymal-like hallmarks associated with SDHB deficiency(17,20). Surprisingly, Western-blot analysis in our cell lines revealed stabilization and massive increase of HIF2α protein levels in *Sdhb-/-* cells, which was not seen in either *Sdhd-/-,* WT or *Sdhd*-R imCC (Fig. 2E). We next performed reduced representation bisulfite sequencing (RRBS) to precisely quantify 5-methyl-cystosine (5mC) modifications along the genome after enrichment for CpG rich regions in the different cell lines. Compared to WT, both *Sdhb* and *Sdhd* KO cells displayed a DNA hypermethylator phenotype, but this phenotype was less pronounced in *Sdhd*-/- cells (Fig. 2F). In total, *Sdhb-/-* cells displayed 6,847 significantly hypermethylated gene-based features (TSS +/- 500 bp and gene bodies) against only 2,564 for *Sdhd*-/- cells (Fig. 2G and Supplementary Table 1). Hypermethylator phenotypes in *Sdhb*-/- and *Sdhd*-/- cells displayed a significant overlap and correlation (Fig. 2H and I), with 1,084 common hypermethylated features representing 42% and 16% of hypermethylated features in *Sdhd*-/- and *Sdhb*-/- imCC, respectively. We next analyzed the transcriptome of all cell lines using RNA-sequencing. Hierarchical clustering of expression profiles across the 1,000 most variant genes (based on standard deviation) showed that *Sdhd*-/- imCC remain closer to wild-type cells and display less gene expression changes than *Sdhb*-/- cells (Fig. 2J). Altogether, these findings indicate that *Sdhd* inactivation induces less DNA methylation and gene expression changes than *Sdhb* deletion. We next aimed at identifying the causes of the seemingly greater inhibition of 2OG-dependent dioxygenases in *Sdhb-/-* cells.

Iron and copper homeostasis are dysregulated in SDH-deficient cells, and especially in Sdhb KO cells

2OG-dependent dioxygenases are iron-containing enzymes. Because SDHB is the iron-sulfur subunit of complex II, we wondered whether its complete loss might lead to disturbances in iron metabolism, which would in turn modulate the activity of 2OG-dependent dioxygenases. We thus used specific fluorescent probes to detect cytosolic and mitochondrial iron in all cell types, as well as assessed iron levels in tumor samples from patients with *SDHB* mutations. We also evaluated mitochondrial copper in all cell types. Indeed, iron and copper are both essential metals with close metabolic interactions that have been known for a long time(29).

We first used the commercial Calcein-AM probe that reveals both Iron(II) and Iron(III) levels, but also other ions such as calcium. This experiment suggested a decrease in global labile iron in SDH-deficient cells compared to WT imCC (Fig. 3A). In order to validate this observation in human PPGL, we performed laser ablation-inductively coupled plasma-mass spectrometry (LA-ICP-MS) in 2 pheochromocytomas carrying *NF1* mutations compared to 2 pheochromocytomas and 2 paragangliomas with *SDHB* gene mutations. We observed that average ^{56}Fe levels were significantly decreased in tumors with *SDHB* mutations (Fig. 3C, D) as compared to tumors with *NF1* mutation (Fig. 3B and Supplementary Fig. 4A). This decrease was greater in *SDHB*-mutated paraganglioma (Fig. 3D) than in *SDHB*-mutated pheochromocytoma (Fig. 3C). These results obtained in tumors from patients consolidate the hypothesis that loss of the SDHB subunit leads to an altered iron metabolism. Calcein-AM probe being poorly specific, we next examined the subcellular localization of Iron(II) using specific probes of both this ion, and specific cell compartments. Unexpectedly, evaluation of the labile pool of cytosolic Iron(II) revealed a significant increase in *Sdhb-/-* cells only (Fig. 3E). This suggests that the calcein-AM data would actually be imputable to a strong decrease in cytosolic levels of Iron(III) in SDH-deficient cells. In opposition, we observed a significant decrease in the mitochondrial pool of chelatable iron (Iron(II)) in both knockout models, decrease which was especially pronounced in *Sdhb-/-* cells and rescued in *Sdhd-R* imCC (Fig. 3F).

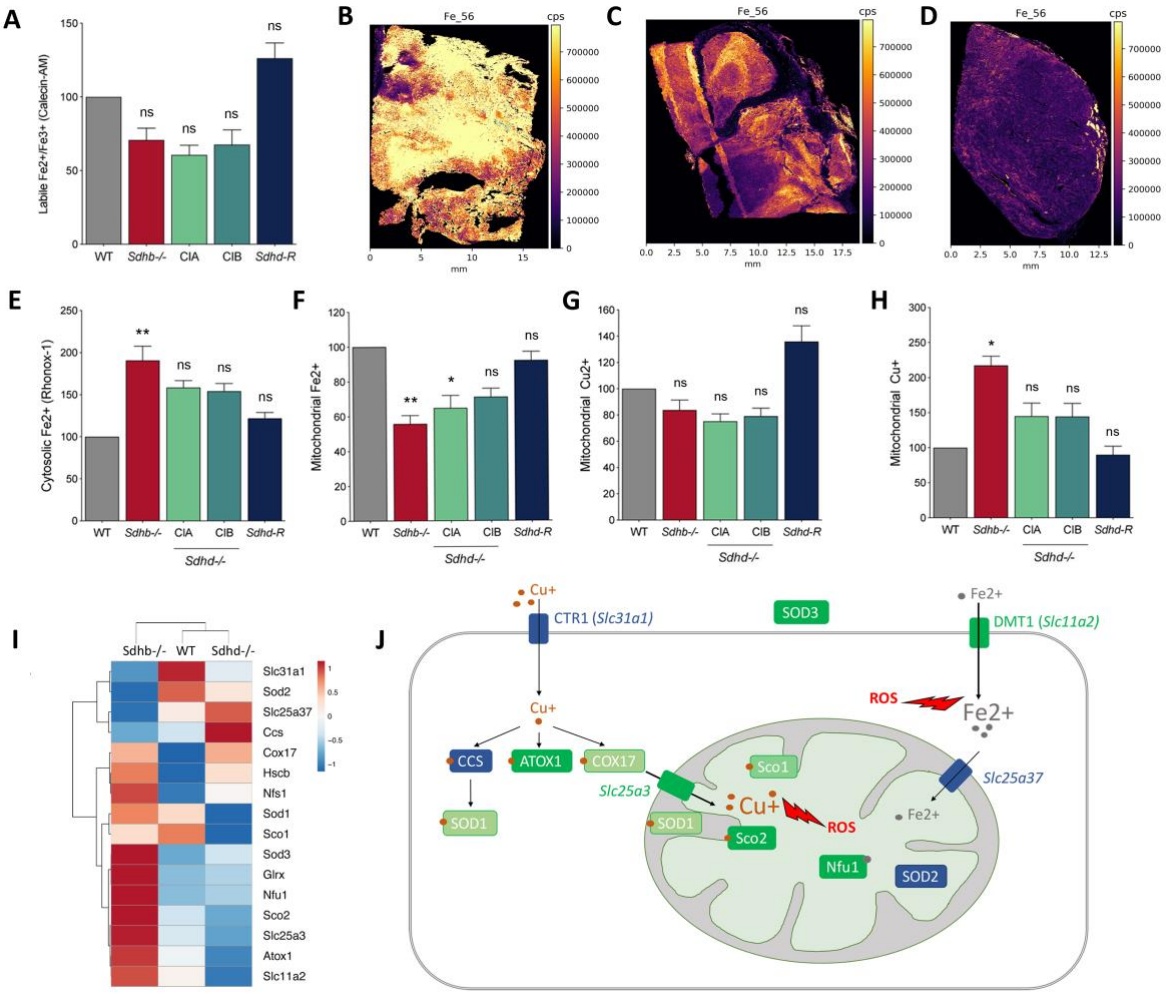

Fig. 3 SDH-deficient cells exhibit significant alterations in iron and copper homeostasis, notably marked in *Sdhb* KO cells. A, Flow cytometry analysis of labile overall iron content using Calcein-AM probe in all imCC cell types (WT, *Sdhb-/-, Sdhd-/-* ClA, *Sdhd-/-*ClB, *Sdhd*-R). **B,** Average ^{56}Fe assessed by LA-ICP-MS in one *NF1* mutated human pheochromocytoma **C,** one *SDHB* mutated human pheochromocytoma and **D,** one *SDHB* mutated human paraganglioma. Images are displayed using the same threshold to enable a direct visual comparison between tumor sections. Flow cytometry analysis were carried out in order to assess **E,** cytosolic Iron(II) content using Rhonox-1 probe ; **F,** mitochondrial Iron(II) content using turn-off Iron(II) probe (69) ; **G,** mitochondrial Cu(II) content using turn-off Cu(II) probe (71) and **H,** mitochondrial Cu(I) content using turn-on Cu(I) probe (72). Bar chart represents an average of three independent experiments. **I,** Heatmap representation of the expression profiles of several critical actors of iron/copper homeostasis in *Sdhb-/-*, WT and *Sdhd-/-* cells, showing significant alterations in *Sdhb* KO cells. Mean level values of actors involved in the iron/copper homeostasis in imCC models were used to perform unsupervised classification. **J,** Diagram highlighting the role played by some iron and copper transporters (DMT1, Slc25a37, CTR1 and Slc25a3) explaining the major alterations induced by *Sdhb* KO in their iron and copper cellular homeostasis. Data shown in **A, E, F, G** and **H** are from three independent experiments, presented as mean ± SEM. Non-parametric one-way ANOVA was used to assess statistical significance; ns, not significant, *P≤0.05, **P≤0.01, ***P≤0.001 relative to WT.

We next evaluated mitochondrial copper levels in all cell types. Concerning the pool of labile mitochondrial Cu(II), no significant changes were observed in the SDH-deficient cells (Fig. 3G), while

mitochondrial Cu(I) was significantly increased in *Sdhb* KO cells only (Fig. 3H). Hence, there was a clear dysregulation in labile iron and copper pools in all SDH deficient cells, a phenotype, which was significantly stronger in *Sdhb-/-* ones. In support of these observations, we evaluated the mRNA expression of several iron and copper transporters as well as of chaperones or different actors of iron/copper homeostasis, which revealed that these pathways were indeed strongly affected in *Sdhb* KO cells (Fig. 3I, J). In particular, these cells showed a differential expression of transporters implicated in the entry of iron and copper in the cell and the mitochondria: high DMT1 (*Slc11a2*) and low Slc25a37 would sustain the increased cytosolic distribution of Iron(II), while low CTR1 (*Slc31a1*) and high Slc25a3, the high mitochondrial Cu(I) levels. Consistently with these observations, human PPGL transcriptome data showed an increase in *DMT1* mRNA levels in SDH tumors as compared with other types of mutated PPGL. SDH tumors also exhibited a slight increase in the expression of other actors involved in iron binding and transport, such as the hypoxia-inducible genes *TF* and *TFRC*. No differences were detected for *TFR2* expression (Supplementary Fig. 3).

Sdhb-deficient cells display increased ROS levels without activation of the NRF2 pathway.

Sdhb-KO cells show increased mitochondrial copper(I) and cytosolic iron(II) levels, which could cause important oxidative stress in these cell compartments(30). An increase in reactive oxygen species (ROS) might also participate to the sustained inhibition of 2OG-dependent dioxygenases activity(31). Flow cytometry analyses of fluorescent probes revealed that *Sdhb*-deficient cells showed increased ROS both in the cytosol (Fig. 4A) and especially in the mitochondria (Fig. 4B). They also displayed a significant increase in lipid peroxidation levels (Fig. 4C). Unexpectedly, none of the *Sdhd*-deficient clones showed any changes in ROS levels as compared to the WT cells. Because *Sdhb-/-* cells display such a significant increase in ROS, we postulated that they would probably show increased anti-oxidant responses, either through superoxide dismutase (SOD) or through activation of the NRF2 pathway. However, the global superoxide dismutase activity did not differ between the different cell types (Supplementary Fig. 4B). Moreover, RNA-seq analysis showed

a significant downregulation of mitochondrial SOD2, thus demonstrating that *Sdhb*-deficient cells do not detoxify the excess in mitochondrial ROS (Fig. 4F).

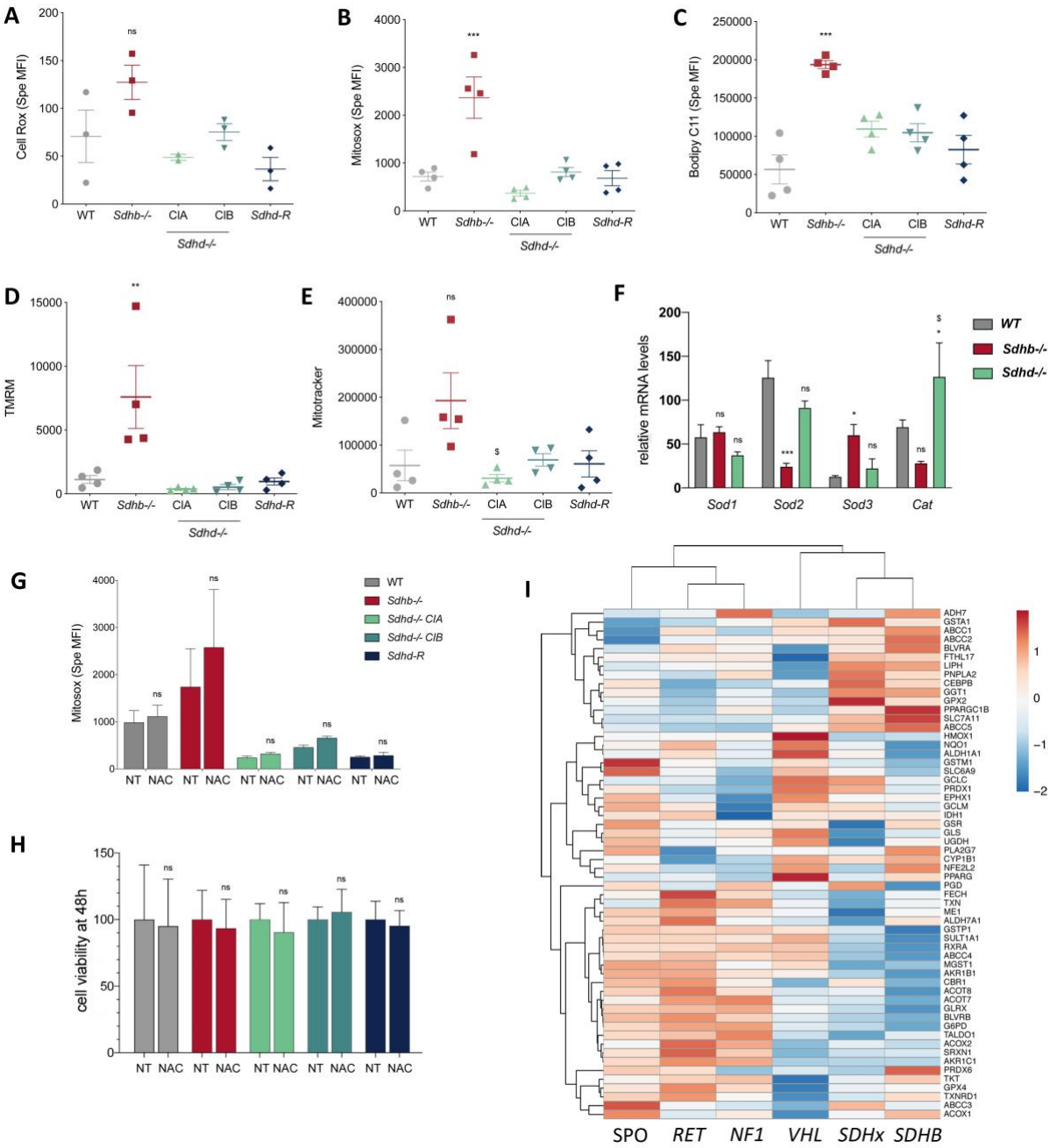

Fig. 4 SDHB-deficient cells display increased ROS levels without activation of the NRF2 pathway. A, Specific MFI using CellROX probe in all imCC cell types. Similar assays were carried out using **B,** Mitosox **C**, Bodipy C11 probe **D**, TMRM and **E**, Mitotracker probes. **F,** Transcriptomic data obtained through RNA-seq analysis showing the mRNA levels of the different forms of superoxide dismutase and catalase, two antioxidant enzymes. SOD1 is located in the cytoplasm, SOD2 in the mitochondrial matrix and SOD3 is the extracellular form of the enzyme. Data are presented as mean ± SEM. **G,** Specific MFI of MitoSOX probe in all imCC models following N-acetyl-cysteine treatment (3 mM) for 48 hours. **H,** Cell survival percentage of all imCC models after treatment with 3 mM of N-acetyl-cysteine (NAC) in comparison to vehicle-treated controls for 48 hours. Data shown are from 3 independent experiments and presented as means ± SEM. In order to assess statistical significance 2-

way ANOVA was used; ns, not significant. **I,** Heatmap representation of the expression of the previously mentioned 58 NRF2-target genes through the transcriptome data of the COMETE collection of human PPGL. Mean values of NRF2 targets levels in the groups of sporadic non-mutated tumors (n=49), *RET*- (n=19), *NF1*- (n=37), *VHL*- (n=40), *SDHA, C, D*- (n=6) and *SDHB*-mutated tumors (n=17) were used to perform unsupervised classification. Data shown in **A, B, C, D** and **E** each dot is representative of an independent experiment (n=4), bar plots show means ± SEM. One-way ANOVA was used to assess statistical significance; ns, not significant, *P≤0.05, **P≤0.01, ***P≤0.001 relative to WT and $P≤0.05 relative to *Sdhb-/-* imCC. In **G** and **H** results shown are from at least three independent experiments. In order to assess statistical significance in **F, G** and **H**, 2-way ANOVA was used; ns, not significant, *P≤0.05, ***P≤0.001.

We performed gene set enrichment analyses using RNA-seq data of 58 NRF2-target genes (Supplementary Table 2) which showed no activation of the pathway in *Sdhb* nor in *Sdhd* KO cells, compared to WT (Supplementary Fig. 4C). In addition, treating the cells with N-acetyl cysteine (NAC) had no effect on the levels of mitochondrial ROS in any of the cell types studied (Fig. 4G), neither affected their proliferation (Fig. 4H). In order to fully validate this observation in the human context, this list of genes was also tested in the transcriptome data of the human PPGL COMETE collection (Fig. 4I). Mean values of NRF2 targets levels in the groups of sporadic non-mutated tumors (n=49), *RET* (n=19), *NF1* (n=37), *VHL* (n=40), *SDHA, C, D*- (n=6) and *SDHB*-mutated tumors (n=17) were used to perform unsupervised classification, which confirmed that the NRF2 pathway is not activated in *SDHB*-deficient tumors. Altogether, these data suggest that in *Sdhb* KO cells, a combination of succinate accumulation, dysregulation of iron and copper homeostasis and high ROS levels may account for the increased inhibition in TET and PHD hydroxylases.

Sdhb-deficient cells have an increased sensitivity to high dose ascorbate

Sdhb-deficient cells displaying high levels of labile Iron(II) (Fig. 3), overexpression of GLUT1 (Supplementary Fig. 2B) and increased ROS (Fig. 4), we postulated that they might present an increased vulnerability to high dose ascorbate or to iron treatment. Treating cells with increasing doses of ferrous iron revealed a specific sensitivity of *Sdhb*-deficient cells. Indeed, after 48 h of treatment, 0.1 mM doses of Iron(II) led to a 60% decrease in *Sdhb-/-* cells survival while it only moderately affected WT, *Sdhd*-KO or *Sdhd*-R cell types (Fig. 5A). More strikingly, ascorbate treatment was highly toxic to *Sdhb* KO cells.

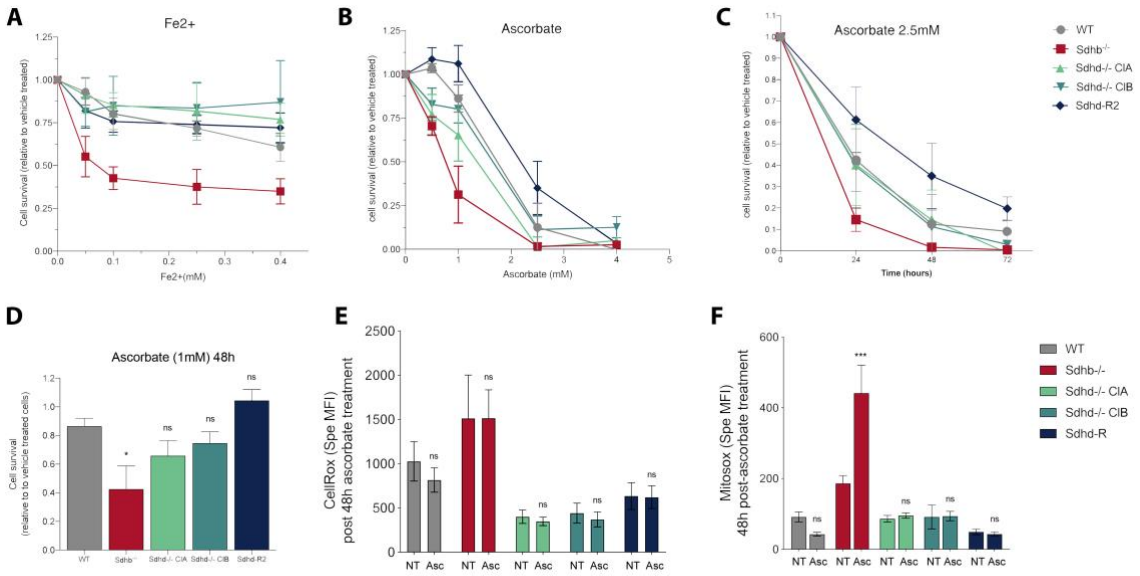

Fig. 5 High dose ascorbate peculiarly affects *Sdhb*-deficient cells through the induction of mitochondrial ROS massive overproduction. A, Dose-response curves showing cell survival of all cell types following 48 hours of treatment with Iron(II) (0.05 mM, 0.1 mM, 0.250 mM and 0.4 mM). **B,** Same as **A** following Ascorbate treatment (0.5 mM, 1 mM, 2.5 mM and 4 mM) showing a complete lethality being reached at 2.5 mM for *Sdhb-/-* imCC. **C,** Time-response curves showing cell survival of all imCC models after treatment with 2.5 mM ascorbate for 24, 48 and 72 hours. **D,** Cell survival percentage of all imCC models after treatment with 1 mM ascorbate for 48 hours. Data for **A, B, C** and **D** are all relative to vehicle-treated controls and presented as means ± SEM (n = 3 independent experiments, with 3 technical replicates/experiment). **E,** Specific MFI of CellROX probe in all imCC models following treatment for 48 hours with either ascorbate 1mM or vehicle (PBS 1X). **F,** Same as **E** using MitoSOX probe. Data from **E** and **F** are mean of at least three independent experiments, presented as mean ± SEM. In **D,** One-way ANOVA was used to assess statistical significance. In **E** and **F,** 2-way ANOVA was performed; ns, not significant, *P≤0.05, ***P≤0.001.

A dose response curve showed that *Sdhb-/-* cells were indeed much more vulnerable to ascorbate with significant increase in cell death appearing from a 1 mM dose onward, a complete lethality being reached at a 2.5 mM ascorbate dose (Fig. 5B). At the higher dose, 85% of *Sdhb*-deficient cell loss was achieved after 24h, while a similar response was only apparent in *Sdhd* and WT cells after 72h (Fig. 5C). To evaluate the mechanism associated with ascorbate-induced lethality, we measured cytosolic and mitochondrial ROS in cells treated for 48 h with 1 mM ascorbate. At such a dose, there was already a significant lethality of *Sdhb*-KO cells and enough cell material was still available to allow the analyses (Fig. 5D). Interestingly, we observed that cytosolic ROS were not modified by ascorbate in any of the cell models (Fig. 5E). In contrast, ascorbate led to a massive increase in mitochondrial ROS, specifically in *Sdhb-/-* cells (Fig. 5F).

Altogether, these data suggest that in *Sdhb*-KO cells ascorbate interacts with the increased Iron(II) labile pool to enhance oxidative stress, leading to rapid cell death.

Discussion

It is well-established that a mutation in the *SDHB* gene is a high risk factor for metastatic PPGL(32) and poor prognosis(6), unlike mutations in other *SDHx* genes (*SDHA*, *SDHC* or *SDHD*) that rarely cause metastatic forms of the disease. This question has been unresolved for 20 years. Many studies have been performed in the past years, mainly using cell lines exhibiting a decrease or complete lack in the expression of *Sdhb.* Thereby, previous work from our team has shown that metastatic SDHB tumors exhibit a NMT phenotype(18,19), associated with increased DNA methylation in comparison to other *SDHx* mutated tumors(20,33). Further, we have recently demonstrated that this hypermethylated profile is due to TET silencing and that the NMT phenotype observed in *SDHB* mutated tumors is the result of synergistic roles of TET repression and pseudohypoxia, through HIF2 activation(20). Although these data have shed light on some mechanisms undeniably involved in the tumorigenesis of *SDHB* mutated tumors, they do not explain the different clinical outcomes observed in patients carrying mutations in the different *SDHx* genes. In the present study, we were able to characterize and compare two physiologically appropriate cellular models exhibiting a complete knock-out in *Sdhb* or *Sdhd* genes, which strikingly recapitulate most of the phenotypic characteristics of *SDHB* and *SDHD*-mutated tumors. Thereby for the first time, we were able to identify the specific mechanisms responsible for the metastatic phenotype associated with *SDHB*-mutated PPGL.

Succinate accumulation is probably the major consequence of SDH loss of activity and increased succinate levels in tumor samples are used as a biomarker of SDH-deficiency in PPGL patients(27,34–36). For a long time, it has therefore been considered to be the main trigger of PPGL tumorigenesis.

450 The role of succinate as an oncometabolite was initially demonstrated in 2005, with the
451 demonstration of its inhibiting role on 2OG-dependent PHD enzymes, leading to the subsequent
452 stabilization of HIFα subunits even under normoxia(37,38). Later, it was demonstrated that succinate
453 is also a major epigenetic modifier, inhibiting TET enzymes and promoting a genome wide
454 hypermethylated profile(17,33,39). It has been suggested that a stronger inhibition of 2OG-
455 dependent dioxygenases observed in *SDHB*-mutated tumors versus tumors with mutations in other
456 *SDHx* genes, might be explained by a fuller inactivation of SDH enzyme associated with higher
457 succinate(27). Here, we firmly invalidate this long-held assumption, both *Sdhb-/-* and *Sdhd-/-* imCC
458 models showing the same loss of SDH activity and similar levels of succinate and fumarate (Fig. 1).
459 Indeed, many of the metabolic characteristics investigated were highly similar between the two cell
460 models suggesting that merely measuring overall steady-state succinate and fumarate levels are
461 inadequate for predicting phenotype, and smaller changes in metabolic function may drive
462 downstream. Surprisingly, HIF2α protein was hardly detectable in *Sdhd*-deficient cells while it was
463 strongly activated in *Sdhb-/-* imCC. This provides further evidence that although aspects of the
464 overall metabolic phenotype were similar between *Sdhb-/-* and *Sdhd-/-* models, as yet unexplored
465 metabolic factors may play a role in the inactivation of the PHD enzymes to stabilize HIF2α . This was
466 unexpected as previous transcriptome analyses of human tumor samples have classified all *SDHx*
467 mutated tumors together with *VHL*-mutated ones in a “pseudohypoxic” cluster(16,17). However,
468 such classifications were based on global transcriptome and obviously included many other
469 pathways. To our knowledge, only three studies have classified PPGL tumors based on the expression
470 of hypoxia-induced genes. In our study, only 3 *SDHD*, 1 *SDHA* and 2 *SDHC*-mutated PPGL were
471 evaluated together with 17 *SDHB*- mutated ones(3). They indeed all clustered together using the
472 expression of 54 HIF-target genes. We have reanalyzed these data, limiting them to the 41 highly
473 expressed ones, and we evaluated their mean expression in *SDHB* versus *SDHD*-mutated tumors.
474 Interestingly, we observed that most genes were overexpressed in SDHB-related tumors while the
475 subset of genes over-represented in *SDHD*-mutated tumors corresponded to genes expressed by

endothelial cells (Supplementary Fig. 5), therefore reflecting the very high vascular density described in these tumors(15,40). Later, Hensen *et al* compared hypoxia-inducible genes in sporadic head and neck PGL (HNPGL) to HNPGL carrying *PGL2* or *SDHD* gene mutations(41). This study was not able to identify any differences in the hypoxic signature of these 3 types of tumors. Finally, Fliedner *et al* evaluated the expression of HIF target genes in a larger collection of *SDHD* (n=14) and *SDHB* (n=15) related PPGL and also revealed some differences between the two types of tumors, with some genes being less overexpressed in *SDHD*-mutated PGL(42). Hence, although it is most probable that, as previously suggested in other studies(15,43–45), *SDHD* tumors display some induction of pseudo-hypoxia *in vivo*, the combination of our *in vitro* data and human PPGL studies does suggest that this effect is at least much more limited in non-*SDHB* mutated cells and can therefore not be imputable to succinate accumulation only.

Our data reveal that while SDHB expression is completely abolished in *Sdhb-/-* cells, a small fraction of SDHB protein remains detectable in *Sdhd-/-* clones, consistently with IHC data on tumors that frequently report a weak diffuse SDHB staining in SDHD-mutated PPGL(24,46). We postulate that the loss in mitochondrial Fe-S clusters present in the SDHB subunit, may be responsible for the significant imbalance in cytosolic and mitochondrial iron and copper distribution, that we observe in SDH-deficient imCC and especially in *Sdhb-/-* cells. This labile iron and mitochondrial cuprous iron overload would in turn be responsible for the overproduction of ROS observed in *Sdhb-/-* cells, thereby indirectly activating pseudohypoxia and DNA methylation. Indeed, it has been previously demonstrated in a number of studies that in the context of excessive ROS levels, these oxidant molecules can act as signals able to trigger the stabilization of Hifα transcription factors in normoxic conditions(47–49),(31). The association between SDH-deficiency and ROS production has been controversial, with some studies showing ROS increase(47,50) and other not(51). Actually, these apparently contradictory data are in total accordance with our observations. Indeed, Selak *et al* first reported the absence of oxidative stress following SDH inactivation, but this was observed in an *SDHD* KD cell model(51). In contrast, Guzy et al. proposed that the mechanism explaining PPGL

tumorigenesis following SDH inhibition was an increase in ROS production, acting as messengers able to activate pseudohypoxic responses and probably resulting in oxidative damage to DNA, genomic instability, and tumorigenesis(47). In that study, an *Sdhb*-Knock Down (KD) model was compared to a *Sdha*-KD one, and ROS increase was only observed in *Sdhb* KD cells. At that time, it was suspected that *SDHA* gene mutations were not associated with PPGL, an assumption that we demonstrated to be untrue several years later (3). Based on these observations, their conclusions were that loss of all but the SDHA subunits of SDH would produce such increase in ROS production, explaining SDHB/C/D-mediated tumorigenesis. In view of the actual knowledge on SDH genetics, the combination of these data with our current observations suggests that ROS production is a specific feature of *SDHB*-mutated cells, and may be responsible, not for SDH-related tumorigenesis in general, but for SDHB-related aggressive phenotype.

Our data suggest that the increased oxidative stress observed in *Sdhb*-deficient cells could be the consequence of the dysregulated iron/copper homeostasis. Indeed, redox-active iron strongly interacts with hydrogen peroxide through the Fenton/Haber-Weiss reaction. This usually slow reaction is catalyzed by labile iron, yielding mainly the highly reactive and toxic hydroxyl radical (•OH) from hydrogen peroxide (H_2O_2) and superoxide ions ($\bullet O_2^-$): Iron(III) + $\bullet O_2^-$ → Iron(II) + O_2 ; Iron(II) + H_2O_2 → Iron(III) + OH^- + •OH (52). Oxidative damage arising from excessive levels of ROS are observed in a variety of pathologies such as neurodegenerative diseases and cancer, and have been linked to malignant transformation, together with an imbalance in iron homeostasis(53). Similar assumptions can be made for copper(54). Our results are also consistent with a recent study demonstrating the role of histone H3-H4 as a copper reductase enzyme that binds Cu(II) and catalyzes its reduction to Cu(I). They showed that active H3-H4 is required for proper utilization of copper for mitochondrial respiration and SOD function. Thereby, the excess of mitochondrial Cu(I) observed here predominantly in *Sdhb-/-* imCC suggests a greater inactivation of H3-H4 and thereby may explain the inhibition of *Sod2* expression and the mitochondrial respiratory deficit observed following Sdhb-deficiency(55).

In this regard, our findings are consistent, although different, with those recently proposed by Liu et al. Using an *Sdhb* KD cell model, these authors also describe ROS accumulation associated with an increase in the intracellular labile iron pool. Surprisingly, these authors observed an increase in iron pool using the calcein probe while in our model, and in human PPGL, this experiment actually showed a decrease in *Sdhb* KO cells. A possible explanation stands in the fact that the model used in the current study is, as the human PPGL studied, a true genetic KO with no SDHB expression, while the model used by Liu *et al* is a KD in which 30% of SDHB protein expression remains. Hence, these different models point to similar pathways, but with major differences in the adaptive responses of the cells. Indeed, Liu et al propose that the iron overload would be due to increased expression of TF and TFR2, while, as previously mentioned such overexpression was not observed in our model. We did observe a slight increase in TF mRNA levels in SDH tumors as compared with other types of mutated PPGL, but not in TFR2. However, in both cases, levels of expression were actually extremely low in all PPGLs and therefore probably not biologically relevant (Supplementary Fig. 3). Furthermore, these authors showed in the same model, that anti-oxidant responses were increased following *SDHB* KD, notably through the upregulation of the nuclear factor erythroid 2-related factor 2 (NRF2)(56). We did not observe any activation of neither the NRF2 pathway nor superoxide dismutase (SOD) activity in any of our different cell types and these data were further validated by our analysis of the transcriptome of human PPGL. Besides, N-acetyl cysteine (NAC) treatment, an inhibitor of the NRF2 pathway, had no effect on the production of mitochondrial ROS by *Sdhb-/-* cells. Hence, it is quite interesting to notice that although similar pathways seem to be affected in the *Sdhb* KO and KD cells (i.e. iron homeostasis, oxidative stress), it seems that the mechanisms and the adaptive responses involved are not similar.

Collectively, these data demonstrate that cells carrying a complete abolition of *Sdhb* gene are not able to neutralize the oxidative damage caused by the mitochondrial ROS excess, through the up-regulation of any intrinsic anti-oxidant pathway. Since, ROS generation seems to be a critical hallmark of SDHB loss, testing an antioxidant treatment on our *Sdhb-/-* model appeared relevant.

Ascorbate offers many assets, as it presents few side effects in healthy tissues, even at pharmacological concentrations and is easy to access. However, although at physiological concentration (micromolar), ascorbate acts as an antioxidant, able to decrease ROS levels(57), it has been shown to have pro-oxidant actions when reaching high concentrations(58). In addition to its strong oxidative role, ascorbate also affects iron homeostasis, as it reduces ferric iron (Iron(III)) in a cycle of reactions leading to the fully oxidized form of ascorbate (DHA), ferrous iron (Iron(II)) and eventually resulting in increased intracellular ROS levels(59,60). Therefore, in a context of redox imbalance associated with an elevated pool of labile iron, ascorbate treatment could lead to unbearably high ROS levels for the cells and thus aggravate an existing oxidative stress burden. Use of ascorbic acid at pharmacologic concentrations was already suggested as a promising therapeutic strategy on various types of tumor cells exhibiting increased ROS levels, increased labile iron and metabolism impairments(53). All the more that, for the past few years many studies have demonstrated the efficacy of ascorbate as an anticancer treatment, killing cancer cells *in vitro*(61,62) and slowing tumor growth *in vivo* (50). In compliance with these reports, our data reveal that high-dose ascorbate treatment led to a higher accumulation of ROS solely in the mitochondria of *Sdhb-/-* imCC, resulting promptly in cell death, thus validating the increased sensitivity of *Sdhb-/-* cells for ascorbate, mediated by ROS overload. Numerous clinical trials are currently evaluating the efficacy of intravenous high-dose pharmacological ascorbate injection for treating different cancer types(60,63). In that context, ascorbate intravenous injections at pharmacological doses appear as a worthy and highly promising therapeutic strategy to treat *SDHB* deficient malignancies, which often exhibit a poor answer to current treatments strategies (radiotherapy, chemotherapy, targeted therapy) and could also be tested in combination with other therapies.

Overall, the comprehensive comparison of the first relevant *Sdhb* and *Sdhd* knock-out cellular models, reveals the common and distinctive pathways used by these cells to adapt to these deficiencies, and highlight specific hallmarks associated with *Sdhb* mutations. Lifting the veil on a long-lasting question, we show that *Sdhb*-deficient cells exhibit stronger PHD and TET inhibition than

their *Sdhd*-deficient counterparts, explaining their aggressive phenotype and mesenchymal morphology. We demonstrate that *Sdhb-/-* imCC manifest a significantly exacerbated imbalance in copper and iron homeostasis resulting in an increased labile iron pool, associated with significant ROS accumulation. High-dose ascorbate treatment of *Sdhb-/-* imCC offers promising results, as it highly aggravated the oxidative stress burden endured by *Sdhb*-deficient cells, thus rising as a potential original therapeutic approach to treat malignant PPGL.

References

1. Baysal BE, Ferrell RE, Willett-Brozick JE, Lawrence EC, Myssiorek D, Bosch A, et al. Mutations in SDHD, a mitochondrial complex II gene, in hereditary paraganglioma. Science. 2000;287:848-51.
2. Astuti D, Latif F, Dallol A, Dahia PL, Douglas F, George E, et al. Gene mutations in the succinate dehydrogenase subunit SDHB cause susceptibility to familial pheochromocytoma and to familial paraganglioma. Am J Hum Genet. 2001;69:49-54.
3. Burnichon N, Briere JJ, Libe R, Vescovo L, Riviere J, Tissier F, et al. SDHA is a tumor suppressor gene causing paraganglioma. Hum Mol Genet. 2010;19:3011–20.
4. Niemann S, Muller U. Mutations in SDHC cause autosomal dominant paraganglioma, type 3. Nat Genet. 2000;26:268-70.
5. Pasini B, Stratakis CA. SDH mutations in tumorigenesis and inherited endocrine tumours: lesson from the phaeochromocytoma-paraganglioma syndromes. Journal of internal medicine. 2009;266:19–42.
6. Amar L, Baudin E, Burnichon N, Peyrard S, Silvera S, Bertherat J, et al. Succinate dehydrogenase B gene mutations predict survival in patients with malignant pheochromocytomas or paragangliomas. J Clin Endocrinol Metab. 2007;92:3822–8.
7. Buffet A, Ben Aim L, Leboulleux S, Drui D, Vezzosi D, Libe R, et al. Positive impact of genetic test on the management and outcome of patients with paraganglioma and/or pheochromocytoma. J Clin Endocrinol Metab. 2019;
8. Hescot S, Curras-Freixes M, Deutschbein T, van Berkel A, Vezzosi D, Amar L, et al. Prognosis of Malignant Pheochromocytoma and Paraganglioma (MAPP-Prono Study): A European Network for the Study of Adrenal Tumors Retrospective Study. J Clin Endocrinol Metab. 2019;104:2367–74.
9. Gimenez-Roqueplo AP, Favier J, Rustin P, Mourad JJ, Plouin PF, Corvol P, et al. The R22X mutation of the SDHD gene in hereditary paraganglioma abolishes the enzymatic activity of complex II in the mitochondrial respiratory chain and activates the hypoxia pathway. Am J Hum Genet. 2001;69:1186-97.
10. Rao JU, Engelke UF, Sweep FC, Pacak K, Kusters B, Goudswaard AG, et al. Genotype-specific differences in the tumor metabolite profile of pheochromocytoma and paraganglioma using untargeted and targeted metabolomics. J Clin Endocrinol Metab. 2015;100:E214-22.
11. Morin A, Letouze E, Gimenez-Roqueplo AP, Favier J. Oncometabolites-driven tumorigenesis: From genetics to targeted therapy. Int J Cancer. 2014;135:2237–48.
12. Müller S, Sindikubwabo F, Cañeque T, Lafon A, Versini A, Lombard B, et al. CD44 regulates epigenetic plasticity by mediating iron endocytosis [Internet]. Cell Biology; 2019 Jul. Available from: http://biorxiv.org/lookup/doi/10.1101/693424
13. Vissers MCM, Kuiper C, Dachs GU. Regulation of the 2-oxoglutarate-dependent dioxygenases and implications for cancer. Biochem Soc Trans. 2014;42:945–51.
14. Kuiper C, Vissers MCM. Ascorbate as a co-factor for fe- and 2-oxoglutarate dependent dioxygenases: physiological activity in tumor growth and progression. Front Oncol. 2014;4:359.
15. Favier J, Briere JJ, Burnichon N, Riviere J, Vescovo L, Benit P, et al. The Warburg effect is genetically determined in inherited pheochromocytomas. PloS one. 2009;4:e7094.
16. Dahia PL, Ross KN, Wright ME, Hayashida CY, Santagata S, Barontini M, et al. A HIF1alpha regulatory loop links hypoxia and mitochondrial signals in pheochromocytomas. PLoS Genet. 2005;1:72–80.
17. Letouze E, Martinelli C, Loriot C, Burnichon N, Abermil N, Ottolenghi C, et al. SDH Mutations Establish a Hypermethylator Phenotype in Paraganglioma. Cancer Cell. 2013;23:739–52.
18. Loriot C, Burnichon N, Gadessaud N, Vescovo L, Amar L, Libe R, et al. Epithelial to Mesenchymal Transition Is Activated in Metastatic Pheochromocytomas and Paragangliomas Caused by SDHB Gene Mutations. J Clin Endocrinol Metab. 2012;97:E954-62.
19. Loriot C, Domingues M, Berger A, Menara M, Ruel M, Morin A, et al. Deciphering the molecular

basis of invasiveness in Sdhb-deficient cells. Oncotarget. 2015;6:32955–65.
20. Morin A, Goncalves J, Moog S, Castro-Vega L-J, Job S, Buffet A, et al. TET-Mediated Hypermethylation Primes SDH-Deficient Cells for HIF2α-Driven Mesenchymal Transition. Cell Rep. 2020;30:4551-4566.e7.
21. Lussey-Lepoutre C, Hollinshead KE, Ludwig C, Menara M, Morin A, Castro-Vega LJ, et al. Loss of succinate dehydrogenase activity results in dependency on pyruvate carboxylation for cellular anabolism. Nature communications. 2015;6:8784.
22. Toledo RA, Burnichon N, Cascon A, Benn DE, Bayley JP, Welander J, et al. Consensus Statement on next-generation-sequencing-based diagnostic testing of hereditary phaeochromocytomas and paragangliomas. Nat Rev Endocrinol. 2017;13:233–47.
23. van Nederveen FH, Gaal J, Favier J, Korpershoek E, Oldenburg RA, de Bruyn EM, et al. An immunohistochemical procedure to detect patients with paraganglioma and phaeochromocytoma with germline SDHB, SDHC, or SDHD gene mutations: a retrospective and prospective analysis. Lancet oncol. 2009;10:764–71.
24. Papathomas TG, Oudijk L, Persu A, Gill AJ, van Nederveen F, Tischler AS, et al. SDHB/SDHA immunohistochemistry in pheochromocytomas and paragangliomas: a multicenter interobserver variation analysis using virtual microscopy: a Multinational Study of the European Network for the Study of Adrenal Tumors (ENS@T). Mod Pathol. 2015;28:807–21.
25. Gimenez-Roqueplo AP, Favier J, Rustin P, Mourad JJ, Plouin PF, Corvol P, et al. The R22X mutation of the SDHD gene in hereditary paraganglioma abolishes the enzymatic activity of complex II in the mitochondrial respiratory chain and activates the hypoxia pathway. Am J Hum Genet. 2001;69:1186–97.
26. Gimenez-Roqueplo AP, Favier J, Rustin P, Rieubland C, Kerlan V, Plouin PF, et al. Functional consequences of a SDHB gene mutation in an apparently sporadic pheochromocytoma. J Clin Endocrinol Metab. 2002;87:4771–4.
27. Lendvai N, Pawlosky R, Bullova P, Eisenhofer G, Patocs A, Veech RL, et al. Succinate-to-fumarate ratio as a new metabolic marker to detect the presence of SDHB/D-related paraganglioma: initial experimental and ex vivo findings. Endocrinology. 2014;155:27–32.
28. Kľučková K, Thakker A, Vettore L, Escribano-Gonzalez C, Hindshaw RL, Tearle JLE, et al. Succinate dehydrogenase deficiency in a chromaffin cell model retains metabolic fitness through the maintenance of mitochondrial NADH oxidoreductase function. FASEB J. 2020;34:303–15.
29. Collins JF, Prohaska JR, Knutson MD. Metabolic crossroads of iron and copper. Nutr Rev. 2010;68:133–47.
30. Videla LA, Fernández V, Tapia G, Varela P. Oxidative stress-mediated hepatotoxicity of iron and copper: role of Kupffer cells. Biometals. 2003;16:103–11.
31. Gerald D, Berra E, Frapart YM, Chan DA, Giaccia AJ, Mansuy D, et al. JunD reduces tumor angiogenesis by protecting cells from oxidative stress. Cell. 2004;118:781–94.
32. Gimenez-Roqueplo AP, Favier J, Rustin P, Rieubland C, Crespin M, Nau V, et al. Mutations in the SDHB gene are associated with extra-adrenal and/or malignant phaeochromocytomas. Cancer Res. 2003;63:5615–21.
33. Killian JK, Kim SY, Miettinen M, Smith C, Merino M, Tsokos M, et al. Succinate dehydrogenase mutation underlies global epigenomic divergence in gastrointestinal stromal tumor. Cancer Discov. 2013;3:648–57.
34. Pollard PJ, Briere JJ, Alam NA, Barwell J, Barclay E, Wortham NC, et al. Accumulation of Krebs cycle intermediates and over-expression of HIF1alpha in tumours which result from germline FH and SDH mutations. Hum Mol Genet. 2005;14:2231–9.
35. Imperiale A, Moussallieh FM, Roche P, Battini S, Cicek AE, Sebag F, et al. Metabolome profiling by HRMAS NMR spectroscopy of pheochromocytomas and paragangliomas detects SDH deficiency: clinical and pathophysiological implications. Neoplasia. 2015;17:55–65.
36. Richter S, Peitzsch M, Rapizzi E, Lenders JW, Qin N, de Cubas AA, et al. Krebs cycle metabolite profiling for identification and stratification of pheochromocytomas/paragangliomas due to

689 succinate dehydrogenase deficiency. J Clin Endocrinol Metab. 2014;99:3903–11.
690 37. Selak MA, Armour SM, MacKenzie ED, Boulahbel H, Watson DG, Mansfield KD, et al. Succinate
691 links TCA cycle dysfunction to oncogenesis by inhibiting HIF-alpha prolyl hydroxylase. Cancer
692 Cell. 2005;7:77–85.
693 38. Briere JJ, Favier J, Benit P, El Ghouzzi V, Lorenzato A, Rabier D, et al. Mitochondrial succinate is
694 instrumental for HIF1alpha nuclear translocation in SDHA-mutant fibroblasts under normoxic
695 conditions. Hum Mol Genet. 2005;14:3263–9.
696 39. Xiao M, Yang H, Xu W, Ma S, Lin H, Zhu H, et al. Inhibition of alpha-KG-dependent histone and
697 DNA demethylases by fumarate and succinate that are accumulated in mutations of FH and
698 SDH tumor suppressors. Genes Dev. 2012;26:1326–38.
699 40. Favier J, Igaz P, Burnichon N, Amar L, Libe R, Badoual C, et al. Rationale for anti-angiogenic
700 therapy in pheochromocytoma and paraganglioma. Endocr Pathol. 2012;23:34–42.
701 41. Hensen EF, Goeman JJ, Oosting J, Van der Mey AG, Hogendoorn PC, Cremers CW, et al. Similar
702 gene expression profiles of sporadic, PGL2-, and SDHD-linked paragangliomas suggest a
703 common pathway to tumorigenesis. BMC Med Genomics. 2009;2:25.
704 42. Fliedner SMJ, Shankavaram U, Marzouca G, Elkahloun A, Jochmanova I, Daerr R, et al. Hypoxia-
705 Inducible Factor 2α Mutation-Related Paragangliomas Classify as Discrete Pseudohypoxic
706 Subcluster. Neoplasia. 2016;18:567–76.
707 43. Lopez-Jimenez E, Gomez-Lopez G, Leandro-Garcia LJ, Munoz I, Schiavi F, Montero-Conde C, et
708 al. Research resource: Transcriptional profiling reveals different pseudohypoxic signatures in
709 SDHB and VHL-related pheochromocytomas. Mol Endocrinol. 2010;24:2382–91.
710 44. Qin N, de Cubas AA, Garcia-Martin R, Richter S, Peitzsch M, Menschikowski M, et al. Opposing
711 effects of HIF1alpha and HIF2alpha on chromaffin cell phenotypic features and tumor cell
712 proliferation: Insights from MYC-associated factor X. Int J Cancer. 2014;135:2054–64.
713 45. Welander J, Andreasson A, Juhlin CC, Wiseman RW, Bäckdahl M, Höög A, et al. Rare germline
714 mutations identified by targeted next-generation sequencing of susceptibility genes in
715 pheochromocytoma and paraganglioma. J Clin Endocrinol Metab. 2014;99:E1352-1360.
716 46. Santi R, Rapizzi E, Canu L, Ercolino T, Baroni G, Fucci R, et al. Potential Pitfalls of SDH
717 Immunohistochemical Detection in Paragangliomas and Phaeochromocytomas Harbouring
718 Germline SDHx Gene Mutation. Anticancer Res. 2017;37:805–12.
719 47. Guzy RD, Sharma B, Bell E, Chandel NS, Schumacker PT. Loss of the SdhB, but Not the SdhA,
720 subunit of complex II triggers reactive oxygen species-dependent hypoxia-inducible factor
721 activation and tumorigenesis. Mol Cell Biol. 2008;28:718–31.
722 48. Guzy RD, Hoyos B, Robin E, Chen H, Liu L, Mansfield KD, et al. Mitochondrial complex III is
723 required for hypoxia-induced ROS production and cellular oxygen sensing. Cell Metab.
724 2005;1:401–8.
725 49. Mansfield KD, Guzy RD, Pan Y, Young RM, Cash TP, Schumacker PT, et al. Mitochondrial
726 dysfunction resulting from loss of cytochrome c impairs cellular oxygen sensing and hypoxic
727 HIF-alpha activation. Cell Metab. 2005;1:393–9.
728 50. Liu Y, Pang Y, Zhu B, Uher O, Caisova V, Huynh T-T, et al. Therapeutic Targeting of SDHB-
729 Mutated Pheochromocytoma/Paraganglioma with Pharmacologic Ascorbic Acid. Clin Cancer
730 Res. 2020;
731 51. Selak MA, Duran RV, Gottlieb E. Redox stress is not essential for the pseudo-hypoxic phenotype
732 of succinate dehydrogenase deficient cells. Biochim Biophys Acta. 2006;1757:567–72.
733 52. Torti SV, Torti FM. Iron and cancer: more ore to be mined. Nat Rev Cancer. 2013;13:342–55.
734 53. Schoenfeld JD, Sibenaller ZA, Mapuskar KA, Wagner BA, Cramer-Morales KL, Furqan M, et al.
735 O2·- and H2O2-Mediated Disruption of Fe Metabolism Causes the Differential Susceptibility of
736 NSCLC and GBM Cancer Cells to Pharmacological Ascorbate. Cancer Cell. 2017;32:268.
737 54. Ravet K, Pilon M. Copper and iron homeostasis in plants: the challenges of oxidative stress.
738 Antioxid Redox Signal. 2013;19:919–32.
739 55. Attar N, Campos OA, Vogelauer M, Cheng C, Xue Y, Schmollinger S, et al. The histone H3-H4
740 tetramer is a copper reductase enzyme. Science. 2020;369:59–64.

741 56. Liu Y, Pang Y, Caisova V, Ding J, Yu D, Zhou Y, et al. Targeting NRF2-Governed Glutathione
742 Synthesis for SDHB-Mutated Pheochromocytoma and Paraganglioma. Cancers (Basel). 2020;12.
743 57. Buettner GR. The pecking order of free radicals and antioxidants: lipid peroxidation, alpha-
744 tocopherol, and ascorbate. Arch Biochem Biophys. 1993;300:535–43.
745 58. Padayatty SJ, Levine M. Vitamin C: the known and the unknown and Goldilocks. Oral Dis.
746 2016;22:463–93.
747 59. Du J, Cullen JJ, Buettner GR. Ascorbic acid: chemistry, biology and the treatment of cancer.
748 Biochim Biophys Acta. 2012;1826:443–57.
749 60. Ngo B, Van Riper JM, Cantley LC, Yun J. Targeting cancer vulnerabilities with high-dose vitamin
750 C. Nat Rev Cancer. 2019;19:271–82.
751 61. Chen Q, Espey MG, Krishna MC, Mitchell JB, Corpe CP, Buettner GR, et al. Pharmacologic
752 ascorbic acid concentrations selectively kill cancer cells: action as a pro-drug to deliver
753 hydrogen peroxide to tissues. Proc Natl Acad Sci USA. 2005;102:13604–9.
754 62. Du J, Martin SM, Levine M, Wagner BA, Buettner GR, Wang S, et al. Mechanisms of ascorbate-
755 induced cytotoxicity in pancreatic cancer. Clin Cancer Res. 2010;16:509–20.
756 63. Nauman G, Gray JC, Parkinson R, Levine M, Paller CJ. Systematic Review of Intravenous
757 Ascorbate in Cancer Clinical Trials. Antioxidants (Basel). 2018;7.
758 64. Hsu PD, Scott DA, Weinstein JA, Ran FA, Konermann S, Agarwala V, et al. DNA targeting
759 specificity of RNA-guided Cas9 nucleases. Nat Biotechnol. 2013;31:827–32.
760 65. Rustin P, Chretien D, Bourgeron T, Gerard B, Rotig A, Saudubray JM, et al. Biochemical and
761 molecular investigations in respiratory chain deficiencies. Clin Chim Acta. 1994;228:35–51.
762 66. Benit P, Goncalves S, Philippe Dassa E, Briere JJ, Martin G, Rustin P. Three spectrophotometric
763 assays for the measurement of the five respiratory chain complexes in minuscule biological
764 samples. Clin Chim Acta. 2006;374:81–6.
765 67. Guo W, Fiziev P, Yan W, Cokus S, Sun X, Zhang MQ, et al. BS-Seeker2: a versatile aligning
766 pipeline for bisulfite sequencing data. BMC Genomics. 2013;14:774.
767 68. Akalin A, Kormaksson M, Li S, Garrett-Bakelman FE, Figueroa ME, Melnick A, et al. methylKit: a
768 comprehensive R package for the analysis of genome-wide DNA methylation profiles. Genome
769 Biol. 2012;13:R87.
770 69. Petrat F, Weisheit D, Lensen M, de Groot H, Sustmann R, Rauen U. Selective determination of
771 mitochondrial chelatable iron in viable cells with a new fluorescent sensor. Biochem J.
772 2002;362:137–47.
773 70. Hirayama, T, Okuda, K, Nagasawa, H. A highly selective turn-onfluorescent probe for iron(II) to
774 visualize labile iron in living cells. Chem Sci. 2013;1250–1256.
775 71. Wang H-H, Xue L, Fang Z-J, Li G-P, Jiang H. A colorimetric and fluorescent chemosensor for
776 copper ions in aqueous media and its application in living cells. New J Chem. 2010;1239–42.
777 72. Dodani SC, Leary SC, Cobine PA, Winge DR, Chang CJ. A targetable fluorescent sensor reveals
778 that copper-deficient SCO1 and SCO2 patient cells prioritize mitochondrial copper homeostasis.
779 J Am Chem Soc. 2011;133:8606–16.

780

Acknowledgements

We thank all members of the Genetics Department, Biological Resources Center and Tumor Bank Platform, Hôpital Européen Georges Pompidou (BB-0033-00063), the Metabolic Tracer Analysis Core (MTAC) at the University of Birmingham for access to their technology platform, as well as the London Metallomics Facility. We thank Dr Stijn J.M. Van Malderen for assistance with shift correction.

Author contributions

J.F., E.L. and D.A.T conceived the study. J.G., A.M., G.G., S.M., C.L.A. designed and performed the experiments, and analyzed the data. S.Mo., K.K., A.P.M., T.J.S., C.L-L., P.B. and A.T. performed the experiments and analyzed the data. J.F., D.A.T., E.L., F.M-G. and R.R. designed the experiments and analyzed the data. J.F. and A-P.G-R. supervised the study. J.F. and J.G. contributed to the management of the project, wrote the manuscript and prepared the figures. E.L. and D.A.T. contributed to the preparation of the manuscript. All the authors discussed the results and reviewed the manuscript.

Experimental procedures

Generation of *Sdhd*$^{-/-}$ Immortalized Mouse Chromaffin Cells by CRISPR-Cas9 method

Targeted gRNA was designed *in silico* by using http://crispr.genome-engineering.org/ as previously described (64). gRNA was transcribed *in vitro* using the kit PrecisionX Cas9 SmartNuclease RNA system (System Biosciences CAS510A-KIT). Briefly, targeted oligonucleotides were annealed to form double strands, and then cloned into SmartNuclease Linearized T7 gRNA Vector. The resulting recombinant vector was linearized by EcoRI digestion. The generated template was used to produce gRNA by *in vitro* transcription. gRNA was then purified (miRNeasy minikit, Qiagen) and its purity was assessed using the Experion RNA StdSens Analysis Kit (BioRad).

Wild-type immortalized mouse chromaffin cells (WT imCC), previously generated by our lab(17), were transfected with 0.6 µg of gRNA (RNA i-MAX (Life Technologies)) and 2µg of Cas9 (System Biosciences CAS940A-1) and 2µg of YFP plasmids (Lipofectamine 2000 (Life Technologies)). Fluorescent cells were cloned by FACS sorting. Clones were screened by direct sequencing of the targeted sequence of murine *Sdhd* gene. Two consecutive transfections were performed: the first generated three heterozygous clones out of 70, and the second performed on heterozygous clones generated 2 homozygous clones out of 288. Mycoplasma contamination was ruled out using the PCR Mycoplasma Test kit I/C (PromKine, PK-CA91-1048).

Sdhd$^{-/-}$ clones transfection by SDHD expressing plasmid

Sdhd$^{-/-}$ clone A was transfected with 2 µg of SDHD-expressing vector (ORIGENE, NM003002) using Lipofectamine 2000 (Life Technologies). Forty-eight hours later, selection was performed with Geneticin (Sigma, G418, 1200 µg/ml) and selected cells were cloned by FACS sorting. Clones were then screened by SDH activity test and by qRT-PCR in order to assess *Sdhd* expression.

824

825 **Direct sequencing of *Sdhd* gene**

826 Direct sequencing of the four exons and exon-intron boundaries of the *Sdhd* gene was performed by
827 Sanger method. Specific primers (available upon request) were designed to amplify small amplicons
828 for *Sdhd* gene sequencing. The sequencing reactions were performed using the BigDye Terminator
829 v3.1 kit (Life Technologies), in an ABI Prism3730XL DNA Analyzer (Perkin Elmer Applied Biosystems,
830 Foster City, CA).

831

832 **Cell culture**

833 imCC were cultured in DMEM high glucose Glutamax (Dulbecco Modified Eagle Medium, Gibco) with
834 10% FBS (Fetal bovine serum, Gibco) and 1% antibiotics (penicillin/streptomycin, Gibco) unless when
835 grown for metabolic or respirometry experiments, in which case they were supplemented with
836 pyruvate (1 mM) and no antibiotics. Cells were grown at 37°C, in 5% CO2. When stated, cells were
837 treated with indicated doses of iron Chloride (Sigma, 372870), L-Ascorbic acid (Sigma, A5960) or 3
838 mM of N-acetyl-cysteine (Sigma, A9165) for 24 h to 72 h.

839

840 **^{13}C-glucose and ^{13}C-glutamine labeling**

841 Cells (3 x 10^5) were seeded onto five wells of a six-well plate and cultured in standard medium for 24
842 h, the remaining well was used as a control containing only medium. Cells were washed in PBS and
843 the medium was then replaced by either fresh DMEM (no glucose, no phenol red) with 10 mM $^{13}C_6$-
844 D-glucose (Sigma) or DMEM (high glucose, no glutamine) supplemented with 2 mM $^{13}C_5$-L-glutamine
845 (Sigma) for 72 h.

846

847

Metabolite extraction

For spent media analysis, 200 µl of cleared media was first extracted. Culture media were then aspirated and cells were washed cold with 0.9% NaCl saline solution before being scraped off the precooled plates into Methanol/water mixture. In all cases, glutaric acid supplied in water was used as internal standard and polar metabolites were extracted using Methanol:H2O:Chloroform at ratio 1:1:1. Briefly, samples were vortexed vigorously, left to shake with all the solvents for 15 min at 4 °C and then centrifuged at 15 000g for 15 min at 4 °C which led to separation into polar and nonpolar fractions. The polar fractions were transferred to new tubes, evaporated to dryness by SpeedVac concentrator and used for Gas Chromatography – Mass Spectrometry (GC-MS) analysis.

GC-MS analysis

The dried extract was first incubated at 95 °C in open tubes and then solubilized in 40 µl of 2% methoxyamine HCl in pyridine followed by 60 minutes incubation at 60°C and subsequently 60 µl N-tertbutyldimethylsilyl-N-methyltrifluoroacetamide with 1% (w/v) tertbutyldimethyl-chlorosilane derivatisation reagent was added. The suspension was incubated for an hour at 60 °C in a well-sealed tube to prevent evaporation. Finally, the samples were centrifuged at 16000 g for 5 minutes and the clear supernatant was transferred to a chromatography vial with a glass insert (Thermo Fisher Scientific) and proceeded immediately to GC-MS analysis.

For analysis of the derivatised samples an Agilent 7890B Series GC/MSD gas chromatograph with a polydimethylsiloxane GC column coupled, with a mass spectrometer (GC-MS) (Agilent Technologies UK Limited, Stockport, UK) was used. Prior to sample analysis the GC-MS was tuned to a full width at half maximum (FWHM) peak width of 0.60 a.m.u. in the mass range of 50 to 650 mass to charge ratio (m/z) using PFTBA tuning solution. 1 µl of sample was injected into the GC-MS in splitless mode with helium carrier gas at a rate of 1.0 ml min^{-1}. The inlet liner containing glass wool was set to a temperature of 270 °C. Oven temperature was set at 100 °C for 1 minute before ramping to 280 °C at

a rate of 5 °C min-1. Temperature was further ramped to 320 °C at a rate of 10 °C min^{-1} held at 320 °C for 5 minutes. Compound detection was carried out in full scan mode in the mass range 50 to 650 m/z, with 2-4 scans sec^{-1}, a source temperature of 250 °C, a transfer line temperature of 280 °C and a solvent delay time of 6.5 minutes. The injector needle was cleaned with acetonitrile three times before measurement commencement and three times following every measurement thereafter. The raw GC-MS data was converted to common data format (CDF) using the acquisition software and further processing of the isotope data including isotope correction and mass isotopomer analysis /batch quantification was performed on metabolite detector software. The raw peak area for each analyte of interest was calculated using the metabolite detector software followed by normalizing the response to the internal standard peak area.

High resolution respirometry

For the measurement in intact state, trypsinised cells were resuspended in cell culture media (4.5g/L glucose + 1 mM pyruvate) and loaded in Oxygraph-O2 k (Oroboros instruments) chamber. After closing the chambers and recording routine respiration, oligomycin (2.5 µM) was added to inhibit ATP synthase. Measurements of the non-phosphorylating electron transfer system (ETS) capacity were obtained through stepwise (0.5 µM) titration of the uncoupler, Carbonyl cyanide 4-(trifluoromethoxy)phenylhydrazone (FCCP). Respiration was inhibited by addition of rotenone (0.5 µM) and antimycin A (2.5 µM) at the end of the experiment. For the measurement in permeabilised state, trypsinised and washed cells were resuspended in respiratory media Mir05 (110 mM sucrose, 60 mM K^+-lactobionate, 0.5 mM EGTA, 3 mM $MgCl_2$, 20 mM taurine, 10 mM KH_2PO_4, 20 mM HEPES, 1g/L BSA essentially fatty acid free, pH 7.1). After closing the chambers and recording respiration on endogenous substrates, digitonin was added to permeabilise the cells. Substrate combinations were used as indicated in the graphs. The concentrations used were 2 mM malate (M), 10 mM glutamate (G) and 20 mM succinate (SUC). In all experiments on permeabilised cells 3 mM ADP was used and

maximum respiratory capacity was reached by stepwise titration of FCCP. Respiration was inhibited by addition of 0.5 µM rotenone and antimycin A (2.5 µM) at the end of the experiment. Values after antimycin A addition were subtracted from all recorded values.

Assessment of enzymatic activities

Respiratory chain activities in subconfluent chromaffin cells were assayed as previously described (65). Malonate-sensitive succinate dehydrogenase (RC complex II; E.C. 1.3.5.1), glycerol 3 phosphate dehydrogenase (EC 1.1.5.3), cyanide-sensitive cytochrome *c* oxidase (RC complex IV; EC 1.9.3.1), malonate-sensitive succinate cytochrome *c* reductase (RC complex II+III; EC 1.3.99.1), and glycerol cytochrome *c* reductase (glycerol 3-phosphate dehydrogenase + RC complex III) were assayed spectrophotometrically at 37°C using a pseudo dual- wavelength Varian CARY50 spectrophotometer (Victoria, Australia) as described previously (66). Protein concentrations were determined by the Bradford method. All chemicals were analytical reagent grade from Sigma Chemical Company.

Quantitative Real-Time PCR

Total RNAs were extracted from cell pellets using RNeasy plus mini-kit (Qiagen) as described by the manufacturer. Reverse transcription was fulfilled using iScript™ cDNA Synthesis Kit (BIO-RAD) during 30 min at 42°C. qRT-PCR was then performed on CFX96™ Real-Time System C1000 Touch™ Thermal Cycler (BIO-RAD) using SuperScript SybrGreen (BioRad). Normalization was performed with 18S amplifications, and comparisons were calculated using the ΔΔCt method. Primers' sequences were as follows:

18S: F 5'-CGCGGTTCTATTTTGTTGGT-3'; R 5'-AACCATAAACGATGCCGAC-3';

Sdhd: F 5'-GGACCAGTGAGAGGGTTGTC-3'; R 5'-AAGCTGAGAGTGCCAAGAGG-3'

Sdhb : F 5'-GCAGCTCCCAGAATCAAAAA-3' ; R 5'-CCAGAGTATTGCCTCCGTTG-3'

Snai1: F 5’-TGGAAAGGCCTTCTCTAGGC-3’; R 5’-AAAAGCACGGTTGCAGTGG-3’

Twist1: F 5’-GACTCCAAGATGGCAAGCTG-3’; R 5’-TTCTCTGGAAACAATGACATCTAGGT-3’

Epas1: F 5’-AGGGCCACAGCAAAGAGAG-3’; R 5’-CATCACGGGATTTCTCCTTC-3’

Mmp9: F 5’-CGGCACGCTGGAATGATC-3’; R 5’- TCGAACTTCGACACTGACAAGAA -3

Col1a1: F 5’-CTCCTGGTATTGCTGGTGCT-3’; R 5’-GGCTCCTCGTTTTCCTTCTT-3’

Col4a2: F 5’-GACCCTGAGGTTAGGAAGGGA-3’; R 5’-TCGGTCCATGATCCCAGTCT-3’

Glut1: F 5’-AAACATGGAACCACCGCTAC-3’; R 5’-GGAGAAGCCCATAAGCACAG-3’

VegfA: F 5’-CTACTGCCGTCCGATTGAG-3’; R 5’-TATGTGCTGGCTTTGGTGAG-3’

Western blot

Total proteins were extracted in RIPA lysis buffer, containing protease and phosphatase inhibitors cocktail (Thermo Fisher, #88669). Protein concentrations were determined with Bradford colorimetric method. Equal quantities of proteins were resolved on NuPAGE® Novex 4–12 % Bis-Tris gradient gel (Invitrogen) and transferred on nitrocellulose membrane. After blocking in PBS-milk solution (5%), membranes were incubated overnight with specific primary antibodies, followed by washing in PBS, 0.05% tween-20 and incubation with corresponding HRP-conjugated (anti-rabbit or anti-mouse) secondary antibodies (Bio-FX). The bound antibodies were revealed by chemiluminescence using ECL (Pierce) and the results read with a LAS-4000 Mini (Fuji). The antibodies used were: anti-actin (1/5000, Sigma-Aldrich, A5316), anti-tubulin (1/2500, Sigma-Aldrich, T9026), anti-HIF2α (1/1000, abcam, #ab8365), and anti-HIF1α (1/1000, Active Motif, ESEE122 #61275), anti-SDHB (1/500, Sigma, HPA002868). The experiment was performed independently three times and representative results are shown.

Fluorescent staining

All Fluorescent staining were performed on cells plated on glass slides until 80% confluence. After a wash in PBS 1X, cells were fixed for 10 min in ice-cold 4% paraformaldehyde. For actin staining, a permeabilization step was performed with proper buffer (0.5% triton X-100, 20 mM Tris-HCl (pH=8), 50 mM NaCl, 3 mM MgCl2, 300 mM sucrose) for 10 min at room temperature. Phalloidin-TRITC toxin (Sigma #P1951) diluted 1/1000 in PBS 1X was incubated for 1h at room temperature and washed before mounting the coverslip in vectashield with Dapi.

For SDHD immunofluorescence, after blocking of aspecific sites for 30 min with PBS 1% BSA 0,1% triton, the slides were incubated, overnight at 4°C, with anti-SDHD antibody (1/200, Sigma SAB3500797) diluted in blocking buffer. Primary antibody was washed and the slides were incubated with the secondary antibody, conjugated with Alexa Fluor 594 (1/2000, Invitrogen) for 1 h at room temperature in the dark and then washed with PBS. Finally, the slides were mounted in Vectashield, containing DAPI, for a blue nuclear staining. Image acquisition was performed using a Confocal SP8 Leica microscope and 12 z-stacks of 0.5 μm were merged.

Cell proliferation assay

50.000 cells were plated on 6-well plates. Growth curves were established by counting cells after three, five and seven days. The experiment was performed three times, in duplicates.

Cell migration assay

Wound scratch assays were performed during 10 hours as previously described (19) and analyzed using ImageJ software. The experiment was performed four times.

Cell adhesion assay

After complete detachment from their plates by trypsin EDTA 0.05 % (Gibco), cells were plated in 6-wells plates. Cell adhesion was evaluated by taking pictures 1 h post-seeding. Adherent and non-adherent cells were identified on the basis of their morphology and the percentage of adhesive cells was calculated. The experiment was performed three times.

RNA-seq analysis

RNA sequencing was performed for 7 samples: 3 *Sdhb*-/-, 2 *Sdhd*-/- and 2 wild-type imCC. RNA samples were enriched for polyadenylated RNA from 5 µg of total RNA, and the enriched samples were used to generate sequencing libraries with the Illumina 'TruSeq Stranded mRNA Sample Prep' kit and associated protocol as provided by the manufacturer. Libraries were sequenced by IntegraGen (Evry, France) on an Illumina HiSeq 2000 as paired-end 75 bp reads. Quality of reads was assessed for each sample using FastQC (http://www.bioinformatics.babraham.ac.uk/projects/fastqc/). Fastq files were aligned to the reference Human genome hg19/GRCh37 or to the reference Mouse genome mm10 with tophat2 (-p 16 -r 150 -g 2 --library-type fr-firststrand). We removed reads mapping to multiple locations. We used HTSeq to obtain the number of reads associated to each gene in the Gencode vM9 (Mouse) database, restricting to protein-coding genes, antisense and lncRNAs. We used the Bioconductor DESeq package to import raw HTSeq counts for each sample into R statistical software and extract the count matrix. After normalizing for library size, we normalized the count matrix by the coding length of genes to compute FPKM scores (number of fragments per kilobase of exon model and millions of mapped reads). We used the Bioconductor DESeq package to obtain size factors and dispersion estimates, and perform differential expression analysis. Hierarchical clustering (Euclidean distance, Ward method) was used to classify samples according to their expression profiles across the 1,000 most variant genes (based on standard deviation).

Reduced Representation Bisulfite Sequencing (RRBS) Analyses

RRBS was performed by Integragen SA (Evry, France), as previously described (17). In short, 4 µg of mouse genomic DNA plus CeGX Sequencing Control (3% W/W) were digested with MspI (NEB). After end-repair, A-tailing, and ligation to methylated Illumina adapters, the library fragments of 40–220 bp were gel isolated, subjected to a double bisulfite conversion using the TrueMethyl 24 kit (Cambridge Epigenetix) for each sample according to the manufacturer's instructions, PCR amplified, and sequenced on an Illumina HiSeq2000 sequencer as paired-end 75 bp reads.

We generated approximately 30 million uniquely aligned reads for each sample, which covered ≈ 1.5 million CpG sites. We used BS-Seeker2 (67) to map RRBS data to the Mouse genome mm10 and retrieve the number of methylated and unmethylated cytosines at each covered CpG site. Methylation rates were then integrated across CpG island (CGI)-based and gene-based features. CGI-based features were defined as follows: CpG islands (from UCSC database Mouse mm10), shores (2 kb on each side of the island) and shelves (2 kb on each side of the shores). DNA methylation outside CpG islands was analyzed by grouping CpG sites not located in CGI-based features every 100kb window. Gene-based features were defined based on Ensembl mus musculus GRCm38.78 assembly. We calculated for each gene the methylation rate across the promoter region (TSS +/- 500bp) and the gene body. We compared methylation rates across all CGI-based and gene-based features. *q* values were computed by comparing the number of methylated and unmethylated reads in each condition using a logistic regression and the SLIM method for p-value adjustment, as implemented in the methylKit package (68). We also calculated the methylation rate difference (delta) between each pair of test and reference sample. We considered as differentially methylated every region with a q-value <0.05 and a methylation delta >0.05 or <-0.05 in at least 80% of test-reference pairs.

Mitochondrial mass and membrane potential assessment using MitoTracker Probe

Cells were seeded onto six-well plates and grown up to 70% confluency. Mitochondrial content per cell line was estimated using MitoTracker Deep Red FM (Thermofisher #M22426). For assessment of mitochondrial membrane potential, cells were stained with tetramethylrhodamine-methyl-ester (TMRM, Thermofisher #T668). Cells were stained with 250 nM MitoTracker Deep Red FM or 100 µM TMRM for 30 min at 37C. Cells were then washed with PBS solution, trypsinized, and resuspended in PBS solution containing 10% FBS for flow cytometric analysis. Flow cytometry data were acquired using an LSR FORTESSA analyzer (BD biosciences).

Mitochondrial Staining using MitoTracker Probe

Cells were seeded onto glass coverslips inside a 24-wells plates and 48 hours later incubated with 250 nM MitoTracker Deep Red FM (Thermofisher #M22426) for 30 min at 37C in the dark. Cells were then fixed in cold acetone for 10 min and rinsed in PBS, before mounting in vectashield with Dapi. Fluorescence was observed using a Confocal SP8 Leica microscope and images were acquired with identical exposure times and settings.

Features of Oxidative Stress

Cells were seeded onto six-well plates and grown up to 70% confluency for 2 days. After what they were directly incubated with fluorescent probes for basal conditions. Cells were washed with PBS, trypsinized and resuspended in PBS solution containing 10% FBS for flow cytometric analysis. Flow cytometry data were acquired using an LSR FORTESSA analyzer (BD biosciences). For ROS quantification upon treatment, cells were treated for 48 hours with 100 µM iron Chloride (Sigma, 372870), 2.5 mM of L-Ascorbic acid (Sigma, A5960) or 3 mM of N-acetyl-cysteine (Sigma, A9165), and then processed, as described above.

Cellular and mitochondrial ROS

Cells were incubated with either 5 µM CellRox Reagent (Thermofisher, #10422) or 5 µM MitoSox (Thermofisher, #M36008) for 30 min at 37°C in the dark.

Lipid Peroxide Product

Cells were incubated with 2 µM Bodipy C11 Reagent (Termofisher, #D3861) for 30 min at 37°C in the dark.

Cellular levels of iron and copper

Metal-specific probes were synthesized as previously described. For mitochondrial copper and iron probes, cells were incubated at 37°C in the dark with the relevant probe prior to being analyzed by flow cytometry using the following probes and conditions: 1 µM turn-off Iron(II) probe (69) (1h) for mitochondrial Iron(II) content; 5 µM Rhonox-1 (turn-on Iron(II)) probe (70) (1h) for cytosolic Iron(II) content ; 1 µM Calcein-AM probe (Thermofisher, #C1430) (1h) for labile overall iron content ; 10 µM turn-off Cu(II) probe (71) (1h) for mitochondrial Cu(II) content ; 1 µM turn-on Cu(I) probe (72) (30min) for mitochondrial Cu(I) content. Cells were trypsinized (TrypLE Express Enzyme, Life Technologies, 12605010) and washed twice with ice cold PBS. Data were recorded on a BD Accuri C6 (BD Biosciences) and processed using Cell Quest (BD Biosciences) and FlowJo (FLOWJO, LLC) software.

Laser ablation-inductively coupled plasma-mass spectrometry (LA-ICP-MS)

For the LA-ICP-MS experiments, an Analyte Excite 193 nm ArF*excimer-based LA system (Teledyne Photon Machines, Bozeman, MT, USA) was used, equipped with the HelEx II two-volume ablation

cell. The LA system was coupled to a Thermo Fisher Scientific iCAP TQ ICP-mass spectrometer (Thermo Fisher Scientific, Waltham, MA, USA) via the Aerosol Rapid Introduction System (ARIS). Tuning of the instrument settings was performed using a NIST SRM 612 glass certified reference material (National Institute for Standards and Technology, Gaithersburg, MD, USA), optimizing for low laser-induced elemental fractionation through monitoring of $^{238}U+/^{232}Th+$ ratios, low oxide formation (<1%) monitoring $^{232}Th^{16}O+/^{232}Th+$ ratios, and high sensitivity for $^{59}Co+$, $^{115}In+$ and $^{238}U+$. LA-ICP-MS images were acquired in a fixed dosage mode, with a vertical and horizontal spatial resolution of 20 µm, a detailed list of sample settings is available in Supplementary Table 3. Formalin-fixed paraffin-embedded tumor tissue sections were dewaxed in xylene immediately prior to imaging, and rehydrated through a descending ethanol series. Two experimental repeats were conducted, each of which consisted of imaging sections from one *NF1* mutant and two *SDHB* mutant tumors (n=6 total tumors interrogated using LA-ICP-MS). Samples were mounted inside a bespoke three slide sample holder of the HelEx II two-volume ablation cell (Teledyne Photon Machines). To correct for instrumental drift, a series of NIST 612 standard ablation scans were performed before and after each tumor image. ICP-MS and positional data were reconstructed using the HDF-based Image Processing software (HDIP, Teledyne Photon Machines Inc., Bozeman, MT, USA). A bespoke pipeline written in Python (version 2.7), was used to generate elemental images from reconstructed data. Negative values, attributed to instrumental noise, were replaced with zeros. All LA-ICP-MS images are displayed using the same threshold to enable a direct visual comparison between tumor sections. Average ^{56}Fe intensities were calculated from pixels containing a positive elemental tissue marker (^{31}P) ensuring background regions did not influence these calculations. For ease of interpretation, ^{56}Fe values for *SDHB* tumors were normalized to their respective *NF1* averages recorded during each experimental repeat. Statistical significance between ^{56}Fe intensities was assessed by Student's t-test.

Statistical analysis

Data are represented as mean (of at least 3 independent experiments) ± SEM (standard error of the mean). Data were analyzed by one-way or 2-way ANOVA. The results were considered to be significant if $p \leq 0.05$. Statistics tests were carried out using the Graph-Pad software.

Enrichment analysis

We used an in-house adaptation of the GSEA method to identify gene sets from the MSigDB database overrepresented among up/down-regulated and hyper/hypomethylated genes.

Data access

The raw and processed RNA-seq and RRBS data sets generated in this study are being deposited to the European Genome Phenome Archive.

Supplementary Figures

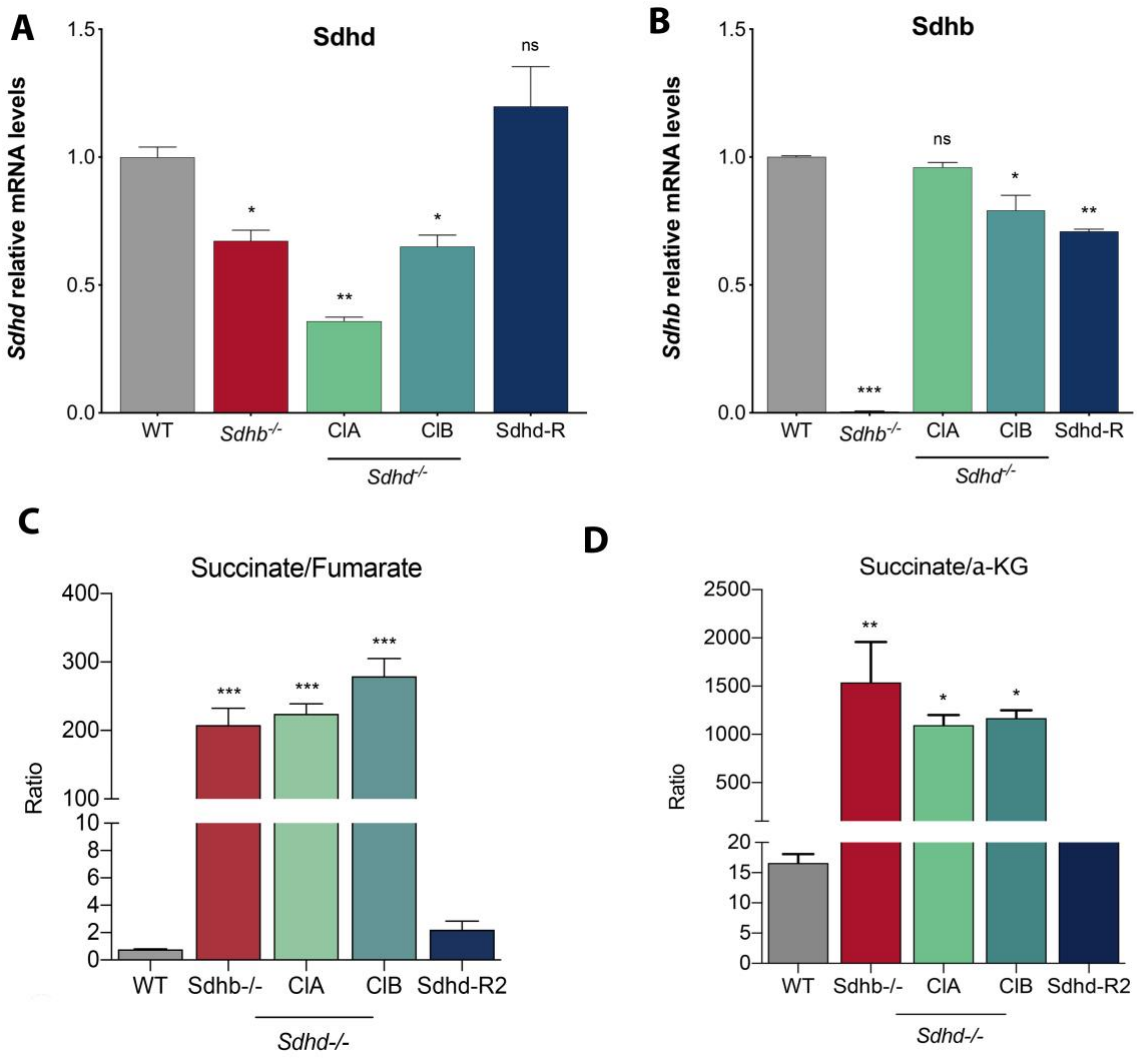

Supplementary Fig. 1 Related to Figure 1. Validation of new *Sdhd* knock-out cell models

A, qRT-PCR analysis of *Sdhd* gene in the indicated cell lines. **B,** qRT-PCR analysis of *Sdhb* gene in the indicated cell lines. For **A and B** data shown are from at least six independent experiments, presented as mean ± SEM. **C,** Succinate to Fumarate ratio and **D,** Succinate to α-ketoglutarate (α-KG) assessed in all the indicated cell lines, using steady-state levels of the former organic acids measured by GS-MS (n=3). Data are shown as mean ± SEM. Student's test was performed to assess statistical significance; ns, not significant, *P≤0.05, **P≤0.01, ***P≤0.001.

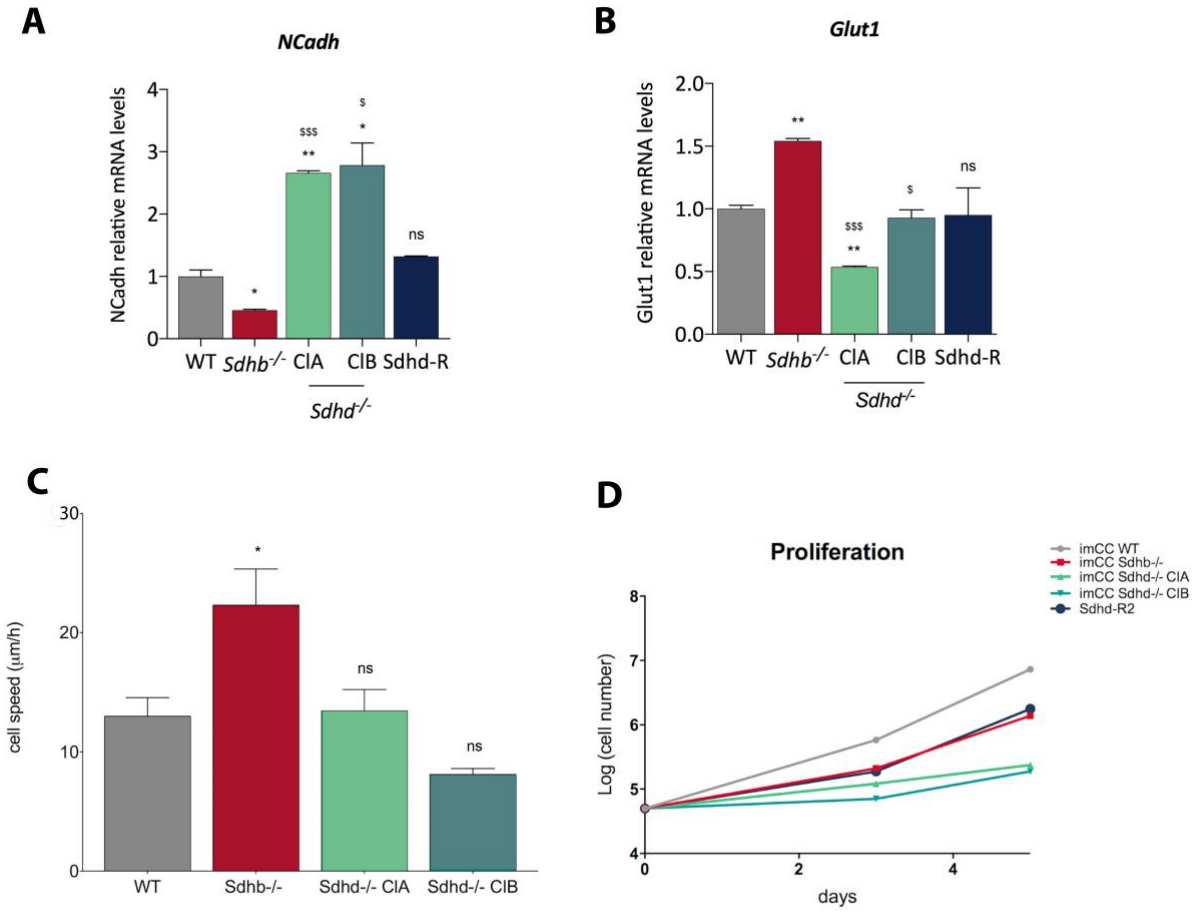

Supplementary Fig. 2 Related to Figure 2. *Sdhb* KO, but not *Sdhd* KO cells exhibit a mesenchymal metastatic phenotype

A, qRT-PCR analysis of *NCadh* gene in the indicated cell lines. **B,** qRT-PCR analysis of *Glut1* gene in the indicated cell lines. For **A and B** data shown are from at least three independent experiments, presented as mean ± SEM. **C,** Individual cell speed was estimated (in µm/hour) by tracking cell nucleus during 12 hours (n=3). **D,** Growth curves of all the indicated cell lines were established by counting cells after three, five and seven days. The experiment was performed three times, in duplicates. Data are shown as mean ± SEM. Student's test was performed to assess statistical significance; ns, not significant, *P≤0.05, **P≤0.01, ***P≤0.001 relative to WT and $P≤0.05, $$$P≤0.001 relative to *Sdhb-/-* imCC.

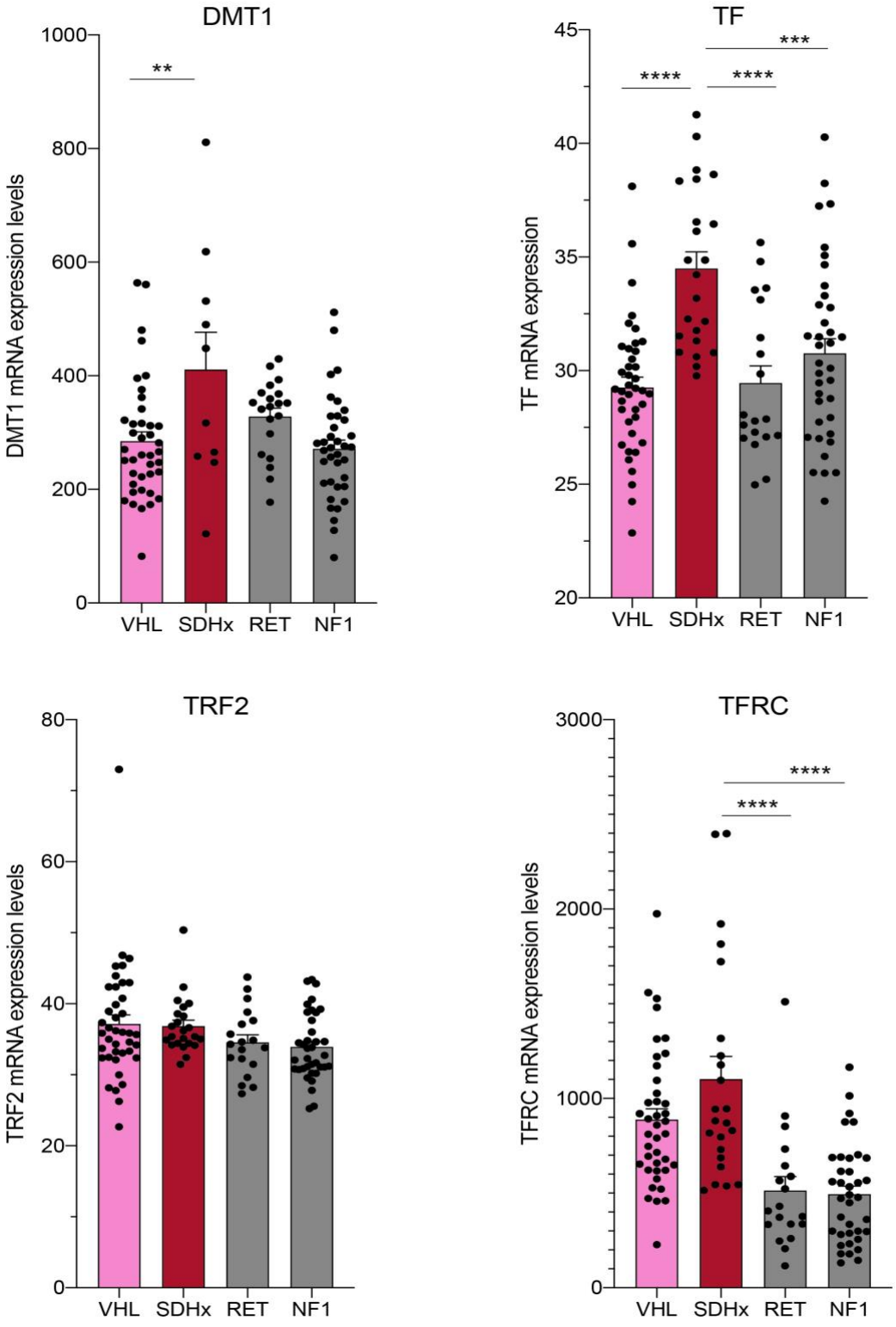

Supplementary Fig. 3 Related to Figure 3. *SDHx*-mutated tumors exhibit slight changes in transferrin (TF) mRNA expression levels in comparison to other types of mutated PPGL

A, Microarray-based expression analysis of several critical actors of cellular iron homeostasis DMT1, TF, TFR2 and TFRC in a cohort of human PPGL, including 40 *VHL*-mutated, 19 *RET*-mutated, 37 *NF1*-mutated and 23 *SDHx*-mutated tumors. Expression clusters have been described in Burnichon et al., 2010. Data are presented as means ± SEM. One-way ANOVA was used to assess statistical significance; **P≤0.01, ***P≤0.001.

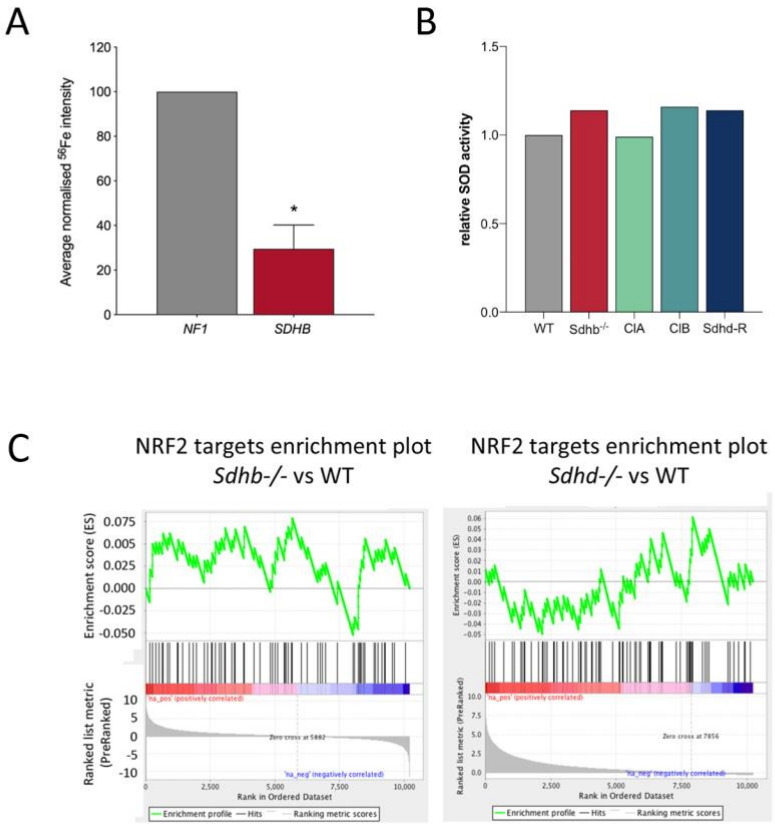

Supplementary Fig. 4 Related to Figure 3 and 4. *SDHB*-mutated PGL exhibit significant decrease in ^{56}Fe and *Sdhb*-deficient cells do not detoxify the excess in mitochondrial ROS

A, Quantification of average ^{56}Fe assessed by LA-ICP-MS in one *NF1* mutated human tumor and two *SDHB* mutated human tumors. ^{56}Fe values for *SDHB* tumors were normalized to their respective *NF1* averages recorded during each experimental repeat. Statistical significance between ^{56}Fe intensities was assessed by Student's t-test; *P≤0.05, **P≤0.01, ***P≤0.001 **B,** Global superoxide dismutase (SOD) activity measured by spectrophotometry in all the indicated cell lines. **C,** Gene set enrichment analyses using RNA-seq data of 58 NRF2-target genes in *Sdhb* and *Sdhd* KO cells versus WT cells.

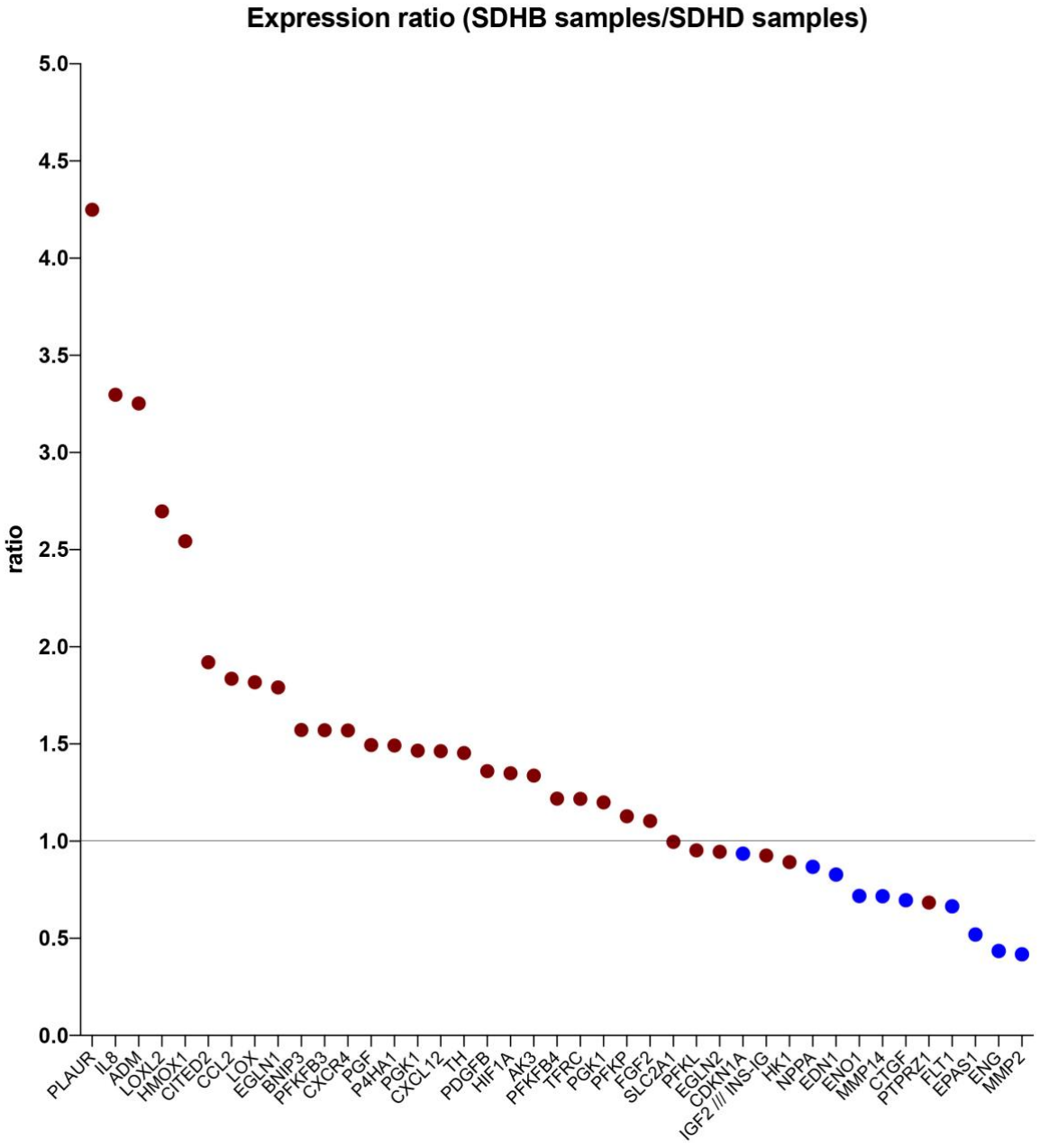

Supplementary Fig. 5 Related to Figure 2. Overexpression of HIF-target genes in *SDHB*-mutated tumors versus *SDHD*-mutated tumors

Ratio between mean expression of 41 highly expressed HIF-target genes in *SDHB* versus *SDHD*-mutated tumors. This analysis includes and compares transcriptomic data from 3 *SDHD* and 17 *SDHB*-mutated tumors. Blue dots indicate genes specifically expressed in endothelial cells.

Supplementary Table 1 Related to Figure 2. Differentially methylated gene-based features in *Sdhb-/-* versus *Sdhd-/-* imCCs

Supplementary Table 2 Related to Figure 4. List of 58 NRF2-target genes used for transcriptomic analyses

Abcc1	ATP-binding cassette, sub-family C (CFTR/MRP), member 1
Abcc2	ATP-binding cassette, sub-family C (CFTR/MRP), member 2
Abcc3	ATP-binding cassette, sub-family C (CFTR/MRP), member 3
Abcc4	ATP-binding cassette, sub-family C (CFTR/MRP), member 4
Abcc5	ATP-binding cassette, sub-family C (CFTR/MRP), member 5
Acot7	acyl-CoA thioesterase 7
Acot8	acyl-CoA thioesterase 8
Acox1	acyl-Coenzyme A oxidase 1, palmitoyl
Acox2	acyl-Coenzyme A oxidase 2, branched chain
Adh7	alcohol dehydrogenase 7 (class IV), mu or sigma polypeptide
Akr1b1	aldo-keto reductase family 1, member B1 (aldose reductase)
Akr1c1	aldo-keto reductase family 1, member C1
Aldh1a1	aldehyde dehydrogenase family 1, subfamily A1
Aldh7a1	aldehyde dehydrogenase family 7, member A1
Blvra	biliverdin reductase A
Blvrb	biliverdin reductase B (flavin reductase (NADPH))
Cbr1	carbonyl reductase 1
Cebpb	CCAAT/enhancer binding protein (C/EBP), beta
Cyp1b1	cytochrome P450, family 1, subfamily b, polypeptide 1
Ephx1	epoxide hydrolase 1, microsomal
Fech	ferrochelatase
Fthl17	ferritin, heavy polypeptide-like 17
G6pd	glucose-6-phosphate dehydrogenase
Gclc	glutamate-cysteine ligase, catalytic subunit
Gclm	glutamate-cysteine ligase, modifier subunit
Ggt1	gamma-glutamyltransferase 1
Glrx	glutaredoxin
Gls	glutaminase
Gpx2	glutathione peroxidase 2
Gpx4	glutathione peroxidase 4
Gsr	glutathione reductase
Gsta1	glutathione S-transferase, alpha 1 (Ya)
Gstm1	glutathione S-transferase, mu 1
Gstp1	glutathione S-transferase, pi 1
Hmox1	heme oxygenase 1
Idh1	isocitrate dehydrogenase 1 (NADP+), soluble
Liph	lipase, member H
Me1	malic enzyme 1, NADP(+)-dependent, cytosolic

Mgst1	microsomal glutathione S-transferase 1
Nfe2l2	nuclear factor, erythroid derived 2, like 2
Nqo1	NAD(P)H dehydrogenase, quinone 1
Pgd	phosphogluconate dehydrogenase
Pla2g7	phospholipase A2, group VII (platelet-activating factor acetylhydrolase, plasma)
Pnpla2	patatin-like phospholipase domain containing 2
Pparg	peroxisome proliferator activated receptor gamma
Ppargc1b	peroxisome proliferative activated receptor, gamma, coactivator 1 beta
Prdx1	peroxiredoxin 1
Prdx6	peroxiredoxin 6
Rxra	retinoid X receptor alpha
Slc6a9	solute carrier family 6 (neurotransmitter transporter, glycine), member 9
Slc7a11	solute carrier family 7 (cationic amino acid transporter, y+ system), member 11
Srxn1	sulfiredoxin 1 homolog (S. cerevisiae)
Sult1a1	sulfotransferase family 1A, phenol-preferring, member 1
Taldo1	transaldolase 1
Tkt	Transketolase
Txn	thioredoxin
Txnrd1	thioredoxin reductase 1
Ugdh	UDP-glucose dehydrogenase

Supplementary Table 3 Related to Figure 3 Methods. Experimental parameters and data acquisition parameters used for LA-ICP-MS imaging.

	Tumors	NIST 612 Scans
Teledyne Photon Machines Analyte Excite		
Energy density (J cm^{-2})	0.5	2.02
Repetition rate (Hz)	125	125
Scan speed (µm s^{-1})	500	500
Beam waist diameter (µm)	20 (Circle)	40 (Circle)
Scanning Mode	Fixed Dosage	Fixed Dosage
Scanning Direction	Uni-directional	Uni-directional
Effective Dosage (shots per position)	5	5
He Carrier gas flow rate (L min^{-1})	0.5	0.5
Thermo Fisher Scientific iCAP TQ ICP-MS		
RF power (W)	1550	1550
Ar plasma gas flow rate (L min -1)	14	14
Ar auxiliary gas flow rate (L min -1)	0.8	0.8
Nebuliser gas flow rate (L min -1)	1.03	1.03
He gas flow rate (L min -1)	3.25	3.25
Acquired m/z ratios (amu)	^{31}P, ^{56}Fe	^{31}P, ^{56}Fe
Respective dwell times (ms)	2.0, 5.8	2.0, 5.8
Total scan cycle time (ms)	40	40

DISCUSSION

L'objectif principal de cette étude était de comparer deux modèles similaires de cellules chromaffines murines mutés sur des gènes *Sdhx* différents, dans le but de mieux comprendre la tumorigenèse SDH-dépendante, mais également d'identifier les mécanismes spécifiquement associés aux mutations *Sdhb,* expliquant ainsi la malignité SDHB-dépendante.

Dans un premier temps, cette étude m'a permis de valider nos modèles d'étude cellulaires, en montrant que les cellules *Sdhb* et *Sdhd* KO ont des phénotypes différents qui récapitulent respectivement les phénotypes des tumeurs humaines avec ces différentes mutations. Ainsi, les imCC *Sdhd* KO ont un comportement beaucoup moins agressif que celui des imCC *Sdhb* KO. En effet, en comparant les cellules *Sdhb* KO aux cellules *Sdhd* KO, j'ai observé que malgré une perte de fonction SDH et une accumulation de succinate similaires, les cellules *Sdhb-/-* présentaient des propriétés prolifératives, migratoires et adhésives significativement accrues, associées à un phénotype mésenchymateux, non retrouvé dans les imCC *Sdhd-/-.* Les études du transcriptome, du méthylome et de la voie de réponse à l'hypoxie auxquelles j'ai procédé dans ces cellules, montrent que les enzymes PHD et TET sont plus fortement inhibées dans les cellules déficientes en SDHB en comparaison à leurs homologues déficientes en SDHD. Or, ces enzymes appartiennent à la grande famille des dioxygénases 2-OG dépendantes, dont l'activité repose sur différents co-facteurs, tels que le 2-oxoglutarate, l'oxygène, l'ascorbate et le fer. Cette observation associée au fait que la sous-unité SDHB constitue la sous-unité fer-souffre (Fe-S) au sein de la SDH, ce qui constitue une différence majeure avec les autres sous-unités de cette même enzyme (SDHA, SDHC et SDHD), m'ont conduit à m'intéresser au métabolisme du fer et du cuivre. J'ai alors émis l'hypothèse que la perte de la sous-unité SDHB pourrait entrainer un déséquilibre majeur de l'homéostasie du fer et du cuivre dans ces cellules. En effet, nos résultats montrent une perte totale de l'expression de la protéine SDHB dans les cellules *Sdhb-/-*, tandis qu'une petite fraction de la protéine SDHB reste détectable dans les imCC *Sdhd-/-,* conformément aux données d'IHC sur les tumeurs humaines qui montrent fréquemment un marquage faible et diffus de SDHB au sein des PPGL avec mutations *SDHD*. Cette différence fondamentale constituait donc une piste particulièrement intéressante pour la compréhension des mécanismes responsables du phénotype métastatique associé aux mutations *Sdhb.* Ces travaux nous ont ainsi permis de mettre en

évidence un déséquilibre significatif de la distribution cytosolique et mitochondriale du fer et du cuivre, particulièrement exacerbé dans les cellules avec un déficit en SDHB. Cette dérégulation de l'homéostasie fer/cuivre résulterait en un excès de fer labile et de cuivre mitochondrial, qui interagiraient à leur tour via la réaction de Fenton/Haber-Weiss, avec certains ROS produits par la chaine respiratoire mitochondriale, dont le peroxyde d'hydrogène très réactif. Cette réaction généralement lente est catalysée par le fer labile également très réactif, entrainant la production du radical hydroxyle hautement réactif et toxique. Ces résultats pourraient expliquer la plus grande inhibition des dioxygénases 2-OG dépendantes observée suite aux mutations du gène *Sdhb.* D'une part, la surcharge en fer labile très réactif pourrait agir en synergie avec le succinate accumulé et ainsi inhiber d'autant plus fortement ces enzymes, ce qui conduirait à l'activation indirecte de la pseudohypoxie et de la méthylation de l'ADN dans ces cellules. D'autre part, les taux élevés de ROS observés dans les cellules *Sdhb-/-* pourraient également être directement responsable de ces phénotypes exacerbés. En effet, plusieurs études ont démontré que dans un contexte oxydant, secondaire à des niveaux excessifs de ROS, ces molécules pourraient agir comme des signaux capables de déclencher la stabilisation des facteurs de transcription Hifα dans des conditions normoxiques.

De plus, les dommages oxydants résultant de l'accumulation significative de ROS sont observés dans une variété de pathologies telles que les maladies neurodégénératives et le cancer, et ont été particulièrement associés à une transformation maligne. Le cuivre semble également être associé à de tels déséquilibres. En effet, le cuivre est nécessaire à la respiration mitochondriale et à la fonction de la superoxide dismutase mitochondriale, une enzyme présentée dans l'introduction et qui participe grandement à la détoxification mitochondriale des ROS. En outre, il a récemment été démontré que l'histone H3-H4 est une enzyme réductase de cuivre essentielle à son utilisation dans les fonctions précédemment mentionnées. Le rôle de l'histone H3-H4 est de lier le Cu^{2+} et de catalyser sa réduction en Cu^{+}. Or, dans l'étude présentée au chapitre 1 de ce manuscrit nous avions évoqué une hyperméthylation de l'histone H3. L'ensemble de ces observations suggèrent donc une inhibition majeure de l'histone H3 au sein des cellules *Sdhb* KO, qui pourrait conduire en une plus grande inactivation de H3-H4 et ainsi expliquerait la surcharge en cuivre, l'inhibition de l'expression de Sod2 et le déficit respiratoire mitochondrial observé suite à un déficit en SDHB.

En outre, les observations faites *in vitro* sur le métabolisme du fer ont pu être validées sur des échantillons humains, grâce à une collaboration avec une équipe de la London Metallomics Facility, ayant mis au point une technique innovatrice : la « Laser ablation-inductively coupled plasma-mass spectrometry (LA-ICP-MS) » permettant la détection du ^{56}Fe au sein de lames de tissus. Nous avons ainsi pu mettre en évidence une déplétion significative en fer sur des lames de tissus provenant d'échantillons de tumeurs de patients. De façon similaire, le dosage du cuivre dans des échantillons de PPGL humains est actuellement en train d'être testé par la même technique.

Le stress oxydant particulièrement marqué, observé dans les imCC *Sdhb-/-* représente sans doute un élément clé du mécanisme responsable du comportement particulièrement agressif de ces cellules, et par conséquent, une cible thérapeutique intéressante. D'autant plus que nos données démontrent que les cellules avec un déficit en SDHB sont incapables d'activer une voie anti-oxydante intrinsèque, ce qui leur permettrait de neutraliser les dommages oxydants causés par l'excès mitochondrial de ROS. Traiter notre modèle d'imCC *Sdhb-/-* avec un antioxydant nous est donc apparu particulièrement pertinent. Ainsi, le traitement des imCC *Sdhb-/-* avec des doses pharmacologiques d'ascorbate, ayant alors une action pro-oxidante, offre des résultats prometteurs, en contribuant à fortement aggraver le fardeau du stress oxydant enduré par les cellules avec un déficit en SDHB.

L'utilisation de ce large éventail de techniques de pointe m'a donc permis de dessiner le mécanisme expliquant comment la perte de différentes sous-unités de la SDH peut conduire à différents phénotypes cellulaires et tumoraux chez les patients. Ces données constituent une étape importante dans la compréhension de la biologie des SDH, d'autant plus qu'il s'agit de la première fois qu'une telle étude comparative est réalisée avec des modèles correspondant à de véritables KO génétiques, comme observé au sein de PPGL humain. Néanmoins, malgré la qualité du modèle utilisé dans la présente étude, celui-ci reste un modèle *in vitro* ce qui constitue l'une des limites principales. En effet, malgré des résultats très prometteurs *in vitro*, de nombreux tests sont encore nécessaires afin de pouvoir transférer le traitement à l'ascorbate chez les patients. Ainsi, une validation de ce traitement *in vivo* dans un modèle intégré de PPGL, est essentielle pour pouvoir considérer une application clinique des résultats de cette étude. Dans cette optique, le traitement à

l'ascorbate est actuellement testé dans des modèles de xénogreffes que nous développons au laboratoire. Ces tests précliniques concluront les travaux effectués au cours de cette étude. A terme, ce traitement pourrait potentiellement être ainsi transféré en clinique chez les patients porteurs des mutations *SDHB* et pourrait représenter une grande avancée thérapeutique dans la prise en charge des patients avec des PGL métastatique.

CHAPITRE 3

Rôle de la matrice extracellulaire dans l'acquisition du phénotype métastatique associé à SDHB

CONTEXTE

Le microenvironnement tumoral est un élément majeur de la progression métastatique, offrant un environnement propice à la colonisation par les cellules tumorales d'un foyer secondaire, à distance de la tumeur primaire. Au sein d'un organisme intégré, l'activation du processus de transition mésenchymateuse, permettant aux cellules tumorales d'acquérir des propriétés migratoires, adhésives et invasives accrues est essentielle mais insuffisante à la formation de métastases. Un microenvironnement adapté, facilitant la migration, l'intravasation, l'adhésion et l'extravasation est également nécessaire. La MEC est l'un des composant du microenvironnement actuellement reconnu comme ayant un impact majeur sur la plasticité des cellules cancéreuses et la progression tumorale.

Les données précédentes de mon équipe d'accueil, ainsi que les travaux présentés lors des deux premiers chapitres de ce manuscrit, démontrent que les cellules et tumeurs avec un déficit en SDHB subissent un processus semblable à une transition neuroendocrino-mésenchymateuse, résultant en un comportement agressif. De plus, mes travaux ont montré *in vitro* que l'activation de HIF2, aboutissant en un phénotype pseudohypoxique, était également spécifique des mutations *Sdhb* et avait ainsi un impact majeur dans le processus d'oncogenèse SDHB-dépendant, responsable du phénotype métastatique. Nous avons évoqué au cours de l'introduction le lien direct existant entre la MEC et la transition mésenchymateuse, ainsi que l'émergence de nouvelles données qui suggèrent une implication collaborative majeure de l'hypoxie et de la MEC dans la progression métastatique. L'hypothèse principale est que l'hypoxie agirait directement sur la composition et l'organisation de la MEC. En outre, l'étude précédente a révélée une inhibition plus importante de certaines dioxygénases dépendantes du 2-OG (TET et PHD) dans les imCC *Sdhb-/-*. Or, les processus de synthèse et de maturation des collagènes, qui constituent les composants majoritaires de la MEC, sont régulés par un autre type d'enzymes appartenant à cette famille, les prolyl-4-hydroxylases du collagène ou CP4H. Nous avons donc émis l'hypothèse que ces enzymes pourraient également être inhibées dans les cellules *Sdhb* KO, ce qui pourrait ainsi conduire à une dérégulation de la composition de la MEC.

La caractéristion de la MEC produite et secrétée *in vitro* par les imCCs *Sdhb-/-* constituait donc une piste particulièrement intéressante pour élucider les mécanismes impliqués dans l'acquisition du phénotype métastatique de ces cellules.

TRAVAUX PERSONNELS

Nous nous sommes donc attachés à l'analyse de la MEC produite et sécrétée *in vitro* par les différentes lignées d'imCCs (WT, *Sdhb-/-* et *Sdhd-/-),* afin d'observer d'éventuelles dérégulations qui pourraient être impliquées dans la progression métastatique associée aux mutations *SDHB.* Dans un premier temps, j'ai utilisé les données transcriptomiques humaines et murines obtenues lors des études précédentes, afin d'observer les niveaux d'expression de gènes codants pour différents composants de la MEC et en particulier des collagènes. Ces données ont été générées respectivement à partir des 188 PPGL issus du réseau national COMETE, dans le cadre du programme CIT pour les tumeurs humaines et à partir de nos modèles cellulaires d'imCC WT, *Sdhd-/-* et *Sdhd-/-* pour les données murines. La rareté de certaines mutations *SDHx,* ne permet pas d'avoir au sein de cohortes d'études, un nombre significatif de tumeurs pour chacune des mutations *SDHx.* Nous disposons en effet de peu de tumeurs SDHD (seulement 3 dans notre transcriptome), qui sont principalement localisées au niveau de la tête et du cou, et ne sont pas systématiquement opérées, et si elles le sont, sont fréquemment embolisées en pré-opératoire ce qui amoindrit de façon significative la qualité du tissu. Ainsi, bien que les données transcriptomiques humaines issues de cette cohorte permettent l'obtention d'analyses comparatives significatives entre les PPGL mutés *SDHx* et les PPGL mutés sur d'autres gènes, il est très difficile d'observer des différences significatives entre les différents types de tumeurs *SDHx.* Par conséquent, l'utilisation des modèles cellulaires reste essentielle pour réaliser de telles études comparatives.

Dans le but de corréler les niveaux d'expression différentielle observés dans nos différents modèles cellulaires, des études de matrisome ont été réalisées. Cette technique consiste à analyser l'ensemble des molécules sécrétées *in vitro* par les imCCs et incorporées dans leur MEC. L'analyse des composants de la MEC a été effectuée sur la plateforme de protéomique de l'Hôpital Cochin (3P5). J'ai procédé à l'extraction et la digestion des matrices produites *in vitro* qui ont ensuite été analysées sur la plateforme de protéomique par spectrométrie de masse. Les résultats obtenus par spectrométrie de masse permettent également d'analyser les niveaux d'hydroxylation des prolines de certains collagènes détectés dans la matrice et donc d'évaluer indirectement l'activité des P4H. Ces analyses très chronophages, sont toujours en cours.

L'objectif principal de ce projet était d'étudier le rôle joué par la matrice dans la tumorigenèse des imCCs avec mutations *Sdhx,* ainsi que d'élucider une éventuelle implication de celle-ci dans la progression métastatique secondaire à une mutation *Sdhb*. J'ai donc poursuivi cette étude par des tests fonctionnels de migration et d'adhésion, réalisés suite à des échanges de matrice entre les différents types d'imCCs.

Enfin, comme nous l'avons vu, le facteur de réponse à l'hypoxie HIF2α, qui est l'un des acteurs majeurs de la transformation métastatique des imCC *Sdhb* KO, semble être étroitement lié au remodelage de la MEC. Nous avons donc cherché à étudier l'impact direct de l'activation de HIF2 sur la MEC des cellules *Sdhb* KO. Nous avons alors étudié un modèle de cellules *Sdhb-/-* dans lesquelles l'utilisation d'un vecteur lentiviral shRNA spécifique avait permis d'inhiber l'expression de *Hif2*α (shHIF2). Ce modèle, décrit pour la première fois dans l'article 1 présenté dans ce manuscrit (Morin et al. 2020), a été généré par Luis Castro-Vega, post-doctorant de mon équipe d'accueil. Nous avions déjà montré que ces cellules présentaient des propriétés migratoires diminuées par rapport aux imCC *Sdhb-/-*, suggérant le rôle majeur de HIF2α dans l'acquisition des propriétés métastatiques secondaire à la perte de SDHB. De façon similaire, Sophie Moog, doctorante de mon laboratoire d'accueil et moi avons réalisés l'extraction et la préparation de la matrice secrétée par ces cellules, dont la composition a ensuite été analysée par la plateforme 3P5. Enfin des tests fonctionnels supplémentaires ont été effectués, afin d'élucider l'impact spécifique de la perte en HIF2α sur la MEC.

Ces résultats feront l'objet d'un troisième article que je signe en co-premier auteure et qui est actuellement en préparation. En attente des derniers résultats d'analyse du matrisome, je présenterai dans ce manuscrit, une première version de l'introduction, des résultats et des méthodes.

ARTICLE 3

Succinate dehydrogenase B deficiency results in extracellular matrix reprogramming to promote a metastatic phenotype

Judith Goncalves*, Sophie Moog*, Mélanie Menara, Céline Loriot, Luis-Jaime Castro-Vega, Catherine Monnot, Laurent Muller, Stéphane Germain, Anne-Paule Gimenez-Roqueplo, Judith Favier

*co-premier auteurs

(Article en préparation)

Succinate dehydrogenase B deficiency results in extracellular matrix reprogramming to promote a metastatic phenotype

Judith GONCALVES[1#], Sophie MOOG[1#], Mélanie MENARA[1], Luis-Jaime CASTRO-VEGA[1], Catherine MONNOT[2], Stéphane GERMAIN[2], Anne-Paule GIMENEZ-ROQUEPLO[1,3], Judith FAVIER[1]

1 Université de Paris, PARCC, INSERM, Equipe Labellisée par la Ligue contre le Cancer, F-75015 Paris, France

2- Collège de France, Center for Interdisciplinary Research in Biology, F-75006 Paris, France

3- Assistance Publique-Hôpitaux de Paris (AP-HP), Hôpital Européen Georges Pompidou, Service de Génétique, F-75015 Paris, France

# Equal contribution

Corresponding author:
Judith Favier
INSERM UMR970
Centre de recherche cardiovasculaire de l'HEGP
56 rue Leblanc 75015 Paris, France
E-mail: judith.favier@inserm.fr
Tel: 00 33 1 53 98 80 41 - Fax: 00 33 1 53 98 79 52

Introduction

Pheochromocytomas (PCC) and paragangliomas (PGL) are rare and highly vascularized neuroendocrine tumors that arise from chromaffin cells of the adrenal medulla and of the autonomous nervous system, respectively (1). Up to 40% of these tumors are caused by mutations in one of the more that 20 pheochromocytoma/paraganglioma (PPGL) predisposing genes identified so far (2). *SDHx* genes mutations represent almost half of the inherited cases. These genes encode the four subunits (A-D) of succinate dehydrogenase (SDH), a tricarboxylic acid enzyme that catalyzes the oxidation of succinate into fumarate (3). *SDHB* gene encodes the catalytic core subunit of SDH. Mutations in this gene are associated with metastatic evolution and poor prognosis while *SDHD* mutations are associated with a very low metastatic risk (4–6). Understanding the mechanisms explaining the peculiar phenotype of SDHB is a major issue, from both a fundamental and a clinical point of view. In previous studies, we showed that *SDHB*-mutated tumors display a particularly marked hypermethylator phenotype as well as epithelial-to-mesenchymal transition (EMT) like specific hallmarks, an embryonic process that promotes metastatic dissemination of cancer cells by increasing their motility and invasiveness (7–9). *In vitro,* we and others have shown that *SDHx* mutations lead to the inactivation of SDH and to the subsequent accumulation of succinate that acts as a competitive inhibitor of 2-oxoglutarate (2-OG) dependent dioxygenases (10) such as HIF prolyl-hydroxylases or DNA and histone demethylases (11). These mediate the pseudohypoxic phenotype as well as some of the EMT-like features observed in SDHB-deficient cells. Recently, we have shown that dysregulation of iron and copper intracellular balance, and increased oxidative stress amplifies this phenotype. Interestingly, the large family of 2-OG dependent dioxygenases also comprises collagen hydroxylases such as prolyl-4-hydroylases (CP4H) that

participate to collagen maturation by catalyzing the hydroxylation of proline residues, but it is not yet known if CP4H are inhibited or not (12–14). Indeed, these modifications by CP4H are essential for the formation of the triple helix and for the stabilization of collagens within the extracellular matrix (ECM) (15–17). Collagen is the most abundant fibrous protein within interstitial ECM and in basement membranes in all animals and constitutes up to 30% of the total proteins in humans and 90% of ECM composition (18). The ECM belongs to the microenvironment with endothelial cells, immunity cells and fibroblasts. It is a dynamic three-dimensional macromolecular network that continuously undergoes remodeling, surrounding cells and which is composed of collagens, proteoglycans, elastin, fibronectin, laminins and others glycoproteins (19). ECM regulates diverse cellular functions such as survival, growth, migration and differentiation, which are vital for maintaining normal homeostasis. In pathologic conditions, especially in cancer, it is well known that ECM remodeling increases the metastatic potential and it is now established that hypoxia can influence this remodeling (20). In this study, we have therefore raised the hypothesis that SDHB-deficiency may modify the composition of the extracellular matrix, which may, in turn, favor the establishment of a microenvironment allowing the metastatic dispersion of malignant cells.

Results

SDHB-deficiency drives major modifications in the ECM composition in human tumors and in immortalized mouse chromaffin cells (imCCs)

To analyze the expression of ECM-associated genes, we used transcriptomic data previously generated from 188 PPGL (25 malignant and 163 benign) included in the French COMETE cohort (21). This collection contains tumors harboring germline and/or somatic mutations in 37 *VHL* gene, 33 *NF1*, 17 *SDHB*, 3 *SDHD* and 15 *RET*. We analyzed the expression data of a selection of 120 genes encoding ECM proteins (corresponding to 188 probes). The unsupervised classification of tumors using this list allowed us to isolate a cluster with high expression, comprising SDHB and VHL tumors, while the SDHD showed lower levels of ECM genes (Figure 1A). Because of the importance of collagens in the composition of the ECM and of the putative inhibition of collagen-hydroxylases by succinate, we next aimed at studying the participation of these proteins in the *Sdhb*-associated phenotype. Transcriptome data generated from human PPGL tissues revealed that the most highly expressed collagens in these tumors were: *COL1A1*, *COL4A2, COL4A1, COL3A1, COL1A2 and COL6A2* (Figure 1B). There were all overexpressed in *VHL* and *SDH*-mutated PPGL (the so-called Cluster 1 tumors) as compared to *NF1* or *RET*-mutated tumors (from the Cluster 2), suggesting a regulation associated with the pseudohypoxic drive previously described in these tumors (22,23). Among them*, COL4A2* was the gene with the most significant increase in SDH-tumors vs Cluster 2 samples. Transcriptome analysis was also carried out *in vitro*, using immortalized mouse chromaffin cells (imCC) invalidated for either *Sdhb* or *Sdhd* genes and their wild-type (WT) counterparts. The previously reported characterization of these cell lines had revealed that *Sdhb*-/- imCCs display an aggressive phenotype supported by a hypermethylator,

pseudohypoxic and oxidative signature, unlike *Sdhd-/-* imCCs that display a "benign" phenotype, reflecting the clinical behaviors of patients bearing these tumors (Goncalves et al., submitted). The transcriptome data generated by RNASeq from imCCs led to very similar results than the ones observed in human (Figure 1C), showing that *Sdhb-/-* cells expressed very high levels of some collagens, such as *Col1a1*, *Col12a1, Col4a2, Col6a1, Col1a2.* Interestingly, transcriptomic data showed that *Sdhb-/-* imCC not only express quantitatively more collagens than its WT or *Sdhd-/-* imCC counterparts*,* but also qualitatively, as these cells express various types of collagens not found in either WT nor *Sdhd-/-* imCC (*Col10a1, Col6a3* and *Col6a2)*. It is also worth noting that unlike *Sdhb-/-* cells, *Sdhd-/-* cells appear to express only a few collagens, even less than WT cells. Collagen 1, 4 and 6 especially appeared to be highly expressed and upregulated following SDHB inactivation in both human PPGL and in the imCC cell line. These results were then validated *in vitro* at the mRNA level by RTqPCR, confirming the strong increase in ColI and ColIVa2 expression in *Sdhb*-KO cells as compared to their WT and *Sdhd-/-* counterparts (Figure 1D, 1E).

We next performed a matrisome analysis in the different cell lines. Matrisome data further revealed a very good correlation between mRNA and protein levels in *Sdhb-/-* cells (Figure 1F,G), showing that the ECM secreted by *Sdhb-/-* cells was mostly composed of Collagen XII, I, X, VI and III. As expected, matrisome data showed that the ECM secreted by *Sdhb-/-* cells is much richer than the one secreted by WT or *Sdhd-/-* cells, which actually happens to be particularly poor (Figure 1H). Surprisingly, the only detectable collagens in the ECM secreted by *Sdhd-/-* cells were collagen XII and VIII at a very low level, the latter being actually absent from the ECM secreted by *Sdhb-/-* cells. In contrast, the comparison of the matrix secreted by *Sdhd-/-* vs WT cells, showed an enrichment, in SDHD-deficient cells, several proteins such as Thrombospondin-1, Tenascin, Plasminogen, Clusterin, Semaphorin 3E or

Serpins. Hence, SDHD-deficient cells ECM is very poor in collagens, but enriched in other unexpected components of the matrix.

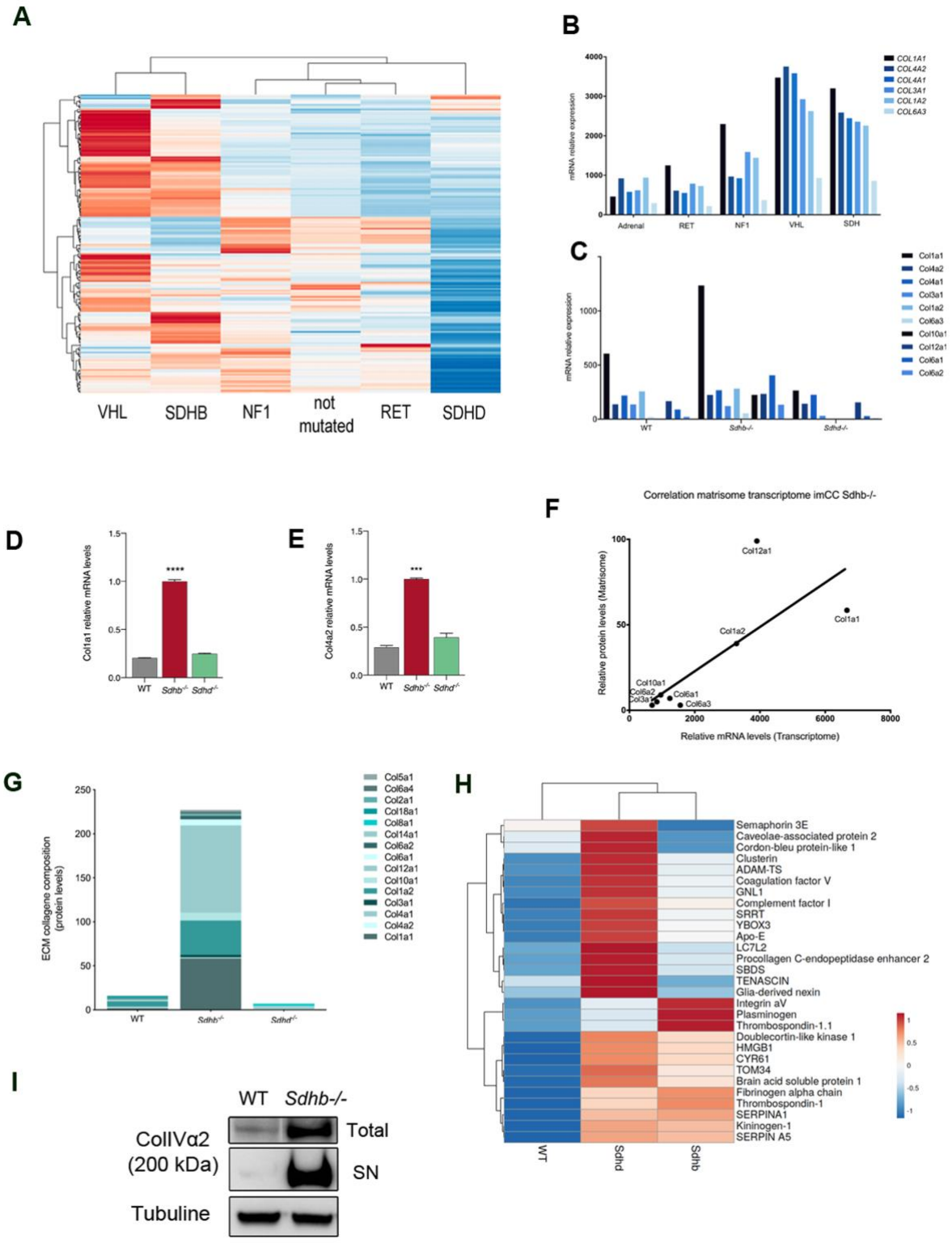

Fig.1: SDHB-deficiency drives major modifications in the ECM composition in human tumors and in immortalized mouse chromaffin cells. A, The unsupervised classification of 188 tumors from COMETE collection using a list of 120 genes encoding ECM proteins isolates a cluster with high

expression, comprising *SDHB* and *VHL* tumors, while the *SDHD* showed lower levels of ECM genes. **B,** Transcriptomic data of human PPGL tissues revealed many overexpressed collagens in *VHL* and *SDH*-mutated PPGL including *COL4A2*, which is the most significant gene increased in SDH-tumors. **C,** Transcriptomic data of imCCs show the overexpression of many collagens in *Sdhb-/-* imCCs versus WT and *Sdhd* KO cells. **D,E,** qRT-PCR analyses show overexpression of *Col1a1* and *Col4a2* in *Sdhb-/-* imCCs in comparison to *Sdhd-/-* and WT imCCs. **F,** Matrisome and transcriptome data revealed a good correlation between proteins and mRNA levels of collagens in *Sdhb-/-* imCCs. **G,** Collagen composition of the ECM secreted by WT, *Sdhb-/-* and *Sdhd-/-* imCCs, showing a massive enrichment in collagens following SDHB deficiency. **H,** Heatmap showing the enrichment in several proteins that form the ECM secreted by *Sdhd-/-* cells in comparison to the ECM secreted by WT cells. **I,** ColIVα2 protein is overexpressed in both whole cells extracts and conditioned media (SN) of *Sdhb-/-* imCCs confirming the good translation and secretion of ColIVα2.

Collagen IV was not detected in the matrisome analysis we performed with these cells, although it was highly overexpressed in transcriptomic data of both human (Figure 1B) and mouse cells (Figure 1C). This observation is probably explained by the fact that ColIVa2 is located in the basal lamina, whose degradation constitutes the first step of metastatic invasion. We thus evaluated the protein levels of Collagen IV by western blot performed on both whole cells extracts and conditioned media of *Sdhb-/-* and WT cell cultures (Figure 1I). We observed a major increase in total ColIVa2 protein levels in *Sdhb-/-* imCC versus WT imCC, together with the presence of ColIVa2 in the supernatant of *Sdhb-/-* imCC solely, thus confirming that ColIVa2 protein was translated and secreted.

Succinate does not inhibit prolyl-4-hydroylases (CP4H)

SDHB-deficient cells show a marked increase in collagens expression and secretion, leading to massive modifications in the composition of their ECM. Collagen maturation occurs inside the endoplasmic reticulum. Hydroxylation of proline residues into 4-hydroxyproline (15), controls the synthesis of collagen and is necessary to form a triple helix of the collagen molecule. It is required for the stability of the fibrillar collagen triple helix at 37°C. Incomplete hydroxylation of proline in the Gly-X-Y sequence results in incorrect formation of the collagen triple helix. In the absence of proline hydroxylation, unfolded chains accumulate within the

endoplasmic reticulum and are expected to be degraded instead of being secreted into the cytoplasm (24).

Previous studies that evaluated the effect of oncometabolites on the activity of collagen hydroxylases used either *in vitro* enzymatic assays (25) or endostatin expression, an antiangiogenic peptide cleaved from collagen XVIII, as a marker of collagen hydroxylases activity (26,27). To our knowledge, it has never truly been shown that succinate, or 2-hydroxyglutarate (in the cases of *IDH* mutated tumors) are able to inhibit the activity of collagen hydroxylases in the cell context, and to decrease collagen synthesis or stability. The substantial presence of collagens in the matrisome of *Sdhb* KO cells, suggests that collagen hydroxylases are still active in these cells, allowing these proteins to go through their maturation process in the endoplasmic reticulum and to be secreted out of the cell. In contrast, Sdhd KO cells show very small amounts of collagens, which may be suggestive of the inactivation of CP4H.

Ongoing analysis are currently being processed, to evaluate peptides sequences analysis with MASCOT software of the fragments of ColI detected by mass spectrometry in the ECM. The first results show the hydroxylation of collagen proline residues in Sdhb KO matrix.

Extracellular matrix of *Sdhb-/-* imCCs supports adhesion and migration properties

To further study the role of ECM *in vitro*, we aimed at differentiating the respective roles of *Sdhb*-/- imCCs themselves and of their extracellular matrix in their adhesive and collective migration abilities. We performed a swap in the extracellular matrix between *Sdhb* KO, *Sdhd* KO and WT cells (28). Briefly, cells were grown on plastic dishes for 4 days, allowing them to secrete their own matrix. Cells were then removed without affecting the ECM and new cells were seeded on top of the ECM. Using this approach, we investigated the behavior of *Sdhb-/-*

imCCs successively on a WT-secreted ECM and on a *Sdhd-/-* secreted ECM and that of WT or *Sdhd-/-* imCCs on the ECM secreted by *Sdhb-/-* cells (Figure 2A, B, C). We showed that *Sdhb-/-* ECM is able to increase both collective migration (Figure 2D) and adhesion (Figure 2E) of WT and *Sdhd-/-* imCCs by nearly 2-fold. Conversely, WT ECM decreases the migration of *Sdhb-/-* imCCs of 20% and slows down a little their adhesion. However, *Sdhd-/-* ECM did not show any effect on the migration or adhesion properties of either *Sdhb-/-* or WT cells, probably due to its peculiar composition. This original assay therefore reveals that *Sdhb-/-* cells produce an ECM which functionally differs from that of WT and *Sdhd-/-* cells favoring some hallmarks of a metastatic phenotype.

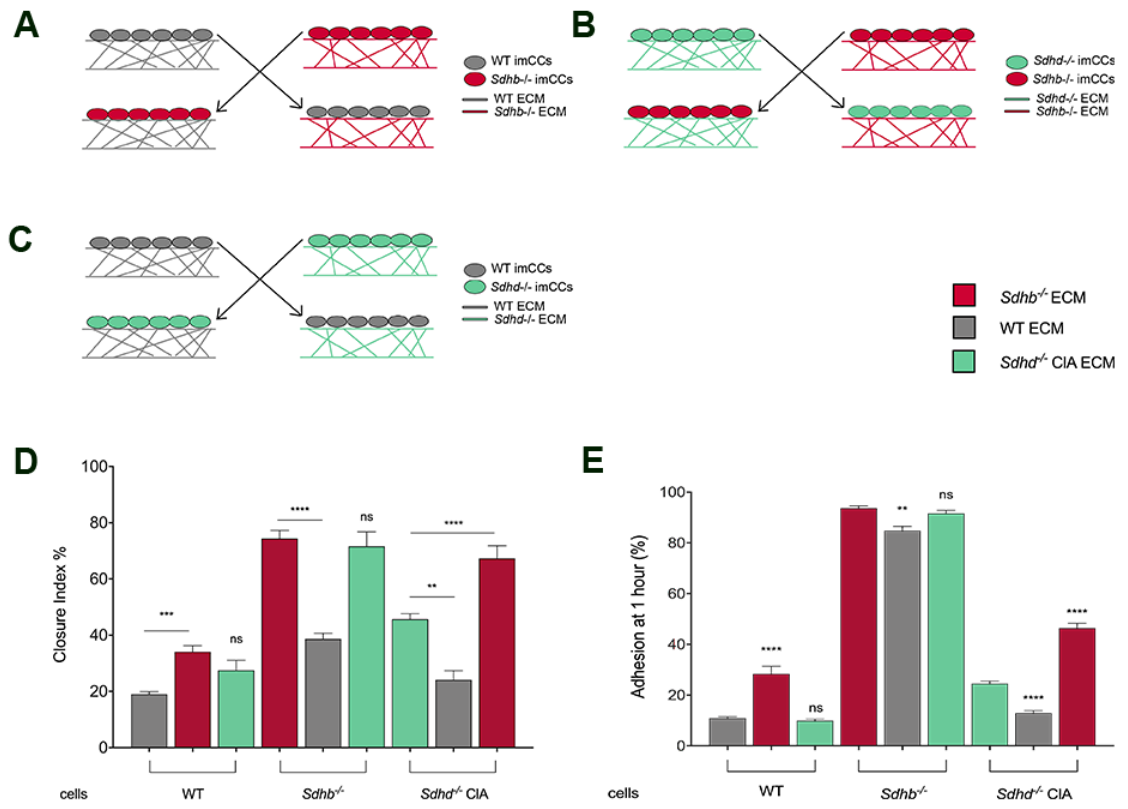

Fig. 2: Extracellular matrix of *Sdhb-/-* imCCs supports adhesion and migration properties. A, B, C, Schematic representation of the principle of the extracellular matrix swap assay, between *Sdhb-/-* imCCs and WT imCCs **(A)**, *Sdhb-/-* imCCs and *Sdhd-/-* **(B)** and between *Sdhd-/-* imCCs and WT imCCs **(C)**. **D,** Collective migration assessed by wound scratch assay showing that the ECM secreted by *Sdhb-/-* imCCs significantly increases migration of WT and *Sdhd-/-* imCCs, while ECM of WT cells decreases migration of *Sdhb-/-* and *Sdhd-/-* imCCs. **E,** Quantification of cell adhesion one hour after plating revealing *Sdhb-/-* secreted ECM significantly increases the adhesion of WT and *Sdhd-/-* imCCs and WT-secreted ECM decreases the adhesion of *Sdhb-/-* and *Sdhd-/-* imCCs.

HIF2α poorly influences the phenotype of the ECM of *Sdhb-/-* cells

We previously showed that *Sdhb-/-* cells, contrary to *Sdhd-/-* and WT cells, exhibit a pseudohypoxic phenotype characterized by a massive accumulation of HIF2α (but not HIF1α) (Goncalves et al., submitted). Recent studies have established a direct link between hypoxia and the properties of the ECM, mainly its composition and organization, which can contribute to the metastatic outcome in several cancers such as breast and lung cancers (20). We therefore wondered what was the role of HIF2α in the ECM production of *Sdhb-/-* cells. In order to explore this hypothesis, we used *Sdhb-/-* cells infected with lentiviruses expressing HIF2α-silencing shRNA (29). We have previously shown that these HIF2α-silenced cells display a decrease in migration while HIF2α loss had only a little impact on the adhesion of SDHB-deficient cells. We first performed a swap in the extracellular matrix between *Sdhb-/-* and *Sdhb-/-* HIF2α-silenced cells and found that the *Sdhb-/-* matrix increases the collective migration of HIF2α silenced cells by more than 2-fold (Figure 3A). The ECM of *Sdhb-/-* HIF2α-silenced cells decreased slightly the migration of *Sdhb-/-* cells without reaching significance. *Sdhb-/-* ECM did not change the adhesion properties of shHIF2α cells, suggesting that adhesion is not mediated by pseudo-hypoxia but by another unknown mechanism (Figure 3B).

To further understand how HIF2α acts on the ECM, we explored the expression of collagen genes and performed a matrisome analysis of these cells. We found, using RT-qPCR, a slight decrease of *Colla1* and a 50% decrease in *ColIVa2* expression in HIF2α silenced cells compared to *Sdhb-/-* cells (Figure 3C). These two genes are the ones that were the most expressed in the transcriptome of *Sdhb-/-* cells. Finally, the matrisome analysis revealed a very similar distribution of the different components of the matrix between *Sdhb-*/- and *Sdhb-/-* HIF2α-

silenced cells. In particular, the types and amounts of Collagens were only poorly influenced by the loss of HIF2α in *Sdhb-/-* cells.

Taking these data together, we showed that pseudo-hypoxia appears to very moderately influence the ECM remodeling of *Sdhb-/-* cells.

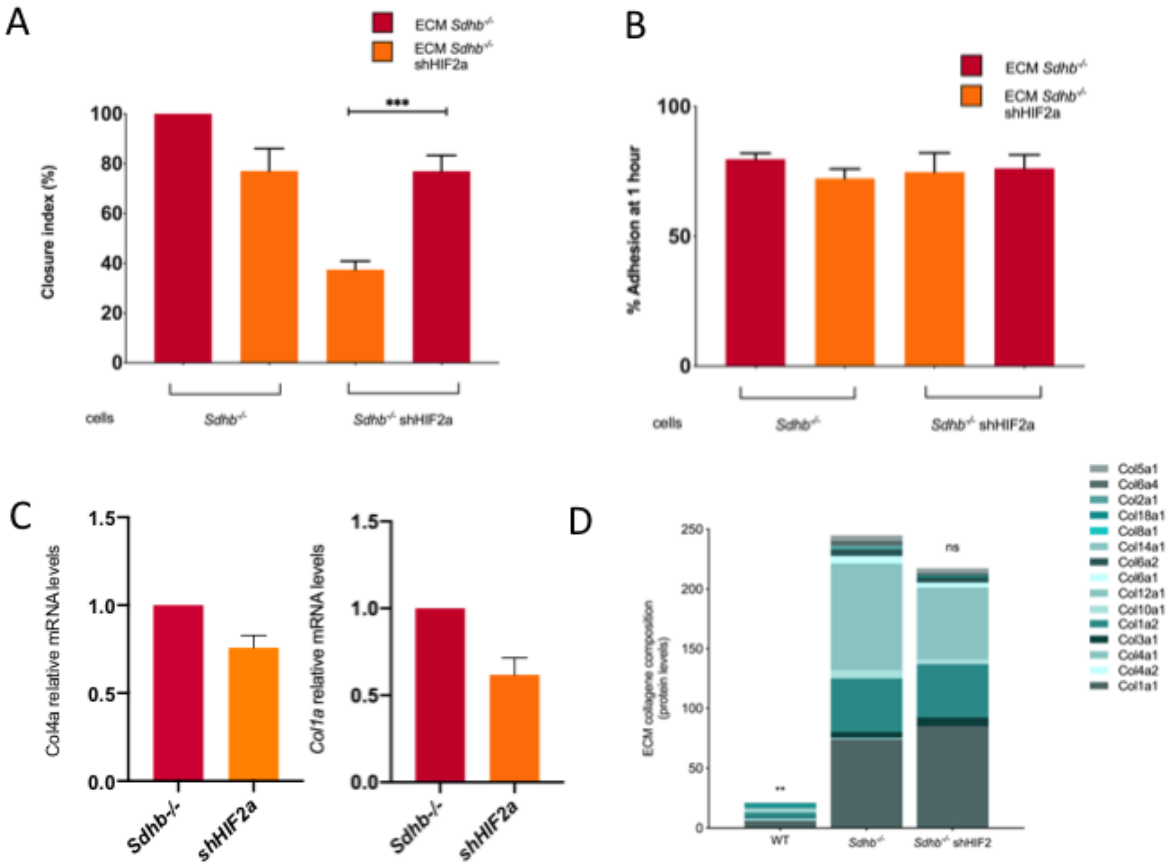

Fig. 3: HIF2α poorly influences the phenotype of the ECM of *Sdhb-/-* cells. A,B,Matrix swap test of *Sdhb-/-* and *Sdhb-/-* HIF2α silenced cells. **A,** Evaluation of collective migration using a wound scratch assay. Migration was assessed after 10h. **B,** Quantification of cell adhesion one hour after plating. **C,** RT-qPCR of Col4a and Col1a expression in *Sdhb-/-* and *Sdhb-/-* shHIF2a cells. **D,** Representation of all the different protein present in the ECM produced by WT, *Sdhb-/-* and *Sdhb-/-* HIF2α silenced cells.

Materiel and methods

Transcriptome

Gene expression profiles were available from a previously published study (21). HG-U133 Plus 2.0 Affymetrix GeneChip data are available online as ArrayExpress entry E-MTAB-733 (http://www.ebi.ac.uk/arrayexpress/). Gene expression profiles of wild-type and *Sdhb-/-* imCC c8 were assessed in duplicates using the GeneChip® Mouse Gene 1.0 ST Array. Data are available as ArrayExpress entry E-MTAB-3403. The list of ECM genes was previously published in the matrisome project, which grouped all ECM-related proteins, detected by mass spectrometry in human and mouse tumors and tissues (http://matrisomeproject.mit.edu/).

Cell culture

WT, *Sdhb*-/- and *Sdhd-/-* immortalized mouse chromaffin cells (imCCs) were generated as described previously (7) (Goncalves et al., submitted) ImCCs were cultivated in DMEM (Dulbecco Modified Eagle Medium, Gibco) with 10% FBS (Fetal bovine serum, Gibco) and 1% antibiotics (penicillin/streptomycin, Gibco). Cells were grown at 37°C and 5% CO_2. Experiments were performed using *Sdhb*-/- imCCs clone 8 and sdhd-/- clone B.

The generation of *Sdhb-/-* with silencing of HIF2α using specific shRNA lentiviral vector were previously described in Morin et al. (29). ShHIF2α clone 9 cells were used for experiments.

Unless specified, all experiments were performed using this regular medium, on regular plastic plates and dishes, without coating.

Preparation of the ECM

Cells were seeded at confluence in 12-wells dishes and grown for 4 days to allow them producing their own extracellular matrix. Culture medium was renewed every day. Cells were then solubilized with 0,5% sodium deoxycholate (Sigma-Aldrich) for 5 minutes on ice and ECM was washed twice with PBS 1X.

Collective migration assay

Culture inserts (Ibidi) were positioned in each well coated with either imCC secreted ECM. New cells, just detached with trypsin-EDTA 0,05% (Gibco) were seeded at confluence on top of coating. After overnight incubation at 37°C and 5% CO_2, culture inserts were removed to create the wound in the cell layer without affecting the coating and cells washed with PBS 1X. Collective migration was followed by taking pictures at time= 0 (T0) and after 10 hours (T10). Relative cell migration was established by calculating the closure index, based on the analysis of at least 25 pictures for each time point and condition, using ImageJ software, as described (7). The experiments were performed in triplicates.

Adhesion assay

Cells were seeded on coated dishes coating. Cell adhesion was followed by taking pictures during 1 hour. Adherent and non-adherent cells were identified on the basis of their morphology (round and refractive cells were considered as non-adherent). The experiments were performed in triplicates.

RTqPCR

Total RNAs were extracted from cell pellet using miRNeasy® Mini Kit (Qiagen) as described by the manufacturer. Reverse transcription was performed using iScript™ cDNA Synthesis Kit

(BIO-RAD) during 5 min at 25°C, 30 min at 42°C and 5 min à 85°C. Thirty (30) µl were added to each sample to a concentration of 10ng/µl. qPCR is performed using CFX96^{TM} Real-Time System C1000 Touch^{TM} Thermal Cycler (BIO-RAD). Normalization was performed with Ubc and B2mg amplifications, and comparisons were calculated using ΔΔCt method. Primers sequences were as follows:

Ubc: F 5'-AGCCCAGTGTTACCACCAAG-3'; R 5'-ACCCAAGAACAAGCAAG-3'

B2mg: F 5'-ATTCACCCCCACTGAGACTG-3'; R 5'-TGCTATTTCTTTCTGCGTGC-3'

Col4a2: F 5'-GACCCTGAGGTTAGGAAGGGA-3' ; R 5'-TCGGTCCATGATCCCAGTCT-3'

Col1a1: F 5'-CTCCTGGTATTGCTGGTGCT-3' ; R 5'- GGCTCCTCGTTTTCCTTCTT-3'

Western blot

Total proteins were extracted, in Tris-EDTA buffer (Tris NaCl pH = 7.4, 0.5% NP-40, 0.5% deoxycholic acid and 5 mM EDTA) containing proteases inhibitors cocktail. Extracellular matrix proteins were extracted from supernatant in 100% trichloroacetic acid (Sigma-Aldrich) overnight. Only total protein concentrations were determined with Bradford colorimetric method and 50µg of proteins were resolved in NuPAGE® Sample Reducing Agent and NuPAGE® LDS Sample Buffer. For extracellular matrix proteins, samples are based on the same cells number and pellets are directly resolved by the same way. Coomassie blue coloration was performed to confirm equal quantites. 50 µg were resolved on NuPAGE® Novex 4–16% Bis-Tris gradient gel or 3-8% Tris-Acetate (Invitrogen), transferred on PVDF membrane. After blocking in PBS-milk solution (5%), membranes were incubated with specific primary antibodies, followed by incubation with corresponding HRP-conjugated secondary antibodies.

Revelation was performed using ECL Plus (Pierce). The antibodies used were: anti-COL4A2 (Santa Cruz Biotechnology, sc-70246) and anti-Tubulin (Sigma-Aldrich, T9026).

Matrisome analysis

Mass spectrometry analyses were performed on a Dionex U3000 RSLC nano-LC system coupled to Orbitrap-Fusion mass spectrometer, all from Thermo Fisher Scientific. The sample was dried using a vacuum concentrator and solubilized in 10% ACN containing 0.1% TFA. One µl was loaded, concentrated and washed for 3 min with the loading buffer (98% H2O, 2% ACN and 0.1% trifluoroacetic acid) on a C18 reverse phase precolumn (3 µm particle size, 100 Å pore size, 75 µm inner diameter, 2 cm length, Dionex, Thermo Fischer Scientific). Peptides were separated on a C18 reverse phase resin (2 µm particle size, 100 Å pore size, 75 µm inner diameter, 25 cm length from Dionex) with a 2-hours gradient from 1% solvent B (80% ACN and 0.085% formic acid in H_2O) and 99% of solvent A (0.1% formic acid in H_2O) to 10% of solvent B for 25 min, 10 to 20 % B for 22 min and 20 to 40% B for 48 min. The mass spectrometers collected data throughout the elution process and operated in a data-dependent scheme with full MS scans acquired with the Orbitrap, followed by 5 seconds to MS/MS HCD spectra detected in the linear trap on the most abundant ions detected. Settings for Orbitrap Fusion were: full MS automatic gain control (AGC): 2.10^5, maximum ion injection time (MIIT): 60 ms, resolution: 6.10^4, m/z range 350-1500 and for MS/MS, AGC: 2.10^4, MIIT: 100 ms, minimum signal threshold: 5000, isolation width: 1.6 m/z, the collision energy of HCD fragmentation was 27%, dynamic exclusion time was set to 30 s. The fragmentation was permitted for precursor with a charge state between 2 and 7. Spectral Processing: the software used to generate .mgf files was Proteome discoverer 1.4.0.288 (Thermo). The Signal to Noise threshold for extraction values was set to 1.5. Database Searching and results filtering: MS/MS spectra were submitted to Mascot (Matrix science) version 2.5.1 search engine (Electrophoresis, 20(18) 3551-67

(1999)). The database used is Swissprot (database 06-2016, 550 552 sequences and 196 472 675 residues) and CRAPome (a Contaminant Repository for Affinity Purification Mass Spectrometry Data, Nat Methods, 10(8): 730–736 (2013), 116 sequences and 38 459 residues). The precursor mass tolerance was set to 4 ppm and the fragment mass tolerance to 0.6 Da. The oxidation of methionines and the hydroxylation of prolin were set as variable modification. The search was restricted to Mus Musculus (16 772 sequences). Enzyme specificity was Trypsin. A filter was applied to the search results and the probability of false positive was kept < 5%. Separate analysis were aligned and compared using the MyPROMS software (Poullet et al. Proteomics 2007 http://onlinelibrary.wiley.com/doi/10.1002/pmic.200600784/abstract). Database searches were performed with Maxquant version 1.5.3.30 (Cox et al., 2014; Cox et al., 2009). The database used was a concatenation of mus musculus sequences from Uniprot- SwissProt database (release 2016-06) and a list of contaminant sequences from Maxquant and CRAPome. The enzyme specifity was trypsin. Variable modifications were acetyl (protein N-term), oxidation (methionine (M)) and hydroxylation (proline (P)). The precursor mass tolerance was set to 4.5 ppm and the fragment mass tolerance was set to 0.5 Da. The minimal length of peptides was seven amino acids. The maximum false-discovery rate (FDR) was set to 0.01 for both the peptides and proteins. Label-free protein quantification (LFQ) was done using both unique and razor peptides. At least 2 such peptides were required for LFQ.

Bibliography

1. Lenders JW, Eisenhofer G, Mannelli M, Pacak K. Phaeochromocytoma. Lancet. 2005/08/23 ed. 2005;366:665–75.
2. Favier J, Amar L, Gimenez-Roqueplo A-P. Paraganglioma and phaeochromocytoma: from genetics to personalized medicine. Nat Rev Endocrinol. 2015;11:101–11.
3. Hederstedt L. Structural biology. Complex II is complex too. Science. 2003/02/01 ed. 2003;299:671–2.
4. Gimenez-Roqueplo A-P, Favier J, Rustin P, Rieubland C, Crespin M, Nau V, et al. Mutations in the SDHB Gene Are Associated with Extra-adrenal and/or Malignant Phaeochromocytomas. Cancer Res. American Association for Cancer Research; 2003;63:5615–21.
5. Amar L, Baudin E, Burnichon N, Peyrard S, Silvera S, Bertherat J, et al. Succinate Dehydrogenase B Gene Mutations Predict Survival in Patients with Malignant Pheochromocytomas or Paragangliomas. J Clin Endocrinol Metab. Oxford Academic; 2007;92:3822–8.
6. Buffet A, Ben Aim L, Leboulleux S, Drui D, Vezzosi D, Libé R, et al. Positive Impact of Genetic Test on the Management and Outcome of Patients With Paraganglioma and/or Pheochromocytoma. J Clin Endocrinol Metab. Oxford Academic; 2019;104:1109–18.
7. Letouzé E, Martinelli C, Loriot C, Burnichon N, Abermil N, Ottolenghi C, et al. SDH Mutations Establish a Hypermethylator Phenotype in Paraganglioma. Cancer Cell. 2013;23:739–52.
8. Loriot C, Burnichon N, Gadessaud N, Vescovo L, Amar L, Libe R, et al. Epithelial to Mesenchymal Transition Is Activated in Metastatic Pheochromocytomas and Paragangliomas Caused by SDHB Gene Mutations. J Clin Endocrinol Metab. 2012/04/12 ed. 2012;97:E954-62.
9. Loriot C, Domingues M, Berger A, Menara M, Ruel M, Morin A, et al. Deciphering the molecular basis of invasiveness in Sdhb-deficient cells. Oncotarget. 2015;6:32955–65.
10. Briere JJ, Favier J, El Ghouzzi V, Djouadi F, Benit P, Gimenez AP, et al. Succinate dehydrogenase deficiency in human. Cell Mol Life Sci. 2005;62:2317–24.
11. Selak MA, Armour SM, MacKenzie ED, Boulahbel H, Watson DG, Mansfield KD, et al. Succinate links TCA cycle dysfunction to oncogenesis by inhibiting HIF-α prolyl hydroxylase. Cancer Cell. 2005;7:77–85.
12. Myllyharju J. Prolyl 4-hydroxylases, the key enzymes of collagen biosynthesis. Matrix Biol. 2003;22:15–24.
13. Myllyharju J. Intracellular Post-Translational Modifications of Collagens. In: Brinckmann J, Notbohm H, Müller PK, editors. Collagen: Primer in Structure, Processing and Assembly [Internet]. Berlin, Heidelberg: Springer; 2005 [cited 2020 Sep 6]. page 115–47. Available from: https://doi.org/10.1007/b103821
14. Myllyharju J, Kivirikko KI. Collagens, modifying enzymes and their mutations in humans, flies and worms. Trends Genet. 2004;20:33–43.
15. Kivirikko KI, Pihlajaniemi T. Collagen hydroxylases and the protein disulfide isomerase subunit of prolyl 4-hydroxylases. Adv Enzymol Relat Areas Mol Biol. 1998;72:325–98.
16. Jimenez S, Harsch M, Rosenbloom J. Hydroxyproline stabilizes the triple helix of chick tendon collagen. Biochem Biophys Res Commun. 1973;52:106–14.

17. Berg RA, Prockop DJ. The thermal transition of a non-hydroxylated form of collagen. Evidence for a role for hydroxyproline in stabilizing the triple-helix of collagen. Biochem Biophys Res Commun. 1973;52:115–20.
18. Kadler KE, Baldock C, Bella J, Boot-Handford RP. Collagens at a glance. J Cell Sci. 2007;120:1955–8.
19. Mouw JK, Ou G, Weaver VM. Extracellular matrix assembly: a multiscale deconstruction. Nat Rev Mol Cell Biol. 2014;15:771–85.
20. Gilkes DM, Semenza GL, Wirtz D. Hypoxia and the extracellular matrix: drivers of tumour metastasis. Nat Rev Cancer. 2014;14:430–9.
21. Burnichon N, Vescovo L, Amar L, Libé R, de Reynies A, Venisse A, et al. Integrative genomic analysis reveals somatic mutations in pheochromocytoma and paraganglioma. Hum Mol Genet. Oxford Academic; 2011;20:3974–85.
22. Dahia PL, Ross KN, Wright ME, Hayashida CY, Santagata S, Barontini M, et al. A HIF1alpha regulatory loop links hypoxia and mitochondrial signals in pheochromocytomas. PLoS Genet. 2005;1:72–80.
23. Favier J, Briere JJ, Burnichon N, Riviere J, Vescovo L, Benit P, et al. The Warburg effect is genetically determined in inherited pheochromocytomas. PLoS One. 2009/09/19 ed. 2009;4:e7094.
24. Lamandé SR, Bateman JF. Procollagen folding and assembly: the role of endoplasmic reticulum enzymes and molecular chaperones. Semin Cell Dev Biol. 1999;10:455–64.
25. Koivunen P, Lee S, Duncan CG, Lopez G, Lu G, Ramkissoon S, et al. Transformation by the (R)-enantiomer of 2-hydroxyglutarate linked to EGLN activation. Nature. 2012;483:484–8.
26. Xiao M, Yang H, Xu W, Ma S, Lin H, Zhu H, et al. Inhibition of alpha-KG-dependent histone and DNA demethylases by fumarate and succinate that are accumulated in mutations of FH and SDH tumor suppressors. Genes & development. 2012/06/09 ed. 2012;26:1326–38.
27. Xu W, Yang H, Liu Y, Yang Y, Wang P, Kim SH, et al. Oncometabolite 2-hydroxyglutarate is a competitive inhibitor of alpha-ketoglutarate-dependent dioxygenases. Cancer Cell. 2011/01/22 ed. 2011;19:17–30.
28. Beckouche N, Bignon M, Lelarge V, Mathivet T, Pichol-Thievend C, Berndt S, et al. The interaction of heparan sulfate proteoglycans with endothelial transglutaminase-2 regulates VEGF165-induced angiogenesis. Science Signaling. 2015;In press.
29. Morin A, Goncalves J, Moog S, Castro-Vega L-J, Job S, Buffet A, et al. TET-Mediated Hypermethylation Primes SDH-Deficient Cells for HIF2α-Driven Mesenchymal Transition. Cell Reports. 2020;30:4551-4566.e7.

DISCUSSION

L'objectif principal de ce projet était d'évaluer l'impact de la matrice extracellulaire (MEC) dans la tumorigenèse des imCCs avec mutations *Sdhx,* et plus particulièrement sur la progression métastatique associée aux mutations sur le gène *Sdhb.*

Dans un premier temps, cette étude nous a permis de mettre en évidence un important remodelage de la MEC produite et sécrétée par les imCC *Sdhb-/-.* Les analyses transcriptomiques menées dans ces cellules montrent une surexpression d'une grande variété de collagènes, en comparaison aux cellules contrôles imCC WT et aux imCC *Sdhd-/-*. Ces observations à l'échelle transcriptomique sont corrélées avec les niveaux protéiques détectées dans la MEC par les études de matrisome. Comme expliqué dans l'introduction de ce manuscrit, la stabilisation de la triple hélice de collagène nécessite l'action de collagènes hydroxylases (dont les P4H) capables de catalyser l'hydroxylation des résidus proline et lysine des fibres de collagène immatures, appelées procollagènes au sein du réticulum endoplasmique des cellules. La présence de nombreux collagènes dans la MEC secrétée *in vitro* par les imCC *Sdhb-/-* traduit donc une bonne activité de ces enzymes, qui sont pourtant des dioxygénases dépendantes du 2-OG. Cette observation démontre pour la première fois dans l'étude des PPGL que, contrairement à ce que l'on attendait, les P4H ne sont pas inhibées par l'accumulation massive de succinate, de ROS et par la dérégulation de l'homéostasie du fer observés dans les imCC *Sdhb-/-*. Ce phénomène inattendu pourrait s'expliquer par les affinités de chacune des dioxygénases pour leurs différents substrats, se traduisant par leurs KM très variés (Tableau 3). Ainsi, les P4H présentent un KM pour le 2-OG dix fois inférieur à celui des PHDs des HIFs, suggérant une moins bonne affinité de ces enzymes pour le 2-OG et expliquant donc que ces enzymes ne soient pas inhibées par le succinate (379). Remarquablement, la MEC produite et sécrétée par leurs homologues cellulaires porteurs d'un KO du gène *Sdhd* apparait au contraire particulièrement appauvrie en collagènes même en comparaison de celle secrétée par les imCC WT. Nos analyses de l'hydroxylation des prolines sont en cours, et permettra de démontrer s'il existe des différences dans l'activité des CP4H dans ces différents modèles.

Les tests fonctionnels de migration et d'adhésion réalisés *in vitro*, suite à des expériences d'échanges de matrice entre nos différents modèles cellulaires ont mis en évidence les propriétés particulières de la MEC des imCC *Sdhb-/-*, capable de favoriser la migration, ainsi

que l'adhésion, des imCC WT et *Sdhd-/-.* Ces résultats révèlent ainsi clairement l'implication de la MEC des imCC *Sdhb-/-* dans les processus métastatiques associés à ce génotype. En revanche, les résultats obtenus dans le modèle *Sdhb-/-* shHIF2a suggèrent une faible participation de la pseudo-hypoxie à ce phénotype matriciel.

Les résultats obtenus lors de cette troisième étude ont donc mis en évidence la capacité des imCC *Sdhb-/-* à modifier leur microenvironnement, en induisant un remodelage de la MEC, pour assurer le maintien de leurs propriétés mésenchymateuses nécessaires au développement de métastases à distance. En plus des analyses d'hydroxylation en cours, l'étude de la matrice des imCC *Sdhb-/-* pourrait être approfondie par l'analyse de la rigidité matricielle. Les enzymes impliquées dans la formation des liaisons supramoléculaires des fibres de collagènes, comme les lysyl-oxydases, sont notamment responsables de cette propriété. Il serait donc intéressant d'analyser la rigidité de la MEC secrétée *in vitro* par les imCCs *Sdhb-/-,* et d'évaluer l'implication des lysyl-oxydases dans le phénotype métastatique, en mesurant notamment l'activité de Loxl4 qui est présente en grande quantité dans le matrisome de ces cellules. De plus, plusieurs études ont montré un lien étroit existant entre la présence de ROS et la composition de la MEC. Étant donné l'accumulation significative de ROS détectée dans les imCC *Sdhb-/-,* l'étude de l'effet des ROS sur la MEC des imCC *Sdhb-/-* pourrait aboutir à une meilleure compréhension des mécanismes mis en œuvre par les imCC *Sdhb-/-* pour modifier leur microenvironnement et ainsi faciliter leur dissémination métastatique. De plus, les ROS pourraient également jouer un rôle sur d'autres composants majeurs du microenvironnement, tels que les fibroblastes ou les cellules immunitaires (247,285). L'évaluation des effets des ROS sur le microenvironnement tumoral imCC *Sdhb-/-* pourrait donc ouvrir la voie à de nouvelles études qui conduiraient à une connaissance plus globale des processus d'oncogenèse induits par un déficit en SDHB.

CONCLUSIONS ET PERSPECTIVES

CONCLUSIONS ET PERSPECTIVES

L'objectif principal de mon projet de thèse était d'élucider les causes de la malignité SDHB-dépendante. L'ensemble de mes travaux de thèse, qui se sont articulés autour de trois grands axes d'études, ont permis d'apporter des réponses conséquentes à cette question majeure dans le domaine de la recherche sur les PPGL, non résolue depuis une vingtaine d'années :

- Le premier axe d'étude a permis d'identifier les mécanismes à l'origine du phénotype hyperméthylateur marqué des PPGL avec une mutation sur le gène *SDHB.* Cette étude a également mis en lumière l'implication de l'hyperméthylation dans l'acquisition des propriétés mésenchymateuses des imCC *Sdhb-/-*, qui favorisent la progression métastatique en synergie avec la pseudo-hypoxie médiée par la stabilisation de HIF2α.

- La deuxième étude présentée dans ce manuscrit a permis d'approfondir les connaissances sur la tumorigenèse secondaire à un défaut de SDH, par la caractérisation et la comparaison, jamais réalisée, de plusieurs modèles cellulaires porteurs de véritables KO de différents gènes *Sdhx (Sdhb* vs *Sdhd).* Cette étude a ainsi permis d'identifier des différences majeures dans les mécanismes moléculaires et cellulaires impliqués, selon le gène *Sdhx* muté et par conséquent a mis en lumière les mécanismes d'oncogenèse spécifiquement impliqués au sein des PPGL mutés *SDHB.* J'ai ainsi a observé que ces phénotypes étaient secondaires à une plus forte inhibition de certaines dioxygénases dépendantes du 2-OG (TETs de l'ADN et PHDs des HIFs) dans les cellules avec un déficit en SDHB. L'accumulation du succinate, qui tient le rôle de principal oncométabolite de la tumorigenèse SDH-dépendante, n'est pas la seule responsable de cette inhibition comme longtemps postulé. En effet, certaines propriétés spécifiquement observées dans les imCC *Sdhb-/-,* en comparaison avec leurs homologues porteuses d'un KO du gène *Sdhd,* seraient responsables de cette inhibition accrue des dioxygénases dépendantes du 2-OG. Ainsi, la perte de la sous-unité SDHB conduit à un stress oxydant élevé, secondaire à une accumulation d'espèces réactives de l'oxygène (ROS), étroitement associé à un déséquilibre de l'homéostasie du fer et du cuivre.

- Enfin, la troisième étude présentée dans ce manuscrit a permis de mettre en lumière l'existence d'une matrice extracellulaire spécifique aux imCCs *Sdhb-/-,* ainsi que l'implication de celle-ci dans l'acquisition du phénotype métastatique des tumeurs avec une mutation *SDHB.*

Mes travaux de thèse ont donc permis d'obtenir des résultats très prometteurs, aussi bien pour la compréhension fondamentale des mécanismes d'oncogenèse liés aux mutations *SDHB*, que pour la prise en charge clinique des patients atteints de PGL héréditaires.

Tout d'abord, l'ascorbate apparait comme une approche thérapeutique potentielle originale pour le traitement des PPGL SDHB-dépendants. En effet, cet antioxydant reconnu offre de nombreux atouts, car il présente peu d'effets secondaires dans les tissus sains, même à des concentrations pharmacologiques et est facile d'accès. L'ascorbate se présentait comme un candidat particulièrement pertinent de par son rôle de co-facteur des dioxygénases dépendantes du 2-OG. Toutefois, c'est son action antinomique sur l'état oxydant des cellules qui s'est révélé particulièrement concluant au cours de mes travaux. Bien qu'il exerce une action anti-oxydante à des concentrations physiologiques (de l'ordre du micromolaire) (380), en étant capable de diminuer les niveaux de ROS, l'ascorbate présente des propriétés pro-oxydantes, lorsqu'il atteint des concentrations élevées (381). Les imCC *Sdhb-/-* montrent une sensibilité accrue pour ce traitement, qui entraine leur mort cellulaire en conduisant à des niveaux de ROS intolérablement élevés pour ces cellules. Ses propriétés pro-oxydantes font donc de l'ascorbate un candidat thérapeutique très prometteur pour le traitement des PPGL mutés *SDHB*, d'autant plus qu'il affecte également l'homéostasie du fer, en interagissant avec la forme ferrique (Fe^{3+}) pour aboutir par un cycle de réactions à la formation de fer ferreux (Fe^{2+}), de la forme oxydée de l'ascorbate (DHA) et de ROS (296,382).

La découverte des mécanismes impliqués dans l'oncogenèse des PPGL SDHB-dépendants a également permis d'ouvrir la voie à d'autres perspectives thérapeutiques prometteuses pour le traitement des formes métastatiques de PPGL. L'hyperméthylation marquée observée dans les cellules et les tumeurs avec une mutation sur le gène *SDHB,* suggère l'utilisation de certains agents déméthylants de l'ADN ou des histones pour le traitement des patients porteurs de ces tumeurs. Ainsi, mon équipe d'accueil a précédemment démontré l'efficacité de la décitabine, un agent capable d'inhiber les ADN-méthyltransférases et associé à la répression des capacités migratoires élevées des imCC *Sdhb-/-* (160). De nouvelles thérapies épigénétiques ont émergées ces dernières années, dont la Guadécitabine, un inhibiteur de la méthylation de l'ADN de deuxième génération, dont l'efficacité a été récemment évaluée lors d'une étude de phase II. Parmi les 9 patients inclus dans cet essai clinique mené par le NIH, 8 présentaient un défaut de SDH ayant conduit à la formation de GIST ou de PGL. Néanmoins, les résultats de

cette étude présentés au cours de l'édition 2020 du congrès international de l'ASCO ne se sont pas avérés concluants.

En outre, le premier article présenté dans ce manuscrit révèle que l'hyperméthylation seule n'est pas suffisante à l'acquisition du phénotype métastatique et que l'activation de la pseudo-hypoxie est également un élément clé. Le facteur HIF2α se présente donc comme une cible thérapeutique particulièrement pertinente pour le traitement des PPGL métastatiques. Après avoir longtemps été considéré comme pharmacologiquement inaccessible, deux antagonistes de HIF2 (PT2385 et PT2977) ont récemment été générés. Ces molécules de petites taille agissent par allostérie pour inhiber la formation du dimère HIF2α/HIF1β et ainsi empêcher leur activité transcriptionnelle (383). Plusieurs études ont récemment rapporté l'efficacité de ces molécules sur l'inhibition de la croissance tumorale *in vitro* et *in vivo* dans le carcinome rénal à cellules claires (ccRCC) (384–386). Plusieurs études de phase II évaluent actuellement l'efficacité du traitement des ccRCC, par ces antagonistes seuls ou en combinaison avec le cabozantinib, un inhibiteur du VEGF ou avec l'évérolimus. Les résultats prometteurs obtenus avec ce traitement dans le ccRCC et l'implication majeure de HIF2α dans les processus d'oncogenèse SDHB-dépendants, suggèrent l'utilisation de ces antagonistes pour le traitement des PPGL avec une mutation *SDHB.* L'efficacité de ces molécules est actuellement en cours d'évaluation *in vitro* dans notre modèle cellulaire d'imCC *Sdhb-/-* et *in vivo* dans des modèles de xénogreffes par une doctorante de mon équipe d'accueil. De plus, nous avons vu lors de la deuxième étude que les imCC *Sdhb-/-* présentent des niveaux d'expression particulièrement élevés de HIF2α, probablement expliqués par l'accumulation de ROS observée dans ces cellules (285,319,387,388). Par conséquent, un traitement associant un antagoniste de HIF2α et de l'ascorbate, pourrait constituer une stratégie thérapeutique potentielle pour le traitement spécifique des PPGL SDHB-dépendants.

L'ensemble des résultats obtenus au cours de ma thèse offrent donc plusieurs perspectives thérapeutiques prometteuses. Cependant, des études plus intégrées, sur des modèles *in vivo* et prenant en compte le microenvironnement tumoral, sont nécessaires pour aboutir à une prise en charge véritablement efficace des patients porteurs de PPGL métastatiques. En effet, comme évoqué dans l'introduction de ce manuscrit, le microenvironnement tumoral est un élément clé de la progression métastatique des cellules tumorales. La troisième étude que j'ai menée au cours de ma thèse a ainsi permis d'amorcer l'étude du microenvironnement

tumoral des PPGL SDHB-dépendants, en analysant l'un de ces composants principaux, la MEC. Cette étude a mis en évidence pour la première fois dans les PPGL, la composition particulière de la MEC produite et sécrétée par les imCC *Sdhb-/-,* qui est notamment beaucoup plus riche en collagènes que celle secrétée par leurs homologues mutés sur le gène *Sdhd.* Ce remodelage de la matrice, lié spécifiquement aux altérations de la sous-unité SDHB, joue également un rôle fonctionnel en favorisant les processus d'adhésion et de migration cellulaire, essentiels à la dissémination métastatique. Ces résultats offrent pour la première fois une vision plus intégrée/globale des processus d'oncogenèse des PPGL et ouvrent ainsi la voie à l'étude du microenvironnement tumoral de ces tumeurs. Toutefois, la MEC ne représente qu'un seul des divers composants du microenvironnement, qui est un ensemble complexe regroupant de nombreux types moléculaires et cellulaires variés. Une étude approfondie de ces différents composants apporterait des connaissances nouvelles sur les mécanismes d'oncogenèse des PPGL mutés *SDHB,* essentielles à la découverte de traitements efficaces pour les patients atteints de PPGL métastatiques.

En outre, mon équipe d'accueil a récemment identifiée une signature de miR spécifique aux PPGL métastatiques de mauvais pronostic. Cette signature est constituée d'un cluster de 4 miR différents (182/96/183 et l'oncomiR-21) (209), qui ont été détectés dans la circulation de patients ainsi que dans le milieu conditionné des imCC *Sdhb-/-*. Plusieurs études ont rapporté que les miR libérés par les cellules cancéreuses avaient un impact sur le microenvironnement tumoral et plus particulièrement sur les cellules immunitaires qui le composent (179,389). Ces observations ont conduit mon équipe d'accueil à émettre l'hypothèse que la sécrétion du cluster de miR, observé dans la circulation des patients atteints de PPGL, pourrait modifier le microenvironnement tumoral et ainsi favoriser la progression métastatique. Cette question constitue l'objectif principal d'un nouveau projet d'étude de mon laboratoire d'accueil. La première étape de ce projet sera d'évaluer les effets de ces 4 miR sur différentes cellules du microenvironnement et notamment sur les cellules immunitaires, telles que les macrophages, les cellules NK et les lymphocytes. Ce projet pourrait ainsi aboutir à des avancées majeures dans la compréhension intégrée des mécanismes impliqués dans la progression métastatique des PPGL. De plus, comme nous l'avons vu au cours de l'introduction, un lien étroit existe entre le recrutement des cellules immunitaires dans le microenvironnement et la MEC. En effet, certains composants de la MEC possèdent des propriétés chimio-attractives qui induisent l'infiltration des macrophages. C'est par exemple le cas des collagènes de type I

(367), présents en grande quantité dans la MEC sécrétée par les cellules avec un déficit en SDHB. De plus, l'hypoxie favorise également l'accumulation des macrophages et affecte grandement leur phénotype en induisant la modification de leurs profils d'expression génique (368–370). Enfin, les macrophages sont grandement impliqués dans l'inflammation, qui constitue l'une des caractéristiques « habilitantes » fondamentales de la progression tumorale, comme définie dès les années 2000 par Weinberg et Hanahan (314). Par conséquent, ces études permettront également une meilleure compréhension du rôle de l'inflammation dans l'oncogenèse des PPGL métastatiques, encore mal connu à l'heure actuelle.

L'ensemble des résultats obtenus suite à ces études devraient ainsi compléter de façon significative les avancées majeures apportés par mes travaux de thèse et pourraient être exploités pour potentialiser les effets des thérapies actuelles et émergentes administrées aux patients atteints de PPGL métastatiques.

BIBLIOGRAPHIE

BIBLIOGRAPHIE

1. Lenders JWM, Kerstens MN, Amar L, Prejbisz A, Robledo M, Taieb D, et al. Genetics, diagnosis, management and future directions of research of phaeochromocytoma and paraganglioma: a position statement and consensus of the Working Group on Endocrine Hypertension of the European Society of Hypertension. Journal of Hypertension. août 2020;38(8):1443–1456.
2. Alesina PF, Walz MK. Adrenal Tumors: Are Gender Aspects Relevant? Visc Med. févr 2020;36(1):15-9.
3. Lo CY, Lam KY, Wat MS, Lam KS. Adrenal pheochromocytoma remains a frequently overlooked diagnosis. American journal of surgery. mars 2000;179(3):212-5.
4. Huber K, Kalcheim C, Unsicker K. The development of the chromaffin cell lineage from the neural crest. Auton Neurosci. 17 nov 2009;151(1):10-6.
5. Bronner ME, LeDouarin NM. Development and evolution of the neural crest: an overview. Dev Biol. 1 juin 2012;366(1):2-9.
6. Adams MS, Bronner-Fraser M. Review: the role of neural crest cells in the endocrine system. Endocrine pathology. Summer 2009;20(2):92-100.
7. Knecht AK, Bronner-Fraser M. Induction of the neural crest: a multigene process. Nat Rev Genet. 2002/06/04 éd. juin 2002;3(6):453-61.
8. Furlan A, Dyachuk V, Kastriti ME, Calvo-Enrique L, Abdo H, Hadjab S, et al. Multipotent peripheral glial cells generate neuroendocrine cells of the adrenal medulla. Science. 07 2017;357(6346).
9. Furlan A, Adameyko I. Schwann cell precursor: a neural crest cell in disguise? Developmental Biology. 1 déc 2018;444:S25-35.
10. Lenders JW, Eisenhofer G, Mannelli M, Pacak K. Phaeochromocytoma. Lancet. 2005/08/23 éd. 20 août 2005;366(9486):665-75.
11. Lee KY, Oh Y-W, Noh HJ, Lee YJ, Yong H-S, Kang E-Y, et al. Extraadrenal paragangliomas of the body: imaging features. AJR Am J Roentgenol. août 2006;187(2):492-504.
12. Lee KY, Oh YW, Noh HJ, Lee YJ, Yong HS, Kang EY, et al. Extraadrenal paragangliomas of the body: imaging features. AJR Am J Roentgenol. 2006/07/25 éd. août 2006;187(2):492-504.
13. T F. Catecholamine biosynthesis and physiological regulation in neuroendocrine cells. Acta Physiol Scand. 1 janv 2000;168(1):1-17.
14. Eisenhofer G, Huynh TT, Hiroi M, Pacak K. Understanding catecholamine metabolism as a guide to the biochemical diagnosis of pheochromocytoma. Reviews in endocrine & metabolic disorders. août 2001;2(3):297-311.
15. Henry JP, Botton D, Sagne C, Isambert MF, Desnos C, Blanchard V, et al. Biochemistry and molecular biology of the vesicular monoamine transporter from chromaffin granules. J Exp Biol. nov 1994;196:251-62.
16. Amara SG, Sonders MS, Zahniser NR, Povlock SL, Daniels GM. Molecular physiology and regulation of catecholamine transporters. Adv Pharmacol. 1998;42:164-8.
17. Nagatsu T, Stjärne L. Catecholamine synthesis and release. Overview. Adv Pharmacol. 1998;42:1-14.
18. Schulz C, Eisenhofer G, Lehnert H. Principles of catecholamine biosynthesis, metabolism and release. Front Horm Res. 2004;31:1-25.
19. Eisenhofer G, Kopin IJ, Goldstein DS. Catecholamine metabolism: a contemporary

view with implications for physiology and medicine. Pharmacol Rev. sept 2004;56(3):331-49.
20. Amar L, Servais A, Gimenez-Roqueplo AP, Zinzindohoue F, Chatellier G, Plouin PF. Year of diagnosis, features at presentation, and risk of recurrence in patients with pheochromocytoma or secreting paraganglioma. J Clin Endocrinol Metab. avr 2005;90(4):2110-6.
21. Plouin PF, Chatellier G, Delahousse M, Rougeot MA, Duclos JM, Pagny JY, et al. [Detection, diagnosis and localization of pheochromocytoma. 77 cases in a population of 21,420 hypertensive patients]. Presse Med. 19 déc 1987;16(44):2211-5.
22. Giavarini A, Chedid A, Bobrie G, Plouin P-F, Hagège A, Amar L. Acute catecholamine cardiomyopathy in patients with phaeochromocytoma or functional paraganglioma. Heart. oct 2013;99(19):1438-44.
23. Capatina C, Ntali G, Karavitaki N, Grossman AB. The management of head-and-neck paragangliomas. Endocr Relat Cancer. oct 2013;20(5):R291-305.
24. Lenders JWM, Duh Q-Y, Eisenhofer G, Gimenez-Roqueplo A-P, Grebe SKG, Murad MH, et al. Pheochromocytoma and Paraganglioma: An Endocrine Society Clinical Practice Guideline. J Clin Endocrinol Metab. 1 juin 2014;99(6):1915-42.
25. Lenders JWM, Pacak K, Walther MM, Linehan WM, Mannelli M, Friberg P, et al. Biochemical diagnosis of pheochromocytoma: which test is best? JAMA. 20 mars 2002;287(11):1427-34.
26. Lenders JW. Biochemical diagnosis of pheochromocytoma and paraganglioma. Annales d'endocrinologie. juin 2009;70(3):161-5.
27. Peaston RT, Graham KS, Chambers E, van der Molen JC, Ball S. Performance of plasma free metanephrines measured by liquid chromatography-tandem mass spectrometry in the diagnosis of pheochromocytoma. Clin Chim Acta. 2 avr 2010;411(7-8):546-52.
28. Weismann D, Peitzsch M, Raida A, Prejbisz A, Gosk M, Riester A, et al. Measurements of plasma metanephrines by immunoassay vs liquid chromatography with tandem mass spectrometry for diagnosis of pheochromocytoma. Eur J Endocrinol. mars 2015;172(3):251-60.
29. Willemsen JJ, Ross HA, Lenders JWM, Sweep FCGJ. Stability of urinary fractionated metanephrines and catecholamines during collection, shipment, and storage of samples. Clin Chem. févr 2007;53(2):268-72.
30. Lenders JWM, Willemsen JJ, Eisenhofer G, Ross HA, Pacak K, Timmers HJLM, et al. Is supine rest necessary before blood sampling for plasma metanephrines? Clin Chem. févr 2007;53(2):352-4.
31. Eisenhofer G, Peitzsch M. Laboratory evaluation of pheochromocytoma and paraganglioma. Clin Chem. déc 2014;60(12):1486-99.
32. Eisenhofer G, Lenders JW, Siegert G, Bornstein SR, Friberg P, Milosevic D, et al. Plasma methoxytyramine: A novel biomarker of metastatic pheochromocytoma and paraganglioma in relation to established risk factors of tumour size, location and SDHB mutation status. Eur J Cancer. 2011/11/01 éd. juill 2012;48(11):1739-49.
33. Rao D, Peitzsch M, Prejbisz A, Hanus K, Fassnacht M, Beuschlein F, et al. Plasma methoxytyramine: clinical utility with metanephrines for diagnosis of pheochromocytoma and paraganglioma. Eur J Endocrinol. août 2017;177(2):103-13.
34. Darr R, Pamporaki C, Peitzsch M, Miehle K, Prejbisz A, Peczkowska M, et al. Biochemical diagnosis of phaeochromocytoma using plasma-free normetanephrine, metanephrine and methoxytyramine: importance of supine sampling under fasting conditions. Clinical endocrinology. avr 2014;80(4):478-86.

35. d'Herbomez M, Forzy G, Bauters C, Tierny C, Pigny P, Carnaille B, et al. An analysis of the biochemical diagnosis of 66 pheochromocytomas. Eur J Endocrinol. mai 2007;156(5):569-75.
36. Gimenez-Roqueplo A-P, Caumont-Prim A, Houzard C, Hignette C, Hernigou A, Halimi P, et al. Imaging work-up for screening of paraganglioma and pheochromocytoma in SDHx mutation carriers: a multicenter prospective study from the PGL.EVA Investigators. J Clin Endocrinol Metab. janv 2013;98(1):E162-173.
37. Bravo EL, Tagle R. Pheochromocytoma: state-of-the-art and future prospects. Endocrine reviews. août 2003;24(4):539-53.
38. Castinetti F, Kroiss A, Kumar R, Pacak K, Taieb D. 15 YEARS OF PARAGANGLIOMA: Imaging and imaging-based treatment of pheochromocytoma and paraganglioma. Endocr Relat Cancer. août 2015;22(4):T135-145.
39. Goldstein DS, Eisenhofer G, Flynn JA, Wand G, Pacak K. Diagnosis and localization of pheochromocytoma. Hypertension. mai 2004;43(5):907-10.
40. Elston MS, Meyer-Rochow GY, Conaglen HM, Clarkson A, Clifton-Bligh RJ, Conaglen JV, et al. Increased SSTR2A and SSTR3 expression in succinate dehydrogenase-deficient pheochromocytomas and paragangliomas. Hum Pathol. mars 2015;46(3):390-6.
41. Timmers HJ, Chen CC, Carrasquillo JA, Whatley M, Ling A, Havekes B, et al. Comparison of 18F-fluoro-L-DOPA, 18F-fluoro-deoxyglucose, and 18F-fluorodopamine PET and 123I-MIBG scintigraphy in the localization of pheochromocytoma and paraganglioma. The Journal of clinical endocrinology and metabolism. déc 2009;94(12):4757-67.
42. Taïeb D, Sebag F, Barlier A, Tessonnier L, Palazzo FF, Morange I, et al. 18F-FDG avidity of pheochromocytomas and paragangliomas: a new molecular imaging signature? J Nucl Med. mai 2009;50(5):711-7.
43. Timmers HJ, Chen CC, Carrasquillo JA, Whatley M, Ling A, Eisenhofer G, et al. Staging and functional characterization of pheochromocytoma and paraganglioma by 18F-fluorodeoxyglucose (18F-FDG) positron emission tomography. J Natl Cancer Inst. 2012/04/21 éd. 2 mai 2012;104(9):700-8.
44. Taïeb D, Timmers HJ, Hindié E, Guillet BA, Neumann HP, Walz MK, et al. EANM 2012 guidelines for radionuclide imaging of phaeochromocytoma and paraganglioma. Eur J Nucl Med Mol Imaging. déc 2012;39(12):1977-95.
45. Treglia G, Cocciolillo F, de Waure C, Di Nardo F, Gualano MR, Castaldi P, et al. Diagnostic performance of 18F-dihydroxyphenylalanine positron emission tomography in patients with paraganglioma: a meta-analysis. Eur J Nucl Med Mol Imaging. juill 2012;39(7):1144-53.
46. King KS, Chen CC, Alexopoulos DK, Whatley MA, Reynolds JC, Patronas N, et al. Functional imaging of SDHx-related head and neck paragangliomas: comparison of 18F-fluorodihydroxyphenylalanine, 18F-fluorodopamine, 18F-fluoro-2-deoxy-D-glucose PET, 123I-metaiodobenzylguanidine scintigraphy, and 111In-pentetreotide scintigraphy. J Clin Endocrinol Metab. sept 2011;96(9):2779-85.
47. Imani F, Agopian VG, Auerbach MS, Walter MA, Imani F, Benz MR, et al. 18F-FDOPA PET and PET/CT accurately localize pheochromocytomas. J Nucl Med. avr 2009;50(4):513-9.
48. Fiebrich H-B, Brouwers AH, Kerstens MN, Pijl MEJ, Kema IP, de Jong JR, et al. 6-[F-18]Fluoro-L-dihydroxyphenylalanine positron emission tomography is superior to conventional imaging with (123)I-metaiodobenzylguanidine scintigraphy, computer tomography, and magnetic resonance imaging in localizing tumors causing catecholamine excess. J Clin Endocrinol Metab. oct 2009;94(10):3922-30.

49. Taïeb D, Pacak K. Genetic Determinants of Pheochromocytoma and Paraganglioma Imaging Phenotypes. J Nucl Med. mai 2020;61(5):643-5.
50. N N, A K, P S, C B, A M, R K. Imaging carotid body chemodectomas with ^{68}Ga-DOTA-NOC PET-CT [Internet]. Vol. 85, The British journal of radiology. Br J Radiol; 2012 [cité 15 sept 2020]. Disponible sur: https://pubmed.ncbi.nlm.nih.gov/22096221/
51. A K, Bl S, C U, A F, Rw G, C U, et al. (68)Ga-DOTATOC PET/CT provides accurate tumour extent in patients with extraadrenal paraganglioma compared to (123)I-MIBG SPECT/CT [Internet]. Vol. 42, European journal of nuclear medicine and molecular imaging. Eur J Nucl Med Mol Imaging; 2015 [cité 15 sept 2020]. Disponible sur: https://pubmed.ncbi.nlm.nih.gov/25134670/
52. Taïeb D, Jha A, Treglia G, Pacak K. Molecular imaging and radionuclide therapy of pheochromocytoma and paraganglioma in the era of genomic characterization of disease subgroups. Endocrine-Related Cancer. 1 nov 2019;26(11):R627-52.
53. Tischler AS, Kimura N, Mcnicol AM. Pathology of pheochromocytoma and extra-adrenal paraganglioma. Ann N Y Acad Sci. août 2006;1073:557-70.
54. McNicol AM. Update on tumours of the adrenal cortex, phaeochromocytoma and extra-adrenal paraganglioma. Histopathology. janv 2011;58(2):155-68.
55. Tischler AS, deKrijger RR. 15 YEARS OF PARAGANGLIOMA: Pathology of pheochromocytoma and paraganglioma. Endocr Relat Cancer. août 2015;22(4):T123-133.
56. Białas M, Okoń K, Dyduch G, Ciesielska-Milian K, Buziak M, Hubalewska-Dydejczyk A, et al. Neuroendocrine markers and sustentacular cell count in benign and malignant pheochromocytomas - a comparative study. Pol J Pathol. juin 2013;64(2):129-35.
57. Bausch B, Tischler AS, Schmid KW, Leijon H, Eng C, Neumann HPH. Max Schottelius: Pioneer in Pheochromocytoma. J Endocr Soc. 1 juill 2017;1(7):957-64.
58. Favier J, Amar L, Gimenez-Roqueplo A-P. Paraganglioma and phaeochromocytoma: from genetics to personalized medicine. Nature Reviews Endocrinology. févr 2015;11(2):101-11.
59. Toledo RA, Qin Y, Cheng Z-M, Gao Q, Iwata S, Silva GM, et al. Recurrent Mutations of Chromatin-Remodeling Genes and Kinase Receptors in Pheochromocytomas and Paragangliomas. Clin Cancer Res. 1 mai 2016;22(9):2301-10.
60. Remacha L, Comino-Méndez I, Richter S, Contreras L, Currás-Freixes M, Pita G, et al. Targeted Exome Sequencing of Krebs Cycle Genes Reveals Candidate Cancer–Predisposing Mutations in Pheochromocytomas and Paragangliomas. Clin Cancer Res. 15 oct 2017;23(20):6315-24.
61. Remacha L, Pirman D, Mahoney CE, Coloma J, Calsina B, Currás-Freixes M, et al. Recurrent Germline DLST Mutations in Individuals with Multiple Pheochromocytomas and Paragangliomas. The American Journal of Human Genetics. 4 avr 2019;104(4):651-64.
62. Buffet A, Morin A, Castro-Vega L-J, Habarou F, Lussey-Lepoutre C, Letouzé E, et al. Germline Mutations in the Mitochondrial 2-Oxoglutarate/Malate Carrier SLC25A11 Gene Confer a Predisposition to Metastatic Paragangliomas. Cancer Res. 15 avr 2018;78(8):1914-22.
63. Cascon A, Comino-Mendez I, Curras-Freixes M, de Cubas AA, Contreras L, Richter S, et al. Whole-exome sequencing identifies MDH2 as a new familial paraganglioma gene. Journal of the National Cancer Institute [Internet]. mai 2015;107(5). Disponible sur: http://www.ncbi.nlm.nih.gov/pubmed/25766404
64. Neumann HP, Berger DP, Sigmund G, Blum U, Schmidt D, Parmer RJ, et al. Pheochromocytomas, multiple endocrine neoplasia type 2, and von Hippel-Lindau disease. N

Engl J Med. 18 nov 1993;329(21):1531-8.
65. Brito JP, Asi N, Bancos I, Gionfriddo MR, Zeballos-Palacios CL, Leppin AL, et al. Testing for germline mutations in sporadic pheochromocytoma/paraganglioma: a systematic review. Clinical Endocrinology. 2015;82(3):338-45.
66. Knudson AG. Mutation and Cancer: Statistical Study of Retinoblastoma. Proc Natl Acad Sci U S A. avr 1971;68(4):820-3.
67. Lammert M, Friedman JM, Kluwe L, Mautner VF. Prevalence of neurofibromatosis 1 in German children at elementary school enrollment. Arch Dermatol. janv 2005;141(1):71-4.
68. Boyd KP, Korf BR, Theos A. Neurofibromatosis type 1. Journal of the American Academy of Dermatology. juill 2009;61(1):1-14; quiz 15-6.
69. Pinson S, Wolkenstein P. [Neurofibromatosis type 1 or Von Recklinghausen's disease]. La Revue de medecine interne / fondee . mars 2005;26(3):196-215.
70. NIH. Neurofibromatosis. Conference statement. National Institutes of Health Consensus Development Conference. Archives of neurology. mai 1988;45(5):575-8.
71. Hersh JH, American Academy of Pediatrics Committee on Genetics. Health supervision for children with neurofibromatosis. Pediatrics. mars 2008;121(3):633-42.
72. Amar L, Bertherat J, Baudin E, Ajzenberg C, Bressac-de Paillerets B, Chabre O, et al. Genetic Testing in Pheochromocytoma or Functional Paraganglioma. JCO. 1 déc 2005;23(34):8812-8.
73. Képénékian L, Mognetti T, Lifante J-C, Giraudet A-L, Houzard C, Pinson S, et al. Interest of systematic screening of pheochromocytoma in patients with neurofibromatosis type 1. Eur J Endocrinol. oct 2016;175(4):335-44.
74. Gruber LM, Erickson D, Babovic-Vuksanovic D, Thompson GB, Young WF, Bancos I. Pheochromocytoma and paraganglioma in patients with neurofibromatosis type 1. Clin Endocrinol (Oxf). janv 2017;86(1):141-9.
75. Bausch B, Koschker AC, Fassnacht M, Stoevesandt J, Hoffmann MM, Eng C, et al. Comprehensive mutation scanning of NF1 in apparently sporadic cases of pheochromocytoma. J Clin Endocrinol Metab. 2006/06/22 éd. sept 2006;91(9):3478-81.
76. Moramarco J, El Ghorayeb N, Dumas N, Nolet S, Boulanger L, Burnichon N, et al. Pheochromocytomas are diagnosed incidentally and at older age in neurofibromatosis type 1. Clin Endocrinol (Oxf). mars 2017;86(3):332-9.
77. Burnichon N, Buffet A, Parfait B, Letouze E, Laurendeau I, Loriot C, et al. Somatic NF1 inactivation is a frequent event in sporadic pheochromocytoma. Human molecular genetics. 2012/09/11 éd. 15 déc 2012;21(26):5397-405.
78. Gieldon L, Masjkur JR, Richter S, Därr R, Lahera M, Aust D, et al. Next-generation panel sequencing identifies NF1 germline mutations in three patients with pheochromocytoma but no clinical diagnosis of neurofibromatosis type 1. Eur J Endocrinol. févr 2018;178(2):K1-9.
79. Maher ER, Neumann HP, Richard S. von Hippel-Lindau disease: a clinical and scientific review. Eur J Hum Genet. juin 2011;19(6):617-23.
80. Crossey PA, Maher ER, Jones MH, Richards FM, Latif F, Phipps ME, et al. Genetic linkage between von Hippel-Lindau disease and three microsatellite polymorphisms refines the localisation of the VHL locus. Hum Mol Genet. mars 1993;2(3):279-82.
81. Maxwell PH, Wiesener MS, Chang GW, Clifford SC, Vaux EC, Cockman ME, et al. The tumour suppressor protein VHL targets hypoxia-inducible factors for oxygen-dependent proteolysis. Nature. 1999/06/03 éd. 20 mai 1999;399(6733):271-5.
82. Favier J, Gimenez-Roqueplo AP. Pheochromocytomas: the (pseudo)-hypoxia

hypothesis. Best practice & research Clinical endocrinology & metabolism. 2010/12/01 éd. déc 2010;24(6):957-68.
83. Binderup MLM, Gimsing S, Kosteljanetz M, Thomsen C, Bisgaard ML. von Hippel-Lindau disease: deafness due to a non-MRI-visible endolymphatic sac tumor despite targeted screening. Int J Audiol. nov 2013;52(11):771-5.
84. Neumann HP, Wiestler OD. Clustering of features of von Hippel-Lindau syndrome: evidence for a complex genetic locus. Lancet. 4 mai 1991;337(8749):1052-4.
85. Lenglet M, Robriquet F, Schwarz K, Camps C, Couturier A, Hoogewijs D, et al. Identification of a new VHL exon and complex splicing alterations in familial erythrocytosis or von Hippel-Lindau disease. Blood. 02 2018;132(5):469-83.
86. Buffet A, Calsina B, Flores S, Giraud S, Lenglet M, Romanet P, et al. Germline mutations in the new E1' cryptic exon of the VHL gene in patients with tumours of von Hippel-Lindau disease spectrum or with paraganglioma. Journal of Medical Genetics [Internet]. 29 janv 2020 [cité 7 juill 2020]; Disponible sur: https://jmg-bmj-com.proxy.insermbiblio.inist.fr/content/early/2020/01/28/jmedgenet-2019-106519
87. Mulligan LM. RET revisited: expanding the oncogenic portfolio. Nat Rev Cancer. mars 2014;14(3):173-86.
88. Mulligan LM, Kwok JB, Healey CS, Elsdon MJ, Eng C, Gardner E, et al. Germ-line mutations of the RET proto-oncogene in multiple endocrine neoplasia type 2A. Nature. 3 juin 1993;363(6428):458-60.
89. Brandi ML, Gagel RF, Angeli A, Bilezikian JP, Beck-Peccoz P, Bordi C, et al. Guidelines for diagnosis and therapy of MEN type 1 and type 2. The Journal of clinical endocrinology and metabolism. déc 2001;86(12):5658-71.
90. Kloos (Chair) RT, Eng C, Evans DB, Francis GL, Gagel RF, Gharib H, et al. Medullary Thyroid Cancer: Management Guidelines of the American Thyroid Association. Thyroid. 26 mai 2009;19(6):565-612.
91. Eng C, Mulligan LM, Healey CS, Houghton C, Frilling A, Raue F, et al. Heterogeneous mutation of the RET proto-oncogene in subpopulations of medullary thyroid carcinoma. Cancer Res. 1996/05/01 éd. 1 mai 1996;56(9):2167-70.
92. Wells SA, Asa SL, Dralle H, Elisei R, Evans DB, Gagel RF, et al. Revised American Thyroid Association guidelines for the management of medullary thyroid carcinoma. Thyroid. juin 2015;25(6):567-610.
93. Boedeker CC, Neumann HPH, Offergeld C, Maier W, Falcioni M, Berlis A, et al. Clinical features of paraganglioma syndromes. Skull Base. janv 2009;19(1):17-25.
94. Neumann HPH, Bausch B, McWhinney SR, Bender BU, Gimm O, Franke G, et al. Germ-Line Mutations in Nonsyndromic Pheochromocytoma. New England Journal of Medicine. 9 mai 2002;346(19):1459-66.
95. Percy MJ, Furlow PW, Lucas GS, Li X, Lappin TR, McMullin MF, et al. A gain-of-function mutation in the HIF2A gene in familial erythrocytosis. N Engl J Med. 2008/01/11 éd. 10 janv 2008;358(2):162-8.
96. Percy MJ, Zhao Q, Flores A, Harrison C, Lappin TR, Maxwell PH, et al. A family with erythrocytosis establishes a role for prolyl hydroxylase domain protein 2 in oxygen homeostasis. Proc Natl Acad Sci U S A. 2006/01/13 éd. 17 janv 2006;103(3):654-9.
97. Ladroue C, Carcenac R, Leporrier M, Gad S, Le Hello C, Galateau-Salle F, et al. PHD2 mutation and congenital erythrocytosis with paraganglioma. N Engl J Med. 2008/12/19 éd. 18 déc 2008;359(25):2685-92.
98. Yang C, Zhuang Z, Fliedner SMJ, Shankavaram U, Sun MG, Bullova P, et al. Germ-line

PHD1 and PHD2 mutations detected in patients with pheochromocytoma/paraganglioma-polycythemia. J Mol Med. janv 2015;93(1):93-104.
99. Zhuang Z, Yang C, Lorenzo F, Merino M, Fojo T, Kebebew E, et al. Somatic HIF2A gain-of-function mutations in paraganglioma with polycythemia. N Engl J Med. 2012/08/31 éd. 6 sept 2012;367(10):922-30.
100. Buffet A, Smati S, Mansuy L, Menara M, Lebras M, Heymann MF, et al. Mosaicism in HIF2A-Related Polycythemia-Paraganglioma Syndrome. The Journal of clinical endocrinology and metabolism. 2013/11/28 éd. févr 2014;99(2):E369-73.
101. Favier J, Buffet A, Gimenez-Roqueplo AP. HIF2A mutations in paraganglioma with polycythemia. The New England journal of medicine. 2012/11/30 éd. 29 nov 2012;367(22):2161; author reply 2161-2.
102. Lorenzo FR, Yang C, Ng Tang Fui M, Vankayalapati H, Zhuang Z, Huynh T, et al. A novel EPAS1/HIF2A germline mutation in a congenital polycythemia with paraganglioma. J Mol Med. avr 2013;91(4):507-12.
103. Comino-Méndez I, de Cubas AA, Bernal C, Álvarez-Escolá C, Sánchez-Malo C, Ramírez-Tortosa CL, et al. Tumoral EPAS1 (HIF2A) mutations explain sporadic pheochromocytoma and paraganglioma in the absence of erythrocytosis. Hum Mol Genet. 1 juin 2013;22(11):2169-76.
104. Opotowsky AR, Moko LE, Ginns J, Rosenbaum M, Greutmann M, Aboulhosn J, et al. Pheochromocytoma and paraganglioma in cyanotic congenital heart disease. J Clin Endocrinol Metab. avr 2015;100(4):1325-34.
105. Vaidya A, Flores SK, Cheng Z-M, Nicolas M, Deng Y, Opotowsky AR, et al. EPAS1 Mutations and Paragangliomas in Cyanotic Congenital Heart Disease. N Engl J Med. 29 2018;378(13):1259-61.
106. Baysal BE, Ferrell RE, Willett-Brozick JE, Lawrence EC, Myssiorek D, Bosch A, et al. Mutations in SDHD, a mitochondrial complex II gene, in hereditary paraganglioma. Science. 2000/02/05 éd. 4 févr 2000;287(5454):848-51.
107. Astuti D, Latif F, Dallol A, Dahia PL, Douglas F, George E, et al. Gene mutations in the succinate dehydrogenase subunit SDHB cause susceptibility to familial pheochromocytoma and to familial paraganglioma. Am J Hum Genet. 2001/06/19 éd. juill 2001;69(1):49-54.
108. Currás-Freixes M, Piñeiro-Yañez E, Montero-Conde C, Apellániz-Ruiz M, Calsina B, Mancikova V, et al. PheoSeq: A Targeted Next-Generation Sequencing Assay for Pheochromocytoma and Paraganglioma Diagnostics. J Mol Diagn. 2017;19(4):575-88.
109. Aim LB, Pigny P, Castro-Vega LJ, Buffet A, Amar L, Bertherat J, et al. Targeted next-generation sequencing detects rare genetic events in pheochromocytoma and paraganglioma. Journal of Medical Genetics. 1 août 2019;56(8):513-20.
110. Baysal BE. Hereditary paraganglioma targets diverse paraganglia. Journal of medical genetics. sept 2002;39(9):617-22.
111. Burnichon N, Rohmer V, Amar L, Herman P, Leboulleux S, Darrouzet V, et al. The succinate dehydrogenase genetic testing in a large prospective series of patients with paragangliomas. The Journal of clinical endocrinology and metabolism [Internet]. 19 mai 2009; Disponible sur: http://www.ncbi.nlm.nih.gov/entrez/query.fcgi?cmd=Retrieve&db=PubMed&dopt=Citation&list_uids=19454582
112. Morin A, Letouze E, Gimenez-Roqueplo AP, Favier J. Oncometabolites-driven tumorigenesis: From genetics to targeted therapy. International journal of cancer Journal international du cancer. 15 nov 2014;135(10):2237-48.

113. Letouze E, Martinelli C, Loriot C, Burnichon N, Abermil N, Ottolenghi C, et al. SDH mutations establish a hypermethylator phenotype in paraganglioma. Cancer cell. 2013/05/28 éd. 10 juin 2013;23(6):739-52.
114. Hederstedt L. Structural biology. Complex II is complex too. Science. 2003/02/01 éd. 31 janv 2003;299(5607):671-2.
115. Pigny P, Vincent A, Cardot Bauters C, Bertrand M, de Montpreville VT, Crepin M, et al. Paraganglioma after maternal transmission of a succinate dehydrogenase gene mutation. J Clin Endocrinol Metab. 2008/01/24 éd. mai 2008;93(5):1609-15.
116. Bayley J-P, Oldenburg RA, Nuk J, Hoekstra AS, van der Meer CA, Korpershoek E, et al. Paraganglioma and pheochromocytoma upon maternal transmission of SDHD mutations. BMC Med Genet. 10 oct 2014;15:111.
117. Burnichon N, Mazzella J-M, Drui D, Amar L, Bertherat J, Coupier I, et al. Risk assessment of maternally inherited SDHD paraganglioma and phaeochromocytoma. J Med Genet. 2017;54(2):125-33.
118. Pasini B, Stratakis CA. SDH mutations in tumorigenesis and inherited endocrine tumours: lesson from the phaeochromocytoma-paraganglioma syndromes. J Intern Med. 2009/06/16 éd. juill 2009;266(1):19-42.
119. Niemann S, Muller U. Mutations in SDHC cause autosomal dominant paraganglioma, type 3. Nat Genet. 2000/11/04 éd. nov 2000;26(3):268-70.
120. Schiavi F, Boedeker CC, Bausch B, Peczkowska M, Gomez CF, Strassburg T, et al. Predictors and prevalence of paraganglioma syndrome associated with mutations of the SDHC gene. JAMA. 2005/10/27 éd. 26 oct 2005;294(16):2057-63.
121. Benn DE, Gimenez-Roqueplo AP, Reilly JR, Bertherat J, Burgess J, Byth K, et al. Clinical presentation and penetrance of pheochromocytoma/paraganglioma syndromes. J Clin Endocrinol Metab. 2005/12/01 éd. mars 2006;91(3):827-36.
122. Cascon A, Landa I, Lopez-Jimenez E, Diez-Hernandez A, Buchta M, Montero-Conde C, et al. Molecular characterisation of a common SDHB deletion in paraganglioma patients. J Med Genet. 2007/12/07 éd. avr 2008;45(4):233-8.
123. Eisenhofer G, Timmers HJ, Lenders JW, Bornstein SR, Tiebel O, Mannelli M, et al. Age at diagnosis of pheochromocytoma differs according to catecholamine phenotype and tumor location. J Clin Endocrinol Metab. 2010/12/15 éd. févr 2011;96(2):375-84.
124. Benn DE, Gimenez-Roqueplo A-P, Reilly JR, Bertherat J, Burgess J, Byth K, et al. Clinical presentation and penetrance of pheochromocytoma/paraganglioma syndromes. J Clin Endocrinol Metab. mars 2006;91(3):827-36.
125. Ricketts CJ, Forman JR, Rattenberry E, Bradshaw N, Lalloo F, Izatt L, et al. Tumor risks and genotype-phenotype-proteotype analysis in 358 patients with germline mutations in SDHB and SDHD. Hum Mutat. 2009/10/06 éd. janv 2010;31(1):41-51.
126. Gimenez-Roqueplo A-P, Favier J, Rustin P, Rieubland C, Crespin M, Nau V, et al. Mutations in the SDHB Gene Are Associated with Extra-adrenal and/or Malignant Phaeochromocytomas. Cancer Res. 1 sept 2003;63(17):5615-21.
127. Amar L, Fassnacht M, Gimenez-Roqueplo AP, Januszewicz A, Prejbisz A, Timmers H, et al. Long-term postoperative follow-up in patients with apparently benign pheochromocytoma and paraganglioma. Horm Metab Res. 2012/02/22 éd. mai 2012;44(5):385-9.
128. Assadipour Y, Sadowski SM, Alimchandani M, Quezado M, Steinberg SM, Nilubol N, et al. SDHB mutation status and tumor size but not tumor grade are important predictors of clinical outcome in pheochromocytoma and abdominal paraganglioma. Surgery.

2017;161(1):230-9.
129. Gimenez-Roqueplo AP, Favier J, Rustin P, Rieubland C, Kerlan V, Plouin PF, et al. Functional consequences of a SDHB gene mutation in an apparently sporadic pheochromocytoma. J Clin Endocrinol Metab. 2002/10/05 éd. oct 2002;87(10):4771-4.
130. King KS, Prodanov T, Kantorovich V, Fojo T, Hewitt JK, Zacharin M, et al. Metastatic Pheochromocytoma/Paraganglioma Related to Primary Tumor Development in Childhood or Adolescence: Significant Link to SDHB Mutations. JCO. 3 oct 2011;29(31):4137-42.
131. Bausch B, Wellner U, Bausch D, Schiavi F, Barontini M, Sanso G, et al. Long-term prognosis of patients with pediatric pheochromocytoma. Endocr Relat Cancer. févr 2014;21(1):17-25.
132. Amar L, Baudin E, Burnichon N, Peyrard S, Silvera S, Bertherat J, et al. Succinate Dehydrogenase B Gene Mutations Predict Survival in Patients with Malignant Pheochromocytomas or Paragangliomas. J Clin Endocrinol Metab. 1 oct 2007;92(10):3822-8.
133. Hescot S, Curras-Freixes M, Deutschbein T, van Berkel A, Vezzosi D, Amar L, et al. Prognosis of Malignant Pheochromocytoma and Paraganglioma (MAPP-Prono Study): A European Network for the Study of Adrenal Tumors Retrospective Study. J Clin Endocrinol Metab. 1 juin 2019;104(6):2367-74.
134. Buffet A, Ben Aim L, Leboulleux S, Drui D, Vezzosi D, Libé R, et al. Positive Impact of Genetic Test on the Management and Outcome of Patients With Paraganglioma and/or Pheochromocytoma. J Clin Endocrinol Metab. 1 avr 2019;104(4):1109-18.
135. Hao HX, Khalimonchuk O, Schraders M, Dephoure N, Bayley JP, Kunst H, et al. SDH5, a gene required for flavination of succinate dehydrogenase, is mutated in paraganglioma. Science. 2009/07/25 éd. 28 août 2009;325(5944):1139-42.
136. Bayley JP, Kunst HP, Cascon A, Sampietro ML, Gaal J, Korpershoek E, et al. SDHAF2 mutations in familial and sporadic paraganglioma and phaeochromocytoma. Lancet oncol. 2010/01/15 éd. avr 2010;11(4):366-72.
137. Kunst HP, Rutten MH, de Monnink JP, Hoefsloot LH, Timmers HJ, Marres HA, et al. SDHAF2 (PGL2-SDH5) and hereditary head and neck paraganglioma. Clin Cancer Res. 2011/01/13 éd. 15 janv 2011;17(2):247-54.
138. Burnichon N, Briere JJ, Libe R, Vescovo L, Riviere J, Tissier F, et al. SDHA is a tumor suppressor gene causing paraganglioma. Hum Mol Genet. 2010/05/21 éd. 1 août 2010;19(15):3011-20.
139. van der Tuin K, Mensenkamp AR, Tops CMJ, Corssmit EPM, Dinjens WN, van de Horst-Schrivers ANA, et al. Clinical Aspects of SDHA-Related Pheochromocytoma and Paraganglioma: A Nationwide Study. J Clin Endocrinol Metab. 01 2018;103(2):438-45.
140. Gill AJ, Hes O, Papathomas T, Šedivcová M, Tan PH, Agaimy A, et al. Succinate dehydrogenase (SDH)-deficient renal carcinoma: a morphologically distinct entity: a clinicopathologic series of 36 tumors from 27 patients. Am J Surg Pathol. déc 2014;38(12):1588-602.
141. Andrews KA, Ascher DB, Pires DEV, Barnes DR, Vialard L, Casey RT, et al. Tumour risks and genotype-phenotype correlations associated with germline variants in succinate dehydrogenase subunit genes SDHB, SDHC and SDHD. J Med Genet. 2018;55(6):384-94.
142. McWhinney SR, Pasini B, Stratakis CA. Familial gastrointestinal stromal tumors and germ-line mutations. N Engl J Med. 2007/09/07 éd. 6 sept 2007;357(10):1054-6.
143. Pasini B, McWhinney SR, Bei T, Matyakhina L, Stergiopoulos S, Muchow M, et al. Clinical and molecular genetics of patients with the Carney-Stratakis syndrome and germline mutations of the genes coding for the succinate dehydrogenase subunits SDHB, SDHC, and

SDHD. Eur J Hum Genet. 2007/08/02 éd. janv 2008;16(1):79-88.
144. Stratakis CA, Carney JA. The triad of paragangliomas, gastric stromal tumours and pulmonary chondromas (Carney triad), and the dyad of paragangliomas and gastric stromal sarcomas (Carney–Stratakis syndrome): molecular genetics and clinical implications. J Intern Med. juill 2009;266(1):43-52.
145. Janeway KA, Kim SY, Lodish M, Nose V, Rustin P, Gaal J, et al. Defects in succinate dehydrogenase in gastrointestinal stromal tumors lacking KIT and PDGFRA mutations. Proc Natl Acad Sci U S A. 2010/12/22 éd. 4 janv 2011;108(1):314-8.
146. Nakahara M, Isozaki K, Hirota S, Miyagawa J-I, Hase-Sawada N, Taniguchi M, et al. A novel gain-of-function mutation of c-kit gene in gastrointestinal stromal tumors. Gastroenterology. 1 nov 1998;115(5):1090-5.
147. Boikos SA, Pappo AS, Killian JK, LaQuaglia MP, Weldon CB, George S, et al. Molecular Subtypes of KIT/PDGFRA Wild-Type Gastrointestinal Stromal Tumors: A Report From the National Institutes of Health Gastrointestinal Stromal Tumor Clinic. JAMA oncology [Internet]. 24 mars 2016; Disponible sur: http://www.ncbi.nlm.nih.gov/pubmed/27011036
148. Oudijk L, Gaal J, Korpershoek E, van Nederveen FH, Kelly L, Schiavon G, et al. SDHA mutations in adult and pediatric wild-type gastrointestinal stromal tumors. Modern pathology : an official journal of the United States and Canadian Academy of Pathology, Inc. 2012/11/24 éd. mars 2013;26(3):456-63.
149. Wagner AJ, Remillard SP, Zhang YX, Doyle LA, George S, Hornick JL. Loss of expression of SDHA predicts SDHA mutations in gastrointestinal stromal tumors. Modern pathology : an official journal of the United States and Canadian Academy of Pathology, Inc. 2012/09/08 éd. févr 2013;26(2):289-94.
150. Killian JK, Miettinen M, Walker RL, Wang Y, Zhu YJ, Waterfall JJ, et al. Recurrent epimutation of SDHC in gastrointestinal stromal tumors. Sci Transl Med. 24 déc 2014;6(268):268ra177.
151. Xekouki P, Szarek E, Bullova P, Giubellino A, Quezado M, Mastroyannis SA, et al. Pituitary Adenoma With Paraganglioma/Pheochromocytoma (3PAs) and Succinate Dehydrogenase Defects in Humans and Mice. J Clin Endocrinol Metab. mai 2015;100(5):E710-9.
152. Xekouki P, Pacak K, Almeida M, Wassif CA, Rustin P, Nesterova M, et al. Succinate dehydrogenase (SDH) D subunit (SDHD) inactivation in a growth-hormone-producing pituitary tumor: a new association for SDH? J Clin Endocrinol Metab. 2011/12/16 éd. mars 2012;97(3):E357-66.
153. Zinn AB, Kerr DS, Hoppel CL. Fumarase Deficiency: A New Cause of Mitochondrial Encephalomyopathy. New England Journal of Medicine. 21 août 1986;315(8):469-75.
154. Bourgeron T, Chretien D, Poggi-Bach J, Doonan S, Rabier D, Letouzé P, et al. Mutation of the fumarase gene in two siblings with progressive encephalopathy and fumarase deficiency. J Clin Invest. juin 1994;93(6):2514-8.
155. Tomlinson IP, Alam NA, Rowan AJ, Barclay E, Jaeger EE, Kelsell D, et al. Germline mutations in FH predispose to dominantly inherited uterine fibroids, skin leiomyomata and papillary renal cell cancer. Nature genetics. 2002/02/28 éd. avr 2002;30(4):406-10.
156. Alam NA, Rowan AJ, Wortham NC, Pollard PJ, Mitchell M, Tyrer JP, et al. Genetic and functional analyses of FH mutations in multiple cutaneous and uterine leiomyomatosis, hereditary leiomyomatosis and renal cancer, and fumarate hydratase deficiency. Human molecular genetics. 2003/05/23 éd. 1 juin 2003;12(11):1241-52.
157. Gardie B, Remenieras A, Kattygnarath D, Bombled J, Lefevre S, Perrier-Trudova V, et

al. Novel FH mutations in families with hereditary leiomyomatosis and renal cell cancer (HLRCC) and patients with isolated type 2 papillary renal cell carcinoma. Journal of medical genetics. 2011/03/15 éd. avr 2011;48(4):226-34.
158. Menko FH, Maher ER, Schmidt LS, Middelton LA, Aittomäki K, Tomlinson I, et al. Hereditary leiomyomatosis and renal cell cancer (HLRCC): renal cancer risk, surveillance and treatment. Fam Cancer. déc 2014;13(4):637-44.
159. Muller M, Ferlicot S, Guillaud-Bataille M, Le Teuff G, Genestie C, Deveaux S, et al. Reassessing the clinical spectrum associated with hereditary leiomyomatosis and renal cell carcinoma syndrome in French FH mutation carriers. Clin Genet. déc 2017;92(6):606-15.
160. Letouzé E, Martinelli C, Loriot C, Burnichon N, Abermil N, Ottolenghi C, et al. SDH Mutations Establish a Hypermethylator Phenotype in Paraganglioma. Cancer Cell. 10 juin 2013;23(6):739-52.
161. Castro-Vega LJ, Buffet A, De Cubas AA, Cascon A, Menara M, Khalifa E, et al. Germline mutations in FH confer predisposition to malignant pheochromocytomas and paragangliomas. Human molecular genetics. 1 mai 2014;23(9):2440-6.
162. Clark GR, Sciacovelli M, Gaude E, Walsh DM, Kirby G, Simpson MA, et al. Germline FH mutations presenting with pheochromocytoma. J Clin Endocrinol Metab. oct 2014;99(10):E2046-2050.
163. Qin Y, Yao L, King EE, Buddavarapu K, Lenci RE, Chocron ES, et al. Germline mutations in TMEM127 confer susceptibility to pheochromocytoma. Nature genetics. mars 2010;42(3):229-33.
164. Abermil N, Guillaud-Bataille M, Burnichon N, Venisse A, Manivet P, Guignat L, et al. TMEM127 screening in a large cohort of patients with pheochromocytoma and/or paraganglioma. The Journal of clinical endocrinology and metabolism. 2012/03/16 éd. mai 2012;97(5):E805-9.
165. Yao L, Schiavi F, Cascon A, Qin Y, Inglada-Perez L, King EE, et al. Spectrum and prevalence of FP/TMEM127 gene mutations in pheochromocytomas and paragangliomas. JAMA. 2010/12/16 éd. 15 déc 2010;304(23):2611-9.
166. Toledo SPA, Lourenço DM, Sekiya T, Lucon AM, Baena MES, Castro CC, et al. Penetrance and clinical features of pheochromocytoma in a six-generation family carrying a germline TMEM127 mutation. J Clin Endocrinol Metab. févr 2015;100(2):E308-318.
167. Qin Y, Deng Y, Ricketts CJ, Srikantan S, Wang E, Maher ER, et al. The tumor susceptibility gene TMEM127 is mutated in renal cell carcinomas and modulates endolysosomal function. Hum Mol Genet. 1 mai 2014;23(9):2428-39.
168. Comino-Mendez I, Gracia-Aznarez FJ, Schiavi F, Landa I, Leandro-Garcia LJ, Leton R, et al. Exome sequencing identifies MAX mutations as a cause of hereditary pheochromocytoma. Nat Genet. 2011/06/21 éd. juill 2011;43(7):663-7.
169. Burnichon N, Cascon A, Schiavi F, Morales NP, Comino-Mendez I, Abermil N, et al. MAX mutations cause hereditary and sporadic pheochromocytoma and paraganglioma. Clinical cancer research : an official journal of the American Association for Cancer Research. 2012/03/29 éd. 15 mai 2012;18(10):2828-37.
170. Grandori C, Cowley SM, James LP, Eisenman RN. The Myc/Max/Mad network and the transcriptional control of cell behavior. Annu Rev Cell Dev Biol. 2000/10/14 éd. 2000;16:653-99.
171. Castro-Vega LJ, Letouzé E, Burnichon N, Buffet A, Disderot P-H, Khalifa E, et al. Multi-omics analysis defines core genomic alterations in pheochromocytomas and paragangliomas. Nature Communications. 27 janv 2015;6(1):6044.

172. Behjati S, Tarpey PS, Presneau N, Scheipl S, Pillay N, Van Loo P, et al. Distinct H3F3A and H3F3B driver mutations define chondroblastoma and giant cell tumor of bone. Nat Genet. déc 2013;45(12):1479-82.
173. Remacha L, Currás-Freixes M, Torres-Ruiz R, Schiavi F, Torres-Pérez R, Calsina B, et al. Gain-of-function mutations in DNMT3A in patients with paraganglioma. Genetics in Medicine. déc 2018;20(12):1644-51.
174. Schlisio S, Kenchappa RS, Vredeveld LC, George RE, Stewart R, Greulich H, et al. The kinesin KIF1Bbeta acts downstream from EglN3 to induce apoptosis and is a potential 1p36 tumor suppressor. Genes Dev. 2008/03/13 éd. 1 avr 2008;22(7):884-93.
175. Yeh IT, Lenci RE, Qin Y, Buddavarapu K, Ligon AH, Leteurtre E, et al. A germline mutation of the KIF1B beta gene on 1p36 in a family with neural and nonneural tumors. Hum Genet. 2008/08/30 éd. oct 2008;124(3):279-85.
176. Welander J, Andreasson A, Juhlin CC, Wiseman RW, Bäckdahl M, Höög A, et al. Rare germline mutations identified by targeted next-generation sequencing of susceptibility genes in pheochromocytoma and paraganglioma. J Clin Endocrinol Metab. juill 2014;99(7):E1352-1360.
177. Flynn A, Benn D, Clifton-Bligh R, Robinson B, Trainer AH, James P, et al. The genomic landscape of phaeochromocytoma. J Pathol. mai 2015;236(1):78-89.
178. Burnichon N, Vescovo L, Amar L, Libé R, de Reynies A, Venisse A, et al. Integrative genomic analysis reveals somatic mutations in pheochromocytoma and paraganglioma. Hum Mol Genet. 15 oct 2011;20(20):3974-85.
179. Fishbein L, Leshchiner I, Walter V, Danilova L, Robertson AG, Johnson AR, et al. Comprehensive Molecular Characterization of Pheochromocytoma and Paraganglioma. Cancer Cell. 13 févr 2017;31(2):181-93.
180. Crona J, Delgado Verdugo A, Maharjan R, Stålberg P, Granberg D, Hellman P, et al. Somatic mutations in H-RAS in sporadic pheochromocytoma and paraganglioma identified by exome sequencing. J Clin Endocrinol Metab. juill 2013;98(7):E1266-1271.
181. Juhlin CC, Stenman A, Haglund F, Clark VE, Brown TC, Baranoski J, et al. Whole-exome sequencing defines the mutational landscape of pheochromocytoma and identifies KMT2D as a recurrently mutated gene. Genes Chromosomes Cancer. sept 2015;54(9):542-54.
182. Crona J, Nordling M, Maharjan R, Granberg D, Stålberg P, Hellman P, et al. Integrative genetic characterization and phenotype correlations in pheochromocytoma and paraganglioma tumours. PLoS ONE. 2014;9(1):e86756.
183. Fishbein L, Khare S, Wubbenhorst B, DeSloover D, D'Andrea K, Merrill S, et al. Whole-exome sequencing identifies somatic ATRX mutations in pheochromocytomas and paragangliomas. Nat Commun. 21 janv 2015;6(1):1-6.
184. Castro-Vega LJ, Lepoutre-Lussey C, Gimenez-Roqueplo AP, Favier J. Rethinking pheochromocytomas and paragangliomas from a genomic perspective. Oncogene. 3 mars 2016;35(9):1080-9.
185. Comino-Méndez I, Tejera ÁM, Currás-Freixes M, Remacha L, Gonzalvo P, Tonda R, et al. ATRX driver mutation in a composite malignant pheochromocytoma. Cancer Genet. 2016;209(6):272-7.
186. Plouin PF, Amar L, Dekkers OM, Fassnacht M, Gimenez-Roqueplo AP, Lenders JWM, et al. European Society of Endocrinology Clinical Practice Guideline for long-term follow-up of patients operated on for a phaeochromocytoma or a paraganglioma. European Journal of Endocrinology. 1 mai 2016;174(5):G1-10.
187. Korpershoek E, Favier J, Gaal J, Burnichon N, van Gessel B, Oudijk L, et al. SDHA

immunohistochemistry detects germline SDHA gene mutations in apparently sporadic paragangliomas and pheochromocytomas. The Journal of clinical endocrinology and metabolism. 2011/07/15 éd. sept 2011;96(9):E1472-6.
188. van Nederveen FH, Gaal J, Favier J, Korpershoek E, Oldenburg RA, de Bruyn EM, et al. An immunohistochemical procedure to detect patients with paraganglioma and phaeochromocytoma with germline SDHB, SDHC, or SDHD gene mutations: a retrospective and prospective analysis. Lancet oncol. 2009/07/07 éd. août 2009;10(8):764-71.
189. Ben Aim L, Pigny P, Castro-Vega LJ, Buffet A, Amar L, Bertherat J, et al. Targeted next-generation sequencing detects rare genetic events in pheochromocytoma and paraganglioma. J Med Genet. 2019;56(8):513-20.
190. NGS in PPGL (NGSnPPGL) Study Group, Toledo RA, Burnichon N, Cascon A, Benn DE, Bayley J-P, et al. Consensus Statement on next-generation-sequencing-based diagnostic testing of hereditary phaeochromocytomas and paragangliomas. Nat Rev Endocrinol. 2017;13(4):233-47.
191. Gill AJ, Benn DE, Chou A, Clarkson A, Muljono A, Meyer-Rochow GY, et al. Immunohistochemistry for SDHB triages genetic testing of SDHB, SDHC, and SDHD in paraganglioma-pheochromocytoma syndromes. Human pathology [Internet]. 16 mars 2010; Disponible sur: http://www.ncbi.nlm.nih.gov/entrez/query.fcgi?cmd=Retrieve&db=PubMed&dopt=Citation&list_uids=20236688
192. Papathomas TG, Oudijk L, Persu A, Gill AJ, van Nederveen F, Tischler AS, et al. SDHB/SDHA immunohistochemistry in pheochromocytomas and paragangliomas: a multicenter interobserver variation analysis using virtual microscopy: a Multinational Study of the European Network for the Study of Adrenal Tumors (ENS@T). Modern pathology : an official journal of the United States and Canadian Academy of Pathology, Inc. juin 2015;28(6):807-21.
193. Menara M, Oudijk L, Badoual C, Bertherat J, Lepoutre-Lussey C, Amar L, et al. SDHD Immunohistochemistry: A New Tool to Validate SDHx Mutations in Pheochromocytoma/Paraganglioma. J Clin Endocrinol Metab. 1 févr 2015;100(2):E287-91.
194. Hoekstra AS, de Graaff MA, Briaire-de Bruijn IH, Ras C, Seifar RM, van Minderhout I, et al. Inactivation of SDH and FH cause loss of 5hmC and increased H3K9me3 in paraganglioma/pheochromocytoma and smooth muscle tumors. Oncotarget. 12 oct 2015;6(36):38777-88.
195. Favier J, Meatchi T, Robidel E, Badoual C, Sibony M, Nguyen AT, et al. Carbonic anhydrase 9 immunohistochemistry as a tool to predict or validate germline and somatic VHL mutations in pheochromocytoma and paraganglioma-a retrospective and prospective study. Mod Pathol. 2020;33(1):57-64.
196. Favier J, Amar L, Gimenez-Roqueplo A-P. Paraganglioma and phaeochromocytoma: from genetics to personalized medicine. Nat Rev Endocrinol. févr 2015;11(2):101-11.
197. Richter S, Gieldon L, Pang Y, Peitzsch M, Huynh T, Leton R, et al. Metabolome-guided genomics to identify mutations in isocitrate dehydrogenase, fumarate hydratase and succinate dehydrogenase genes in pheochromocytoma and paraganglioma. Genet Med. mars 2019;21(3):705-17.
198. Wallace PW, Conrad C, Brückmann S, Pang Y, Caleiras E, Murakami M, et al. Metabolomics, machine learning and immunohistochemistry to predict succinate dehydrogenase mutational status in phaeochromocytomas and paragangliomas. The Journal of Pathology. 2020;251(4):378-87.

199. Imperiale A, Moussallieh FM, Roche P, Battini S, Cicek AE, Sebag F, et al. Metabolome profiling by HRMAS NMR spectroscopy of pheochromocytomas and paragangliomas detects SDH deficiency: clinical and pathophysiological implications. Neoplasia. janv 2015;17(1):55-65.
200. Lussey-Lepoutre C, Bellucci A, Morin A, Buffet A, Amar L, Janin M, et al. In Vivo Detection of Succinate by Magnetic Resonance Spectroscopy as a Hallmark of SDHx Mutations in Paraganglioma. Clinical cancer research : an official journal of the American Association for Cancer Research. 1 mars 2016;22(5):1120-9.
201. Lussey-Lepoutre C, Bellucci A, Burnichon N, Amar L, Buffet A, Drossart T, et al. Succinate detection using in vivo 1H-MR spectroscopy identifies germline and somatic SDHx mutations in paragangliomas. Eur J Nucl Med Mol Imaging. juin 2020;47(6):1510-7.
202. Chrisoulidou A, Kaltsas G, Ilias I, Grossman AB. The diagnosis and management of malignant phaeochromocytoma and paraganglioma. Endocr Relat Cancer. 2007/10/05 éd. sept 2007;14(3):569-85.
203. Goldstein RE, O'Neill JA, Holcomb GW, Morgan WM, Neblett WW, Oates JA, et al. Clinical experience over 48 years with pheochromocytoma. Ann Surg. juin 1999;229(6):755-64; discussion 764-766.
204. Park J, Song C, Park M, Yoo S, Park SJ, Hong S, et al. Predictive Characteristics of Malignant Pheochromocytoma. Korean J Urol. avr 2011;52(4):241-6.
205. Ayala-Ramirez M, Feng L, Johnson MM, Ejaz S, Habra MA, Rich T, et al. Clinical risk factors for malignancy and overall survival in patients with pheochromocytomas and sympathetic paragangliomas: primary tumor size and primary tumor location as prognostic indicators. J Clin Endocrinol Metab. mars 2011;96(3):717-25.
206. Schovanek J, Martucci V, Wesley R, Fojo T, del Rivero J, Huynh T, et al. The size of the primary tumor and age at initial diagnosis are independent predictors of the metastatic behavior and survival of patients with SDHB-related pheochromocytoma and paraganglioma: a retrospective cohort study. BMC Cancer. 21 juill 2014;14:523.
207. Agarwal A, Mehrotra PK, Jain M, Gupta SK, Mishra A, Chand G, et al. Size of the tumor and pheochromocytoma of the adrenal gland scaled score (PASS): can they predict malignancy? World J Surg. déc 2010;34(12):3022-8.
208. Kimura N, Takayanagi R, Takizawa N, Itagaki E, Katabami T, Kakoi N, et al. Pathological grading for predicting metastasis in phaeochromocytoma and paraganglioma. Endocr Relat Cancer. juin 2014;21(3):405-14.
209. Calsina B, Castro-Vega LJ, Torres-Pérez R, Inglada-Pérez L, Currás-Freixes M, Roldán-Romero JM, et al. Integrative multi-omics analysis identifies a prognostic miRNA signature and a targetable miR-21-3p/TSC2/mTOR axis in metastatic pheochromocytoma/paraganglioma. Theranostics. 2019;9(17):4946-58.
210. Zhang J, Cong R, Zhang Q, Zeng T, Song R, Meng X. Integrative analysis of ceRNA network and DNA methylation associated with gene expression in malignant pheochromocytomas: a study based on The Cancer Genome Atlas. Translational Andrology and Urology. 10 mars 2020;9(2):344-54.
211. Job S, Georges A, Burnichon N, Buffet A, Amar L, Bertherat J, et al. Transcriptome Analysis of lncRNAs in Pheochromocytomas and Paragangliomas. J Clin Endocrinol Metab. 1 mars 2020;105(3):898-907.
212. Job S, Draskovic I, Burnichon N, Buffet A, Cros J, Lépine C, et al. Telomerase Activation and ATRX Mutations Are Independent Risk Factors for Metastatic Pheochromocytoma and Paraganglioma. Clin Cancer Res. 15 janv 2019;25(2):760-70.

213. Plouin PF, Duclos JM, Soppelsa F, Boublil G, Chatellier G. Factors associated with perioperative morbidity and mortality in patients with pheochromocytoma: analysis of 165 operations at a single center. The Journal of clinical endocrinology and metabolism. avr 2001;86(4):1480-6.
214. Pacak K. Preoperative management of the pheochromocytoma patient. J Clin Endocrinol Metab. nov 2007;92(11):4069-79.
215. Castinetti F, Qi X-P, Walz MK, Maia AL, Sansó G, Peczkowska M, et al. Outcomes of adrenal-sparing surgery or total adrenalectomy in phaeochromocytoma associated with multiple endocrine neoplasia type 2: an international retrospective population-based study. Lancet Oncol. mai 2014;15(6):648-55.
216. Volkin D, Yerram N, Ahmed F, Lankford D, Baccala A, Gupta GN, et al. Partial adrenalectomy minimizes the need for long-term hormone replacement in pediatric patients with pheochromocytoma and von Hippel-Lindau syndrome. J Pediatr Surg. nov 2012;47(11):2077-82.
217. Lim J-Y, Kim J, Kim SH, Lee S, Lim YC, Kim JW, et al. Surgical treatment of carotid body paragangliomas: outcomes and complications according to the shamblin classification. Clin Exp Otorhinolaryngol. juin 2010;3(2):91-5.
218. Adjalle R, Plouin PF, Pacak K, Lehnert H. Treatment of malignant pheochromocytoma. Hormone and metabolic research = Hormon- und Stoffwechselforschung = Hormones et metabolisme. 2009/08/13 éd. sept 2009;41(9):687-96.
219. Dupin C, Lang P, Dessard-Diana B, Simon J-M, Cuenca X, Mazeron J-J, et al. Treatment of head and neck paragangliomas with external beam radiation therapy. Int J Radiat Oncol Biol Phys. 1 juin 2014;89(2):353-9.
220. Liscak R, Urgosik D, Chytka T, Simonova G, Novotny J, Vymazal J, et al. Leksell Gamma Knife radiosurgery of the jugulotympanic glomus tumor: long-term results. J Neurosurg. déc 2014;121 Suppl:198-202.
221. Gilbo P, Morris CG, Amdur RJ, Werning JW, Dziegielewski PT, Kirwan J, et al. Radiotherapy for benign head and neck paragangliomas: a 45-year experience. Cancer. 1 déc 2014;120(23):3738-43.
222. Cao KI, Feuvret L, Herman P, Bolle S, Jouffroy T, Goudjil F, et al. Protontherapy of head and neck paragangliomas: A monocentric study. Cancer/Radiothérapie. 1 févr 2018;22(1):31-7.
223. Baudin E, Habra MA, Deschamps F, Cote G, Dumont F, Cabanillas M, et al. Therapy of endocrine disease: treatment of malignant pheochromocytoma and paraganglioma. Eur J Endocrinol. sept 2014;171(3):R111-122.
224. van Hulsteijn LT, Niemeijer ND, Dekkers OM, Corssmit EPM. (131)I-MIBG therapy for malignant paraganglioma and phaeochromocytoma: systematic review and meta-analysis. Clin Endocrinol (Oxf). avr 2014;80(4):487-501.
225. Huang H, Abraham J, Hung E, Averbuch S, Merino M, Steinberg SM, et al. Treatment of malignant pheochromocytoma/paraganglioma with cyclophosphamide, vincristine, and dacarbazine: recommendation from a 22-year follow-up of 18 patients. Cancer. 15 oct 2008;113(8):2020-8.
226. Ayala-Ramirez M, Feng L, Habra MA, Rich T, Dickson PV, Perrier N, et al. Clinical benefits of systemic chemotherapy for patients with metastatic pheochromocytomas or sympathetic extra-adrenal paragangliomas: insights from the largest single-institutional experience. Cancer. 1 juin 2012;118(11):2804-12.
227. Nomura K, Kimura H, Shimizu S, Kodama H, Okamoto T, Obara T, et al. Survival of

Patients with Metastatic Malignant Pheochromocytoma and Efficacy of Combined Cyclophosphamide, Vincristine, and Dacarbazine Chemotherapy. J Clin Endocrinol Metab. 1 août 2009;94(8):2850-6.
228. Hadoux J, Favier J, Scoazec JY, Leboulleux S, Al Ghuzlan A, Caramella C, et al. SDHB mutations are associated with response to temozolomide in patients with metastatic pheochromocytoma or paraganglioma. International journal of cancer Journal international du cancer. 1 déc 2014;135(11):2711-20.
229. Favier J, Briere JJ, Burnichon N, Riviere J, Vescovo L, Benit P, et al. The Warburg effect is genetically determined in inherited pheochromocytomas. PLoS One. 2009/09/19 éd. 2009;4(9):e7094.
230. Pollard PJ, El-Bahrawy M, Poulsom R, Elia G, Killick P, Kelly G, et al. Expression of HIF-1alpha, HIF-2alpha (EPAS1), and their target genes in paraganglioma and pheochromocytoma with VHL and SDH mutations. J Clin Endocrinol Metab. 2006/09/07 éd. nov 2006;91(11):4593-8.
231. Eisenhofer G, Walther MM, Huynh TT, Li ST, Bornstein SR, Vortmeyer A, et al. Pheochromocytomas in von Hippel-Lindau syndrome and multiple endocrine neoplasia type 2 display distinct biochemical and clinical phenotypes. J Clin Endocrinol Metab. 2001/05/10 éd. mai 2001;86(5):1999-2008.
232. Favier J, Igaz P, Burnichon N, Amar L, Libe R, Badoual C, et al. Rationale for anti-angiogenic therapy in pheochromocytoma and paraganglioma. Endocrine pathology. 2011/12/21 éd. mars 2012;23(1):34-42.
233. Hahn NM, Reckova M, Cheng L, Baldridge LA, Cummings OW, Sweeney CJ. Patient with malignant paraganglioma responding to the multikinase inhibitor sunitinib malate. J Clin Oncol. 2008/12/10 éd. 20 janv 2009;27(3):460-3.
234. Jimenez C, Cabanillas ME, Santarpia L, Jonasch E, Kyle KL, Lano EA, et al. Use of the tyrosine kinase inhibitor sunitinib in a patient with von Hippel-Lindau disease: targeting angiogenic factors in pheochromocytoma and other von Hippel-Lindau disease-related tumors. J Clin Endocrinol Metab. 2008/11/20 éd. févr 2009;94(2):386-91.
235. Joshua AM, Ezzat S, Asa SL, Evans A, Broom R, Freeman M, et al. Rationale and evidence for sunitinib in the treatment of malignant paraganglioma/pheochromocytoma. The Journal of clinical endocrinology and metabolism. 2008/11/13 éd. janv 2009;94(1):5-9.
236. Park KS, Lee JL, Ahn H, Koh JM, Park I, Choi JS, et al. Sunitinib, a novel therapy for anthracycline- and cisplatin-refractory malignant pheochromocytoma. Japanese journal of clinical oncology. 2009/03/07 éd. mai 2009;39(5):327-31.
237. Ayala-Ramirez M, Chougnet CN, Habra MA, Palmer JL, Leboulleux S, Cabanillas ME, et al. Treatment with sunitinib for patients with progressive metastatic pheochromocytomas and sympathetic paragangliomas. The Journal of clinical endocrinology and metabolism. 2012/09/12 éd. nov 2012;97(11):4040-50.
238. O'Kane GM, Ezzat S, Joshua AM, Bourdeau I, Leibowitz-Amit R, Olney HJ, et al. A phase 2 trial of sunitinib in patients with progressive paraganglioma or pheochromocytoma: the SNIPP trial. British Journal of Cancer. juin 2019;120(12):1113-9.
239. Jimenez C, Fazeli S, Román-Gonzalez A. Antiangiogenic therapies for pheochromocytoma and paraganglioma. Endocr Relat Cancer. juill 2020;27(7):R239-54.
240. Herrmann E, Bierer S, Wülfing C. Update on systemic therapies of metastatic renal cell carcinoma. World J Urol. juin 2010;28(3):303-9.
241. Dahia PL, Ross KN, Wright ME, Hayashida CY, Santagata S, Barontini M, et al. A HIF1alpha regulatory loop links hypoxia and mitochondrial signals in pheochromocytomas.

PLoS Genet. juill 2005;1(1):72-80.
242. Eisenhofer G, Huynh TT, Pacak K, Brouwers FM, Walther MM, Linehan WM, et al. Distinct gene expression profiles in norepinephrine- and epinephrine-producing hereditary and sporadic pheochromocytomas: activation of hypoxia-driven angiogenic pathways in von Hippel-Lindau syndrome. Endocr Relat Cancer. 2004/12/23 éd. déc 2004;11(4):897-911.
243. Lopez-Jimenez E, Gomez-Lopez G, Leandro-Garcia LJ, Munoz I, Schiavi F, Montero-Conde C, et al. Research resource: Transcriptional profiling reveals different pseudohypoxic signatures in SDHB and VHL-related pheochromocytomas. Mol Endocrinol. 2010/10/29 éd. déc 2010;24(12):2382-91.
244. Calsina B, Currás-Freixes M, Buffet A, Pons T, Contreras L, Letón R, et al. Role of MDH2 pathogenic variant in pheochromocytoma and paraganglioma patients. Genetics in Medicine. déc 2018;20(12):1652-62.
245. Halliwell B. Oxidative stress and neurodegeneration: where are we now? Journal of Neurochemistry. 2006;97(6):1634-58.
246. Halliwell B, Gutteridge JMC. Free Radicals in Biology and Medicine. Oxford University Press; 2015. 961 p.
247. Costa A, Scholer-Dahirel A, Mechta-Grigoriou F. The role of reactive oxygen species and metabolism on cancer cells and their microenvironment. Semin Cancer Biol. avr 2014;25:23-32.
248. Gorrini C, Harris IS, Mak TW. Modulation of oxidative stress as an anticancer strategy. Nat Rev Drug Discov. déc 2013;12(12):931-47.
249. Finkel T. Signal Transduction by Mitochondrial Oxidants. J Biol Chem. 10 févr 2012;287(7):4434-40.
250. Apel K, Hirt H. Reactive oxygen species: metabolism, oxidative stress, and signal transduction. Annu Rev Plant Biol. 2004;55:373-99.
251. Murphy MP. How mitochondria produce reactive oxygen species. Biochem J. 1 janv 2009;417(1):1-13.
252. Balaban RS, Nemoto S, Finkel T. Mitochondria, oxidants, and aging. Cell. 25 févr 2005;120(4):483-95.
253. Sena LA, Chandel NS. Physiological roles of mitochondrial reactive oxygen species. Mol Cell. 26 oct 2012;48(2):158-67.
254. Cairns RA, Harris IS, Mak TW. Regulation of cancer cell metabolism. Nat Rev Cancer. févr 2011;11(2):85-95.
255. Brand MD. The sites and topology of mitochondrial superoxide production. Exp Gerontol. août 2010;45(7-8):466-72.
256. Jensen PK. Antimycin-insensitive oxidation of succinate and reduced nicotinamide-adenine dinucleotide in electron-transport particles. I. pH dependency and hydrogen peroxide formation. Biochim Biophys Acta. 10 août 1966;122(2):157-66.
257. Forman HJ, Kennedy JA. Role of superoxide radical in mitochondrial dehydrogenase reactions. Biochem Biophys Res Commun. 8 oct 1974;60(3):1044-50.
258. Loschen G, Azzi A, Richter C, Flohé L. Superoxide radicals as precursors of mitochondrial hydrogen peroxide. FEBS Lett. 15 mai 1974;42(1):68-72.
259. Janssen-Heininger YMW, Mossman BT, Heintz NH, Forman HJ, Kalyanaraman B, Finkel T, et al. Redox-based regulation of signal transduction: principles, pitfalls, and promises. Free Radic Biol Med. 1 juill 2008;45(1):1-17.
260. Li W, Kong A-N. Molecular mechanisms of Nrf2-mediated antioxidant response. Mol Carcinog. févr 2009;48(2):91-104.

261. Sporn MB, Liby KT. NRF2 and cancer: the good, the bad and the importance of context. Nat Rev Cancer. 19 2012;12(8):564-71.
262. Taguchi K, Motohashi H, Yamamoto M. Molecular mechanisms of the Keap1–Nrf2 pathway in stress response and cancer evolution. Genes Cells. févr 2011;16(2):123-40.
263. Meister A. Glutathione deficiency produced by inhibition of its synthesis, and its reversal; applications in research and therapy. Pharmacol Ther. 1991;51(2):155-94.
264. Meister A. Selective modification of glutathione metabolism. Science. 29 avr 1983;220(4596):472-7.
265. Murphy MP. Mitochondrial thiols in antioxidant protection and redox signaling: distinct roles for glutathionylation and other thiol modifications. Antioxidants & Redox Signaling. 15 mars 2012;16(6):476-95.
266. Bouayed J, Bohn T. Exogenous antioxidants--Double-edged swords in cellular redox state: Health beneficial effects at physiologic doses versus deleterious effects at high doses. Oxid Med Cell Longev. août 2010;3(4):228-37.
267. Wilson JX. Regulation of vitamin C transport. Annu Rev Nutr. 2005;25:105-25.
268. Manz DH, Blanchette NL, Paul BT, Torti FM, Torti SV. Iron and cancer: recent insights. Ann N Y Acad Sci. 2016;1368(1):149-61.
269. Hentze MW, Muckenthaler MU, Galy B, Camaschella C. Two to tango: regulation of Mammalian iron metabolism. Cell. 9 juill 2010;142(1):24-38.
270. Torti SV, Torti FM. Iron and cancer: more ore to be mined. Nat Rev Cancer. mai 2013;13(5):342-55.
271. Chen Q, Espey MG, Krishna MC, Mitchell JB, Corpe CP, Buettner GR, et al. Pharmacologic ascorbic acid concentrations selectively kill cancer cells: action as a pro-drug to deliver hydrogen peroxide to tissues. Proc Natl Acad Sci USA. 20 sept 2005;102(38):13604-9.
272. Du J, Martin SM, Levine M, Wagner BA, Buettner GR, Wang S, et al. Mechanisms of ascorbate-induced cytotoxicity in pancreatic cancer. Clin Cancer Res. 15 janv 2010;16(2):509-20.
273. Rawal M, Schroeder SR, Wagner BA, Cushing CM, Welsh JL, Button AM, et al. Manganoporphyrins increase ascorbate-induced cytotoxicity by enhancing H2O2 generation. Cancer Res. 15 août 2013;73(16):5232-41.
274. Duarte TL, Almeida GM, Jones GDD. Investigation of the role of extracellular H2O2 and transition metal ions in the genotoxic action of ascorbic acid in cell culture models. Toxicol Lett. 5 avr 2007;170(1):57-65.
275. Sakagami H, Satoh K, Fukuchi K, Gomi K, Takeda M. Effect on an iron-chelator on ascorbate-induced cytotoxicity. Free Radic Biol Med. 1997;23(2):260-70.
276. Buettner GR, Jurkiewicz BA. Catalytic metals, ascorbate and free radicals: combinations to avoid. Radiat Res. mai 1996;145(5):532-41.
277. Clément MV, Ramalingam J, Long LH, Halliwell B. The in vitro cytotoxicity of ascorbate depends on the culture medium used to perform the assay and involves hydrogen peroxide. Antioxid Redox Signal. févr 2001;3(1):157-63.
278. Mastrangelo D, Massai L, Fioritoni G, Coco F. Vitamin C Against Cancer. In 2017.
279. Chandel NS, Maltepe E, Goldwasser E, Mathieu CE, Simon MC, Schumacker PT. Mitochondrial reactive oxygen species trigger hypoxia-induced transcription. Proc Natl Acad Sci USA. 29 sept 1998;95(20):11715-20.
280. Bell EL, Chandel NS. Mitochondrial oxygen sensing: regulation of hypoxia-inducible factor by mitochondrial generated reactive oxygen species. Essays Biochem. 2007;43:17-27.

281. Jones RG, Thompson CB. Tumor suppressors and cell metabolism: a recipe for cancer growth. Genes Dev. 1 mars 2009;23(5):537-48.
282. Hu Y, Rosen DG, Zhou Y, Feng L, Yang G, Liu J, et al. Mitochondrial manganese-superoxide dismutase expression in ovarian cancer: role in cell proliferation and response to oxidative stress. J Biol Chem. 25 nov 2005;280(47):39485-92.
283. Min JY, Lim S-O, Jung G. Downregulation of catalase by reactive oxygen species via hypermethylation of CpG island II on the catalase promoter. FEBS Lett. 3 juin 2010;584(11):2427-32.
284. Teoh-Fitzgerald MLT, Fitzgerald MP, Jensen TJ, Futscher BW, Domann FE. Genetic and epigenetic inactivation of extracellular superoxide dismutase promotes an invasive phenotype in human lung cancer by disrupting ECM homeostasis. Mol Cancer Res. janv 2012;10(1):40-51.
285. Toullec A, Gerald D, Despouy G, Bourachot B, Cardon M, Lefort S, et al. Oxidative stress promotes myofibroblast differentiation and tumour spreading. EMBO Mol Med. juin 2010;2(6):211-30.
286. Kim HM, Haraguchi N, Ishii H, Ohkuma M, Okano M, Mimori K, et al. Increased CD13 expression reduces reactive oxygen species, promoting survival of liver cancer stem cells via an epithelial-mesenchymal transition-like phenomenon. Ann Surg Oncol. juill 2012;19 Suppl 3:S539-548.
287. Diehn M, Cho RW, Lobo NA, Kalisky T, Dorie MJ, Kulp AN, et al. Association of reactive oxygen species levels and radioresistance in cancer stem cells. Nature. 9 avr 2009;458(7239):780-3.
288. Martindale JL, Holbrook NJ. Cellular response to oxidative stress: signaling for suicide and survival. J Cell Physiol. juill 2002;192(1):1-15.
289. Xu D, Rovira II, Finkel T. Oxidants painting the cysteine chapel: redox regulation of PTPs. Dev Cell. mars 2002;2(3):251-2.
290. Guzy RD, Sharma B, Bell E, Chandel NS, Schumacker PT. Loss of the SdhB, but Not the SdhA, subunit of complex II triggers reactive oxygen species-dependent hypoxia-inducible factor activation and tumorigenesis. Mol Cell Biol. 2007/10/31 éd. janv 2008;28(2):718-31.
291. Selak MA, Duran RV, Gottlieb E. Redox stress is not essential for the pseudo-hypoxic phenotype of succinate dehydrogenase deficient cells. Biochim Biophys Acta. 2006/06/27 éd. mai 2006;1757(5-6):567-72.
292. Cervera AM, Apostolova N, Crespo FL, Mata M, McCreath KJ. Cells silenced for SDHB expression display characteristic features of the tumor phenotype. Cancer research. 1 juin 2008;68(11):4058-67.
293. Pollard PJ, Briere JJ, Alam NA, Barwell J, Barclay E, Wortham NC, et al. Accumulation of Krebs cycle intermediates and over-expression of HIF1alpha in tumours which result from germline FH and SDH mutations. Hum Mol Genet. 2005/07/01 éd. 1 août 2005;14(15):2231-9.
294. Saito Y, Ishii K, Aita Y, Ikeda T, Kawakami Y, Shimano H, et al. Loss of SDHB Elevates Catecholamine Synthesis and Secretion Depending on ROS Production and HIF Stabilization. Neurochem Res. 1 avr 2016;41(4):696-706.
295. P G, T E, E P, V G, L C, A C, et al. Functional study in a yeast model of a novel succinate dehydrogenase subunit B gene germline missense mutation (C191Y) diagnosed in a patient affected by a glomus tumor. Hum Mol Genet. 4 mars 2009;18(10):1860-8.
296. Ngo B, Van Riper JM, Cantley LC, Yun J. Targeting cancer vulnerabilities with high-dose vitamin C. Nat Rev Cancer. 2019;19(5):271-82.

297. Hoffman MA, Ohh M, Yang H, Klco JM, Ivan M, Kaelin WG Jr. von Hippel-Lindau protein mutants linked to type 2C VHL disease preserve the ability to downregulate HIF. Human molecular genetics. 1 mai 2001;10(10):1019-27.
298. Jaakkola P, Mole DR, Tian YM, Wilson MI, Gielbert J, Gaskell SJ, et al. Targeting of HIF-alpha to the von Hippel-Lindau ubiquitylation complex by O2-regulated prolyl hydroxylation. Science. 2001;292(5516):468-72.
299. Müller S, Sindikubwabo F, Cañeque T, Lafon A, Versini A, Lombard B, et al. CD44 regulates epigenetic plasticity by mediating iron endocytosis. bioRxiv. 9 juill 2019;693424.
300. Vissers MCM, Kuiper C, Dachs GU. vita. Biochem Soc Trans. août 2014;42(4):945-51.
301. Kuiper C, Vissers MCM. Ascorbate as a Co-Factor for Fe- and 2-Oxoglutarate Dependent Dioxygenases: Physiological Activity in Tumor Growth and Progression. Front Oncol [Internet]. 10 déc 2014 [cité 29 août 2020];4. Disponible sur: https://www.ncbi.nlm.nih.gov/pmc/articles/PMC4261134/
302. Myllyharju DJ. Prolyl 4-hydroxylases, key enzymes in the synthesis of collagens and regulation of the response to hypoxia, and their roles as treatment targets. Annals of Medicine. 1 janv 2008;40(6):402-17.
303. Kietzmann T, Mennerich D, Dimova EY. Hypoxia-Inducible Factors (HIFs) and Phosphorylation: Impact on Stability, Localization, and Transactivity. Front Cell Dev Biol [Internet]. 23 févr 2016 [cité 30 août 2020];4. Disponible sur: https://www.ncbi.nlm.nih.gov/pmc/articles/PMC4763087/
304. Pollard PJ, Wortham NC, Tomlinson IP. The TCA cycle and tumorigenesis: the examples of fumarate hydratase and succinate dehydrogenase. Ann Med. 2004/01/08 éd. 2003;35(8):632-9.
305. Selak MA, Armour SM, MacKenzie ED, Boulahbel H, Watson DG, Mansfield KD, et al. Succinate links TCA cycle dysfunction to oncogenesis by inhibiting HIF-α prolyl hydroxylase. Cancer Cell. 1 janv 2005;7(1):77-85.
306. Sciacovelli M, Gonçalves E, Johnson TI, Zecchini VR, da Costa ASH, Gaude E, et al. Fumarate is an epigenetic modifier that elicits epithelial-to-mesenchymal transition. Nature. sept 2016;537(7621):544-7.
307. Carmeliet P, Dor Y, Herbert JM, Fukumura D, Brusselmans K, Dewerchin M, et al. Role of HIF-1alpha in hypoxia-mediated apoptosis, cell proliferation and tumour angiogenesis. Nature. 1998;394(6692):485-90.
308. Loriot C, Domingues M, Berger A, Menara M, Ruel M, Morin A, et al. Deciphering the molecular basis of invasiveness in Sdhb-deficient cells. Oncotarget. 20 oct 2015;6(32):32955-65.
309. Ferrara N, Gerber HP, LeCouter J. The biology of VEGF and its receptors. Nat Med. juin 2003;9(6):669-76.
310. Seagroves TN, Ryan HE, Lu H, Wouters BG, Knapp M, Thibault P, et al. Transcription factor HIF-1 is a necessary mediator of the pasteur effect in mammalian cells. Molecular and cellular biology. mai 2001;21(10):3436-44.
311. Hu CJ, Wang LY, Chodosh LA, Keith B, Simon MC. Differential roles of hypoxia-inducible factor 1alpha (HIF-1alpha) and HIF-2alpha in hypoxic gene regulation. Molecular and cellular biology. déc 2003;23(24):9361-74.
312. Warburg O. On respiratory impairment in cancer cells. Science (New York, NY. 10 août 1956;124(3215):269-70.
313. Bartrons R, Caro J. Hypoxia, glucose metabolism and the Warburg's effect. Journal of bioenergetics and biomembranes. juin 2007;39(3):223-9.

314. Hanahan D, Weinberg RA. Hallmarks of cancer: the next generation. Cell. 2011/03/08 éd. 4 mars 2011;144(5):646-74.
315. Kim JW, Tchernyshyov I, Semenza GL, Dang CV. HIF-1-mediated expression of pyruvate dehydrogenase kinase: a metabolic switch required for cellular adaptation to hypoxia. Cell metabolism. mars 2006;3(3):177-85.
316. Papandreou I, Cairns RA, Fontana L, Lim AL, Denko NC. HIF-1 mediates adaptation to hypoxia by actively downregulating mitochondrial oxygen consumption. Cell metabolism. mars 2006;3(3):187-97.
317. Wigfield SM, Winter SC, Giatromanolaki A, Taylor J, Koukourakis ML, Harris AL. PDK-1 regulates lactate production in hypoxia and is associated with poor prognosis in head and neck squamous cancer. British journal of cancer. 17 juin 2008;98(12):1975-84.
318. Fukuda R, Zhang H, Kim JW, Shimoda L, Dang CV, Semenza GL. HIF-1 regulates cytochrome oxidase subunits to optimize efficiency of respiration in hypoxic cells. Cell. 6 avr 2007;129(1):111-22.
319. Scortegagna M, Ding K, Oktay Y, Gaur A, Thurmond F, Yan LJ, et al. Multiple organ pathology, metabolic abnormalities and impaired homeostasis of reactive oxygen species in Epas1-/- mice. Nat Genet. déc 2003;35(4):331-40.
320. Unwin RD, Craven RA, Harnden P, Hanrahan S, Totty N, Knowles M, et al. Proteomic changes in renal cancer and co-ordinate demonstration of both the glycolytic and mitochondrial aspects of the Warburg effect. Proteomics. 2003/08/19 éd. août 2003;3(8):1620-32.
321. Hervouet E, Demont J, Pecina P, Vojtiskova A, Houstek J, Simonnet H, et al. A new role for the von Hippel-Lindau tumor suppressor protein: stimulation of mitochondrial oxidative phosphorylation complex biogenesis. Carcinogenesis. mars 2005;26(3):531-9.
322. Craven RA, Stanley AJ, Hanrahan S, Dods J, Unwin R, Totty N, et al. Proteomic analysis of primary cell lines identifies protein changes present in renal cell carcinoma. Proteomics. mai 2006;6(9):2853-64.
323. Keith B, Johnson RS, Simon MC. HIF1α and HIF2α: sibling rivalry in hypoxic tumor growth and progression. Nat Rev Cancer. 15 déc 2011;12(1):9-22.
324. Bruick RK. Expression of the gene encoding the proapoptotic Nip3 protein is induced by hypoxia. Proceedings of the National Academy of Sciences of the United States of America. 1 août 2000;97(16):9082-7.
325. Raval RR, Lau KW, Tran MG, Sowter HM, Mandriota SJ, Li JL, et al. Contrasting properties of hypoxia-inducible factor 1 (HIF-1) and HIF-2 in von Hippel-Lindau-associated renal cell carcinoma. Molecular and cellular biology. juill 2005;25(13):5675-86.
326. Lee S, Nakamura E, Yang H, Wei W, Linggi MS, Sajan MP, et al. Neuronal apoptosis linked to EglN3 prolyl hydroxylase and familial pheochromocytoma genes: developmental culling and cancer. Cancer Cell. août 2005;8(2):155-67.
327. Bishop T, Gallagher D, Pascual A, Lygate CA, de Bono JP, Nicholls LG, et al. Abnormal sympathoadrenal development and systemic hypotension in PHD3-/- mice. Mol Cell Biol. mai 2008;28(10):3386-400.
328. Kluckova K, Sticha M, Cerny J, Mracek T, Dong L, Drahota Z, et al. Ubiquinone-binding site mutagenesis reveals the role of mitochondrial complex II in cell death initiation. Cell Death & Disease. mai 2015;6(5):e1749-e1749.
329. Grimm S. Respiratory chain complex II as general sensor for apoptosis. Biochimica et Biophysica Acta (BBA) - Bioenergetics. 1 mai 2013;1827(5):565-72.
330. Hwang M-S, Rohlena J, Dong L-F, Neuzil J, Grimm S. Powerhouse down: Complex II

dissociation in the respiratory chain. Mitochondrion. 1 nov 2014;19:20-8.
331. Ricci J-E, Gottlieb RA, Green DR. Caspase-mediated loss of mitochondrial function and generation of reactive oxygen species during apoptosis. J Cell Biol. 6 janv 2003;160(1):65-75.
332. Berger SL, Kouzarides T, Shiekhattar R, Shilatifard A. An operational definition of epigenetics. Genes & Development. 1 avr 2009;23(7):781-3.
333. Killian JK, Kim SY, Miettinen M, Smith C, Merino M, Tsokos M, et al. Succinate dehydrogenase mutation underlies global epigenomic divergence in gastrointestinal stromal tumor. Cancer discovery. 2013/04/04 éd. juin 2013;3(6):648-57.
334. Cervera AM, Bayley J-P, Devilee P, McCreath KJ. Inhibition of succinate dehydrogenase dysregulates histone modification in mammalian cells. Molecular Cancer. 22 oct 2009;8:89.
335. Tahiliani M, Koh KP, Shen Y, Pastor WA, Bandukwala H, Brudno Y, et al. Conversion of 5-methylcytosine to 5-hydroxymethylcytosine in mammalian DNA by MLL partner TET1. Science (New York, NY). 15 mai 2009;324(5929):930-5.
336. Ito S, D'Alessio AC, Taranova OV, Hong K, Sowers LC, Zhang Y. Role of Tet proteins in 5mC to 5hmC conversion, ES-cell self-renewal and inner cell mass specification. Nature. 26 août 2010;466(7310):1129-33.
337. van Duinen N, Corssmit EPM, de Jong WHA, Brookman D, Kema IP, Romijn JA. Plasma levels of free metanephrines and 3-methoxytyramine indicate a higher number of biochemically active HNPGL than 24-h urinary excretion rates of catecholamines and metabolites. Eur J Endocrinol. sept 2013;169(3):377-82.
338. Sakai T, Toguchida J, Ohtani N, Yandell DW, Rapaport JM, Dryja TP. Allele-specific hypermethylation of the retinoblastoma tumor-suppressor gene. American Journal of Human Genetics. mai 1991;48(5):880-8.
339. Herman JG, Baylin SB. Gene silencing in cancer in association with promoter hypermethylation. The New England Journal of Medicine. 20 nov 2003;349(21):2042-54.
340. Favier J, Letouze E. [Mutations in succinate dehydrogenase and DNA methylation]. Medecine sciences : M/S. 2013/12/21 éd. déc 2013;29(12):1092-4.
341. Sulkowski PL, Sundaram RK, Oeck S, Corso CD, Liu Y, Noorbakhsh S, et al. Krebs-cycle-deficient hereditary cancer syndromes are defined by defects in homologous-recombination DNA repair. Nature Genetics. août 2018;50(8):1086-92.
342. Sulkowski PL, Oeck S, Dow J, Economos NG, Mirfakhraie L, Liu Y, et al. Oncometabolites suppress DNA repair by disrupting local chromatin signalling. Nature. juin 2020;582(7813):586-91.
343. Pang Y, Lu Y, Caisova V, Liu Y, Bullova P, Huynh T-T, et al. Targeting NAD+/PARP DNA Repair Pathway as a Novel Therapeutic Approach to SDHB-Mutated Cluster I Pheochromocytoma and Paraganglioma. Clin Cancer Res. 15 2018;24(14):3423-32.
344. Myllyharju J. Intracellular Post-Translational Modifications of Collagens. In: Brinckmann J, Notbohm H, Müller PK, éditeurs. Collagen: Primer in Structure, Processing and Assembly [Internet]. Berlin, Heidelberg: Springer; 2005 [cité 6 sept 2020]. p. 115-47. (Topics in Current Chemistry). Disponible sur: https://doi.org/10.1007/b103821
345. Gelse K, Pöschl E, Aigner T. Collagens—structure, function, and biosynthesis. Advanced Drug Delivery Reviews. 28 nov 2003;55(12):1531-46.
346. Jimenez S, Harsch M, Rosenbloom J. Hydroxyproline stabilizes the triple helix of chick tendon collagen. Biochem Biophys Res Commun. 1 mai 1973;52(1):106-14.
347. Berg RA, Prockop DJ. The thermal transition of a non-hydroxylated form of collagen. Evidence for a role for hydroxyproline in stabilizing the triple-helix of collagen. Biochem

Biophys Res Commun. 1 mai 1973;52(1):115-20.
348. Walmsley AR, Batten MR, Lad U, Bulleid NJ. Intracellular retention of procollagen within the endoplasmic reticulum is mediated by prolyl 4-hydroxylase. J Biol Chem. 21 mai 1999;274(21):14884-92.
349. Gilkes DM, Semenza GL, Wirtz D. Hypoxia and the extracellular matrix: drivers of tumour metastasis. Nat Rev Cancer. 2014;14(6):430-9.
350. Hulmes DJS. Building collagen molecules, fibrils, and suprafibrillar structures. J Struct Biol. févr 2002;137(1-2):2-10.
351. Bonfanti L, Mironov AA, Martínez-Menárguez JA, Martella O, Fusella A, Baldassarre M, et al. Procollagen Traverses the Golgi Stack without Leaving the Lumen of Cisternae: Evidence for Cisternal Maturation. Cell. 23 déc 1998;95(7):993-1003.
352. Beck K, Boswell BA, Ridgway CC, Bächinger HP. Triple helix formation of procollagen type I can occur at the rough endoplasmic reticulum membrane. J Biol Chem. 30 août 1996;271(35):21566-73.
353. Prockop DJ, Kivirikko KI. Collagens: molecular biology, diseases, and potentials for therapy. Annu Rev Biochem. 1995;64:403-34.
354. Myllyharju J, Kivirikko KI. Collagens, modifying enzymes and their mutations in humans, flies and worms. Trends Genet. janv 2004;20(1):33-43.
355. Boot-Handford RP, Tuckwell DS. Fibrillar collagen: the key to vertebrate evolution? A tale of molecular incest. Bioessays. févr 2003;25(2):142-51.
356. Kalluri R. Basement membranes: structure, assembly and role in tumour angiogenesis. Nat Rev Cancer. juin 2003;3(6):422-33.
357. Khoshnoodi J, Cartailler J-P, Alvares K, Veis A, Hudson BG. Molecular Recognition in the Assembly of Collagens: Terminal Noncollagenous Domains Are Key Recognition Modules in the Formation of Triple Helical Protomers. J Biol Chem. 15 déc 2006;281(50):38117-21.
358. Lin CQ, Bissell MJ. Multi-faceted regulation of cell differentiation by extracellular matrix. The FASEB Journal. 1993;7(9):737-43.
359. Egeblad M, Rasch MG, Weaver VM. Dynamic interplay between the collagen scaffold and tumor evolution. Curr Opin Cell Biol. oct 2010;22(5):697-706.
360. Semenza GL. Cancer-stromal cell interactions mediated by hypoxia-inducible factors promote angiogenesis, lymphangiogenesis, and metastasis. Oncogene. 29 août 2013;32(35):4057-63.
361. Casazza A, Di Conza G, Wenes M, Finisguerra V, Deschoemaeker S, Mazzone M. Tumor stroma: a complexity dictated by the hypoxic tumor microenvironment. Oncogene. 3 avr 2014;33(14):1743-54.
362. Wyckoff JB, Wang Y, Lin EY, Li J, Goswami S, Stanley ER, et al. Direct visualization of macrophage-assisted tumor cell intravasation in mammary tumors. Cancer Res. 15 mars 2007;67(6):2649-56.
363. Conklin MW, Eickhoff JC, Riching KM, Pehlke CA, Eliceiri KW, Provenzano PP, et al. Aligned collagen is a prognostic signature for survival in human breast carcinoma. Am J Pathol. mars 2011;178(3):1221-32.
364. Provenzano PP, Eliceiri KW, Campbell JM, Inman DR, White JG, Keely PJ. Collagen reorganization at the tumor-stromal interface facilitates local invasion. BMC Med. 26 déc 2006;4(1):38.
365. Provenzano PP, Inman DR, Eliceiri KW, Trier SM, Keely PJ. Contact guidance mediated three-dimensional cell migration is regulated by Rho/ROCK-dependent matrix reorganization. Biophys J. déc 2008;95(11):5374-84.

366. Levental KR, Yu H, Kass L, Lakins JN, Egeblad M, Erler JT, et al. Matrix crosslinking forces tumor progression by enhancing integrin signaling. Cell. 25 nov 2009;139(5):891-906.
367. Kaplan G. In vitro differentiation of human monocytes. Monocytes cultured on glass are cytotoxic to tumor cells but monocytes cultured on collagen are not. J Exp Med. 1 juin 1983;157(6):2061-72.
368. Wels J, Kaplan RN, Rafii S, Lyden D. Migratory neighbors and distant invaders: tumor-associated niche cells. Genes Dev. 1 mars 2008;22(5):559-74.
369. Murdoch C, Giannoudis A, Lewis CE. Mechanisms regulating the recruitment of macrophages into hypoxic areas of tumors and other ischemic tissues. Blood. 15 oct 2004;104(8):2224-34.
370. Cramer T, Yamanishi Y, Clausen BE, Förster I, Pawlinski R, Mackman N, et al. HIF-1alpha is essential for myeloid cell-mediated inflammation. Cell. 7 mars 2003;112(5):645-57.
371. Wynn TA, Barron L. Macrophages: master regulators of inflammation and fibrosis. Semin Liver Dis. août 2010;30(3):245-57.
372. Joyce JA, Pollard JW. Microenvironmental regulation of metastasis. Nat Rev Cancer. avr 2009;9(4):239-52.
373. Paget S. The distribution of secondary growths in cancer of the breast. 1889. Cancer Metastasis Rev. août 1989;8(2):98-101.
374. Reymond N, d'Água BB, Ridley AJ. Crossing the endothelial barrier during metastasis. Nature Reviews Cancer. déc 2013;13(12):858-70.
375. Lendvai N, Pawlosky R, Bullova P, Eisenhofer G, Patocs A, Veech RL, et al. Succinate-to-Fumarate Ratio as a New Metabolic Marker to Detect the Presence of SDHB/D-related Paraganglioma: Initial Experimental and Ex Vivo Findings. Endocrinology. janv 2014;155(1):27-32.
376. Richter S, Peitzsch M, Rapizzi E, Lenders JW, Qin N, de Cubas AA, et al. Krebs cycle metabolite profiling for identification and stratification of pheochromocytomas/paragangliomas due to succinate dehydrogenase deficiency. The Journal of clinical endocrinology and metabolism. oct 2014;99(10):3903-11.
377. Loriot C, Burnichon N, Gadessaud N, Vescovo L, Amar L, Libe R, et al. Epithelial to Mesenchymal Transition Is Activated in Metastatic Pheochromocytomas and Paragangliomas Caused by SDHB Gene Mutations. J Clin Endocrinol Metab. 2012/04/12 éd. juin 2012;97(6):E954-62.
378. Thiery JP. Epithelial-mesenchymal transitions in tumour progression. Nature reviews. juin 2002;2(6):442-54.
379. Kundu S. Co-operative intermolecular kinetics of 2-oxoglutarate dependent dioxygenases may be essential for system-level regulation of plant cell physiology. Front Plant Sci [Internet]. 2015 [cité 17 sept 2020];6. Disponible sur: https://www.frontiersin.org/articles/10.3389/fpls.2015.00489/full
380. Buettner GR. The pecking order of free radicals and antioxidants: lipid peroxidation, alpha-tocopherol, and ascorbate. Arch Biochem Biophys. 1 févr 1993;300(2):535-43.
381. Padayatty SJ, Levine M. Vitamin C: the known and the unknown and Goldilocks. Oral Dis. sept 2016;22(6):463-93.
382. Du J, Cullen JJ, Buettner GR. Ascorbic acid: chemistry, biology and the treatment of cancer. Biochim Biophys Acta. déc 2012;1826(2):443-57.
383. Scheuermann TH, Stroud D, Sleet CE, Bayeh L, Shokri C, Wang H, et al. Isoform-Selective and Stereoselective Inhibition of Hypoxia Inducible Factor-2. J Med Chem. 13 août 2015;58(15):5930-41.

384. Xu R, Wang K, Rizzi JP, Huang H, Grina JA, Schlachter ST, et al. 3-[(1 *S* ,2 *S* ,3 *R*)-2,3-Difluoro-1-hydroxy-7-methylsulfonylindan-4-yl]oxy-5-fluorobenzonitrile (PT2977), a Hypoxia-Inducible Factor 2α (HIF-2α) Inhibitor for the Treatment of Clear Cell Renal Cell Carcinoma. J Med Chem. 8 août 2019;62(15):6876-93.
385. Chen W, Hill H, Christie A, Kim MS, Holloman E, Pavia-Jimenez A, et al. Targeting Renal Cell Carcinoma with a HIF-2 antagonist. Nature. 3 nov 2016;539(7627):112-7.
386. Cho H, Du X, Rizzi JP, Liberzon E, Chakraborty AA, Gao W, et al. On-Target Efficacy of a HIF2α Antagonist in Preclinical Kidney Cancer Models. Nature. 3 nov 2016;539(7627):107-11.
387. Saito S, Lin Y-C, Tsai M-H, Lin C-S, Murayama Y, Sato R, et al. Emerging roles of hypoxia-inducible factors and reactive oxygen species in cancer and pluripotent stem cells. Kaohsiung J Med Sci. juin 2015;31(6):279-86.
388. Gerald D, Berra E, Frapart YM, Chan DA, Giaccia AJ, Mansuy D, et al. JunD reduces tumor angiogenesis by protecting cells from oxidative stress. Cell. 17 sept 2004;118(6):781-94.
389. Pinato DJ, Black JR, Trousil S, Dina RE, Trivedi P, Mauri FA, et al. Programmed cell death ligands expression in phaeochromocytomas and paragangliomas: Relationship with the hypoxic response, immune evasion and malignant behavior. Oncoimmunology [Internet]. 4 août 2017 [cité 19 sept 2020];6(11). Disponible sur: https://www.ncbi.nlm.nih.gov/pmc/articles/PMC5674959/

ANNEXES

ARTICLE 4

Synergistic Highly Potent Targeted Drug Combinations in Different Pheochromocytoma Models Including Human Tumor Cultures

Maria Fankhauser, Nicole Bechmann, Michael Lauseker, Judith Goncalves, Judith Favier, Barbara Klink, Doreen William, Laura Gieldon, Julian Maurer, Gerald Spöttl, Petra Rank, Thomas Knösel, Michael Orth, Christian G. Ziegler, Elke Tatjana Aristizabal Prada, German Rubinstein, Martin Fassnacht, Christine Spitzweg, Ashley B. Grossman, Karel Pacak, Felix Beuschlein, Stefan R. Bornstein, Graeme Eisenhofer, Christoph J. Auernhammer, Martin Reincke, Svenja Nölting

Endocrinology. 2019 Nov 1;160(11):2600-2617.

Synergistic Highly Potent Targeted Drug Combinations in Different Pheochromocytoma Models Including Human Tumor Cultures

Maria Fankhauser,[1]* Nicole Bechmann,[2]* Michael Lauseker,[3] Judith Goncalves,[4,5,6] Judith Favier,[4,5] Barbara Klink,[7,8,9] Doreen William,[9] Laura Gieldon,[7,9,10,11] Julian Maurer,[1] Gerald Spöttl,[1] Petra Rank,[1] Thomas Knösel,[12] Michael Orth,[13] Christian G. Ziegler,[14] Elke Tatjana Aristizabal Prada,[1] German Rubinstein,[1] Martin Fassnacht,[15] Christine Spitzweg,[1] Ashley B. Grossman,[16,17] Karel Pacak,[18] Felix Beuschlein,[1,19] Stefan R. Bornstein,[14] Graeme Eisenhofer,[2,14] Christoph J. Auernhammer,[1] Martin Reincke,[1] and Svenja Nölting[1]

[1]Medizinische Klinik und Poliklinik IV, Klinikum der Universität, LMU München, 80337 Munich, Germany; [2]Institute for Clinical Chemistry and Laboratory Medicine, University Hospital Carl Gustav Carus at Technische Universität Dresden, 01069 Dresden, Germany; [3]Institute for Medical Information Sciences, Biometry, and Epidemiology, Campus Grosshadern, Ludwig-Maximilians-University of Munich, 81377 Munich, Germany; [4]Institut National de la Santé et de la Recherche Médicale, UMR970, Paris-Cardiovascular Research Center, Equipe Labellisée par la Ligue contre le Cancer, F-75015 Paris, France; [5]Université Paris Descartes, Sorbonne Paris Cité, Faculté de Médecine, F-75006 Paris, France; [6]Université Paris Diderot, Sorbonne Paris Cité, F-75013 Paris, France; [7]Institute for Clinical Genetics, Faculty of Medicine Carl Gustav Carus, TU Dresden, 01307 Dresden, Germany; [8]National Center of Genetics, Laboratoire National de Santé, 1, L-3555 Dudelange, Luxembourg; [9]German Cancer Consortium, 01307 Dresden, Germany; [10]German Cancer Research Center, 69120 Heidelberg, Germany; [11]Core Unit for Molecular Tumor Diagnostics, National Center for Tumor Diseases, 69120 Heidelberg, Germany; [12]Institute of Pathology, Ludwig-Maximilians-University, 80337 Munich, Germany; [13]Department of Radiation Oncology, University Hospital, LMU Munich, 81377 Munich, Germany; [14]Department of Medicine III, University Hospital Carl Gustav Carus Dresden, 01307 Dresden, Germany; [15]Department of Medicine I, Division of Endocrinology and Diabetology, University Hospital, University of Würzburg, 97080 Würzburg, Germany; [16]Oxford Centre for Diabetes, Endocrinology and Metabolism, University of Oxford, Oxford OX3 7LE, United Kingdom; [17]Royal Free Hospital ENETS Centre of Excellence, London NW3 2QG, United Kingdom; [18]*Eunice Kennedy Shriver* National Institute of Child Health and Human Development, National Institutes of Health, Bethesda, Maryland 20892; and [19]Klinik für Endokrinologie, Diabetologie und Klinische Ernährung, Universitätsspital Zürich, 8091 Zurich, Switzerland

ORCiD numbers: 0000-0002-7064-590X (S. Nölting).

There are no officially approved therapies for metastatic pheochromocytomas apart from ultratrace ^{131}I-metaiodbenzylguanidine therapy, which is approved only in the United States. We have, therefore, investigated the antitumor potential of molecular-targeted approaches in murine pheochromocytoma cell lines [monocyte chemoattractant protein (MPC)/monocyte chemoattractant protein/3-(4,5-Dimethylthiazol-2-yl)-2,5-diphenyltetrazolium bromide (MTT)], immortalized mouse chromaffin *Sdhb*$^{-/-}$ cells, three-dimensional pheochromocytoma tumor models (MPC/MTT spheroids), and human pheochromocytoma primary cultures. We identified the specific phosphatidylinositol-3-kinase α inhibitor BYL719 and the mammalian target of rapamycin inhibitor everolimus as the most effective combination in all models. Single treatment with clinically relevant

ISSN Online 1945-7170

Received 30 May 2019. Accepted 14 July 2019.
First Published Online 19 July 2019

*M. Fankhauser and N.B. contributed equally to this work.

Abbreviations: CVD, cyclophosphamide, vincristine, dacarbazine; DMSO, dimethyl sulfoxide; imCC, immortalized mouse chromaffin cells; MPC, monocyte chemoattractant protein; mTORC1, mammalian target of rapamycin; MTT, 3-(4,5-Dimethylthiazol-2-yl)-2,5-diphenyltetrazolium bromide; NET, neuroendocrine tumor; NGS, next-generation sequencing; PARP, poly(ADP-ribose) polymerase; PCC, pheochromocytoma; PGL, paraganglioma; PI3K, phosphatidylinositol-3-kinase; *TET1*, tet methylcytosine dioxygenase; TKI, tyrosine kinase inhibitor; VEGFR, vascular endothelial growth factor receptor; WT, wild-type.

doses of BYL719 and everolimus significantly decreased MPC/MTT and *Sdhb*$^{-/-}$ cell viability. A targeted combination of both inhibitors synergistically reduced MPC and *Sdhb*$^{-/-}$ cell viability and showed an additive effect on MTT cells. In MPC/MTT spheroids, treatment with clinically relevant doses of BYL719 alone or in combination with everolimus was highly effective, leading to a significant shrinkage or even a complete collapse of the spheroids. We confirmed the synergism of clinically relevant doses of BYL719 plus everolimus in human pheochromocytoma primary cultures of individual patient tumors with BYL719 attenuating everolimus-induced AKT activation. We have thus established a method to assess molecular-targeted therapies in human pheochromocytoma cultures and identified a highly effective combination therapy. Our data pave the way to customized combination therapy to target individual patient tumors. **(*Endocrinology* 160: 2600–2617, 2019)**

Pheochromocytomas (PCCs) and paragangliomas (PGLs) are rare neuroendocrine, catecholamine-producing tumors that originate from the adrenal medulla or extra-adrenal paraganglia. About 10% of PCCs and 35% to 40% of PGLs are metastatic (1–9). The prognosis of patients with metastatic PCC/PGL is poor, with a 5-year survival rate of 63% (10). Current therapeutic approaches for metastatic PCC/PGL, such as radionuclide therapy with ^{131}I-metaiodbenzylguanidine, peptide receptor radionuclide therapy (11), or chemotherapy, are (apart from ultratrace ^{131}I-metaiodbenzylguanidine, which has been approved only in the United States) not officially approved and are limited in their effectiveness, as recently reviewed (12). Therefore, novel therapeutic strategies are urgently needed.

The standard chemotherapy regimen for PCC/PGLs is CVD (cyclophosphamide, vincristine, dacarbazine). Inhibitors of the DNA repair enzyme poly(ADP-ribose) polymerase (PARP) have been demonstrated to potentiate DNA damaging effects of alkylating chemotherapeutic agents, such as dacarbazine or temozolomide (13–15), both being metabolized to the same active metabolite (16). Therefore, combining standard chemotherapy with a PARP inhibitor might be a promising novel therapeutic approach.

Another therapeutic approach is to define the aberrant molecular pathways in such tumors, which can then be targeted by specific therapy. Germline mutations can be identified in ~30% to 40% of patients with PCC/PGL, with an equal number showing somatic mutations in more than 20 well-characterized susceptibility genes (17, 18). These different mutations can be separated into three main molecular clusters [summarized in Fig. 1 and recently reviewed (19)]:

(i) The pseudohypoxic signaling cluster (cluster-1) is related to mutations of genes encoding for proteins that are associated with significant regulation of the hypoxia signaling pathway; these include mutations in genes encoding for hypoxia-inducible factor-2α (*HIF2A*), Krebs cycle enzymes such as succinate dehydrogenase subunits [*SDHx* (*SDHA, SDHB, SDHC, SDHD*)], succinate dehydrogenase complex assembly factor-2 (*SDHAF2*), fumarate hydratase (*FH*), malate dehydrogenase 2 (*MDH2*), and isocitrate dehydrogenase 1 (*IDH1*). This pathway includes mutations in von Hippel–Lindau tumor suppressor (*VHL*) and egl-9 prolyl hydroxylase-1 and -2 (*EGLN1/2*) genes. Such mutations promote HIF-α stabilization and accumulation resulting in, among other effects, increased angiogenesis via changes in vascular endothelial growth factor-1 and -2 receptors (VEGFR1/2) and platelet-derived growth factor-β receptor transcription.

(ii) The kinase signaling cluster (cluster-2) is related to mutations of genes encoding for proteins that belong to the phosphatidylinositol-3-kinase (PI3K)/mammalian target of rapamycin (mTORC1) pathway/receptor kinase signaling and comprises mutations in the rearranged-during-transfection (*RET*) proto-oncogene, neurofibromin 1 (*NF1*) tumor suppressor, *H-RAS* and *K-RAS* proto-oncogenes, transmembrane protein 127 (*TMEM127*), and Myc-associated factor X (*MAX*).

(iii) Most recently, the Wnt signaling cluster (cluster-3) has been described as being of pathological significance.

The multitargeted receptor tyrosine kinase inhibitor (TKI) sunitinib has antiangiogenic and antiproliferative potential due to inhibition of VEGFR1/2, platelet-derived growth factor-β receptor, and RET and has been approved for the treatment of renal cell carcinomas, pancreatic neuroendocrine tumors (NETs), and gastrointestinal stromal tumors. Sunitinib is currently being investigated in a randomized placebo-controlled phase II clinical trial in patients with PCC/PGL, for which recruitment has been completed (FIRST-MAPPP, clinical trial no. NCT01371201).

The mTORC1 inhibitor everolimus, currently used in the treatment of breast cancer, renal cell carcinoma, and NETs, showed poor efficacy when used alone in PCC/PGLs (20). However, one patient with an *SDHB* mutation who was treated with the combination of low

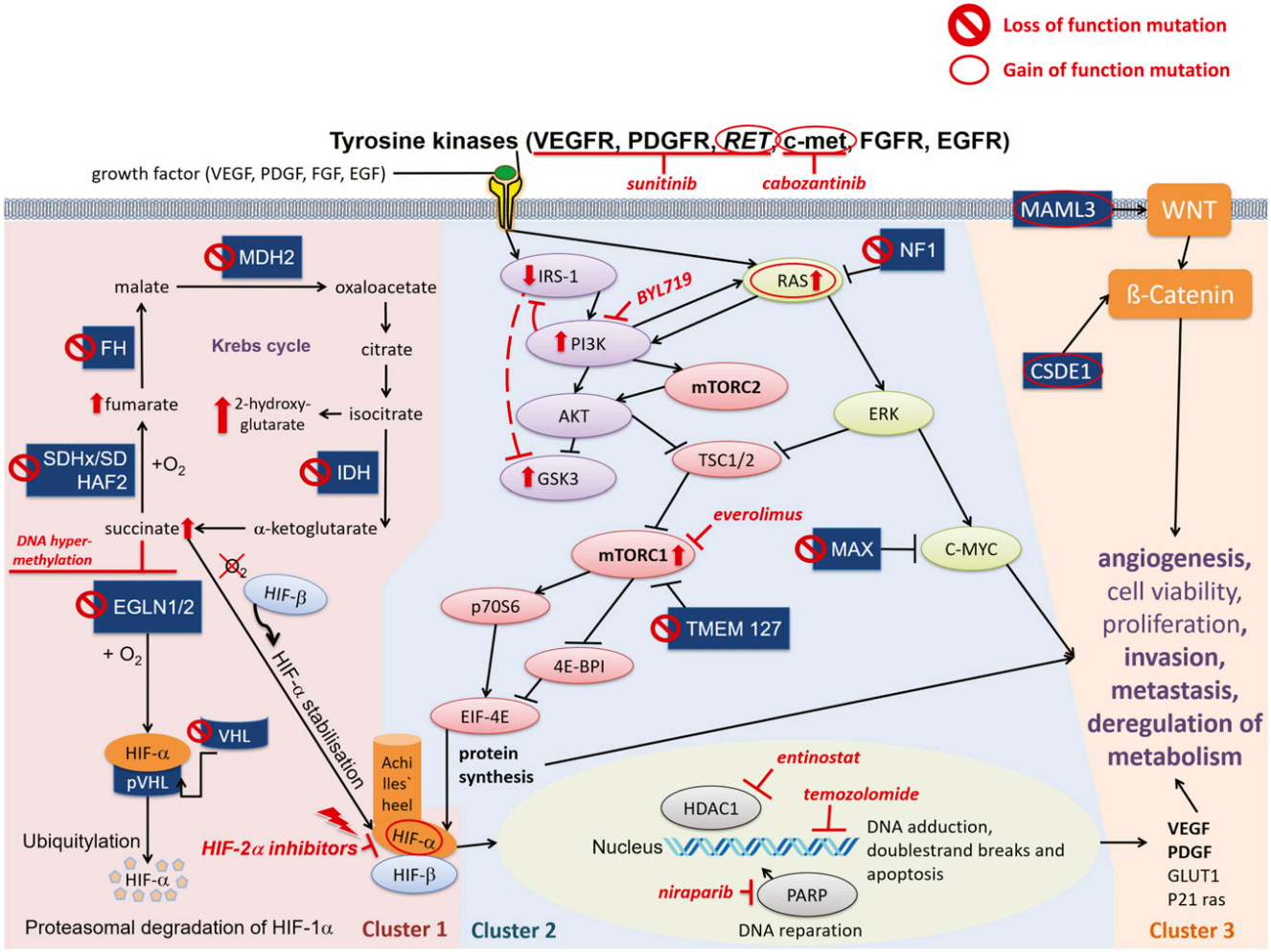

Figure 1. Cluster-1, cluster-2, and cluster-3, with molecular-targeted therapeutic options. Cluster-1: The pseudo-hypoxic signaling cluster includes mutations in genes encoding for hypoxia-inducible factor 2-α (*HIF2A*), Krebs-cycle enzymes such as succinate dehydrogenase subunits [*SDHx* (*SDHA*, *SDHB*, *SDHC*, *SDHD*)], succinate dehydrogenase complex assembly factor-2 (*SDHAF2*), fumarate hydratase (*FH*), malate dehydrogenase 2 (*MDH2*), and isocitrate dehydrogenase (*IDH*), and including von Hippel–Lindau tumor suppressor (*VHL*) and egl-9 prolyl hydroxylase 1 and 2 (*EGLN1/2*). Cluster-2: The kinase signaling cluster comprises mutations in the rearranged-during-transfection (*RET*) proto-oncogene, neurofibromin 1 (*NF1*) tumor suppressor, *H-RAS* and *K-RAS* proto-oncogenes, transmembrane protein 127 (*TMEM127*), and Myc-associated factor X (*MAX*). Receptor tyrosine kinases (among others, RET, VEGFR, c-met) activate insulin receptor substrate 1 (IRS-1), which recruits the phosphatidylinositol-3-kinase (PI3K). PI3K activates AKT, which inhibits tuberous sclerosis proteins 1/2 (TSC1/2), leading to disinhibition/activation of the mammalian target of rapamycin (mTORC1); mTORC1 phosphorylates and activates various proteins, including p70S6 kinase (p70S6K), by which p70S6 is phosphorylated. Activated p70S6 promotes cell growth, proliferation, cell survival, and leads, among other effects, to the protein synthesis of HIF-1α, which favors angiogenesis [VEGF/platelet-derived growth factor (PDGF)] transcription, among others], invasion, and metastasis under hypoxic or pseudo-hypoxic conditions. AKT also inhibits glycogen synthase kinase 3 (GSK3). Persistent activation of PI3K leads to feedback downregulation of IRS-1, which may lead to GSK3 disinhibition/activation. The RAS/RAF/ERK pathway is also activated by tyrosine kinases (RET, among others) and activates mTORC1. *NF1* mutations lead to disinhibition/activation of RAS. *TMEM127* mutations lead to disinhibition/activation of mTORC1. The tumor suppressor MAX antagonizes Myc-dependent cell survival, proliferation, and angiogenesis: mutations lead to increased cell proliferation and angiogenesis. Cluster-3: The Wnt signaling cluster comprises somatic mutations in cold shock domain containing E1 (*CSDE1*) and the mastermind-like transcriptional coactivator 3 (*MAML3*) fusion genes. ⦸, pheochromocytoma-promoting loss-of-function mutation of a tumor suppressor gene; ○, pheochromocytoma-promoting gain-of-function mutation of a proto-oncogene. ↑, increase/upregulation; ⊥, inhibition; ↓, activation.

doses of the mTORC1 inhibitor rapamycin and the TKI sunitinib showed long-term disease control (21).

In an *in vivo* breast cancer mouse model, the mTORC1 inhibitor everolimus has shown synergistic effects together with the PI3Kα inhibitor BYL719 (alpelisib) and overcame BYL719 resistance (22). The clinical phase III approval study SOLAR-1 investigating BYL719 in patients with breast cancer has reached its final endpoints (23). Moreover, BYL719 overcame everolimus resistance in a stably everolimus-resistant pancreatic NET cell line model (24). Therefore, combining different targeted drugs may strongly enhance their therapeutic potential and prevent the development of resistance.

Based on these data, we have investigated the antitumor potential of a variety of both targeted and chemotherapeutic agents and their combinations and their impact on cellular signaling pathways in well-validated murine PCC

cell line models and a murine *Sdhb* knock-out ($Sdhb^{-/-}$) cell line (the best available cell line models for highly aggressive *SDHB*-mutated paragangliomas), three-dimensional murine PCC spheroids, and human PCC primary cultures to identify novel therapeutic options.

Materials and Methods

Cell lines

Murine monocyte chemoattractant protein (MPC) (MPC 4/30/PRR) (25) and 3-(4,5-Dimethylthiazol-2-yl)-2,5-diphenyltetrazolium bromide (MTT) (26) cell lines were cultured as described previously (27) in DMEM/F12 (1:1) (Life Technologies, Karlsruhe, Germany) supplemented with 10% fetal bovine serum (Biochrom, Berlin, Germany), 1% penicillin/streptomycin (Life Technologies), and 0.4% amphotericin B (Biochrom) at 5% CO_2 and 37°C. Cells were counted by an automated cell counter (Countess; Invitrogen, Darmstadt, Germany). MPC/MTT cells were confirmed for species identity by cytochrome C oxidase I DNA barcoding and for strain identity by comparing short tandem repeats from these cell lines with short tandem repeats of identity-confirmed counterparts as described previously (28). These analyses were performed by the Deutsche Sammlung von Mikroorganismen und Zellkulturen (Braunschweig, Germany).

Immortalized mouse chromaffin cells both wild-type (WT) and $Sdhb^{-/-}$ (29) were cultured in DMEM Glutamax (Gibco) with 10% fetal bovine serum (Gibco) and 1% penicillin/streptomycin (Gibco) at 37°C in 5% CO_2.

Inhibitors

Everolimus, BYL719, sunitinib, temozolomide, niraparib (PARP inhibitor), cabozantinib (a TKI inhibiting c-met/VEGFR2/c-KIT/FLT3/RET/TIE2), and entinostat (a histone deacetylase 1/3 inhibitor) were purchased from Selleckchem (Munich, Germany). All drugs were dissolved in dimethyl sulfoxide (DMSO) (D8418; Sigma) and diluted in 0.2% BSA/PBS. DMSO was used as the vehicle (DMSO control) equal to the highest dose of each single experiment and had no effect on cell viability up to concentrations of 0.2% (1:500) DMSO.

Dose finding: Clinically relevant doses

Treatment doses of 10 to 25 nM everolimus were chosen because the plasma levels in patients on daily therapy with 10 mg everolimus range between ~8 nM (c_{min} after 2 weeks of daily exposure to 10 mg everolimus) and 59 nM (c_{2h} after 12 weeks of daily exposure to 10 mg everolimus) (30).

Concentrations of 2.5 to 10 μM BYL719 used in our experiments are also clinically relevant: In patients with advanced solid malignancies, median BYL719 plasma concentrations between 2 and 11 μM were found 2 to 8 hours post dose with 1-month daily oral standard therapy with 300 to 450 mg BYL719 (31).

We used 0.5 to 2 μM sunitinb in MPC/MTT cells and in human PCC cultures. Administration of 50 mg sunitinib per day leads to plasma concentrations of 0.1 to 0.2 μM (32). Thus, we only used a slightly higher dose as our starting concentration.

We used 0.5 to 2 μM cabozantinib in MPC/MTT cells and 1 to 10 μM cabozantinib in human PCC cultures. Administration of 20 to 60 mg of cabozantinib per day leads to plasma concentrations of 0.7 to 2.2 μM (33).

Human PCC primary cultures

This study was approved by the European Network for the Study of Adrenal Tumors, and informed consent was obtained from each patient. Primary tumor tissues were isolated from adrenal glands of six patients with PCC, and lymph node/uterus metastases were isolated from one patient with metastatic PGL (n = 7). Specimens were taken immediately after surgery and placed into Petri dishes filled with PBS. Tissue was separated into 0.5-mm pieces. Diced tissue was resuspended in 10 mL collagenase (Biochrom) and incubated at 37°C for 60 minutes. Subsequently, 2 mL pure fetal calf serum were added to inactivate the collagenase, and tumor tissue was centrifuged at 1100 rpm for 5 minutes. The supernatant was removed, and the pellet was gently resuspended in erythrocyte lysis buffer. After incubation for 7 minutes, centrifugation was repeated, the supernatant was removed, and the pellet was resuspended in DMEM/F12 supplemented with 10% fetal calf serum, 1% penicillin/streptomycin, and 0.4% amphotericin B. The suspension was filtered through a 70-μm sieve, and cells were counted and seeded into 96- or 6-well plates. After 3 to 5 days of incubation, cells were treated with everolimus, BYL719, sunitinib, temozolomide, niraparib, cabozantinib, or entinostat. After 48 or 72 hours, cell viability was analyzed. To confirm chromaffin cell origin, we used Western blot analysis of synaptophysin after 24 hours, as described below.

Cell viability

MPC/MTT cells were seeded into 96-well plates at densities of 2000 cells per well, grown for 24 hours, and treated with different concentrations of sunitinib, BYL719, and cabozantinib, either alone or in combination with everolimus. Furthermore, cells were treated with niraparib alone or in combination with temozolomide or with entinostat alone. Metabolic activity was assessed by the Cell Titer Blue® cell viability assay (no. G8081; Promega, Madison, WI) after 48, 72, and 120 hours of drug incubation. Cells were incubated for 4 hours with Cell Titer Blue® solution; fluorescence was measured at 560/590 nm using a GLOMAX plate reader (Promega).

Cell cycle analysis

The cell cycle was analyzed (Accuri C6 Analysis; BD Biosciences, San Jose, CA) as previously described (24). For flow cytometric analysis, cells were incubated for 24 hours with BYL719, everolimus, and sunitinib alone or in combination.

Apoptosis

Apoptosis was measured after 24 hours of treatment with BYL719, everolimus, and sunitinib, alone or in combination, using the Apo-One homogeneous caspase3/7-Assay kit (no. G7790; Promega) as previously described (24).

Cytotoxicity by crystal violet assay

A total of 2.5×10^3 cells per well were seeded into 48-well plates and treated for 72 hours (everolimus, BYL719, combination or vehicle). Crystal violet assay was then performed as previously described (34). Values were standardized to the vehicle absorbance at 24 hours and expressed as cell viability.

Cell viability curves were established. Experiments were performed three times in duplicate.

Spheroid cultivation and treatment

Generation and cultivation of MPC/MTT cell spheroids was conducted as described previously (35, 36). Four days after spheroid generation, spheroids were treated with sunitinib or BYL719 alone or in combination with everolimus. Afterward, spheroid growth was monitored for 14 days (single treatment). During cultivation, medium was replaced every 3 to 4 days. A fractionated treatment regimen was used by additional treatment of the spheroids on days 7, 11, and 14.

Protein extraction and Western blot analysis

Cells were seeded into 10-cm plates and grown for 24 hours in complete medium before incubation with sunitinib and BYL719, either alone or in combination with everolimus, for 24 or 48 hours. Duplicate wells were used for each concentration of drug. Western blotting was conducted as described previously (37) using the following primary and secondary antibodies and their dilutions: pAktT (Ser473) (dilution: 1:20,000) (RRID: AB_2315049) (38), AKT (dilution: 1:5000) (RRID: AB_329827) (39), p4EBP1 (Ser65) (dilution: 1:2000) (RRID: AB_330947) (40), 4EBP1 (dilution: 1:1000) (RRID: AB_2097841) (41), p53 (dilution: 1:1000) (RRID: AB_10695803) (42), cyclin D1 (dilution: 1:1000) (RRID: AB_2259616) (43), cyclin D3 (dilution: 1:2000) (RRID: AB_2070801) (44), pp70S6K (Thr389) (dilution: 1:1000) (RRID: AB_330944) (45), p70S6K (dilution: 1:5000) (RRID: AB_390722) (46), pS6 (Ser240/244) (dilution: 1:200,000) (RRID: AB_10694233) (47), S6 (dilution: 1:20,000) (RRID: AB_331355) (48), pGSK3α/β (Ser21/9) (dilution: 1:5000) (RRID: AB_329830) (49), GSK3α/β (dilution: 1:1000) (RRID: AB_10547140) (50), CDK1/cdc2 (POH1) (dilution: 1:1000) (RRID: AB_2074795) (51), Chk1 (2G1D5) (dilution: 1:1000) (RRID: AB_2080320) (52) (Cell Signaling, Danvers, MA), IRS-1 (dilution: 1:5000) (RRID: AB_2536328) (53), pIRS-1 (Ser312) (dilution: 1:5000) (RRID: AB_2533767) (54) (Invitrogen, Carlsbad, CA), actin (dilution: 1:10,000) (RRID: AB_476744) (55) (Sigma-Aldrich, St. Louis, MO), and synaptophysin clone SY38 (dilution: 1:1000) (RRID: AB_95187) (56) (Merck-Millipore, Darmstadt, Germany). Western blot quantification was performed, and a representative blot of three independent experiments is shown.

Multigene panel next-generation sequencing

Testing for disease-causing variants in PCC/PGL-associated genes was performed by targeted next-generation sequencing (NGS), as described previously (57), using a custom-designed multigene panel based on the TruSeq® Nano DNA Library Prep Kit (Illumina, San Diego, CA).

The panel comprises 84 genes, including more than 20 genes associated with PCC/PGL (58), and was shown to be suitable for analysis of blood and formalin-fixed paraffin-embedded or fresh frozen tumor tissue. DNA was isolated from formalin-fixed paraffin-embedded tumor tissue samples. Library preparation was done according to the manufacturer's instructions, and 150 nt paired-end sequencing was carried out with a minimum median coverage of 1000-fold on a NextSeq500 sequencer (Illumina). Data analysis was performed using the Biomedical Genomics Workbench 5.0 (Qiagen) as described previously (59). Settings for variant calling in tumor tissue were adapted using a low-frequency variant detection algorithm with a required minimum frequency of 5%, three reads supporting the variant, and a required minimum coverage of 10 reads.

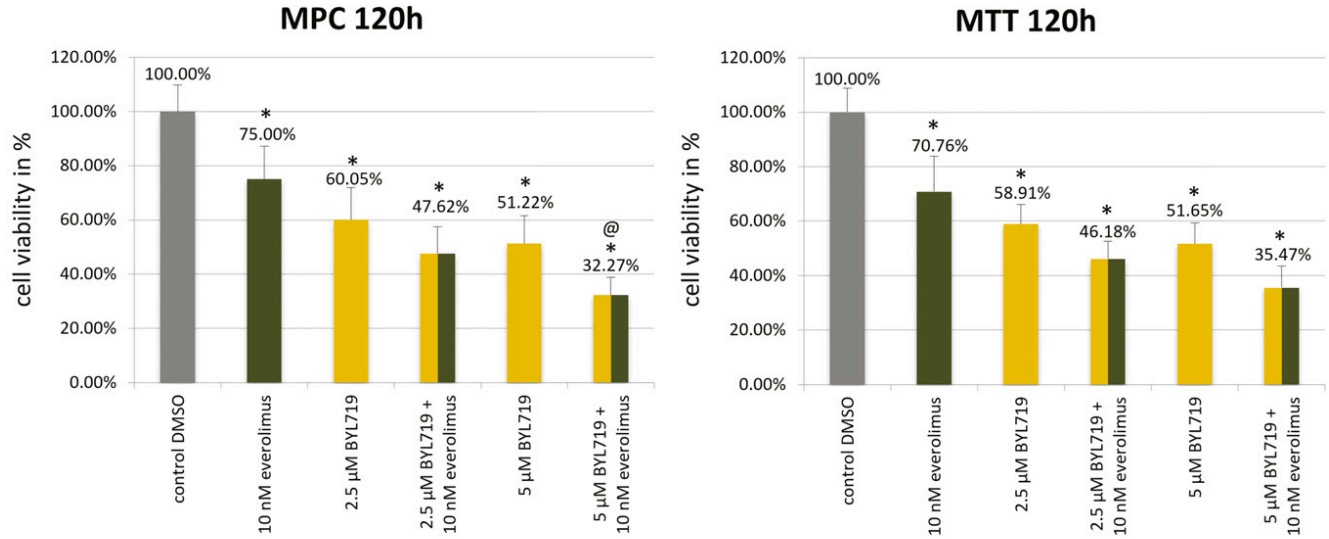

@ Synergistic effect of BYL719/everolimus in MPC cells
* Significant decrease of cell viability compared to control DMSO

Figure 2. Significant MPC/MTT cell viability reduction by clinically relevant doses of BYL719, everolimus, and by the combination of both after 120 h. The arithmetic means and standard deviation of at least three independent experiments are shown. @The BYL719/everolimus combination treatment was statistically synergistic in MPC cells and additive in MTT cells. *Statistically significant differences in comparison with the DMSO control ($P < 0.05$).

Statistical analysis

Results are displayed as mean ± SD of at least three independent experiments. Each cell viability experiment consisted of at least six samples per concentration and incubation time. Cell viability in the monocyte chemoattractant protein/3-(4,5-Dimethylthiazol-2-yl)-2,5-diphenyltetrazolium bromide experiments was modeled via a linear mixed model with random effects for trial and fixed effects for substances and their interactions. For the human primary cultures, we used a linear mixed model for the natural logarithm of the viability. Synergism was assessed as described previously (60) and was confirmed when both single effects were significant, the interaction effect was significant, and all regression coefficients were negative. When both single effects were significant and the interaction effect was not significant, it was defined as an "additive" effect.

For spheroid data, the diameter of the spheroids was modeled via a quasi-Poisson mixed model with random effects for trial and spheroid. Temporal correlation was modeled via a continuous AR(1) correlation structure. Besides the main effects, the model included a quadratic term for the day since starting and interactions between time and substances. All significance tests were performed within the respective model.

Calculations were performed using R 3.5.1 (R Foundation for Statistical Computing, Vienna, Austria). Significance was assessed at $P < 0.05$. Due to the exploratory character of this work, we did not adjust any P values for multiple testing.

Results

MPC/MTT cells

Cell viability after different drug treatments

Treatment (120 hours) with clinically relevant doses of BYL719 (2.5 μM/5 μM) and everolimus (10 nM) significantly diminished MPC/MTT cell viability compared with the control (Fig. 2); combination treatment with 5 μM BYL719 and 10 nM everolimus synergistically reduced MPC and additively MTT reduced cell viability (Fig. 2).

Treatment with sunitinib (1 μM/2 μM) and everolimus (10 nM) significantly reduced MPC/MTT cell viability compared with the control (Fig. 3). Combination treatment synergistically reduced MPC (1 μM/2 μM sunitinib plus 10 nM everolimus) and MTT (2 μM sunitinib plus 10 nM everolimus) cell viability (Fig. 3).

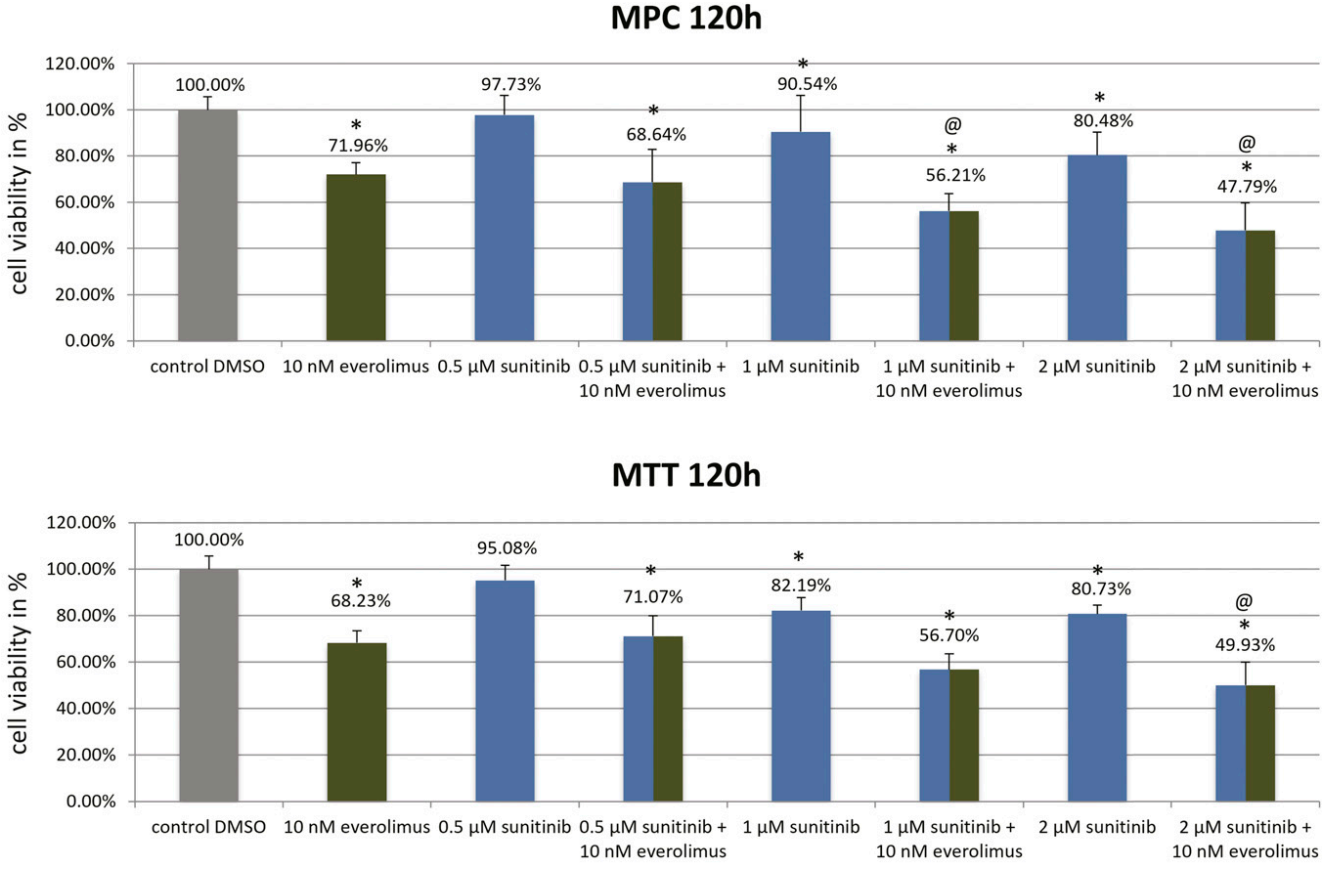

Figure 3. Significant MPC/MTT cell viability reduction by sunitinib, everolimus, and by the combination of both after 120 h. The arithmetic means and SD of at least three independent experiments are shown. [@]Sunitinib/everolimus combination treatment was statistically synergistic in both cell lines. *Statistically significant differences in comparison with the DMSO control ($P < 0.05$).

Cabozantinib (1 μM/2 μM) significantly reduced MPC/MTT cell viability (58) but was not synergistic with everolimus (data not shown).

Niraparib (0.5 μM/1 μM) and temozolomide (100 μM/250 μM) singly significantly reduced MPC/MTT cell viability compared with the control (Fig. 4). Combination of 0.5 to 1.0 μM niraparib plus 100 μM temozolomide, or 0.5 μM niraparib plus 250 μM temozolomide, synergistically diminished MTT, but not MPC, cell viability (Fig. 4).

For all the following experiments in MPC/MTT cells and spheroids, we investigated only the most promising combinations (BYL719/everolimus and sunitinib/everolimus).

Cell cycle and apoptosis

BYL719 (5 μM), everolimus (10 nM), and sunitinib (1 μM/2 μM) significantly increased the G1 cell cycle phase in MPC cells compared with the control (Fig. 5). In MTT cells, everolimus (10 nM) and sunitinib (1 μM/2 μM) significantly increased the G1 cell cycle phase. In both cell lines, BYL719/everolimus or sunitinib/everolimus combination treatments further enhanced G1-phase cell cycle arrest compared with single treatments (Fig. 5). The sub-G1 phase and Western blot quantification can be viewed in materials saved to an online repository (58).

Apoptosis was investigated by caspase assay. In both cell lines, significant apoptosis induction was observed

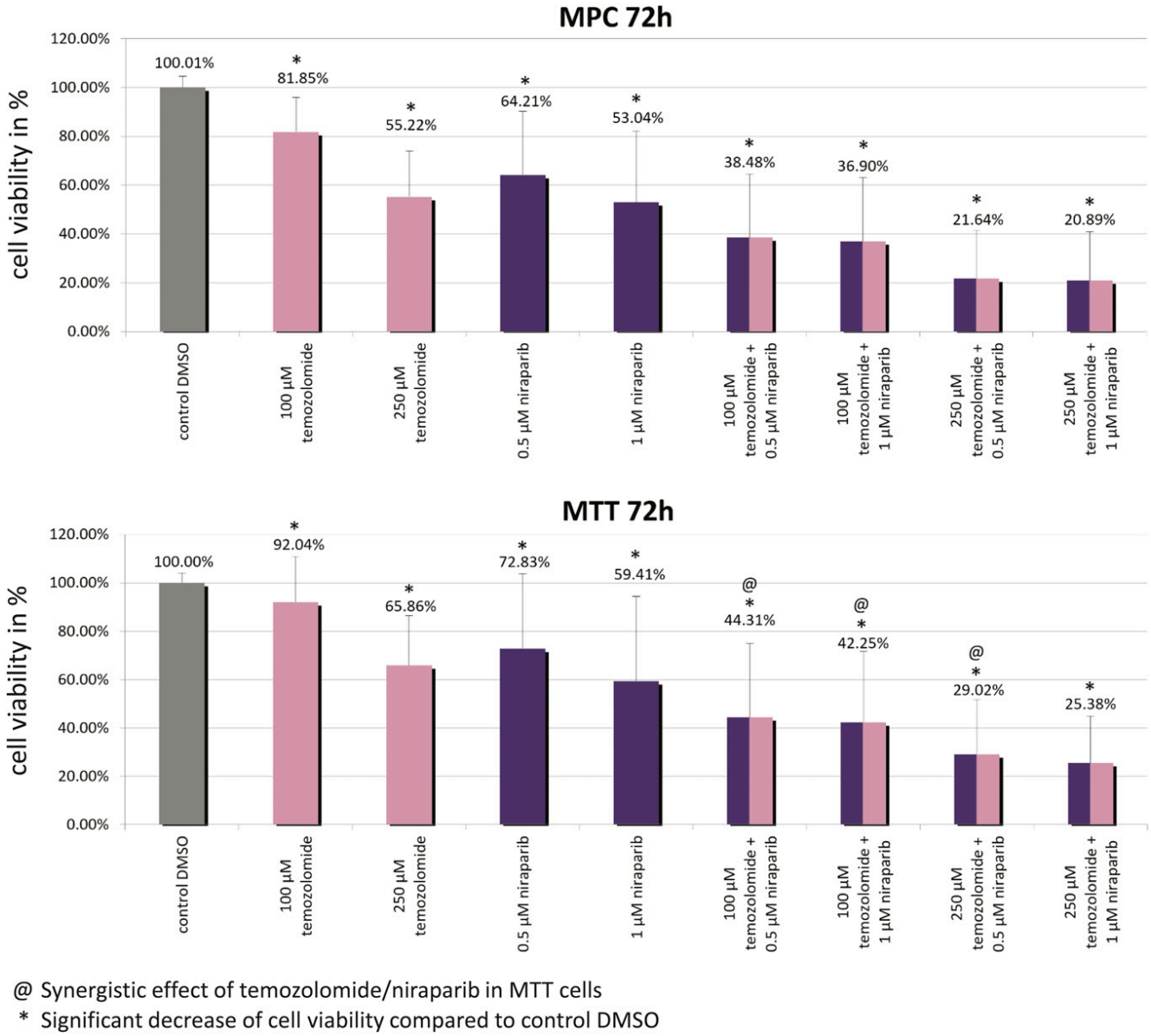

Figure 4. Significant MPC/MTT cell viability reduction by niraparib, by temozolomide, and by the combination of both after 72 h. [@]The niraparib/temozolomide combination was statistically synergistic in MTT cells but not in MPC cells. *Statistically significant differences in comparison with the DMSO control ($P < 0.05$).

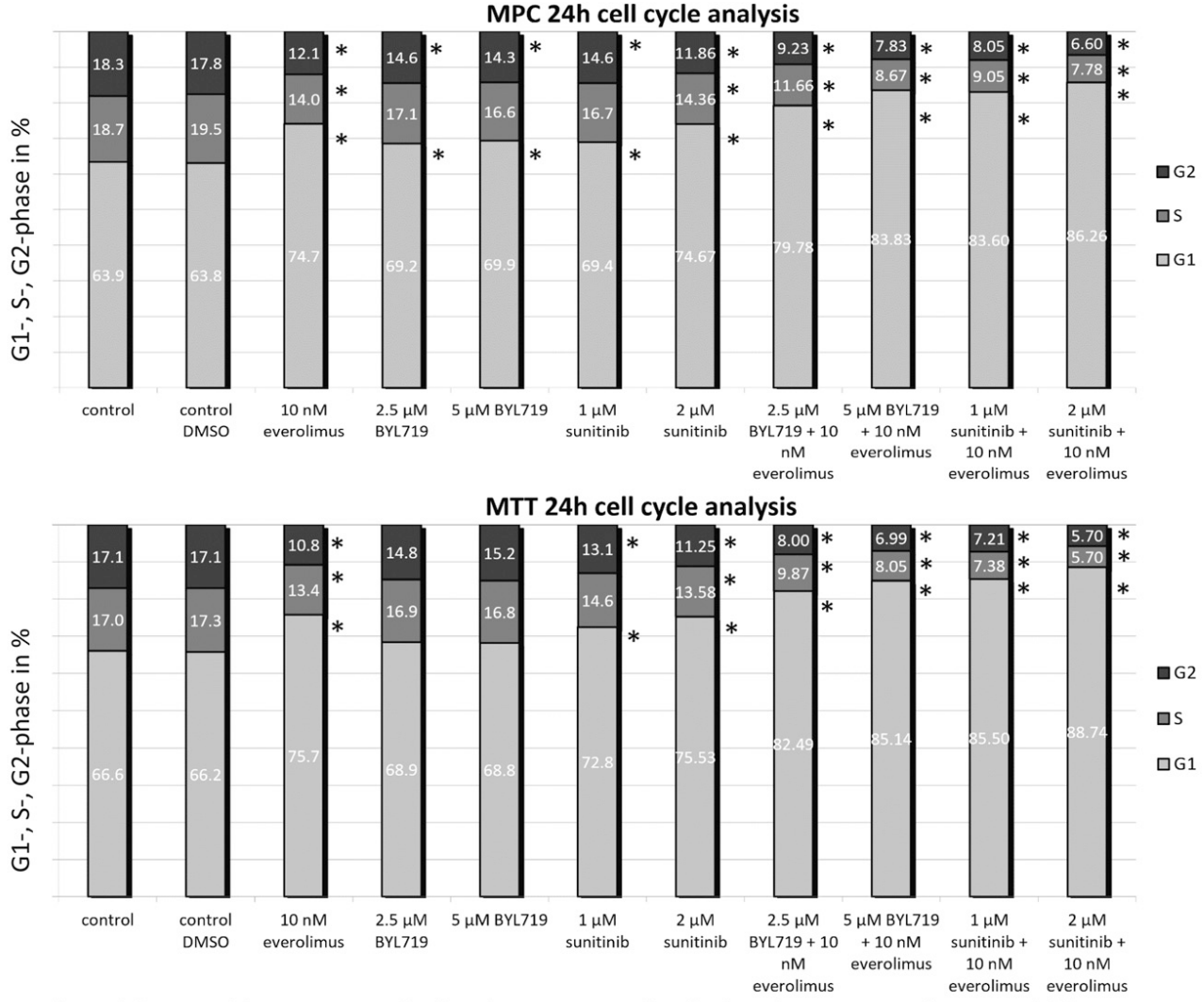

Figure 5. Cell cycle analysis via flow cytometric analysis. Significant induction of a G1-phase cell cycle arrest in MPC cells by BYL719, everolimus, or sunitinib alone and (even stronger) by the BYL719/everolimus and sunitinib/everolimus combination treatments at 24 h of treatment. Significant induction of a G1-phase cell cycle arrest in MTT cells by everolimus (10 nM) and sunitinib (1 µM/2 µM) and (even stronger) by the BYL719/everolimus and sunitinib/everolimus combination treatment at 24 h of treatment. The arithmetic means and SD of at least three independent experiments are shown. *Statistically significant differences in comparison with the DMSO control ($P < 0.05$).

after BYL719 treatment alone (2.5 µM/5 µM), after BYL719/everolimus combination treatment, and (to a lesser extent) after the sunitinib/everolimus combination treatment (Fig. 6).

Western blot analysis

Western blot results of MPC/MTT cells are shown in Fig. 7. Western blot quantification can be viewed in materials saved to an online repository (58). Everolimus is known to inhibit mTORC1/p70S6K and thereby activate AKT. Indeed, everolimus and each combination treatment inhibited p70S6K and S6 in MPC/MTT cells; 4EBP1, another mTORC1 effector, was inhibited by everolimus, BYL719, and each combination treatment. PI3K/AKT_{S473} was activated in response to everolimus, inhibited by BYL719, and unaffected by sunitinib. The BYL719/everolimus combination attenuated everolimus-induced PI3K/AKT_{S473} activation to the level of the untreated control. The sunitinib/everolimus combination did not effectively attenuate everolimus-induced PI3K/AKT_{S473} activation. Although most of the effects were seen at the highest doses tested, these are still low clinically relevant doses (clinically relevant doses of BYL719 are 2 to 11 µM and of everolimus are 8 to 59 nM).

PI3K/AKT phosphorylates and thereby inhibits GSK3 (61). Persistent activation of PI3K leads to feedback downregulation of IRS-1, which may lead to GSK3 disinhibition/activation (62). GSK3α/β phosphorylation and thereby inhibition led to a significant decrease in NET cell viability (63). In this study BYL719 and everolimus alone led to GSK3 inhibition

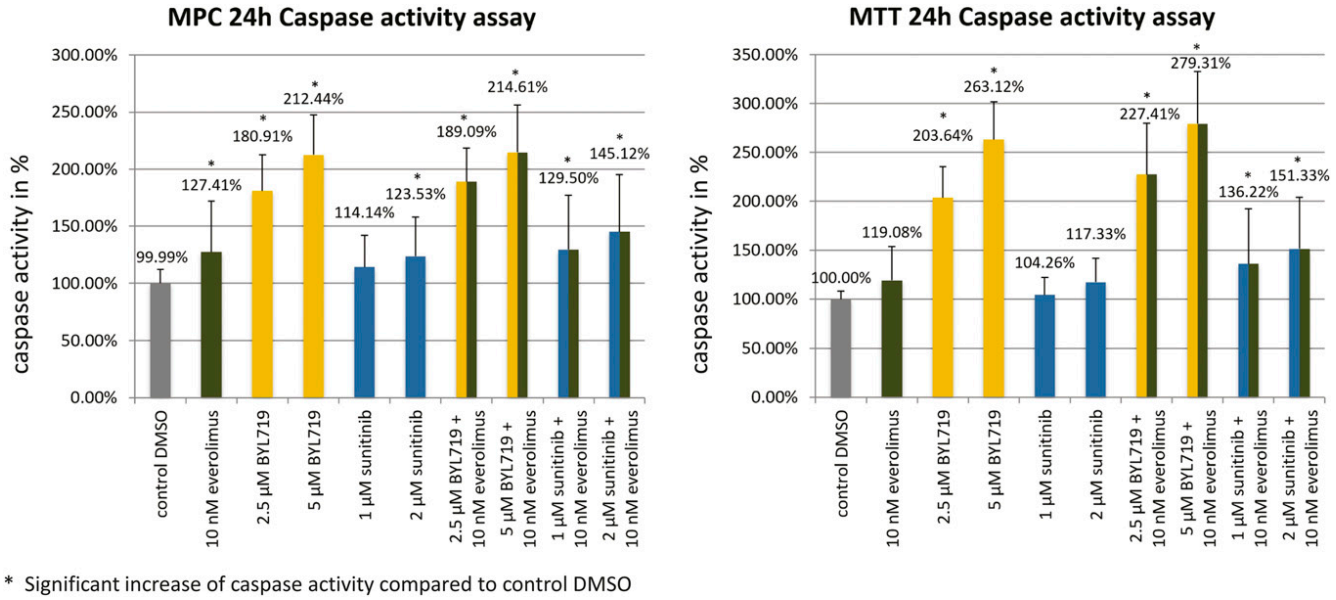

Figure 6. Mean caspase-3/-7 activity in percent ± SD in MPC/MTT cell lines after 24 h of incubation with different drugs. In both cell lines, significant apoptosis induction was observed after BYL719 treatment alone, after BYL719/everolimus combination treatment, and (to a lesser extent) after sunitinib/everolimus combination treatment. The arithmetic means and SD of at least three independent experiments are shown. *Statistically significant differences in comparison with the DMSO control ($P < 0.05$).

in MPC/MTT cells, and combination treatment even more strongly inhibited GSK3. The sunitinib/everolimus combination also led to GSK3 inhibition, compared with the control and single treatment in MTT cells, but inhibited GSK3β to a lesser extent than the BYL719/everolimus combination. BYL719 alone, everolimus alone, and the BYL719/everolimus combination treatment promoted IRS-1 upregulation in MPC/MTT cells as a potential mechanism of GSK3 inhibition.

Consistent with induction of G1 cell cycle arrest, Cyclin D1 and D3 decreased after BYL719/everolimus and sunitinib/everolimus combination treatments in MPC/MTT cells.

Sdhb$^{-/-}$ immortalized mouse chromaffin cells

Patients with PCC/PGL carrying mutations in *SDHB* often show increased incidence of an early-onset, increased metastatic risk and thus a poor prognosis (64). Effective treatment strategies for these patients are missing. Therefore, we have investigated the impact of BYL719 (2.5 µM) and everolimus (10 nM) alone or in combination on immortalized mouse chromaffin cells (imCCs) with and without expression of *Sdhb*. *Sdhb*$^{-/-}$ imCCs carry a true knockout of the *Sdhb* gene, leading to the absence of SDHB protein and complete inhibition of SDH activity (29). Both everolimus and BYL719 alone significantly reduced *Sdhb*$^{-/-}$ cell viability compared with the vehicle, with a synergistic effect of the combination at 72 hours (Fig. 8). Moreover, BYL719 treatment alone had a significantly stronger inhibitory effect on *Sdhb*$^{-/-}$ imCC viability compared with WT imCC viability after 48 and 72 hours of treatment, but the combination treatment was no more effective in *Sdhb*$^{-/-}$ than in the WT cells after 72 hours of treatment (Fig. 8).

MPC/MTT cell spheroids

Tumor cell spheroids are characterized by an oxygen and nutrient gradient and provide an excellent *in vitro* model for drug screening regarding their antitumor activity. Fractionated treatment with clinically relevant doses of BYL719 (5 µM) led to significant shrinkage of MPC/MTT spheroids, compared with the spheroid sizes at the beginning (day 4), and in several cases led to complete spheroid collapse (day 16) (Fig. 9) (58). Fractionated treatment with clinically relevant doses of everolimus (25 nM) significantly inhibited MPC/MTT spheroid growth (Fig. 9) (58). These effects were enhanced by the BYL719/everolimus combination, leading to a significant shrinkage or an early complete collapse of MPC/MTT spheroids in several experiments (days 9 and 14, respectively) (Fig. 9). Although the DMSO control had an average diameter of 585 ± 50.2 µm (MPC) and 500 ± 166.3 µm (MTT) after 18 days, fractionated treatment with 25 nM everolimus plus 5 µM BYL719 led to a significantly smaller average spheroid diameters of 59.5 ± 68.8 µm (MPC) and 62.7 ± 42.3 µm (MTT), respectively. Fractionated treatment with sunitinib only slowed spheroid growth down (58). In MPC spheroids, sunitinib enhanced the efficacy of everolimus (58), but this effect was not

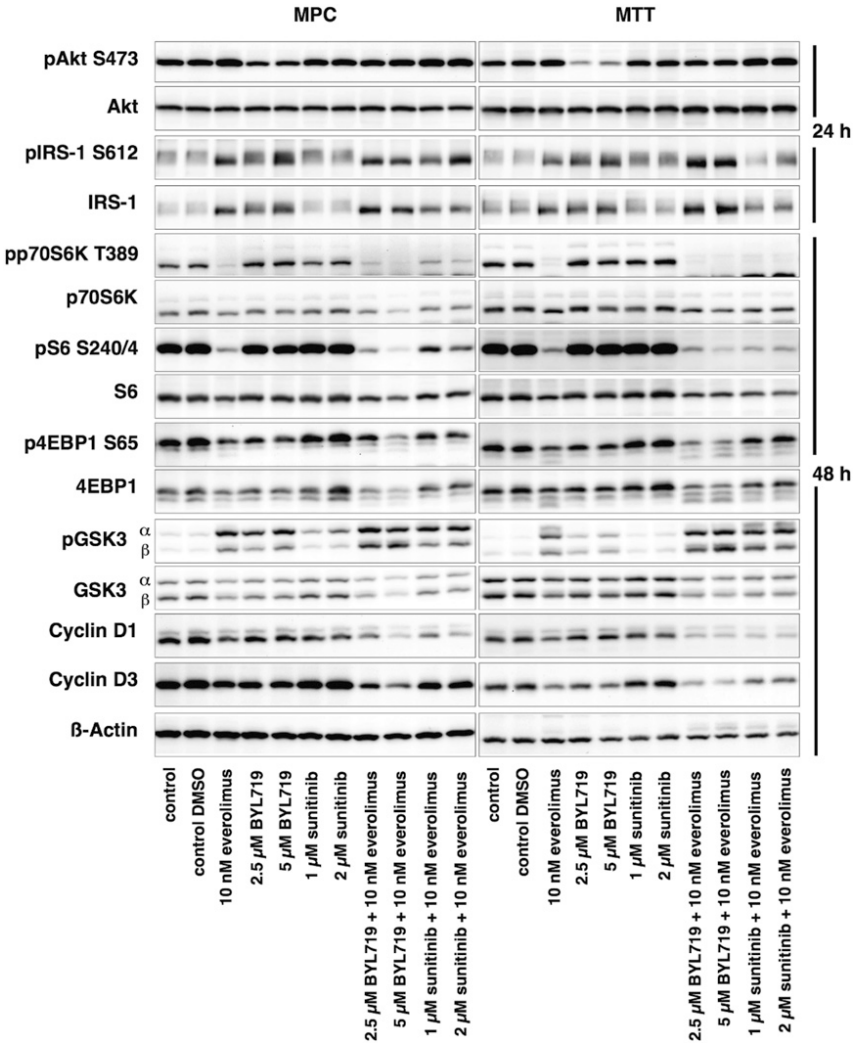

Figure 7. Western blot analysis of MPC/MTT cell lines after 24 or 48 h of incubation with different drugs. Inhibition of p70S6K, S6, 4EBP1, and GSK3 signaling, attenuation of everolimus-induced AKT activation, IRS-1 upregulation, and cyclin D1/D3 downregulation after BYL719/everolimus combination treatment. A representative blot of three independently performed experiments is shown.

seen in MTT spheroids after fractionated treatment (58). Fractionated treatment was more effective than single treatment. No spheroid regrowth was seen after BYL719 single treatment.

Human primary cultures

Clinical, histological, and genetic characteristics

We generated primary cultures from seven patients with PCC/PGL and confirmed tumor identity by detecting synaptophysin as a well-established PCC/PGL marker (30).

Tumors from patients 1, 2, 4, and 6 showed criteria associated with an adverse prognosis, including capsule invasion, vascular invasion, a size of >5 cm, or a Ki-67 of 5% (Table 1), although they were not metastatic. Patient 7 had a metastatic PGL.

Targeted NGS (Table 1) showed disease-causing *NF1* mutations in tumors of patients 2 and 3, in line with cluster-2 tumors. These were likely somatic mutations; in neither patient was germline testing available, but neither patient showed clinical stigmata of neurofibromatosis. However, to exclude the possibility of a hereditary PPGL syndrome, pathogenic variants identified in tumor tissue would need to be analyzed in corresponding blood samples as well.

In tumor tissue from patient 7, we identified a missense variant of unknown significance in the tet methylcytosine dioxygenase (*TET1*) gene, a demethylase involved in epigenetic regulation and gene activation. In the tumor tissues from patients 1 and 4, no known disease-causing susceptibility mutation was identified by NGS. NGS was not performed on tumor tissues from patients 5 and 6.

Primary cell culture viability after different drug treatments

We have statistically combined all human tumor cultures in which combination treatments were tested (tumor cultures from six patients, n = 6).

In all combination-treated human primary cultures (n = 6), clinically relevant doses of BYL719 (2.5 μM/5 μM) and everolimus (10 nM) significantly reduced viability, and the combination of 5μM BYL719 and 10 nM everolimus was highly effective and synergistic ($P < 0.05$) (Fig. 10).

Sunitinib (2 μM) significantly decreased primary culture viability but was not synergistic with everolimus (Fig. 10).

We could not test combination treatments in the primary cultures from patient 7 because there was insufficient tissue material. Sunitinib (1 to 8 μM) and clinically relevant doses of BYL719 (2.5 to 10 μM) separately decreased viability of the primary cultures from patient 7 (58).

Furthermore, we tested entinostat (1 to 10 μM), cabozantinib (1 to 10 μM), niraparib (5 to 10 μM), and temozolomide (100 to 250 μM) in primary cultures from five patients with PCC. Entinostat (1 to 10 μM), cabozantinib (1 to 10 μM), and niraparib (5 to 10 μM) significantly decreased primary culture viability, but temozolomide had no effect (Fig. 11).

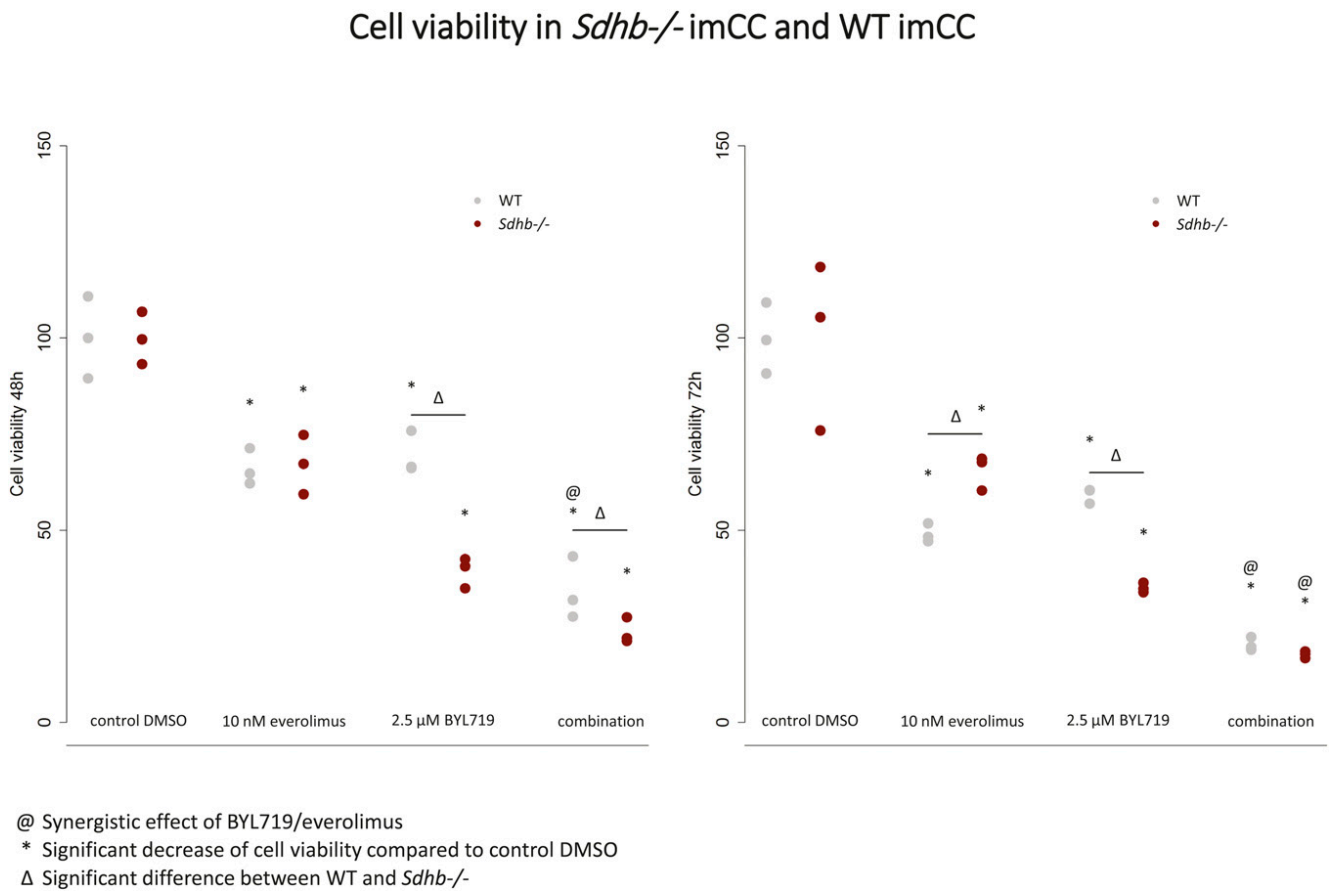

Figure 8. Significant reduction of cell viability after BYL719 and everolimus treatment in immortalized mouse chromaffin WT and $Sdhb^{-/-}$ cells at 48 and 72 h, with a synergistic effect (@) of the combination in both cell lines at 72 h and a substantially stronger effect of BYL719 alone in the $Sdhb^{-/-}$ compared with the WT cells. $^{\Delta}$Significant difference between WT and $Sdhb^{-/-}$. *Statistically significant differences in comparison with the DMSO control ($P < 0.05$).

Western blot analysis

We had sufficient human primary culture material from patients 2, 3, and 5 for performing detailed Western blot analysis of these primary cultures; the results are shown in Fig. 12. Western blot quantification of the treatments performed identically in all three primary cultures (control DMSO, 10 nM everolimus, 2 µM BYL719, BYL719/everolimus combination) can be viewed in materials saved to an online repository (58). Supplemental Table 2 (58) shows all the values of the Western blot quantification of all primary culture Western blots. The mTORC1 effector proteins p70S6K and S6 were strongly inhibited by everolimus and by each combination treatment at 24 hours; 4EBP1, another mTORC1 effector protein, was inhibited by everolimus and the BYL719/everolimus combination treatment. AKT_{S473} was activated in response to everolimus, and this activation was attenuated by the addition of BYL719 in the primary cultures from patients 3 and 5. In contrast to the mouse cell lines, inhibition of GSK3 by BYL719 or by combination treatments could not be shown, possibly due to a shorter treatment time of 24 hours. However, after a longer incubation time of 48 hours, the protein concentration of the primary cultures was too low for Western blot detection. P53 was moderately downregulated by the everolimus/BYL719 combination. Consistent with a G1-phase cell cycle arrest, combination treatments were associated with downregulation of the cell cycle promoting markers cyclin D3, CDK1 cdc2 (patient 3), and chk1 (patients 3 and 5).

Discussion

We have shown that targeted combination treatment with clinically relevant doses of the PI3Kα inhibitor BYL719 and the mTORC1 inhibitor everolimus exhibited strong synergistic antitumor potential in PCC cell lines and especially $Sdhb^{-/-}$ cells and in human PCC primary cultures. In MPC/MTT three-dimensional spheroids, this combination treatment led to dramatic spheroid shrinkage or to a complete spheroid collapse in several experiments. The BYL719/everolimus combination was the most effective treatment we have tested in PCC spheroids.

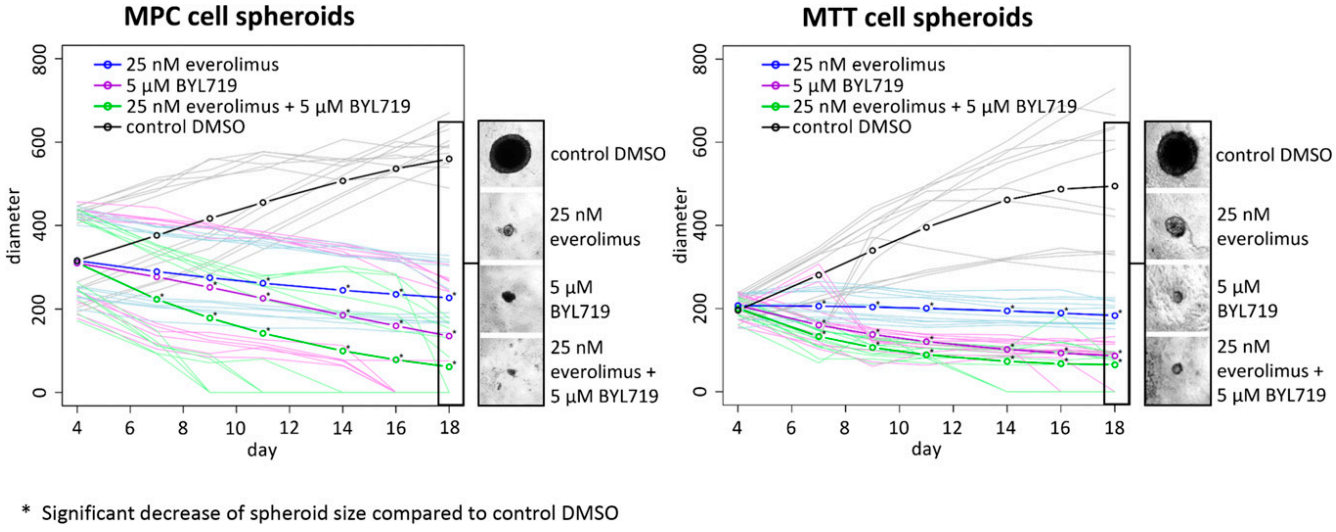

Figure 9. Significant MPC/MTT spheroid shrinkage or complete spheroid collapse after fractionated treatment with 5 µM BYL719, even stronger shrinkage, as compared with BYL719 alone, or an early complete collapse of the spheroids in several experiments after fractionated treatment with the BYL719/everolimus combination and spheroid growth inhibition after fractionated treatment with 25 nM everolimus. Spheroids were treated with different concentrations of BYL719 and everolimus after completed spheroid formation (day 4) and on days 7, 11, and 14 (fractionated treatment). Growth was monitored over 18 d. The arithmetic means and all single values of each experiment of at least three independent experiments are shown. *Statistically significant different results in comparison with the DMSO control ($P < 0.05$).

Everolimus has been approved for the treatment of NETs in many countries (65–67). Similarly to PCC/PGL with increased PI3K/AKT/mTORC1 activation (68), gastroenteropancreatic NETs show frequent PI3K/AKT/mTORC1 overactivation (69, 70). However, everolimus alone showed disappointing results in a small study of patients with PCC/PGL (20). Compensatory IRS-1/PI3K/AKT disinhibition/activation in response to mTORC1/p70S6K inhibition is the known short-term mechanism of everolimus resistance (71–75). Indeed, we found strong everolimus-induced PI3K/AKT activation in PCC cell lines and human primary cultures. In different NET cell lines, the PI3Kα inhibitor BYL719 showed synergism with everolimus at clinically relevant doses (24, 76) and overcame long-term everolimus resistance in human pancreatic NET cells (24). In a breast cancer model, everolimus also acted synergistically with BYL719 and delayed the development of resistance to BYL719 *in vitro* and *in vivo* (22). Consistently, we showed in our murine PCC cell lines and in two different human PCC cultures that addition of BYL719 attenuated everolimus-induced AKT activation, which may

Table 1. Clinical and Histological Characteristics of the Human PCC/PGL Primary Cultures From Seven Different Patients

Patient	Age	Sex	Tumor	Metastatic	Histology and Criteria of Malignancy	Ki-67 (%)	NGS of the Tumors
1	82	M	Adrenal pheochromocytoma	No	Tumor size: 1.5 cm; capsule invasion	1–2	No known susceptibility mutation
2	50	M	Adrenal pheochromocytoma	No	Tumor size: 12.9 cm; nuclear pleomorphism	1–2	*NF1* mutation
3	73	F	Adrenal pheochromocytoma	No	Tumor size: 3.9 cm; nuclear and cell pleomorphism	2	*NF1* mutation
4	26	M	Adrenal pheochromocytoma	No	Tumor size: 3.2 cm; vascular invasion, anisonucleosis, cell inclusions	5	No known susceptibility mutation
5	65	M	Adrenal pheochromocytoma	No	Tumor size: 5 cm	<1	Not assessed
6	60	M	Adrenal pheochromocytoma	No	Tumor size: 5.5 cm; capsule invasion, vascular invasion	<1	Not assessed
7	30	F	Uterus metastasis	Yes	Tumor size: 5.3 cm	20	Variant of unknown significance in *TET1*
			Lymph node metastasis	Yes	Tumor size: 2.5 cm	20	

Abbreviations: F, female; M, male.

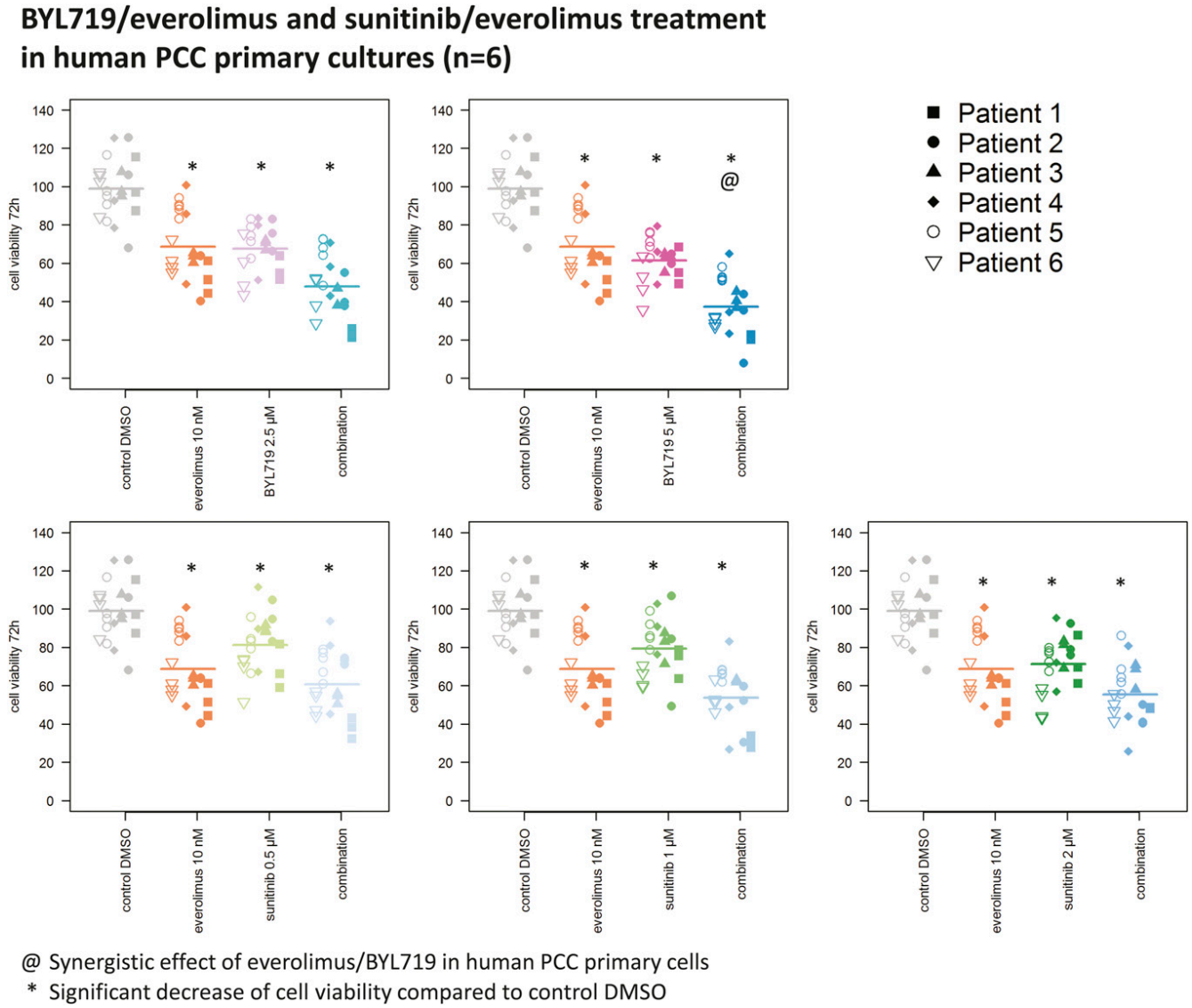

Figure 10. Significant reduction of human PCC primary culture viability (n = 6) by clinically relevant doses of BYL719, everolimus, and the combination of BYL719 plus everolimus at 72 h of treatment, showing a synergistic effect (@) of 5 µM BYL719 plus 10 nM everolimus. A significant reduction of human PCC primary culture viability (n = 6) by sunitinib and the combination of sunitinib plus everolimus is seen at 72 h. Sunitinib and everolimus did not act synergistically. The arithmetic means and all single values of six human PCC cultures from six different patients are shown. *Statistically significant different results in comparison with the DMSO control ($P < 0.05$).

contribute to the synergism of both drugs. As also observed in human NET cells (24, 76), BYL719/everolimus combination treatment led to synergistic inhibition of GSK3 in PCC cell lines, possibly as a consequence of IRS-1 upregulation. IRS-1 has previously been shown to inhibit GSK3 via different signaling pathways (61, 77, 78), and GSK3 inhibition has shown antitumor potential in human NET cell lines (63).

In our murine cell lines, the BYL719/everolimus combination induced a substantial G1-phase cell cycle arrest that was more prominent than in each single-drug treatment. Consistently, the BYL719/everolimus combination led to cyclin D1/D3 downregulation in PCC cell lines and human primary cultures.

In contrast to other PI3K inhibitors, such as NVP-BEZ235 or BKM120, BYL719 is most likely to become clinically available. The phase III approval study SOLAR-1 evaluating BYL719 (alpelisib) in metastatic breast cancer has reached its final endpoints (23). Another phase IB trial is evaluating the safety of BYL719 (alpelisib) plus everolimus in advanced breast, renal cell, and pancreatic cancer, including pancreatic NETs (clinical trial no. NCT02077933).

Sunitinib is being evaluated in a randomized, prospective, placebo-controlled clinical phase II trial in PCC/PGL (FIRST-MAPPP, NCT01371202), which has completed recruitment. A synergistic effect of sunitinib and everolimus was shown in MPC/MTT cell lines at doses exceeding clinical relevance but not in human primary cultures. This may be in part due to additional

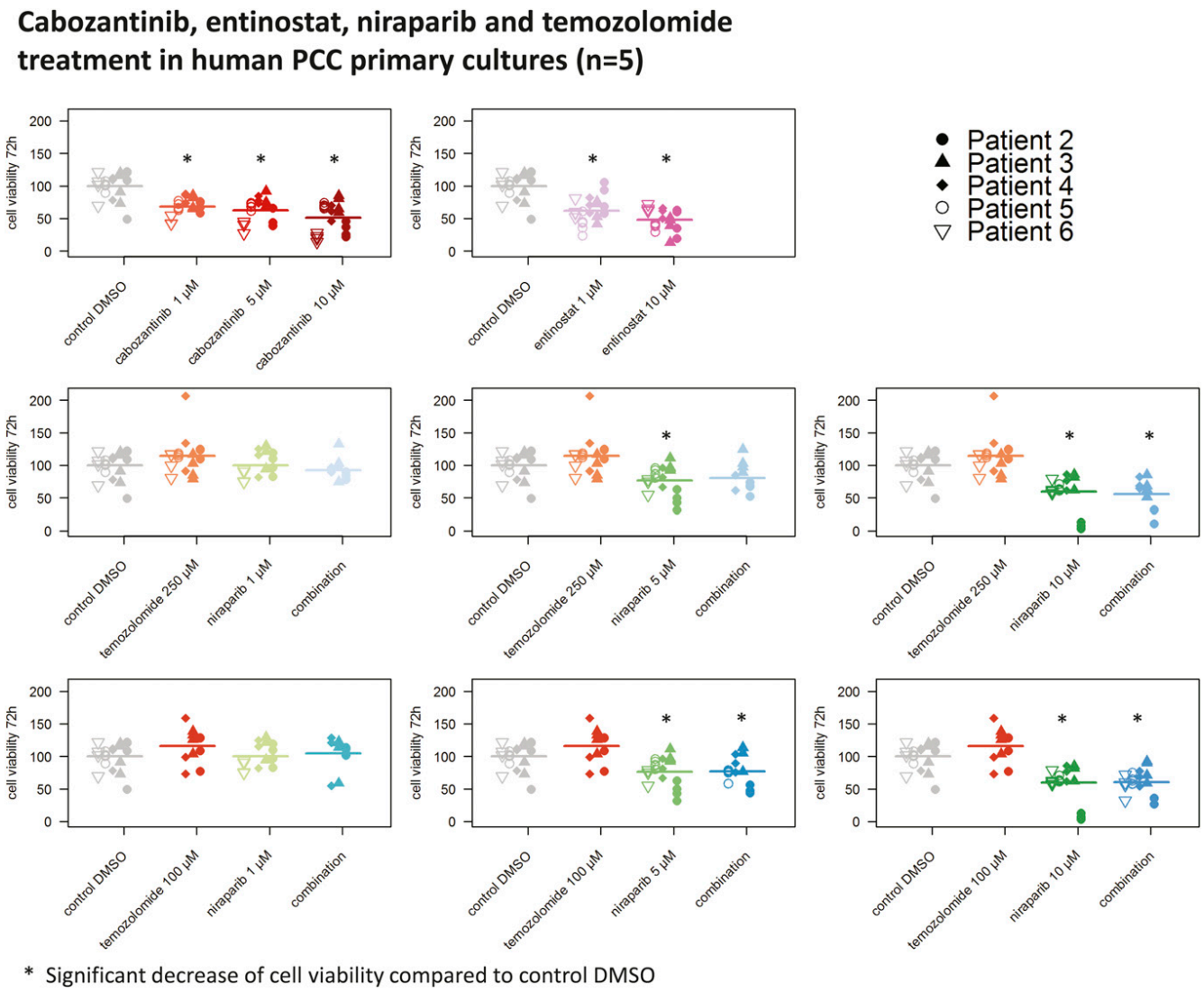

Figure 11. Substantial reduction of human PCC primary culture viability (n = 5) by cabozantinib, entinostat, and niraparib, but not temozolomide, at 72 h of treatment. The arithmetic means and all single values of five human PCC primary cultures from five patients are shown. *Statistically significant different results in comparison with the DMSO control ($P < 0.05$).

antiangiogenic activity of sunitinib *in vivo*, which cannot be mimicked by cell culture. However, BYL719/everolimus combination treatment seems to be more promising, as compared with sunitinib/everolimus *in vitro*. Nevertheless, one case in the literature notes a patient with the *SDHB* mutation who received the mTORC1 inhibitor rapamycin in combination with sunitinib and experienced long-term disease control (21).

The combination of niraparib with temozolomide was synergistic in the MTT cells but not in human primary cultures. PARP inhibition by niraparib suppresses DNA repair and sensitizes tumors to alkylating DNA-damaging agents (14, 79, 80), thus synergizing with temozolomide in the murine PCC cell lines. Consistent with this, in an allograft PCC mouse model, a PARP inhibitor sensitized PCCs to temozolomide (15). However, temozolomide showed an absence of efficacy in human primary cultures, whereas niraparib and entinostat were effective in primary cultures. This implicates fundamental differences of drug effects between murine cell lines and human primary cultures, rendering additional confirmatory drug testing in human primary cultures even more important.

Cabozantinib showed significant efficacy in PCC cell lines and human primary cultures at clinically relevant doses but no synergism with everolimus. The PCC cell lines and human primary cultures displayed a weaker response to cabozantinib alone, as compared with everolimus/BYL719 combination treatment. Our data suggest that dual PI3K/mTORC1 inhibition might be more effective at lower doses with less toxicity. As a next step, we will investigate the most promising combination of everolimus/BYL719 *in vivo* in a suitable PCC allograft model.

The success of the different molecular-targeted therapies alone and in combination depends on the individual

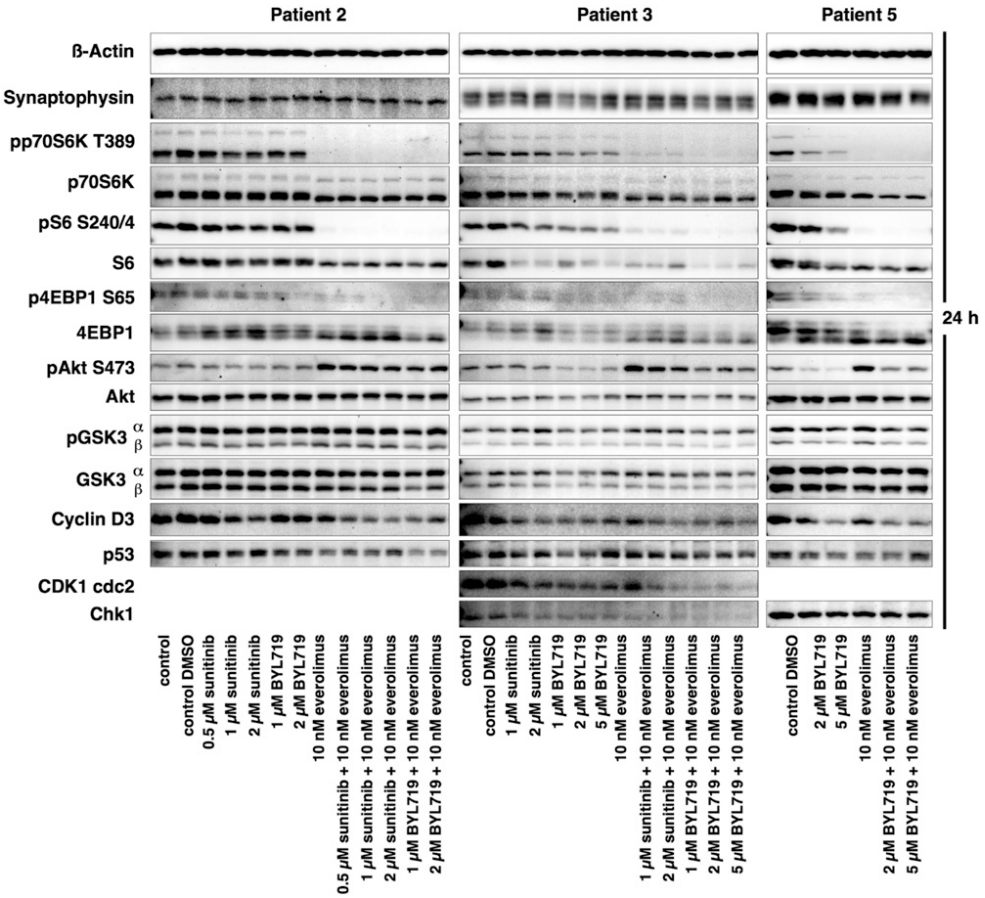

Figure 12. Western blot analysis of the human primary cultures from patients 2, 3, and 5 after 24 h of incubation with different drugs. There was strong synaptophysin expression in all primary cultures. There was strong inhibition of mTORC1/p70S6K and 4EBP1 signaling by everolimus and all combination treatments, attenuation of everolimus-induced AKT activation by the combination treatment in the primary cultures from patients 3 and 5 and downregulation of cyclin D3, CDK1 cdc2 (patient 3), chk1 (patients 3 and 5), and p53 by the combination treatment. GSK3 showed no clear differences, most likely due to suboptimal incubation times.

molecular aberrations of each tumor, as shown in other tumor types (81). For example, the tumors from patients 2 and 3 are associated with *NF1* mutations leading to MEK/RAS/ERK and mTORC1 overactivation (82–84). Accordingly, both tumor cultures responded well to mTORC1 and PI3Kα inhibition by everolimus and BYL719, respectively, and especially to the combination, with attenuation of everolimus-induced AKT activation by BYL719. This suggests that, among others, *NF1*-mutated tumors, which are frequently present among sporadic PCCs (85), should respond to these targeted drugs. In the PGL of patient 7, who had an unusual metastatic phenotype, no disease-causing variants were identified in any of the known PCC/PGL susceptibility genes; however, a variant of unknown significance in *TET1*, a DNA demethylase, was found, which presents a potential candidate gene that needs further investigation in the future.

In summary, we have established a method to investigate molecular-targeted agents in human PCC primary cultures of individual patient tumors and have correlated drug efficacy with signaling pathway alterations. The established protocol for *ex vivo* treatment of human PCC/PGL primary cultures with different molecular-targeted drugs allows screening for appropriate treatment approaches for each patient. In addition, we identified dual mTORC1/PI3Kα inhibition by the everolimus/BYL719 combination treatment as clinically relevant, highly effective synergistic targeted therapy in all the PCC models investigated, including human tumor cultures.

Acknowledgments

The authors thank Susanne Schmid (study nurse) for her excellent work and Isabel Poser and Daniela Stanke for excellent technical assistance.

Financial Support: This work was funded by Deutsche Forschungsgemeinschaft within the CRC/Transregio 205/1 "The Adrenal: Central Relay in Health and Disease" (to N.B., B.K., C.G.Z., M.F., F.B., S.R.B., G.E., and M.R.) and by the Intramural Research Program of the National Institutes of Health, National Institute of Child Health and Human Development.

Clinical Trial Information: ClinicalTrials.gov nos. NCT01371201 (registered 10 June 2011) and NCT02077933 (registered 14 March 2014).

Additional Information

Correspondence: Svenja Nölting, MD, Med. Klinik und Poliklinik IV, Klinikum der Universität München, Ziemssenstraße 1, 80336 Munich, Germany. E-mail: svenja.noelting@med.uni-muenchen.de.

Disclosure Summary: A.B.G. has received research funding from AAA and lecture fees from Ipsen, Roche, and HRA Pharma. C.J.A. has received research contracts from Ipsen, Novartis, and ITM Solucin; lecture honorarium from Ipsen, Novartis, and Falk Foundation; and advisory board honorarium from Novartis. S.N. has received research contracts from Novartis and lecture fees from Ipsen. The remaining authors have nothing to disclose.

Data Availability: All data generated or analyzed during this study are included in this published article or in the data repositories listed in References.

References and Notes

1. Remine WH, Chong GC, Van Heerden JA, Sheps SG, Harrison EG, Jr. Current management of pheochromocytoma. *Ann Surg*. 1974; **179**(5):740–748.
2. Proye CA, Vix M, Jansson S, Tisell LE, Dralle H, Hiller W. "The" pheochromocytoma: a benign, intra-adrenal, hypertensive, sporadic unilateral tumor. Does it exist? *World J Surg*. 1994;**18**(4):467–472.
3. Goldstein RE, O'Neill JA, Jr, Holcomb GW III, Morgan WM III, Neblett WW III, Oates JA, Brown N, Nadeau J, Smith B, Page DL, Abumrad NN, Scott HW, Jr. Clinical experience over 48 years with pheochromocytoma. *Ann Surg*. 1999;**229**(6):755–764, discussion 764–766.
4. Mannelli M, Ianni L, Cilotti A, Conti A. Pheochromocytoma in Italy: a multicentric retrospective study. *Eur J Endocrinol*. 1999; **141**(6):619–624.
5. John H, Ziegler WH, Hauri D, Jaeger P. Pheochromocytomas: can malignant potential be predicted? *Urology*. 1999;**53**(4):679–683.
6. Edström Elder E, Hjelm Skog AL, Höög A, Hamberger B. The management of benign and malignant pheochromocytoma and abdominal paraganglioma. *Eur J Surg Oncol*. 2003;**29**(3):278–283.
7. Amar L, Servais A, Gimenez-Roqueplo AP, Zinzindohoue F, Chatellier G, Plouin PF. Year of diagnosis, features at presentation, and risk of recurrence in patients with pheochromocytoma or secreting paraganglioma. *J Clin Endocrinol Metab*. 2005;**90**(4):2110–2116.
8. Feng F, Zhu Y, Wang X, Wu Y, Zhou W, Jin X, Zhang R, Sun F, Kasoma Z, Shen Z. Predictive factors for malignant pheochromocytoma: analysis of 136 patients. *J Urol*. 2011;**185**(5):1583–1590.
9. Park J, Song C, Park M, Yoo S, Park SJ, Hong S, Hong B, Kim CS, Ahn H. Predictive characteristics of malignant pheochromocytoma. *Korean J Urol*. 2011;**52**(4):241–246.
10. Hamidi O, Young WF, Jr, Gruber L, Smestad J, Yan Q, Ponce OJ, Prokop L, Murad MH, Bancos I. Outcomes of patients with metastatic phaeochromocytoma and paraganglioma: A systematic review and meta-analysis. *Clin Endocrinol (Oxf)*. 2017;**87**(5):440–450.
11. Mak IYF, Hayes AR, Khoo B, Grossman A. Peptide receptor radionuclide therapy as a novel treatment for metastatic and invasive phaeochromocytoma and paraganglioma. *Neuroendocrinology*. (in press).
12. Nölting S, Grossman A, Pacak K. Metastatic phaeochromocytoma: spinning towards more promising treatment options. *Exp Clin Endocrinol Diabetes*. 2019;**127**(2-3):117–128.
13. Ray Chaudhuri A, Nussenzweig A. The multifaceted roles of PARP1 in DNA repair and chromatin remodelling. *Nat Rev Mol Cell Biol*. 2017;**18**(10):610–621.
14. de Murcia JM, Niedergang C, Trucco C, Ricoul M, Dutrillaux B, Mark M, Oliver FJ, Masson M, Dierich A, LeMeur M, Walztinger C, Chambon P, de Murcia G. Requirement of poly(ADP-ribose) polymerase in recovery from DNA damage in mice and in cells. *Proc Natl Acad Sci USA*. 1997;**94**(14):7303–7307.
15. Pang Y, Lu Y, Caisova V, Liu Y, Bullova P, Huynh TT, Zhou Y, Yu D, Frysak Z, Hartmann I, Taïeb D, Pacak K, Yang C, Yang C. Targeting NAD+/PARP DNA repair pathway as a novel therapeutic approach to SDHB-mutated cluster I pheochromocytoma and paraganglioma. *Clin Cancer Res*. 2018;**24**(14):3423–3432.
16. Koumarianou A, Kaltsas G, Kulke MH, Oberg K, Strosberg JR, Spada F, Galdy S, Barberis M, Fumagalli C, Berruti A, Fazio N. Temozolomide in advanced neuroendocrine neoplasms: pharmacological and clinical aspects. *Neuroendocrinology*. 2015;**101**(4): 274–288.
17. Luchetti A, Walsh D, Rodger F, Clark G, Martin T, Irving R, Sanna M, Yao M, Robledo M, Neumann HP, Woodward ER, Latif F, Abbs S, Martin H, Maher ER. Profiling of somatic mutations in phaeochromocytoma and paraganglioma by targeted next generation sequencing analysis. *Int J Endocrinol*. 2015;**2015**:138573.
18. Burnichon N, Vescovo L, Amar L, Libé R, de Reynies A, Venisse A, Jouanno E, Laurendeau I, Parfait B, Bertherat J, Plouin PF, Jeunemaitre X, Favier J, Gimenez-Roqueplo AP. Integrative genomic analysis reveals somatic mutations in pheochromocytoma and paraganglioma. *Hum Mol Genet*. 2011;**20**(20):3974–3985.
19. Jochmanova I, Pacak K. Genomic landscape of pheochromocytoma and paraganglioma. *Trends Cancer*. 2018;**4**(1):6–9.
20. Druce MR, Kaltsas GA, Fraenkel M, Gross DJ, Grossman AB. Novel and evolving therapies in the treatment of malignant phaeochromocytoma: experience with the mTOR inhibitor everolimus (RAD001). *Horm Metab Res*. 2009;**41**:697–702.
21. Ayala-Ramirez M, Chougnet CN, Habra MA, Palmer JL, Leboulleux S, Cabanillas ME, Caramella C, Anderson P, Al Ghuzlan A, Waguespack SG, Deandreis D, Baudin E, Jimenez C. Treatment with sunitinib for patients with progressive metastatic pheochromocytomas and sympathetic paragangliomas. *J Clin Endocrinol Metab*. 2012;**97**(11):4040–4050.
22. Elkabets M, Vora S, Juric D, Morse N, Mino-Kenudson M, Muranen T, Tao J, Campos AB, Rodon J, Ibrahim YH, Serra V, Rodrik-Outmezguine V, Hazra S, Singh S, Kim P, Quadt C, Liu M, Huang A, Rosen N, Engelman JA, Scaltriti M, Baselga J. mTORC1 inhibition is required for sensitivity to PI3K p110α inhibitors in PIK3CA-mutant breast cancer. *Sci Transl Med*. 2013;**5**(196): 196ra99.
23. André F, Ciruelos E, Rubovszky G, Campone M, Loibl S, Rugo HS, Iwata H, Conte P, Mayer IA, Kaufman B, Yamashita T, Lu YS, Inoue K, Takahashi M, Pápai Z, Longin AS, Mills D, Wilke C, Hirawat S, Juric D; SOLAR-1 Study Group. Alpelisib for *PIK3CA*-mutated, hormone receptor-positive advanced breast cancer. *N Engl J Med*. 2019;**380**(20):1929–1940.
24. Aristizabal Prada ET, Spöttl G, Maurer J, Lauseker M, Koziolek EJ, Schrader J, Grossman A, Pacak K, Beuschlein F, Auernhammer CJ, Nölting S. The role of GSK3 and its reversal with GSK3 antagonism in everolimus resistance. *Endocr Relat Cancer*. 2018;**25**(10): 893–908.
25. Powers JF, Evinger MJ, Tsokas P, Bedri S, Alroy J, Shahsavari M, Tischler AS. Pheochromocytoma cell lines from heterozygous neurofibromatosis knockout mice. *Cell Tissue Res*. 2000;**302**(3): 309–320.
26. Martiniova L, Lai EW, Elkahloun AG, Abu-Asab M, Wickremasinghe A, Solis DC, Perera SM, Huynh T-T, Lubensky IA, Tischler AS, Kvetnansky R, Alesci S, Morris JC, Pacak K. Characterization of an animal model of aggressive metastatic pheochromocytoma linked to a specific gene signature. *Clin Exp Metastasis*. 2009;**26**(3):239–250.

27. Nölting S, Garcia E, Alusi G, Giubellino A, Pacak K, Korbonits M, Grossman AB. Combined blockade of signalling pathways shows marked anti-tumour potential in phaeochromocytoma cell lines. *J Mol Endocrinol*. 2012;**49**(2):79–96.
28. Almeida JL, Hill CR, Cole KD. Mouse cell line authentication. *Cytotechnology*. 2014;**66**(1):133–147.
29. Letouzé E, Martinelli C, Loriot C, Burnichon N, Abermil N, Ottolenghi C, Janin M, Menara M, Nguyen AT, Benit P, Buffet A, Marcaillou C, Bertherat J, Amar L, Rustin P, De Reyniès A, Gimenez-Roqueplo AP, Favier J. SDH mutations establish a hypermethylator phenotype in paraganglioma. *Cancer Cell*. 2013; **23**(6):739–752.
30. Budde K, Zonnenberg BA, Frost M, Cheung W, Urva S, Brechenmacher T, Stein K, Chen D, Kingswood JC, Bissler JJ. Pharmacokinetics and pharmacodynamics of everolimus in patients with renal angiomyolipoma and tuberous sclerosis complex or lymphangioleiomyomatosis. *Br J Clin Pharmacol*. 2016;**81**(5): 958–970.
31. De Buck SS, Jakab A, Boehm M, Bootle D, Juric D, Quadt C, Goggin TK; Buck SSd. Population pharmacokinetics and pharmacodynamics of BYL719, a phosphoinositide 3-kinase antagonist, in adult patients with advanced solid malignancies. *Br J Clin Pharmacol*. 2014;**78**(3):543–555.
32. Faivre S, Delbaldo C, Vera K, Robert C, Lozahic S, Lassau N, Bello C, Deprimo S, Brega N, Massimini G, Armand J-P, Scigalla P, Raymond E. Safety, pharmacokinetic, and antitumor activity of SU11248, a novel oral multitarget tyrosine kinase inhibitor, in patients with cancer. *J Clin Oncol*. 2006;**24**(1):25–35.
33. Miles D, Jumbe NL, Lacy S, Nguyen L. Population pharmacokinetic model of cabozantinib in patients with medullary thyroid carcinoma and its application to an exposure-response analysis. *Clin Pharmacokinet*. 2016;**55**(1):93–105.
34. Feoktistova M, Geserick P, Leverkus M. Crystal violet assay for determining viability of cultured cells. *Cold Spring Harb Protoc*. 2016;**2016**(4):pdb.prot087379.
35. Bechmann N, Ehrlich H, Eisenhofer G, Ehrlich A, Meschke S, Ziegler CG, Bornstein SR. Anti-tumorigenic and anti-metastatic activity of the sponge-derived marine drugs aeroplysinin-1 and isofistularin-3 against pheochromocytoma in vitro. *Mar Drugs*. 2018;**16**(5):E172.
36. Bechmann N, Poser I, Seifert V, Greunke C, Ullrich M, Qin N, Walch A, Peitzsch M, Robledo M, Pacak K, Pietzsch J, Richter S, Eisenhofer G. Impact of extrinsic and intrinsic hypoxia on catecholamine biosynthesis in absence or presence of Hif2α in pheochromocytoma cells. *Cancers (Basel)*. 2019;**11**(5):594.
37. Reuther C, Heinzle V, Spampatti M, Vlotides G, de Toni E, Spöttl G, Maurer J, Nölting S, Göke B, Auernhammer CJ. Cabozantinib and tivantinib, but not INC280, induce antiproliferative and antimigratory effects in human neuroendocrine tumor cells in vitro: evidence for 'off-target' effects not mediated by c-Met inhibition. *Neuroendocrinology*. 2016;**103**(3-4):383–401.
38. RRID:AB_2315049, https://scicrunch.org/resolver/RRID:AB_2315049.
39. RRID:AB_329827, https://scicrunch.org/resolver/RRID:AB_329827.
40. RRID:AB_330947, https://scicrunch.org/resolver/RRID:AB_330947.
41. RRID:AB_2097841, https://scicrunch.org/resolver/RRID:AB_2097841.
42. RRID:AB_10695803, https://scicrunch.org/resolver/RRID:AB_10695803.
43. RRID:AB_2259616, https://scicrunch.org/resolver/RRID:AB_2259616.
44. RRID:AB_2070801, https://scicrunch.org/resolver/RRID:AB_2070801.
45. RRID:AB_330944, https://scicrunch.org/resolver/RRID:AB_330944.
46. RRID:AB_390722, https://scicrunch.org/resolver/RRID:AB_390722.
47. RRID:AB_10694233, https://scicrunch.org/resolver/RRID:AB_10694233.
48. RRID:AB_331355, https://scicrunch.org/resolver/RRID:AB_331355.
49. RRID:AB_329830, https://scicrunch.org/resolver/RRID:AB_329830.
50. RRID:AB_10547140, https://scicrunch.org/resolver/RRID:AB_10547140.
51. RRID:AB_2074795, https://scicrunch.org/resolver/RRID:AB_2074795.
52. RRID:AB_2080320, https://scicrunch.org/resolver/RRID:AB_2080320.
53. RRID:AB_2536328, https://scicrunch.org/resolver/RRID:AB_2536328.
54. RRID:AB_2533767, https://scicrunch.org/resolver/RRID:AB_2533767.
55. RRID:AB_476744, https://scicrunch.org/resolver/RRID:AB_476744.
56. RRID:AB_95187, https://scicrunch.org/resolver/RRID:AB_95187.
57. Gieldon L, William D, Hackmann K, Jahn W, Jahn A, Wagner J, Rump A, Bechmann N, Nölting S, Knösel T, Gudziol V, Constantinescu G, Masjkur J, Beuschlein F, Timmers HJ, Canu L, Pacak K, Robledo M, Aust D, Schröck E, Eisenhofer G, Richter S, Klink B. Optimizing genetic workup in pheochromocytoma and paraganglioma by integrating diagnostic and research approaches. *Cancers (Basel)*. 2019;**11**(6):E809.
58. Fankhauser M, Bechmann N, Lauseker M, Goncalves J, Favier J, Klink B, William D, Gieldon L, Maurer J, Spöttl G, Rank P, Knösel T, Orth M, Ziegler CG, Aristizabal Prada ET, Rubinstein G, Fassnacht M, Spitzweg C, Grossman AB, Pacak K, Beuschlein F, Bornstein SR, Eisenhofer G, Auernhammer CJ, Reincke M, Nölting S. Data from: Synergistic highly potent targeted drug combinations in different pheochromocytoma models including human tumor cultures. Secure Synology Webstorage NAS 2019. Deposited 7 May 2019. https://emds-nas.quickconnect.to/d/s/496975158882345550/sUrm8NYh5szKPD5NacKzaoXM18OrpRiV-TyKA5VWc5QY_.
59. Rump A, Benet-Pages A, Schubert S, Kuhlmann JD, Janavičius R, Macháčková E, Foretová L, Kleibl Z, Lhota F, Zemankova P, Betcheva-Krajcir E, Mackenroth L, Hackmann K, Lehmann J, Nissen A, DiDonato N, Opitz R, Thiele H, Kast K, Wimberger P, Holinski-Feder E, Emmert S, Schröck E, Klink B. Identification and functional testing of ERCC2 mutations in a multi-national cohort of patients with familial breast- and ovarian cancer. *PLoS Genet*. 2016;**12**(8):e1006248.
60. Slinker BK. The statistics of synergism. *J Mol Cell Cardiol*. 1998; **30**(4):723–731.
61. Maurer U, Preiss F, Brauns-Schubert P, Schlicher L, Charvet C. GSK-3: at the crossroads of cell death and survival. *J Cell Sci*. 2014; **127**(7):1369–1378.
62. Pirola L, Bonnafous S, Johnston AM, Chaussade C, Portis F, Van Obberghen E. Phosphoinositide 3-kinase-mediated reduction of insulin receptor substrate-1/2 protein expression via different mechanisms contributes to the insulin-induced desensitization of its signaling pathways in L6 muscle cells. *J Biol Chem*. 2003;**278**(18): 15641–15651.
63. Aristizabal Prada ET, Weis C, Orth M, Lauseker M, Spöttl G, Maurer J, Grabowski P, Grossman A, Auernhammer CJ, Nölting S. GSK3α/β: a novel therapeutic target for neuroendocrine tumors. *Neuroendocrinology*. 2018;**106**(4):335–351.
64. Timmers HJ, Kozupa A, Eisenhofer G, Raygada M, Adams KT, Solis D, Lenders JW, Pacak K. Clinical presentations, biochemical phenotypes, and genotype-phenotype correlations in patients with succinate dehydrogenase subunit B-associated pheochromocytomas and paragangliomas. *J Clin Endocrinol Metab*. 2007;**92**(3):779–786.
65. Pavel ME, Hainsworth JD, Baudin E, Peeters M, Hörsch D, Winkler RE, Klimovsky J, Lebwohl D, Jehl V, Wolin EM, Öberg K, Van Cutsem E, Yao JC; RADIANT-2 Study Group. Everolimus plus octreotide long-acting repeatable for the treatment of advanced neuroendocrine tumours associated with carcinoid syndrome (RADIANT-2): a randomised, placebo-controlled, phase 3 study. *Lancet*. 2011;**378**(9808):2005–2012.
66. Yao JC, Shah MH, Ito T, Bohas CL, Wolin EM, Van Cutsem E, Hobday TJ, Okusaka T, Capdevila J, de Vries EGE, Tomassetti P, Pavel ME, Hoosen S, Haas T, Lincy J, Lebwohl D, Öberg K; RAD001 in Advanced Neuroendocrine Tumors, Third Trial (RADIANT-3) Study Group. Everolimus for advanced pancreatic neuroendocrine tumors. *N Engl J Med*. 2011;**364**(6):514–523.
67. Yao JC, Fazio N, Singh S, Buzzoni R, Carnaghi C, Wolin E, Tomasek J, Raderer M, Lahner H, Voi M, Pacaud LB, Rouyrre N, Sachs C, Valle JW, Fave GD, Van Cutsem E, Tesselaar M, Shimada Y, Oh D-Y, Strosberg J, Kulke MH, Pavel ME; RAD001 in Advanced Neuroendocrine Tumours, Fourth Trial (RADIANT-4) Study Group. Everolimus for the treatment of advanced, non-functional neuroendocrine tumours of the lung or gastrointestinal

tract (RADIANT-4): a randomised, placebo-controlled, phase 3 study. *Lancet*. 2016;**387**(10022):968–977.
68. Fassnacht M, Weismann D, Ebert S, Adam P, Zink M, Beuschlein F, Hahner S, Allolio B. AKT is highly phosphorylated in pheochromocytomas but not in benign adrenocortical tumors. *J Clin Endocrinol Metab*. 2005;**90**(7):4366–4370.
69. Briest F, Grabowski P. PI3K-AKT-mTOR-signaling and beyond: the complex network in gastroenteropancreatic neuroendocrine neoplasms. *Theranostics*. 2014;**4**(4):336–365.
70. Pavel M. Translation of molecular pathways into clinical trials of neuroendocrine tumors. *Neuroendocrinology*. 2013;**97**(1): 99–112.
71. O'Reilly KE, Rojo F, She QB, Solit D, Mills GB, Smith D, Lane H, Hofmann F, Hicklin DJ, Ludwig DL, Baselga J, Rosen N. mTOR inhibition induces upstream receptor tyrosine kinase signaling and activates Akt. *Cancer Res*. 2006;**66**(3):1500–1508.
72. Carracedo A, Ma L, Teruya-Feldstein J, Rojo F, Salmena L, Alimonti A, Egia A, Sasaki AT, Thomas G, Kozma SC, Papa A, Nardella C, Cantley LC, Baselga J, Pandolfi PP. Inhibition of mTORC1 leads to MAPK pathway activation through a PI3K-dependent feedback loop in human cancer. *J Clin Invest*. 2008; **118**(9):3065–3074.
73. Zitzmann K, Rüden J, Brand S, Göke B, Lichtl J, Spöttl G, Auernhammer CJ. Compensatory activation of Akt in response to mTOR and Raf inhibitors: a rationale for dual-targeted therapy approaches in neuroendocrine tumor disease. *Cancer Lett*. 2010; **295**(1):100–109.
74. Svejda B, Kidd M, Kazberouk A, Lawrence B, Pfragner R, Modlin IM. Limitations in small intestinal neuroendocrine tumor therapy by mTor kinase inhibition reflect growth factor-mediated PI3K feedback loop activation via ERK1/2 and AKT. *Cancer*. 2011; **117**(18):4141–4154.
75. Passacantilli I, Capurso G, Archibugi L, Calabretta S, Caldarola S, Loreni F, Delle Fave G, Sette C. Combined therapy with RAD001 e BEZ235 overcomes resistance of PET immortalized cell lines to mTOR inhibition. *Oncotarget*. 2014;**5**(14):5381–5391.
76. Nölting S, Rentsch J, Freitag H, Detjen K, Briest F, Möbs M, Weissmann V, Siegmund B, Auernhammer CJ, Aristizabal Prada ET, Lauseker M, Grossman A, Exner S, Fischer C, Grötzinger C, Schrader J, Grabowski P; GERMAN NET-Z study group. The selective PI3Kα inhibitor BYL719 as a novel therapeutic option for neuroendocrine tumors: Results from multiple cell line models. *PLoS One*. 2017;**12**(8):e0182852.
77. Cohen P, Frame S. The renaissance of GSK3. *Nat Rev Mol Cell Biol*. 2001;**2**(10):769–776.
78. Wada A. GSK-3 inhibitors and insulin receptor signaling in health, disease, and therapeutics. *Front Biosci*. 2009;**14**:1558–1570.
79. Genther Williams SM, Kuznicki AM, Andrade P, Dolinski BM, Elbi C, O'Hagan RC, Toniatti C. Treatment with the PARP inhibitor, niraparib, sensitizes colorectal cancer cell lines to irinotecan regardless of MSI/MSS status. *Cancer Cell Int*. 2015;**15**(1):14.
80. Kanjanapan Y, Lheureux S, Oza AM. Niraparib for the treatment of ovarian cancer. *Expert Opin Pharmacother*. 2017;**18**(6): 631–640.
81. Hagemann IS, Devarakonda S, Lockwood CM, Spencer DH, Guebert K, Bredemeyer AJ, Al-Kateb H, Nguyen TT, Duncavage EJ, Cottrell CE, Kulkarni S, Nagarajan R, Seibert K, Baggstrom M, Waqar SN, Pfeifer JD, Morgensztern D, Govindan R. Clinical next-generation sequencing in patients with non-small cell lung cancer. *Cancer*. 2015;**121**(4):631–639.
82. Johannessen CM, Reczek EE, James MF, Brems H, Legius E, Cichowski K. The NF1 tumor suppressor critically regulates TSC2 and mTOR [published correction appears in *Proc Natl Acad Sci USA*. 2005;**102**(44):16119]. *Proc Natl Acad Sci USA*. 2005; **102**(24):8573–8578.
83. Johannessen CM, Johnson BW, Williams SM, Chan AW, Reczek EE, Lynch RC, Rioth MJ, McClatchey A, Ryeom S, Cichowski K. TORC1 is essential for NF1-associated malignancies. *Curr Biol*. 2008;**18**(1):56–62.
84. Martin GA, Viskochil D, Bollag G, McCabe PC, Crosier WJ, Haubruck H, Conroy L, Clark R, O'Connell P, Cawthon RM, et al. The GAP-related domain of the neurofibromatosis type 1 gene product interacts with ras p21. *Cell*. 1990;**63**(4):843–849.
85. Welander J, Söderkvist P, Gimm O. The NF1 gene: a frequent mutational target in sporadic pheochromocytomas and beyond. *Endocr Relat Cancer*. 2013;**20**(4):C13–C17.

ARTICLE 5

Succinate dehydrogenase deficiency in a chromaffin cell model retains metabolic fitness through the maintenance of mitochondrial NADH oxidoreductase function

Katarína Kľučková, Alpesh Thakker, Lisa Vettore, Cristina Escribano-Gonzalez, Rebecca L Hindshaw, Jacqueline L E Tearle, Judith Goncalves, Baksho Kaul, Gareth G Lavery, Judith Favier, Daniel A Tennant

FASEB J. 2020 Jan;34(1):303-315.

Received: 14 June 2019 | Revised: 17 September 2019 | Accepted: 8 October 2019

DOI: 10.1096/fj.201901456R

RESEARCH ARTICLE

THE FASEB JOURNAL

Succinate dehydrogenase deficiency in a chromaffin cell model retains metabolic fitness through the maintenance of mitochondrial NADH oxidoreductase function

Katarína Kľučková[1] | Alpesh Thakker[1] | Lisa Vettore[1] | Cristina Escribano-Gonzalez[1] | Rebecca L. Hindshaw[1] | Jacqueline L. E. Tearle[1] | Judith Goncalves[2] | Baksho Kaul[1] | Gareth G. Lavery[1] | Judith Favier[2] | Daniel A. Tennant[1]

[1]Institute of Metabolism and Systems Research, College of Medical and Dental Sciences, University of Birmingham, Birmingham, UK

[2]Université de Paris, PARCC, INSERM, Equipe Labellisée par la Ligue contre le Cancer, Paris, France

Correspondence
Judith Favier, PARCC, European Georges Pompidou Hospital, 56 rue Leblanc, 75015 Paris, France.
Email: judith.favier@inserm.fr

Daniel A. Tennant, Institute of Metabolism and Systems Research, College of Medical and Dental Sciences, University of Birmingham, Birmingham B15 2TT, UK.
Email: d.tennant@bham.ac.uk

Present address
Katarína Kľučková, Barts Cancer Institute, Queen Mary University of London, London, UK

Abstract

Mutations in succinate dehydrogenase (SDH) lead to the development of tumors in a restricted subset of cell types, including chromaffin cells and paraganglia. The molecular basis for this specificity is currently unknown. We show that loss of SDH activity in a chromaffin cell model does not perturb complex I function, retaining the ability to oxidize NADH within the electron transport chain. This activity supports continued oxidation of substrates within the tricarboxylic acid (TCA) cycle. However, due to the block in the TCA cycle at SDH, the high glutamine oxidation activity is only maintained through an efflux of succinate. We also show that although the mitochondria of SDH-deficient cells are less active per se, their higher mass per cell results in an overall respiratory rate that is comparable with wild-type cells. Finally, we observed that when their mitochondria are uncoupled, SDH-deficient cells are unable to preserve their viability, suggesting that the mitochondrial metabolic network is unable to compensate when exposed to additional stress. We therefore show that in contrast to models of SDH deficiency based on epithelial cells, a chromaffin cell model retains aspects of metabolic "health," which could form the basis of cell specificity of this rare tumor type.

Abbreviations: DTNB, 5,5′-dithiobis-(2-nitrobenzoic acid); ETC, electron transport chain; ETF, electron transfer flavoprotein; FA, fatty acids; FAO, fatty acid oxidation; FCCP, carbonyl cyanide 4-(trifluoromethoxy)phenylhydrazone; GIST, gastrointestinal stromal tumors; imCC, immortalized murine chromaffin cells; MAF, mouse adrenal fibroblasts; ME2, malic enzyme 2; NAD^+, nicotinamide adenine dinucleotide; NADH, reduced NAD^+; OAA, oxaloacetate; PCK2, phosphoenolpyruvate carboxykinase; PDH E1α, pyruvate dehydrogenase E1α subunit; PDK1/4, PDH kinase 1/4; PPGL, pheochromocytoma and paraganglioma; RIPA, radioimmunoprecipitation assay; ROS, reactive oxygen species; SDHA-D, succinate dehydrogenase subunits A-D; SRB, sulforhodamine B; TCA, tricarboxylic acid; TMRE, Tetramethylrhodamine ethyl ester; UCP2, uncoupling protein 2.

Jacqueline L. E. Tearle, EMBL Australia Single Molecule Science, School of Medical Sciences, Lowy Cancer Research Centre, UNSW, Sydney, Australia

Funding information
Paradifference; Wellcome Trust (Wellcome), Grant/Award Number: 104612/Z/14/Z; Cancer Research UK (CRUK), Grant/Award Number: C42109/A26982 and C42109/A24891

KEYWORDS
electron transport chain, metabolism, mitochondria, pheochromocytoma, succinate dehydrogenase

1 | INTRODUCTION

Succinate dehydrogenase (SDH), also known as complex II (CII) of the electron transport chain (ETC), has a unique function within the mitochondrial metabolic network, being part of both the ETC and the tricarboxylic acid (TCA) cycle. As such, SDH activity was thought to be universally required for cell proliferation and survival. However, loss of any one of the four subunits of this enzyme leads to the development of rare tumor types including pheochromocytoma and paraganglioma (PPGL), gastrointestinal stromal tumors (GIST), and cases of renal cancer.[1] The function of SDH within the mitochondrial matrix is to oxidize succinate to fumarate with the resulting electrons reducing the ubiquinone pool of the ETC. SDH deficiency therefore results in a well-characterized increase in succinate levels in the matrix, which on reaching the cytosol inhibits members of the 2-oxoglutarate-dependent dioxygenase family of enzymes, eliciting epigenetic changes and pseudohypoxic signaling that are likely the major drivers of tumorigenesis.[2,3]

However, despite being originally described in 2000,[4] little is still known concerning how loss of SDH function can be tolerated, and why only in a highly restricted number of cell types. Although loss of function mutations in SDHB-D subunits is almost entirely restricted to oncogenesis, the first description of a loss of function mutation in SDHA was described in neurodegenerative disease, causing Leigh syndrome.[1,5,6] Importantly, the mutations observed in Leigh syndrome are distinct from those reported in tumors, suggesting that mutations in different members of the complex, and indeed different regions of SDHA may have distinct effects on the overall biochemistry of SDH. Indeed, using a model of SDH loss based on deletion of *Sdhb* in a kidney epithelial cell line, it was recently shown that tumor-specific mutations of SDH can compromise activity of complex I,[7,8] while those observed in Leigh syndrome do not.[8] However, data from SDH-deficient PPGL and a chromaffin cell-based model with reduced (knocked-down) Sdhb expression reported around the same time suggested that it may not be the case in this model.[9] The existence of models of SDH deficiency using different cell types therefore provides an opportunity to resolve the question regarding the tissue specificity of tumorigenesis arising from loss of this metabolic enzyme.

It is clear from recent studies in multiple cell models of SDH deficiency that aspects of the TCA cycle retain function.[7,8,10] There is therefore considerable plasticity within the mitochondrial metabolic network, although it is likely that this comes at a cost to the cell—a well-described consequence being the increased production of reactive oxygen species (ROS). These molecules are produced as a result of the dependence of mitochondrial metabolism on redox active reactions. Mitochondrial respiration is based on molecular oxygen accepting electrons that arise from two reduced pyridine nucleotides; NADH and $FADH_2$, which are themselves most often generated through dehydrogenase reactions within the TCA cycle. Loss or reduction of the ability to oxidize these pyridines, as observed in conditions such as hypoxia as well as loss of SDH function, restricts the capability of the TCA cycle to generate the necessary substrates for macromolecule synthesis, such as aspartate.[7,10-12]

It therefore remains unclear what the cellular or microenvironmental conditions are that permit the continued viability and proliferation required for tumorigenesis despite loss of SDH function. We report here that in contrast to epithelial cell models of SDH loss, chromaffin cells lacking SDH retain complex I function, and are capable of oxidizing diverse substrates that may contribute to the metabolic fitness of the cells. However, this comes at a cost to the cell, as they demonstrate little spare respiratory capacity and are highly sensitive to mitochondrial uncoupling. We therefore suggest that at least part of the reason for the restriction of SDH mutation-driven tumors to specific cell types may be due to the retention of complex I activity, reducing the need to remodel the metabolic network associated with the $NADH:NAD^+$ redox pair, allowing continued viability and proliferation.

2 | MATERIALS AND METHODS

2.1 | Cell culture and chemicals

Previously characterized immortalized mouse chromaffin cell lines deficient in *Sdhb* ($Sdhb^{-/-}$ CL6 and CL8) as well

as their *Sdhb*$^{+/+}$ counterparts were maintained in Dulbecco's Modified Eagle Medium (DMEM) supplemented with 10% fetal bovine serum (FBS) and 1 mM pyruvate. The same cell culture conditions were used for the mouse adrenal fibroblasts (MAF), *Sdhb*$^{+/+}$ and *Sdhb*$^{-/-}$. All chemicals, including DMEM and FBS, were from Sigma-Aldrich unless stated otherwise. Brightfield images were taken using an EVOS FL (Thermo Scientific), at 10× magnification.

2.2 | High-resolution respirometry

For the measurement in intact state, trypsinized cells were resuspended in cell culture media (4.5 g/L glucose + 1 mM pyruvate) and loaded in an Oxygraph-2k (Oroboros instruments) chamber. After closing the chambers and recording routine respiration, oligomycin (2.5 μM) was added to inhibit ATP synthase. Measurements of the non-phosphorylating electron transfer system (ETS) capacity were obtained through stepwise (0.5 μM) titration of the uncoupler, carbonyl cyanide 4-(trifluoromethoxy)phenylhydrazone (FCCP). Respiration was inhibited by addition of rotenone (0.5 μM) and antimycin A (2.5 μM) at the end of the experiment. For the measurement in permeabilized state, trypsinized and washed cells were resuspended in respiratory media Mir05 (110 mM sucrose, 60 mM K^+-lactobionate, 0.5 mM EGTA, 3 mM $MgCl_2$, 20 mM taurine, 10 mM KH_2PO_4, 20 mM HEPES, 1 g/L BSA [essentially fatty acid free], pH 7.1). After closing the chambers and recording respiration on endogenous substrates, digitonin was added to permeabilize the cells. Substrate combinations were used as indicated in the graphs. The concentrations used were 2 mM malate (Mal), 10 mM glutamate (Glu), 5 mM pyruvate (Pyr), and 10 mM succinate (suc). For fatty acid oxidation (FAO) assessment, limiting malate was used at concentration 0.05 mM and either 40 μM palmitoylcarnitine or 200 μM octanoylcarnitine. In all experiments on permeabilized cells, 3 mM ADP was used and maximum respiratory capacity was reached by stepwise titration of FCCP. Respiration was inhibited by addition of 0.5 μM rotenone and antimycin A (2.5 μM) in the end of the experiment. Values after antimycin A addition were subtracted from all recorded values. For the experiments with ^{13}C tracers, FCCP and inhibitors were omitted. For mitochondrial measurements, the permeabilization step was omitted.

2.3 | Mitochondrial membrane potential measurement

Trypsinized cells were resuspended in Mir05 medium at 0.5 mg/mL protein concentration on ice, and supplemented with 20 nM Tetramethylrhodamine ethyl ester dye (TMRE; Santa Cruz) and respiratory substrates as indicated at concentrations as for the respirometry measurements, before being permeabilized with 0.1 μg digitonin per μg protein for 5 minutes at room temperature and immediately measured on Fortessa LSR-II flow cytometer (Beckton Dickinson). Each set of samples was assessed in three states: untreated (just TMRE and respiratory substrates), state 3 (+3 mM ADP), and uncoupled (100 μM FCCP). The relative mitochondrial membrane potential was determined from the difference of the coupled phosphorylating condition with ADP and the depolarized value.

2.4 | Mitochondrial mass evaluation

Cells in culture were incubated for 20 minutes with 100 nM MitoTracker Green (Thermo Fisher Scientific), before trypsinization, washing (PBS), and resuspension in PBS supplemented with MitoTracker Green (100 nM). Where shown, cells were pre-incubated with FCCP (100 μM) to depolarize the mitochondria 5 minutes before being incubated with MitoTracker Green. The fluorescence signal was assessed using Fortessa LSR-II flow cytometer (Beckton Dickinson), and mitochondrial mass expressed relative to fluorescence signal in *Sdhb*$^{+/+}$ cells.

For citrate synthase activity, 1×10^6 trypsinized cells were washed with PBS and frozen before lysis in 200 μL of 50 mM Tris (pH 8) with 4 × freeze-thaw cycles in liquid nitrogen/water bath. The assay was performed on 5 μL of cleared supernatant added to 90 μL of reaction buffer (0.1 mM DTNB, 0.3 mM Acetyl CoA, 0.1% Triton X-100 in 100 mM Tris-HCl, pH 8) in 96-well plate. The baseline absorbance was measured in Fluostar Omega plate reader (BMG Labtech) at 412 nm for 15 minutes, then 5 μL of 10 mM oxaloacetate was added and the absorbance measured for further 15 minutes. Baseline signal was subtracted from the signal measured after oxaloacetate addition.

2.5 | ATP assessment

Measurement of cellular ATP was performed using a bioluminescent assay (Sigma; FLAA) as per manufacturer's instructions. 24 hours before measurement, cells were seeded at 2×10^3 per well in a 96-well plate. Where shown, oligomycin (2.5 μM) was added 10 minutes prior to lysis. After removal of media, cells were washed in PBS (pH 7.4) and lysed in 50 μL of buffer. 100 μL of ATP assay was added to all wells before luminescence was read (BMG PHERAstar). Data were normalized to total protein per well using a BCA assay (ThermoFisher Scientific).

2.6 | Total cell protein and cell size evaluation

1×10^6 trypsinized cells were washed with PBS and lysed in 60 μL of RIPA buffer for 30 minutes. Protein concentration in the cleared supernatant was determined using the BCA protein method (Thermo Fisher Scientific). For cell size evaluation, cells were measured in the CASY TT cell counter and their diameter was recorded.

2.7 | Immunoblotting

Cells were lysed in modified RIPA buffer before dilution and quantitation using a bicinchoninic acid (BCA) assay. Lysates were diluted in Laemmli buffer before using 25 μg for electrophoretic separation using SDS-PAGE. After blotting onto nitrocellulose membrane, the following antibodies were used to identify expression of cellular proteins: ACTB, OGDH (Proteintech; #15212-1-AP), PDH E1α (Proteintech; 18068-1-AP), PDHK1 (Cell Signaling; #3820), PDK4 (Proteintech; 12949-1-AP), and PGC1α (Cell Signaling #3820). Images were digitally acquired using a ChemiDoc XRS+ System (Bio Rad).

2.8 | Cell growth assay

Cell growth was assayed using the Sulforhodamine-B (SRB) assay. Cells were plated day before the treatment and after 3 days growth in the presence of the drug cells were fixed in the plates by addition of 20% ice cold trichloracetic acid (TCA) for at least 30 minutes. Fixed cells were then washed with water, left to dry and stained with 0.4% SRB dye dissolved in 1% acetic acid. Superfluous dye was washed off with 1% acetic acid and when dry, dissolved in 50 mM Tris-HCl pH 8 and the absorbance measured on Fluostar Omega plate reader (BMG Labtech) at 510 nm.

2.9 | Mitochondria isolation

Mitochondria were isolated using modified methodology described by Frezza et al.[13] Briefly, trypsinized and washed cells were homogenized for 5 minutes in isolation buffer (200 mM sucrose, 10 mM Tris-MOPS, 1 mM EGTA-Tris; pH 7) using glass/Teflon homogenizer at speed 1000 rpm. Homogenate was then centrifuged at 600 *g* for 10 minutes, pellet discarded, and supernatant centrifuged at 3000 *g* for 5 minutes. Mitochondria in the supernatant were then pelleted at 10 000 *g* for 15 minutes. Pelleted mitochondria were resuspended in ~50 μL of isolation buffer and let stand on ice for at least 1 hour before their respiration was assessed. During this time, protein concentration was determined by BCA protein method (Thermo Fisher Scientific).

2.10 | ^{13}C labeling

Cells were prepared as described for the respirometry measurements and after plasma membrane permeabilization with digitonin, 3 mM ADP and ^{13}C labeled (all CK isotopes) and unlabeled respiratory substrates were added as indicated (1 mM malate, 10 mM glutamate, 5 mM pyruvate, and 3 mM glutamine) and left to respire in opened Oxygraph-2k chambers for 40 minutes. Then the chambers were closed again, respiration signal recorded and cytochrome c was added to check for mitochondrial integrity. Contents of the chambers were collected in precooled Eppendorf tubes, centrifuged at 10 000 *g* for 5 minutes, washed once with ice-cold saline, and frozen immediately on dry ice. For cell-based ^{13}C labeling, $^{13}C_{16}$-palmitic acid (50 μM) or $^{13}C_5$ glutamine (2 mM; all CK Isotopes) were added to cells for 3 days in "flux media"; DMEM powder (Sigma) supplied with sodium bicarbonate as per manufacturer's instructions, 10% FBS and unlabeled forms of glucose and/or glutamine depending on the ^{13}C-enriched nutrient employed. After the incubation period, cells were washed with saline and scraped off the precooled plates into methanol/H_2O mixture. For spent media analysis, 200 μL of cleared media was extracted. In all cases, 0.5 μg/sample of D-6 glutaric acid (CDN Isotopes) supplied in H_2O was used as internal standard and polar metabolites were extracted using Methanol:H_2O:Chloroform at ratio 1:1:1. Briefly, samples were vortexed vigorously, left to shake with all the solvents for 15 minutes at 4°C and then centrifuged for 15 minutes at 16 000 *g*. The upper polar phase was collected and evaporated in the Savant vacuum system (Thermo Fisher Scientific) and used for Gas Chromatography—Mass Spectrometry (GC-MS) analysis.

2.11 | GC-MS analysis

The dried extract was first incubated at 95°C in open tubes and then solubilized in 40 μL of 2% methoxyamine HCl in pyridine followed by 60 minutes incubation at 60°C and subsequently 60 μL N-tertbutyldimethylsilyl-N-methyltrifluoroacetamide with 1% (w/v) tertbutyldimethyl-chlorosilane derivatization reagent was added. The suspension was incubated for an hour at 60°C in a well-sealed tube to prevent evaporation. Finally, the samples were centrifuged at 16 000 *g* for 5 minutes and the clear supernatant was transferred to a chromatography vial with a glass insert (Thermo Fisher Scientific) and processed immediately to GC-MS analysis. For analysis of the derivatized samples, an Agilent 7890B Series GC/MSD gas chromatograph with a polydimethylsiloxane GC column coupled,

with a mass spectrometer (GC-MS) (Agilent Technologies UK Limited, Stockport, UK) was used. Prior to sample analysis, the GC-MS was tuned to a full width at half maximum (FWHM) peak width of 0.60 a.m.u. in the mass range of 50-650 mass to charge ratio (m/z) using PFTBA tuning solution. 1 μL of sample was injected into the GC-MS in splitless mode with helium carrier gas at a rate of 1.0 mL min^{-1}. The inlet liner containing glass wool was set to a temperature of 270°C. Oven temperature was set at 100°C for 1 minute before ramping to 280°C at a rate of 5°C min^{-1}. Temperature was further ramped to 320°C at a rate of 10°C min^{-1} held at 320°C for 5 minutes. Compound detection was carried out in full scan mode in the mass range 50-650 m/z, with 2-4 scans sec^{-1}, a source temperature of 250°C, a transfer line temperature of 280°C and a solvent delay time of 6.5 minutes. The injector needle was cleaned with acetonitrile three times before measurement commencement and three times following every measurement thereafter. The raw GC-MS data were converted to common data format using the acquisition software and further processing of the isotope data including isotope correction and mass isotopomer analysis/batch quantification was performed on metabolite detector software. The raw peak area for each analyte of interest was calculated using the metabolite detector software followed by normalizing the response to the internal standard peak area.

2.12 | Gene expression data

Gene expression profiles of human tumors were available from a previous study, in which 186 fully genotyped PPGL were analyzed.[14,15] The data are shown for a subset of these samples carrying germline and somatic mutations in RET (n = 19), NF1 (n = 37), VHL (n = 40) or SDHx (n = 23) genes, as well as two samples of normal adrenal medulla. HG-U133 Plus 2.0 Affymetrix GeneChip data from this previous study are available online as ArrayExpress entry E-MTAB-733 (http://www.ebi.ac.uk/arrayexpress/). Gene expression profiles of wild-type and *Sdhb*$^{-/-}$ MAF and imCC (CL6 and CL8) were assessed in duplicates using the GeneChip® Mouse Gene 1.0 ST Array.[10] Data are available as ArrayExpress entry E-MTAB-3403. Principal component analysis (PCA) and hierarchical clustering were performed using ClustVis software[16] with default settings using a gene list of 35 PGC1a target genes and metabolic enzymes. Heatmap shows data filtered for genes showing a >1.5-fold difference between WT and KO imCC.

2.13 | Statistical analysis

One-way or two-way ANOVA was used to assess statistical significance; $*P \leq .05$, $**P \leq .01$, $***P \leq .001$, $****P \leq .0001$.

3 | RESULTS

Tumor-associated mutations in SDH, all of which result in loss of oxidative enzymatic activity, lead to tumor formation in a restricted set of cell types—most often chromaffin cells and paraganglia. Previous studies performed in epithelial cell types suggested that mutations in SDH subunits that underpin tumor formation lead to loss of complex I activity and a restricted metabolic phenotype.[8,17] We therefore sought to confirm whether this metabolic phenotype was also observed in a physiologically relevant model derived from chromaffin cells compared to a genetically identical model derived from a non-tumor-forming cell type, adrenal fibroblasts (MAFs).[10] We first assessed oxygen consumption of intact cells and found that although loss of SDH activity in the MAF model decreased oxygen consumption consistent with that previously reported (Figure 1A), SDH-deficient chromaffin cells (imCC) retained a similar respiratory phenotype to their wild-type counterparts (Figure 1B). Interestingly, in both cell models, loss of SDH resulted in no change in ATP synthesis-independent respiration (Figure 1A,B). However, maximal capacity of the electron transport chain (FCCP-uncoupled respiration) was greatly reduced in both SDH-mutated cell models (Figure 1A,B), suggesting that use of electrons in ATP synthesis was reduced independently of cell type. We therefore assessed cellular ATP content between wild-type and SDH-deficient cells, and found that indeed it was significantly lower in both SDH-deficient cell models. To test reliance of the cells on the mitochondrial ATP synthase, we incubated them with the inhibitor, oligomycin, and observed that the wild-type cells were able to compensate with increased glycolytic ATP production, resulting in no net change in cellular ATP (Figure 1C). Interestingly, although the SDH-deficient MAFs also showed a similar ATP content after oligomycin, the SDH-deficient imCC cells demonstrated a significant increase in ATP (Figure 1C). These data demonstrate that the ATP synthase is instead working in reverse in this cell model, hydrolyzing ATP to contribute to the maintenance of the transmembrane proton gradient, much like previously observed in ischemia.[18,19]

To assess mitochondrial respiratory phenotype independently of the cytosol, permeabilized cells were incubated with saturating concentrations of respiratory substrates for complex I, and subsequently complex II. ADP-stimulated (state 3) complex I-supported respiration was found to be lower in the SDH-deficient MAF model compared to wild-type controls, again in contrast to the chromaffin cell model (Figure 1D,E). However, in both models, the expected loss of succinate-driven (complex II) activity was observed in SDH-deficient cells. These data suggest that the loss of complex I activity observed in intact SDH-deficient cells may be through an alteration in the generation or availability of NADH for complex I activity, rather than an

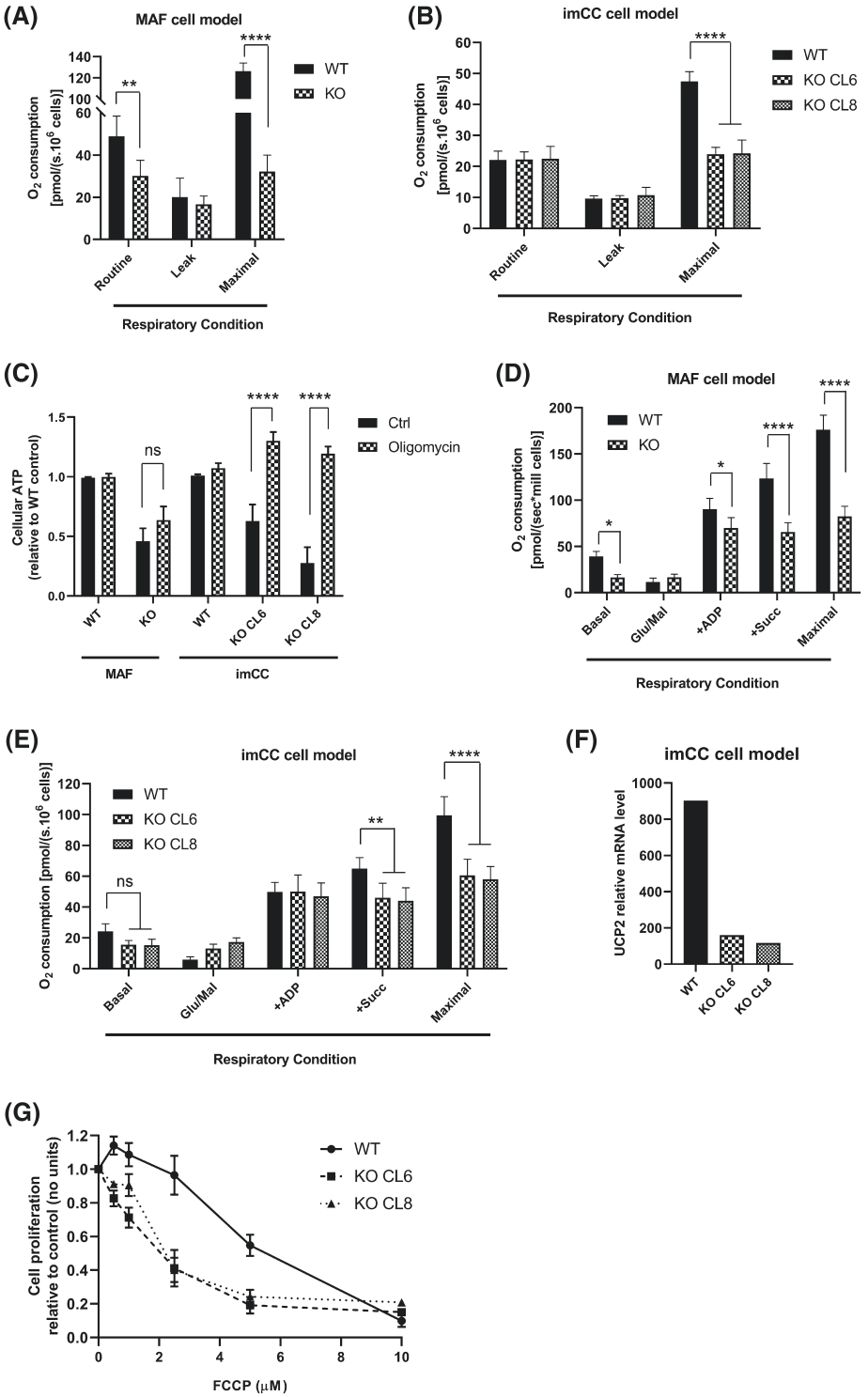

FIGURE 1 A and B, Respiration of intact MAF (A) or imCC (B) cells. Leak was determined through the use of oligomycin (2.5 μM), while maximal condition was defined through addition of FCCP in 0.5 μM steps until maximal rate was observed. Results shown are from 4 (MAF) or 3 (imCC) independent experiments, presented as mean ± SD. Two-way ANOVA was used to assess statistical significance; $^{**}P < .01$, $P < .001$, $^{****}P < .0001$. C, ATP content in both imCC and MAF cell lines, in the presence or absence of oligomycin (2.5 μM, pre-incubated for 10 minutes before lysis), presented as a mean of at least four independent experiments, each in technical triplicate ± SEM. Ns; not significant, $^{****}P < .0001$. D and E, Respiration (oxygen consumption) of permeabilized MAF (D) and imCC (E) cells in basal (Mir05) medium. Additions as follows: Glu/Mal; glutamate (10 mM) and malate (2 mM), ADP (3 mM), Succ; succinate (10 mM) or maximal; FCCP titrated in 0.5 μM steps. Results shown are from four independent experiments, presented as mean ± SD. ns; not significant, $^{*}P < .05$, $^{**}P < .01$, $^{****}P < .0001$. F, UCP2 mRNA expression showing that both Sdhb-deficient clones have >80% reduction in UCP2 expression. G, Effect of the proton ionophore FCCP on cell growth over 3 days in culture. Results are from three independent experiments performed in triplicate, presented as mean ± SEM

inherent defect of mitochondria. Consistent with the data from intact cells, loss of maximal respiratory phenotype (FCCP-stimulated) was observed in permeabilized cells (on complex I and II substrates; Figure 1D,E). These data, alongside those suggesting a reversal of the ATP synthase (Figure 1C) suggested that SDH-deficient cells may be sensitive to uncoupling of the respiratory chain. Indeed, expression of the uncoupling protein, UCP2 was significantly reduced in the SDH-deficient cell models, consistent with this hypothesis (Figure 1F and Supplementary Figure 1A). Importantly, when UCP2 levels were compared between SDH-mutated and non-SDH-mutated patient tumor samples, only the former exhibited reduced expression (Supplementary Figure 1B), confirming that this was a phenotype only relevant to SDH-deficient tumors. We therefore incubated both wild-type and SDH-deficient cells with increasing concentrations of FCCP before assessing cell number after 3 days. We observed a significant sensitization of the SDH-deficient cells, with an LD_{50} around 50% lower than that of wild-type cells (Figure 1G).

Despite the clear similarities between the MAF and imCC cell models, a significant difference was observed in complex I activity between models, with imCC cells retaining activity and the MAF cell model demonstrating a significant reduction in function, as previously described (Figure 1A,B,D,E).[8,17] This suggested that this cell type was able to retain a more wild-type like TCA cycle activity in the absence of SDH compared to the MAFs, which could confer at least part of the tissue specificity of SDH mutant tumors. The respiratory phenotype of the imCCs was therefore investigated in more detail. Previous studies have suggested that the cytosolic redox balance is altered in SDH-deficient cells, and that the addition of exogenous pyruvate can support metabolic function.[7] In addition to supporting cytosolic redox, pyruvate has also been shown as a carbon source in the mitochondria of SDH-deficient cells,[7,10] supporting proliferation (Supplementary Figure 2A). We therefore investigated complex I-linked respiration in permeabilized SDH-deficient cells in the presence of exogenous pyruvate and found that although respiration was unchanged, maximal respiratory capacity was increased (Figure 2A). This suggested that pyruvate oxidation within the mitochondria may be limiting in SDH-deficient cells, perhaps due to a significant demand for oxaloacetate through carboxylation to produce aspartate.[7,10] These data suggested that SDH-deficient imCC cells are not deficient in complex I function, due to the fact that the oxidative decarboxylation of pyruvate is used to reduce NAD^+ to NADH. We therefore tested this using an alternative NADH-producing substrate—fatty acids (FA). During the course of mitochondrial β-oxidation, FA are stepwise degraded to acetyl CoA units. Each of these steps produces $FADH_2$ and NADH, which contribute electrons to the respiratory chain via the electron transport flavoprotein (ETF) and complex I. Using either octanoyl- or palmitoyl-carnitine, we found that both FA are efficient respiratory substrates for SDH-deficient cells (Figure 2B,C). Indeed, respiration on palmitoyl-carnitine exceeded that of the wild-type cells. These measurements provide further confirmation of complex I functionality in SDH-deficient cells and suggest that FA could be an energetic fuel in the absence of full SDH function. This is supported by the fact that SDH-deficient cells showed increased susceptibility to the FA oxidation inhibitor etomoxir (Supplementary Figure 2B), although they showed little difference in the incorporation of palmitate-derived ^{13}C-labeled acetyl CoA units into TCA cycle (Supplementary Figure 2C).

Due to the apparent differences in respiratory capacity and sensitivity to uncoupling, we investigated whether permeabilized SDH-deficient cells maintained a high mitochondrial membrane potential in the presence of saturating concentrations of respiratory substrates. This appeared to be the case (Figure 2D), but when normalized to increased mitochondrial content using MitoTracker Green (Figure 2E), no difference was observed (Figure 2F). Importantly, we confirmed that MitoTracker Green staining was unaffected by mitochondrial membrane potential (Supplementary Figure 2D). As mitochondrial content can also be assessed using citrate synthase activity, this was also examined as an independent measurement, but found not to vary between wild-type and SDH-deficient cells (Figure 2G). These results suggested that SDH-deficient cells may upregulate their mitochondrial mass to compensate for reduced metabolic efficiency arising through mechanisms such as ROS-mediated damage of matrix proteins, or reduced matrix protein content—the latter resulting in a less dense matrix. Respiratory experiments performed on isolated mitochondria support this observation, as these show decreased respiration on glutamate/malate combination and similar respiration in the presence of glutamate/malate/pyruvate when expressed per mitochondrial protein (Figure 2H). Importantly, SDH-deficient cells are larger than their wild-type counterparts (Figure 2I and Supplementary Figure 2E,F)—consistent with them containing enlarged mitochondria (Figure 2E). We therefore investigated whether SDH-deficient cells increase PGC1a expression as a marker of increased mitochondrial biogenesis, but found instead decreased expression (Supplementary Figure 2G). These data suggest that the change in mitochondrial mass is unlikely to be due to increased biogenesis, but more likely due to matrix swelling as a result of metabolic dysfunction.

To investigate the metabolic pathways that SDH-deficient cells use to support complex I-linked respiration in more depth, we investigated the metabolism of $^{13}C_4$-malate supplied to permeabilized cells as before (G+M; Figure 3A), but incubated for 45 minutes—a time point previously shown to approach steady state.[20] Although

limited incorporation of ^{13}C from malate was observed in succinate (Figure 3B), which is most likely due to the presence of unlabeled glutamate, we observed similar labeling of m + 4 citrate between wild-type and SDH-deficient cells, indicative of citrate synthase activity. This was confirmed by similar levels of the m + 6 citrate isotopomer, which is the product of the condensation of $^{13}C_4$-oxaloacetate (OAA) and $^{13}C_2$-acetyl CoA (Figure 3C). Labeling of acetyl CoA occurs through oxidation of labeled pyruvate, which itself is derived either from OAA or malate through the action of

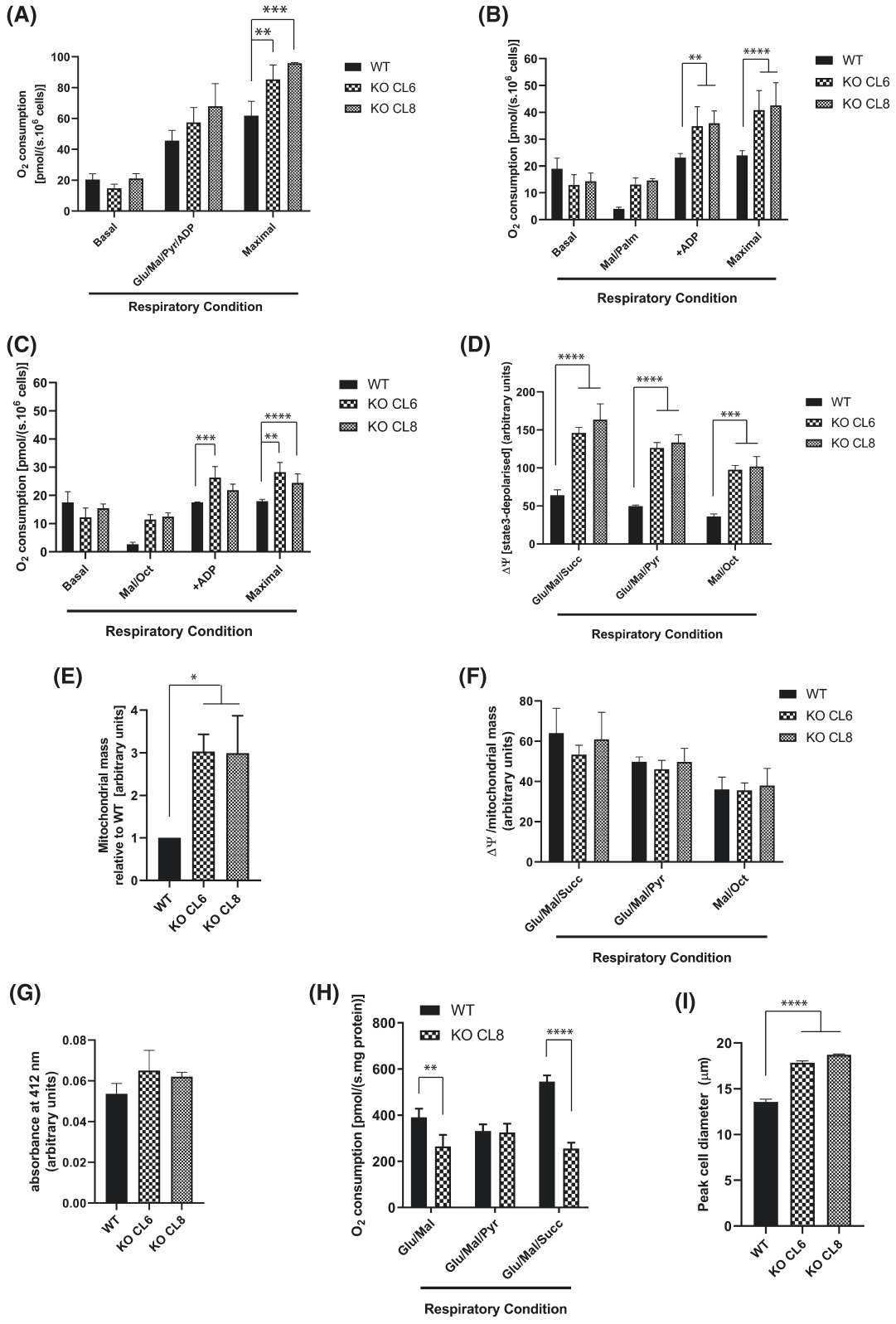

FIGURE 2 A, Respiration (oxygen consumption) of permeabilized imCCs in basal state (Mir05 medium), or with the following additions: Glu/Mal/Pyr/ADP; glutamate (10 mM), malate (2 mM) and pyruvate (5 mM), ADP (3 mM), followed by FCCP to stimulate maximal respiration. $*P < .05$, $**P < .01$ (two-way ANOVA, Dunnett's post-test). B and C, Respiration of fatty acids—palmitate (B) and octanoate (C). Palmitoylcarnitine (40 μM) or octanoylcarnitine (200 μM) were added with limiting concentrations of malate (0.05 mM), with ADP (3 mM), followed by FCCP (maximal) to stimulate maximal respiration as above. $**P < .01$, $***P < .001$, $****P < .001$ (two-way ANOVA, Dunnett's post-test). D, Mitochondrial membrane potential ($\Delta\psi$) assessed in the presence of indicated substrates. The substrates were: 10 mM glutamate (Glu), 2 mM malate (Mal), 5 mM pyruvate (Pyr), 10 mM succinate (Succ), or 200 μM octanoylcarnitine and 0.05 M malate (Mal/Oct). $***P < .001$, $****P < .001$ (two-way ANOVA, Dunnett's post-test). E, Mitochondrial mass assessed with 100 nM of $\Delta\psi$ insensitive dye MitoTracker Green. $P < .05$ (t test with Welch's correction). F, $\Delta\psi$ normalized to mitochondrial mass ([data shown in D]/[data shown in E]). G, Citrate synthase activity assessed per cell number. H, Respiration of isolated mitochondria in the presence of 3 mM ADP and different substrate combinations as indicated. The substrates were 10 mM glutamate (Glu), 2 mM malate (Mal), 5 mM pyruvate (Pyr), and 10 mM succinate (Succ). $**P < .01$, $****P < .0001$ (two-way ANOVA, Dunnett's post-test). I, Cell size presented as peak diameter (PDI) of the cells in suspension. $****P < .0001$. Results shown are from 3 to 4 independent experiments and presented as mean ± SD, apart from G and I, which were 4 and 3 independent samples, respectively

mitochondrial phosphoenolpyruvate carboxykinase (PCK2) or malic enzyme (ME2) activities, respectively (Figure 3A). High levels of pyruvate-forming activity in these conditions were confirmed through the presence of the m + 3 isotopomer of alanine (Figure 3D).[21] We and others have previously shown upregulation of pyruvate carboxylase in SDH-deficient cells and tumors, which would support anaplerotic pyruvate use in the mitochondria.[7,10] In light of the results above, we investigated the expression of enzymes involved in central carbon metabolism in the mitochondria, and observed a number with significant differential changes in mRNA expression between MAF and imCC model (Supplementary Figure 3A). Given that PDHA1 and PDK4, two enzymes involved in the regulation of pyruvate oxidation, demonstrated altered expression, we assessed them at the protein level and found that they were both significantly downregulated, but in both cell models (Supplementary Figure 3B). These data suggest that changes in pyruvate oxidation that may occur downstream of these alterations in protein expression are unlikely to explain cell type-specific metabolic alterations observed.

To investigate TCA cycle pathways downstream of citrate, we omitted glutamate from the system and used either a combination of $^{13}C_4$-malate and unlabeled pyruvate (Figure 3E), or $^{13}C_5$-glutamine/unlabeled malate (Figure 3I). When $^{13}C_4$-malate was supplied together with unlabeled pyruvate, clear evidence of citrate synthase activity in both cell lines was observed (m + 4 isotopomer), which constituted 90% of the total citrate pool in SDH-deficient cells and 70% in wild-type (Figure 3F). Continued oxidation of citrate to yield succinate appeared to be higher in SDH-deficient cells compared to wild-type cells (m + 2 succinate isotopomer; Figure 3G) confirming the absence of any metabolic defect in the TCA cycle between citrate synthase and SDH, and therefore efficient NADH-oxidizing activity in the SDH-deficient chromaffin cells. The mass isotopomer distribution is independent of pool size so this difference is expected to be independent of the truncation of the TCA cycle in SDH-deficient cells and concomitant succinate accumulation. In both cell lines, 90% of all fumarate was synthesized through fumarate hydratase activity, suggestive of relatively low SDH activity even in wild-type chromaffin cells (Figure 3H). When the permeabilized cells were incubated with unlabeled malate in combination with $^{13}C_5$ glutamine, around 80% of all citrate was unlabeled in SDH-deficient cells while this was ~60% in wild-type cells, the predominant isotopomers arose from TCA cycle oxidation activity (m + 2 and m + 4 isotopomers; Figure 3J). Interestingly, although glutamine-derived glutamate was similar in both conditions (Figure 3K), downstream production of succinate was increased in SDH-deficient cells, as expected (Figure 3L). These results suggest that the respiratory substrates provided to mitochondria in selectively permeabilized cells are metabolized in a similar manner independent of SDH function. We have previously shown that expression of many of the enzymes involved in the reductive carboxylation of glutamine is altered independently of cell model at the mRNA level.[10] Due to the increased glutamate oxidation observed, we investigated the expression of 2-oxoglutarate (α-ketoglutarate) dehydrogenase (OGDH), part of the OGDH complex, and a critical control point for glutamate oxidation within TCA cycle. We found that it was not substantially altered in either cell model (Supplementary Figure 3C).

It was recently shown that after pharmacological inhibition of SDH, complex I-dependent respiration was preserved due to glutamine oxidation accompanied by succinate efflux out of mitochondria and the cell.[8] It was further suggested that this mechanism sustains respiration in cells with neurodegeneration-associated *SDHA* mutation and suggested that the ability to use this normally redundant metabolic shunt may explain the different phenotype in SDH-mutations-associated tumors versus neurodegenerative disorders.[8] In our study, we report that respiration was found to be similar between wild-type and SDH-deficient chromaffin cells (Figure 1B) due to a maintenance of complex I activity. We therefore investigated whether succinate efflux specifically supported glutamine oxidation in our model. We incubated SDH-deficient cells with $^{13}C_5$-glutamine, and indeed observed a high rate of glutamine-derived succinate efflux, with close to 75% of all

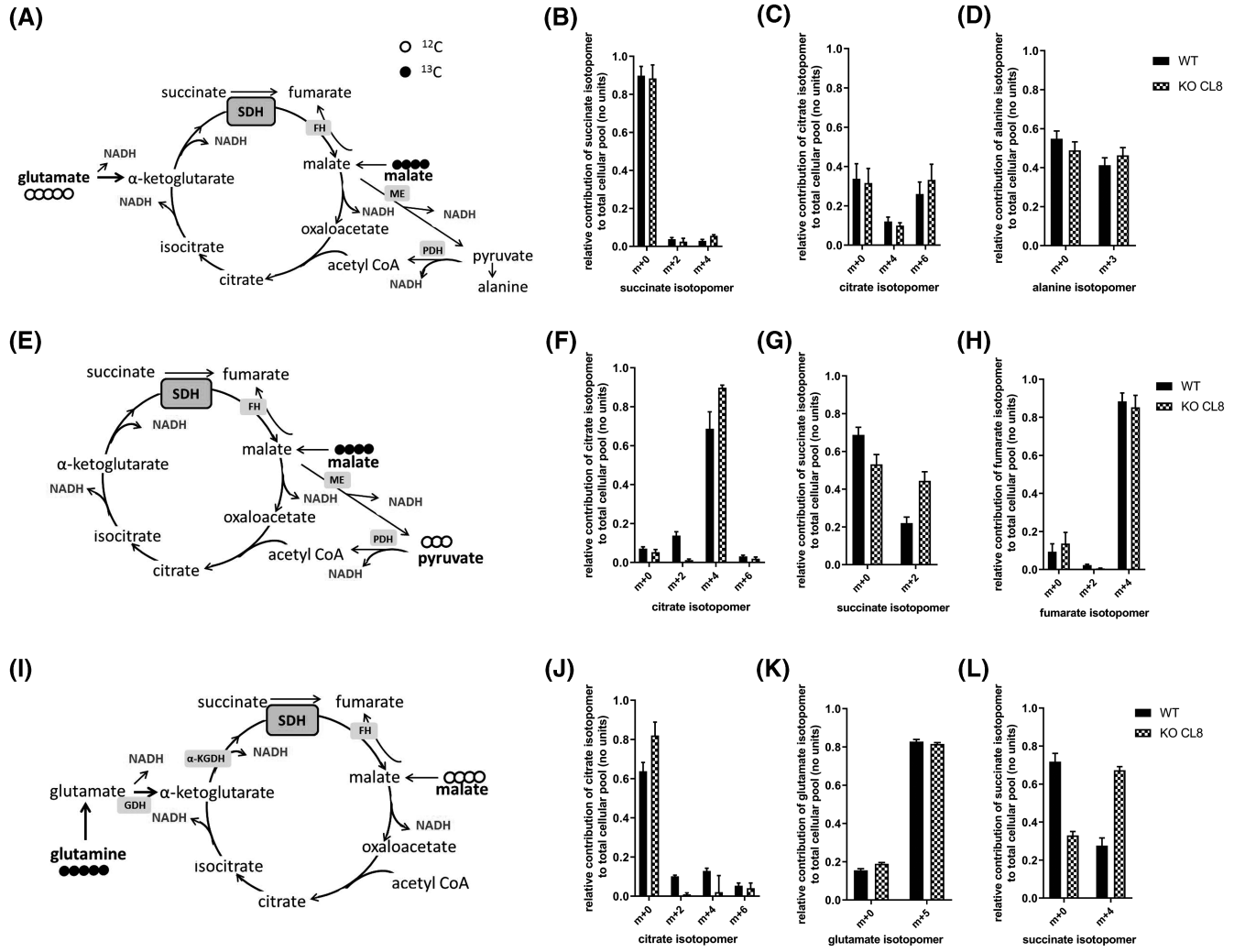

FIGURE 3 Metabolism of ^{13}C labeled respiratory substrates. A, Scheme of TCA cycle with SDH enzyme (yellow box) and accompanying redox reaction producing NADH (highlighted in blue) during the labeling experiment with $^{13}C_4$ malate and non-labeled glutamate in the Oxygraph-2k. Black full circles represent ^{13}C carbon atoms. B-D, Relative contribution of succinate (B), citrate (C), and alanine (D) isotopomers to total cellular pool in the Oxygraph-2k labeling experiment with 1 mM $^{13}C_4$ malate and unlabeled 10 mM glutamate. E, Scheme of TCA cycle with SDH enzyme (yellow box) and accompanying redox reaction producing NADH (highlighted in blue) during the labeling experiment with $^{13}C_4$ malate and non-labeled pyruvate in the Oxygraph-2k. Black full circles represent ^{13}C carbon atoms. F-H, Relative contribution of citrate (F), succinate (G), and fumarate (H) isotopomers to total cellular pool in the Oxygraph-2k labeling experiment with 1 mM $^{13}C_4$ malate and non-labeled 5 mM pyruvate. I, Scheme of TCA cycle with SDH enzyme (yellow box) and accompanying redox reaction producing NADH (highlighted in blue) during the labeling experiment with $^{13}C_5$ glutamine and non-labeled malate in the Oxygraph-2k. Black full circles represent ^{13}C carbon atoms. J-L, Relative contribution of citrate (J), glutamate (K), and succinate (L) isotopomers to total cellular pool in the Oxygraph-2k labeling experiment with 3 mM $^{13}C_5$ glutamine with non-labeled 1 mM malate. Data shown are a product of 2-3 independent experiments performed in duplicate and individual results pooled for final evaluation presented as mean ± SD

cellular succinate arising from glutamine (compared to 32% in wild-type cells; Figure 4A), which was also observed in the medium (Figure 4B,C). This suggests that glutamine oxidation is highly active in the chromaffin model of *Sdhb* loss, and could explain the sustained respiration observed. Consistent with their increased glutamine requirement, inhibition of glutaminolysis with BPTES, a potent inhibitor of glutaminase, reduced growth or increased cell death of SDH-deficient cells more efficiently than in their wild-type counterparts (Figure 4D).

4 | DISCUSSION

SDH-mutated tumors arise from one of very few cell types, which include chromaffin cells, paraganglia, and gastrointestinal stromal cells.[22] Given that these cell types have not been shown to have a higher inherent rate of mutation than others, it suggests that they are able to tolerate loss of this central metabolic enzyme while other cell types cannot. Indeed, this is a common theme in tumors driven by mutations in metabolic enzymes: loss of fumarate hydratase

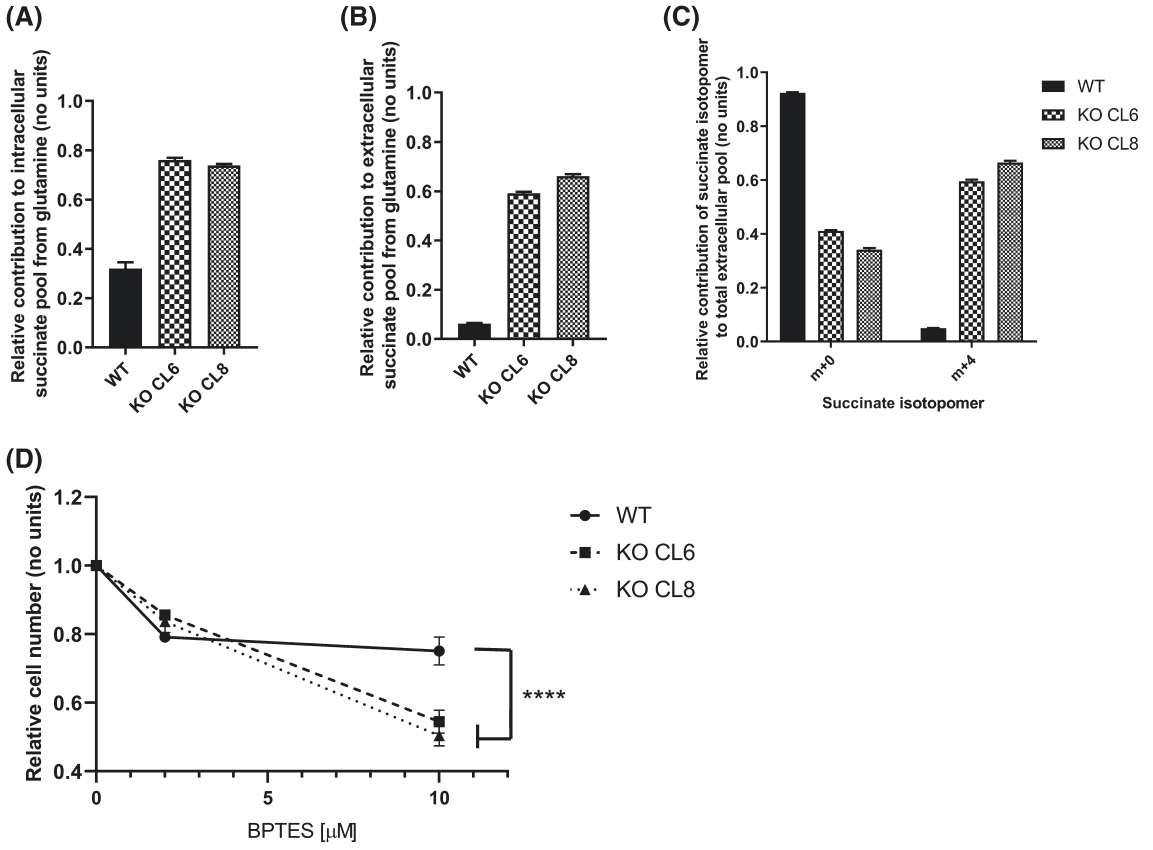

FIGURE 4 Glutamine oxidation and succinate efflux in *Sdhb*$^{-/-}$ cells. A, Relative contribution to intracellular succinate pool from $^{13}C_5$ glutamine. B, Relative contribution to effluxed succinate pool from $^{13}C_5$ glutamine. C, Relative contribution of succinate isotopomers to total extracellular succinate pool from $^{13}C_5$ glutamine. D, Cell growth over period of 3 days in the presence of 2 or 10 μM BPTES. In (A-C), experiments were done in tetraplicate and results shown are presented as mean ± SD. In (D) 4, independent experiments were done in triplicate and results are shown as mean ± SEM. One-way ANOVA was used to assess statistical significance; ****$P \leq .0001$

is observed to arise most frequently in myocytes of the smooth muscle and renal epithelium while oncogenic mutations in isocitrate dehydrogenase 1 are most often observed in tumors arising from glial cells, myeloid cells, and chondrocytes.[22]

This study represents the first to investigate comprehensively mitochondrial metabolic function after loss of *Sdhb*, in chromaffin cells. It is important to note that many of the metabolic phenotypes observed in the chromaffin model described here and published previously mirror those described in other *Sdhb*$^{-/-}$ models based on non-physiologically relevant cell types; adrenal fibroblast (described here), renal,[7,8] and breast epithelia.[17] In these models, both respiration of intact cells and complex I-specific activity were found to be lower in SDH-deficient cells compared with wild-type (Figure 1).[7,8,17] We show here that this is not the case in a chromaffin cell-derived model, which retains complex I function and a respiratory activity comparable to wild-type cells. Furthermore, it appears that they maintain the supply of acetyl co-A through a combination of pyruvate and fatty acid oxidation. However, our data also suggest that when FA oxidation is inhibited, SDH-deficient chromaffin cells are unable to compensate with additional contribution from pyruvate, which is most likely due to inhibition of pyruvate dehydrogenase by HIF-dependent upregulation of the inhibitory kinase, pyruvate dehydrogenase kinase 1 (Supplementary Figure 3B).[23] Finally, we also provide evidence to suggest that in the imCC cell model, the mitochondrial ATP synthase functions as an ATP-hydrolyzing proton pump, in contrast to the MAF cell model. This is consistent with the increased sensitivity of these SDH-deficient cells to the ionophore, FCCP (Figure 1G), which dissipates the proton gradient and therefore likely increases the rate of mitochondrial ATP hydrolysis to a rate that is unsustainable for the cells.

It is important to note that some of the respiratory phenotype observed in the chromaffin model is likely due to the increased mitochondrial mass observed that was not apparent in the breast epithelial model.[17] Increased mitochondrial mass downstream of SDH deficiency is consistent with previous observations made in *SDH*-mutated

PPGL, which are characterized by the presence of significant number of defective mitochondria.[24,25] Indeed, a similar mitochondrial morphology and increase in mass was observed in other SDHB-mutated tumor types as well as in *Sdhb*$^{+/-}$ mice.[26,27] However, this increase may come at a cost to the cell; the mitochondria themselves are less efficient, and even small increases in electron flow were found to result in a reduction in viability (Figure 1G). Importantly, the clear differences between the chromaffin and non-chromaffin cell models observed in this study are also reflected in previous studies using these models, where glucose and glutamine oxidation, which generate NADH, were retained in the *Sdhb*$^{-/-}$ chromaffin cell model, which was less apparent in the epithelial cell models.[7,10]

It is therefore clear from the cell model data both previously published and presented here that, in parallel with the etiology of SDHB-deficient tumors, the tissue of origin of the SDH-deficient cell may be critical to their ability to cope with loss of SDH activity. We suggest that at least some of this is likely due to the retention of complex I function, which maintains a more favorable NAD^+:NADH, reducing the need for additional metabolic re-wiring. The respiration of SDH-deficient cells is supported by increased but incomplete glutamine oxidation. However, this is not sufficient to ensure reserve respiratory capacity and these cells show high sensitivity toward inhibition of glutaminolysis and mitochondrial uncoupling, features which could be taken advantage of for future therapeutic potential.

ACKNOWLEDGMENTS

We would like to thank Professor Mark Viant and Dr Stefan Schade for the use and assistance with the CASY cell counter. We thank Professors Ed Rainger and David Hodson and Mr Nick Fine for kindly providing reagents. KK, AT, and JG are supported by the Paradifference Foundation, LV, CEG, and BK are supported by Cancer Research UK (C42109/A26982 and C42109/A24891) and GGL holds a Wellcome Trust Senior Fellowship (104612/Z/14/Z).

AUTHORS CONTRIBUTIONS

K. Kľučková, C. Escribano-Gonzalez, L. Vettore, R.L. Hindshaw, J.L.E. Tearle, and B. Kaul performed research; J. Goncalves and G.G. Lavery prepared and supplied reagents; K. Kľučková, C. Escribano-Gonzalez, L. Vettore, R.L. Hindshaw, J.L.E. Tearle, A. Thakker, J. Favier, and D.A. Tennant processed and analyzed data; K. Kľučková, J. Favier, and D.A. Tennant designed the research and wrote the manuscript.

CONFLICT OF INTEREST

The authors declare no conflicts of interest.

REFERENCES

1. Bardella C, Pollard PJ, Tomlinson I. SDH mutations in cancer. *Biochim Biophys Acta*. 2011;1807:1432-1443.
2. Letouze E, Martinelli C, Loriot C, et al. SDH mutations establish a hypermethylator phenotype in paraganglioma. *Cancer Cell*. 2013;23:739-752.
3. Selak MA, Armour SM, MacKenzie ED, et al. Succinate links TCA cycle dysfunction to oncogenesis by inhibiting HIF-alpha prolyl hydroxylase. *Cancer Cell*. 2005;7:77-85.
4. Baysal BE, Ferrell RE, Willett-Brozick JE, et al. Mutations in SDHD, a mitochondrial complex II gene, in hereditary paraganglioma. *Science*. 2000;287:848-851.
5. Bourgeron T, Rustin P, Chretien D, et al. Mutation of a nuclear succinate dehydrogenase gene results in mitochondrial respiratory chain deficiency. *Nat Genet*. 1995;11:144-149.
6. Burnichon N, Briere JJ, Libe R, et al. SDHA is a tumor suppressor gene causing paraganglioma. *Hum Mol Genet*. 2010;19:3011-3020.
7. Cardaci S, Zheng L, MacKay G, et al. Pyruvate carboxylation enables growth of SDH-deficient cells by supporting aspartate biosynthesis. *Nat Cell Biol*. 2015;17:1317-1326.
8. Lorendeau D, Rinaldi G, Boon R, et al. Dual loss of succinate dehydrogenase (SDH) and complex I activity is necessary to recapitulate the metabolic phenotype of SDH mutant tumors. *Metab Eng*. 2017;43:187-197.
9. Pang Y, Lu Y, Caisova V, et al. Targeting NAD(+)/PARP DNA Repair Pathway as a Novel Therapeutic Approach to SDHB-Mutated Cluster I Pheochromocytoma and Paraganglioma. *Clin Cancer Res*. 2018;24:3423-3432.
10. Lussey-Lepoutre C, Hollinshead KE, Ludwig C, et al. Loss of succinate dehydrogenase activity results in dependency on pyruvate carboxylation for cellular anabolism. *Nat Commun*. 2015;6:8784.
11. Birsoy K, Wang T, Chen WW, Freinkman E, Abu-Remaileh M, Sabatini DM. An essential role of the mitochondrial electron transport chain in cell proliferation is to enable aspartate synthesis. *Cell*. 2015;162:540-551.
12. Sullivan LB, Gui DY, Hosios AM, Bush LN, Freinkman E, Vander Heiden MG. Supporting aspartate biosynthesis is an essential function of respiration in proliferating cells. *Cell*. 2015;162:552-563.
13. Frezza C, Cipolat S, Scorrano L. Organelle isolation: functional mitochondria from mouse liver, muscle and cultured fibroblasts. *Nat Protoc*. 2007;2:287-295.
14. Ben Aim L, Pigny P, Castro-Vega LJ, et al. Targeted next-generation sequencing detects rare genetic events in pheochromocytoma and paraganglioma. *J Med Genet*. 2019;56:513-520.
15. Burnichon N, Vescovo L, Amar L, et al. Integrative genomic analysis reveals somatic mutations in pheochromocytoma and paraganglioma. *Hum Mol Genet*. 2011;20:3974-3985.
16. Metsalu T, Vilo J. ClustVis: a web tool for visualizing clustering of multivariate data using Principal Component Analysis and heatmap. *Nucleic Acids Res*. 2015;43:W566-W570.
17. Bezawork-Geleta A, Wen H, Dong L, et al. Alternative assembly of respiratory complex II connects energy stress to metabolic checkpoints. *Nat Commun*. 2018;9:2221.
18. Rouslin W. Protonic inhibition of the mitochondrial oligomycin-sensitive adenosine 5′-triphosphatase in ischemic and autolyzing cardiac muscle. Possible mechanism for the mitigation of ATP hydrolysis under nonenergizing conditions. *J Biol Chem*. 1983;258:9657-9661.

19. Garlick PB, Radda GK, Seeley PJ. Studies of acidosis in the ischaemic heart by phosphorus nuclear magnetic resonance. *Biochem J*. 1979;184:547-554.
20. Nonnenmacher Y, Palorini R, d'Herouel AF, et al. Analysis of mitochondrial metabolism in situ: Combining stable isotope labeling with selective permeabilization. *Metab Eng*. 2017;43:147-155.
21. Christen S, Lorendeau D, Schmieder R, et al. Breast cancer-derived lung metastases show increased pyruvate carboxylase-dependent anaplerosis. *Cell Rep*. 2016;17:837-848.
22. Laurenti G, Tennant DA. Isocitrate dehydrogenase (IDH), succinate dehydrogenase (SDH), fumarate hydratase (FH): three players for one phenotype in cancer? *Biochem Soc Trans*. 2016;44:1111-1116.
23. Kim JW, Tchernyshyov I, Semenza GL, Dang CV. HIF-1-mediated expression of pyruvate dehydrogenase kinase: a metabolic switch required for cellular adaptation to hypoxia. *Cell Metab*. 2006;3:177-185.
24. Douwes Dekker PB, Hogendoorn PC, Kuipers-Dijkshoorn N, et al. SDHD mutations in head and neck paragangliomas result in destabilization of complex II in the mitochondrial respiratory chain with loss of enzymatic activity and abnormal mitochondrial morphology. *J Pathol*. 2003;201:480-486.
25. D'Antongiovanni V, Martinelli S, Richter S, et al. The microenvironment induces collective migration in SDHB-silenced mouse pheochromocytoma spheroids. *Endocr Relat Cancer*. 2017;24:555-564.
26. Housley SL, Lindsay RS, Young B, et al. Renal carcinoma with giant mitochondria associated with germ-line mutation and somatic loss of the succinate dehydrogenase B gene. *Histopathology*. 2010;56:405-408.
27. Szarek E, Ball ER, Imperiale A, et al. Carney triad, SDH-deficient tumors, and Sdhb+/- mice share abnormal mitochondria. *Endocr Relat Cancer*. 2015;22:345-352.

SUPPORTING INFORMATION

Additional supporting information may be found online in the Supporting Information section.

How to cite this article: Kľučková K, Thakker A, Vettore L, et al. Succinate dehydrogenase deficiency in a chromaffin cell model retains metabolic fitness through the maintenance of mitochondrial NADH oxidoreductase function. *The FASEB Journal*. 2020;34:303–315. https://doi.org/10.1096/fj.201901456R

REVUE 1

Rodent models of pheochromocytoma, parallels in rodent and human tumorigenesis

Charlotte Lussey-Lepoutre, Alexandre Buffet, Aurélie Morin, Judith Goncalves, Judith Favier

Cell Tissue Res. 2018 May;372(2):379-392.

Cell and Tissue Research (2018) 372:379–392
https://doi.org/10.1007/s00441-018-2797-y

REVIEW

Rodent models of pheochromocytoma, parallels in rodent and human tumorigenesis

Charlotte Lussey-Lepoutre[1,2] · Alexandre Buffet[2,3] · Aurélie Morin[2,3] · Judith Goncalves[2,3] · Judith Favier[2,3]

Received: 10 November 2017 / Accepted: 16 January 2018 / Published online: 9 February 2018

Abstract

Paragangliomas and pheochromocytomas are rare neuroendocrine tumors characterized by a large spectrum of hereditary predisposition. Based on gene expression profiling classification, they can be classically assigned to either a hypoxic/angiogenic cluster (cluster 1 including tumors with mutations in *SDHx*, *VHL* and *FH* genes) or a kinase-signaling cluster (cluster 2 consisting in tumors related to *RET*, *NF1*, *TMEM127* and *MAX* genes mutations, as well as most of the sporadic tumors). The past 15 years have seen the emergence of an increasing number of genetically engineered and grafted models to investigate tumorigenesis and develop new therapeutic strategies. Among them, only cluster 2-related predisposed models have been successful but grafted models are however available to study cluster 1-related tumors. In this review, we present an overview of existing rodent models targeting predisposition genes involved or not in human pheochromocytoma/paraganglioma susceptibility and their contribution to the improvement of pheochromocytoma experimental research.

Keywords Pheochromocytoma · Paraganglioma · Mouse models

Introduction

Pheochromocytoma (PCC) and paraganglioma (PGL) are rare neuroendocrine tumors that arise in chromaffin cells of the adrenal medulla and in sympathetic and parasympathetic paraganglia, respectively. Nearly 40% of patients with pheochromocytoma and/or paraganglioma (PPGL) carry a germline mutation in one of the 13 PPGL predisposing genes identified so far (Favier et al. 2014), including *RET* (leading to multiple endocrine neoplasia type 2A and 2B), *NF1* (causing neurofibromatosis type 1), *VHL* (Von Hippel Lindau disease) and *SDHx* genes (*SDHA*, *SDHB*, *SDHC*, *SDHD*, *SDHAF2*, responsible for hereditary PGL syndrome). Other rare cases involve germline or mosaic mutations in the *FH*, *TMEM127*, *MAX*, *HIF2A* and *MDH2* genes (Cascon et al. 2015; Castro-Vega et al. 2015; Dahia 2014; Favier et al. 2014). In addition, somatic mutations have been reported in 30% of cases, involving the *VHL*, *RET*, *NF1*, *HIF2A*, *ATRX* and *HRAS* genes (Castro-Vega et al. 2015). With the exception of *RET* and *HIF2A* that act as oncogenes, all PPGL susceptibility genes are tumor suppressor genes: patients carry a heterozygous germline mutation and tumor development occurs following a somatic second hit that leads to loss of heterozygosity (LOH) and to the subsequent inactivation of the gene's function.

Over the past few years, gene expression profiling of these rare tumors enabled discovering new PPGL predisposition genes (Burnichon et al. 2010; Cascon et al. 2015; Comino-Mendez et al. 2011; Favier et al. 2012; Letouze et al. 2013; Qin et al. 2010) and classifying PPGLs by classically assigning them to either a hypoxic/angiogenic cluster (cluster 1) or a kinase-signaling cluster (cluster 2) (Burnichon et al. 2011; Dahia et al. 2005; Eisenhofer et al. 2004; Favier et al. 2009; Lopez-Jimenez et al. 2010). Cluster 1 contains all *SDH*x-, *VHL*- and *FH*-mutated tumors (Castro-Vega et al. 2014; Letouze et al. 2013). Cluster 2 comprises tumors related to *RET*, *NF1*, *TMEM127* and *MAX* genes mutations, as well as most of the sporadic tumors.

Between 10% (PCC) to 40% (PGL) of patients will present a malignant progression of their disease, defined by the occurrence of the first metastasis (Lenders et al. 2014) and with a 5-

✉ Judith Favier
judith.favier@inserm.fr

[1] Université Pierre et Marie Curie, Faculté de Médecine, Service de Médecine Nucléaire Hôpital Pitié-Salpêtrière, Paris, France

[2] INSERM UMR970, Paris-Cardiovascular Research Center, Equipe Labellisée Ligue Contre le Cancer, 56 rue Leblanc, F-75015 Paris, France

[3] Sorbonne Paris Cité, Faculté de Médecine, Université Paris Descartes, F-75006 Paris, France

year survival rate below 50%. Mutations in the *SDHB* gene are associated with metastatic, aggressive forms of PPGL (Amar et al. 2007; Gimenez-Roqueplo et al. 2003). Indeed, more than one third of patients with metastatic PPGL carry a germline *SDHB* mutation and half of *SDHB*-mutated patients will ultimately develop a metastatic disease.

Many genetically engineered and grafted mouse models have been generated to investigate the mechanisms of PPGL tumorigenesis, develop new diagnostic biomarkers or test innovative therapeutic strategies. Existing mouse models include mutations on *c-mos*, *Ret*, *ErbB2* and *B-Raf* proto-oncogenes (Lai et al. 2007; Schulz et al. 1992; Smith-Hicks et al. 2000; Urosevic et al. 2011) and inactivation of *Nf1*, *Rb*, *Trp53 Vhl*, *Sdhd*, *Pten* and *InK4a* tumor suppressor genes (Bayley et al. 2009; Gnarra et al. 1997; Haase et al. 2001; Jacks et al. 1994; Korpershoek et al. 2009; Ma et al. 2003; Nikitin et al. 1999; Piruat et al. 2004; You et al. 2002). This review focuses on these existing models aiming at deciphering human tumor development and improving malignant PPGL early diagnosis and treatment.

Predisposed mouse models

Cluster 1

The cluster C1 comprises tumors carrying mutations on *SDHx*, *FH*, *VHL* and *HIF2A* genes. Genes overexpressed in the C1 cluster promote a "pseudo-hypoxic" signature secondary to the direct capacity of *SDHx* and *VHL*-mutated cells to stabilize hypoxia-inducible factors (HIFs) in normoxic conditions, thereby stimulating angiogenesis, proliferation and glycolysis pathways (Favier et al. 2009). *VHL* encodes a member of an E3 ubiquitin ligase complex that addresses HIFα proteins to proteasomal degradation in normoxia. *SDHA-D* genes encode the four subunits of succinate dehydrogenase (SDH) or mitochondrial complex II, an enzyme located at the crossroads between the mitochondrial electron transport chain and the tricarboxylic acid (TCA) cycle (Lancaster and Simon 2002). In PPGL patients carrying a germline heterozygous mutation on a *SDHx* gene, somatic loss of the remaining allele induces a complete SDH loss-of-function, which results in the accumulation of its substrate, succinate in the tumor. Succinate acts as an oncometabolite that is suspected to mediate the tumorigenic effects related to *SDHx* mutations (Letouze et al. 2013): its accumulation inhibits prolyl-hydroxylases activity that finally results in the abnormal stabilization of HIFαs under normoxic conditions (Briere et al. 2005). *SDHx* mutations also impair DNA and histone demethylation processes. Succinate inhibits TET DNA and JmJC histones demethylases, leading to global DNA and histones hypermethylation that has important consequences on gene expression (Letouze et al. 2013). *FH* is also a tumor suppressor gene involved in the TCA cycle, encoding fumarase (or fumarate hydratase), which converts fumarate into malate. As for SDH-related PPGL, fumarate accumulation acts as an oncometabolite (Castro-Vega et al. 2014; Letouze et al. 2013) (Morin et al. 2014) leading to a global histone and DNA hypermethylation in *FH*-related paragangliomas, a high rate of malignancy and a poor prognosis. Altogether these findings underlie the medical need for a reliable preclinical model of "cluster 1-like" tumors.

The (desperate) quest for an SDH-deficient mouse model

Piruat et al. published the first report of SDH complex inactivation in a mouse model in 2004 (Piruat et al. 2004). In this model, the homozygous knockout (KO) of *Sdhd* was lethal at an embryonic stage (E7) while heterozygous *Sdhd* inactivation induces a slight hyperplasia of the carotid body (CB) and a significant increase of spontaneous CB activity under normoxic conditions but without any CB PGL nor PCC (Piruat et al. 2004). Several years later, a second *Sdhd*-knockout mouse model was generated. They observed the same results even after crossing them with a strain knocked-out for a candidate imprinted modifier gene ($H19^{+/-}$ mice) in order to mimic the "imprinted" inheritance of *SDHD* tumorigenesis observed in human (Bayley et al. 2009). Finally, two conditional *Sdhd* KO were reported. One allowed a tissue-specific Sdhd deletion driven by the tyrosine hydroxylase promoter in the catecholaminergic system and the other one a tamoxifen-induced LOH at adulthood. None of these models resulted in PPGL. In contrast, they led to a reduced size of carotid bodies and to decreased cell numbers in the adrenal medulla (Diaz-Castro et al. 2012).

Two different teams reported negative results regarding engineering a *Sdhb*-deficient mouse model (Lepoutre-Lussey et al. 2015; Maher III et al. 2011).

Maher et al. did not observe any PPGL development in their heterozygous constitutional *Sdhb*-deficient mouse model, even after crossing them with a mouse deficient for *Bub 1*, *a* gene playing a key role in the mitotic checkpoint (Maher III et al. 2011).

As embryonic death of nullizygous *Sdhb* mice was predictable, our strategy was to use the Cre-Lox system to generate both a constitutive and a conditional inactivation of the gene. To that aim, LoxP sites were inserted on both sides of *Sdhb* exon 2 (Lepoutre-Lussey et al. 2015; Letouze et al. 2013). The constitutive knockout model was obtained by crossing *Sdhb*-floxed mice with PGK-Crem mice and two tissue-specific conditional KO models were generated using tyrosine hydroxylase-Cre (TH-Cre), expected to drive Cre recombinase expression in all catecholaminergic cells (Gelman et al. 2003) or human Prostate-Specific Antigen-Cre (PSA-Cre), supposedly specific of the prostate in human but actually driving expression in the adrenal medulla in

mouse (Korpershoek et al. 2009). Unfortunately, after a long-life follow-up of a large cohort including heterozygous constitutive and tissue specific Sdhb KO mice, no indication of chromaffin tumor development was apparent in any animal (Lepoutre-Lussey et al. 2015).

In a second step, because of the failure of the pure *Sdhb* KO model, we crossed them under a *Pten* KO background, which was previously reported to be predisposed to PCC (You et al. 2002), in order to generate a metastatic PCC experimental model harboring an inactivation of the Sdhb gene. At 10 months, 37% of the double conditional KO homozygous for Sdhb deletion mice (Ptenlox/lox, Sdhblox/lox, PSA-Cre and Pten+/lox, Sdhblox/lox, PSA-Cre) developed a PCC (instead of more than 70% in the Pten+/− KO mouse model) but in contrast with human tumors (Pollard et al. 2005), no accumulation of succinate was detected in any of these tumors suggesting the absence of Sdhb deletion in the tumor. This result, together with the lower incidence of PCC, suggest a cellular lethality of Sdhb complete KO in mouse, as shown for the *Sdhd* conditional KO (Diaz-Castro et al. 2012). The generation of a predisposed SDH-related model of PGL or PCC probably requires a "second hit" that would allow paraganglioma tumorigenesis in rodents.

Vhl- and *Fh*-deficient mice

The Von Hippel Lindau disease is a rare autosomal dominant hereditary neoplastic syndrome caused by mutations in the *VHL* tumor suppressor gene, which are responsible for a predisposition to renal cell carcinoma (RCC), retinal or central nervous system hemangioblastomas, pancreatic cysts and PPGL (Kim and Kaelin 2004).

The homozygous KO of *Vhl* in mice results in embryonic lethality secondary to a lack of placental vasculogenesis (Gnarra et al. 1997), while the phenotype of heterozygous *Vhl* mice is strongly dependent on their genetic background. Indeed, no phenotype was observed in $Vhl^{+/-}$ mice bred in a mixed C57BL6/c129 genetic background (Gnarra et al. 1997), while $Vhl^{+/-}$ in a BALB/c129 background developed cavernous liver hemangiomas with a high phenotypic penetrance (Haase et al. 2001). Several tissue-specific V*hl* KO models were generated (first in the liver (Haase et al. 2001) and then in the kidney, epidermis, thymus…) leading to several vascular tumors and renal cysts (for review see Haase 2005). Although about 90% of clear cell renal cell carcinomas (RCC) harbor biallellic inactivation of *VHL* (Sato et al. 2013), most of renal cell-specific *Vhl* KO failed to develop RCC. Recently, Harlander et al. showed that the development of RCC in *Vhl*-deficient mice needed the combination of 2 other combined deletions in *Trp53* and *Rb1* genes suggesting that *Vhl* deficiency is not sufficient for RCC formation (Harlander et al. 2017).

To our knowledge, only one specific *Vhl* KO in catecholaminergic cells was generated using the TH promoter (Macias et al. 2014). Interestingly, in contrast with the expected role of *VHL* as a tumor suppressor gene in human, conditional *Vhl* inactivation in catecholaminergic mouse cells did not lead to a tumor development but in the contrary to an important atrophy of targeted organs such as CB, adrenomedulla and sympathetic ganglia. These impairments were also associated with intolerance to hypoxia in the absence of hypoxia-induced CB hypertrophy in adult mice (Macias et al. 2014). These results were confirmed, to a lesser extend but always without any PPGL development, with a conditional *Vhl* KO during adulthood thanks to an inducible conditional KO ($TH\text{-}CRE^{ER}\text{-}VHL^{KO}$) (Macias et al. 2014).

Germline mutations in the tumor suppressor gene *FH* predispose in human to Reed syndrome, also known as Hereditary leiomyomatosis and renal cell cancer (HLRCC) (Tomlinson et al. 2002; Toro et al. 2003). This autosomal dominant disease associates smooth muscle tumors (leiomyomas) in the skin (more than 70% of *FH*-mutation carriers develop cutaneous leiomyoma) and uterus (about 82% of women develop uterine leiomyoma). Affected patients are at risk of developing benign renal cysts and type 2 papillary renal carcinoma. Recently, we demonstrated that *FH* gene germline mutations can also predispose to PPGL (Letouze et al. 2013) and, as in patients with *SDHB* mutation, lead to malignant or multiple forms of the disease (Castro-Vega et al. 2014; Clark et al. 2014).

Pollard et al. generated a mouse model of FH deficiency with a particular interest in kidney cancer development (Pollard et al. 2007). Again, $Fh1^{-/-}$ mice died during early embryogenesis, while tissue-specific targeting of *Fh1* in the kidney ($Fh1^{lox/lox}$;Ksp1.3/Cre animals), results in renal cysts but no RCC, as a direct consequence of HIF1α (and HIF2α) overexpression (Pollard et al. 2007) but without a clear demonstration of the link between tumor development and activation of the hypoxic pathway while the phenotype observed in *Fh* KO mice is not rescued but even worsened by the inactivation of HIF1 (Adam et al. 2011). No specific *Fh* inactivation in the adrenal medulla has been performed so far.

Cluster 2A

Cluster C2A comprises *RET*-, *NF1*-, *MAX*- and *TMEM127*-mutated tumors, as well as most sporadic tumors, including the recently described hotspot somatic mutation in *HRAS* (Castro-Vega et al. 2015). These tumors display activation of the RAS/mitogen-activated protein kinase (MAPK) and IGF1 signaling pathways, predisposing in human to the development of usually benign PCC with a very low incidence of PGL and malignant tumors (Table 1, Fig. 1).

Table 1 Rodent models of pheochromocytomas

Model type	Human expression cluster	Human syndrome	Gene	Mouse model	PPGL (%) and age of onset	Other phenotype	Cell lines	References
Genetically predisposed mouse models	Cluster 1	No model						
	Cluster 2	NF1	*NF1*	*Nf1−/−*	–	Embryonic lethal (E13.5)	–	Jacks 1994
				Nf1+/−	PCC (10–20%), 15–28 months	Myeloid leukemia		
					–	–	MPC	Powers 2000
		MEN2B	*RET*	Met918Thr (het)	Chromaffin cell hyperplasia (16%)	C-cell hyperplasia (up to 41% at 12 months)	–	Smith-Hicks 2000
				Met918Thr (homo)	PCC (100%), 6–10 months	C-cell hyperplasia (up to 60% at 10 months)	–	
							–	
		Retinoblastoma	*Rb*	*Rb +/−*	PCC 71% (14% bilateral) 12 months	C-cell thyroid carcinomas 81% 12 months. Pituitary, parathyroid, lung, pancreas tumors	–	Nikitin 1999
				Rb1F2/F2:Trp53F2–10/F2–10:TEC1	Bilateral PCC (100%), 4 months		–	Tonks 2010
		None	*c-mos*	Transgenic	Bilateral PCC (58%), 8 months	C-cell thyroid carcinomas; gliosis; axonal degeneration	–	Schultz 1992
		None	*B-Raf*	*B-RafV600E*	PCC and PGL (80%), 5 months	Cardio-faciocutaneous syndrome		Urosevic 2011
		None	*CerS2*	*CerS2$^{GT/GT}$ (CerS2null)*	Medullary hyperplasia (100%) Bilateral PCC (54%)	Hepatopathy, emphysema, demyelination	–	Park 2015
		None	*ErbB2*	PB-*ErbB2*	Adrenal hypertrophy (5%) PCC (5% of males), 15 months	Prostate intraepithelial neoplasia	–	Lai 2007
		Cowden syndrome	*PTEN*	*Ink4a Arf+/+; Pten+/−*	PCC (24%), 10.5 months	Prostate, breast and endometrial hyperplasia. Lymphoma; pulmonary and colon carcinoma sarcoma	–	You 2002
				Ink4a Arf+/−; Pten+/−	PCC (57%), 7.5 months			
				Ink4a Arf−/−; Pten+/−	PCC (59%), 6 months			
				PSA-Cre; *Pten*loxP/loxP	PCC from 30%, 7–9 months to 100%, 15–16 months	Prostate tumors	–	Korpershoek 2009
Xeno- and allografted tumors	Cluster 1	Familial PGL	*SDHB*	Allograft *Sdhb −/−*	Subcutaneous tumors	–	Immortalized mouse chromaffin cells "ImCC"	Lussey-Lepoutre 2016
				Xenograft ShRNA-*SDHB*	Subcutaneous tumors	–	143B human osteosarcoma	Guzy 2008

Table 1 (continued)

Model type	Human expression cluster	Human syndrome	Gene	Mouse model	PPGL (%) and age of onset	Other phenotype	Cell lines	References
				Xenograft human PGL and a human PGL-liver metastasis	Small subcutaneous tumors	–	–	Powers 2017
	Cluster 2	NF1	*NF1*	Allograft *Nf1*+/–	Subcutaneous and metastatic tumors	–	Mouse PCC cells "MPC"	Ohta 2008
					Metastatic tumors	–	Mouse tumor tissue "MTT"	Martiniova 2009
		Familial PCC	*MAX*	Xenograft *Max* −/−	Subcutaneous tumors	–	Rat PC 12 cells	Denorme 2015
		Sporadic PGL	–	Xenograft human sporadic PGL	Small subcutaneous tumors	–	–	Powers 2017

PCC pheochromocytoma, *PGL* paraganglioma, *NF1* neurofibromatosis type 1, *MEN* multiple endocrine neoplasia

Genes linked to PPGL predisposition in human

Nf1 *NF1* is a very large gene (60 exons) (Viskochil et al. 1990) encoding neurofibromin, a repressor of the RAS–RAF–MAPK signaling cascade. Heterozygous mutations in this gene were identified in the early nineties as being responsible for neurofibromatosis type 1, also known as Von Recklinghausen disease, one of the most frequent autosomic disorders (prevalence of 1 in 3000 to 1 in 4000 people in the general population and a high penetrance) characterized by pigmentary abnormalities and neoplastic growth of neural crest-derived cells, such as multiple dermal neurofibromas and very rarely PCC (0.1–5.7% of patients with NF1) (Gutmann et al. 1997).

As an important tumor suppressor, homozygous deletion of Nf1 in mouse leads to embryonic lethality. The heterozygous Nf1 knockout mouse model partially mimics the human syndrome as mice develop PCC (but at a much higher frequency, ~ 10–20% lifetime incidence) without any neurofibromas (Jacks et al. 1994). However, an interesting observation with this model is that, as already observed in the Vhl mice, the great influence of the genetic background. Indeed, PCC only arose in mice with a mixed genetic background (Powers et al. 2000). One possible explanation for this is the varying levels of neurofibromin expression depending on the mouse strain. Indeed, strain-dependent tissue-specific modifiers may modulate Nf1 expression to levels comparable to that of mutation of one *Nf1* allele. Hence, haploinsufficient models may be extremely different from one another depending on the genetic background (Hawes et al. 2007).

Ret *RET is a* proto-oncogene encoding a tyrosine kinase receptor activating, after binding of its ligands, the PI3K–AKT and MAPK–ERK signaling pathways (Ibanez 2013; Wagner et al. 2012). Gain-of-function mutations in *RET* proto-oncogene cause multiple endocrine neoplasia type 2 (MEN2), a rare autosomal dominant disorder comprising 2 syndromes: MEN2A, associating medullary thyroid carcinoma, PCC and hyperparathyroidism and caused by several germline mutations frequently affecting codon 634 and MEN 2B (accounting only for 5% of MEN2 cases) defined by severe medullary thyroid carcinoma, PCC, Marfanoid habitus, mucosal neuromas and ganglioneuromatosis of the gut and the intestine and exclusively secondary to a unique point mutation at codon 918 (M918T) (Carlson et al. 1994) .

Only one PCC model was secondary to a direct activating mutation (Met918thr) of the *RET* proto-oncogene, the mutation involved in MEN2B in human (Smith-Hicks et al. 2000). At 6 months, 100% of the homozygous RetMEN2B mice developed a PCC. In contrast with the human phenotype, these mice developed thyroid C-cell hyperplasia (the presumed precursor of carcinoma in human) but no MTC (Smith-Hicks et al. 2000). MEN 2A mouse models secondary

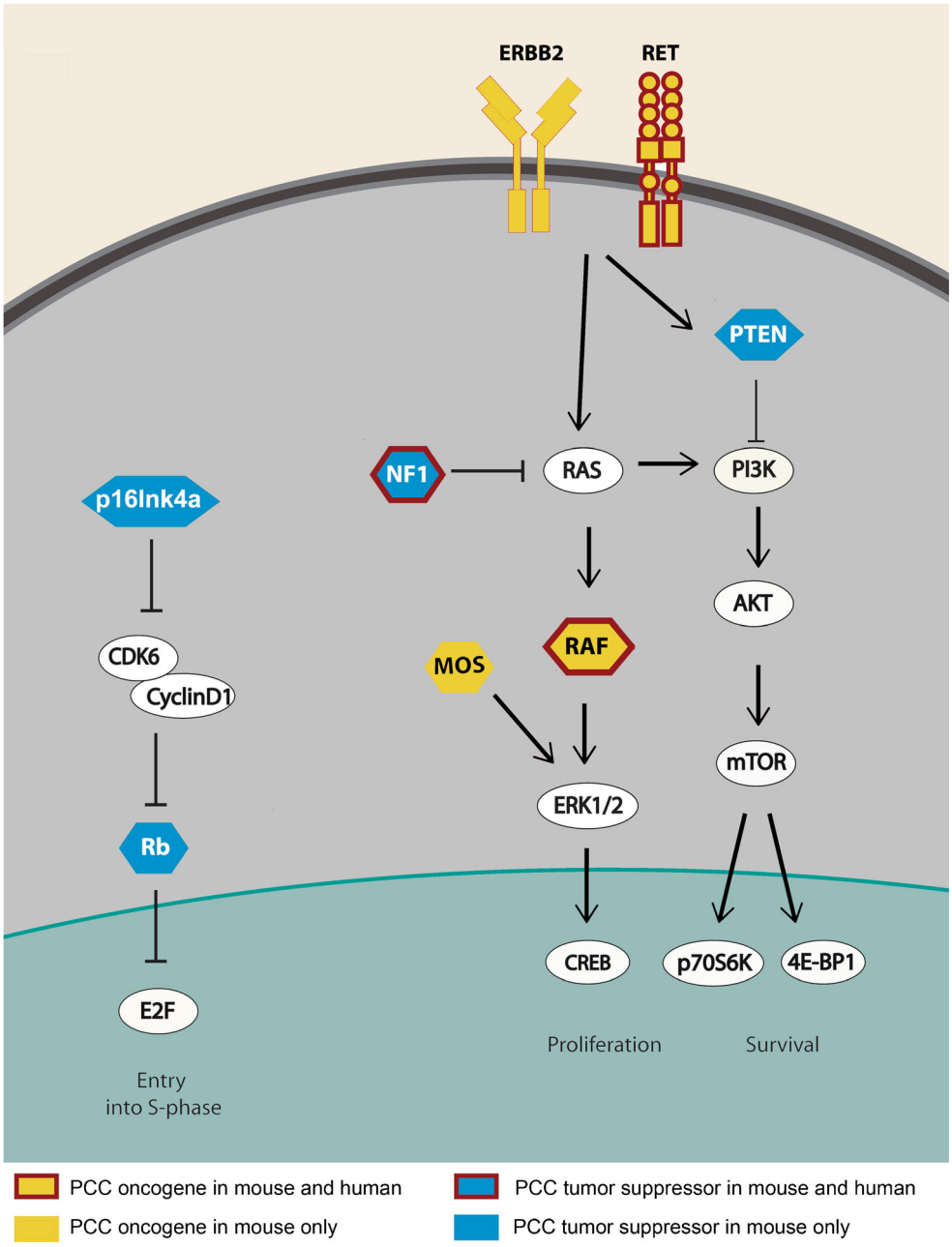

Fig. 1 Signaling pathways associated with the development of pheochromocytomas in mouse

to RET mutations affecting codon 634 predispose to MTC but without chromaffin tumor (Michiels et al. 1997; Reynolds et al. 2001). These different phenotypes may be explained by the different consequences of MEN 2A and MEN 2B causing mutations. Indeed, all MEN 2 mutations result in a stimulation of RET tyrosine kinase receptor but through different mechanisms of activation. MEN 2A 634 mutations involve cysteine residues in the RET extracellular domain resulting in ligand-independent dimerization and constitutive activation of the phosphorylating cascade. In contrast, the M918T substitution seems to convert the substrate-binding pocket of RET to resemble those of non-receptor src-related tyrosine kinases. More recently, it was shown to increase intrinsic kinase activity, partially release kinase autoinhibition and facilitate ligand-independent phosphorylation of 2B-RET receptors (Gujral et al. 2006).

Predisposing genes in mice without parallel human PPGL disease: *c-mos*, *Rb*, *B-Raf*, *Pten/InK4a*, *p53*, *Rb*, *ErbB2* and *CerS2*

Other genetically engineered mice with mutations not associated with PPGL susceptibility in humans have surprisingly been shown to be predisposed to PPGL.

The very first report of a PCC mouse model was linked to the RET signaling pathway, when Schultz et al. studied four

lines of transgenic *c-mos* mice in 1992 (Schulz et al. 1992). In addition to severe neurological defects and lens abnormalities, three of these *mos* transgenic lines presented neuroendocrine tumors similar to the human MEN2 associating a high frequency of bilateral PCC (58%) with MTC. Thereafter, a mouse with a heterozygous loss-of-function mutation of the retinoblastoma tumor suppressor (*Rb*+/−) developed a phenotype combining MTC and 71% of PCC (14% bilateral) (Nikitin et al. 1999). This later pathway is strongly associated with PCC in mouse as the dual loss of *Rb1* and *Trp53* in the adrenal medulla (using a Tyrosinase promoter driven Cre) also leads to PCC, without metastasis (Tonks et al. 2010).

Mutations in the *PTEN* tumor suppressor gene (involved in the negative regulation of the PI3K/AKT signaling pathway) have as main consequences in humans the Cowden syndrome associating several tumors (hamartomas, breast, thyroid and endometrium cancers) but no PCC (Puc et al. 2006; van Nederveen et al. 2006). Co-existing inactivation of *PTEN* and of *INK4a*, (which encodes 2 tumor suppressors (p16INK4a and p19ARF) that regulate p53 and pRb pathways) are observed in several human cancers, although not yet in PPGL (Ali et al. 1999). The heterozygous inactivation of *Pten* predisposes to a broad spectrum of cancers in mice including PCC in 23% of cases at 7 months, a frequency that rises to 60% when *Pten* and *Ink4a* are co-inactivated. Furthermore, this is one of the rare mouse models predisposing to malignant PCC, with around 15% of malignancy (lung metastasis) (You et al. 2002).

Surprisingly prostate cancer studies led to two tissue-specific PCC mouse models using technologies driven by supposedly specific prostate promoters that actually leak in the mouse adrenal medulla. First, Korpershoek et al. reported the conditional *Pten* KO driven by a PSA (prostate-specific antigen)-Cre recombinase. These mice are predisposed to PCC with an incidence of 78% in males, a number of whom with pulmonary metastases (Korpershoek et al. 2009; Ma et al. 2003). The same group also generated a double conditional KO mouse by crossing the *Pten* conditional KO with a Trp53 conditional KO previously generated by Marino et al. (2000). This model is more severe with a higher frequency of metastatic PCC (up to 67% lung metastases) and with a younger age of onset (4–5 months vs 11 months) (Korpershoek et al. 2012).

The second model results from an ectopic expression of an activated *ErbB2* transgene, driven by the minimal rat probasin promoter (PB). The activation of this tyrosine kinase receptor results in a decrease in the PTEN signaling pathway together with an increase in cycline D1 levels and leads to bilateral PCC in approximately 5% of male mice (Lai et al. 2007).

BRAF encodes a serine/threonine protein kinase involved in the RAS-RAF-MEK-ERK signaling pathway. The BRAF V600E mutation is the most common activating mutation in cancer, leading to constitutive BRAF kinase activity, phosphorylation of MEK and ERK kinases and sustained MAPK pathway signaling. *BRAF* V600E somatic mutations have been identified in several solid tumors, including malignant melanoma, colorectal cancer, differentiated thyroid cancers, breast and lung carcinomas, with a usually poor prognosis (Davies et al. 2002; Ikenoue et al. 2003; Namba et al. 2003). This mutation is not directly involved in human hereditary PPGL but around 10% of sporadic PCC have recently been shown to carry a somatic mutation in H-RAS (Castro-Vega et al. 2015; Crona et al. 2013; Oudijk et al. 2014). Interestingly, it was recently shown that mice expressing the hypomorphic B-RafV600E allele are predisposed to PPGL (Urosevic et al. 2011). Very interestingly, this is the first model that develops a high incidence (80% at 5 months of age) of both PGL and PCC with a 20% rate of metastatic phenotype.

Finally, the *CerS2* gene, encoding ceramide synthase 2, an enzyme involved in sphingolipid (SL) biosynthesis, has recently been implicated in PCC predisposition in mice (Park et al. 2015). Indeed, the CerS2 null mice, which are unable to synthetize very long-chain ceramides, develop lesions in several organs (hepatopathy, emphysema, demyelination) and are prone to bilateral PCC in more than 50% at 19 months of age with a 100% of medullary hyperplasia. The mechanism responsible for PCC tumorigenesis is not known but appears to be linked with changes in the SL profile with a reduction level of very long-chain SL together with an accumulation of long-chain SL and sphinganine that lead to the inhibition of mitochondrial complex IV activity and subsequent oxidative stress (Zigdon et al. 2013). Nevertheless, none of the classical signaling pathways usually incriminated in PPGL development seem to be involved: no upregulation of HIF-1α, no phosphorylation of Akt or mTor (Park et al. 2015). In human, only one patient harboring a deletion in one allele of *CerS2* has been reported with no evidence of PCC occurrence (Mosbech et al. 2014).

Conclusions on predisposed mouse models

The struggle for developing animal models of PPGL predisposition has shown that mice and men display some similarities but also major differences. Hence, all the models that have been successful are related to cluster 2 tumors and cause pheochromocytomas, with the exception of some paragangliomas in B-*Raf*$^{+/LSLV600E}$ mice. These mutations that mostly promote the activation of the MAPK and AKT/mTOR pathways do seem to be strongly oncogenic in adrenal chromaffin cells in mouse (Fig. 1). Actually, their impact is even more important than in humans as some genes of these pathways such as *Pten*, *c-mos*, *Rb*, *Erbb2* cause PCC in mouse but have not been associated with PCC predisposition in patients. To the best of our knowledge, none of the knockout mice of the cluster 1 mutated genes has ever been described with PPGL. Actually, at least 90% of tumors developed in SDH

patients are paragangliomas, which appears to be extremely rare in rodents. This may partly explain the failure in generating SDH-related tumors in mouse. However, *VHL*-mutated patients mostly develop PCC and PGL in only 20% of cases or so. Hence, it appears that the pathways associated with tumorigenesis in cluster 1 related tumors (pseudo-hypoxia in both SDH and VHL and DNA hypermethylation in SDH but also, to a lesser extent in VHL tumors) seem to be poorly efficient to promote tumorigenesis in mice. The reason for this discrepancy is quite puzzling but difficult to investigate experimentally. Whether it is linked to the genetic backgrounds used to generate these animals or to the lack of an associated chromosomal event, not reproduced in these models, is still a question that has not been properly addressed and that may provide some answers. Anyhow, the urge to generate such models has led researchers in the field to develop graft models using mouse or human cells.

Grafted mouse models

In a grafted model, human (xenograft) or animal (xeno-/allograft) cancer cells are transplanted either under the skin (ectopic) or into the organ of tumor origin (orthotopic) using immunodeficient rodents such as athymic nude mice or severely compromised immunodeficient (SCID) mice. Metastatic models can further be developed by injecting cells into the circulation (through the tail vein or in the heart) or in the spleen, the latter leading to a typical liver tropism. As compared with naturally occurring tumors, these models generally show a rapid tumor growth with an easy follow-up in particular for ectopic grafts. Although very useful for preclinical studies, most of these models do not recapitulate the typical slow growth of PPGL in humans and do not mimic the natural history of the tumor. In addition, they imply the use of immunodeficient mice and are thus inappropriate for studying the role of the immune microenvironment and the use of biotherapies targeting the immune checkpoint. Anyhow, the recent development of several cell lines and graft models has allowed significant advances in the understanding of PPGL tumorigenesis and in the launching of preclinical studies.

Allografted models

The first mouse model was developed by allografting the mouse pheochromocytoma cells (MPC) derived from an *Nf1* KO mouse tumor (Powers et al. 2000). This mouse model of metastatic PCC was established using intravenously injected MPC cells leading to metastatic lesions predominantly in the liver, 4 weeks after injection (Ohta et al. 2008). One year after, the same team obtained an allografted mouse model with a more aggressive phenotype by injecting into athymic mice the mouse tumor tissue (MTT) cells derived from an MPC liver metastasis (Martiniova et al. 2009). These two allografted models were extensively characterized by multimodality imaging confirming the metastatic phenotype, with a particular tropism for the liver (Giubellino et al. 2012; Martiniova et al. 2009, 2009, 2010, 2011) and both models appear to be suitable for preclinical studies (Martiniova et al. 2011; Pacak et al. 2012). More recently, the MPC cell line was stably transduced with a far-red-flurorescent-tagged lentivirus (MPC-mCherry cell line) and subcutaneously allografted to nude mice in order to elaborate a mouse model suitable for preclinical studies without the need for dedicated small animal imaging strategies only available in specialized research centers (Ullrich et al. 2014).

Nevertheless, there was still an unmet medical need for experimental models of cluster 1-related tumors that would reproduce malignant PPGL caused by *SDHB* mutations. Hence, because of the failure to develop a predisposed SDH-related animal model, our lab recently generated an allografted mouse model by subcutaneous injection of immortalized mouse chromaffin cells (imCC) (Letouze et al. 2013) carrying a homozygous knockout of the *Sdhb* gene into the fat-pad of female NMRI-nu mice (Lussey-Lepoutre et al. 2015). This mouse model reproduces the succinate accumulation and the particular vascular pattern observed in human *SDHx*-dependent PPGL. However, imCC have lost some differentiation markers of chromaffin cells and are likely not secreting anymore. Another allograft model has also been reported using *Sdhb−/−* renal cells (Cardaci et al. 2015).

Xenografted mouse models

One xenograft mouse model has recently been generated using rat pheochromocytoma PC12 cells injected subcutaneously into athymic Swiss nude nu/nu mice with a tumor development observed about 14 days after implantation. PC12 cells are historically the first cell line elaborated from an irradiated rat that spontaneously developed a PCC (Greene and Tischler 1976). About 20 years after, a deletion in *Max*, a gene also involved in human PCC (cluster C2) was identified as potentially responsible for tumorigenesis in these cells (Hopewell and Ziff 1995).

An adequate experimental model for a preclinical study would have been human xenograft of primary or metastatic PPGL. An interesting xenograft model using shRNA mediated *SDHB* knock-down in 143B human osteosarcoma cells was generated by Guzy et al. (2008). Interestingly, they found an acceleration of tumor growth when inhibiting *SDHB*. Nevertheless, this model is not *stricto* sensu a PCC mouse model since the cell type is not derived from a chromaffin tissue. Unfortunately, generating such a model appears to be challenging and until now, only one human xenografted model has been reported (Powers et al. 2017). Indeed, Powers et al. succeeded in growing xenografts of human PPGL in a

particular strain of immunodeficient mice: NOD-scid gamma (NGS) mice, which lack functional B cells, T cells and NK cells, paving the way for a new hope in this quest. Nevertheless, a limit of these human xenografts is that their progression is extremely slowly. Therefore, while they might faithfully replicate the growth rate of PPGL in their human hosts, which is often measured in years for a single doubling, this also makes them impractical for reproducible studies.

Did rodent models give new insights in the human PPGL struggle?

The objective of developing animal models includes deciphering tumorigenesis, developing new diagnosis tools and testing new therapeutic strategies in vivo, in conditions as close as possible to the human pathology.

Tumorigenesis

Surprisingly, PCC predisposed models in mouse have been only minimally utilized for mechanistic studies following their initial reports. Indeed, the molecular pathways implicated in cluster 2 tumors are mostly very well known, with the activation of the canonical signaling pathways involving MAPK or mTOR. In contrast, the more puzzling cluster 1 group of tumors could never be reproduced in a rodent knockout model and has therefore not beneficiated from such tools, allowing the study of the tumor's natural history. Current knowledge on these tumors, such as the identification of the pseudohypoxic pathway or the hypermethylator phenotype, have basically been obtained through the study of human tumor samples, or using in vitro cell lines. Xenograft models have however allowed some progress in the demonstration of the functionality of these pathways in vivo. Indeed, Guzy et al. demonstrated that targeting the hypoxic response in *Sdhb* knockdown cells did lead to a reduction of their growth in immunodeficient mice (Guzy et al. 2008).

Innovating diagnosis tools and therapeutic preclinical studies

The recent development of numerous graft models has allowed the launching of an increasing number of preclinical and in vivo imaging studies. One main advance in PPGL imaging issued from a preclinical model was the development last year of a new method to detect succinate accumulation in vivo by proton magnetic resonance spectroscopy (^{1}H-MRS) (Lussey-Lepoutre et al. 2015). Indeed, SDH inactivation leads to a massive accumulation of succinate that, assessed on surgically resected tissues, is a highly specific biomarker of *SDHx*-mutated tumors (Pollard et al. 2005; Rao et al. 2013; Richter et al. 2014). We optimized a pulse ^{1}H-MRS sequence to measure succinate in the allografted mouse model of *Sdhb*-deficient tumors. Following this initial preclinical step, we demonstrated, in patients, the feasibility of detecting succinate in vivo by ^{1}H-MRS as a very specific biomarker of *SDHx* mutations and as a quantifiable surrogate marker putatively enabling to monitor early response to treatment (Lussey-Lepoutre et al. 2015).

Other reports studied functional imaging with the ultimate objective of radionuclide therapy. *Martinova* et al. showed an increased uptake in ^{123}MIBG (meta-iodobenzylguanidine) and 18F–Fluorodopamine detected by scintigraphy in the metastatic allografted MPC mouse model following treatment with histone deacetylase (HDAC) inhibitors (Martiniova et al. 2011). HDAC inhibitors actually amplified the amount of norepinephrine transporter expressed in the tumors, potentially enhancing the efficacy of ^{131}MIBG therapy, one current therapeutic option in malignant PPGL (Martiniova et al. 2011). Nevertheless, until now, no therapeutic combination of HDAC and ^{131}MIBG therapy has been published either in this mouse model or in patients.

As a neuroendocrine tumor, PPGL abundantly express somatostatin receptor (sst) promoting great interest for new imaging using Gallium-68 labeled somatostatin analogues that recently showed interesting performance for PPGL evaluation (Archier et al. 2016; Janssen et al. 2015; Janssen et al. 2016; Kroiss et al. 2013, 2015). These good results support peptide receptor-targeting radionuclide therapies, mostly tested in gastroenteropancreatic neuroendocrine tumors (Strosberg et al. 2017) but also in metastatic or inoperable PPGL, although only in small series (Forrer et al. 2008; Puranik et al. 2015; Zovato et al. 2012). Recently, a German team demonstrated promising results of ^{177}Lu-Dotatate therapy in parallel to a high rate of ^{64}Cu-DOTATATE tumor uptake visualized on microPET imaging in the MPC-mCherry allografted mouse model (Ullrich et al. 2014), hence providing a basis for future clinical trials (Ullrich et al. 2016).

A few studies tested specific therapeutic agents in in vivo models. The effect of AZD8055 (an mTORC1/2 inhibitor) was assessed in the metastatic model established with MTT cells expressing Luciferase and monitored by in vivo bioluminescence imaging (Giubellino et al. 2013). This showed a reduction in the primary tumor burden as well as of the number of lung and liver metastases. The same authors reported the effects of HSP90 inhibitors in the metastatic spread of MTT cells injected in the tail vein of immunodeficient mice (Isaacs et al. 2002) and showed a reduction of HIF1 levels, suggesting that such inhibitor may be of interest for the management of cluster 1 pseudohypoxic PPGL. Finally, Denorme et al. used the xenograft model of PC12 cells to study the effect of the anti-angiogenic molecules, sorafenib and sunitinib (which is still being evaluated in clinical trials in patients (http://clinicaltrials.gov/show/NCT01371201 and https://clinicaltrials.gov/ct2/show/NCT00843037)) and showed that

both molecules promoted a reduction in microvessel density and of tumor growth (Denorme et al. 2014).

Conclusion and perspectives

In conclusion, the past 10 or 15 years have seen the emergence of an increasing number of models and studies that have been able to generate a pertinent and efficient animal model of PPGL that allows studying their natural history and launching preclinical assays. These studies have now demonstrated that if mice are strongly susceptible to the development of cluster 2-like pheochromocytomas (mediated by activating mutations in *Ret*, *Erbb2*, *Raf* or *c-mos* or by knockout of *Nf1*, *Rb*, *Pten*, *p16Ink4a*), it is still impossible to generate a cluster 1-like model through knockouts of *Sdhx*, *Fh*, or *Vhl* genes. For now, allografts with murine cell lines remain the only feasible option to study in vivo the behavior of such tumors. The recent progress allowed by the TALEN, CRISPR/Cas9, or induced pluripotent stem cells (iPSCs) technologies will surely promote, in the next future, an acceleration of such models. The Tischler Lab has already generated heterozygous *Sdhb*+/− rats that may be more prone to the development of SDH-related PPGL. Also, new mouse or human chromaffin or PPGL cell lines or grafts will eventually become available to permit experimental research for the treatment of this rare disease.

The international pheochromocytoma/paraganglioma research consortium PRESSOR encourages and attempts to foster collaboration on development of new experimental models. The webpage of the PRESSOR Tumor Models working Group can be accessed at www.PRESSOR.org.

References

Adam J, Hatipoglu E, O'Flaherty L, Ternette N, Sahgal N, Lockstone H, Baban D, Nye E, Stamp GW, Wolhuter K, Stevens M, Fischer R, Carmeliet P, Maxwell PH, Pugh CW, Frizzell N, Soga T, Kessler BM, El-Bahrawy M, Ratcliffe PJ, Pollard PJ (2011) Renal cyst formation in Fh1-deficient mice is independent of the Hif/Phd pathway: roles for fumarate in KEAP1 succination and Nrf2 signaling. Cancer Cell 20:524–537

Ali IU, Schriml LM, Dean M (1999) Mutational spectra of PTEN/MMAC1 gene: a tumor suppressor with lipid phosphatase activity. J Natl Cancer Inst 91:1922–1932

Amar L, Baudin E, Burnichon N, Peyrard S, Silvera S, Bertherat J, Bertagna X, Schlumberger M, Jeunemaitre X, Gimenez-Roqueplo AP, Plouin PF (2007) Succinate dehydrogenase B gene mutations predict survival in patients with malignant pheochromocytomas or paragangliomas. J Clin Endocrinol Metab 92:3822–3828

Archier A, Varoquaux A, Garrigue P, Montava M, Guerin C, Gabriel S, Beschmout E, Morange I, Fakhry N, Castinetti F, Sebag F, Barlier A, Loundou A, Guillet B, Pacak K, Taieb D (2016) Prospective comparison of (68)Ga-DOTATATE and (18)F-FDOPA PET/CT in patients with various pheochromocytomas and paragangliomas with emphasis on sporadic cases. Eur J Nucl Med Mol Imaging 43:1248–1257

Bayley JP, van Minderhout I, Hogendoorn PC, Cornelisse CJ, van der Wal A, Prins FA, Teppema L, Dahan A, Devilee P, Taschner PE (2009) Sdhd and SDHD/H19 knockout mice do not develop paraganglioma or pheochromocytoma. PLoS One 4:e7987

Briere JJ, Favier J, Benit P, El Ghouzzi V, Lorenzato A, Rabier D, Di Renzo MF, Gimenez-Roqueplo AP, Rustin P (2005) Mitochondrial succinate is instrumental for HIF1alpha nuclear translocation in SDHA-mutant fibroblasts under normoxic conditions. Hum Mol Genet 14:3263–3269

Burnichon N, Briere JJ, Libe R, Vescovo L, Riviere J, Tissier F, Jouanno E, Jeunemaitre X, Benit P, Tzagoloff A, Rustin P, Bertherat J, Favier J, Gimenez-Roqueplo AP (2010) SDHA is a tumor suppressor gene causing paraganglioma. Hum Mol Genet 19:3011–3020

Burnichon N, Vescovo L, Amar L, Libe R, de Reynies A, Venisse A, Jouanno E, Laurendeau I, Parfait B, Bertherat J, Plouin PF, Jeunemaitre X, Favier J, Gimenez-Roqueplo AP (2011) Integrative genomic analysis reveals somatic mutations in pheochromocytoma and paraganglioma. Hum Mol Genet 20:3974–3985

Cardaci S, Zheng L, MacKay G, van den Broek NJ, MacKenzie ED, Nixon C, Stevenson D, Tumanov S, Bulusu V, Kamphorst JJ, Vazquez A, Fleming S, Schiavi F, Kalna G, Blyth K, Strathdee D, Gottlieb E (2015) Pyruvate carboxylation enables growth of SDH-deficient cells by supporting aspartate biosynthesis. Nat Cell Biol 17:1317–1326

Carlson KM, Dou S, Chi D, Scavarda N, Toshima K, Jackson CE, Wells SA Jr, Goodfellow PJ, Donis-Keller H (1994) Single missense mutation in the tyrosine kinase catalytic domain of the RET protooncogene is associated with multiple endocrine neoplasia type 2B. Proc Natl Acad Sci U S A 91:1579–1583

Cascon A, Comino-Mendez I, Curras-Freixes M, de Cubas AA, Contreras L, Richter S, Peitzsch M, Mancikova V, Inglada-Perez L, Perez-Barrios A, Calatayud M, Azriel S, Villar-Vicente R, Aller J, Setien F, Moran S, Garcia JF, Rio-Machin A, Leton R, Gomez-Grana A, Apellaniz-Ruiz M, Roncador G, Esteller M, Rodriguez-Antona C, Satrustegui J, Eisenhofer G, Urioste M, Robledo M (2015) Whole-exome sequencing identifies MDH2 as a new familial paraganglioma gene. J Natl Cancer Inst 107

Castro-Vega LJ, Buffet A, De Cubas AA, Cascon A, Menara M, Khalifa E, Amar L, Azriel S, Bourdeau I, Chabre O, Curras-Freixes M, Franco-Vidal V, Guillaud-Bataille M, Simian C, Morin A, Leton R, Gomez-Grana A, Pollard PJ, Rustin P, Robledo M, Favier J, Gimenez-Roqueplo AP (2014) Germline mutations in FH confer predisposition to malignant pheochromocytomas and paragangliomas. Hum Mol Genet 23:2440–2446

Castro-Vega LJ, Lepoutre-Lussey C, Gimenez-Roqueplo AP, Favier J (2015) Rethinking pheochromocytomas and paragangliomas from a genomic perspective. Oncogene

Castro-Vega LJ, Letouze E, Burnichon N, Buffet A, Disderot PH, Khalifa E, Loriot C, Elarouci N, Morin A, Menara M, Lepoutre-Lussey C, Badoual C, Sibony M, Dousset B, Libe R, Zinzindohoue F, Plouin PF, Bertherat J, Amar L, de Reynies A, Favier J, Gimenez-Roqueplo AP (2015) Multi-omics analysis defines core genomic alterations in pheochromocytomas and paragangliomas. Nat Commun 6:6044

Clark GR, Sciacovelli M, Gaude E, Walsh DM, Kirby G, Simpson MA, Trembath RC, Berg JN, Woodward ER, Kinning E, Morrison PJ, Frezza C, Maher ER (2014) Germline FH mutations presenting with pheochromocytoma. J Clin Endocrinol Metab 99:E2046–E2050

Comino-Mendez I, Gracia-Aznarez FJ, Schiavi F, Landa I, Leandro-Garcia LJ, Leton R, Honrado E, Ramos-Medina R, Caronia D, Pita G, Gomez-Grana A, de Cubas AA, Inglada-Perez L, Maliszewska A, Taschin E, Bobisse S, Pica G, Loli P, Hernandez-Lavado R, Diaz JA, Gomez-Morales M, Gonzalez-Neira A, Roncador G, Rodriguez-Antona C, Benitez J, Mannelli M,

Opocher G, Robledo M, Cascon A (2011) Exome sequencing identifies MAX mutations as a cause of hereditary pheochromocytoma. Nat Genet 43:663–667

Crona J, Delgado Verdugo A, Maharjan R, Stalberg P, Granberg D, Hellman P, Bjorklund P (2013) Somatic mutations in H-RAS in sporadic pheochromocytoma and paraganglioma identified by exome sequencing. J Clin Endocrinol Metab 98:E1266–E1271

Dahia PL (2014) Pheochromocytoma and paraganglioma pathogenesis: learning from genetic heterogeneity. Nat Rev Cancer 14:108–119

Dahia PL, Ross KN, Wright ME, Hayashida CY, Santagata S, Barontini M, Kung AL, Sanso G, Powers JF, Tischler AS, Hodin R, Heitritter S, Moore F, Dluhy R, Sosa JA, Ocal IT, Benn DE, Marsh DJ, Robinson BG, Schneider K, Garber J, Arum SM, Korbonits M, Grossman A, Pigny P, Toledo SP, Nose V, Li C, Stiles CD (2005) A HIF1alpha regulatory loop links hypoxia and mitochondrial signals in pheochromocytomas. PLoS Genet 1:72–80

Davies H, Bignell GR, Cox C, Stephens P, Edkins S, Clegg S, Teague J, Woffendin H, Garnett MJ, Bottomley W, Davis N, Dicks E, Ewing R, Floyd Y, Gray K, Hall S, Hawes R, Hughes J, Kosmidou V, Menzies A, Mould C, Parker A, Stevens C, Watt S, Hooper S, Wilson R, Jayatilake H, Gusterson BA, Cooper C, Shipley J, Hargrave D, Pritchard-Jones K, Maitland N, Chenevix-Trench G, Riggins GJ, Bigner DD, Palmieri G, Cossu A, Flanagan A, Nicholson A, Ho JW, Leung SY, Yuen ST, Weber BL, Seigler HF, Darrow TL, Paterson H, Marais R, Marshall CJ, Wooster R, Stratton MR, Futreal PA (2002) Mutations of the BRAF gene in human cancer. Nature 417:949–954

Denorme M, Yon L, Roux C, Gonzalez BJ, Baudin E, Anouar Y, Dubessy C (2014) Both sunitinib and sorafenib are effective treatments for pheochromocytoma in a xenograft model. Cancer Lett 352:236–244

Diaz-Castro B, Pintado CO, Garcia-Flores P, Lopez-Barneo J, Piruat JI (2012) Differential impairment of catecholaminergic cell maturation and survival by genetic mitochondrial complex II dysfunction. Mol Cell Biol 32:3347–3357

Eisenhofer G, Huynh TT, Pacak K, Brouwers FM, Walther MM, Linehan WM, Munson PJ, Mannelli M, Goldstein DS, Elkahloun AG (2004) Distinct gene expression profiles in norepinephrine- and epinephrine-producing hereditary and sporadic pheochromocytomas: activation of hypoxia-driven angiogenic pathways in von Hippel-Lindau syndrome. Endocr Relat Cancer 11:897–911

Favier J, Amar L, Gimenez-Roqueplo A (2014) Paraganglioma and phaeochromocytoma: from genetics to personalized medicine. Nat Rev Endocrinol

Favier J, Briere JJ, Burnichon N, Riviere J, Vescovo L, Benit P, Giscos-Douriez I, De Reynies A, Bertherat J, Badoual C, Tissier F, Amar L, Libe R, Plouin PF, Jeunemaitre X, Rustin P, Gimenez-Roqueplo AP (2009) The Warburg effect is genetically determined in inherited pheochromocytomas. PLoS One 4:e7094

Favier J, Buffet A, Gimenez-Roqueplo AP (2012) HIF2A mutations in paraganglioma with polycythemia. N Engl J Med 367:2161 **author reply 2161-2162**

Forrer F, Riedweg I, Maecke HR, Mueller-Brand J (2008) Radiolabeled DOTATOC in patients with advanced paraganglioma and pheochromocytoma. The quarterly journal of nuclear medicine and molecular imaging: official publication of the Italian Association of Nuclear Medicine 52:334–340

Gelman DM, Noain D, Avale ME, Otero V, Low MJ, Rubinstein M (2003) Transgenic mice engineered to target Cre/loxP-mediated DNA recombination into catecholaminergic neurons. Genesis 36: 196–202

Gimenez-Roqueplo AP, Favier J, Rustin P, Rieubland C, Crespin M, Nau V, Khau Van Kien P, Corvol P, Plouin PF, Jeunemaitre X, Network C (2003) Mutations in the SDHB gene are associated with extra-adrenal and/or malignant phaeochromocytomas. Cancer Res 63: 5615–5621

Giubellino A, Bullova P, Nolting S, Turkova H, Powers JF, Liu Q, Guichard S, Tischler AS, Grossman AB, Pacak K (2013) Combined inhibition of mTORC1 and mTORC2 signaling pathways is a promising therapeutic option in inhibiting pheochromocytoma tumor growth: in vitro and in vivo studies in female athymic nude mice. Endocrinology 154:646–655

Giubellino A, Woldemichael GM, Sourbier C, Lizak MJ, Powers JF, Tischler AS, Pacak K (2012) Characterization of two mouse models of metastatic pheochromocytoma using bioluminescence imaging. Cancer Lett 316:46–52

Gnarra JR, Ward JM, Porter FD, Wagner JR, Devor DE, Grinberg A, Emmert-Buck MR, Westphal H, Klausner RD, Linehan WM (1997) Defective placental vasculogenesis causes embryonic lethality in VHL-deficient mice. Proc Natl Acad Sci U S A 94:9102–9107

Greene LA, Tischler AS (1976) Establishment of a noradrenergic clonal line of rat adrenal pheochromocytoma cells which respond to nerve growth factor. Proc Natl Acad Sci U S A 73:2424–2428

Gujral TS, Singh VK, Jia Z, Mulligan LM (2006) Molecular mechanisms of RET receptor-mediated oncogenesis in multiple endocrine neoplasia 2B. Cancer Res 66:10741–10749

Gutmann DH, Aylsworth A, Carey JC, Korf B, Marks J, Pyeritz RE, Rubenstein A, Viskochil D (1997) The diagnostic evaluation and multidisciplinary management of neurofibromatosis 1 and neurofibromatosis 2. JAMA 278:51–57

Guzy RD, Sharma B, Bell E, Chandel NS, Schumacker PT (2008) Loss of the SdhB, but not the SdhA, subunit of complex II triggers reactive oxygen species-dependent hypoxia-inducible factor activation and tumorigenesis. Mol Cell Biol 28:718–731

Haase VH (2005) The VHL tumor suppressor in development and disease: functional studies in mice by conditional gene targeting. Semin Cell Dev Biol 16:564–574

Haase VH, Glickman JN, Socolovsky M, Jaenisch R (2001) Vascular tumors in livers with targeted inactivation of the von Hippel-Lindau tumor suppressor. Proc Natl Acad Sci U S A 98:1583–1588

Harlander S, Schonenberger D, Toussaint NC, Prummer M, Catalano A, Brandt L, Moch H, Wild PJ, Frew IJ (2017) Combined mutation in Vhl, Trp53 and Rb1 causes clear cell renal cell carcinoma in mice. Nat Med

Hawes JJ, Tuskan RG, Reilly KM (2007) Nf1 expression is dependent on strain background: implications for tumor suppressor haploinsufficiency studies. Neurogenetics 8:121–130

Hopewell R, Ziff EB (1995) The nerve growth factor-responsive PC12 cell line does not express the Myc dimerization partner Max. Mol Cell Biol 15:3470–3478

Ibanez CF (2013) Structure and physiology of the RET receptor tyrosine kinase. Cold Spring Harbor Perspect in Biol 5

Ikenoue T, Hikiba Y, Kanai F, Tanaka Y, Imamura J, Imamura T, Ohta M, Ijichi H, Tateishi K, Kawakami T, Aragaki J, Matsumura M, Kawabe T, Omata M (2003) Functional analysis of mutations within the kinase activation segment of B-Raf in human colorectal tumors. Cancer Res 63:8132–8137

Isaacs JS, Jung YJ, Mimnaugh EG, Martinez A, Cuttitta F, Neckers LM (2002) Hsp90 regulates a von Hippel Lindau-independent hypoxia-inducible factor-1 alpha-degradative pathway. J Biol Chem 277: 29936–29944

Jacks T, Shih TS, Schmitt EM, Bronson RT, Bernards A, Weinberg RA (1994) Tumour predisposition in mice heterozygous for a targeted mutation in Nf1. Nat Genet 7:353–361

Janssen I, Blanchet EM, Adams K, Chen CC, Millo C, Herscovitch P, Taieb D, Kebebew E, Lehnert H, Fojo AT, Pacak K (2015) Superiority of [68Ga]-DOTATATE PET/CT to other functional imaging modalities in the localization of SDHB-associated metastatic pheochromocytoma and paraganglioma. Clin Cancer Res: Off J Am Assoc Cancer Res

Janssen I, Chen CC, Millo CM, Ling A, Taieb D, Lin FI, Adams KT, Wolf KI, Herscovitch P, Fojo AT, Buchmann I, Kebebew E, Pacak K

(2016) PET/CT comparing (68)Ga-DOTATATE and other radiopharmaceuticals and in comparison with CT/MRI for the localization of sporadic metastatic pheochromocytoma and paraganglioma. Eur J Nucl Med Mol Imaging 43:1784–1791

Kim WY, Kaelin WG (2004) Role of VHL gene mutation in human cancer. Journal of clinical oncology : official journal of the American Society of Clinical Oncology 22:4991–5004

Korpershoek E, Kloosterhof NK, Ziel-van der Made A, Korsten H, Oudijk L, Trapman J, Dinjens WN, de Krijger RR (2012) Trp53 inactivation leads to earlier phaeochromocytoma formation in pten knockout mice. Endocr Relat Cancer 19:731–740

Korpershoek E, Loonen AJ, Corvers S, van Nederveen FH, Jonkers J, Ma X, Ziel-van der Made A, Korsten H, Trapman J, Dinjens WN, de Krijger RR (2009) Conditional Pten knock-out mice: a model for metastatic phaeochromocytoma. J Pathol 217:597–604

Kroiss A, Putzer D, Frech A, Decristoforo C, Uprimny C, Gasser RW, Shulkin BL, Url C, Widmann G, Prommegger R, Sprinzl GM, Fraedrich G, Virgolini IJ (2013) A retrospective comparison between 68Ga-DOTA-TOC PET/CT and 18F-DOPA PET/CT in patients with extra-adrenal paraganglioma. Eur J Nucl Med Mol Imaging 40:1800–1808

Kroiss A, Shulkin BL, Uprimny C, Frech A, Gasser RW, Url C, Gautsch K, Madleitner R, Nilica B, Sprinzl GM, Gastl G, Fraedrich G, Virgolini IJ (2015) (68)Ga-DOTATOC PET/CT provides accurate tumour extent in patients with extraadrenal paraganglioma compared to (123)I-MIBG SPECT/CT. Eur J Nucl Med Mol Imaging 42:33–41

Lai EW, Rodriguez OC, Aventian M, Cromelin C, Fricke ST, Martiniova L, Lubensky IA, Lisanti MP, Picard KL, Powers JF, Tischler AS, Pacak K, Albanese C (2007) ErbB-2 induces bilateral adrenal pheochromocytoma formation in mice. Cell Cycle 6:1946–1950

Lancaster CR, Simon J (2002) Succinate:quinone oxidoreductases from epsilon-proteobacteria. Biochim Biophys Acta 1553:84–101

Lenders JW, Duh QY, Eisenhofer G, Gimenez-Roqueplo AP, Grebe SK, Murad MH, Naruse M, Pacak K, Young WF Jr, Endocrine S (2014) Pheochromocytoma and paraganglioma: an endocrine society clinical practice guideline. J Clin Endocrinol Metab 99:1915–1942

Lepoutre-Lussey C, Thibault C, Buffet A, Morin A, Badoual C, Benit P, Rustin P, Ottolenghi C, Janin M, Castro-Vega LJ, Trapman J, Gimenez-Roqueplo AP, Favier J (2015) From Nf1 to Sdhb knockout: successes and failures in the quest for animal models of pheochromocytoma. Mol Cell Endocrinol

Letouze E, Martinelli C, Loriot C, Burnichon N, Abermil N, Ottolenghi C, Janin M, Menara M, Nguyen AT, Benit P, Buffet A, Marcaillou C, Bertherat J, Amar L, Rustin P, De Reynies A, Gimenez-Roqueplo AP, Favier J (2013) SDH mutations establish a hypermethylator phenotype in paraganglioma. Cancer Cell 23:739–752

Lopez-Jimenez E, Gomez-Lopez G, Leandro-Garcia LJ, Munoz I, Schiavi F, Montero-Conde C, de Cubas AA, Ramires R, Landa I, Leskela S, Maliszewska A, Inglada-Perez L, de la Vega L, Rodriguez-Antona C, Leton R, Bernal C, de Campos JM, Diez-Tascon C, Fraga MF, Boullosa C, Pisano DG, Opocher G, Robledo M, Cascon A (2010) Research resource: transcriptional profiling reveals different pseudohypoxic signatures in SDHB and VHL-related pheochromocytomas. Mol Endocrinol 24:2382–2391

Lussey-Lepoutre C, Bellucci A, Morin A, Buffet A, Amar L, Janin M, Ottolenghi C, Zinzindohoue F, Autret G, Burnichon N, Robidel E, Banting B, Fontaine S, Cuenod CA, Benit P, Rustin P, Halimi P, Fournier L, Gimenez-Roqueplo AP, Favier J, Tavitian B (2015) In vivo detection of succinate by magnetic resonance spectroscopy as a Hallmark of SDHx mutations in paraganglioma. Clin Cancer Res: Off J Am Assoc Cancer Res

Ma W, Tessarollo L, Hong SB, Baba M, Southon E, Back TC, Spence S, Lobe CG, Sharma N, Maher GW, Pack S, Vortmeyer AO, Guo C, Zbar B, Schmidt LS (2003) Hepatic vascular tumors, angiectasis in multiple organs, and impaired spermatogenesis in mice with conditional inactivation of the VHL gene. Cancer Res 63:5320–5328

Macias D, Fernandez-Aguera MC, Bonilla-Henao V, Lopez-Barneo J (2014) Deletion of the von Hippel-Lindau gene causes sympathoadrenal cell death and impairs chemoreceptor-mediated adaptation to hypoxia. EMBO molecular medicine 6:1577–1592

Maher III LJ, Smith EH, Rueter EM, Becker NA, Bida JP, Nelson-Holte M, Piruat Palomo JI, García-Flores P, López-Barneo O, Van Deursen J (2011) Mouse models of human familial paraganglioma. In: Martin JF (ed) Pheochromocytoma—a new view of the old problem. InTech

Marino S, Vooijs M, van Der Gulden H, Jonkers J, Berns A (2000) Induction of medulloblastomas in p53-null mutant mice by somatic inactivation of Rb in the external granular layer cells of the cerebellum. Genes Dev 14:994–1004

Martiniova L, Kotys MS, Thomasson D, Schimel D, Lai EW, Bernardo M, Merino MJ, Powers JF, Ruzicka J, Kvetnansky R, Choyke PL, Pacak K (2009) Noninvasive monitoring of a murine model of metastatic pheochromocytoma: a comparison of contrast-enhanced microCT and nonenhanced MRI. Journal of magnetic resonance imaging : JMRI 29:685–691

Martiniova L, Lai EW, Elkahloun AG, Abu-Asab M, Wickremasinghe A, Solis DC, Perera SM, Huynh TT, Lubensky IA, Tischler AS, Kvetnansky R, Alesci S, Morris JC, Pacak K (2009) Characterization of an animal model of aggressive metastatic pheochromocytoma linked to a specific gene signature. Clin Exp Metastasis 26:239–250

Martiniova L, Lai EW, Thomasson D, Kiesewetter DO, Seidel J, Merino MJ, Kvetnansky R, Pacak K (2009) Animal model of metastatic pheochromocytoma: evaluation by MRI and PET. Endocr Regul 43:59–64

Martiniova L, Lu J, Chiang J, Bernardo M, Lonser R, Zhuang Z, Pacak K (2011) Pharmacologic modulation of serine/threonine phosphorylation highly sensitizes PHEO in a MPC cell and mouse model to conventional chemotherapy. PLoS One 6:e14678

Martiniova L, Perera SM, Brouwers FM, Alesci S, Abu-Asab M, Marvelle AF, Kiesewetter DO, Thomasson D, Morris JC, Kvetnansky R, Tischler AS, Reynolds JC, Fojo AT, Pacak K (2011) Increased uptake of [(1)(2)(3)I]meta-iodobenzylguanidine, [(1)(8)F]fluorodopamine, and [(3)H]norepinephrine in mouse pheochromocytoma cells and tumors after treatment with the histone deacetylase inhibitors. Endocr Relat Cancer 18:143–157

Martiniova L, Schimel D, Lai EW, Limpuangthip A, Kvetnansky R, Pacak K (2010) In vivo micro-CT imaging of liver lesions in small animal models. Methods 50:20–25

Michiels FM, Chappuis S, Caillou B, Pasini A, Talbot M, Monier R, Lenoir GM, Feunteun J, Billaud M (1997) Development of medullary thyroid carcinoma in transgenic mice expressing the RET protooncogene altered by a multiple endocrine neoplasia type 2A mutation. Proc Natl Acad Sci U S A 94:3330–3335

Morin A, Letouze E, Gimenez-Roqueplo AP, Favier J (2014) Oncometabolites-driven tumorigenesis: from genetics to targeted therapy. Int J Cancer 135:2237–2248

Mosbech MB, Olsen AS, Neess D, Ben-David O, Klitten LL, Larsen J, Sabers A, Vissing J, Nielsen JE, Hasholt L, Klein AD, Tsoory MM, Hjalgrim H, Tommerup N, Futerman AH, Moller RS, Faergeman NJ (2014) Reduced ceramide synthase 2 activity causes progressive myoclonic epilepsy. Annals of clinical and translational neurology 1:88–98

Namba H, Nakashima M, Hayashi T, Hayashida N, Maeda S, Rogounovitch TI, Ohtsuru A, Saenko VA, Kanematsu T, Yamashita S (2003) Clinical implication of hot spot BRAF mutation, V599E, in papillary thyroid cancers. J Clin Endocrinol Metab 88:4393–4397

Nikitin AY, Juarez-Perez MI, Li S, Huang L, Lee WH (1999) RB-mediated suppression of spontaneous multiple neuroendocrine

neoplasia and lung metastases in Rb+/− mice. Proc Natl Acad Sci U S A 96:3916–3921

Ohta S, Lai EW, Morris JC, Pang AL, Watanabe M, Yazawa H, Zhang R, Green JE, Chan WY, Sirajuddin P, Taniguchi S, Powers JF, Tischler AS, Pacak K (2008) Metastasis-associated gene expression profile of liver and subcutaneous lesions derived from mouse pheochromocytoma cells. Mol Carcinog 47:245–251

Oudijk L, de Krijger RR, Rapa I, Beuschlein F, de Cubas AA, Dei Tos AP, Dinjens WN, Korpershoek E, Mancikova V, Mannelli M, Papotti M, Vatrano S, Robledo M, Volante M (2014) H-RAS mutations are restricted to sporadic pheochromocytomas lacking specific clinical or pathological features: data from a multi-institutional series. J Clin Endocrinol Metab 99:E1376–E1380

Pacak K, Sirova M, Giubellino A, Lencesova L, Csaderova L, Laukova M, Hudecova S, Krizanova O (2012) NF-kappaB inhibition significantly upregulates the norepinephrine transporter system, causes apoptosis in pheochromocytoma cell lines and prevents metastasis in an animal model. International journal of cancer Journal international du cancer 131:2445–2455

Park WJ, Brenner O, Kogot-Levin A, Saada A, Merrill AH Jr, Pewzner-Jung Y, Futerman AH (2015) Development of pheochromocytoma in ceramide synthase 2 null mice. Endocr Relat Cancer 22:623–632

Piruat JI, Pintado CO, Ortega-Saenz P, Roche M, Lopez-Barneo J (2004) The mitochondrial SDHD gene is required for early embryogenesis, and its partial deficiency results in persistent carotid body glomus cell activation with full responsiveness to hypoxia. Mol Cell Biol 24: 10933–10940

Pollard PJ, Briere JJ, Alam NA, Barwell J, Barclay E, Wortham NC, Hunt T, Mitchell M, Olpin S, Moat SJ, Hargreaves IP, Heales SJ, Chung YL, Griffiths JR, Dalgleish A, McGrath JA, Gleeson MJ, Hodgson SV, Poulsom R, Rustin P, Tomlinson IP (2005) Accumulation of Krebs cycle intermediates and over-expression of HIF1alpha in tumours which result from germline FH and SDH mutations. Hum Mol Genet 14:2231–2239

Pollard PJ, Spencer-Dene B, Shukla D, Howarth K, Nye E, El-Bahrawy M, Deheragoda M, Joannou M, McDonald S, Martin A, Igarashi P, Varsani-Brown S, Rosewell I, Poulsom R, Maxwell P, Stamp GW, Tomlinson IP (2007) Targeted inactivation of fh1 causes proliferative renal cyst development and activation of the hypoxia pathway. Cancer Cell 11:311–319

Powers JF, Evinger MJ, Tsokas P, Bedri S, Alroy J, Shahsavari M, Tischler AS (2000) Pheochromocytoma cell lines from heterozygous neurofibromatosis knockout mice. Cell Tissue Res 302:309–320

Powers JF, Pacak K, Tischler AS (2017) Pathology of human pheochromocytoma and paraganglioma xenografts in NSG mice. Endocr Pathol 28:2–6

Puc J, Placha G, Wocial B, Podsypanina K, Parsons R, Gaciong Z (2006) Analysis of PTEN mutation in non-familial pheochromocytoma. Ann N Y Acad Sci 1073:317–331

Puranik AD, Kulkarni HR, Singh A, Baum RP (2015) Peptide receptor radionuclide therapy with (90)Y/ (177)Lu-labelled peptides for inoperable head and neck paragangliomas (glomus tumours). Eur J Nucl Med Mol Imaging 42:1223–1230

Qin Y, Yao L, King EE, Buddavarapu K, Lenci RE, Chocron ES, Lechleiter JD, Sass M, Aronin N, Schiavi F, Boaretto F, Opocher G, Toledo RA, Toledo SP, Stiles C, Aguiar RC, Dahia PL (2010) Germline mutations in TMEM127 confer susceptibility to pheochromocytoma. Nat Genet 42:229–233

Rao JU, Engelke UF, Rodenburg RJ, Wevers RA, Pacak K, Eisenhofer G, Qin N, Kusters B, Goudswaard AG, Lenders JW, Hermus AR, Mensenkamp AR, Kunst HP, Sweep FC, Timmers HJ (2013) Genotype-specific abnormalities in mitochondrial function associate with distinct profiles of energy metabolism and catecholamine content in pheochromocytoma and paraganglioma. Clinical cancer research : an official journal of the American Association for Cancer Research 19:3787–3795

Reynolds L, Jones K, Winton DJ, Cranston A, Houghton C, Howard L, Ponder BA, Smith DP (2001) C-cell and thyroid epithelial tumours and altered follicular development in transgenic mice expressing the long isoform of MEN 2A RET. Oncogene 20:3986–3994

Richter S, Peitzsch M, Rapizzi E, Lenders JW, Qin N, de Cubas AA, Schiavi F, Rao JU, Beuschlein F, Quinkler M, Timmers HJ, Opocher G, Mannelli M, Pacak K, Robledo M, Eisenhofer G (2014) Krebs cycle metabolite profiling for identification and stratification of pheochromocytomas/paragangliomas due to succinate dehydrogenase deficiency. J Clin Endocrinol Metab 99:3903–3911

Sato Y, Yoshizato T, Shiraishi Y, Maekawa S, Okuno Y, Kamura T, Shimamura T, Sato-Otsubo A, Nagae G, Suzuki H, Nagata Y, Yoshida K, Kon A, Suzuki Y, Chiba K, Tanaka H, Niida A, Fujimoto A, Tsunoda T, Morikawa T, Maeda D, Kume H, Sugano S, Fukayama M, Aburatani H, Sanada M, Miyano S, Homma Y, Ogawa S (2013) Integrated molecular analysis of clear-cell renal cell carcinoma. Nat Genet 45:860–867

Schulz N, Propst F, Rosenberg MP, Linnoila RI, Paules RS, Kovatch R, Ogiso Y, Vande Woude G (1992) Pheochromocytomas and C-cell thyroid neoplasms in transgenic c-mos mice: a model for the human multiple endocrine neoplasia type 2 syndrome. Cancer Res 52:450–455

Smith-Hicks CL, Sizer KC, Powers JF, Tischler AS, Costantini F (2000) C-cell hyperplasia, pheochromocytoma and sympathoadrenal malformation in a mouse model of multiple endocrine neoplasia type 2B. EMBO J 19:612–622

Strosberg J, El-Haddad G, Wolin E, Hendifar A, Yao J, Chasen B, Mittra E, Kunz PL, Kulke MH, Jacene H, Bushnell D, O'Dorisio TM, Baum RP, Kulkarni HR, Caplin M, Lebtahi R, Hobday T, Delpassand E, Van Cutsem E, Benson A, Srirajaskanthan R, Pavel M, Mora J, Berlin J, Grande E, Reed N, Seregni E, Oberg K, Lopera Sierra M, Santoro P, Thevenet T, Erion JL, Ruszniewski P, Kwekkeboom D, Krenning E, Investigators N-T (2017) Phase 3 trial of 177Lu-Dotatate for midgut neuroendocrine tumors. N Engl J Med 376:125–135

Tomlinson IP, Alam NA, Rowan AJ, Barclay E, Jaeger EE, Kelsell D, Leigh I, Gorman P, Lamlum H, Rahman S, Roylance RR, Olpin S, Bevan S, Barker K, Hearle N, Houlston RS, Kiuru M, Lehtonen R, Karhu A, Vilkki S, Laiho P, Eklund C, Vierimaa O, Aittomaki K, Hietala M, Sistonen P, Paetau A, Salovaara R, Herva R, Launonen V, Aaltonen LA, Multiple Leiomyoma C (2002) Germline mutations in FH predispose to dominantly inherited uterine fibroids, skin leiomyomata and papillary renal cell cancer. Nat Genet 30:406–410

Tonks ID, Mould AW, Schroder WA, Cotterill A, Hayward NK, Walker GJ, Kay GF (2010) Dual loss of rb1 and Trp53 in the adrenal medulla leads to spontaneous pheochromocytoma. Neoplasia 12:235–243

Toro JR, Nickerson ML, Wei MH, Warren MB, Glenn GM, Turner ML, Stewart L, Duray P, Tourre O, Sharma N, Choyke P, Stratton P, Merino M, Walther MM, Linehan WM, Schmidt LS, Zbar B (2003) Mutations in the fumarate hydratase gene cause hereditary leiomyomatosis and renal cell cancer in families in North America. Am J Hum Genet 73:95–106

Ullrich M, Bergmann R, Peitzsch M, Cartellieri M, Qin N, Ehrhart-Bornstein M, Block NL, Schally AV, Pietzsch J, Eisenhofer G, Bornstein SR, Ziegler CG (2014) In vivo fluorescence imaging and urinary monoamines as surrogate biomarkers of disease progression in a mouse model of pheochromocytoma. Endocrinology 155:4149–4156

Ullrich M, Bergmann R, Peitzsch M, Zenker EF, Cartellieri M, Bachmann M, Ehrhart-Bornstein M, Block NL, Schally AV, Eisenhofer G, Bornstein SR, Pietzsch J, Ziegler CG (2016) Multimodal somatostatin receptor theranostics using [(64)Cu]Cu

−/[(177)Lu]Lu-DOTA-(Tyr(3))octreotate and AN-238 in a mouse pheochromocytoma model. Theranostics 6:650–665

Urosevic J, Sauzeau V, Soto-Montenegro ML, Reig S, Desco M, Wright EM, Canamero M, Mulero F, Ortega S, Bustelo XR, Barbacid M (2011) Constitutive activation of B-Raf in the mouse germ line provides a model for human cardio-facio-cutaneous syndrome. Proc Natl Acad Sci U S A 108:5015–5020

van Nederveen FH, Perren A, Dannenberg H, Petri BJ, Dinjens WN, Komminoth P, de Krijger RR (2006) PTEN gene loss, but not mutation, in benign and malignant phaeochromocytomas. J Pathol 209: 274–280

Viskochil D, Buchberg AM, Xu G, Cawthon RM, Stevens J, Wolff RK, Culver M, Carey JC, Copeland NG, Jenkins NA et al (1990) Deletions and a translocation interrupt a cloned gene at the neurofibromatosis type 1 locus. Cell 62:187–192

Wagner SM, Zhu S, Nicolescu AC, Mulligan LM (2012) Molecular mechanisms of RET receptor-mediated oncogenesis in multiple endocrine neoplasia 2. Clinics 67(Suppl 1):77–84

You MJ, Castrillon DH, Bastian BC, O'Hagan RC, Bosenberg MW, Parsons R, Chin L, DePinho RA (2002) Genetic analysis of Pten and Ink4a/Arf interactions in the suppression of tumorigenesis in mice. Proc Natl Acad Sci U S A 99:1455–1460

Zigdon H, Kogot-Levin A, Park JW, Goldschmidt R, Kelly S, Merrill AH Jr, Scherz A, Pewzner-Jung Y, Saada A, Futerman AH (2013) Ablation of ceramide synthase 2 causes chronic oxidative stress due to disruption of the mitochondrial respiratory chain. J Biol Chem 288:4947–4956

Zovato S, Kumanova A, Dematte S, Sansovini M, Bodei L, Di Sarra D, Casagranda E, Severi S, Ambrosetti A, Schiavi F, Opocher G, Paganelli G (2012) Peptide receptor radionuclide therapy (PRRT) with 177Lu-DOTATATE in individuals with neck or mediastinal paraganglioma (PGL). Hormone and metabolic research = Hormon- und Stoffwechselforschung = Hormones et metabolisme 44:411–414

REVUE 2

Emerging molecular markers of metastatic pheochromocytomas and paragangliomas

Judith Goncalves, Charlotte Lussey-Lepoutre, Judith Favier, Anne-Paule Gimenez-Roqueplo, Luis Jaime Castro-Vega

Ann Endocrinol (Paris). 2019 Jun;80(3):159-162.

Annales d'Endocrinologie 80 (2019) 159–162

Disponible en ligne sur ScienceDirect www.sciencedirect.com

Elsevier Masson France EM|consulte www.em-consulte.com

Klotz communication 2019: New insights into the pathophysiology and treatment of Neuroendocrine Tumors

Emerging molecular markers of metastatic pheochromocytomas and paragangliomas

Judith Goncalves[a,b], Charlotte Lussey-Lepoutre[a,c], Judith Favier[a,b], Anne-Paule Gimenez-Roqueplo[a,b,d], Luis Jaime Castro-Vega[a,b,*]

[a] Inserm, UMR970, équipe labellisée Ligue Contre le Cancer, Paris-Cardiovascular Research Center, 75015 Paris, France
[b] Faculté de médecine, PRES Sorbonne Paris-Cité, Paris-Descartes University, 75006 Paris, France
[c] Department of Nuclear Medicine, Pitié-Salpêtrière Hospital, Sorbonne University, 75013 Paris, France
[d] Genetics Department, hôpital européen Georges-Pompidou, AP–HP, 75015, Paris, France

ARTICLE INFO

Keywords:
Pheochromocytoma
Paraganglioma
Metastasis
Biomarkers

ABSTRACT

Metastatic pheochromocytoma/paraganglioma (PPGL) represents a major clinical challenge due to limitations in accurate diagnostic tools and effective treatments. Currently, patients classified at high-risk by means of clinical, biochemical and genetic criteria, require a lifelong monitoring, while it remains difficult to determine the metastatic potential of PPGL only on the basis of histopathological features. Thus, tumor molecular markers that improve the risk stratification of these patients are needed. In the past few years, we have witnessed an unprecedented molecular characterization of PPGL, which led to the emergence of promising candidate biomarkers predictive of metastatic behavior. Here, we briefly discuss these breakthroughs and provide some insights for the prospective implementation of molecular markers of metastatic PPGL in the clinical setting in years to come.

Keywords :
Phéochromocytome
Paragangliome
Métastase
Biomarqueurs

RÉSUMÉ

Les phéochromocytomes et paragangliomes (PPGL) métastatiques posent de difficiles problèmes de diagnostic, pronostic, traitement et surveillance à long terme. La découverte de marqueurs moléculaires tumoraux est donc essentielle pour mieux définir le risque d'évolution métastatique des patients. Au cours des dernières années, nous avons assisté à une caractérisation moléculaire sans précédent des PPGL, qui a conduit à l'émergence de biomarqueurs candidats prometteurs, prédictifs du comportement métastatique. Dans cette revue, nous exposons et discutons ces avancées et l'application clinique potentielle de ces biomarqueurs moléculaires de PPGL métastatiques dans un futur proche.

1. Clinicopathological aspects of metastatic PPGL

Pheochromocytoma and paraganglioma (PPGL) are rare neuroendocrine tumors which arise in the sympathetic and parasympathetic paraganglia. Most of these tumors are not life-threatening and can be easily cured by surgery, whereas up to 20% may become metastatic [1]. The clinical outcome of patients with metastatic PPGL is highly variable. More than 40% of patients present with metastases at the time of diagnosis while others up to 50 years afterwards [2,3]. The overall 5-year survival rate of these patients varies between 34% and 60% [4]. Surgery can improve the prognosis [5], but if the primary tumor is unresectable, rapid disease progression is observed [3]. Standard chemotherapeutic regimen with cyclophosphamide, vincristine, and dacarbazine, or radionuclide therapy with 131 Iodine-radiolabelled metaiodobenzylguanidine only result in partial responses [6,7]. Thus, clinical trials testing targeted therapies such as tyrosine kinase inhibitors are underway [8].

Clinical, biochemical and genetic factors associated with metastatic PPGL comprise tumor location (extra-adrenal), large tumor size, high levels of plasma methoxytyramine and urinary dopamine, and germline mutations in SDHB, FH and SLC25A11 genes [1,9–12]. Carriers of mutations in other PPGL susceptibility

* Corresponding author. Inserm, UMR970, équipe labellisée Ligue Contre le Cancer, Paris-Cardiovascular Research Center, 75015 Paris, France.
E-mail address: luis-jaime.castro-vega@inserm.fr (L.J. Castro-Vega).

https://doi.org/10.1016/j.ando.2019.04.003
0003-4266/

genes have a lower risk [13,14]. Higher mortality is associated with male sex, older age at the time of diagnosis, synchronous metastases, large tumor size, elevated dopamine, SDHB status and not undergoing primary tumor resection [3,15]. Of note, the implementation of genetic testing in routine has greatly improved the management and clinical outcome of patients with SDHx/VHL mutations [16]. In marked contrast, there is no accurate mean to estimate the risk of developing a metastatic disease in patients with apparently sporadic PPGL, which would be helpful to guide their clinical management.

Histopathological features suggestive of metastatic behavior are the basis of the grade score systems PASS (Pheochromocytoma of the Adrenal Gland Scaled Score) [17] and GAPP (The Grading system for Adrenal Pheochromocytoma and Paraganglioma) [18]. However, low sensitivity and specificity [19] as well as significant inter and intra-observer variabilities preclude their implementation. The recent WHO classification of endocrine tumors pointed out that given the absence of reliable histopathologic criteria to distinguish "malignant" from "benign" PPGL, these two historically used terms should be abolished [20]. It was also emphasized that only the evidence of metastatic lesions, but not locally invasive or recurrent tumors defines metastatic PPGL. Since all PPGL presumably have a metastatic potential, molecular markers able to predict tumor aggressiveness are urgently needed.

2. Earliest molecular markers

Initial efforts made use of immunohistochemistry and RT-qPCR to evaluate the expression of candidate markers including cell proliferation antigen Ki-67/MIB-1 [21–23], c-Erb2 [23,24], angiogenic factors EPAS1 and VEGF [25,26], CD34 (for assessment of vascular architecture) [25], TERT [22,27], metastasis suppressors nm23-H1, TIMP-4, BRMS-1, TXNIP, CRSP-3 and E-Cad [28,29], epithelial-to-mesenchymal transition (EMT) inducers (Snail and Twist) [30,31], stemness factor OCT4 [32], activation of the mammalian target of rapamycin mTOR pathway [33] and neuroendocrine gene transcripts in liquid biopsies [34]. In addition, fewer number of S-100 + sustentacular cells [35], hypermethylation of the p16INK4A promoter [36,37], albeit modestly correlated with expression at mRNA and protein levels, and a CpG island methylator phenotype (CIMP) determined by examination of a panel of genes using pyrosequencing [38] have been also suggested as markers of metastatic PPGL.

Although these exploratory studies indicated that metastatic PPGL may undergo increased proliferation and alterations of both differentiation and tissue architecture, they presented several methodological, technical and analytical limitations to draw conclusions. For instance, in most of them, the number of biosamples included was too small, and in the cases in which the genotype could be determined, the SDHB status appeared as a potential confounding factor. Markers evaluated by immunohistochemistry such as c-Erb2, CD34, OCT4 and S-100 could not be reproduced in subsequent independent series [39–42]. Dependency on the experience of the observer and antibodies differences may account for discrepancies when using this technique. Automated quantitative imaging systems can be used for a better evaluation of immunohistochemical markers. Variability of results based on RT-qPCR, on the other hand, is high, particularly when assessing low abundant transcripts such as the metastasis suppressor genes or the transcripts present in the circulation. Droplet digital PCR (ddPCR), a highly sensitive technique for assessment of gene expression, is recommended nowadays to circumvent this problem. Nonetheless, detection of transcripts such as TERT may render a false-positive result due to tumor lymphocytic infiltration. The potential utility of some of these earliest biomarkers as well as the discovery of new ones started to emerge upon the arrival of more comprehensive studies of large cohorts of PPGL intended to perform an unbiased molecular characterization.

3. Emergent molecular markers

Recent integrative genomic studies enabled to propose a molecular classification of PPGL into two main subtypes (cluster 1 and cluster 2) characterized by germline or somatic mutations in susceptibility genes or in recently identified drivers [43]. SDHx/FH/SLC25A11-related PPGL, which is the group of genetically defined tumors with the higher metastatic potential, exhibit global DNA hypermethylation, transcriptional signatures of EMT and angiogenesis/hypoxia signaling pathways and overexpression of miRNA cluster 182/96/183, miR-210 and miR-483. VHL/EPAS1-related tumors have intermediate methylation levels, a glycolytic profile, and similar to SDHx-related PPGL, also display a pseudohypoxic phenotype with overexpression of the hypoxic marker miR-210. NF1/RET/TMEM127/MAX/HRAS/MET/FGFR1-related tumors are characterized by global hypomethylation, downregulation of miRNA cluster DLK-MEG3 and overactivation of RAS/MAPK and IGF1 signaling pathways. A new molecular group was recently described, characterized by MAML3 gene fusions and CSDE1 somatic mutations linked to activation of the Wnt signaling pathway [44].

Regarding metastatic PPGL, initial genomic studies reported that these tumors harbor high frequency of recurrent copy number alterations yet at large-scale [45,46] as well as underexpression of > 85% genes, probably linked to its undifferentiated pattern [47]. More recently, the TCGA study suggested MAML3 fusion gene, somatic mutations in ATRX and SETD2 genes and high somatic mutation rate as novel markers of aggressive and/or metastatic PPGL [44]. Expression data from this cohort further highlighted overactivation of cell cycle and regulation of actin cytoskeleton pathways [48] as well as overexpression of PDL-2 strongly correlated with genes reflecting an immune-exhausted T cell response [49]. The TCGA study also confirmed that SDHB mutation, global hypermethylation and Ki-67 immunoreactivity were associated with poor clinical outcome. Nonetheless, since no multivariate analyses were provided, it is difficult to ascertain the prognostic value of the newly identified markers compared to the SDHB status. In fact, ATRX mutations were initially reported to be frequent, yet not restricted to SDHB-related tumors [50]. Interestingly, besides ATRX mutations, a hotspot mutation in the TERT promoter (C228T), which could not be captured by whole-exome sequencing analyses, was associated with the metastatic progression of SDHB-related tumors [51,52].

Given that TERT and ATRX are mutually exclusive telomere maintenance mechanisms [53], it raised the question as to whether immortalization could be a prognostic factor, after all, most PPGL are indolent. To address this issue, we undertook a comprehensive analysis of immortalization in a series of 200 tumors collected by the French COMETE network [54]. We showed that, in fact, only 20% of PPGL get immortalized by either telomerase activation or the alternative lengthening of telomeres (ALT) mechanism. Of note, different genomic alterations leading to the transcriptional activation of TERT comprising not only promoter mutation but also promoter hypermethylation and copy number gains, along with ATRX mutations, accounted for about 70% of metastatic PPGL thus appearing as independent risk factors strongly associated with both metastasis-free and overall survivals. The receiver operating characteristic analysis yielded an area under the curve (AUC) of 0.84, demonstrating that these alterations perform more accurately than the SDHB status (AUC 0.70) on the ability to discriminate metastatic from non-metastatic PPGL. Although this study was devoid of independent validation, parallel observations support these findings

[50–52,55,56]. Notably, immortalization-related mechanisms have also been reported to guide stratification and diagnosis in high risk neuroblastoma [57] and glioma [58], two other neural crest-derived tumors.

Taking into account the potential of non-coding RNAs as prognostic markers [59], we have also evaluated long non-coding RNAs (lncRNAs) using a mining-approach of transcriptome data from the same French COMETE cohort (unpublished observations). Remarkably, we identified one putative lncRNA whose expression is dramatically reduced in metastatic tumors. This transcript accurately discriminated (AUC 0.95) metastatic from non-metastatic tumors with SDHx mutations and was significantly associated with short metastasis-free survival. Moreover, multivariate cox proportional hazards regression analyses for metastasis-free survival revealed this transcript as an independent risk factor associated with poor clinical outcome of SDHx mutation-carriers. Importantly, this transcript was further validated in an independent yet small series of SDHx-related tumors. It is expected that more classes of ncRNAs linked to metastatic PPGL will be discovered using RNA-seq approaches in the years to come.

Two powerful collaborative studies led by Dr. Mercedes Robledo and carried out thanks to the European Network for the Study of Adrenal Tumors (ENS@T) enabled the discovery of additional informative markers. One of these studies consisted on the analysis of compiled miRNA profiling data (450 tumors in total; follow-up period 35 years) and enabled the identification of a six-miRNA metastatic signature strongly correlated with time to progression, irrespective of SDHB status (unpublished data). In fact, combined analysis of two of those miRNAs yielded an AUC of 0.80 which was largely better than the SDHB status (AUC 0.63) in this study. Moreover, this signature was validated in an independent series of 49 formalin-fixed paraffin-embedded (FFPE) tissue specimens and partially retrieved as circulating miRNA in patients' liquid biopsies, particularly during the progressive phase of the metastatic disease (unpublished observations). The second study consisted on the analysis of compiled methylome data from 277 tumors [60] including 48 metastatic PPGL. The authors successfully identified hypermethylation in the promoter of the RDBP (negative elongation factor complex member E) gene as a promising biomarker of metastatic PPGL significantly associated with time to progression, even after correcting for SDHB genotype. Further validation was provided in an independent series of 33 FFPE tumors including 19 metastatic. Although this finding was not reproduced by another group, it should be noted that this second study analyzed a smaller PPGL cohort ($N = 39$), including 10 metastatic tumors only from cluster 1 [61].

4. Conclusions and future perspectives

The current international guidelines for the clinical management of patients operated for a PPGL recommend the assessment of plasma or urinary metanephrines every year to screen for local or metastatic recurrences or new tumors, and also define a category of patients at high-risk of developing a metastatic disease (young patients and those with a genetic disease, a large tumor and/or a paraganglioma) for whom a lifelong annual follow-up is required [62]. It is worth noting that while genetic testing readily improved the outcome of patients at high-risk such as SDHB mutation carriers [16], patients with sporadic tumors still don't benefit of molecular markers for their risk stratification.

Earliest studies of candidate prognostic markers had several selection biases including small cohorts, undetermined genetic predispositions (some studies were conducted before the advent of genetic testing), variable or unreported follow-up times and regimen of surveillance, different definitions of metastatic PPGL and no statistical analyses to adequately assess the outcomes of patients. In the last few years, molecular characterization of large series of PPGL with well-annotated clinical and genetic data, led to the discovery of promising markers, able to predict the metastatic behavior of both SDHB-mutated and sporadic tumors and so there is exciting opportunity to further leverage these advances. The time is ripe for launching prospective multicentre studies in a real-life clinical scenario, aimed at comparing the diagnostic/prognostic performance of those novel markers. Thus, a prognostication model of metastatic PPGL could be developed by combining the most reliable clinical, genetic and molecular risk factors.

It is expected that tumor biomarkers may become integral to management strategies in metastatic patients in the era of cancer precision medicine. However, as reliable biomarkers arrive, new challenges are expected. For instance, assessment of molecular markers in cases with multiple tumors would be difficult in routine practice. Moreover, likewise other human cancers, metastatic PPGL display a high degree of genetic [63] and epigenetic [61] heterogeneity. Therefore, a single biopsy may not capture the complete molecular landscape of an evolving tumor. To evaluate disease progression, assessment of molecular markers in liquid biopsies will be more appropriate. In this regard, circulating miRNAs and detection of individual mutations in cell-free DNA by means of ddPCR already holds significant promise. We believe that implementation of molecular markers of metastatic PPGL in the near future will be useful to improve risk stratification, to guide patient care, and consequently to reduce the associated medico-economic costs of long-term surveillance.

Disclosure of interest

The authors declare that they have no competing interest.

Acknowledgements

Work in the Genetics and Metabolism of Rare Cancers Lab is supported by past and current grants from European Commission FP7 Research and Innovation Funding Program for 2007–2013 (n° 259735), Horizon 2020 (n° 633983); *Institut National du Cancer* and *Direction Générale de l'Offre de Soins* (DGOS), *Programme de Recherche Translationnelle en cancérologie* (PRT-K 2014, COMETE-TACTIC, INCa_DGOS_8663); *Agence Nationale de la Recherche* (ANR-2011-JCJC-00701 MODEOMAPP); *Alliance nationale pour les sciences de la vie et de la santé* (AVIESAN); *Plan Cancer : appel à projets Épigénétique et Cancer 2013* (EPIG201303 METABEPIC), the Cancer Research for Personalized Medicine – CARPEM project (*Site de Recherche Intégré sur le Cancer* – SIRIC) and The Paradifference Foundation. The group is supported by the *Ligue Nationale contre le Cancer* (*Équipe Labellisée*). We apologize to all colleagues whose important contributions could not be cited due to space limitations.

References

[1] Ayala-Ramirez M, et al. Clinical risk factors for malignancy and overall survival in patients with pheochromocytomas and sympathetic paragangliomas: primary tumor size and primary tumor location as prognostic indicators. J Clin Endocrinol Metab 2011;96:717–25.
[2] Hamidi O, et al. Malignant Pheochromocytoma and Paraganglioma: 272 Patients Over 55 Years. J Clin Endocrinol Metab 2017;102:3296–305.
[3] Hamidi O, et al. Outcomes of patients with metastatic phaeochromocytoma and paraganglioma: A systematic review and meta-analysis. Clin Endocrinol (Oxf) 2017;87:440–50.
[4] Pacak K, et al. Pheochromocytoma: recommendations for clinical practice from the First International Symposium October 2005. Nat Clin Pract Endocrinol Metab 2007;3:92–102.
[5] Roman-Gonzalez A, et al. Impact of surgical resection of the primary tumor on overall survival in patients with metastatic pheochromocytoma or sympathetic paraganglioma. Ann Surg 2018;268:172–8.

[6] Niemeijer ND, Alblas G, van Hulsteijn LT, Dekkers OM, Corssmit EP. Chemotherapy with cyclophosphamide, vincristine and dacarbazine for malignant paraganglioma and pheochromocytoma: systematic review and meta-analysis. Clin Endocrinol (Oxf) 2014;81:642–51.
[7] Baudin E, et al. Therapy of endocrine disease: treatment of malignant pheochromocytoma and paraganglioma. Eur J Endocrinol 2014;171:R111–22.
[8] Nolting S, Grossman A, Pacak K, Metastatic Phaeochromocytoma:. Spinning towards more promising treatment options. Exp Clin Endocrinol Diabetes 2019;127:117–28.
[9] Eisenhofer G, et al. Plasma methoxytyramine: a novel biomarker of metastatic pheochromocytoma and paraganglioma in relation to established risk factors of tumour size, location and SDHB mutation status. Eur J Cancer 2012;48:1739–49.
[10] Amar L, et al. Succinate dehydrogenase B gene mutations predict survival in patients with malignant pheochromocytomas or paragangliomas. J Clin Endocrinol Metab 2007;92:3822–8.
[11] Castro-Vega LJ, et al. Germline mutations in FH confer predisposition to malignant pheochromocytomas and paragangliomas. Hum Mol Genet 2014;23:2440–6.
[12] Buffet A, et al. Germline mutations in the Mitochondrial 2-Oxoglutarate/Malate carrier SLC25A11 gene confer a predisposition to metastatic paragangliomas. Cancer Res 2018;78:1914–22.
[13] Bausch B, Borozdin W, Neumann HP, European-American Pheochromocytoma Study, G. Clinical and genetic characteristics of patients with neurofibromatosis type 1 and pheochromocytoma. N Engl J Med 2006;354:2729–31.
[14] Crona J, et al. Genotype-phenotype correlations in pheochromocytoma and paraganglioma. Endocr Relat Cancer 2019.
[15] Turkova H, et al. characteristics and outcomes of metastatic sdhb and sporadic pheochromocytoma/paraganglioma: an national institutes of health study. Endocr Pract 2016;22:302–14.
[16] Buffet A, et al. Positive impact of genetic test on the management and outcome of patients with paraganglioma and/or pheochromocytoma. J Clin Endocrinol Metab 2019;104:1109–18.
[17] Thompson LD. Pheochromocytoma of the Adrenal gland Scaled Score (PASS) to separate benign from malignant neoplasms: a clinicopathologic and immunophenotypic study of 100 cases. Am J Surg Pathol 2002;26:551–66.
[18] Kimura N, et al. Pathological grading for predicting metastasis in phaeochromocytoma and paraganglioma. Endocr Relat Cancer 2014;21:405–14.
[19] Stenman A, Zedenius J, Juhlin CC. The Value of histological algorithms to predict the malignancy potential of pheochromocytomas and abdominal paragangliomas-a meta-analysis and systematic review of the literature. Cancers (Basel) 2019;11.
[20] Lloyd RV OR, K.G., Rosai J. WHO classification of tumours: pathology and genetics of tumours of endocrine organs. (2017).
[21] Clarke MR, Weyant RJ, Watson CG, Carty SE. Prognostic markers in pheochromocytoma. Hum Pathol 1998;29:522–6.
[22] Elder EE, et al. KI-67 AND hTERT expression can aid in the distinction between malignant and benign pheochromocytoma and paraganglioma. Mod Pathol 2003;16:246–55.
[23] Tavangar SM, et al. Immunohistochemical expression of Ki67, c-erbB-2, and c-kit antigens in benign and malignant pheochromocytoma. Pathol Res Pract 2010;206:305–9.
[24] Castilla-Guerra L, et al. Expression and prognostic value of c-erbB-2 oncogene product in human phaeochromocytomas. Histopathology 1997;31:144–9.
[25] Favier J, Plouin PF, Corvol P, Gasc JM. Angiogenesis and vascular architecture in pheochromocytomas: distinctive traits in malignant tumors. Am J Pathol 2002;161:1235–46.
[26] Salmenkivi K, Heikkila P, Liu J, Haglund C, Arola J. VEGF in 105 pheochromocytomas: enhanced expression correlates with malignant outcome. APMIS 2003;111:458–64.
[27] Boltze C, et al. Expression profile of the telomeric complex discriminates between benign and malignant pheochromocytoma. J Clin Endocrinol Metab 2003;88:4280–6.
[28] Ohta S, et al. Downregulation of metastasis suppressor genes in malignant pheochromocytoma. Int J Cancer 2005;114:139–43.
[29] Saffar H, et al. Expression of galectin-3, nm-23, and cyclooxygenase-2 could potentially discriminate between benign and malignant pheochromocytoma. Am J Clin Pathol 2011;135:454–60.
[30] Waldmann J, et al. Expression of the transcription factor snail and its target gene twist are associated with malignancy in pheochromocytomas. Ann Surg Oncol 2009;16:1997–2005.
[31] Hayry V, et al. High frequency of SNAIL-expressing cells confirms and predicts metastatic potential of phaeochromocytoma. Endocr Relat Cancer 2009;16:1211–8.
[32] Alexander RE, Cheng L, Grignon DJ, Idrees M. Cytoplasmic staining of OCT4 is a highly sensitive marker of adrenal medullary-derived tissue. Am J Surg Pathol 2013;37:727–33.
[33] Chaux A, et al. Immunohistochemical evidence of dysregulation of the mammalian target of rapamycin pathway in primary and metastatic pheochromocytomas. Urology 2012;80 [736 e7-12].
[34] Peczkowska M, et al. The clinical utility of circulating neuroendocrine gene transcript analysis in well-differentiated paragangliomas and pheochromocytomas. Eur J Endocrinol 2017;176:143–57.
[35] Unger P, et al. S100 protein-positive sustentacular cells in malignant and locally aggressive adrenal pheochromocytomas. Arch Pathol Lab Med 1991;115:484–7.
[36] Kiss NB, et al. Methylation of the p16INK4A promoter is associated with malignant behavior in abdominal extra-adrenal paragangliomas but not pheochromocytomas. Endocr Relat Cancer 2008;15:609–21.
[37] Kiss NB, et al. Acquired hypermethylation of the P16INK4A promoter in abdominal paraganglioma: relation to adverse tumor phenotype and predisposing mutation. Endocr Relat Cancer 2013;20:65–78.
[38] Geli J, et al. Global and regional CpG methylation in pheochromocytomas and abdominal paragangliomas: association to malignant behavior. Clin Cancer Res 2008;14:2551–9.
[39] de Krijger RR, et al. Prognostic value of p53, bcl-2, and c-erbB-2 protein expression in phaeochromocytomas. J Pathol 1999;188:51–5.
[40] Oudijk L, et al. Vascular pattern analysis for the prediction of clinical behaviour in pheochromocytomas and paragangliomas. PLoS One 2015;10:e0121361.
[41] Oudijk L, et al. Immunohistochemical expression of stem cell markers in pheochromocytomas/paragangliomas is associated with SDHx mutations. Eur J Endocrinol 2015;173:43–52.
[42] Białas MOK, Dyduch G, Ciesielska-Milian K, Buziak M, Hubalewska-Dydejczyk A, Sobrinho-Simoes M. Neuroendocrine markers and sustentacular cell count in benign and malignant pheochromocytomas – a comparative study. Pol J Pathol 2013;64:129–35.
[43] Castro-Vega LJ, Lepoutre-Lussey C, Gimenez-Roqueplo AP, Favier J. Rethinking pheochromocytomas and paragangliomas from a genomic perspective. Oncogene 2016;35:1080–9.
[44] Fishbein L, et al. Comprehensive molecular characterization of pheochromocytoma and paraganglioma. Cancer Cell 2017;31:181–93.
[45] Sandgren J, et al. Recurrent genomic alterations in benign and malignant pheochromocytomas and paragangliomas revealed by whole-genome array comparative genomic hybridization analysis. Endocr Relat Cancer 2010;17:561–79.
[46] Petri BJ, et al. Frequent loss of 17p, but no p53 mutations or protein overexpression in benign and malignant pheochromocytomas. Mod Pathol 2008;21:407–13.
[47] Brouwers FM, et al. Gene expression profiling of benign and malignant pheochromocytoma. Ann N Y Acad Sci 2006;1073:541–56.
[48] Suh YJ, Choe JY, Park HJ. Malignancy in pheochromocytoma or paraganglioma: integrative analysis of 176 cases in TCGA. Endocr Pathol 2017;28:159–64.
[49] Pinato DJ, et al. Programmed cell death ligands expression in phaeochromocytomas and paragangliomas: relationship with the hypoxic response, immune evasion and malignant behavior. Oncoimmunology 2017;6:e1358332.
[50] Fishbein L, et al. Whole-exome sequencing identifies somatic ATRX mutations in pheochromocytomas and paragangliomas. Nat Commun 2015;6:6140.
[51] Liu T, et al. The activating TERT promoter mutation C228T is recurrent in subsets of adrenal tumors. Endocr Relat Cancer 2014;21:427–34.
[52] Papathomas TG, et al. Telomerase reverse transcriptase promoter mutations in tumors originating from the adrenal gland and extra-adrenal paraganglia. Endocr Relat Cancer 2014;21:653–61.
[53] Reddel RR. Telomere maintenance mechanisms in cancer: clinical implications. Curr Pharm Des 2014;20:6361–74.
[54] Job S, et al. Telomerase activation and atrx mutations are independent risk factors for metastatic pheochromocytoma and paraganglioma. Clin Cancer Res 2019;25:760–70.
[55] Svahn F, et al. Telomerase reverse transcriptase promoter hypermethylation is associated with metastatic disease in abdominal paraganglioma. Clin Endocrinol (Oxf) 2018;88:343–5.
[56] Dwight T, et al. TERT structural rearrangements in metastatic pheochromocytomas. Endocr Relat Cancer 2018;25:1–9.
[57] Ackermann S, et al. A mechanistic classification of clinical phenotypes in neuroblastoma. Science 2018;362:1165–70.
[58] Pekmezci M, et al. Adult infiltrating gliomas with WHO 2016 integrated diagnosis: additional prognostic roles of ATRX and TERT. Acta Neuropathol 2017;133:1001–16.
[59] Ching T, et al. Pan-Cancer Analyses Reveal Long Intergenic Non-Coding RNAs Relevant to Tumor Diagnosis, Subtyping and Prognosis. EBioMedicine 2016;7:62–72.
[60] de Cubas AA, et al. DNA Methylation profiling in pheochromocytoma and paraganglioma reveals diagnostic and prognostic markers. Clin Cancer Res 2015;21:3020–30.
[61] Backman S, et al. Global DNA methylation analysis identifies two discrete clusters of pheochromocytoma with distinct genomic and genetic alterations. Sci Rep 2017;7:44943.
[62] Plouin PF, et al. European Society of Endocrinology Clinical Practice Guideline for long-term follow-up of patients operated on for a phaeochromocytoma or a paraganglioma. Eur J Endocrinol 2016;174:G1–10.
[63] Crona J, et al. Spatiotemporal Heterogeneity characterizes the genetic landscape of pheochromocytoma and defines early events in tumorigenesis. Clin Cancer Res 2015;21:4451–60.

REVUE 3

An update on adult forms of hereditary pheochromocytomas and paragangliomas

Charles Dariane, Judith Goncalves, Marc-Olivier Timsit, Judith Favier

(Article accepté en septembre dans la revue Current Opinion in Oncology)

REVIEW

An update on adult forms of hereditary pheochromocytomas and paragangliomas

Charles Dariane[a], *Judith Goncalves*[b], *Marc-Olivier Timsit*[a,b], *and Judith Favier*[b]

Purpose of review
Pheochromocytomas and paragangliomas (PPGL) display a strong genetic determinism with 40% of inherited forms. The purpose of this review is to provide an update on current knowledge on adult forms of hereditary PPGL and their management.

Recent findings
PPGL are genetically-driven in 70% of cases, with germline and/or somatic mutations identified in more than 20 genes. Although eight new susceptibility genes have recently emerged, mutations on *SDHx* genes remain the most frequent. In addition to *SDHB,* mutations in *SLC25A11, FH* and *MDH2* may predispose to a metastatic disease and somatic alterations including TERT and ATRX mutations, and the differential expression on noncoding RNAs are also associated with the occurrence of metastases.
The biochemical diagnosis remains the mainstay of functional PPGL and does not differ between hereditary PPGL while the choice of the best nuclear imaging approach is dictated by the tumor type and can be influenced by the presence of a germline mutation (18F-DOPA PET/CT for cluster 2 mutation and ^{68}Ga-DOTATATE PET/CT for cluster 1 mutation).

Summary
A systematic genetic testing and counselling is recommended for all PPGL patients and should lead to conservative surgery and an adapted follow up, in case of hereditary form.

Keywords
driver mutations, genetic determinism, paraganglioma, pheochromocytoma

INTRODUCTION

Pheochromocytomas and paragangliomas (PPGL) are rare neuroendocrine, catecholamine-secreting tumors that arise from chromaffin cells of the adrenal medulla (pheochromocytomas, PCC) or from sympathetic and parasympathethic ganglia (paragangliomas, PGL). Clinical symptoms of the disease are common between adrenal and extra-adrenal forms and are determined by excessive secretion of catecholamines (norepinephrine, epinephrine, and dopamine) or tumoral syndrome in case of malignant form or cervical PGL [1,2]. When located in the thoraco-abdomino-pelvic space, PGL are functional and hormone-secreting in 85% of cases, whereas they are nonsecreting in 90% of cases when located in the cervical space or the skull base [3].

Although mostly benign, about 15% undergo a metastatic evolution. One of the main specificities of PPGL is their strong genetic determinism. Over the past 20 years, more than 15 susceptibility genes have been identified (Fig. 1). Most are tumor suppressors (including *NF1, VHL, SDHx, FH, TMEM127, MAX, SCL25A11*), and a few are oncogenes (*RET* and *EPAS1*) [4]. They predispose to either syndromic, early, multiple, or malignant forms of PPGL [3,5] (Table 1). A germline mutation in one of these genes is found in 40% of all cases [3,6], making PPGL the most commonly inherited tumor in human [5]. Mutations on *SDHx* genes (*SDHA, SDHB, SDHC, SDHD, SDHAF2*) account for over half of the mutations found in patients with hereditary PPGL. They

[a]Service d'urologie, Hôpital européen Georges-Pompidou, Université de Paris and [b]Université de Paris, PARCC, INSERM, Equipe Labellisée par la Ligue contre le Cancer, Paris, France

Correspondence to Judith Favier, PhD, Genetics and Metabolism of Rare Cancers team, INSERM, UMR970, Paris-Cardiovascular Research Center, 56 rue Leblanc, 75015 Paris, France. Tel: +33 1 53 98 80 41; e-mail: judith.favier@inserm.fr

Curr Opin Oncol 2020, 32:000–000
DOI:10.1097/CCO.0000000000000694

KEY POINTS

- PPGL are frequently inherited with around 20 susceptibility genes identified.
- 40% of all cases are explained by the identification of a germline mutation, and 30% by a somatic mutation.
- Somatic mutations and differential expression of microRNAs and lncRNAs are associated with the development of metastatic forms of the disease.
- Biochemical diagnosis should be confirmed by conventional and nuclear imaging, and the choice of the optimal radiopharmaceutical can be guided by the genetic background.
- Genetic investigation is mandatory to personalize surgery and adapt patient's and relatives' management and follow-up.

encode the different subunits and the assembly factor of succinate dehydrogenase (SDH), a mitochondrial enzyme involved in the tricarboxylic acid (TCA) cycle and the electron transport chain. Genotype–phenotype correlations have emerged in patients with mutations in PPGL predisposing genes [7]. Distinct biochemical, molecular and clinical presentations have been shown, depending on the driver genes mutated [8,9]. Transcriptomic studies led on international tumor collections, have classified PPGL in three main clusters [10,11], each related to different tumorigenesis mechanisms. The pseudohypoxic cluster (C1) includes tumors with mutations in TCA cycle related genes and *VHL*. Abnormal stabilization of hypoxia-inducible factors (HIFα) is explained by the lack of ubiquitination in PPGL with VHL loss-of-function, or, in *SDHx* or *FH*-mutated cases, by the accumulation of oncometabolites, such as succinate or fumarate, which act as competitive inhibitors of 2-OG dependent dioxygenases such as the HIF-prolylhydroxylases (PHDs) [12,13]. Accumulation of these oncometabolites also inhibits DNA (TET) and histone (JmjC) demethylases, resulting in global DNA hypermethylation and chromatin structural modifications [14▪]. Such epigenetic changes result in the downregulation of many genes including tumor-suppressor genes, genes involved in metastasis propagation and genes responsible for chromaffin differentiation, explaining their norepinephrine secretion [15]. The kinase signaling cluster (C2) is characterized by the activation of the MAPK and mTOR pathways. This subtype gathers tumors with germline and somatic mutations in *RET*, *NF1, TMEM127, MAX*, and *HRAS* genes. Most of the time, these mutations predispose to epinephrine-secreting PCC. Finally, a third cluster has emerged from The Cancer Genome Atlas (TCGA) transcriptomic studies. It is characterized by the activation of the Wnt/β-catenin pathway. The tumors gathered in this subtype are driven by a fusion gene including Mastermind Like Transcriptional Coactivator 3 and have a predominantly adrenal location. These PPGL display mixed noradrenergic and adrenergic secretion and may be linked to metastatic or recurrent disease [10,11,16–19].

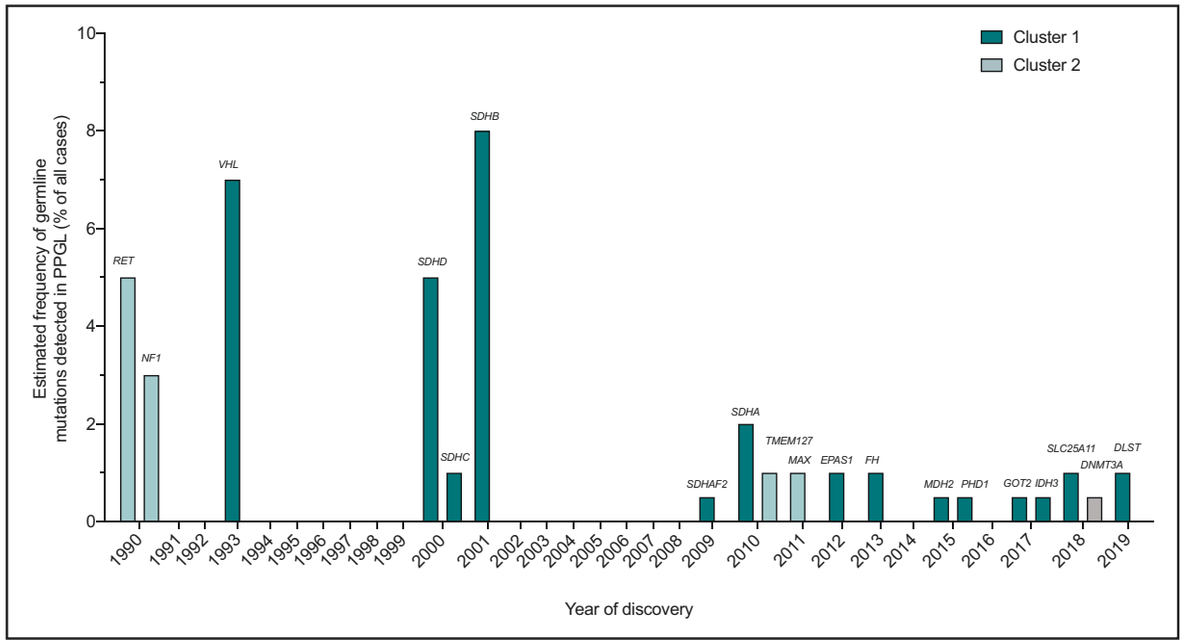

FIGURE 1. PPGL susceptibility genes: Year of discovery and frequency of mutations.

Table 1. PPGL susceptibility genes

Gene	Year of discovery	Protein function	Expression cluster	Clinical presentation	Risk of metastasis
RET	1990	Tyrosine kinase receptor	Cluster 2	MEN2 syndrome (PCC, MTC)	low
NF1	1990	Neurofibromin 1, negative regulator of the RAS signaling pathway	Cluster 2	NF1 syndrome (multiple PCC, neurofibromas, Lisch nodules, axillary and inguinal freckling osseous lesions, optic glioma, sarcomas, GIST, ccRCC)	low
VHL	1993	Von Hippel-Lindau protein	Cluster 1B	VHL syndrome (PCC, APGL, ccRCC, central nervous system or retinal haemangioblastomas, renal and pancreatic cysts, pancreatic neuroendocrine tumors, endolymphatic sac tumors, and epididymal cystadenomas)	low
SDHD	2000	Anchoring subunit D of SDH	Cluster 1A	Multiple HNPGL, GIST, ccRCC, PA	low
SDHC	2000	Anchoring subunit C of SDH	Cluster 1A	HNPGL, GIST, RCC	low
SDHB	2001	Catalytic subunit B of SDH	Cluster 1A	TAPPGL, GIST, RCC, PA	high
SDHAF2	2009	Assembly factor of SDH	Cluster 1A	HNPGL	low
SDHA	2010	Catalytic subunit A of SDH	Cluster 1A	HNPGL, GIST, RCC, PA	low
TMEM127	2010	Negative regulator of mTOR pathway	Cluster 2	Multiple PCC, ccRCC	low
MAX	2011	Leucine zipper type trancription factor	Cluster 2	Multiple PCC, renal oncocytoma	low
EPAS1	2012	Alpha subunit of the hypoxia inducible factor 2	Cluster 1B	PCC, TAPPGL, polycythemia, somatostatinoma	low
FH	2013	Fumarate dehydrogenase	Cluster 1A	TAPPGL, Leiomyoma, RCC	high
MDH2	2015	Mitochondrial malate dehydrogenase	Cluster 1A	Multiple PCC, TAPPGL	high
PHD1	2015	Alpha-ketoglutarate-dependent hydroxylase	Cluster 1B	Multiple PGL, early onset of polycythemia	low
GOT2	2017	Glutamic-oxaloacetic transaminase	Cluster 1A	Multiple TAPPGL	high ?
IDH3	2017	NAD- specific isocitrate dehydrogenase 3	Cluster 1A?	HNPGL, AML	?
SLC25A11	2018	Mitochondrial 2-oxoglutarate/malate carrier	Cluster 1A	TAPPGL	high
DNMT3A	2018	DNA methyltransferase		HNPGL, AML	low
DLST	2019	E2 subunit of mitochondrial a-ketoglutarate dehydrogenase (OGDH)	Cluster 1A	Multiple TAPPGL	low

AML, acute myeloid leukemia; ccRCC, clear cell renal cell carcinoma; GIST, gastrointestinal stromal tumor; HNPGL, head and neck; MEN2, multiple endocrine neoplasia type 2; MTC, medullary thyroid carcinoma; NF1 syndrome, neurofibromatosis type 1; PA, pituitary adenoma; PCC, pheochromocytoma; SDH, succinate dehydrogenase; TAPPGL, thoracic, abdominal or pelvic paraganglioma; VHL syndrome, von Hippel-Lindau syndrome.

Current guidelines advise to propose a genetic screening to all patients with PPGL, especially because the identification of a germline mutation in one of these genes greatly influences patients follow-up [20,21]. The purpose of this review is to give an update on the knowledge acquired in recent years on the biology and management of hereditary PPGL.

NEW PHEOCHROMOCYTOMAS AND PARAGANGLIOMAS SUSCEPTIBILITY GENES

In the last 5 years, new susceptibility genes have been identified, mainly through the use of whole-exome sequencing (WES) in patients with multiple or familial PPGLs (Fig. 1; Table 1). Some of these genes are involved in mitochondrial metabolism (*MDH2, GOT2, SLC25A11*, and *DLST*) [22–25,26▪] and are thought to belong to cluster 1; some others are implicated in MAPK signaling pathways (*MET* and *MERTK*) [10,16] bringing these mutations closer to cluster 2 and finally some genes are involved in DNA methylation (*H3F3A, DNMT3A*) [16,27,28]. It should be noted that mutations on these genes have been identified in a very limited number of cases.

MDH2 is the fourth PPGL susceptibility gene encoding an enzyme from the TCA cycle, malate dehydrogenase. It catalyzes the oxidation of L-malate to oxaloacetate and is involved in the malate-aspartate shuttle (MAS), which is critical for cellular respiration. A first germline mutation was identified in a patient with multiple metastatic PPGLs secreting norepinephrine [29]. Since, four other patients with an *MDH2* mutation have been described. They presented early forms of PPGL, often multiple and metastatic in 40% of cases [23,29].

GOT2 encodes the mitochondrial glutamic-oxaloacetic transaminase, also involved in the MAS, where it catalyzes the conversion of oxaloacetate to aspartate. A gain of function mutation in *GOT2* was described in a patient with metastatic and multiple PPGLs, thanks to an next-generation sequencing (NGS) panel targeting genes involved in mitochondrial metabolism [24].

SLC25A11 is another tumor suppressor gene playing a major role in the MAS. It encodes the 2-oxoglutarate-malate transporter, which allows the transport of malate from the mitochondria to the cytosol. To date, germline mutations in this gene have been described in eight patients, 70% of whom presented a metastatic phenotype [25,26▪].

Finally, the *DLST* tumor suppressor gene encodes the dihydrolipoamide S-succinyl-transferase protein which constitutes the E2 subunit of the α-ketoglutarate dehydrogenase (OGDH). This enzymatic complex catalyzes the conversion of α-ketoglutarate to succinyl-CoA in the TCA cycle. *DLST* mutations were first identified in eight unrelated individuals and are thought to result in OGDH dysfunction and subsequent higher α-ketoglutarate to fumarate ratio, likely responsible for PPGL development in these patients. Four of these patients presented multiple PPGL [26▪].

MET is an oncogene predisposing mainly to type 1 papillary renal cell carcinoma. Somatic mutations in this gene had been identified in PPGLs and a germline mutation was recently discovered in a family of PCC carriers [10,16]. In 2016, a germline mutation in the *MERTK* gene was identified in two patients with medullary thyroid carcinoma (CMT) and PPGLs [16]. Like *RET*, *MET*, and *MERTK* both encode tyrosine kinase receptor.

A recurrent hot spot mutation in the *H3F3A* gene, encoding histone H3.3, has been described in two young patients with multiple PPGL [16]. These two patients also carried giant cell tumors of the bone, with which the mutation appears to be systematically associated.

Finally, WES allowed the identification of two gain-of-function germline mutations in *DNMT3A*, in two patients with multiple PPGL and one with a familial history [27]. *DNMT3A* encodes a DNA methyltransferase responsible for DNA methylation patterns.

VALIDATION OF GENETIC VARIANTS IN PHEOCHROMOCYTOMAS AND PARAGANGLIOMAS SUSCEPTIBILITY GENES

Genetic testing being systematically recommended to patients with PPGL, several approaches have been developed to estimate the pathogenicity of variants of uncertain significance (VUS) identified in patients/tumors. Following SDHB, SDHA, and SDHD immunohistochemistries (IHC) that have been developed to validate *SDHx* variants [30,31], negative FH immunostaining has recently been described in *FH*-mutated tumors [32,33], whereas tumors with *SLC25A11* and *DLST* mutations show OGC and DLST negative immunostainings, respectively [25,26▪]. In contrast, *GOT2*-mutated PPGLs exhibit a positive immunostaining, reflecting the higher GOT2 expression observed in these tumors [24]. Furthermore, a strong correlation between a positive membrane immunostaining for CA9 and *VHL* mutations (germline or somatic) has also been recently described in PPGL [34▪].

Metabolomic studies also constitute a relevant strategy to support genetic variant interpretation in the cases of mitochondrial related mutations [6].

Metabolites assessment by liquid-chromatography-mass-spectrometry (LCMS) allows the identification of rare cases of PPGLs with germline mutations in *FH* and somatic mutations in *IDHx* and *SDHx* genes [35▪]. A recent comparative study showed that LCMS displayed a higher specificity than SDHB IHC, with a similar sensitivity to detect SDH mutations. It showed the strong complementarity of both techniques supporting the use of both strategies for good patient management [36].

Finally, magnetic resonance spectroscopy (^{1}H-MRS) has proven to be particularly effective to detect succinate accumulation in patients [37,38]. Following proof-of-concept studies, a recent validation study performed on 50 patients with PPGL demonstrated the high diagnostic performance of this approach in *SDHx* mutation carriers [39▪].

RECENT ADVANCES IN TUMOR GENETICS AND GENOMICS OF PHEOCHROMOCYTOMAS AND PARAGANGLIOMAS

In the past years, targeted NGS and WES revealed a high prevalence of somatic mutations in sporadic PPGLs. Half of these cases were secondary to a somatic mutation in *RET*, *VHL*, or *NF1* genes [40,41]. Somatic mutations have been identified in several PPGL predisposing genes, such as *RET, VHL, EPAS1, NF1*, and *SDHB*, but also in *HRAS* and *TP53*. These mutations are responsible for around 30% of PPGLs with no identified germline mutation, bringing the rate of genetically determined PPGLs up to 70% [11]. Recently, a study using a custom-designed NGS targeted panel highlighted some rare cases mosaic germline mutations and revealed the existence of *SDHx* somatic variants [42]. Remarkably, two tumors with somatic *SDHD* variants were also identified, following succinate detection by ^{1}H-MRS [39▪].

Moreover, recent data suggest that somatic alterations in genes involved in telomere preservation and cellular immortalization (i.e. *ATRX* or *TERT*) participate to metastatic evolution of the disease. These mutations are often found in *SDHB*-related PPGL [11,14▪,43]. *Job et al.* [14▪] recently showed that telomerase activation and *ATRX* mutations are independent factors of poor prognosis and should be assessed in order to identify potentially metastatic PPGLs, especially in tumors at high risk of progression such as those with *SDHB* or *FH* mutations. In addition, a signature cluster of six miRNAs (miR-21-3p, miR-183-5p, miR-182-5p, miR-96-5p, miR-551b-3p, and miR-202-5p) was associated with higher metastatic risk in patients with PPGL. Liquid biopsies also exhibited higher levels of five of these miRNAs. Notably, miR-21-3p is associated with mTOR pathway activation and correlates with a predictive signature of positive response to mTOR inhibitor in PPGLs and other cancers [44▪].

Finally, long-noncoding RNA (lncRNA) were recently associated with PPGL transcriptional dysregulation. Four lncRNA appeared to correlate with the different PPGL mRNA expression clusters. One lncRNA (GenBank: BC063866) is peculiarly thought to constitute an independent risk factor of malignancy and poor clinical outcome in *SDHx*-mutated patients. These lncRNA and miRNAs thereby appear as innovative biomarkers for the detection of potentially metastatic PPGL [45,46].

ADVANCES IN THE UNDERSTANDING OF SDHB-RELATED ONCOGENESIS

Mutations in *SDHB* are the main predictor of metastatic evolution in PPGL [47,48]. Recent studies have shed light on some of the mechanisms involved in the acquisition of metastatic features of *SDHB*-mutated cells (Fig. 2). First, synergistic effects of TET inhibition and pseudohypoxia have been revealed [49▪], and the implication of iron overload and oxidative stress [50], resulting in innovative therapeutic targets in SDH-associated malignancies. Moreover, *SDHB* mutations have been associated with increased PARP-dependent DNA repair, known to repair single-strand DNA breaks [51]. Succinate accumulation has also been shown to disrupt the homologous recombination DNA-repair pathway through the inhibition of lysine demethylase KDM4B, in *SDHx*-mutated tumors [52,53▪▪].

UPDATE ON THE CLINICAL MANAGEMENT OF PATIENTS WITH PHEOCHROMOCYTOMAS AND PARAGANGLIOMAS

Diagnosis: biochemical and imaging hallmarks of hereditary pheochromocytomas and paragangliomas

The classical clinical presentations (triad of concomitant headache, sweating, and palpitations; or hypertension) can lead to suspicion of PPGL, which need to be confirmed on a biochemical analysis of hormonal concentrations, followed by anatomic localization of the tumors. Commonly, PPGL can also be suspected when an incidental adrenal tumor is found on abdominal imaging or in the context of hereditary renal cell carcinoma (*VHL*, *FH* mutations, or SDH-deficient renal carcinoma). Early diagnosis is crucial, because of the cardiovascular risks caused by excess secretion of catecholamines, and in case of

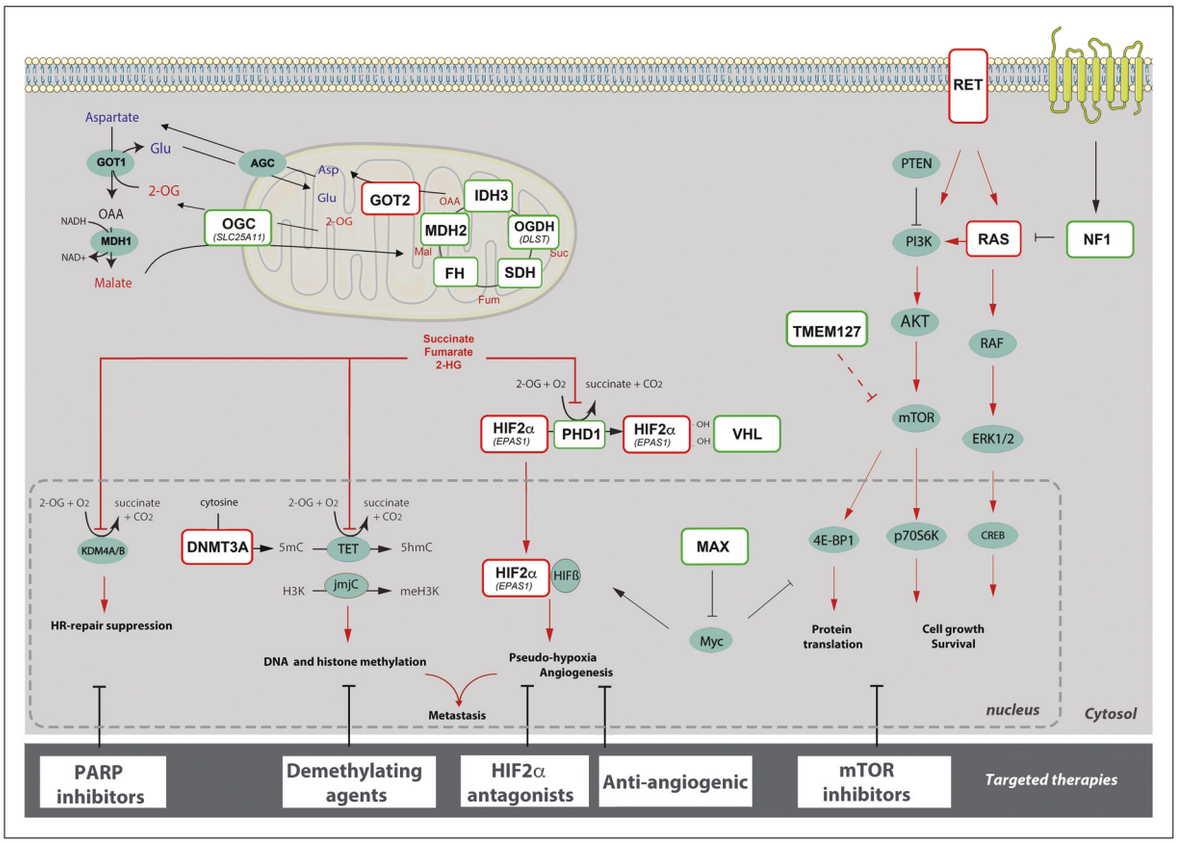

FIGURE 2. Oncogenic pathways in hereditary PPGL. Mechanisms of tumorigenesis associated with mutations in oncogenes (red) or tumor suppressor genes (green) predisposing to PPGL and their associated targeted therapeutic approaches.

hereditary predisposition, by the risk of development of multiple and sometimes metastatic tumors [3].

The biochemical diagnosis remains the mainstay of functional PPGL and does not differ between hereditary patients with PPGL, although the biochemical phenotype can orientate genetic testing with cluster 1 tumors showing a noradrenergic phenotype (norepinephrine and normetanephrine secretion because of a decrease in PNMT enzyme secretion) and cluster 2 tumors leading to an adrenergic secretion (epinephrine and metanephrine secretion). Recent guidelines recommend that initial testing for PPGL should include measurements of plasma free or urinary fractionated metanephrines [54▪▪], and that consideration should be given to preanalytical factors (such as α- and β-blockers which can be like other medications responsible for false-positive results). Some authors recommend a collection on a urine sample (as random 'spot' urinary metanephrines) to simplify patient management [55] or simply the plasma dosage however leading to a 15% rate of false-positive [56]. Usually, functional PPGL diagnosis is highly likely when concentrations of hormones are found to be more than three-fold the superior value in a high-risk patient (e.g. the one with a genetic predisposition); however, any elevation of metanephrine fraction should be carefully followed, and measurements repeated. It has also to be noticed that the plasma measurement of 3-methoxytyramine (3-MT) represents a prognostic marker of metastatic PPGL and presents sometimes an isolated elevation in case of head-and-neck PGL (HNPGL) [57].

Imaging is then performed to locate the tumor(s) [58] and to search for metastasis, when malignant PPGL is suspected. Indeed, in 2017, the WHO concluded that all PPGL, even without apparent metastases, have a malignant potential [59,60]. Malignancy is then defined by objective metastatic spread on imaging (either in lymph nodes, bones, lung, or liver) and is more likely to occur in patients with large PCC, sympathetic paragangliomas, and norepinephrine-secreting tumors. Even in localized diseases, a continual follow-up is required given the risk of recurrence and metastatic spread. The presence of a mutation in *SDHB, FH*, or *SLC25A11* should prone the clinician to a closer follow-up of

patients, and a life-long follow-up in case of *SDHB* mutation, because this mutation lead to metastatic evolution in 50% of cases with a penetrance of 50% at age 50. In case of mutation in *SDHx*, patients present a risk of developing a gastro-intestinal stromal tumor (particularly *SDHA* and *SDHC*), or a renal cell carcinoma (in case of mutation in *SDHB*), and multiple cervical paragangliomas (in case of mutation in *SDHD*). Renal cell carcinomas should also be searched for in case of germline *FH* or *VHL* mutations.

The choice of the best diagnostic imaging approach is dictated by the type of tumor and can also be influenced by the presence of a germline mutation. PPGLs linked to *NF1/RET/MAX/TMEM127* and *VHL* mutations are almost always confined to the adrenal medulla and are well differentiated. A specific algorithm of follow-up should also be defined based on the specific type of mutation. Nuclear imaging is usually combined to conventional imaging (i.e. CT scan and MRI). It can also be useful when hormones concentrations are normal, or when conventional imaging is negative. The choice of the optimal radiopharmaceutical can be guided by tumor location (tightly linked to embryologic origin) and genetic background [61,62]. In case of apparently sporadic PCC or inherited PCC linked to *NF1/RET/MAX*/TMEM127 (cluster 2) and *VHL* (cluster 1, except *SDHx*), the 18F-DOPA PET/CT should be preferred (and ^{68}Ga-DOTATATE PET/CT in second choice). The ^{68}Ga-DOTATATE PET/CT (DOTATATE corresponds to somatostatin analogs labeled with diagnostic radionuclides) should be favored in case of HNPGL, or in case of extra-adrenal sympathetic or multifocality or metastatic disease or in case of *SDHB, FH*, or *SLC25A11* variants [61]. ^{123}I-MIBG (metaiodobenzylguanidine) scintigraphy can be useful in case of adrenal lesion evocative for PCC but with nonconclusive biochemical results or medications interferences. It should be restricted to this indication or when radiopharmaceutical MIBG-based therapy is to follow (metastatic cases).

Treatment of pheochromocytomas and paragangliomas

For localized hormone-secreting PPGL, the surgical excision remains the mainstay of management. Tumor removal reduces both immediate consequences of catecholamine excess and distant vascular and myocardial complications. Most PPGL are curable by surgery when localized, with a recurrence-free survival estimated at 1% per year per patient [63].

Regarding the surgical approach, recent guidelines recommend minimally invasive surgery for most PCC (i.e. laparoscopic radical adrenalectomy) [21,54▪▪]. In case of bilateral tumors or genetic predisposition (particularly in MEN2 syndrome from cluster 2), a partial adrenalectomy or a tumorectomy can be discussed. Some authors have reported outpatient adrenalectomy as a well tolerated minimally invasive approach without increase risk of 30-day complications or readmission in appropriately selected candidates [64]. Regarding abdominal paraganglioma (such as retroperitoneal paraganglioma or bladder paraganglioma), a laparoscopic tumorectomy is preferred, if technically feasible [58]. An open resection is proposed particularly in case of large tumors more than 6 cm or multifocal tumors, to prevent from rupture or dissemination [21,54▪▪]. For large nonsecreting HNPGL, predictable sympathetic sequelae can lead to contra-indicate a surgery, leading to a radiation therapy decision.

In case of metastatic status (around 10–15% of all cases), overall survival decreased to 62% at 5 years, with no consensual management because it is a rare condition with lack of prospective data. Tumor morbidity is related to their size, location, hormonal activity, vascular nature, and rate of progression. Systemic therapies for this indication are limited and remain mainly palliative with a limited efficacy [65▪]. Only high-specific-activity iodine-131 MIBG is approved in the Unites States for treatment of MIBG-avid metastatic PPGL, and not all patients are candidates for this radiopharmaceutical [19]. These patients always need to be discussed in expert board meetings since surgery to decrease the tumor burden, radiation therapy, chemotherapy, embolization, metabolic radiation, MIBG, or specific therapy can be proposed.

Recently, genomics and metabolomics advances have made it possible to envisage the use of targeted therapies and precision medicine in metastatic PPGL and particularly *SDHB* patients, by targeting angiogenesis, hypermethylation, pseudo-hypoxia, and the metabolic reprogramming. In an attempt to take advantage of the angiogenic and proliferative pathways that are activated by the genetic alterations driving PPGL (mainly cluster 1 patients), antiangiogenic therapies (e.g. sunitinib) have been explored in patients with progressive PPGL with a progression-free survival of 13.4 months but with a very low objective response rate [66▪]. HIF2α antagonists have also appeared to be good candidates for the treatment of metastatic PPGL in particular those included in cluster 1 [67].

Standard chemotherapy regimen of cyclophosphamide–dacarbazine–vincristine (CVD) is recommended for metastatic PPGL with a partial response in about 37% [68], however temozolamide (the oral form of dacarbazine) seems to have higher response rate in patients with *SDHB* mutations and patients

with hypermethylator phenotypes [69]. Another therapy (PARP inhibitor) has been evaluated alone or in addition to temozolamide in patients with *SDHB* mutations, based on the fact that the overproduction of succinate have been found to suppress DNA-repair pathway [51].

Finally, considering that the mTOR signaling pathway has been implicated through *TMEM127* gene mutation, mTOR inhibitor everolimus have been tested in patient with *NF1* mutation, but so far not proven to be effective.

CONCLUSION

PCC and PGL are rare tumors, most often benign, that can lead to an excess of catecholamines. The strong genetic determinism associated with these tumors make it essential to systematically proceed to genetic investigation for patients with PPGL. The substantial progress made in the knowledge of PPGL genetics and tumorigenesis in recent years significantly improved the management and the follow-up of patients with inherited PPGL, and their relatives [5,70▪]. In fact, although *SDHB* mutation carriers were initially considered to have a poorer prognosis than patients with non-*SDHB* metastatic PPGL [71,72], a recent study has questioned this statement and showed that in a cohort of 169 patients with metastatic PPGL, those bearing *SDHB* mutation did not have a worse prognosis [65▪]. This inconsistency may be explained by the great progress made in the past decade in monitoring *SDHB*-mutated patients [65▪,70▪]. However, a continual follow-up is required given the risk of recurrence and metastatic spread.

Acknowledgements

None.

Financial support and sponsorship

None.

Conflicts of interest

The authors declare no competing interest.

REFERENCES AND RECOMMENDED READING

Papers of particular interest, published within the annual period of review, have been highlighted as:

- ▪ of special interest
- ▪▪ of outstanding interest

1. Tevosian SG, Ghayee HK. Pheochromocytomas and paragangliomas. Endocrinol Metab Clin North Am 2019; 48:727–750.
2. Thompson LDR, Gill AJ, Asa SL, *et al.* Dataset for the reporting of pheochromocytoma and paraganglioma: explanations and recommendations of the Guidelines from the International Collaboration on Cancer Reporting (ICCR). Hum Pathol 2020. S0046-8177(20)30084-8.
3. Cornu E, Belmihoub I, Burnichon N, *et al.* [Phaeochromocytoma and paraganglioma]. Rev Med Interne 2019; 40:733–741.
4. Neumann HPH, Bausch B, McWhinney SR, *et al.* Germ-line mutations in nonsyndromic pheochromocytoma. N Engl J Med 2002; 346:1459–1466.
5. Buffet A, Burnichon N, Favier J, *et al.* An overview of 20 years of genetic studies in pheochromocytoma and paraganglioma. Best Pract Res Clin Endocrinol Metab 2020; 34:101416.
6. Favier J, Amar L, Gimenez-Roqueplo A-P. Paraganglioma and phaeochromocytoma: from genetics to personalized medicine. Nat Rev Endocrinol 2015; 11:101–111.
7. Crona J, Lamarca A, Ghosal S, *et al.* Genotype-phenotype correlations in pheochromocytoma and paraganglioma: a systematic review and individual patient meta-analysis. Endocr Relat Cancer 2019; 26:539–550.
8. Crona J, Taïeb D, Pacak K. New perspectives on pheochromocytoma and paraganglioma: toward a molecular classification. Endocr Rev 2017; 38:489–515.
9. Neumann HP, Young WF, Krauss T, *et al.* 65 YEARS OF THE DOUBLE HELIX: genetics informs precision practice in the diagnosis and management of pheochromocytoma. Endocr Relat Cancer 2018; 25:T201–T219.
10. Castro-Vega LJ, Letouzé E, Burnichon N, *et al.* Multiomics analysis defines core genomic alterations in pheochromocytomas and paragangliomas. Nat Commun 2015; 6:6044.
11. Fishbein L, Leshchiner I, Walter V, *et al.* Comprehensive molecular characterization of pheochromocytoma and paraganglioma. Cancer Cell 2017; 31:181–193.
12. Selak MA, Armour SM, MacKenzie ED, *et al.* Succinate links TCA cycle dysfunction to oncogenesis by inhibiting HIF-α prolyl hydroxylase. Cancer Cell 2005; 7:77–85.
13. Sciacovelli M, Gonçalves E, Johnson TI, *et al.* Fumarate is an epigenetic modifier that elicits epithelial-to-mesenchymal transition. Nature 2016; 537:544–547.
14. ▪ Job S, Draskovic I, Burnichon N, *et al.* Telomerase activation and ATRX mutations are independent risk factors for metastatic pheochromocytoma and paraganglioma. Clin Cancer Res 2019; 25:760–770.

This paper demonstrates that TERT activation, through different possible mechanisms such as promoter mutation, chromosome gain, or methylation, and ATRX mutations are two somatic genetic events that are significantly associated with the development of metastases in SDHB-mutated or FH-mutated patients with PPGL.

15. van Duinen N, Corssmit EPM, de Jong WHA, *et al.* Plasma levels of free metanephrines and 3-methoxytyramine indicate a higher number of biochemically active HNPGL than 24-h urinary excretion rates of catecholamines and metabolites. Eur J Endocrinol 2013; 169:377–382.
16. Toledo RA, Qin Y, Cheng Z-M, *et al.* Recurrent mutations of chromatin-remodeling genes and kinase receptors in pheochromocytomas and paragangliomas. Clin Cancer Res 2016; 22:2301–2310.
17. Bausch B, Schiavi F, Ni Y, *et al.* Clinical characterization of the pheochromocytoma and paraganglioma susceptibility genes SDHA, TMEM127, MAX, and SDHAF2 for gene-informed prevention. JAMA Oncol 2017; 3: 1204–1212.
18. Welander J, Łysiak M, Brauckhoff M, *et al.* Activating FGFR1 mutations in sporadic pheochromocytomas. World J Surg 2018; 42:482–489.
19. Dahia P, Clifton-Bligh R, Gimenez-Roqueplo A-P, *et al.* Metastatic pheochromocytoma and paraganglioma: proceedings of the MEN2019 workshop. Endocr Relat Cancer 2020; 27:T41–T52.
20. Plouin PF, Amar L, Dekkers OM, *et al.* European Society of Endocrinology Clinical Practice Guideline for long-term follow-up of patients operated on for a phaeochromocytoma or a paraganglioma. Eur J Endocrinol 2016; 174:G1–G10.
21. Lenders JWM, Duh Q-Y, Eisenhofer G, *et al.* Pheochromocytoma and paraganglioma: an endocrine society clinical practice guideline. J Clin Endocrinol Metab 2014; 99:1915–1942.
22. Cascón A, Comino-Méndez I, Currás-Freixes M, *et al.* Whole-exome sequencing identifies MDH2 as a new familial paraganglioma gene. J Natl Cancer Inst 2015; 107:djv053.
23. Calsina B, Currás-Freixes M, Buffet A, *et al.* Role of MDH2 pathogenic variant in pheochromocytoma and paraganglioma patients. Genet Med 2018; 20:1652–1662.
24. Remacha L, Comino-Méndez I, Richter S, *et al.* Targeted exome sequencing of krebs cycle genes reveals candidate cancer-predisposing mutations in pheochromocytomas and paragangliomas. Clin Cancer Res 2017; 23 :6315–6324.
25. Buffet A, Morin A, Castro-Vega L-J, *et al.* Germline mutations in the mitochondrial 2-oxoglutarate/malate carrier SLC25A11 gene confer a predisposition to metastatic paragangliomas. Cancer Res 2018; 78:1914–1922.
26. ▪ Remacha L, Pirman D, Mahoney CE, *et al.* Recurrent germline DLST mutations in individuals with multiple pheochromocytomas and paragangliomas. Am J Hum Genet 2019; 104:651–664.

This paper reports the first PPGL cases with germline mutations in the DLST gene, encoding another TCA cycle enzyme, OGDH

27. Remacha L, Currás-Freixes M, Torres-Ruiz R, *et al.* Gain-of-function mutations in DNMT3A in patients with paraganglioma. Genet Med 2018; 20: 1644–1651.

28. Welander J, Andreasson A, Juhlin CC, *et al.* Rare germline mutations identified by targeted next-generation sequencing of susceptibility genes in pheochromocytoma and paraganglioma. J Clin Endocrinol Metab 2014; 99:E1352–E1360.
29. Cascon A, Comino-Mendez I, Curras-Freixes M, *et al.* Whole-exome sequencing identifies MDH2 as a new familial paraganglioma gene. J Natl Cancer Inst 2015; 107:.
30. Papathomas TG, Oudijk L, Persu A, *et al.* SDHB/SDHA immunohistochemistry in pheochromocytomas and paragangliomas: a multicenter interobserver variation analysis using virtual microscopy: a Multinational Study of the European Network for the Study of Adrenal Tumors (ENS@T). Mod Pathol 2015; 28:807–821.
31. Menara M, Oudijk L, Badoual C, *et al.* SDHD immunohistochemistry: a new tool to validate SDHx mutations in pheochromocytoma/paraganglioma. J Clin Endocrinol Metab 2015; 100:E287–E291.
32. Castro-Vega LJ, Buffet A, De Cubas AA, *et al.* Germline mutations in FH confer predisposition to malignant pheochromocytomas and paragangliomas. Hum Mol Genet 2014; 23:2440–2446.
33. Udager AM, Magers MJ, Goerke DM, *et al.* The utility of SDHB and FH immunohistochemistry in patients evaluated for hereditary paraganglioma-pheochromocytoma syndromes. Hum Pathol 2018; 71:47–54.
34. ▪ Favier J, Meatchi T, Robidel E, *et al.* Carbonic anhydrase 9 immunohistochemistry as a tool to predict or validate germline and somatic VHL mutations in pheochromocytoma and paraganglioma-a retrospective and prospective study. Mod Pathol 2020; 33:57–64.
This paper demonstrates that CA9 protein analysis should be added to the arsenal of immunohistochemistries used to validate the pathogenicity of genetic variants identified in patients with PPGL.
35. ▪ Richter S, Gieldon L, Pang Y, *et al.* Metabolome-guided genomics to identify mutations in isocitrate dehydrogenase, fumarate hydratase and succinate dehydrogenase genes in pheochromocytoma and paraganglioma. Genet Med 2019; 21:705–717.
This study demonstrates the utility of metabolomics to validate genetic variants in genes encoding TCA cycle enzymes in patients with PPGL.
36. Wallace PW, Conrad C, Brückmann S, *et al.* Metabolomics, machine learning and immunohistochemistry to predict succinate dehydrogenase mutational status in phaeochromocytomas and paragangliomas. J Pathol 2020; 251:378–387.
37. Imperiale A, Moussallieh FM, Roche P, *et al.* Metabolome profiling by HRMAS NMR spectroscopy of pheochromocytomas and paragangliomas detects SDH deficiency: clinical and pathophysiological implications. Neoplasia 2015; 17:55–65.
38. Lussey-Lepoutre C, Bellucci A, Morin A, *et al.* In vivo detection of succinate by magnetic resonance spectroscopy as a hallmark of SDHx mutations in paraganglioma. Clin Cancer Res 2016; 22:1120–1129.
39. ▪ Lussey-Lepoutre C, Bellucci A, Burnichon N, *et al.* Succinate detection using in vivo 1H-MR spectroscopy identifies germline and somatic SDHx mutations in paragangliomas. Eur J Nucl Med Mol Imaging 2020; 47:1510–1517.
In a cohort of 50 patients with PPGL, this study validates the specificity and sensitivity of in vivo tumor detection of succinate with 1H-MRS for the identification of SDH mutated patients/tumors.
40. Urbini M, Nannini M, Astolfi A, *et al.* Whole exome sequencing uncovers germline variants of cancer-related genes in sporadic pheochromocytoma. Int J Genom 2018; 2018:e6582014https://www.hindawi.com/journals/ijg/2018/6582014/.
41. Burnichon N, Vescovo L, Amar L, *et al.* Integrative genomic analysis reveals somatic mutations in pheochromocytoma and paraganglioma. Hum Mol Genet 2011; 20:3974–3985.
42. Ben Aim L, Pigny P, Castro-Vega LJ, *et al.* Targeted next-generation sequencing detects rare genetic events in pheochromocytoma and paraganglioma. J Med Genet 2019; 56:513–520.
43. Fishbein L, Khare S, Wubbenhorst B, *et al.* Whole-exome sequencing identifies somatic ATRX mutations in pheochromocytomas and paragangliomas. Nat Commun 2015; 6:1–6.
44. ▪ Calsina B, Castro-Vega LJ, Torres-Pérez R, *et al.* Integrative multiomics analysis identifies a prognostic miRNA signature and a targetable miR-21-3p/TSC2/mTOR axis in metastatic pheochromocytoma/paraganglioma. Theranostics 2019; 9:4946–4958.
This large European collaborative study evaluated the miRnome of 443 PPGL and identified a signature of six miRNAs associated with metastatic risk and time to progression, five of which were also detected in patients' liquid biopsies.
45. Job S, Georges A, Burnichon N, *et al.* Transcriptome analysis of lncRNAs in pheochromocytomas and paragangliomas. J Clin Endocrinol Metab 2020; 105:898–907.
46. Zhang J, Cong R, Zhang Q, *et al.* Integrative analysis of ceRNA network and DNA methylation associated with gene expression in malignant pheochromocytomas: a study based on The Cancer Genome Atlas. Transl Androl Urol 2020; 9:344–354.
47. Amar L, Bertherat J, Baudin E, *et al.* Genetic testing in pheochromocytoma or functional paraganglioma. J Clin Oncol 2005; 23:8812–8818.
48. Gimenez-Roqueplo A-P, Favier J, Rustin P, *et al.* Mutations in the SDHB gene are associated with extra-adrenal and/or malignant phaeochromocytomas. Cancer Res 2003; 63:5615–5621.
49. ▪ Morin A, Goncalves J, Moog S, *et al.* TET-mediated hypermethylation primes SDH-deficient cells for HIF2α-driven mesenchymal transition. Cell Rep 2020; 30:4551–4566.e7.
This paper demonstrates how TET inhibition acts in synergy with HIF2A stabilization to allow SDHB-deficient cells to acquire metastatic properties.
50. Liu Y, Pang Y, Zhu B, *et al.* Therapeutic targeting of SDHB-mutated pheochromocytoma/paraganglioma with pharmacologic ascorbic acid. Clin Cancer Res 2020; 26:3868–3880.
51. Pang Y, Lu Y, Caisova V, *et al.* Targeting NAD+/PARP DNA repair pathway as a novel therapeutic approach to SDHB-mutated cluster i pheochromocytoma and paraganglioma. Clin Cancer Res 2018; 24:3423–3432.
52. Sulkowski PL, Sundaram RK, Oeck S, *et al.* Krebs-cycle-deficient hereditary cancer syndromes are defined by defects in homologous-recombination DNA repair. Nat Genet 2018; 50:1086–1092.
53. ▪▪ Sulkowski PL, Oeck S, Dow J, *et al.* Oncometabolites suppress DNA repair by disrupting local chromatin signalling. Nature 2020; 582:586–591.
In this study, the authors deciphered the pathway by which oncometabolites disrupt DNA repair. They show that oncometabolite-induced inhibition of the lysine demethylase KDM4B results in aberrant hypermethylation of histone 3 lysine 9 at loci surrounding DNA breaks, masking a local H3K9 trimethylation signal that is essential for the proper execution of homology-dependent repair.
54. ▪▪ Lenders JWM, Kerstens MN, Amar L, *et al.* Genetics, diagnosis, management and future directions of research of phaeochromocytoma and paraganglioma: a position statement and consensus of the Working Group on endocrine hypertension of the European society of hypertension. J Hypertens 2020; 38:1443–1456.
In this study, a group of experts from the European Society of Hypertension propose a document that summarizes the current knowledge in epidemiology, genetics, diagnosis, treatment and surveillance of PPGL.
55. Sbardella E, Maunsell Z, May CJH, *et al.* Random 'spot' urinary metanephrines compared with 24-h-urinary and plasma results in phaeochromocytomas and paragangliomas. Eur J Endocrinol 2020; 183:129–139.
56. Sawka AM, Prebtani AP, Thabane L, *et al.* A systematic review of the literature examining the diagnostic efficacy of measurement of fractionated plasma free metanephrines in the biochemical diagnosis of pheochromocytoma. BMC Endocr Disord 2004; 4:2.
57. Rao D, Peitzsch M, Prejbisz A, *et al.* Plasma methoxytyramine: clinical utility with metanephrines for diagnosis of pheochromocytoma and paraganglioma. Eur J Endocrinol 2017; 177:103–113.
58. Wang EY, Pak JS, Virk RK, *et al.* Bladder preservation for patients with bladder paragangliomas: case series and review of the literature. Urology 2020; 143:194–205.
59. Lam AK-Y. Update on adrenal tumours in 2017 World Health Organization (WHO) of endocrine tumours. Endocr Pathol 2017; 28:213–227.
60. Kimura N, Takekoshi K, Naruse M. Risk stratification on pheochromocytoma and paraganglioma from laboratory and clinical medicine. J Clin Med 2018; 7:242.
61. Taïeb D, Pacak K. Genetic determinants of pheochromocytoma and paraganglioma imaging phenotypes. J Nucl Med 2020; 61:643–645.
62. Janssen I, Chen CC, Millo CM, *et al.* PET/CT comparing (68)Ga-DOTATATE and other radiopharmaceuticals and in comparison with CT/MRI for the localization of sporadic metastatic pheochromocytoma and paraganglioma. Eur J Nucl Med Mol Imaging 2016; 43:1784–1791.
63. Amar L, Lussey-Lepoutre C, Lenders JWM, *et al.* Management of endocrine disease: recurrence or new tumors after complete resection of pheochromocytomas and paragangliomas: a systematic review and meta-analysis. Eur J Endocrinol 2016; 175:R135–145.
64. Gartland RM, Fuentes E, Fazendin J, *et al.* Safety of outpatient adrenalectomy across 3 minimally invasive approaches at 2 academic medical centers. Surgery 2020. S0039-6060(20)30170-7.
65. ▪ Hescot S, Curras-Freixes M, Deutschbein T, *et al.* Prognosis of malignant pheochromocytoma and paraganglioma (MAPP-Prono Study): a european network for the study of adrenal tumors retrospective study. J Clin Endocrinol Metab 2019; 104:2367–2374.
In this retrospective multicenter study, the authors searched for prognostic parameters of overall survival in metastatic patients with PPGL. Surprisingly, they do not confirm SDHB mutations as a major prognostic parameter in metastatic patients. Whether this is because of differences in the follow-up of patients remains an open question.
66. ▪ O'Kane GM, Ezzat S, Joshua AM, *et al.* A phase 2 trial of sunitinib in patients with progressive paraganglioma or pheochromocytoma: the SNIPP trial. Br J Cancer 2019; 120:1113–1119.
This is the first report of a phase 2 clinical trial using the antiangiogenic agents sunitinib in PPGL.
67. Toledo RA. New HIF2α inhibitors: potential implications as therapeutics for advanced pheochromocytomas and paragangliomas. Endocr Relat Cancer 2017; 24:C9–C19.
68. Niemeijer ND, Alblas G, van Hulsteijn LT, *et al.* Chemotherapy with cyclophosphamide, vincristine and dacarbazine for malignant paraganglioma and pheochromocytoma: systematic review and meta-analysis. Clin Endocrinol (Oxf) 2014; 81:642–651.
69. Hadoux J, Favier J, Scoazec J-Y, *et al.* SDHB mutations are associated with response to temozolomide in patients with metastatic pheochromocytoma or paraganglioma. Int J Cancer 2014; 135:2711–2720.

70. Buffet A, Ben Aim L, Leboulleux S, *et al.* Positive impact of genetic test on the ■ management and outcome of patients with paraganglioma and/or pheochromocytoma. J Clin Endocrinol Metab 2019; 104:1109–1118.
This study compared the outcome of PPGL patients with SDH and VHL mutations, depending on the delay of obtention of genetic testing. It reveals that the early knowledge of genetic status modifies the follow-up of patients, and thereby, significantly improve their prognosis.

71. Amar L, Baudin E, Burnichon N, *et al.* Succinate dehydrogenase B gene mutations predict survival in patients with malignant pheochromocytomas or paragangliomas. J Clin Endocrinol Metab 2007; 92:3822–3828.

72. King KS, Prodanov T, Kantorovich V, *et al.* Metastatic pheochromocytoma/paraganglioma related to primary tumor development in childhood or adolescence: significant link to SDHB mutations. J Clin Oncol 2011; 29:4137–4142.